Mathématiques et Applications 79

Pierre Saramito

Complex fluids

Modeling and Algorithms

SMAI

Springer

Mathématiques et Applications

Directeurs de la collection:
M. Hoffmann et V. Perrier

79

More information about this series at http://www.springer.com/series/2966

MATHÉMATIQUES & APPLICATIONS

Comité de Lecture 2012–2016/Editorial Board 2012–2016

Directeurs de la collection
M. HOFFMANN et V. PERRIER

Pierre Saramito

Complex fluids

Modeling and Algorithms

Springer

Pierre Saramito
Laboratoire Jean Kuntzmann
Centre National de la Recherche
Scientifique
Université Grenoble Alpes
Grenoble
France

ISSN 1154-483X ISSN 2198-3275 (electronic)
Mathématiques et Applications
ISBN 978-3-319-44361-4 ISBN 978-3-319-44362-1 (eBook)
DOI 10.1007/978-3-319-44362-1

Library of Congress Control Number: 2016947484

Mathematics Subject Classification (2010): 35, 76, 65, 68

This Springer imprint is published by Springer Nature
The registered company is Springer International Publishing AG
The registered company address is: Gewerbestrasse 11, 6330 Cham, Switzerland

À Claire

Preface

Water and air behave in a similar way and their flow can be described in a very accurate way by the Navier–Stokes equations. Others fluids behave differently: they cannot be described by the Navier–Stokes equations. Fluids that can be described by the Navier–Stokes equations are called Newtonian fluids, and all the others are called non-Newtonian or complex fluids. Most common fluids, such as toothpaste, hair gel, mayonnaise, liquid foam, cement, and blood are complex fluids. Molten plastics are also complex fluids. The success of the forming process depends on the knowledge of the material's properties. Geophysical fluids, such as mud flows, volcanic lava, glaciers, and snow avalanches are also complex fluids and the hazard assessment uses softwares that are based on complex fluid models. In biology, the optimization of arterial graft requires the knowledge of the behavior of the flow of blood, also a complex fluid.

Goals The object of this book is twofold: modeling and algorithms. The first goal of this book is to present in a comprehensive text the modeling of complex fluids. Complex fluid models are introduced by increasing the level of complexity, and the relations between all the models are addressed using hierarchical diagrams. The second goal is to present an up-to-date mathematical and numerical analysis of the corresponding equations and to propose several practical numerical algorithms for the approximation of the solutions. The various numerical methods presented here are then suitable for implementation on computers, using some finite element libraries. These numerical methods are able to compute velocities, pressures, and stresses at each position and at each time when explicit computations are no more possible for complex geometries and flow conditions. Numerous examples of practical flow computations are presented along with this book. Software implementations are based on the Rheolef finite element library [283–285] developed by the author. Rheolef is a free software available as a standard package under the Debian and Ubuntu GNU/Linux systems and that can be installed from source code on others systems.

Audience This book is primarily intended for undergraduate students and researchers in applied mathematics, engineering sciences, computational mechanics, and physics. The reader is assumed to be familiar with computational methods

such as finite differences and finite elements, together with the corresponding variational formulations of partial differential equations. Special care has been devoted to making the material as much self-contained as possible. The general level of the book is best suited for an undergraduate-level course which can be built by drawing on some of the present chapters. The material is actually an elaboration on the lecture notes by the author for an undergraduate course on complex fluids at Grenoble University and ENSIMAG. Some of the topics covered in this book stem from recent work by the authors, e.g., on the logarithm of conformation tensor formulation of viscoelastic fluids and the joint work with Bernabeu on inertia effects in viscoplastic flows and also the joint work with Cheddadi and Graner for the elaboration of elastoviscoplastic models and their numerical resolution.

Outline Newtonian fluids and the Navier–Stokes equations are presented in Chap. 1. Newtonian fluids constitute the basis on which are developed more complex models. This first chapter also introduces some concepts, notations, and numerical methods that are reused all along this book: the continuum mechanics theory (Sects. 1.1–1.3), the method of characteristics for the time discretization and two algorithms for the resolution of the underlying linear system, the so-called Stokes problem. Chapter 2 covers various quasi-Newtonian fluids: it is a first step inside complex fluids. Quasi-Newtonian fluids are defined by a nonconstant viscosity law that depends upon the velocity gradient. Two numerical algorithms are presented in order to solve this nonlinearity: the fixed point method and the Newton method. Chapter 3 addresses viscoplastic fluids: these complex fluids are defined by a non-differentiable energy of dissipation function and the corresponding constitutive equations are highly nonlinear. Two main classes of numerical algorithms are presented: the regularization method and the augmented Lagrangian algorithm. This second approach uses some convex analysis tools introduced in the chapter. Chapter 4 is dedicated to viscoelastic fluids. This chapter starts with the concept of frame-invariant tensor derivatives. An operator splitting method allows to develop a second order in time algorithm, the so-called θ-scheme. An alternative numerical approach is also presented: it is based on a change of variable, with the new variable defined in terms of the logarithm of the conformation tensor. Chapter 5 deals with elastoviscoplastic fluids that combines nonlinearities presented in the two previous chapters. Elastoviscoplastic fluid models are obtained with the help of a thermodynamical framework with internal variables. These complex fluid models could be organized in a hierarchical view, shown on Fig. 1. This diagram also draws the dependencies upon the chapters of the book. Chapter 1 contains prerequisites (Sects. 1.1–1.4) for all others chapters. Then Chaps. 2, 3 and 4 could be read independently. Chapter 5 presents a synthesis of all complex fluid models of the previous chapters together with a new one that combines their complexities. All chapters share a similar outline: introductory sections leads to the problem statement. Then, the fluid model is presented through Poiseuille and Couette flows, which can be solved explicitly. Next, numerical methods are presented together with examples of computations dealing with complex flow conditions for which no explicit solution is available. Some concluding remarks close each chapter. These notes furnish references and historical complements together with some alternative

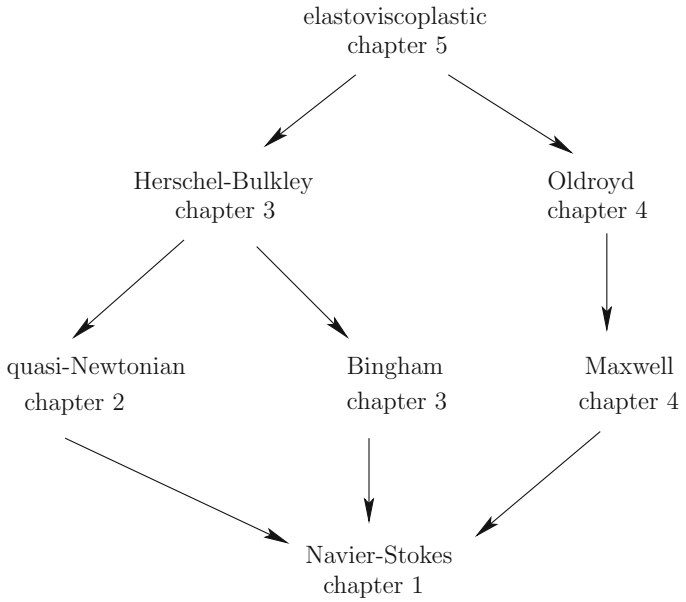

Fig. 1 Complex fluids: a hierarchy of models

methods when available. A bibliography of more than 300 entries and an index closes the book. The literature on complex fluids is so vast that this bibliography is by no means exhaustive. We hope that the selected entries provide the reader with additional information to examine in more deep the topics covered herein and to explore new ones.

Acknowledgments The author is grateful to several colleagues for their constructive remarks that helped to improve the manuscript. In particular, my warmest thanks go to Véronique Dansereau, Ibrahim Cheddadi, François Graner, and Franck Pigeonneau. I am also thankful to Thierry Colin and Valérie Perrier for offering me the opportunity to publish this book in the *mathématiques and applications* collection and to the two anonymous reviewers for their careful reading of the book and their comments that helped to improve the book.

Grenoble, France Pierre Saramito

Contents

Notations

Ω	Flow domain
$\partial\Omega$	Boundary of the flow domain
$\boldsymbol{n}$	Outer unit normal on $\partial\Omega$
ρ	Mass density
$\boldsymbol{u}$	Velocity vector
σ_{tot}	Cauchy stress tensor
p	Pressure
$\nabla\boldsymbol{u}$	$= \left(\frac{\partial u_i}{\partial x_j}\right)_{1 \le i,j \le 3}$ Gradient of velocity tensor
$D(\boldsymbol{u})$	$= (\nabla\boldsymbol{u} + \nabla\boldsymbol{u}^T)/2$ Rate of deformation tensor
$W(\boldsymbol{u})$	$= (\nabla\mathbf{u} - \nabla\mathbf{u}^T)/2$ Vorticity tensor
$\boldsymbol{u}.\boldsymbol{v}$	$= \sum_{i=1}^{3} u_i v_i$ Dot product, for any vectors
$\lvert\boldsymbol{v}\rvert$	$= (\boldsymbol{v}.\boldsymbol{v})^{\frac{1}{2}}$ Vector norm
$\sigma : \tau$	$= \sum_{i,j=1}^{3} \sigma_{i,j}\tau_{i,j}$ Double dot product, for any tensors
$\lvert\tau\rvert$	$= \left(\frac{\tau:\tau}{2}\right)^{\frac{1}{2}}$ Tensor norm
$\dot{\gamma}$	$= \lvert 2D(\boldsymbol{u})\rvert$ Shear rate
$\boldsymbol{I}$	Identity tensor
$\text{tr}(\tau)$	$= \sum_{i=1}^{3} \tau_{i,i}$ Trace of a tensor
$\text{dev}(\tau)$	$= \tau - (1/3)\text{tr}(\tau)\boldsymbol{I}$, Deviatoric part of a tensor
$\mathbb{R}^{3\times3}_{s}$	$= \left\{\tau \in \mathbb{R}^{3\times3} \ ; \ \tau = \tau^T\right\}$, The set of 3×3 symmetric matrices
$\mathbb{R}^{3\times3}_{s*+}$	The set of 3×3 symmetric positive definite matrices
$\boldsymbol{u} \otimes \boldsymbol{v}$	$= (u_i v_j)_{1 \le i,j \le 3}$ Tensorial product of two vectors
η	Viscosity
K	Consistency
n	Power law index
σ_0	Yield stress
μ	Elastic modulus

λ	Relaxation time
a	Interpolation parameter of the Gordon–Schowalters tensor derivative
Re	Reynolds number
Bi	Bingham number
We	Weissenberg number
α	Viscosity ratio, for a polymer solution with a viscous solvent

Chapter 1
Navier–Stokes Equation

This chapter starts with two general principles: the mass and momentum conservations, valid for any fluid, complex or not, which will be used all along this book. The two corresponding sections introduce some basic notations and concepts such as the velocity vector and the stress tensor. The fundamental Reynolds and Stokes formula are also presented here, together with the Cauchy theorem. The constitutive equation of a Newtonian fluid is then analyzed: it closes the Navier–Stokes system of equations. Theoretical results available for these equations are recalled before computing some explicit solutions for two simple cases of major practical interest: the Poiseuille and Couette flows. In the general case of complex geometries and boundary conditions, no explicit solutions are available. Several methods for computing approximations of the solutions are covered in this chapter. The time discretization based on the method of characteristics is presented first. Next, with the help of variational formulations, we deal with the discretization in space. Two discretization methods are examined: the staggered grid finite difference and the finite element. For the resolution of the mixed linear system, both a direct and an iterative algorithm are addressed. Finally, numerical approximations of the solution of the Navier–Stokes equations are presented for the driven cavity problem.

1.1 Conservation of Mass

Let us introduce first some basic notations, that will be used all along this book. The flow domain $\Omega \subset \mathbb{R}^3$ is an open bounded subset of the three dimensional physical space. The *density* of the fluid ρ is a function, defined at any time $t \geqslant 0$ and at any location $\boldsymbol{x} \in \Omega$ of the flow domain and its value, always positive, is denoted by $\rho(t, \boldsymbol{x})$. The assumption that ρ exists is a *continuum* hypothesis: it does not hold at the microscopic scale, when considering the molecular structure of the matter. At macroscopic scales, this assumption is extremely accurate. The fluid *velocity* is a three component real vector, denoted as $\boldsymbol{u}(t, \boldsymbol{x}) = (u_i(t, \boldsymbol{x}))_{1 \leqslant i \leqslant 3}$ and the vector field is simply denoted by $\boldsymbol{u}$ (see Fig. 1.1). We assume that the functions ρ and $\boldsymbol{u}$ are

P. Saramito, *Complex fluids*, Mathématiques et Applications 79,
DOI 10.1007/978-3-319-44362-1_1

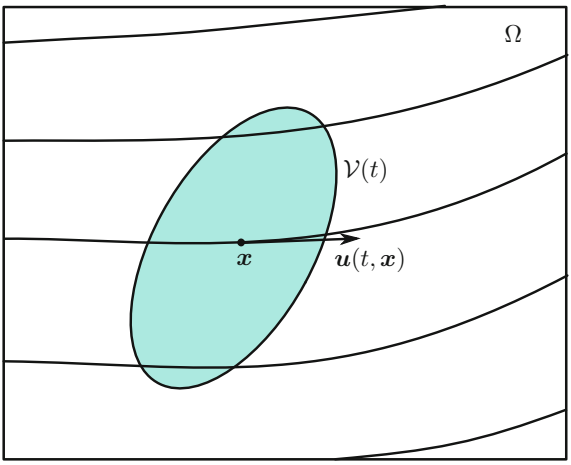

Fig. 1.1 Representation of the flow in continuum mechanics

sufficiently smooth so that the standard operations of calculus can be performed on them.

Postulate 1.1 *(conservation of mass – non-local form)*
The mass of the fluid is conserved along the time inside any material system transported by the velocity field.

Our first aim is to express this postulate by using mathematical notations. An arbitrary material system is represented by a bounded subset $\mathcal{V}(t) \subset \Omega$ that is transported by the fluid in the flow domain Ω at any time $t \geqslant 0$. The conservation of mass principle equivalently postulates that, at any time $t \geqslant 0$, the mass variation inside $\mathcal{V}(t)$ is zero.

$$\frac{d}{dt}\left(\int_{\mathcal{V}(t)} \rho(t,\boldsymbol{x})\,\mathrm{d}x\right) = 0 \tag{1.1}$$

This conservation of mass principle could also be rewritten in a local form instead of inside an arbitrary subdomain $\mathcal{V}(t)$. For this purpose, we need some tools to write global equations in a local form. Observe also that the domain of integration $\mathcal{V}(t)$ depends on time: the time derivative and the integration could not be swapped directly. This swap requires introducing additional terms as presented in the forthcoming Reynolds formula as well as the concept of *divergence*.

Definition 1.1 (*divergence of a vector field*)
Let $(0, x_1, x_2, x_3)$ denote the Cartesian coordinate system. For any vector field $\boldsymbol{v}$, defined in Ω, its *divergence* is defined by:

$$\operatorname{div} \boldsymbol{v} = \sum_{i=1}^{3} \frac{\partial v_i}{\partial x_i}$$

Theorem 1.1 (Reynolds transport formula)
Let $\boldsymbol{u}$ be any vector field defined in Ω and let $\mathcal{V}(t) \subset \Omega$ be any bounded subset transported by $\boldsymbol{u}$. For any function φ, defined at any time and at any point of Ω, we have

$$\frac{\mathrm{d}}{\mathrm{d}t}\left(\int_{\mathcal{V}(t)} \varphi(t,\boldsymbol{x})\,\mathrm{d}x\right) = \int_{\mathcal{V}(t)} \left(\frac{\partial \varphi}{\partial t} + \operatorname{div}(\varphi\,\boldsymbol{u})\right)\mathrm{d}x \tag{1.2}$$

Proof This is a classical theorem of continuum mechanics: see e.g. [85, p. 26], [52, p. 10], [307, p. 19] or [35, p. 5] for the proof. □

In order to establish the local expression of the conservation of mass, we use a density argument, introduced here.

Definition 1.2 (*set of dense parts of a domain*)
Let $\Omega \subset \mathbb{R}^d$, $d = 1, 2, 3$, be an open bounded subset of a d-dimensional physical space. Let $\mathcal{P}(\Omega)$ denotes the set of all possible parts of Ω. Then, $\mathcal{D} \subset \mathcal{P}(\Omega)$, a set of parts of Ω is said to be *dense* in Ω when for all $\boldsymbol{x} \in \Omega$ and for all $\mathcal{V} \subset \Omega$ containing $\boldsymbol{x}$, there exists an open part $\omega \in \mathcal{D}$ such that $\boldsymbol{x} \in \omega$ and $\omega \subset \mathcal{V}$.

There are many examples of a set of dense parts of Ω. The more classical example is the set of all open balls contained in Ω. Another example is the set of all open parallelepipeds whose faces are parallel to the axes of a Cartesian coordinate system. Indeed, in any open ball centered in $\boldsymbol{x}$, we can inscribe an open parallelepiped centered in $\boldsymbol{x}$, Also, the set of all open tetrahedrons whose faces are parallel to four fixed and different planes is another valid example of set of dense parts of Ω.

Lemma 1.1 (from global to local by density)
Let $\Omega \subset \mathbb{R}^d$, $d = 1, 2, 3$, be an open bounded subset of a d-dimensional physical space. Let $\mathcal{D}$ be a set of dense parts of Ω. For all $\varphi \in C^0\left(\bar{\Omega}\right)$, we have

$$\int_{\mathcal{V}} \varphi(\boldsymbol{x})\,\mathrm{d}x = 0, \quad \forall \mathcal{V} \in \mathcal{D} \implies \varphi = 0 \text{ in } \Omega$$

Proof By contraposition, suppose that there exists $\boldsymbol{x}_0 \in \Omega$ such that $\varphi(\boldsymbol{x}_0) = \alpha \neq 0$. Let us suppose first $\alpha > 0$. Since φ is continuous, there exists a sufficiently small vicinity $\mathcal{V}_0 \in \mathcal{D}$ containing $\boldsymbol{x}_0$ such that $\operatorname{meas}(\mathcal{V}_0) > 0$ and

$$\frac{\alpha}{2} \leqslant \varphi(\boldsymbol{x}), \quad \forall \boldsymbol{x} \in \mathcal{V}_0$$

Integrating over $\mathcal{V}_0$ yields

$$0 < \frac{\alpha \operatorname{meas}(\mathcal{V}_0)}{2} \leqslant \int_{\mathcal{V}} \varphi(\boldsymbol{x})\,\mathrm{d}x$$

This is in contradiction with the hypothesis. When $\alpha < 0$, set $\tilde{\varphi} = -\varphi$ and $\tilde{\alpha} = -\alpha$: it also leads to the same contradiction and thus $\varphi = 0$. □

Then, we have all the required tools and we are able to establish the local form of the conservation of mass.

Theorem 1.2 (conservation of mass – local form)

$$\frac{\partial \rho}{\partial t} + \operatorname{div}(\rho \boldsymbol{u}) = 0 \ \ in \ \ ]0, +\infty[\times \Omega \tag{1.3}$$

Proof Let us apply the Reynolds formula (1.2) with $\varphi = \rho$. The conservation of mass (1.1) becomes

$$\int_{\mathcal{V}(t)} \left(\frac{\partial \rho}{\partial t} + \operatorname{div}(\rho \boldsymbol{u}) \right) \mathrm{d}x = 0$$

This relation is true at any time $t > 0$ and for any subdomain $\mathcal{V}(t) \subset \Omega$. Thus, from Lemma 1.1, the relation is true locally at any point in Ω and the proof is complete. □

1.2 Conservation of Momentum

The conservation of momentum admits the following general expression (see e.g. [307, p. 32] or [85, p. 38]).

Postulate 1.2 *(conservation of momentum – non-local form)*
There exists at least one chronology and frame of reference, called Galilean, such that at each time and for every material system, the time derivative of the torque of the momentum is equal to the torque of the forces applied to the system.

It was first postulated in 1667 by Newton in its celebrated book, reedited in 1726 [220]. The previous reference is in Latin: see e.g. its French translation [221, 222] written in 1759 by du Châtelet or its English [223] one, written in 1846 by Motte. This postulate is also called the second fundamental law and the fundamental law of dynamics. The time derivative of the momentum is also called the acceleration.

Remark 1.1 (*Galilean frames*)
The conservation of momentum is not invariant by changing to a non-Galilean frame, e.g. if we add to a constant translation motion a solid rotation with respect to a Galilean frame. Indeed, a rotation or a non-constant translation changes the acceleration. This postulate assumes the existence of at least one Galilean frame. In practice, it could only be approximative and its choice depends upon the application: e.g. relative to the Earth or to some stars. This choice was discussed in 1902 by Poincaré [242], in the conclusion of its third chapter, as "*Nous adoptons [ce postulat] parce que certaines expériences nous ont montré qu'il serait commode*" (We adopt this postulate because some experiments have shown that it would be convenient). Non-Galilean frames of reference are often considered in celestial mechanics, in meteorology or oceanography, or for rigid body mechanics. In these cases, it is necessary to add to

the forces applied to the system some other suitable terms related to the acceleration, e.g. the Coriolis pseudo-force.

Our first aim is to express this postulate by using mathematical notations. Let us denotes $t \geqslant 0$ the time of the Galilean chronology and assume that the Cartesian coordinate system $(0, x_1, x_2, x_3)$ is associated to a Galilean frame. Let $\mathcal{V}(t) \subset \Omega$ be any material system, transported by the velocity field $\boldsymbol{u}$. Before we continue, we need some auxiliary notations and definitions.

Definition 1.3 (*wedge product of two vectors*)
The *wedge product* of two vectors $\boldsymbol{a} = (a_i)_{1\leqslant i\leqslant 3}$ and $\boldsymbol{b} = (b_i)_{1\leqslant i\leqslant 3} \in \mathbb{R}^3$ is denoted by $\boldsymbol{a} \wedge \boldsymbol{b}$ and is defined by

$$\boldsymbol{a} \wedge \boldsymbol{b} = \begin{pmatrix} a_2 b_3 - a_3 b_2 \\ a_3 b_1 - a_1 b_3 \\ a_1 b_2 - a_2 b_1 \end{pmatrix}$$

The *density of momentum* is defined by $\rho \boldsymbol{u}$. The *torque of the momentum* of the system $\mathcal{V}(t)$ is expressed by two quantities:

$$\begin{aligned} &(1) \text{ its linear resultant : } \int_{\mathcal{V}(t)} \rho(t, \boldsymbol{x})\, \boldsymbol{u}(t, \boldsymbol{x})\, \mathrm{d}x \\ &(2) \text{ its angular resultant : } \int_{\mathcal{V}(t)} \rho(t, \boldsymbol{x})\, \boldsymbol{u}(t, \boldsymbol{x}) \wedge \boldsymbol{x}\, \mathrm{d}x \end{aligned}$$

Next, there are two categories of applied forces: volume forces, acting inside the system $\mathcal{V}(t)$ and surface forces, acting on its boundary $\partial\mathcal{V}(t)$. Volume forces on the small and arbitrary volume $\mathcal{V}(t)$ represent external forces, acting at distance, while surface forces are due to internal forces acting inside the fluid, as $\mathcal{V}(t) \subset \Omega$ is inside the flow domain. Let us denote by $\rho \boldsymbol{g}$ in $\mathcal{V}(t)$, the density of volume forces. For instance, when representing gravity forces, $\boldsymbol{g}$ is the gravity acceleration vector. Others external forces acting on $\mathcal{V}(t)$ can be added, e.g. magnetic forces due to a magnetic field. These forces depend upon specificities of the problem under consideration. The density of surface forces acting on the boundary $\partial\mathcal{V}(t)$ at position $\boldsymbol{x}$ admits the general form $\boldsymbol{s}(\boldsymbol{x}, \boldsymbol{n})$, called the *normal stress vector*. Here, $\boldsymbol{n}$ denotes the *outer unit normal* vector to the boundary $\partial\mathcal{V}(t)$ at position $\boldsymbol{x}$. Surface forces express for instance the pressures and friction between molecules at the microscopic scale. Note that there exists in some mechanical textbooks a different convention for the unit normal $\boldsymbol{n}$, as the *inner* unit normal: which implies a change of sign in formulas for the corresponding terms. Based on theses definitions, we are able to express the conservation of momentum for the system $\mathcal{V}(t)$ at any time t. Two relations can be written, the conservation of linear momentum and the conservation of angular momentum:

$$\frac{\mathrm{d}}{\mathrm{d}t}\left(\int_{\mathcal{V}(t)} \rho\, \boldsymbol{u}\, \mathrm{d}x\right) = \int_{\mathcal{V}(t)} \rho\, \boldsymbol{g}\, \mathrm{d}x + \int_{\partial\mathcal{V}(t)} \boldsymbol{s}(\boldsymbol{x}, \boldsymbol{n})\, \mathrm{d}s \tag{1.4}$$

$$\frac{\mathrm{d}}{\mathrm{d}t}\left(\int_{\mathcal{V}(t)} \rho\,\boldsymbol{u}\wedge\boldsymbol{x}\,\mathrm{d}x\right)=\int_{\mathcal{V}(t)}\rho\,\boldsymbol{g}\wedge\boldsymbol{x}\,\mathrm{d}x+\int_{\partial\mathcal{V}(t)}\boldsymbol{s}(\boldsymbol{x},\boldsymbol{n})\wedge\boldsymbol{x}\,\mathrm{d}s \tag{1.5}$$

Our next aim is to express these relations in local form. To do so, we need to introduce some additional definitions and notations.

Definition 1.4 (*tensor product of two vectors*)
The tensor product of any vectors $\boldsymbol{a}$ and $\boldsymbol{b}\in\mathbb{R}^3$, denoted as $\boldsymbol{a}\otimes\boldsymbol{b}$, is a 3×3 real matrix:

$$\boldsymbol{a}\otimes\boldsymbol{b}=(a_ib_j)_{1\leqslant i,j\leqslant 3}$$

Definition 1.5 (*tensor field*)
A *tensor* field $\boldsymbol{\tau}$ is a 3×3 real matrix-valued function, defined at any time $t>0$ and $\boldsymbol{x}\in\Omega$ by $\boldsymbol{\tau}(t,\boldsymbol{x})=(\tau_{i,j}(t,\boldsymbol{x}))_{1\leqslant i,j\leqslant 3}$.

Definition 1.6 (*divergence of a tensor*)
The divergence of a tensor field $\boldsymbol{\tau}$, defined in Ω, is the vector field defined by:

$$\mathbf{div}\,\boldsymbol{\tau}=\left(\sum_{j=1}^{3}\frac{\partial\tau_{i,j}}{\partial x_j}\right)_{1\leqslant i\leqslant 3}$$

It means that the divergence of a tensor is a vector whose components are the divergence of the rows of the tensor.

From Theorem 1.1 and using these notations, we obtain the following vectorial version of the Reynolds formula.

Corollary 1.1 (Reynolds transport formula – vectorial version)

$$\frac{\mathrm{d}}{\mathrm{d}t}\left(\int_{\mathcal{V}(t)}\boldsymbol{q}(t,\boldsymbol{x})\,\mathrm{d}x\right)=\int_{\mathcal{V}(t)}\left(\frac{\partial\boldsymbol{q}}{\partial t}+\mathbf{div}(\boldsymbol{q}\otimes\boldsymbol{u})\right)\mathrm{d}x \tag{1.6}$$

Let us apply (1.6) with $\boldsymbol{q}=\rho\boldsymbol{u}$ representing the density of momentum. Then, the conservation of linear momentum (1.4) writes

$$\int_{\mathcal{V}(t)}\left(\frac{\partial(\rho\boldsymbol{u})}{\partial t}+\mathbf{div}(\rho\boldsymbol{u}\otimes\boldsymbol{u})-\rho\boldsymbol{g}\right)\mathrm{d}x=\int_{\partial\mathcal{V}(t)}\boldsymbol{s}(\boldsymbol{x},\boldsymbol{n})\,\mathrm{d}s \tag{1.7}$$

We now concentrate on the right-hand-side of Eq. (1.7). The following Cauchy theorem expresses the density of surface forces $\boldsymbol{s}(\boldsymbol{x},\boldsymbol{n})$ in a simple and elegant way. As the time has no importance for this result, it is presented as time independent. Next, we will be able to transform the boundary integral over $\partial\mathcal{V}(t)$ into a volume integral in $\mathcal{V}(t)$, thanks to the Stokes formula.

Theorem 1.3 (existence of the Cauchy stress tensor)
Let $\Omega\subset\mathbb{R}^3$ be an open bounded subset of the three dimensional space. Let $\boldsymbol{f}$ be

a bounded vector field defined in Ω *and* $\boldsymbol{s}$ *be a continuous vector field, defined in* $\Omega \times S$ *where* $S = \{\boldsymbol{\nu} \in \mathbb{R}^3;\ |\boldsymbol{\nu}| = 1\}$ *denotes the unit sphere. Assume that*

$$\int_{\partial \mathcal{V}} \boldsymbol{s}(\boldsymbol{x}, \boldsymbol{n})\, \mathrm{d}s = \int_{\mathcal{V}} \boldsymbol{f}(\boldsymbol{x})\, \mathrm{d}x, \quad \forall \mathcal{V} \subset \Omega \tag{1.8}$$

where $\boldsymbol{n}$ *denotes the unit outward normal on* $\partial\mathcal{V}$*. Then,* $\boldsymbol{s}$ *could be extended with respect to its second argument from* S *to* $\mathbb{R}^3$ *as a linear operator, i.e. there exists a tensor* $\boldsymbol{\sigma}_{\text{tot}}$*, called the* Cauchy stress tensor*, such that*

$$\boldsymbol{s}(\boldsymbol{x}, \boldsymbol{\nu}) = \boldsymbol{\sigma}_{\text{tot}}(\boldsymbol{x})\, \boldsymbol{\nu} \tag{1.9}$$

for all $\boldsymbol{x} \in \Omega$ *and* $\boldsymbol{\nu} \in \mathbb{R}^3$.

Proof The Cauchy's original proof is in two steps. The first step shows the principle of the action and the reaction. It was first postulated in 1667 by Newton [220] and is also called the Newton's third fundamental law (*actio* = *reactio*). Later, in 1827, it has been directly proved by Cauchy [44] in its Theorem 1. The second step of the proof shows the linearity of the operator and the existence of the tensor and was showed in 1827 by Cauchy in the same paper (see also [43]).

Step 1: action and reaction – Consider any $\boldsymbol{x}_0 \in \Omega$ and any $\boldsymbol{\nu} \in S$. Let $\varepsilon > 0$ and $\mathcal{V} = \{\boldsymbol{y} \in \mathbb{R}^3;\ |\boldsymbol{y} - \boldsymbol{x}_0| < \varepsilon\}$ be the ball centered in $\boldsymbol{x}_0$ with radius ε. As Ω is an open set, there exists a radius $\varepsilon_0 > 0$ sufficiently small such that for all $\varepsilon < \varepsilon_0$ we have $\mathcal{V} \subset \Omega$. Let $P = \{\boldsymbol{y} \in \mathbb{R}^3;\ (\boldsymbol{y} - \boldsymbol{x}_0).\boldsymbol{\nu} = 0\}$ be the plane passing in $\boldsymbol{x}_0$ and whose normal is $\boldsymbol{\nu}$. This plane cuts $\mathcal{V}$ in two half spheres denoted as $\mathcal{V}_1$ and $\mathcal{V}_2$, as shown on Fig. 1.2, such that the outer normal on $\partial\mathcal{V}_1 \cap P$ is $\boldsymbol{\nu}$ and that on $\partial\mathcal{V}_2 \cap P$ is $-\boldsymbol{\nu}$. Let us apply (1.8) successively to $\mathcal{V}$, $\mathcal{V}_1$ and $\mathcal{V}_2$. We obtain

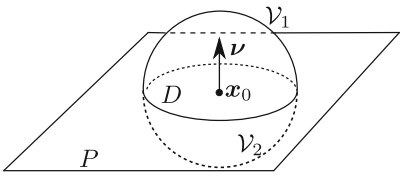

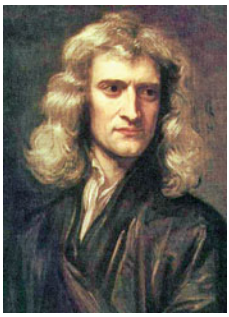

Isaac
Newton
1687

Augustin
Cauchy
1823, 1827

Fig. 1.2 (*left*) Cauchy's proof of the Newton's action and reaction principle. (*middle*) Portrait of Newton in 1689 by Godfrey Kneller. (*right*) Lithography of Cauchy around 1840 by Zéphirin Belliard after a painting by Jean Roller

$$\int_{\partial\mathcal{V}} \boldsymbol{s}(\boldsymbol{x},\boldsymbol{n})\,\mathrm{d}s = \int_{\mathcal{V}} \boldsymbol{f}(\boldsymbol{x})\,\mathrm{d}x$$
$$\int_{\partial\mathcal{V}_1\cap P} \boldsymbol{s}(\boldsymbol{x},\boldsymbol{\nu})\,\mathrm{d}s + \int_{\partial\mathcal{V}_1\setminus P} \boldsymbol{s}(\boldsymbol{x},\boldsymbol{n})\,\mathrm{d}s = \int_{\mathcal{V}_1} \boldsymbol{f}(\boldsymbol{x})\,\mathrm{d}x$$
$$\int_{\partial\mathcal{V}_2\cap P} \boldsymbol{s}(\boldsymbol{x},-\boldsymbol{\nu})\,\mathrm{d}s + \int_{\partial\mathcal{V}_2\setminus P} \boldsymbol{s}(\boldsymbol{x},\boldsymbol{n})\,\mathrm{d}s = \int_{\mathcal{V}_2} \boldsymbol{f}(\boldsymbol{x})\,\mathrm{d}x$$

As $\overline{\mathcal{V}} = \overline{\mathcal{V}_1} \cup \overline{\mathcal{V}_2}$ and $\overline{\partial\mathcal{V}} = \overline{\partial\mathcal{V}_1\setminus P} \cup \overline{\partial\mathcal{V}_2\setminus P}$, subtracting the two last relations from the first one leads to

$$\int_D \left(\boldsymbol{s}(\boldsymbol{x},\boldsymbol{\nu}) + \boldsymbol{s}(\boldsymbol{x},-\boldsymbol{\nu})\right)\,\mathrm{d}s = 0$$

where $D = \partial\mathcal{V}_1 \cap P = \partial\mathcal{V}_2 \cap P$ denotes the disc living on the plane P, centered in $\boldsymbol{x}_0$ and with radius ε, as shown on Fig. 1.2. Note that $D = \{\boldsymbol{y} \in \mathbb{R}^3;\ (\boldsymbol{y}-\boldsymbol{x}_0).\boldsymbol{\nu} = 0 \text{ and } |\boldsymbol{y}-\boldsymbol{x}_0| < \varepsilon\}$. As this is true for any disc D, any $\boldsymbol{x}_0 \in \Omega$ and $\boldsymbol{\nu} \in S$, from Lemma 1.1 we get

$$\boldsymbol{s}(\boldsymbol{x},\boldsymbol{\nu}) = -\boldsymbol{s}(\boldsymbol{x},-\boldsymbol{\nu})\ \ \forall \boldsymbol{x} \in \Omega,\ \ \forall \boldsymbol{\nu} \in S \tag{1.10}$$

This is the local form of the action and reaction principle: from each part of the disc D, the subregion $\mathcal{V}_1$ acting on $\mathcal{V}_2$ applies an action opposite to the actions of $\mathcal{V}_2$ on $\mathcal{V}_1$, which is called reaction.

Step 2: linearity – Consider the Cartesian coordinate system $(0, x_1, x_2, x_3)$. Next, consider any $\boldsymbol{x}_0 = (x_{0,i})_{1\leqslant i\leqslant 3} \in \Omega$ and any $\boldsymbol{\nu} = (\nu_j)_{1\leqslant j\leqslant 3} \in S$. Suppose, without loss of generality, that $\nu_j > 0$ for all $j = 1, 2, 3$. Let $\varepsilon > 0$ and $\mathcal{V} = \{\boldsymbol{y} \in \mathbb{R}^3;\ y_i > x_{0,i}, i = 1, 2, 3 \text{ and } (\boldsymbol{y}-\boldsymbol{x}_0).\boldsymbol{\nu} < \varepsilon\}$ be a small tetrahedron, as represented on Fig. 1.3. As Ω is an open set, then ε could be chosen sufficiently small such that $\mathcal{V} \subset \Omega$. Let $\mathcal{F}_j = \{\boldsymbol{y} \in \mathbb{R}^3;\ y_j = x_{0,j} \text{ and } (\boldsymbol{y}-\boldsymbol{x}_0).\boldsymbol{\nu} < \varepsilon\}$, $j = 1, 2, 3$ be the three faces of the tetrahedron that are parallel to the axis and $\mathcal{F}_4 = \{\boldsymbol{y} \in \mathbb{R}^3;\ y_j > x_{0,j},\ j = 1, 2, 3 \text{ and } (\boldsymbol{y}-\boldsymbol{x}_0).\boldsymbol{\nu} = \varepsilon\}$ its fourth face. Observe that the outward unit normal to $\mathcal{F}_j$ is $-\boldsymbol{e}_j$, $1 \leqslant j \leqslant 3$ and those of $\mathcal{F}_4$ is $\boldsymbol{\nu}$. Let us apply (1.8):

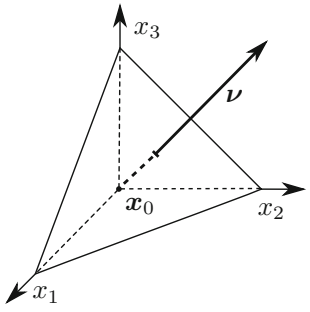

Fig. 1.3 Cauchy's small tetrahedron

$$\sum_{j=1}^{3} \int_{\mathcal{F}_j} \boldsymbol{s}(\boldsymbol{x}, -\boldsymbol{e}_j)\, \mathrm{d}s + \int_{\mathcal{F}_4} \boldsymbol{s}(\boldsymbol{x}, \boldsymbol{\nu})\, \mathrm{d}s = \int_{\mathcal{V}} \boldsymbol{f}(\boldsymbol{x})\, \mathrm{d}x \tag{1.11}$$

On one hand, (1.10) yields $\boldsymbol{s}(\boldsymbol{x}, -\boldsymbol{e}_j) = -\boldsymbol{s}(\boldsymbol{x}, \boldsymbol{e}_j)$ for all $\boldsymbol{x} \in \mathcal{F}_j$ and for all $j = 1, 2, 3$. On the other hand, since $\boldsymbol{s}$ is continuous with respect to its first variable $\boldsymbol{s}(\boldsymbol{x}, \boldsymbol{e}_j) = \boldsymbol{s}(\boldsymbol{x}_0, \boldsymbol{e}_j) + \boldsymbol{r}_j(\varepsilon)$ for all $\boldsymbol{x} \in \partial\mathcal{V}$ with $\lim_{\varepsilon \to 0} \boldsymbol{r}_j(\varepsilon) = 0$. Conversely, on the last face for all $\boldsymbol{x} \in \mathcal{F}_4$ we have $\boldsymbol{s}(\boldsymbol{x}, \boldsymbol{\nu}) = \boldsymbol{s}(\boldsymbol{x}_0, \boldsymbol{\nu}) + \boldsymbol{r}_4(\varepsilon)$ with $\lim_{\varepsilon \to 0} \boldsymbol{r}_4(\varepsilon) = 0$. Some elementary computations show that $\mathrm{meas}(\mathcal{F}_4) = \varepsilon^2/(2\nu_1\nu_2\nu_3)$, $\mathrm{meas}(\mathcal{F}_j) = \nu_j\, \mathrm{meas}(\mathcal{F}_4)$, $j = 1, 2, 3$. Then, dividing (1.11) by $\mathrm{meas}(\mathcal{F}_4)$ and rearranging yields:

$$\boldsymbol{s}(\boldsymbol{x}_0, \boldsymbol{\nu}) - \sum_{j=1}^{3} \nu_j\, \boldsymbol{s}(\boldsymbol{x}_0, \boldsymbol{e}_j) = \frac{1}{\mathrm{meas}(\mathcal{F}_4)} \int_{\mathcal{V}} \boldsymbol{f}(\boldsymbol{x})\, \mathrm{d}x + \sum_{j=1}^{3} \nu_j\, \boldsymbol{r}_j(\varepsilon) - \boldsymbol{r}_4(\varepsilon)$$

Recall that $\boldsymbol{f}$ is bounded, from theorem's hypothesis. Thus, there exists a constant $C > 0$ such that the absolute value of the sum of $\boldsymbol{f}$ over $\mathcal{V}$ is bounded by $\mathrm{meas}(\mathcal{V})\, C$. Next, after some computations, $\mathrm{meas}(\mathcal{V}) = (\varepsilon/3)\, \mathrm{meas}(\mathcal{F}_4)$ and the previous relation yields

$$\left| \boldsymbol{s}(\boldsymbol{x}_0, \boldsymbol{\nu}) - \sum_{j=1}^{3} \nu_j\, \boldsymbol{s}(\boldsymbol{x}_0, \boldsymbol{e}_j) \right| \leqslant \frac{C\,\varepsilon}{3} + \left| \sum_{j=1}^{3} \nu_j\, \boldsymbol{r}_j(\varepsilon) - \boldsymbol{r}_4(\varepsilon) \right|$$

Observe that the left-hand-side is independent of ε while the right-hand-side tends to zero when $\varepsilon \to 0$. Let us introduce the notation $\sigma_{i,j}(\boldsymbol{x}_0) = \boldsymbol{s}(\boldsymbol{x}_0, \boldsymbol{e}_j).\boldsymbol{e}_i$ for all i, j, $1 \leqslant i, j \leqslant 3$. Then

$$\boldsymbol{s}(\boldsymbol{x}_0, \boldsymbol{\nu}) = \sum_{i,j=1}^{3} \sigma_{i,j}(\boldsymbol{x}_0)\, \nu_j\, \boldsymbol{e}_i, \quad \forall \boldsymbol{x}_0 \in \Omega, \quad \forall \boldsymbol{\nu} \in S$$

This expression could be immediately extended from all $\boldsymbol{\nu} \in S$ to all $\boldsymbol{\nu} \in \mathbb{R}^3$ and this extended expression is obviously linear in $\boldsymbol{\nu}$. Finally, the Cauchy stress tensor is simply defined by $\boldsymbol{\sigma}_{\mathrm{tot}} = (\sigma_{i,j})_{1 \leqslant i,j \leqslant 3}$. □

Let us apply the Cauchy theorem 1.3 to the density of volume forces

$$\boldsymbol{f} = \frac{\partial(\rho \boldsymbol{u})}{\partial t} + \mathbf{div}(\rho \boldsymbol{u} \otimes \boldsymbol{u}) - \rho \boldsymbol{g}$$

Then, relation (1.7) becomes, with expression (1.9) of the surface forces in terms of the Cauchy stress tensor:

$$\int_{\mathcal{V}(t)} \left(\frac{\partial(\rho \boldsymbol{u})}{\partial t} + \mathbf{div}(\rho \boldsymbol{u} \otimes \boldsymbol{u}) - \rho \boldsymbol{g} \right) \mathrm{d}x = \int_{\partial\mathcal{V}(t)} \boldsymbol{\sigma}_{\mathrm{tot}} \boldsymbol{n}\, \mathrm{d}s \tag{1.12}$$

We are now looking to transform the boundary integral in the right-hand-side into a volume integral. This will be done with the help of the forthcoming Stokes formula, that will be generalized to tensors.

Theorem 1.4 (integral in space – Gauss)
For any subset $\mathcal{V} \subset \Omega$ and any sufficiently regular function φ defined in $\mathcal{V}$, we have

$$\int_{\mathcal{V}} \frac{\partial \varphi}{\partial x_i} \, \mathrm{d}x = \int_{\partial \mathcal{V}} \varphi \, n_i \, \mathrm{d}s, \quad \forall i = 1, 2, 3$$

where $\boldsymbol{n} = (n_i)_{1 \leqslant i \leqslant 3}$ denotes the outward unit normal vector on $\partial \mathcal{V}$ in the Cartesian coordinate system $(0, x_1, x_2, x_3)$.

Proof This is a classical result of continuum mechanics and differential geometry. See e.g. [153, p. 634] for a proof. □

Corollary 1.2 (divergence formula – Green–Ostrogradsky, Stokes)
For any subset $\mathcal{V} \subset \Omega$ and any sufficiently regular vector field $\boldsymbol{v}$ defined in $\mathcal{V}$, the sum of its divergence is related to its flux across the boundary as:

$$\int_{\mathcal{V}} \operatorname{div} \boldsymbol{v} \, \mathrm{d}x = \int_{\partial \mathcal{V}} \boldsymbol{v}.\boldsymbol{n} \, \mathrm{d}s \tag{1.13}$$

where $\boldsymbol{n}$ is the outward unit normal vector on $\partial \mathcal{V}$.

Proof This classical result of continuum mechanics is a direct consequence of the previous Gauss theorem: using $\varphi = v_i$ where $\boldsymbol{v} = (v_i)_{1 \leqslant i \leqslant 3}$ and summing over i yields the result. □

Corollary 1.3 (divergence formula – tensorial extension)
For any subset $\mathcal{V} \subset \Omega$ and any sufficiently regular tensor $\boldsymbol{\tau}$ defined in $\mathcal{V}$, we have

$$\int_{\mathcal{V}} \mathbf{div}\, \boldsymbol{\tau} \, \mathrm{d}x = \int_{\partial \mathcal{V}} \boldsymbol{\tau}\, \boldsymbol{n} \, \mathrm{d}s \tag{1.14}$$

where $\boldsymbol{n}$ is the outward unit normal vector on $\partial \mathcal{V}$.

Proof This result is directly obtained from (1.13) by using as $\boldsymbol{v}$ any column vector of $\boldsymbol{\tau}$ and then summing. □

Using (1.14) with $\boldsymbol{\tau} = \boldsymbol{\sigma}_{tot}$, the relation (1.12) becomes

$$\int_{\mathcal{V}(t)} \left(\frac{\partial(\rho \boldsymbol{u})}{\partial t} + \mathbf{div}(\rho \boldsymbol{u} \otimes \boldsymbol{u} - \boldsymbol{\sigma}_{\mathrm{tot}}) - \rho \boldsymbol{g} \right) \mathrm{d}x = 0$$

This relation is true at any time $t > 0$ and for any subdomain $\mathcal{V}(t) \subset \Omega$. Thus, from Lemma 1.1, the relation is true locally at any point in Ω and we obtain a local expression of the conservation of linear momentum:

$$\frac{\partial(\rho \boldsymbol{u})}{\partial t} + \mathbf{div}(\rho \boldsymbol{u} \otimes \boldsymbol{u} - \boldsymbol{\sigma}_{\text{tot}}) = \rho \boldsymbol{g} \ \text{ in } \ ]0, +\infty[\times \Omega \tag{1.15}$$

Observe the rearrangement:

$$\begin{aligned} &\frac{\partial(\rho \boldsymbol{u})}{\partial t} + \mathbf{div}(\rho \boldsymbol{u} \otimes \boldsymbol{u}) \\ &= \frac{\partial \rho}{\partial t} \boldsymbol{u} + \rho \frac{\partial \boldsymbol{u}}{\partial t} + \operatorname{div}(\rho \boldsymbol{u})\, \boldsymbol{u} + \rho (\boldsymbol{u}.\nabla)\boldsymbol{u} \\ &= \rho \left(\frac{\partial \boldsymbol{u}}{\partial t} + (\boldsymbol{u}.\nabla)\boldsymbol{u} \right) + \left(\frac{\partial \rho}{\partial t} + \operatorname{div}(\rho \boldsymbol{u}) \right) \boldsymbol{u} \end{aligned} \tag{1.16}$$

where $(\boldsymbol{u}.\nabla)\boldsymbol{u}$ denotes the following vector

$$(\boldsymbol{u}.\nabla)\boldsymbol{u} = \left(\sum_{j=1}^{3} u_j \frac{\partial u_i}{\partial x_j} \right)_{1 \leqslant i \leqslant 3}$$

Note that the parenthesis are required here for $(\boldsymbol{u}.\nabla)$, since the expression $\boldsymbol{u}.\nabla\boldsymbol{u}$ could also denote the left multiplication by the vector $\boldsymbol{u}$ of the tensor $\nabla\boldsymbol{u}$, i.e.

$$\boldsymbol{u}.(\nabla \boldsymbol{u}) = \left(\sum_{i=1}^{3} u_i \frac{\partial u_i}{\partial x_j} \right)_{1 \leqslant j \leqslant 3} \neq (\boldsymbol{u}.\nabla)\boldsymbol{u}$$

Here, the *gradient of velocity* tensor, denoted by $\nabla\boldsymbol{u}$, is defined by

$$\nabla \boldsymbol{u} = \left(\frac{\partial u_i}{\partial x_j} \right)_{1 \leqslant i,j \leqslant 3}$$

Note that some textbooks adopt a different convention for the definition of $\nabla\boldsymbol{u}$ as $\left(\frac{\partial u_j}{\partial x_i} \right)_{1 \leqslant i,j \leqslant 3}$ i.e. the transposed tensor.

Using the conservation of mass (1.3), the last term of the right-hand-side in (1.16) is zero and

$$\frac{\partial(\rho \boldsymbol{u})}{\partial t} + \mathbf{div}(\rho \boldsymbol{u} \otimes \boldsymbol{u}) = \rho \left(\frac{\partial \boldsymbol{u}}{\partial t} + (\boldsymbol{u}.\nabla)\boldsymbol{u} \right)$$

Replacing in (1.15), we obtain the following alternate formulation of the conservation of linear momentum.

Theorem 1.5 (conservation of linear momentum – local form)

$$\rho \left(\frac{\partial \boldsymbol{u}}{\partial t} + (\boldsymbol{u}.\nabla)\boldsymbol{u} \right) - \mathbf{div}\, \boldsymbol{\sigma}_{\text{tot}} = \rho \boldsymbol{g} \ \textit{in} \ ]0, +\infty[\times \Omega \tag{1.17}$$

Finally, the conservation of angular momentum (1.5) leads to the following result.

Theorem 1.6 (symmetry of the Cauchy stress tensor)
The Cauchy stress tensor $\boldsymbol{\sigma}_{\text{tot}}$ *is symmetric at any time in* Ω.

Proof Applying the Reynolds formulas (1.6) with $\boldsymbol{q} = \rho \boldsymbol{u} \wedge \boldsymbol{x}$ to the left-hand-side of (1.5) and then, the expression (1.9) of the density of surface forces $\boldsymbol{s}(\boldsymbol{x}, \boldsymbol{n})$ from the Cauchy theorem 1.3, we obtain, after some rearrangements:

$$\int_{\partial \mathcal{V}(t)} (\boldsymbol{\sigma}_{\text{tot}} \boldsymbol{n}) \wedge \boldsymbol{x} \, \mathrm{d}s = \int_{\mathcal{V}(t)} \boldsymbol{f} \wedge \boldsymbol{x} \, \mathrm{d}x \tag{1.18}$$

where, for convenience, we have introduced the notation:

$$\boldsymbol{f} = \frac{\partial(\rho \boldsymbol{u})}{\partial t} + \mathbf{div}(\rho \boldsymbol{u} \otimes \boldsymbol{u}) - \rho \boldsymbol{g}$$

Let $\boldsymbol{\sigma}_{\text{tot}} = (\sigma_{i,j})_{1 \leqslant i,j \leqslant 3}$ and $\boldsymbol{n} = (n_j)_{1 \leqslant j \leqslant 3}$ be expressed by their components in the $(0, x_1, x_2, x_3)$ Cartesian coordinate system. Then, after expansion, the term $(\boldsymbol{\sigma}_{\text{tot}} \boldsymbol{n}) \wedge \boldsymbol{x}$ can be rearranged as $(\boldsymbol{\sigma}_{\text{tot}} \boldsymbol{n}) \wedge \boldsymbol{x} = \boldsymbol{\tau} \boldsymbol{n}$ where $\boldsymbol{\tau}$ is the tensor whose j-th column vector $\boldsymbol{\tau}_j$, $j = 1, 2, 3$ is given by

$$\boldsymbol{\tau}_j = \begin{pmatrix} x_3 \sigma_{2,j} - x_2 \sigma_{3,j} \\ x_1 \sigma_{3,j} - x_3 \sigma_{1,j} \\ x_2 \sigma_{1,j} - x_1 \sigma_{2,j} \end{pmatrix}$$

With this notation, (1.18) becomes:

$$\int_{\partial \mathcal{V}(t)} \boldsymbol{\tau} \boldsymbol{n} \, \mathrm{d}s = \int_{\mathcal{V}(t)} \boldsymbol{f} \wedge \boldsymbol{x} \, \mathrm{d}x$$

We are now able to transform the integral on the boundary into an integral over the whole domain by applying the divergence formula (1.14) to the left-hand-side:

$$\int_{\mathcal{V}(t)} (\mathbf{div}\, \boldsymbol{\tau} - \boldsymbol{f} \wedge \boldsymbol{x}) \, \mathrm{d}x \tag{1.19}$$

Then, after expansion on the components, the term $\mathbf{div}\, \boldsymbol{\tau}$ can be rearranged as $\mathbf{div}\, \boldsymbol{\tau} = \boldsymbol{r} + \mathbf{div}\, \boldsymbol{\sigma}_{\text{tot}} \wedge \boldsymbol{x}$ where $\boldsymbol{r}$ denotes the following vector:

$$\boldsymbol{r} = \begin{pmatrix} \sigma_{2,3} - \sigma_{3,2} \\ \sigma_{3,1} - \sigma_{1,3} \\ \sigma_{1,2} - \sigma_{2,1} \end{pmatrix}$$

With these notations, and after replacing the notation $\boldsymbol{f}$ by its definition and using the local expression (1.15) of the conservation of linear momentum, (1.19) becomes successively,

$$\begin{aligned}\int_{\mathcal{V}(t)} \boldsymbol{r}\,\mathrm{d}x &= \int_{\mathcal{V}(t)} (\boldsymbol{f} - \mathbf{div}\,\boldsymbol{\sigma}_{\mathrm{tot}}) \wedge \boldsymbol{x}\,\mathrm{d}x \\ &= \int_{\mathcal{V}(t)} \left(\frac{\partial(\rho \boldsymbol{u})}{\partial t} + \mathbf{div}(\rho \boldsymbol{u} \otimes \boldsymbol{u} - \boldsymbol{\sigma}_{\mathrm{tot}}) - \rho \boldsymbol{g} \right) \wedge \boldsymbol{x}\,\mathrm{d}x \\ &= 0\end{aligned}$$

This relation is true at any time $t > 0$ and for any subdomain $\mathcal{V}(t) \subset \Omega$. Thus, from Lemma 1.1, the relation is true locally: $\boldsymbol{r} = 0$ in $]0, +\infty[\times\Omega$ which means, from the definition of $\boldsymbol{r}$ that the Cauchy stress tensor $\boldsymbol{\sigma}_{\mathrm{tot}}$ is symmetric at any time in Ω. □

1.3 Constitutive Equation

In the two previous sections, we have obtained two equations, the conservation of mass (1.3) and momentum (1.17). Conversely, there are three unknowns: ρ, the density, $\boldsymbol{u}$, the velocity and $\boldsymbol{\sigma}_{\mathrm{tot}}$ the symmetric Cauchy stress tensor. Thus, there is a problem: the system is not closed and can not be solved. Note that there are vector and tensor valued equations and unknowns: counting scalars leads to 10 scalar unknowns and 4 scalar equations. A tensor valued equation should therefore be added in order for the system to be closed. The remedy is to add a relation between $\boldsymbol{\sigma}_{\mathrm{tot}}$ and $\boldsymbol{u}$ that describes the kind of material under consideration: this additional relation is called the *constitutive equation*. Indeed, the mass and momentum conservation equations are true for all materials, and we have never yet clarified which kind of material is considered.

The main idea of a *Newtonian fluid* is to provide a linear relation between $\boldsymbol{u}$ and $\boldsymbol{\sigma}_{\mathrm{tot}}$. It is the simplest relation that we can consider. Various more complex and non-linear constitutive relations will be introduced all along this book, from Chap. 2–5, and all the associated fluids will be called non-Newtonian fluids. Let us first introduce some notations and definitions.

Definition 1.7 (*trace of a tensor*)
The *trace* of a 3×3 matrix or tensor $\boldsymbol{\tau}$ is defined by

$$\mathrm{tr}(\boldsymbol{\tau}) = \sum_{i=1}^{3} \tau_{i,i} \tag{1.20}$$

Let us denote by $\boldsymbol{I} = (\delta_{i,j})_{1 \leqslant i,j \leqslant 3}$ the *identity* 3×3 matrix, that interprets also as a constant tensor field, where $\delta_{i,j}$ denotes the Kronecker symbol, i.e. $\delta_{i,i} = 1$ and $\delta_{i,j} = 0, i \neq j$.

Definition 1.8 (*deviator of a tensor*)
The *deviator*, also called the deviatoric part, of a 3×3 real matrix or tensor $\boldsymbol{\tau}$ is defined by

$$\mathrm{dev}(\boldsymbol{\tau}) = \boldsymbol{\tau} - \frac{1}{3}\mathrm{tr}(\boldsymbol{\tau})\, \boldsymbol{I} \tag{1.21}$$

The remaining term $\frac{1}{3}\mathrm{tr}(\boldsymbol{\tau})\, \boldsymbol{I}$ is called the *spherical part* of the tensor.

Property 1.1 (trace of the deviator)
The trace of the deviator is zero:

$$\mathrm{tr}(\mathrm{dev}(\boldsymbol{\tau})) = 0, \quad \forall \boldsymbol{\tau} \in \mathbb{R}^{3\times 3}$$

Definition 1.9 (*decomposition of the Cauchy stress tensor*)
The Cauchy stress tensor admits the following decomposition

$$\boldsymbol{\sigma}_{\mathrm{tot}} = \boldsymbol{\sigma} - p\, \boldsymbol{I} \tag{1.22}$$

where $\boldsymbol{\sigma} = \mathrm{dev}(\boldsymbol{\sigma}_{\mathrm{tot}})$ is the *stress deviator* and $p = -\frac{1}{3}\mathrm{tr}(\boldsymbol{\sigma}_{\mathrm{tot}})$ is the *pressure*.

Definition 1.10 (*rate of deformation*)
The *rate of deformation* is defined as the symmetric part of the gradient of velocity tensor

$$D(\boldsymbol{u}) = \frac{\nabla \boldsymbol{u} + \nabla \boldsymbol{u}^T}{2}$$

Definition 1.11 (*vorticity tensor*)
The *vorticity tensor*, associated to the velocity field $\boldsymbol{u}$, is denoted by $W(\boldsymbol{u})$ and is defined as the antisymmetric part of the gradient of velocity tensor:

$$W(\boldsymbol{u}) = \frac{\nabla \boldsymbol{u} - \nabla \boldsymbol{u}^T}{2} \tag{1.23}$$

It represents the rotation of the fluid.

Definition 1.12 (*Newtonian fluid*)
The fluid is said Newtonian when the stress deviator $\boldsymbol{\sigma}$ is proportional to the rate of deformation with a constant coefficient, η, called the *viscosity*, such that

$$\boldsymbol{\sigma} = 2\eta\, \mathrm{dev}\,(D(\boldsymbol{u})) \tag{1.24}$$

As we will see, thermodynamics impose that $\eta > 0$. The most common examples of Newtonian fluids are air, water, honey and oils. There are numerous applications for numerical computations involving air and water: weather and climate change predictions, flood control, car and airplane shape optimizations, etc. Oils are involved in many industrial processes such as lubrication. There are also numerous examples of fluids of the everyday life that are not Newtonian, i.e. for which the previous

relation is not satisfied, for instance bread dough, clay, cements, toothpaste, gels, blood, etc. These fluids are the subject of the next chapters.

Property 1.2 (decomposition of the rate of deformation)
For any vector field $\boldsymbol{u}$*, we have*

$$\begin{aligned} \mathrm{tr}(D(\boldsymbol{u})) &= \mathrm{div}(\boldsymbol{u}) \\ \mathrm{dev}(D(\boldsymbol{u})) &= D(\boldsymbol{u}) - \frac{1}{3}\mathrm{div}(\boldsymbol{u})\, \boldsymbol{I} \end{aligned}$$

From this expression of $\mathrm{dev}(D(\boldsymbol{u}))$, the relation (1.24) becomes

$$\boldsymbol{\sigma} = 2\eta D(\boldsymbol{u}) - \frac{2\eta}{3}\mathrm{div}(\boldsymbol{u})\, \boldsymbol{I}$$

and then, from (1.22), the constitutive equation for a Newtonian fluid is, in terms of the Cauchy stress tensor:

$$\boldsymbol{\sigma}_{\mathrm{tot}} = 2\eta\, D(\boldsymbol{u}) - \left(p + \frac{2\eta}{3}\mathrm{div}(\boldsymbol{u})\right) \boldsymbol{I} \tag{1.25}$$

Let us summarize. There are three equations, namely the conservations of mass (1.3) and momentum (1.17) and the constitutive equation (1.25), and there are four unknowns: ρ, the density, $\boldsymbol{u}$, the velocity, p, the pressure, and $\boldsymbol{\sigma}_{\mathrm{tot}}$ the Cauchy stress tensor. Note that there are vector and tensor valued equations and unknowns: counting scalars leads to 11 scalar unknowns and 10 scalar equations. An equation is therefore still missing. The typical remedy is to add a scalar constitutive equation for ρ, e.g. a relation between ρ and p. For gases like the air, a common relation between the density and the pressure is $\rho = c_0 p^{\gamma}$ where c_0 and γ are two given constants. This relation expresses that the fluid is *compressible*: the density is related to the pressure.

1.4 Incompressible Navier–Stokes Equations

For liquids like water or oils, we assume that ρ is a given positive constant. In this case, the fluid is said *incompressible*: it means that the density is constant and independent of the pressure. This is a common assumption for most liquids considered in this book. A generalization is to suppose that ρ depends upon another variable, e.g. the temperature for non-isothermal fluids. For simplicity, we suppose in this chapter that the temperature is constant. Assuming that ρ is constant allows making an important simplification; the conservation of mass (1.3) reduces to the following incompressibility relation $\mathrm{div}\, \boldsymbol{u} = 0$. Then, the constitutive equation (1.25) writes: $\boldsymbol{\sigma}_{\mathrm{tot}} = 2\eta D(\boldsymbol{u}) - p\, \boldsymbol{I}$. Note that $\mathbf{div}\, \boldsymbol{\sigma}_{\mathrm{tot}} = \mathbf{div}(2\eta D(\boldsymbol{u})) - \nabla p$. These simplifications for incompressible Newtonian fluids allows eliminating $\boldsymbol{\sigma}_{\mathrm{tot}}$ and reducing the

system to two equations and two unknowns: the velocity $\boldsymbol{u}$ and the pressure p. The problem could be closed with suitable initial and boundary conditions.

(P): find $\boldsymbol{u}$ and p defined in $]0, T[\times\Omega$ such that

$$\rho\left(\frac{\partial \boldsymbol{u}}{\partial t} + (\boldsymbol{u}.\nabla)\boldsymbol{u}\right) - \mathbf{div}(2\eta D(\boldsymbol{u})) + \nabla p = \rho \boldsymbol{g} \text{ in }]0, T[\times\Omega \tag{1.26a}$$

$$-\mathrm{div}(\boldsymbol{u}) = 0 \text{ in }]0, T[\times\Omega \tag{1.26b}$$

$$\boldsymbol{u}(t=0) = \boldsymbol{u}_0 \text{ in } \Omega \tag{1.26c}$$

$$\boldsymbol{u} = \boldsymbol{u}_\Gamma \text{ on }]0, T[\times\partial\Omega \tag{1.26d}$$

where $\boldsymbol{u}_0$ and $\boldsymbol{u}_\Gamma$ are given initial and boundary conditions and $T > 0$ is the final time for the computation. The boundary condition (1.26d) assumes that the velocity is known on the boundary. It is the so-called Dirichlet boundary condition. As the velocity is divergence-free, the boundary data $\boldsymbol{u}_\Gamma$ is expected to satisfy a compatibility condition. Indeed, from the divergence formula (Corollary 1.2, p. 10):

$$\int_{\partial\Omega} \boldsymbol{u}.\boldsymbol{n}\,\mathrm{d}s = \int_{\partial\Omega} \mathrm{div}(\boldsymbol{u})\,\mathrm{d}x = 0$$

Thus, the boundary data $\boldsymbol{u}_\Gamma$ should satisfy:

$$\int_{\partial\Omega} \boldsymbol{u}_\Gamma.\boldsymbol{n}\,\mathrm{d}s = 0 \tag{1.27}$$

This relation interprets simply as: since the material is incompressible, the integrated inflow $\boldsymbol{u}_\Gamma.\boldsymbol{n} < 0$ through the boundary should be globally compensated by integrated outflow $\boldsymbol{u}_\Gamma.\boldsymbol{n} > 0$.

Remark 1.2 (*Mixed Dirichlet–Neumann boundary conditions*)
Alternate boundary conditions could be considered. A common alternative is a Neumann condition, that prescribes the normal component $\boldsymbol{\sigma}_{\mathrm{tot}}\,\boldsymbol{n}$ of the Cauchy stress on the boundary. This alternative is common for free surface or symmetry conditions, or when a prescribed force is imposed on the fluid boundary. Also, a Dirichlet condition could be imposed on a part of the boundary and a Neumann one on its complementary in $\partial\Omega$.

Remark 1.3 (*non-uniqueness of the pressure*)
If $(\boldsymbol{u}, p)$ is a solution of (1.26a)–(1.26d) then, for any real constant C, $(\boldsymbol{u}, p + C)$ is also a solution. It means that the pressure is non-unique and determined up to an additive constant. When the Dirichlet condition (1.26d) is replaced by a Neumann condition $\boldsymbol{\sigma}_{\mathrm{tot}}\boldsymbol{n} = 0$ on $\partial\Omega$, as $\boldsymbol{\sigma}_{\mathrm{tot}} = -p\,\boldsymbol{I} + 2\eta D(\boldsymbol{u})$ involves the pressure, then this constant is fully determined by the Neumann boundary condition and the pressure is unique. The pressure is also unique when using mixed boundary conditions: one part of the boundary is associated to a Dirichlet condition and the other to a Neumann condition.

Note the identity $\mathbf{div}(2D(\boldsymbol{u})) = \Delta\boldsymbol{u} + \nabla(\operatorname{div}\boldsymbol{u})$, where Δ denotes the Laplace operator. Using the incompressibility relation (1.26b), and considering the viscosity η constant, the conservation of momentum (1.26a) writes

$$\rho\left(\frac{\partial \boldsymbol{u}}{\partial t} + (\boldsymbol{u}.\nabla)\boldsymbol{u}\right) - \eta\,\Delta\boldsymbol{u} + \nabla p = \rho\boldsymbol{g}$$

This simplification is often used in incompressible Navier–Stokes equations. In this book, (1.26a) is the preferred expression, as in the next chapters, these equations will be extended to the case when η is non-constant.

Theorem 1.7 (existence and uniqueness – Navier–Stokes equations)

- *There exists a time $T^* > 0$ that depends on the data ($\boldsymbol{u}_0$, etc.) such that there exists a unique solution, defined in $[0, T^*]$, and this solution is continuous in time.*
- *If the problem is reduced to a two-dimensional flow domain (e.g. there is an invariant direction), the previous result is valid in all $[0, T]$.*

This is the main existence and uniqueness result for the solution of the Navier–Stokes equations. The initial proof of this result is due to Leray in 1934 [184]. For a precise statement of this theorem and more recent presentation of the proof, see Lions [190], Temam [306, p. 22] or Boyer and Fabrie [35, p. 352]. In the three-dimensional case, when $T^* < T$, there is no guaranty that there is a unique solution in all $[0, T]$, Thus, the theory is yet incomplete for the general three-dimensional case: its proof, or the proof of its impossibility, is the subject of one of the seven millennium prize problems that were stated by the Clay mathematics institute in 2000. A correct solution to this problems would be awarded one million US dollars prize.

The study of the behavior of fluids (gas or liquids) started at least with Archimède in the antic Greece. With Newton, in the 17th century, developed the mathematical setting of physics and the fundamental laws of the dynamics. In 1738, Bernoulli [22] (Fig. 1.4) introduced the energy conservation of a non-viscous fluid (the $\eta = 0$ case). The previous reference was written in Latin: see [23] for an English translation. Next, d'Alembert and Euler developed the equations for a non-viscous fluid, the so-called Euler equations. In 1749, d'Alembert [2] introduced in its initial manuscript, submitted for a mathematical award, two new and fundamental ideas: the velocity field and the partial derivatives. The work was still incomplete, as the incompressibility was not treated correctly, and he did not win the prize. In 1755, Euler published [96] a more complete presentation of the problem, based on the d'Alembert one, and including the pressure field, that was necessary to impose the incompressibility constraint. See [97] for an English translation of the original Euler paper, written in French. In 1752, d'Alembert pointed out that, with such a description, a body immersed in a fluid would be able to move without any resistance: this paradox opposing common experience. In 1823, Navier [218] introduced the concept of friction at the molecular level, corresponding at the continuous level with the viscous term $\eta > 0$ in our present equations. Navier was inspired by the heat equation and by its second order diffusion term for incorporating the friction effect into the Euler equations. A

Daniel Bernoulli 1738 | Jean le Rond d'Alembert 1749 | Leonhard Euler 1755 | Henri Navier 1820 | Gabriel Stokes 1845 | Jean Leray 1934

Fig. 1.4 History of the Navier–Stokes equations. From *left* to *right* Daniel Bernoulli, painting by Joh. Niklaus Groth in 1790; Jean le Rond d'Alembert, painting by Maurice Quentin de la Tour in 1753; Leonhard Euler, painting by Jakob Emanuel Handmann in 1756; Henri Navier, a bust at *école des ponts et chausées* in Paris; Gabriel Stokes, photo by Fradelle and Young; Jean Leray, photo by Jacobs Konrad at Oberwolfach in 1961 (copyright MFO, CC-by-SA 2.0 DE)

recent historical presentation of the elaboration of these equations can be found in the nice book by Darrigol [75], who mentions on p. 101: "*Navier's theory received little contemporary attention. The Navier–Stokes equation was rediscovered or rederived at least four times, by Cauchy in 1823, by Poisson in 1829, by Saint-Venant in 1837, and by Stokes in 1845 [298]. Each new discoverer either ignored or denigrated his predecessors' contribution. Each had his own way to justify the equation, although they all exploited the analogy between elasticity and viscous flow.*" Nevertheless, the Navier–Stokes equations was then completed, and the d'Alembert paradox was solved. The first mathematical result concerning the well-posedness of these equations is due to Leray in 1934. The first idea is to look for explicit solutions to these equations. Except in some very specific cases, such as Poiseuille and Couette flows (see the next sections) this approach is doomed to fail. The next step is to search for some approximations, for instance as the sum of trigonometric series. More recently, the numerical approximation of the solutions was developed, based on computer features together with finite difference and finite element methods.

1.5 Example: Poiseuille Flow

The velocity profile of a Newtonian flow in a circular pipe was derived experimentally in 1838 by Poiseuille [243], a physicist and physiologist, and, independently in 1839, by Hagen a physicist and hydraulic engineer. It applies to a laminar Newtonian fluid flowing between two parallel plates or through a long cylindrical pipe of constant circular cross section (see Fig. 1.5). Poiseuille was interested by blood flow in capillaries and veins. While these authors obtained the mathematical expression of the velocity profile from experimental observations, the solution could be derived directly from the Navier–Stokes equations. This derivation is presented in this section. For simplicity, we consider first the flow between parallel plates, as the computation for a cylindrical pipe is similar. Assume that the flow is laminar,

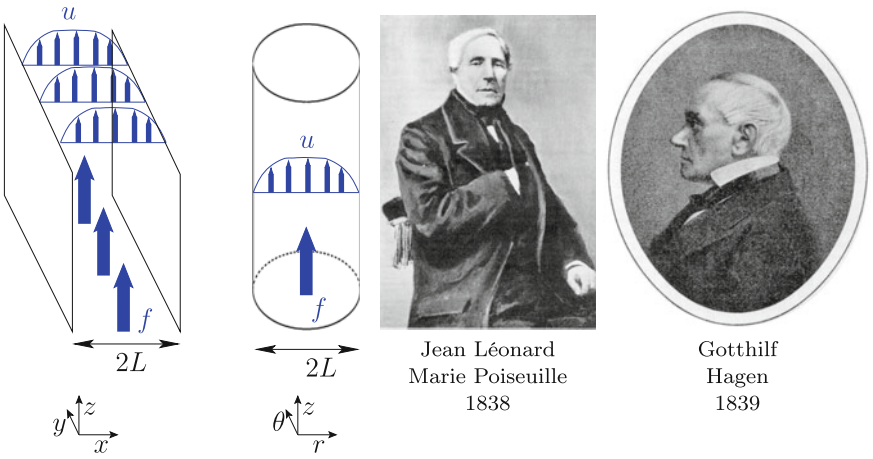

Fig. 1.5 Poiseuille flow in a circular pipe or between parallel plates. (*left*) schematic view; (*center*) Jean Léonard Marie Poiseuille, photo by an unknown author; (*right*) Gotthilf Hagen, photo published in Zentralblatt der Bauverwaltung, XIX(39), p. 237, 1899

i.e. sufficiently slow. Note that, when the flow rate is above a threshold, the fluid flow is no more laminar but turbulent, and the velocity and pressure can no more be obtained by the present explicit computation. Consider the Cartesian coordinate system (x, y, z). When the flow is laminar, it is everywhere parallel to the plates, i.e. $\boldsymbol{u}(\boldsymbol{x}) = (0, 0, u_z(x))$. and the pressure does not vary in the horizontal cross sections (parallel to the plane $0xy$), i.e. p depends only upon z. By invariance of translation along the z axis, the pressure variation $\mathrm{d}p/\mathrm{d}z$ is constant along the z axis. Thus, assume that $p(x, y, z) = -fz + p_0$ with a given $f > 0$ and $p_0 \in \mathbb{R}$. The gradient of velocity tensor writes:

$$\nabla \boldsymbol{u} = \begin{pmatrix} 0 & 0 & 0 \\ 0 & 0 & 0 \\ u_z' & 0 & 0 \end{pmatrix}$$

Problem (1.26a)–(1.26d) reduces, in the stationary case, to

(P): find $u_z :]-L, L[\longrightarrow \mathbb{R}$ such that

$$\begin{cases} -\eta u_z'' = f \text{ in }]-L, L[\\ u_z(-L) = u_z(L) = 0 \end{cases}$$

where L is the half distance between the plates. The first equation corresponds to the conservation of momentum projected on the z axis and the second equation, to the non-slip boundary condition at the plates. Note that the inertia term $(\boldsymbol{u}.\nabla)\boldsymbol{u}$ is zero. Indeed, $\boldsymbol{u} = u_z\, \boldsymbol{e}_z$ while ∇ contains just one component $\partial/\partial x$ in the $\boldsymbol{e}_x$ direction and then the operator $\boldsymbol{u}.\nabla$ is zero. There are three physical parameters in this problem:

L, the half distance between the plates, f, the pressure force and η, the viscosity. This dependency upon physical parameters could be simplified by a linear change of variable called the *dimensional analysis*. The new dimensionless quantities are denoted with tildes:

$$\tilde{x} = \frac{x}{L} \text{ and } \tilde{u}(\tilde{x}) = \frac{u_z(L\tilde{x})}{U}$$

where $U > 0$ will be chosen later. After this change of variable, the problem becomes:
(P): find $\tilde{u} :]-1, 1[\longrightarrow \mathbb{R}$ such that

$$\begin{cases} -\dfrac{\eta U}{f L^2}\tilde{u}'' = 1 \text{ in }]-1, 1[\\ \tilde{u}(-1) = \tilde{u}(1) = 0 \end{cases}$$

Then, choose $U = fL^2/\eta$: the factor in the first equation disappears and there is no more physical parameter in this dimensionless problem: it means that the solution of the original problem is invariant up to a linear change of variable. Finally, after integration and using the boundary conditions, we obtain

$$\tilde{u}(\tilde{x}) = \frac{1 - \tilde{x}^2}{2}, \quad \forall \tilde{x} \in [-1, 1]$$

and, going back to dimensional quantities, this result writes

$$u_z(x) = \frac{f}{2\eta}(L^2 - x^2), \quad \forall x \in [-L, L]$$

Let us turn to the case of a flow in a circular pipe. Let $(0, r, \theta, z)$ be the cylindrical coordinate system, such that Oz is the axis of the pipe. When laminar, the flow is everywhere parallel to this axis, i.e. $\boldsymbol{u}(\boldsymbol{x}) = (0, 0, u_z(r))$. and the pressure does not vary in the cross sections, i.e. p depends only upon z. By invariance by translation along the z axis, the pressure variation $\mathrm{d}p/\mathrm{d}z$ is constant along the z axis. Thus, assume that $p(x, y, z) = -fz + p_0$ with a given $f > 0$ and $p_0 \in \mathbb{R}$. The gradient of velocity tensor writes:

$$\nabla \boldsymbol{u} = \begin{pmatrix} 0 & 0 & 0 \\ 0 & 0 & 0 \\ u_z' & 0 & 0 \end{pmatrix}$$

Problem (1.26a)–(1.26d) reduces, in the stationary case, to
(P): find $u_z :]0, L[\longrightarrow \mathbb{R}$ such that

$$\begin{cases} -\dfrac{\eta}{r}\left(r u_z'\right)' = f \text{ in }]0, L[\\ u_z'(0) = 0 \text{ and } u_z(L) = 0 \end{cases}$$

The first equation is the conservation of momentum expressed in cylindrical coordinates and projected onto the z axis. It is completed by the symmetry on the axis and by the non-slip boundary condition along the pipe wall. Note that the inertia term also vanishes. A dimensional analysis shows that there is no physical parameter in this dimensionless problem, i.e. problem is invariant up to a linear change of variable. After integration, the solution is

$$u_z(r) = \frac{f}{4\eta}(L^2 - r^2), \quad \forall r \in [0, L]$$

Note that the solution in a pipe could be obtained from the solution between parallel planes by replacing f by $f/2$. Note also that these solutions are parabolic: the parabolic nature of the velocity profile was first observed experimentally by Poiseuille and Hagen and could be obtained directly from the Navier–Stokes equations. When the fluid is no more laminar, e.g. for higher velocities, turbulence appears and the hypothesis that the velocity is parallel to the plates or to the pipe axis, is no longer valid. In 1883, Reynolds [259] studied the transition to turbulence of the Poiseuille flow for a Newtonian fluid.

1.6 Example: Couette Flow

In 1823, Navier [218] established equations expressing the movement of a fluid while taking into account internal friction. In 1845, Stokes [298, p. 304] suggested an experimental setup with a flow between to concentric and rotating cylinders. Maurice Couette realized the corresponding apparatus in 1887, during his doctoral thesis preparation [64]: he performed an experimental verification of the Navier theory together with the effective and accurate measurement of internal friction coefficient of liquids, which was not yet referred to as the viscosity. The original Couette's apparatus is shown on Fig. 1.6. Today, such apparatus is referred to as a Couette viscosimeter. The space between the two cylinders is filled with a viscous fluid and a cylinder, either the inner or the outer one, is rotated. When the cylinder velocity is not too large, the flow is laminar and the velocity remains parallel to the cylinders. When the velocity becomes large, this result is no more valid and the flow becomes turbulent. For a laminar flow, the velocity writes $\boldsymbol{u} = (0, u_\theta(r), 0)$ in the cylindrical coordinate system (r, θ, z). By introducing the angular velocity $\omega(r)$ such that $u_\theta(r) = r\,\omega(r)$ for any $r \in [r_1, r_2]$, the gradient of velocity writes

$$\nabla \boldsymbol{u} = \begin{pmatrix} 0 & 0 & 0 \\ r\omega' & 0 & 0 \\ 0 & 0 & 0 \end{pmatrix}$$

Note that the inertia term $(\boldsymbol{u}.\nabla)\boldsymbol{u} = (r\omega^2, 0, 0)$ is not vanishing, due to the centripetal acceleration term in cylindrical coordinates. There are two main experimental

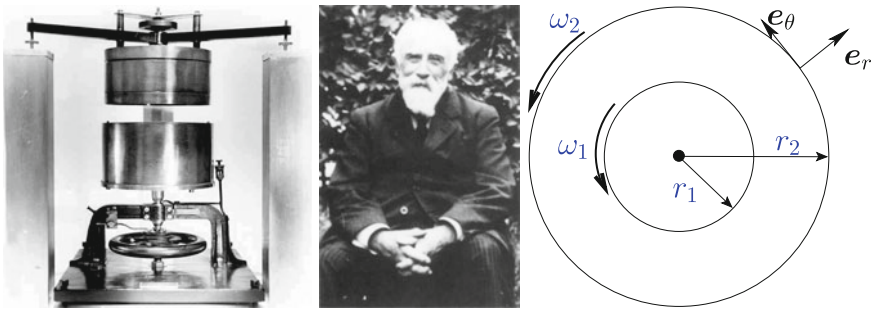

Fig. 1.6 (*left*) Couette's original apparatus (photo from [239]); (*center*) Maurice Couette, photo at Angers university, while doing a measurement with a cathetometer (photo from [239]); (*right*) schematic view

setups: one in which the torque is prescribed, and one in which the angular velocity is prescribed.

Imposed torque – The stationary Navier–Stokes equations, together with an imposed torque on the inner cylinder and an imposed angular velocity on the outer one, lead to the following problem:

(P): find ω, defined in $]r_1, r_2[$, and p, defined in $]r_1, r_2[\times]0, z_0[$, such that

$$\rho\, r\, \omega^2 - \frac{\partial p}{\partial r} = 0 \quad \text{in }]r_1, r_2[\times]0, z_0[\tag{1.28a}$$

$$-\frac{\eta}{r^2}\left(r^3\omega'\right)' = 0 \quad \text{in }]r_1, r_2[\tag{1.28b}$$

$$-\frac{\partial p}{\partial z} = -\rho g \quad \text{in }]r_1, r_2[\times]0, z_0[\tag{1.28c}$$

$$\eta\, r_1 \omega'(r_1) = -f \text{ and } \omega(r_2) = \omega_2 \tag{1.28d}$$

Here, r_1 and r_2 denotes the radius of the inner and outer cylinders, respectively (see Fig. 1.8). The three first equations are the projections of the conservation of momentum in cylindrical coordinates on the r, θ and z axis, respectively. Here, ω_2 is the angular velocity of the outer cylinder and f is a stress boundary data on the inner one. From a mathematical point of view there is a Neumann boundary condition on the inner cylinder and a Dirichlet one on the outer cylinder. From mechanical point of view, the data f corresponds to apply a torque F in the vertical direction on the inner cylinder $\Gamma_1 = \{(r_1, \theta, z);\ 0 \leqslant \theta \leqslant 2\pi,\ 0 \leqslant z \leqslant z_0\}$ where z_0 is the height of the inner cylinder. From the action and reaction property (1.10), the vertical torque exerted by the cylinder on the fluid is equal and opposite to the torque exerted by the fluid on the cylinder:

$$F = -\left(\int_{\Gamma_1} (\boldsymbol{\sigma}_{\text{tot}}\boldsymbol{n}) \wedge \boldsymbol{x}\, \mathrm{d}s\right).\boldsymbol{e}_z = -2\pi z_0 r_1^2 \sigma_{r\theta}(r_1) \tag{1.29}$$

From the constitutive equation (1.25) of a Newtonian fluid we have $\sigma_{r\theta}(r_1) = \eta\, r_1\omega'(r_1)$ and from (1.28d) we have $\eta\, r_1\omega'(r_1) = -f$. Then $F = 2\pi z_0 r_1^2 f$ or equivalently, the boundary condition data f expresses in terms of the imposed mechanical torque F as $f = F/(2\pi z_0 r_1^2)$. The previous problem counts seven physical parameters: η, f, ω_2, r_1, r_2, ρ and g. In order to reduce the number of parameters, let us perform a dimensional analysis. As usual, the dimensionless quantities are denoted with tildes:

$$\tilde{r} = \frac{r}{r_2},\ \tilde{z} = \frac{z}{r_2},\ \ \tilde{\omega}(\tilde{r}) = \frac{\omega(r_2\tilde{r}) - \omega_2}{W},\ \ \tilde{p}(\tilde{r},\tilde{z}) = \frac{p(r_2\tilde{r}, r_2\tilde{z})}{\Sigma} \tag{1.30}$$

where the characteristic stress is $\Sigma = f$ and the characteristic angular velocity W is such that $\Sigma = \eta W$ i.e. $W = f/\eta$. Based on this change of variables, the dimensionless problem writes:

(P): find $\tilde{\omega}$, defined in $]\beta, 1[$, and $\tilde{p}$, defined in $]\beta, 1[\times]0, \gamma[$, such that

$$Re\,\tilde{r}\,\tilde{\omega}^2 - \frac{\partial \tilde{p}}{\partial \tilde{r}} = 0 \quad \text{in }]\beta, 1[\times]0, \gamma[\tag{1.31a}$$

$$-\frac{1}{\tilde{r}^2}\left(\tilde{r}^3\tilde{\omega}'\right)' = 0 \quad \text{in }]\beta, 1[\tag{1.31b}$$

$$-\frac{\partial \tilde{p}}{\partial \tilde{z}} = -\frac{Re}{Fr^2} \quad \text{in }]\beta, 1[\times]0, \gamma[\tag{1.31c}$$

$$\beta\omega'(\beta) = -1 \text{ and } \omega(1) = 0 \tag{1.31d}$$

Clearly, the equations for $\tilde{\omega}$ and $\tilde{p}$ are decoupled and $\tilde{p}$ can be estimated in a second time by integrating (1.31a) and (1.31c). The problem of computing the angular velocity, through (1.31b) and (1.31d), involves only one dimensionless number: the geometry confinement $\beta = r_1/r_2 \in]0, 1[$. The two Eqs. (1.31a) and (1.31c) for the pressure involve three additional dimensionless numbers: the Reynolds $Re = \rho W^2 r_2^2/\Sigma = \rho f r_2^2/\eta^2$, the Froude $Fr = (Wr_2)/\sqrt{gr_2} = (f/\eta)\sqrt{r_2/g}$ and the cylinder vertical extension $\gamma = z_0/r_2$.

Integrating (1.31b) we get $\tilde{\omega}'(\tilde{r}) = -c\tilde{r}^{-3}$ where c is an integration constant. From the Neumann boundary condition (1.31d) at $\tilde{r} = \beta$ we get $c = \beta^2$. A second integration with the Dirichlet boundary condition (1.31d) at $\tilde{r} = 1$ yields

$$\tilde{\omega}(\tilde{r}) = \frac{\beta^2}{2}\left(\tilde{r}^{-2} - 1\right)$$

Then, the pressure is obtained by integrating (1.31a) and (1.31c).

$$\begin{aligned}\tilde{p}(\tilde{r},\tilde{z}) &= Re\int_{\beta}^{\tilde{r}} \tilde{\omega}(\tilde{r})\,\tilde{r}\,\mathrm{d}\tilde{r} + p_0\\ &= \frac{Re\,\beta^2}{8\tilde{r}^2}\left((\tilde{r}^2-\beta^2)\left(1+\beta^2\tilde{r}^2\right) - 4\beta^2\tilde{r}^2\log\left(\frac{\tilde{r}}{\beta}\right)\right)\\ &\quad + \frac{Re\,\tilde{z}}{Fr^2} + \tilde{p}_0 \end{aligned} \tag{1.32}$$

From (1.31a) we have $\partial\tilde{p}/\partial\tilde{r} > 0$ and then, the fluid is pushed in the direction of the outer cylinder. The first term is the centripetal acceleration, with Re factor, the second one is the weight liquid effect and the last one, $\tilde{p}_0$, is an integration constant, as the pressure is defined up to a constant. Note that this is the required pressure to keep the upper surface of the fluid horizontal. When the surface is not held horizontal but is free, this function will determine the shape of the free surface (see Fig. 1.7 right). The dimensional solution is then simply obtained by $\omega(r) = \omega_2 + f\tilde{\omega}(r/r_2)/\eta$, $u_\theta(r) = r\,\omega(r)$ and $p(r,z) = f\,\tilde{p}(r/r_2, z/r_2)$. Expanding, we have

$$u_\theta(r) = \omega_2 r + \frac{f\,r}{2\eta}\left(\left(\frac{r_1}{r}\right)^2 - \left(\frac{r_1}{r_2}\right)^2\right)$$

The solution is represented on Fig. 1.7.

Imposed angular velocity – The previous problem was associated to a Neumann boundary condition that amounts to imposing the torque on the inner cylinder. Another common problem consists in replacing the Neumann condition at $r = r_1$ by a Dirichlet condition:

$$\omega(r_1) = \omega_1 \text{ and } \omega(r_2) = \omega_2$$

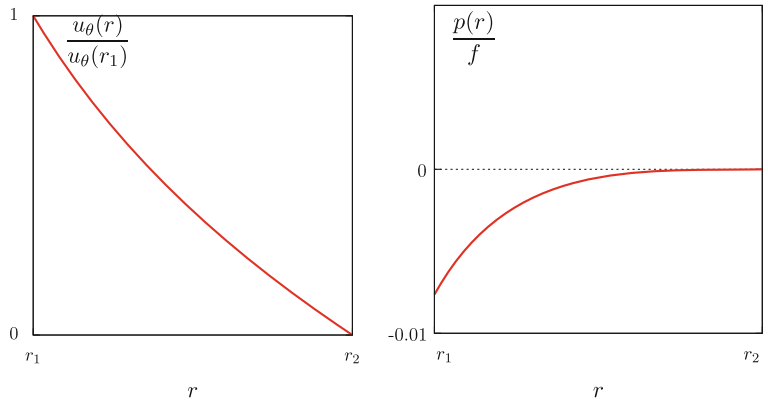

Fig. 1.7 Couette flow of a Newtonian fluid ($\beta = 1/2$): (*left*) velocity; (*right*) pressure ($Re = 1$)

This amounts to imposing the angular velocity of the cylinder inner. The problem counts seven physical parameters: η, ω_1, ω_2, r_1, r_2, ρ and g. Let $W = \omega_1 - \omega_2$ and $\Sigma = \eta(\omega_1 - \omega_2)$ be the characteristic angular velocity and stress, respectively. With these characteristic data, the dimensionless quantities are then still defined by (1.30). The boundary condition (1.31d) of the dimensionless problem becomes

$$\tilde{\omega}(\beta) = 1 \text{ and } \tilde{\omega}(1) = 0 \tag{1.33}$$

The dimensionless problem is defined by (1.31a)–(1.31c) and (1.33). Note that the computation of $\tilde{\omega}$ is still decoupled to that of $\tilde{p}$, which can be computed in a second time. The reduced problem (1.31b) and (1.33) for computing the angular velocity involves only one dimensionless number, the geometry confinement. After integration, we get the following explicit expression of the angular velocity

$$u_\theta(r) = \omega_2 r + \frac{(\omega_1 - \omega_2)\, r}{1 - \left(\frac{r_1}{r_2}\right)^2} \left(\left(\frac{r_1}{r}\right)^2 - \left(\frac{r_1}{r_2}\right)^2 \right)$$

and the computation of the pressure is similar as in the previous case. The Couette's original apparatus was designed for measuring the torque F on the inner cylinder when $\omega_1 = 0$ and $\omega_2 > 0$ was imposed. In that case, the ratio of the torque by the outer cylinder angular velocity is

$$\frac{F}{\omega_2} = -\frac{2\pi\, r_1^2 z_0\, \sigma_{r\theta}(r_1)}{\omega_2} = -\left(\frac{4\pi r_1^2 r_2^2 z_0}{r_2^2 - r_1^2} \right) \eta$$

Note that this ratio is independent of the angular velocity ω_2 and is proportional to the viscosity. This relation, predicted by the Navier–Stokes equations, was accurately verified by the Couette experimental measurements. Moreover, the coefficient factor depends only upon r_1, r_2 and z_0 that are related to the dimension of the geometry, and this apparatus is an efficient method for measuring the viscosity.

The case $\omega_1 > 0$ and $\omega_2 = 0$ was used in 1923 by Taylor [305] to explore the limit angular velocity for the stable laminar solution. For sufficiently large Reynolds numbers, the solution develops three dimensional patterns. This limit is well-known today and the mathematical properties of the Navier–Stokes equations at large Reynolds numbers has been systematically explored for this particular flow in 1994 in the beautiful book by Chossat and Iooss [53].

For more complex geometries or flow conditions, explicit solutions are not possible and numerical approximations of the solutions is developed instead: this is the aim of the following sections.

1.7 Time Discretization

In this section, the time derivative of the velocity is approximated using a finite difference scheme based on the method of characteristics. This method requires two new concepts, the concept of a characteristic line, also called trajectory, and the concept of Lagrangian derivative.

Definition 1.13 (*characteristic line – trajectory*)
For any velocity field $\boldsymbol{u}$, any $t_0 \in [0, T]$ and $\boldsymbol{x}_0 \in \Omega$, let $X(t_0, \boldsymbol{x}_0;\ t)$ be the position at time $t \in [0, T]$ of a fluid particle that is at position $\boldsymbol{x}_0$ at time t_0. The *characteristic* is the parametrized line $(X(t_0, \boldsymbol{x}_0;\ t))_{t\in[0,T]}$, defined as the unique solution of the following Cauchy problem:

$$\frac{\partial X}{\partial t}(t_0, \boldsymbol{x}_0;\ t) = \boldsymbol{u}(t, X(t_0, \boldsymbol{x}_0;\ t)), \quad \forall t \in]0, T[\tag{1.34a}$$

$$X(t_0, \boldsymbol{x}_0;\ t_0) = \boldsymbol{x}_0 \tag{1.34b}$$

The characteristic line represents the *trajectory* passing at time t_0 at position $\boldsymbol{x}_0$. The existence and the continuity of the characteristics defined by (1.34a)–(1.34b) follow from the Cauchy–Lipschitz theorem (see e.g. [183, p. 31]), assuming that the velocity field is sufficiently regular.

Definition 1.14 (*Lagrangian derivative along the flow* $\boldsymbol{u}$)
For any function φ defined in $[0, T] \times \Omega$, we denote $\dfrac{D\varphi}{Dt}$ the Lagrangian derivative of φ, defined by

$$\frac{D\varphi}{Dt} = \frac{\partial \varphi}{\partial t} + (\boldsymbol{u}.\nabla)\varphi$$

A major property is the relation between the Lagrange derivative and a total time derivative of a composition involving the characteristic.

Property 1.3 (Lagrange derivatives and characteristic)
For any sufficiently regular function φ defined in $[0, T] \times \Omega$, the Lagrange derivative satisfies, for all $(t_0, \boldsymbol{x}_0) \in]0, T[\times\Omega$ and $t \in]0, T[$:

$$\frac{D\varphi}{Dt}(t, X(t_0, \boldsymbol{x}_0;\ t)) = \frac{\mathrm{d}}{\mathrm{d}t}\{\varphi(t, X(t_0, \boldsymbol{x}_0;\ t))\}$$

The proof is simply obtained by the composition of the derivatives. A finite difference approximation of the total derivative is then possible: it is the principle of the method of characteristics. Let us now decompose the time interval $[0, T]$ as the union of subintervals:

$$[0, T] = \bigcup_{m=0}^{M} [t_m, t_{m+1}]$$

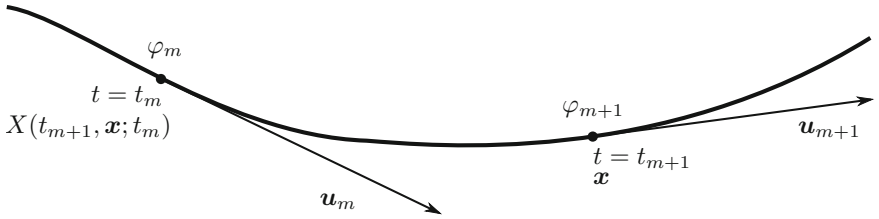

Fig. 1.8 Trajectory of the fluid particle

where $t_m = m\Delta t$ and $\Delta t = T/M$ is the time step. The situation is represented on Fig. 1.8. Here, $X(t_{m+1}, \boldsymbol{x};\ t_m)$ denotes the position of the fluid material at time t_m which was at $\boldsymbol{x}$ at time $t = t_{m+1}$. Note that we are tracking the trajectories backward. In order to compare the convergence order of different schemes, we introduce some usual notations.

Definition 1.15 (*big-$\mathcal{O}$ notation at the vicinity of zero*)
A function f is a big-$\mathcal{O}$ of another function g when Δt tends to zero, and is denoted by $f(\Delta t) = \mathcal{O}(g(\Delta t))$ if and only if there exists a constant $C > 0$ and $\Delta t_0 > 0$ such that $f(\Delta t) \leqslant C\, g(\Delta t)$ for all $\Delta t \leqslant \Delta t_0$.

Property 1.4 (first order approximation of the total derivative)
For any sufficiently regular function φ defined in $[0, T] \times \Omega$, a first order approximation of the Lagrange derivative writes

$$\frac{D\varphi}{Dt}(t_{m+1}, \boldsymbol{x}) = \frac{\varphi(t_{m+1}, \boldsymbol{x}) - \varphi\,(t_m, X_m(\boldsymbol{x}))}{\Delta t} + \mathcal{O}(\Delta t)$$

for all $m \in \{0, \ldots, M\}$ and $\boldsymbol{x} \in \Omega$, where

$$X_m(\boldsymbol{x}) = \boldsymbol{x} - \Delta t\ \boldsymbol{u}(t_m, \boldsymbol{x})$$

is a second order approximation of $X(t_{m+1}, \boldsymbol{x};\ t_m)$ and where $\mathcal{O}(\Delta t)$ denotes higher order terms.

Proof Using a forward first order scheme for approximating the Cauchy problem (1.34a)–(1.34b) when t_0 is replaced by t_{m+1} yields, for all $\boldsymbol{x} \in \Omega$:

$$\begin{cases} \dfrac{X(t_{m+1}, \boldsymbol{x};\ t_{m+1}) - X(t_{m+1}, \boldsymbol{x};\ t_m)}{\Delta t} + \mathcal{O}(\Delta t) = \boldsymbol{u}(t_m, \boldsymbol{x}) \\ X(t_{m+1}, \boldsymbol{x};\ t_{m+1}) = \boldsymbol{x} \end{cases}$$

which leads to $X(t_{m+1}, \boldsymbol{x};\ t_m) = X_m(\boldsymbol{x}) + \mathcal{O}(\Delta t^2)$. Then, a Taylor expansion of $\phi(t) = \varphi(t, X(t_{m+1}, \boldsymbol{x};\ t)$ versus t at $t = t_{m+1}$ yields

$$\frac{D\varphi}{Dt}(t_{m+1}, \boldsymbol{x}) = \frac{\varphi(t_{m+1}, \boldsymbol{x}) - \varphi\,(t_m, X(t_{m+1}, \boldsymbol{x}; t_m))}{\Delta t} + \mathcal{O}(\Delta t)$$

Another Taylor expansion of φ with respect to its second argument leads to $\varphi(t_m, X(t_{m+1}, \boldsymbol{x}; t_m)) = \varphi(t_m, X_m(\boldsymbol{x})) + \mathcal{O}(\Delta t^2)$ which completes the proof. □

A direct application is to rewrite the inertia term in the left-hand-side of (1.26a) as

$$\frac{D\boldsymbol{u}}{Dt} = \frac{\partial \boldsymbol{u}}{\partial t} + (\boldsymbol{u}.\nabla)\boldsymbol{u}$$

Then

$$\frac{D\boldsymbol{u}}{Dt}(t_{m+1}, x) = \frac{\boldsymbol{u}(t_{m+1}, x) - \boldsymbol{u}(t_m, X_m(\boldsymbol{x}))}{\Delta t} + \mathcal{O}(\Delta t)$$

For convenience, the Navier–Stokes equations can be reduced using a general formulation and the problem writes

$$\begin{aligned} \mathcal{M}\frac{D\mathcal{U}}{Dt} + \mathcal{F}(\mathcal{U}) &= 0 \\ \mathcal{M}(\mathcal{U} - \mathcal{U}_0) &= 0 \end{aligned}$$

This first order differentiation formula leads to a first order implicit scheme for the abstract problem.

Algorithm 1.1 (*first order implicit scheme – abstract version*)

- $m = 0$: let $\mathcal{U}_0$, the initial condition, being given
- $m \geqslant 0$: let $\mathcal{U}_m$ being known, find $\mathcal{U}_{m+1}$ such that

$$\mathcal{M}\frac{\mathcal{U}_{m+1} - \mathcal{U}_m \circ X_m}{\Delta t} + \mathcal{F}(\mathcal{U}_{m+1}) = 0$$

The Navier–Stokes system corresponds to the following setting:

$$\mathcal{U} = \begin{pmatrix} \boldsymbol{u} \\ p \end{pmatrix}, \quad \mathcal{U}_0 = \begin{pmatrix} \boldsymbol{u}_0 \\ 0 \end{pmatrix}, \quad \mathcal{M} = \mathrm{diag}(\rho, 0),$$
$$\mathcal{F}(\mathcal{U}) = \begin{pmatrix} -\mathbf{div}(2\eta D(\boldsymbol{u})) + \nabla p - \rho \boldsymbol{g} \\ -\mathrm{div}\, \boldsymbol{u} \end{pmatrix}$$

Algorithm 1.2 (*first order implicit scheme – Navier–Stokes equations*)

- $m = 0$: let $\boldsymbol{u}_0$, the initial condition, being given
- $m \geqslant 0$: let $\boldsymbol{u}_m$ being known, find $\boldsymbol{u}_{m+1}$ and p_{m+1} such that

$$\frac{\rho}{\Delta t}\boldsymbol{u}_{m+1} - \mathbf{div}(2\eta D(\boldsymbol{u}_{m+1})) + \nabla p_{m+1} = \rho \boldsymbol{g} + \frac{\rho}{\Delta t}\boldsymbol{u}_m \circ X_m \text{ in } \Omega \quad (1.35a)$$
$$-\mathrm{div}\, \boldsymbol{u}_{m+1} = 0 \text{ in } \Omega \quad (1.35b)$$
$$\boldsymbol{u}_{m+1} = \boldsymbol{u}_\Gamma(t_{m+1}) \text{ on } \partial\Omega \quad (1.35c)$$

where $X_m(\boldsymbol{x}) = \boldsymbol{x} - \Delta t\ \boldsymbol{u}_m(\boldsymbol{x})$.

Theorem 1.8 (first order approximation)
The sequence $(\boldsymbol{u}_m, p_m)_{m\geqslant 0}$ *defined by recurrence in Algorithm 1.2 converges to a solution of the Navier–Stokes equations* (1.26a)–(1.26d) *and is a first order approximation in time of the solution.*

Proof See [241, 299]. □

For practical applications, we would prefer a higher order scheme. Numerical experiments with important inertia effects show that a second order scheme, when combined with second order in space approximation for the velocity, is much more efficient than a first order one (see e.g. [109, 294]). Let us consider now the following second order backward differentiation formula (BDF2), defined for all $\phi \in C^2([0, T])$ by:

$$\frac{\mathrm{d}\phi}{\mathrm{d}t}(t) = \frac{3\phi(t) - 4\phi(t - \Delta t) + \phi(t - 2\Delta t)}{2\Delta t} + \mathcal{O}(\Delta t^2), \quad \forall t > 0$$

Property 1.5 (second order approximation of the total derivative)
For any sufficiently regular function φ *defined in* $[0, T] \times \Omega$*, a second order approximation of the Lagrange derivative writes*

$$\frac{D\varphi}{Dt}(t_{m+1}, \boldsymbol{x}) = \frac{3\varphi(t_{m+1}, \boldsymbol{x}) - 4\varphi\,(t_m, X_m(\boldsymbol{x})) + \varphi\,(t_{m-1}, X_{m-1}(\boldsymbol{x}))}{2\Delta t} + \mathcal{O}(\Delta t^2)$$

where

$$\begin{aligned} X_m(\boldsymbol{x}) &= \boldsymbol{x} - \Delta t\, \tilde{\boldsymbol{u}}_{m+1}(\boldsymbol{x}) \\ X_{m-1}(\boldsymbol{x}) &= \boldsymbol{x} - 2\Delta t\, \tilde{\boldsymbol{u}}_{m+1}(\boldsymbol{x}) \\ \tilde{\boldsymbol{u}}_{m+1} &= 2\boldsymbol{u}(t_m) - \boldsymbol{u}(t_{m-1}) \end{aligned}$$

Proof Observe that $\tilde{\boldsymbol{u}}_{m+1}$ is a second order extrapolation at t_{m+1} of the velocity field $\boldsymbol{u}$, based on $\boldsymbol{u}(t_m)$ and $\boldsymbol{u}(t_{m-1})$. Then, following the argument of the proof of Property 1.4. $X_m(\boldsymbol{x})$ and $X_{m-1}(\boldsymbol{x})$ are third order approximations of $X(t_{m+1}, \boldsymbol{x}; t_m)$ and $X(t_{m+1}, \boldsymbol{x}; t_{m-1})$, respectively. The result is then obtained by two Taylor expansions, as in the proof of Property 1.4. □

Algorithm 1.3 (*second order implicit scheme – Navier–Stokes equations*)

- $m = 0$: let $\boldsymbol{u}_0$, the initial condition, being given and let $\boldsymbol{u}_{-1} = \boldsymbol{u}_0$
- $m \geqslant 0$: let $\boldsymbol{u}_m$ and $\boldsymbol{u}_{m-1}$ being known, find $\boldsymbol{u}_{m+1}$ and p_{m+1} such that

$$\frac{3\rho}{4\Delta t}\boldsymbol{u}_{m+1} - \mathbf{div}(2\eta D(\boldsymbol{u}_{m+1})) + \nabla p_{m+1} = \rho\boldsymbol{g} + \frac{2\rho}{\Delta t}\boldsymbol{u}_m \circ X_m - \frac{\rho}{2\Delta t}\boldsymbol{u}_{m-1} \circ X_{m-1} \text{ in } \Omega \tag{1.36a}$$

$$-\operatorname{div} \boldsymbol{u}_{m+1} = 0 \text{ in } \Omega \tag{1.36b}$$

$$\boldsymbol{u}_{m+1} = \boldsymbol{u}_\Gamma(t_{m+1}) \text{ on } \partial\Omega \tag{1.36c}$$

where

$$X_m(\boldsymbol{x}) = \boldsymbol{x} - \Delta t\, \tilde{\boldsymbol{u}}_{m+1}(\boldsymbol{x})$$
$$X_{m-1}(\boldsymbol{x}) = \boldsymbol{x} - 2\Delta t\, \tilde{\boldsymbol{u}}_{m+1}(\boldsymbol{x})$$
$$\tilde{\boldsymbol{u}}_{m+1} = 2\boldsymbol{u}_m - \boldsymbol{u}_{m-1}$$

Theorem 1.9 (second order approximation)
The sequence $(\boldsymbol{u}_m, p_m)_{m\geqslant 0}$ *defined by recurrence in Algorithm 1.3 converges to a solution of the Navier–Stokes equations* (1.26a)–(1.26d) *and is a second order approximation in time of the solution.*

Proof See [33] for a complete proof. □

1.8 Stokes Problem

Both first and second order implicit schemes lead to a sequence of similar linear systems: dropping the $m+1$ subscripts, these linear systems write:

(P): find $\boldsymbol{u}$ and p, defined in Ω, such that

$$\kappa\boldsymbol{u} - \mathbf{div}\,(2\eta D(\boldsymbol{u})) + \nabla p = \boldsymbol{f} \text{ in } \Omega \tag{1.37a}$$

$$-\operatorname{div} \boldsymbol{u} = 0 \text{ in } \Omega \tag{1.37b}$$

$$\boldsymbol{u} = \boldsymbol{u}_\Gamma \text{ on } \partial\Omega \tag{1.37c}$$

where $\kappa \geqslant 0$, $\eta > 0$, $\boldsymbol{f}$ and $\boldsymbol{u}_\Gamma$ are given. For the first order scheme, we have $\kappa = \rho/\Delta t$ and $\boldsymbol{f} = \rho\boldsymbol{g} + \frac{\rho}{\Delta t}\boldsymbol{u}_m \circ X_m$. Conversely, for the second order one, $\kappa = 3\rho/(2\Delta t)$ and $\boldsymbol{f} = \rho\boldsymbol{g} + \frac{2\rho}{\Delta t}\boldsymbol{u}_m \circ X_m - \frac{\rho}{2\Delta t}\boldsymbol{u}_{m-1} \circ X_{m-1}$. Moreover, when $\kappa = 0$ and $\boldsymbol{f} = \rho\boldsymbol{g}$, this system corresponds to the stationary Navier–Stokes equations when inertia terms are neglected. This is the so-called Stokes problem. Note that it is an improper name, as it is Navier who first introduced the viscous term into the Euler equations and was later followed by Stokes (see Sect. 1.4).

There are many methods for building practical approximations of the solution of the problem: finite differences, finite elements, spectral methods, etc. Most of them

build on a discretization of the flow domain Ω. Based on a regular grid discretization, the finite difference approach performs some approximations of the derivatives in the equations. Most of the others methods, such as the finite element method, are based on a less regular discretization of the domain, the finite element mesh. These approaches are more flexible than the finite difference method for dealing with complex flow geometries. The finite element method requires a *variational formulation* of the problem. Thus, let us turn to the variational formulation of the Stokes problem. Equation (1.37a) is multiplied by any *test function* $\boldsymbol{v}$ satisfying $\boldsymbol{v} = 0$ on $\partial\Omega$. The result is then integrated over Ω, leading to

$$\int_\Omega \kappa \boldsymbol{u}.\boldsymbol{v}\,\mathrm{d}x - \int_\Omega \mathbf{div}(2\eta D(\boldsymbol{u})).\boldsymbol{v}\,\mathrm{d}x + \int_\Omega \nabla p.\boldsymbol{v}\,\mathrm{d}x = \int_\Omega \boldsymbol{f}.\boldsymbol{v}\,\mathrm{d}x \tag{1.38}$$

Definition 1.16 (*double dot product*)
For any 3×3 matrix or tensor $\boldsymbol{\sigma}$ and $\boldsymbol{\tau}$, the double dot product $\boldsymbol{\sigma} : \boldsymbol{\tau}$ is defined by

$$\boldsymbol{\sigma} : \boldsymbol{\tau} = \sum_{i=1}^{3}\sum_{j=1}^{3} \sigma_{i,j}\tau_{i,j} \tag{1.39}$$

Property 1.6 (generalized integration by part)
For any sufficiently regular function p and vector field $\boldsymbol{v}$, defined in Ω, we have

$$\int_\Omega \nabla p.\boldsymbol{v}\,\mathrm{d}x + \int_\Omega p\,\mathrm{div}\,\boldsymbol{v}\,\mathrm{d}x = \int_{\partial\Omega} p\,\boldsymbol{v}.\boldsymbol{n}\,\mathrm{d}s \tag{1.40a}$$

For any sufficiently regular symmetric tensor field $\boldsymbol{\tau}$, defined in Ω, we have

$$\int_\Omega D(\boldsymbol{v}) : \boldsymbol{\tau}\,\mathrm{d}x + \int_\Omega \boldsymbol{v}.\mathbf{div}(\boldsymbol{\tau})\,\mathrm{d}x = \int_{\partial\Omega} \boldsymbol{v}.(\boldsymbol{\tau}\,\boldsymbol{n})\,\mathrm{d}s \tag{1.40b}$$

Proof Recall the divergence formula (Corollary 1.3, p. 11):

$$\int_{\partial\Omega} \boldsymbol{w}.\boldsymbol{n}\,\mathrm{d}s = \int_\Omega \mathrm{div}\,\boldsymbol{w}\,\mathrm{d}x,\ \forall \boldsymbol{w}$$

Choosing $\boldsymbol{w} = p\,\boldsymbol{v}$, for any p and $\boldsymbol{v}$ and expanding leads to the result. The tensorial case is simply obtained by summation of a vectorial extension of the previous relation. □

Recall that the test function $\boldsymbol{v}$ satisfies $\boldsymbol{v} = 0$ on $\partial\Omega$: then (1.40a) reduces to

$$\int_\Omega \nabla p.\boldsymbol{v}\,\mathrm{d}x = -\int_\Omega p\,\mathrm{div}\,\boldsymbol{v}\,\mathrm{d}x$$

Then, (1.38) becomes:

$$\int_\Omega \kappa \boldsymbol{u}.\boldsymbol{v}\,\mathrm{d}x - \int_\Omega \mathbf{div}(2\eta D(\boldsymbol{u})).\boldsymbol{v}\,\mathrm{d}x - \int_\Omega p\,\mathrm{div}\,\boldsymbol{v}\,\mathrm{d}x = \int_\Omega \boldsymbol{f}.\boldsymbol{v}\,\mathrm{d}x \tag{1.41}$$

Next, using (1.40b) with $\boldsymbol{\tau} = 2\eta D(\boldsymbol{u})$ and the fact that $\boldsymbol{v} = 0$ on $\partial\Omega$, leads to

$$-\int_\Omega \mathbf{div}(2\eta D(\boldsymbol{u})).\boldsymbol{v}\,\mathrm{d}x = \int_\Omega 2\eta D(\boldsymbol{u}) : D(\boldsymbol{v})\,\mathrm{d}x$$

Then, (1.41) becomes:

$$\int_\Omega \kappa \boldsymbol{u}.\boldsymbol{v}\,\mathrm{d}x + \int_\Omega 2\eta D(\boldsymbol{u}) : D(\boldsymbol{v})\,\mathrm{d}x - \int_\Omega p\,\mathrm{div}\,\boldsymbol{v}\,\mathrm{d}x = \int_\Omega \boldsymbol{f}.\boldsymbol{v}\,\mathrm{d}x \tag{1.42}$$

Equation (1.37b) is also multiplied by any test function q and the result is integrated over Ω:

$$-\int_\Omega q\,\mathrm{div}\,\boldsymbol{u}\,\mathrm{d}x \tag{1.43}$$

Relations (1.42)–(1.43) are true for any sufficiently regular test functions $\boldsymbol{v}$ and q satisfying $\boldsymbol{v} = 0$ on $\partial\Omega$: this is the variational formulation of the Stokes problem.

We are now able to be more precise about the *sufficient regularity* of the test functions. Our aim is to ensure that all the integrals involved in (1.42)–(1.43) are convergent. The regularity assumptions are introduced via some *functional spaces*. First, let us introduce some standard Lebesgue and Hilbert functional spaces (see e.g. [36]).

Definition 1.17 (*Lebesgue functional spaces*)

$$L^1(\Omega) = \left\{\varphi : \Omega \to \mathbb{R};\ \int_\Omega |\varphi|\,\mathrm{d}x < +\infty\right\}$$
$$L^2(\Omega) = \left\{\varphi : \Omega \to \mathbb{R};\ \varphi^2 \in L^1(\Omega)\right\}$$

Definition 1.18 (*Hilbert functional space*)

$$H^1(\Omega) = \left\{\varphi \in L^2(\Omega);\ \nabla\varphi \in \left(L^2(\Omega)\right)^3\right\}$$
$$H_0^1(\Omega) = \left\{\varphi \in H^1(\Omega);\ \varphi = 0 \text{ on } \partial\Omega\right\}$$

In the previous definition of $H_0^1(\Omega)$, the boundary $\partial\Omega$ is assumed to be smooth enough, more precisely, continuously differentiable. See [36], p. 287, for its generalization to the case when $\partial\Omega$ is not smooth enough.

The following functional spaces are related to the velocity and the pressure, respectively:

$$V(\boldsymbol{u}_\Gamma) = \left\{\boldsymbol{w} \in \left(H^1(\Omega)\right)^3;\ \boldsymbol{w} = \boldsymbol{u}_\Gamma \text{ on } \partial\Omega\right\} \tag{1.44a}$$

$$L_0^2(\Omega) = \left\{ q \in L^2(\Omega);\ \int_\Omega q \,\mathrm{d}x = 0 \right\} \tag{1.44b}$$

Note that the pressure space $L_0^2(\Omega)$ contains a zero average constraint: as the pressure is defined up to an additive constant (see Remark 1.3, p. 16), this constraint sets this constant. Then the pressure is uniquely defined. The variational formulation of the Stokes problem together with appropriate functional spaces writes:

(FV): find $\boldsymbol{u} \in V(\boldsymbol{u}_\Gamma)$ and $p \in L_0^2(\Omega)$ such that

$$\begin{aligned} \int_\Omega \{\kappa\, \boldsymbol{u}.\boldsymbol{v} + 2\eta D(\boldsymbol{u}) : D(\boldsymbol{v})\} \,\mathrm{d}x - \int_\Omega p \,\mathrm{div}\, \boldsymbol{v} \,\mathrm{d}x &= \int_\Omega \boldsymbol{f}.\boldsymbol{v} \,\mathrm{d}x \\ - \int_\Omega q \,\mathrm{div}\, \boldsymbol{u} \,\mathrm{d}x &= 0 \end{aligned}$$

for all $\boldsymbol{v} \in V(0)$ and $q \in L_0^2(\Omega)$. Note that, for non-homogeneous boundary conditions, the velocity belongs to the space $V(\boldsymbol{u}_\Gamma)$ while its associated test function belongs to $V(0)$.

This problem can be reformulated in an abstract and more compact way that shows some structural properties of the Stokes problem more clearly. The following linear and bilinear forms are introduced:

$$\begin{aligned} a(\boldsymbol{u}, \boldsymbol{v}) &= \int_\Omega \{\kappa\, \boldsymbol{u}.\boldsymbol{v} + 2\eta D(\boldsymbol{u}) : D(\boldsymbol{v})\} \,\mathrm{d}x, \quad \forall \boldsymbol{u}, \boldsymbol{v} \in \left(H^1(\Omega)\right)^3 \\ b(\boldsymbol{v}, q) &= -\int_\Omega q \,\mathrm{div}\, \boldsymbol{v} \,\mathrm{d}x, \quad \forall q \in L^2(\Omega),\ \forall \boldsymbol{v} \in \left(H^1(\Omega)\right)^3 \\ \ell(\boldsymbol{v}) &= \int_\Omega \boldsymbol{f}.\boldsymbol{v} \,\mathrm{d}x, \quad \forall \boldsymbol{v} \in \left(H^1(\Omega)\right)^3 \end{aligned}$$

The variational formulation reads:

(FV): find $\boldsymbol{u} \in V(\boldsymbol{u}_\Gamma)$ and $p \in L_0^2(\Omega)$ such that

$$\begin{cases} a(\boldsymbol{u},\ \boldsymbol{v}) + b(\boldsymbol{v},\ p) = \ell(\boldsymbol{v}),\ \forall \boldsymbol{v} \in V(0) \\ b(\boldsymbol{u},\ q) \qquad\qquad\quad = 0, \quad \forall q \in L_0^2(\Omega) \end{cases} \tag{1.45}$$

Let us introduce finally the kernel of the divergence operator:

$$\begin{aligned} K(\boldsymbol{u}_\Gamma) &= \left\{ \boldsymbol{w} \in V(\boldsymbol{u}_\Gamma);\ b(\boldsymbol{w}, q) = 0,\ \forall q \in L_0^2(\Omega) \right\} \\ &= \{ \boldsymbol{w} \in V(\boldsymbol{u}_\Gamma);\ \mathrm{div}\, \boldsymbol{w} = 0 \} \end{aligned} \tag{1.46}$$

The variational formulation reduces to:

(FV): find $\boldsymbol{u} \in K(\boldsymbol{u}_\Gamma)$ such that

$$a(\boldsymbol{u},\ \boldsymbol{v}) = \ell(\boldsymbol{v}),\ \forall \boldsymbol{v} \in K(0) \tag{1.47}$$

Thus, the Stokes problem can be expressed as a standard linear problem on the kernel of the divergence operator $K(\boldsymbol{u}_\Gamma)$. The following definition and lemma will help us showing that this problem is well-posed.

Definition 1.19 (*coercivity*)
The bilinear form $a(.,.)$ is *coercive* in $\left(H_0^1(\Omega)\right)^3$ if and only if

$$\exists \alpha > 0 \ / \ a(\boldsymbol{u}, \boldsymbol{u}) \geqslant \alpha \|\boldsymbol{u}\|_{1,2,\Omega}^2, \ \forall \boldsymbol{u} \in \left(H_0^1(\Omega)\right)^3$$

Lemma 1.2 (symmetric part of vector gradient norm inequality)

$$\|2D(\boldsymbol{u})\|_{L^2(\Omega)} \geqslant c_0 \|\boldsymbol{u}\|_{H^1(\Omega)}, \quad \forall \boldsymbol{u} \in \left(H_0^1(\Omega)\right)^3$$

where $c_0 > 0$ is a constant depending only upon Ω.

Proof This result follows from the Korn inequality, which is a classical result of functional analysis. See e.g. [86, p. 115] or [119, p. 86]. □

Remark 1.4 (*equivalence norms on H_0^1*)
The previous result is not obvious as $\|2D(\boldsymbol{u})\|_{L^2(\Omega)}$ involves only the symmetric part of the velocity gradient while $\|\boldsymbol{u}\|_{H^1(\Omega)}$ involves the full gradient. Note that the inverse inequality is evident and

$$\|\boldsymbol{u}\|_{H^1(\Omega)} \geqslant \|2D(\boldsymbol{u})\|_{L^2(\Omega)} \geqslant c_0 \|\boldsymbol{u}\|_{H^1(\Omega)}, \quad \forall \boldsymbol{u} \in \left(H_0^1(\Omega)\right)^3$$

Then, $a(.,.)^{1/2}$ is a norm in H_0^1 equivalent to $\|.\|_{H^1(\Omega)}$.

Theorem 1.10 (existence and uniqueness of velocity for the Stokes problem)
Assume that the boundary $\partial\Omega$ and the data $\boldsymbol{u}_\Gamma$ and $\boldsymbol{f}$ are smooth enough. More precisely, assume that the boundary $\partial\Omega$ is continuously differentiable, that the boundary data $\boldsymbol{u}_\Gamma \in \left(H^{\frac{1}{2}}(\Omega)\right)^3$ and satisfies the compatibility condition (1.27) *and that the right-hand-side $\boldsymbol{f} \in \left(H^{-1}(\Omega)\right)^3$. Then, the Stokes problem* (1.47) *admits a unique solution $\boldsymbol{u} \in K(\boldsymbol{u}_\Gamma)$.*

Proof A direct proof can be found in [119, p. 80]. Let us give the main steps of the proof. From [119, p. 24], Lemma 2.2, there exists $\tilde{\boldsymbol{u}}_0 \in \left(H^1(\Omega)\right)^3$ such that $\operatorname{div} \tilde{\boldsymbol{u}}_0 = 0$ in Ω and $\tilde{\boldsymbol{u}}_0 = \boldsymbol{u}_\Gamma$ on $\partial\Omega$. Then, with the change of unknown $\tilde{\boldsymbol{u}} = \boldsymbol{u} - \tilde{\boldsymbol{u}}_0$, the problem reduces to the case of a homogeneous Dirichlet boundary condition $\tilde{\boldsymbol{u}} =$ on $\partial\Omega$ together with a modified right-hand-side $\widetilde{\boldsymbol{f}} = \boldsymbol{f} - \kappa\tilde{\boldsymbol{u}} + \mathbf{div}\,(2\eta D(\tilde{\boldsymbol{u}}))$. Next, since from Lemma 1.2, the bilinear form $a(.,.)$ is coercive with a coercivity constant $\alpha = \eta c_0$, the result follows from the Lax–Milgram theorem [179]. See e.g. [36, p. 140] for a recent proof of the Lax–Milgram theorem. □

The existence and uniqueness of the mixed velocity–pressure variational formulation of the Stokes problem (1.45) is also a classical result (see e.g. [119, p. 80]).

The last step consists in the discretization of the space $K(\boldsymbol{u}_\Gamma)$ in order to get a finite dimensional linear system, suitable for computational treatment. In 1981, Hecht [139] proposed a discretization of the space $K(\boldsymbol{u}_\Gamma)$ by using piecewise polynomials, i.e. a space of piecewise polynomial velocities that satisfy the divergence free constraint. In 2015, Perrier et al. [163] proposed a promising divergence-free wavelet basis. Nevertheless, these approaches are not easy to implement and research in the field of building finite dimensional spaces with an explicit divergence free basis is still in progress. Most popular finite element approaches presented in the last few decades base on the mixed velocity–pressure variational formulation (1.45) together with a discretization of both velocity and pressure spaces by piecewise polynomials.

Remark 1.5 (*Mixed Dirichlet–Neumann boundary conditions*)
Instead of the Dirichlet condition $\boldsymbol{u} = \boldsymbol{u}_\Gamma$ on the entire boundary $\partial\Omega$, assume that it is imposed only on a part $\Gamma_d \subset \partial\Omega$ while a Neumann condition $\boldsymbol{\sigma}_{\text{tot}}\boldsymbol{n} = \boldsymbol{f}_\Gamma$ is imposed on Γ_n, the complementary of Γ_d in $\partial\Omega$, where $\boldsymbol{f}_\Gamma$ is a given vector field defined on Γ_n (see also Remark 1.2, p. 16). This is a very common situation in practical flow problems. In that case, the definition (1.44a) of the space $V(\boldsymbol{u}_\Gamma)$ is replaced by

$$V(\boldsymbol{u}_\Gamma) = \left\{ \boldsymbol{w} \in \left(H^1(\Omega)\right)^3 ;\ \boldsymbol{w} = \boldsymbol{u}_\Gamma \text{ on } \Gamma_d \right\}$$

As $\boldsymbol{\sigma}_{\text{tot}} = -p\,\boldsymbol{I} + 2\eta D(\boldsymbol{u})$ involves the pressure, the Neumann condition on Γ_n fixes the undetermined additive constant for the pressure and the functional space $L^2_0(\Omega)$ for the pressure is replaced simply by $L^2(\Omega)$. Relation (1.41) writes also for all test function $\boldsymbol{v} \in V(0)$:

$$\int_\Omega \kappa\,\boldsymbol{u}.\boldsymbol{v}\,\mathrm{d}x - \int_\Omega \mathbf{div}(\boldsymbol{\sigma}_{\text{tot}}).\boldsymbol{v}\,\mathrm{d}x = \int_\Omega \boldsymbol{f}.\boldsymbol{v}\,\mathrm{d}x$$

After an integration by part, using Property 1.6 with $\boldsymbol{\tau} = \boldsymbol{\sigma}_{\text{tot}}$, we obtain

$$\int_\Omega \kappa\,\boldsymbol{u}.\boldsymbol{v}\,\mathrm{d}x + \int_\Omega \boldsymbol{\sigma}_{\text{tot}} : D(\boldsymbol{v})\,\mathrm{d}x - \int_{\partial\Omega} (\boldsymbol{\sigma}_{\text{tot}}\boldsymbol{n}).\boldsymbol{v}\,\mathrm{d}s = \int_\Omega \boldsymbol{f}.\boldsymbol{v}\,\mathrm{d}x$$

Next, let us expand $\boldsymbol{\sigma}_{\text{tot}} = -p\,\boldsymbol{I} + 2\eta D(\boldsymbol{u})$ and use $\boldsymbol{v} = 0$ on Γ_d and $\boldsymbol{\sigma}_{\text{tot}}\boldsymbol{n} = \boldsymbol{f}_\Gamma$ on Γ_n for the boundary term, we get:

$$\int_\Omega \kappa\,\boldsymbol{u}.\boldsymbol{v}\,\mathrm{d}x + \int_\Omega 2\eta D(\boldsymbol{u}) : D(\boldsymbol{v})\,\mathrm{d}x - \int_\Omega p\,\mathrm{div}\,\boldsymbol{v}\,\mathrm{d}x = \int_\Omega \boldsymbol{f}.\boldsymbol{v}\,\mathrm{d}x + \int_{\Gamma_n} \boldsymbol{f}_\Gamma.\boldsymbol{v}\,\mathrm{d}s$$

Finally, the bilinear forms $a(.,.)$ and $b(.,.)$ are unchanged in the variational formulation. The only changes when using mixed Dirichlet–Neumann boundary conditions are the functional spaces for the velocity and the pressure and the right-hand-side $\ell(.)$, replaced by:

$$\ell(\boldsymbol{v}) = \int_{\Omega} \boldsymbol{f}.\boldsymbol{v}\,\mathrm{d}x + \int_{\Gamma_n} \boldsymbol{f}_{\Gamma}.\boldsymbol{v}\,\mathrm{d}s, \quad \forall \boldsymbol{v} \in \left(H^1(\Omega)\right)^3$$

1.9 Mixed Velocity–Pressure Discretization

The velocity space $V(\boldsymbol{u}_{\Gamma})$ defined in (1.44a) is a subset of $\left(H^1(\Omega)\right)^3$: its discretization by continuous and piecewise polynomial functions is totally standard. Note that the Dirichlet boundary conditions can be easily handled when using continuous and piecewise approximations. Conversely, the pressure space $L^2_0(\Omega)$ defined in (1.44b) contains a constraint: since the pressure is defined up to an additive constant, a zero average constraint is added into the pressure space. Nevertheless, the space $L^2_0(\Omega)$ is non-standard while the space $L^2(\Omega)$, without this constraint, is completely standard. The practical issue is to externalize this zero average constraint and approximate the $L^2(\Omega)$ space.

Let us introduce the bilinear form

$$c(p,\mu) = \mu \int_{\Omega} p\,\mathrm{d}x, \quad \forall p \in L^2(\Omega),\ \forall \mu \in \mathbb{R}$$

The zero average constraint would be satisfied when $c(p,\mu) = 0$ for all $\mu \in \mathbb{R}$. This constraint is imposed by introducing a *Lagrange multiplier* $\lambda \in \mathbb{R}$ and the following *Lagrangian*, defined for all $\boldsymbol{u} \in \left(H^1(\Omega)\right)^3$, $p \in L^2(\Omega)$ and $\lambda \in \mathbb{R}$:

$$L(\boldsymbol{u},\ p, \lambda) = \frac{1}{2}a(\boldsymbol{u},\ \boldsymbol{u}) + b(\boldsymbol{u},\ p) + c(p,\lambda) - \ell(\boldsymbol{u})$$

Note that the pressure appears as the Lagrange multiplier associated to the zero-divergence for the velocity. The variational formulation is rewritten into the following *saddle point* formulation (see Fig. 1.9):

$$(\boldsymbol{u},\ p,\ \lambda) = \underset{\boldsymbol{v}\in V(\boldsymbol{u}_{\Gamma})}{\arg\inf} \ \underset{\substack{q\in L^2(\Omega)\\ \mu\in\mathbb{R}}}{\sup} \ L(\boldsymbol{v},\ q,\ \mu)$$

The saddle point is sometimes called the *mountain pass*. Our aim is to characterize the saddle point of this Lagrangian. This requires some additional mathematical tools, especially the derivation of the Lagrangian L versus its arguments when these arguments are functions, such as $\boldsymbol{u}$ and p. This derivation could be performed by the notion of Gâteaux derivative that extends the notion of directional derivative.

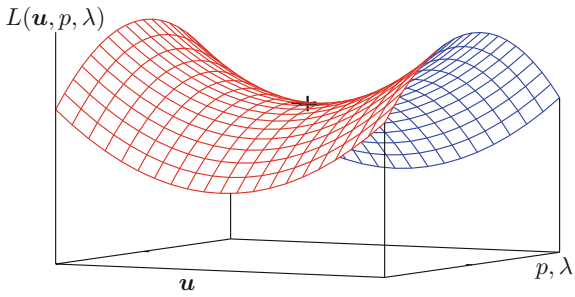

Fig. 1.9 Saddle point of a Lagrangian

Definition 1.20 (*Gâteaux derivative*)
For all derivative direction $\boldsymbol{v} \in \left(H^1(\Omega)\right)^3$, the Gâteaux derivative of L versus $\boldsymbol{u}$ in the direction $\boldsymbol{v}$ is defined by:

$$\frac{\partial L}{\partial \boldsymbol{u}}(\boldsymbol{u},\, p,\, \lambda).(\boldsymbol{v}) = \lim_{\varepsilon \to 0} \frac{L(\boldsymbol{u} + \varepsilon \boldsymbol{v},\, p,\, \lambda) - L(\boldsymbol{u},\, p,\, \lambda)}{\varepsilon}$$

Conversely, we are able to define the directional derivatives of L versus p and λ.

Theorem 1.11 (characterization of the saddle point)
The Lagrangian L is differentiable, unbounded, convex in $\boldsymbol{u}$ and linear in (p, λ). Its saddle-point $(\boldsymbol{u},\, p,\, \lambda)$ is the unique point where all the partial derivatives vanishes:

$$\frac{\partial L}{\partial \boldsymbol{u}} = \frac{\partial L}{\partial p} = \frac{\partial L}{\partial \lambda} = 0$$

This is a classical result of optimization theory, see e.g. [263] for the proof. It remains to compute the directional derivatives. First, the derivative in the $\boldsymbol{u}$ direction:

$$\begin{aligned}
&\frac{\partial L}{\partial \boldsymbol{u}}(\boldsymbol{u},\, p,\, \lambda).(\boldsymbol{v}) \\
&= \lim_{\varepsilon \to 0} \frac{1}{\varepsilon} \left(\frac{1}{2} a(\boldsymbol{u} + \varepsilon \boldsymbol{v},\, \boldsymbol{u} + \varepsilon \boldsymbol{v}) + b(\boldsymbol{u} + \varepsilon \boldsymbol{v},\, p) - \ell(\boldsymbol{u} + \varepsilon \boldsymbol{v}) \right. \\
&\qquad \left. - \frac{1}{2} a(\boldsymbol{u},\, \boldsymbol{u}) - b(\boldsymbol{u},\, p) + \ell(\boldsymbol{u}) \right) \\
&= a(\boldsymbol{u},\, \boldsymbol{v}) + b(\boldsymbol{v},\, p) - \ell(\boldsymbol{v})
\end{aligned}$$

Also, the directional derivatives in the p and λ directions:

$$\begin{aligned}
\frac{\partial L}{\partial p}(\boldsymbol{u},\, p,\, \lambda).(q) &= b(\boldsymbol{u}, q) + c(q, \lambda) \\
\frac{\partial L}{\partial \lambda}(\boldsymbol{u},\, p,\, \lambda).(\mu) &= c(p, \mu)
\end{aligned}$$

By grouping these expressions of the directional derivatives, we obtain a more explicit characterization of the saddle point.

Corollary 1.4 (characterization of the saddle point)
The saddle point $(\boldsymbol{u}, p, \lambda) \in V(\boldsymbol{u}_\Gamma) \times L^2(\Omega) \times \mathbb{R}$ *is characterized by*

$$\left\{\begin{array}{lll} a(\boldsymbol{u}, \boldsymbol{v}) + b(\boldsymbol{v}, p) & & = \ell(\boldsymbol{v}) \\ b(\boldsymbol{u}, q) & + c(q, \lambda) & = 0 \\ c(p, \mu) & & = 0 \end{array}\right. \tag{1.48}$$

for all $\boldsymbol{v} \in V(0)$, $q \in L^2(\Omega)$ *and* $\mu \in \mathbb{R}$.

This characterization appears as a variant of the (1.45) mixed variational formulation: it involves one supplementary scalar unknown $\lambda \in \mathbb{R}$, while all functional spaces are now fully standard and can be more easily discretized. Recall that when using mixed Dirichlet–Neumann boundary conditions, the zero average constraint is not imposed and the bilinear form $c(.,.)$ and corresponding multiplier λ are omitted (see Remark 1.3, p. 16). The principle of the discretization is to choose two finite dimensional spaces:

$$X_h \subset H^1(\Omega)^3 \quad \text{and} \quad Q_h \subset L^2(\Omega)$$

and then set

$$V_h(\boldsymbol{u}_{h,\Gamma}) = \left\{\boldsymbol{w}_h \in X_h;\ \boldsymbol{w}_h = \boldsymbol{u}_{h,\Gamma} \text{ on } \partial\Omega\right\}$$

where $\boldsymbol{u}_{h,\Gamma}$ denotes the Lagrange interpolate of $\boldsymbol{u}_\Gamma$ on the boundary. The finite dimensional approximate problem is then simply obtained by replacing in (1.48) the infinite dimensional spaces $V(\boldsymbol{u}_\Gamma)$ and $L^2(\Omega)$ by their finite dimensional counterpart X_h and Q_h.

$(FV)_h$: find $(\boldsymbol{u}_h, p_h, \lambda) \in V_h(\boldsymbol{u}_\Gamma) \times Q_h \times \mathbb{R}$ such that

$$\left\{\begin{array}{lll} a(\boldsymbol{u}_h, \boldsymbol{v}) + b(\boldsymbol{v}, p_h) & & = \ell(\boldsymbol{v}) \\ b(\boldsymbol{u}_h, q) & + c(q, \lambda) & = 0 \\ c(p_h, \mu) & & = 0 \end{array}\right. \tag{1.49}$$

for all $\boldsymbol{v} \in V_h(0)$, $q \in Q_h$ and $\mu \in \mathbb{R}$.

This is a linear, finite dimensional and well-posed system and $\boldsymbol{u}_h$ and p_h are now unique and computable. The main question is now to be sure that $(\boldsymbol{u}_h, p_h)$ are valid approximations of the solution $(\boldsymbol{u}, p)$. This is not an obvious task: for some choice of the velocity–pressure space pair (X_h, Q_h), the approximation $(\boldsymbol{u}_h, p_h)$ do converge to the solution $(\boldsymbol{u}, p)$ when the mesh size h tends to zero, but for slightly different choices, it does not converge. For instance, the simplest choice, the piecewise linear and continuous approximation of both velocity and pressure, does not lead to a convergent sequence with mesh refinement. For years, practical experiences identified some velocity–pressure pairs of spaces that led to convergent approximations. In 1965, Harlow and Welch [138] proposed a staggered grid finite difference method

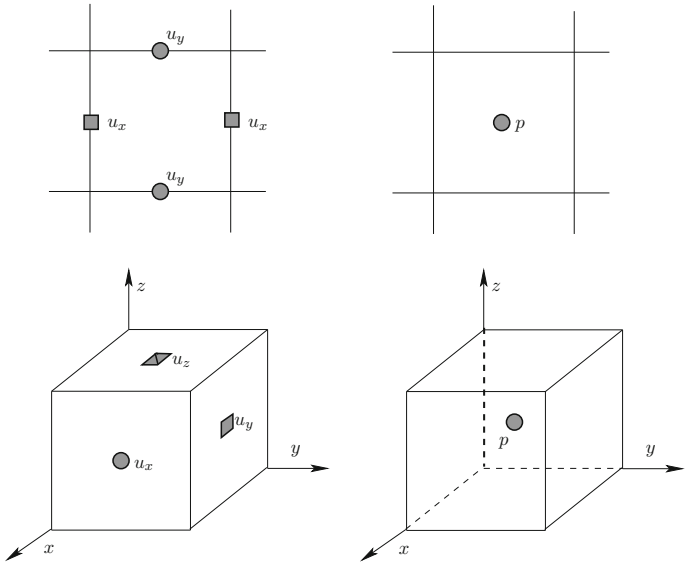

Fig. 1.10 The Harlow and Welch staggered grid finite difference [138]

that became very popular for the discretization of flow problems (see Fig. 1.10). The velocity components are located at the middle of edges in two dimensions and at the center of faces in three dimensions. This way, the finite difference approximation of the divergence of a velocity field is second order at the center of a cell, where pressure are approximated. This robust scheme was implemented in many software developed during this period, and many of them are still in use today, e.g. for meteorology and oceanography. In 1973, Taylor and Hood [304] exhibited a successful finite element pair: a piecewise quadratic approximation of the velocity and a piecewise linear approximation for the pressure (see Fig. 1.11). Nevertheless, these choices were non-intuitive and a general mechanism for building a convergent method was unclear. In 1974, Brezzi [37] presented a mathematical analysis of the situation in a very general framework of the approximation of the saddle point of a Lagrangian. He exhibited a necessary and sufficient condition of convergence. This condition expresses how the velocity and pressure spaces may be approximated, satisfying a compatibility condition.

Theorem 1.12 (Convergence of the approximate Stokes solution)
Let $(\boldsymbol{u}, p)$ *be the solution of the Stokes problem* (1.48) *and* $(\boldsymbol{u}_h, p_h)$ *be the solution of its finite dimensional counterpart* (1.49)*. Then*

$$\lim_{h \to 0} (\boldsymbol{u}_h, p_h) = (\boldsymbol{u}, p)$$

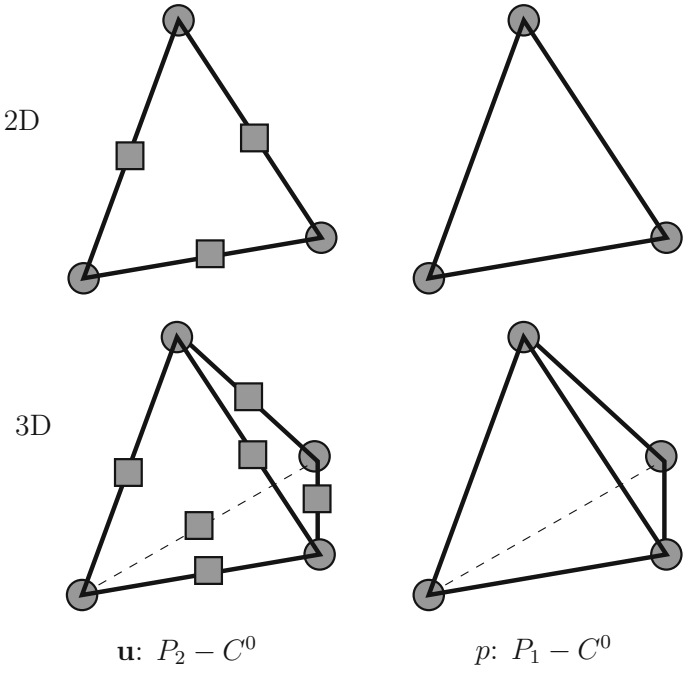

Fig. 1.11 The Taylor-Hood finite elements [304]

if and only if

$$\exists \beta > 0 \ \textit{such that} \ \forall h > 0, \quad \inf_{q_h \in Q_h} \sup_{\boldsymbol{v}_h \in X_h} \frac{b(\boldsymbol{v}_h,\, q_h)}{\|\boldsymbol{v}_h\|_{H^1}\, \|q_h\|_{L^2}} \geqslant \beta$$

and β is independent of the mesh size h.

A more recent proof of this theorem can be found in the book of Brezzi and Fortin [38] that presents an exhaustive list of convergent pairs of velocity–pressure spaces for the Stokes problem. Note that the constant β in the theorem may be independent of h: this compatibility condition is not fully explicit and the proof that a pair $(X_h,\, Q_h)$ satisfies this condition is often difficult to establish. Nevertheless, this mathematical approach is rigorous and clarifies a very confusing period. Moreover, the Harlow and Welch [138] staggered grid finite difference method has been showed to satisfy this condition and was extended to arbitrary unstructured meshes by Girault and Raviart [119] in the context of incompressible finite element methods, the so-called Raviart–Thomas element.

1.10 Direct Resolution of the Stokes Problem

For simplicity, let us consider the Taylor and Hood finite element [304] (see Fig. 1.11).

$$X_h = \{\boldsymbol{v}_h \in \left(C^0(\bar{\Omega})\right)^3 ;\ \boldsymbol{v}_{h|K} \in (P_2)^3,\ \forall K \in \mathscr{T}_h\}$$
$$Q_h = \{q_h \in C^0(\bar{\Omega});\ q_{h|K} \in P_1,\ \forall K \in \mathscr{T}_h\}$$

where $\mathscr{T}_h$ denotes a finite element mesh. Let $n_p = \dim(Q_h)$ be the dimension of the space Q_h and $(\xi_i)_{1 \leqslant i \leqslant n_p}$ be its basis. Any element $p_h \in Q_h$ can be represented on this basis, e.g.:

$$p_h(\boldsymbol{x}) = \sum_{j=1}^{n_p} p_j \xi_j(\boldsymbol{x}), \quad \boldsymbol{x} \in \Omega$$

where $(p_j)_{1 \leqslant j \leqslant n_p} \in \mathbb{R}^{n_p}$. We consider here a Lagrange *nodal basis* of these spaces. It means that we associate to each basis function ξ_j, $0 \leqslant j \leqslant n_p$ a node $\boldsymbol{x}_j \in \bar{\Omega}$ such that $\xi_j(\boldsymbol{x}_i) = \delta_{i,j}$, $1 \leqslant i, j \leqslant n_p$, where $\delta_{i,j}$ denotes the Kronecker symbol, i.e. $\delta_{i,i} = 1$ and $\delta_{i,j} = 0$, $i \neq j$. Note that $p_h(\boldsymbol{x}_j) = p_j$, $1 \leqslant j \leqslant n_p$. Such a nodal basis is represented on Fig. 1.12 in elevation view for a two-dimensional mesh.

Conversely, let $n_u = \dim(X_h)$ and $(\varphi_i)_{1 \leqslant i \leqslant n_u}$ be a nodal basis of X_h. In order to treat the Dirichlet boundary condition, let $n_s < n_u$ be the number of internal nodes that belong to the interior of the flow domain Ω, and $n_u - n_s$ be the number of boundary nodes, that belong to $\partial\Omega$. Without loss of generality, we assume that nodes are numbered such that boundary nodes appear last. For any $\boldsymbol{u}_h \in X_h$, we have the decomposition

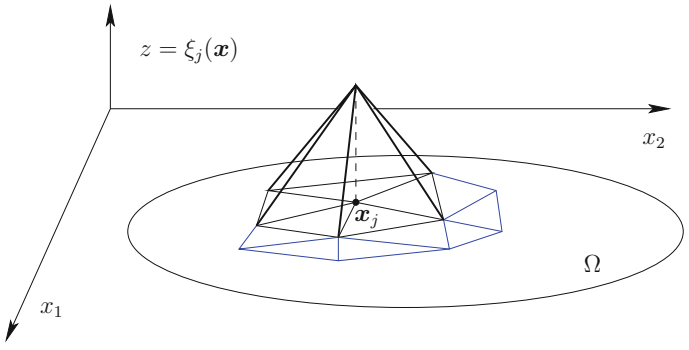

Fig. 1.12 Lagrange nodal basis function in elevation view

$$\boldsymbol{u}_h(\boldsymbol{x}) = \sum_{j=1}^{n_s} u_j \boldsymbol{\varphi}_j(\boldsymbol{x}) + \sum_{j=n_s+1}^{n_u} \bar{u}_j \boldsymbol{\varphi}_j(\boldsymbol{x})$$

Here, $(\bar{u}_j)_{n_s+1 \leqslant j \leqslant n_u}$ corresponds to the Dirichlet boundary condition $\boldsymbol{u}_\Gamma$ at the boundary nodes. Replacing $\boldsymbol{u}_h$ and p_h in (1.49) by their development on the basis and choosing a test function $\boldsymbol{v}_h = \boldsymbol{\varphi}_i$, $1 \leqslant i \leqslant n_s$ and $q_h = \xi_i$, $1 \leqslant i \leqslant n_p$, we obtain the following linear system.

$(S)_h$: find $U = (u_i)_{1 \leqslant i \leqslant n_s} \in \mathbb{R}^{n_s}$, $P = (p_i)_{1 \leqslant i \leqslant n_p} \in \mathbb{R}^{n_p}$ and $\lambda \in \mathbb{R}$ such that

$$\begin{pmatrix} A & B^T & 0 \\ B & 0 & C \\ 0 & C^T & 0 \end{pmatrix} \begin{pmatrix} U \\ P \\ \lambda \end{pmatrix} = \begin{pmatrix} F \\ G \\ 0 \end{pmatrix}$$

where $A = (a_{i,j})_{1 \leqslant i,j \leqslant n_s}$, $B = (b_{i,j})_{1 \leqslant i \leqslant n_s, 1 \leqslant j \leqslant n_p}$, $C = (c_i)_{1 \leqslant i \leqslant n_p}$, $F = (f_i)_{1 \leqslant i \leqslant n_s}$ and $G = (g_i)_{1 \leqslant i \leqslant n_p}$ with

$$\begin{aligned} a_{i,j} &= a(\boldsymbol{\varphi}_i, \boldsymbol{\varphi}_j), \quad 1 \leqslant i, j \leqslant n_s \\ b_{i,j} &= b(\boldsymbol{\varphi}_i, \xi_j), \quad 1 \leqslant i \leqslant n_s, \ 1 \leqslant j \leqslant n_p \\ c_i &= c(\xi_i, 1), \quad 1 \leqslant i \leqslant n_p \\ f_i &= \ell(\boldsymbol{\varphi}_i) - \sum_{j=n_s+1}^{n_u} a(\boldsymbol{\varphi}_j, \boldsymbol{\varphi}_i)\bar{u}_j, \quad 1 \leqslant i \leqslant n_s \\ g_i &= -\sum_{j=n_s+1}^{n_u} b(\boldsymbol{\varphi}_j, \boldsymbol{\varphi}_i)\bar{u}_j, \quad 1 \leqslant i \leqslant n_p \end{aligned}$$

Note that the right-hand-sides $F \in \mathbb{R}^{n_s}$ and $G \in \mathbb{R}^{n_p}$ involve the values $(\bar{u}_j)_{n_s+1 \leqslant j \leqslant n_u}$ of the Dirichlet boundary condition $\boldsymbol{u}_\Gamma$ at the boundary nodes. Figure 1.13 shows a two-dimensional finite element mesh and the associated matrix for the Laplace operator with Dirichlet boundary conditions, as discretized by continuous and piecewise linear elements. Non-zero elements are represented in black and zero elements are in white. Note that the matrix is *sparse*. The number of non-zero entries in each line is bounded by a constant that is independent of the size of the mesh. Its typical value is six for two-dimensional meshes and twenty for a three-dimensional one, independently of the mesh size, which could be very large. Thus, an efficient computer representation of such sparse matrices conserves only non-zero elements: for a $n \times n$ matrix, the memory requirement reduces from n^2 to a liner function of n. See [282] for a detailed implementation of sparse matrices and applications to finite elements.

The sparse matrix is symmetric and non-singular: it can be factorized as LDL^T, where D is diagonal and L is lower triangular and unitary. This direct method performs two distinct steps: the *factorization* $A = LDL^T$, and the *resolution* itself $(LDL^T)x = b$, that involves three sub-steps, solving successively $Lz = b$, then $Dy = z$ and finally $L^T x = y$. Figure 1.14 represent the non-zero elements of the lower triangular part L for both natural and optimized *numbering*. Note the

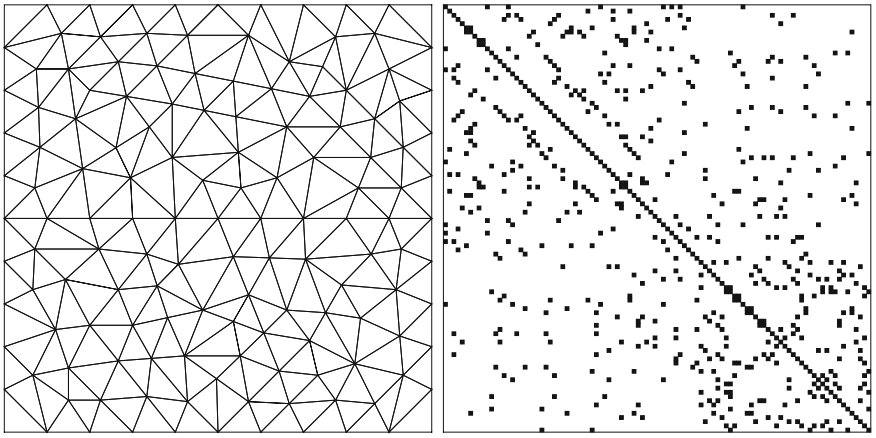

Fig. 1.13 Finite element mesh $\mathscr{T}_h$ (*left*) and the corresponding sparse matrix A (*right*)

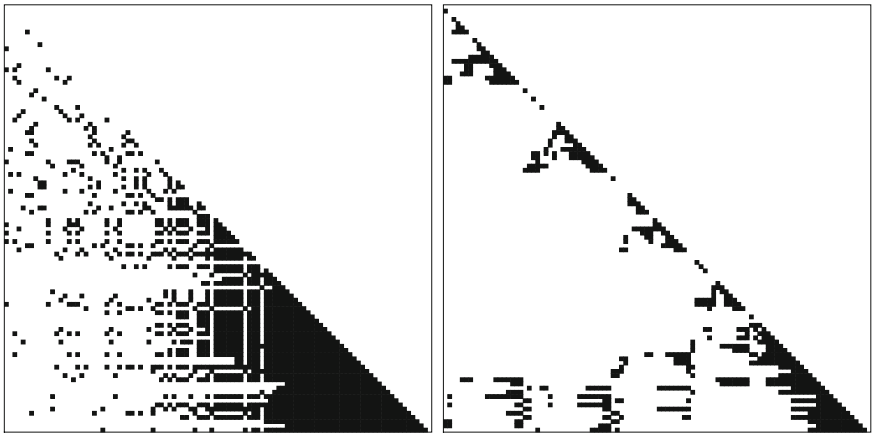

Fig. 1.14 Sparse factorization $A = LDL^T$: renumbering and filling with natural (*left*) and optimized (*right*) numberings

propagation of non-zero elements due to the factorization, called *fillin*. Note also its reduction when using a specific optimized numbering. Thus, the efficiency of the direct method strongly depends upon the ordering strategy for the fillin reduction. For a regular grid and in the two-dimensional case, there exists a specific ordering called nested dissection [114, 115] that minimizes the fillin of the sparse matrix during the factorization. For the three-dimensional case this ordering is called nested multisection [4]. These numbering algorithms extend to general finite element meshes (see [284], Sect. 1.10). Asymptotic evaluation of the computing time versus n, the size of the sparse matrix, is then possible and is given in Fig. 1.15 for the two steps of the resolution and versus the dimension $d = 1, 2, 3$ of the geometry. In the

d	factorize	solve
1	n	n
2	$n^{3/2}$	$n \log n$
3	n^2	$n^{4/3}$

Fig. 1.15 Direct solver: asymptotic computing time versus n, the size of the sparse matrix, and d, the geometry dimension

one-dimensional case, the method is optimal for both the factorization and the resolution. In the two-dimensional case, the computing time for the factorization is $\mathcal{O}(n^{3/2})$ while the resolution $\mathcal{O}(n)$ is dramatically lower. For both Algorithms 1.2, p. 28, and 1.3, p. 29, the factorization of the matrix associated to the Stokes subproblem could be performed at once before starting the time stepping loop. Then, at each time step, successive systems could be solved for different right-hand-sides. Thus, the direct method is advantageous in the two-dimensional case. In the three dimensional case, the situation is different. The computing time of the factorization is $\mathcal{O}(n^2)$, which is much more time consuming and the resolution $\mathcal{O}(n^{4/3})$ is also not advantageous. Later, we will study more efficient iterative solvers. The forthcoming Sect. 1.12 presents the resolution of the Stokes and Navier–Stokes problems using the `Rheolef` library [284, 286] that implements all these efficient algorithms for sparse matrices. But beforehand, we have to study the evaluation of the right-hand-sides of the Stokes subproblems during the resolution of the Navier–Stokes equation with the method of characteristics.

1.11 Space Discretization of Characteristics

When using the discretized version of the first order implicit scheme Algorithm 1.2, p. 28, or its second order variant Algorithm 1.3, p. 29, there is some practical difficulties in evaluating the right-hand-side $\ell(.)$ of the variational formulation of the Stokes subproblems. These difficulties are not obvious, as they are specific to the discrete formulation: they do not appear in the continuous version of the problem. Let us consider for simplicity the first order Algorithm 1.2, as its variants present similar difficulties. Let $\boldsymbol{u}_{h,m}$ denote the known velocity at the m-th step of the discrete version of the algorithm. Then, the right-hand-side of the variational formulation is defined for all $\boldsymbol{v}_h \in X_h$ by

$$\ell(\boldsymbol{v}_h) = \int_\Omega \rho\, \boldsymbol{g}.\boldsymbol{v}_h(\boldsymbol{x})\,\mathrm{d}x + \int_\Omega \frac{\rho}{\Delta t}\boldsymbol{u}_{h,m}(X_m(\boldsymbol{x})).\boldsymbol{v}_h(\boldsymbol{x})\,\mathrm{d}x$$

Recall that both $\boldsymbol{g}$, $\boldsymbol{u}_{h,m}$ and $X_{h,m}(\boldsymbol{x}) = \boldsymbol{x} - \Delta t\, \boldsymbol{u}_{h,m}(\boldsymbol{x})$ are known, so $l(.)$ is clearly computable. The first term is standard and does not present any difficulty. Let us focus on the second one. For evaluation the right-hand-side vector $(f_i)_{1\leqslant i\leqslant n_s}$ of the linear system, the test function $\boldsymbol{v}_h$ is replaced by any basis function $\boldsymbol{\varphi}_i \in X_h$, $1 \leqslant i \leqslant n_s$ associated to an internal node i, and the sum over Ω is computed as a sum over all

elements K of the mesh $\mathcal{T}_h$:

$$\begin{aligned} f_i &= \int_\Omega \frac{\rho}{\Delta t} \boldsymbol{u}_{m,h}(X_{h,m}(\boldsymbol{x})).\varphi_i(\boldsymbol{x})\,\mathrm{d}x \\ &= \sum_{K\in\mathcal{T}_h} \int_K \frac{\rho}{\Delta t} \boldsymbol{u}_{h,m}(X_{h,m}(\boldsymbol{x})).\varphi_i(\boldsymbol{x})\,\mathrm{d}x \end{aligned}$$

Note that, while both $\boldsymbol{u}_{h,m}$, $X_{h,m}$ and φ_i are piecewise polynomials, the composition $\boldsymbol{u}_{h,m} \circ X_{h,m}$ is not in general polynomial in all $K \in \mathcal{T}_h$. Thus, the integral cannot be evaluated exactly: practical evaluations use an approximation based on a quadrature formula:

$$\begin{aligned} f_{i,K} &= \int_K \frac{\rho}{\Delta t} \boldsymbol{u}_{h,m}(X_{h,m}(\boldsymbol{x})).\varphi_i(\boldsymbol{x})\,\mathrm{d}x \\ &\approx \sum_{q=0}^{n_q} \frac{\rho}{\Delta t} \boldsymbol{u}_{h,m}(X_{h,m}(\boldsymbol{x}_{q,K})).\varphi_i(\boldsymbol{x}_{q,K})\,\omega_{q,K} \end{aligned} \tag{1.50}$$

where $(\boldsymbol{x}_{q,K},\ \omega_{q,K})_{1\leqslant q\leqslant n_q}$ is the set of nodes and weights of the quadrature formula on K. The choice of the quadrature formula is of major importance. In 1988, Morton et al. [210] have pointed out that in most cases, quadrature rules lead to unstable schemes and, in 2006, Bermudez et al. [17] analyzed several quadrature formula and showed that the Gauss–Lobatto formulas lead to the most stable method. Let us focus on the practical evaluation (1.50). The right-hand-side is evaluated by an outer loop on all the elements K in the mesh and inner loop on the set of internal nodes in K, that is denoted by inode(K).

Algorithm 1.4 (*right-hand-side assembly*)
$f_i := 0, \quad 1 \leqslant i \leqslant n$
for all $K \in \mathcal{T}_h$
  for all $i \in$ inode(K) **do**
    evaluate $f_{i,K}$ *from* (1.50)
    $f_i := f_i + f_{i,K}$
  end do
end for

Let us study the asymptotic computing time of this algorithm versus the mesh size $n_e = \mathrm{card}(\mathcal{T}_h)$. The number of internal nodes per element card(inode(K)) is generally small as compared to the mesh size n_e, e.g. 6 for a P_2 triangular element in two dimension and 10 for a P_2 tetrahedron in three dimension. We assume that card(inode(K)) is bounded by a constant independent upon n_e. Thus, this algorithm performs $\mathcal{O}(n_e)$ evaluations of $f_{i,K}$ from (1.50). Each evaluation is a sum of n_q terms involving $\boldsymbol{u}_{h,m}(X_{h,m}(\boldsymbol{x}_{q,K}))$, $1 \leqslant q \leqslant n_q$ where n_q is the size of the quadrature formula. The difficulty is to evaluate $\boldsymbol{u}_{h,m}(X_{h,m}(\boldsymbol{x}_{q,K}))$ in a practical way. Recall that the approximate characteristic foot is given by $X_{h,m}(\boldsymbol{x}) = \boldsymbol{x} - \Delta t\, \boldsymbol{u}_{h,m}(\boldsymbol{x})$ for the

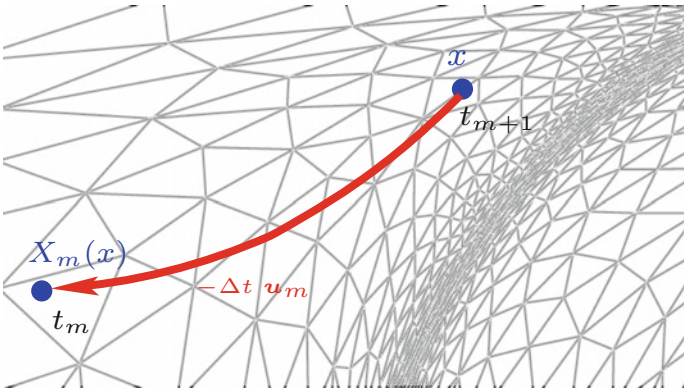

Fig. 1.16 Interpolating at the characteristic foot $X_m(\boldsymbol{x})$

first order algorithm and by a similar formula for its higher order variants. While $\boldsymbol{x}_{q,K} \in K$, in general $X_{h,m}(\boldsymbol{x}_{q,K}) \notin K$, as shown on Fig. 1.16. The displacement by $-\Delta t\, \boldsymbol{u}_{h,m}(\boldsymbol{x})$ could travel across the mesh far from element K depending upon Δt and the local value of the velocity field $\boldsymbol{u}_{h,m}$. Thus, an element K' containing $\boldsymbol{y} = X_{h,m}(\boldsymbol{x}_{q,K})$ should be searched in all the mesh $\mathcal{T}_h$. Then, the restriction of $\boldsymbol{u}_{h,m}$ to this element K' is a polynomial and it suffices to interpolate it at $\boldsymbol{y} \in K'$.

Algorithm 1.5 (*search – simple and inefficient*)
found := **false**
for all $K' \in \mathcal{T}_h$ **and while not** *found* **do**
if $\boldsymbol{y} \in K'$ **then**
found := **true**
end if
end for

This algorithm performs on average $n_e/2$ tests such that $\boldsymbol{y} \in K'$, and n_e tests in the worst case. Evaluation such as $\boldsymbol{u}_{h,m}(X_m(\boldsymbol{x}_{q,K}))$ should be performed for all $K \in \mathcal{T}_h$, all $i \in \text{inode}(K)$ and all $q \in \{1, \ldots, n_q\}$. The size n_q of the quadrature formula is generally related to the polynomial degree and we assume that n_q is bounded by a constant independent upon the mesh size n_e. For instance, for a triangular element, $n_q = 3$ for the first Gauss–Lobatto quadrature formula, also called the trapezoidal rule, and $n_q = 7$ for its second order variant, also called the Simpson formula. It means that the total cost for the evaluation of the right-hand-side $(f_i)_{1 \leqslant i \leqslant n_s}$ of the Stokes subproblem with this search Algorithm 1.5 is $\mathcal{O}(n_e^2)$. We can assume that the mesh size n_e and the matrix size n are asymptotically proportionals. Let us consider a two-dimensional problem. The linear system is factorized once with a computing time $\mathcal{O}(n^{3/2})$ (see Fig. 1.15), and then, at each time step of the first order implicit Algorithm 1.2, the right-hand side is evaluated in time $\mathcal{O}(n^2)$ and then the system is solved in time $\mathcal{O}(n\ \log(n))$. Thus, the computing time is asymptotically dominated

by the search algorithm. This is extremely inefficient. Let us improve the situation in the one-dimensional case before studying the multi-dimensional cases.

Uniform mesh – Let $\Omega =]a, b[$ where $a, b \in \mathbb{R}$. We consider a uniform subdivision in $N \geqslant 1$ elements. The i-th element is $K_i = [a+i/N,\ a+(i+1)/N]$, $0 \leqslant i \leqslant N-1$ and the mesh $\mathcal{T}_h$ is defined as the union of all these elements. The element containing $y \in [a, b]$ is K_i where

$$i = \min\left(\left\lfloor \left(\frac{y-a}{b-a}\right) N \right\rfloor,\ N-1\right)$$

where $\lfloor . \rfloor$ denotes the integral part of a real number. The min function acts only when $y = b$, avoiding $i = N$. This method extends to the d-dimensional case, $d \geqslant 1$ when Ω is a rectangle or a parallelepiped. Let $\Omega = \prod_{k=1}^{d}]a_k, b_k[$ with $a_k, b_k \in \mathbb{R}$, $1 \leqslant k \leqslant d$. All elements of the uniform mesh are denoted by using multi-index:

$$K_{i_1,\ldots,i_d} = \prod_{k=1}^{d} \left[a_k + \frac{i_k}{N_k}, a_k + \frac{i_k+1}{N_k} \right]$$

where $0 \leqslant i_k \leqslant N_k - 1$ and $1 \leqslant k \leqslant d$. The mesh size is then $n_e = \prod_{k=1}^{d} N_k$.

Algorithm 1.6 (*search – uniform grid*)
for k := 1 **to** d **do**

$$i_k = \min\left(\left\lfloor \left(\frac{y_k - a_k}{b_k - a_k}\right) N_k \right\rfloor,\ N_k - 1\right)$$

end for
$K' := K_{i_1,\ldots,i_d}$

The computing time is $\mathcal{O}(1)$, i.e. a constant independent of the mesh size. Then, the computing time for the evaluation of the right-hand-side of the Stokes subproblems involving characteristics is asymptotically $\mathcal{O}(n_e)$, which is optimal, as the size of the right-hand-side is $n_s = \mathcal{O}(n_e)$. This simplicity and efficiency explains that the method of characteristics and its Lagrangian variants (particle in cells, vortex, etc.) are very popular on rectangular or parallelepiped domains: these methods are then combined with the finite difference staggered grids proposed by Harlow and Welch [138]. This approach extends to the finite element context with non-uniform and non-structured meshes.

Non-uniform structured mesh – Let us start with the one-dimensional case before generalizing. Let $x_0 = a < x_1 < \cdots < x_N = b$ be an arbitrary subdivision of $\Omega =]a, b[$ where $a, b \in \mathbb{R}$. The i-th element is $K_i = [x_i, x_{i+1}]$, $0 \leqslant i \leqslant N-1$ and the mesh $\mathcal{T}_h$ is defined as the union of all these elements. We do as when searching for a word in a dictionary: we open the book roughly in the middle, then look if the word is found before or after that page. Next, we reiterate the process by searching on the first

half book if the word is before, or on the second half otherwise, so on until reaching the page containing the word. This method exploits the fact that words in the dictionary are sorted in alphabetical order. Observe that vertices $x_0, x_1, \ldots, x_N$ are also sorted by increasing order. Searching K_i containing $y \in [a, b]$ can be performed in a similar way in this ordered list also called *binary search* (see e.g. [170, Sect. 6.2.1]).

Algorithm 1.7 (*search – binary search in an ordered list*)

$i_{\min} := 0$
$i_{\max} := N - 1$
while $i_{\min} < i_{\max}$ **do**
  $i := \lfloor (i_{\min} + i_{\max})/2 \rfloor$
  if $x \leqslant x_i$ **then**
    $i_{\max} := i$
  else
    $i_{\min} := i$
  end if
end while

The computing time is $\mathcal{O}(\log N)$ on average. This algorithm extends to the multi-dimensional case with a structured non-uniform mesh when the domain is a rectangle or a parallelepiped. Let $\Omega = \prod_{k=1}^{d}]a_k, b_k[$ with $a_k, b_k \in \mathbb{R}$, $1 \leqslant k \leqslant d$. For any k, $0 \leqslant k \leqslant d$, let $x_{0,k} = a_k < x_{1,k} < \cdots < x_{N_k,k} = b_k$ be an arbitrary subdivision in the k-th direction. All elements of the structured mesh are denoted by using multi-index: $K_{i_1,\ldots,i_d} = \prod_{k=1}^{d} \left[x_{i_k,k}, x_{i_{k+1},k}\right]$ where $0 \leqslant i_k \leqslant N_k - 1$ and $1 \leqslant k \leqslant d$. The mesh size is then $n_e = \prod_{k=1}^{d} N_k$. The multi-dimensional search algorithm is then obtained by performing a binary search in all the d directions and the computational time for one search is on average $\mathcal{O}(\log N_1 + \cdots + \log N_d) = \mathcal{O}(\log n_e)$. Assume that the mesh size n_e and the matrix size n are asymptotically proportional and let us consider a two-dimensional problem. The evaluation of a n-sized right-hand-side vector requires $\mathcal{O}(n)$ searches and its computing time is then $\mathcal{O}(n \log(n))$. The linear system is factorized only once with a computing time $\mathcal{O}(n^{3/2})$ and then, at each step of the first order implicit Algorithm 1.2, the right-hand side is evaluated in time $\mathcal{O}(n \log(n))$ and then the system is also solved in time $\mathcal{O}(n \log(n))$. Thus, the computing time at each iteration is $\mathcal{O}(n \log(n))$ and there is no need to do a more efficient search as the computing time would be dominated by the system solve step. In the three-dimensional case, the system solve has $\mathcal{O}(n^{4/3})$ which dominates the search. Thus, this search approach is efficient in two and three dimensions.

General unstructured mesh – The general one-dimensional case is completely solved by the previous paragraph, using the binary search algorithm. Hence, let us turn to the two- and -three dimensional cases. In two dimensions, the data are not sorted and building a multi-dimensional sorted list is not an obvious task. The idea is to perform at each level a binary search in each direction, with the help of an auxiliary data structure called a *quadtree*, that is represented on Fig. 1.17. This

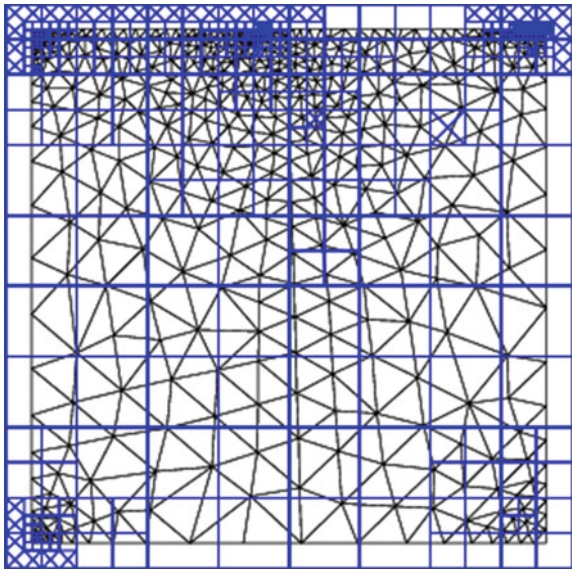

Fig. 1.17 Quadtree search data structure in a general unstructured mesh

idea was presented in 1974 by Finkel et Bentley [101]. A clear description of this data structure can be found in [275]. The CGAL computational geometry algorithm library [45] is a C++ free software library that implements such geometrical search algorithms. As in the one dimensional case, the average computing time is $\mathcal{O}(\log n_e)$ which is optimal for our purpose. An efficient implementation of all these sparse matrix, geometric search, interpolation and assembly algorithm is non-trivial for general unstructured meshes: the `Rheolef` library [284, 286] proposes such an efficient implementation. Its search algorithms base on the CGAL library. The next section presents the resolution of the Stokes and Navier–Stokes problems using `Rheolef`.

1.12 Example: Driven Cavity Flow

The flow of a Newtonian fluid in a two-dimensional driven cavity flow is considered in this section: the cavity is a square whose side length is L. A plate at the top of the cavity moves with a constant speed U and generates a rotation of the fluid in the cavity. The gravity effects are assumed to be negligible, i.e. the right-hand side of (1.26a) is replaced by zero. Together with the flow parameters U and L, the Navier–Stokes equations (1.26a)–(1.26d) involves two additional parameters: the density ρ and the viscosity η. Thus the problem has four parameters. This dependency upon

dimensional parameters could be simplified by a dimensional analysis. The new dimensionless quantities are denoted with tildes:

$$\tilde{\boldsymbol{x}} = \frac{\boldsymbol{x}}{L}, \quad \tilde{\boldsymbol{u}}(\tilde{\boldsymbol{x}}) = \frac{\boldsymbol{u}(L\tilde{\boldsymbol{x}})}{U}, \quad \tilde{t} = \frac{L}{U}t \quad \text{and} \quad \tilde{p}(\tilde{\boldsymbol{x}}) = \frac{\eta U}{L}\, p(L\tilde{\boldsymbol{x}})$$

Let $\tilde{\Omega} =]0, 1[^2$ and $\tilde{T} = LT/U$. After this change of unknown, problem (1.26a)–(1.26d) becomes:

(P): find $\boldsymbol{u}$ and p defined in $]0, T[\times\Omega$ such that

$$\begin{aligned} Re\left(\frac{\partial\tilde{\boldsymbol{u}}}{\partial\tilde{t}} + (\tilde{\boldsymbol{u}}.\tilde{\nabla})\tilde{\boldsymbol{u}}\right) - \tilde{\mathbf{div}}(2\tilde{D}(\tilde{\boldsymbol{u}})) + \tilde{\nabla}\tilde{p} &= 0 \ \text{ in } \ ]0, \tilde{T}[\times\tilde{\Omega} \\ -\tilde{\mathrm{div}}(\tilde{\boldsymbol{u}}) &= 0 \ \text{ in } \ ]0, \tilde{T}[\times\tilde{\Omega} \\ \tilde{\boldsymbol{u}}(0) &= 0 \ \text{ in } \ \tilde{\Omega} \\ \tilde{\boldsymbol{u}} &= \tilde{\boldsymbol{u}}_\Gamma \ \text{ on } \ ]0, \tilde{T}[\times\partial\tilde{\Omega} \end{aligned}$$

where $\tilde{\nabla}$, $\tilde{D}$, $\tilde{div}$ and $\tilde{\mathbf{div}}$ denote derivatives with respect to $\tilde{\boldsymbol{x}}$ and

$$Re = \frac{\rho U L}{\eta}$$

is the Reynolds number. This number was used for the first time in 1883 by Reynolds [259] when studying the transition to turbulence for a Poiseuille flow of a Newtonian fluid. The initial condition is zero and the boundary condition is also zero except on the top boundary $\tilde{\boldsymbol{u}}_\Gamma = \boldsymbol{e}_x$ in the Cartesian coordinate system $(0, x, y)$. Finally, this dimensionless formulation of the problem involves only one dimensionless number Re instead of the four parameters ρ, η, U and L.

Figure 1.18 presents the implementation with the C++ `Rheolef` [284, 286] library when $Re = 0$, i.e. the so-called Stokes problem. Note the correspondence between the variational formulation (on the right) and the C++ code. This correspondence improves the readability of the code. Moreover, this code is very short and counts about 15 lines. This readability and compactness are definitive advantages of `Rheolef`. `Rheolef` is a free software that is available as a standard package under the Debian and Ubuntu GNU/Linux systems and could be installed from the source code on others systems.

Figure 1.19 shows the solution of the driven cavity flow when $Re = 0$, for both the two- and three-dimensional cases, as obtained with the previous code shown on Fig. 1.18. Note that the same code is able to compute both the two and three dimensional solution of the problem, which is an additional advantage of using the `Rheolef` library. In the two-dimensional case, both the velocity field and the associated stream function are represented. The stream function coincides with the trajectory for a stationary solution: it brings important informations about the flow

```
int main (int argc, char** argv) {
  geo omega (argv[1]);
  space Qh (omega, "P1");
  space Xh (omega, "P2", "vector");
  Xh.block ("boundary");
  trial u(Xh), p(Qh); test v(Xh), q(Qh);
  form a = integrate (2*ddot(D(u),D(v)));
  form b = integrate (-q*div(u));
  form m = integrate (p*q);
  field uh (Xh, 0), ph (Qh, 0);
  uh[1]["top"] = 0;
  solver_abtb stokes (a.uu(), b.uu(), m.uu());
  stokes.solve(-a.ub()*uh.b(), -b.ub()*uh.b(),
      uh.set_u(), ph.set_u());
  cout ≪ catchmark("u") ≪ uh
       ≪ catchmark("p") ≪ ph;
}
```

Let $\Omega \subset \mathbb{R}^d, \quad d = 1, 2, 3$

$$Q_h = \{q \in L^2(\Omega);\ q_{|K} \in P_1,\ \forall K \in \mathcal{T}_h\}$$

$$X_h = \{\mathbf{v} \in H^1(\Omega)^d;\ \mathbf{v}_{|K} \in (P_2)^d,\ \forall K \in \mathcal{T}_h\}$$

$\forall\ \mathbf{u},\ \mathbf{v}$, et p, q, define:

$$a(\mathbf{u}, \mathbf{v}) = \int_\Omega 2D(\mathbf{u}) : D(\mathbf{v})$$

$$b(\mathbf{u}, q) = -\int_\Omega q \operatorname{div} \mathbf{u}$$

$$m(p, q) = \int_\Omega p\, q$$

find $\mathbf{u} \in X_h$, $\mathbf{u}_h = 0$ on $\partial\Omega$, and $p_h \in Q_h$ s. t.

$$a(\mathbf{u}_h, \mathbf{v}_h) + b(\mathbf{v}_h, p) = 0$$

$$b(\mathbf{u}_h, q) = 0$$

$$\forall \mathbf{v}_h \in X_h, \mathbf{v}_h = 0 \text{ sur } \partial\Omega,\ \forall q_h \in Q_h$$

Fig. 1.18 Implementation of a Stokes solver with `Rheolef` [284, 286]

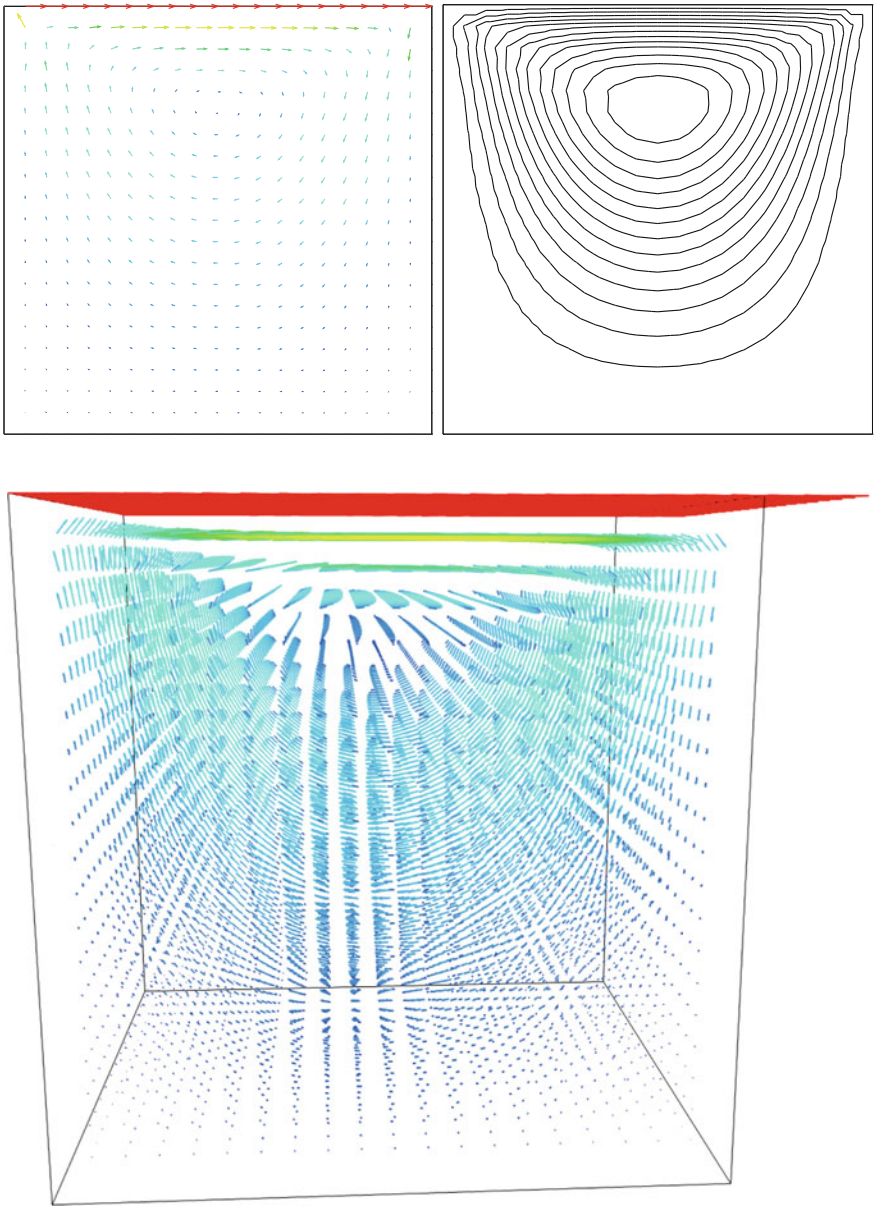

Fig. 1.19 Stokes flow in the driven cavity: velocity and stream function (from [284])

and is of common usage for the graphical representation of fluid flows. For a two-dimensional problem, the stream function is a scalar field defined such that $\boldsymbol{u} = \mathbf{curl}(\psi)$ where $\mathbf{curl}(.)$ is the vector operator defined in the Cartesian $(0, x, y)$ system by

$$\mathbf{curl}(\psi) = \begin{pmatrix} \dfrac{\partial \psi}{\partial y} \\ -\dfrac{\partial \psi}{\partial x} \end{pmatrix}$$

Note that the stream function is defined up to an additive constant. Since ψ is constant along the boundary for the driven cavity flow, it is convenient to choose $\psi = 0$ on $\partial\Omega$ in order to set the value this constant. Let us introduce the curl of a vector be the scalar operator that describes the fluid rotation

$$\mathrm{curl}(\boldsymbol{u}) = \frac{\partial u_y}{\partial x} - \frac{\partial u_x}{\partial y}$$

Then $\mathrm{curl}(\mathbf{curl}(\psi)) = -\Delta\psi$ and the stream function ψ is characterized, for any given $\boldsymbol{u}$, as the unique solution of the following Poisson problem with homogeneous Dirichlet boundary conditions:

$$\begin{aligned} -\Delta\psi &= \mathrm{curl}(\boldsymbol{u}) \text{ in } \Omega \\ \psi &= 0 \text{ on } \partial\Omega \end{aligned}$$

Figure 1.20 shows the solution of the Navier–Stokes equations for various Reynolds numbers. This solution is computed with Algorithm 1.1, as implemented in `Rheolef` [284, 286], combined with an auto-adaptive mesh procedure based on the bidimensional anisotropic mesh generator `bamg` [140]. This adaptive mesh procedure allows to accurately catch the recirculation zones, as represented with the use of the stream function. When Re increases, the solution becomes unsymmetric, the center of the primary recirculating vortex in the cavity shifts downstream and right while the vortex develops at the right bottom corner.

For higher Reynolds number, Shen [294] showed in 1991 that the flow converges to a stationary state for Reynolds numbers up to 10 000; for Reynolds numbers larger than a critical value $10\,000 < Re_1 < 10\,500$ and less than another critical value $15\,000 < Re_2 < 16\,000$, these authors found that the flow becomes periodic in time which indicates a Hopf bifurcation; the flow loses time periodicity for $Re \geq Re_2$. In 1998, Ould Salihi [232] found a loss of stationarity between 10 000 and 20 000. In 2002, Auteri et al. [6] estimated the critical value for the apparition of the first instability to $Re_1 \approx 8018$. In 2005, this result was informed by [113]: these authors estimated Re_1 close to 8000, in agreement with [6]. Also, in 2005, Erturk et al. [94] computed steady driven cavity solutions up to $Re \leqslant 21\,000$. Such direct computations of stationary solutions at high Reynolds numbers was also performed

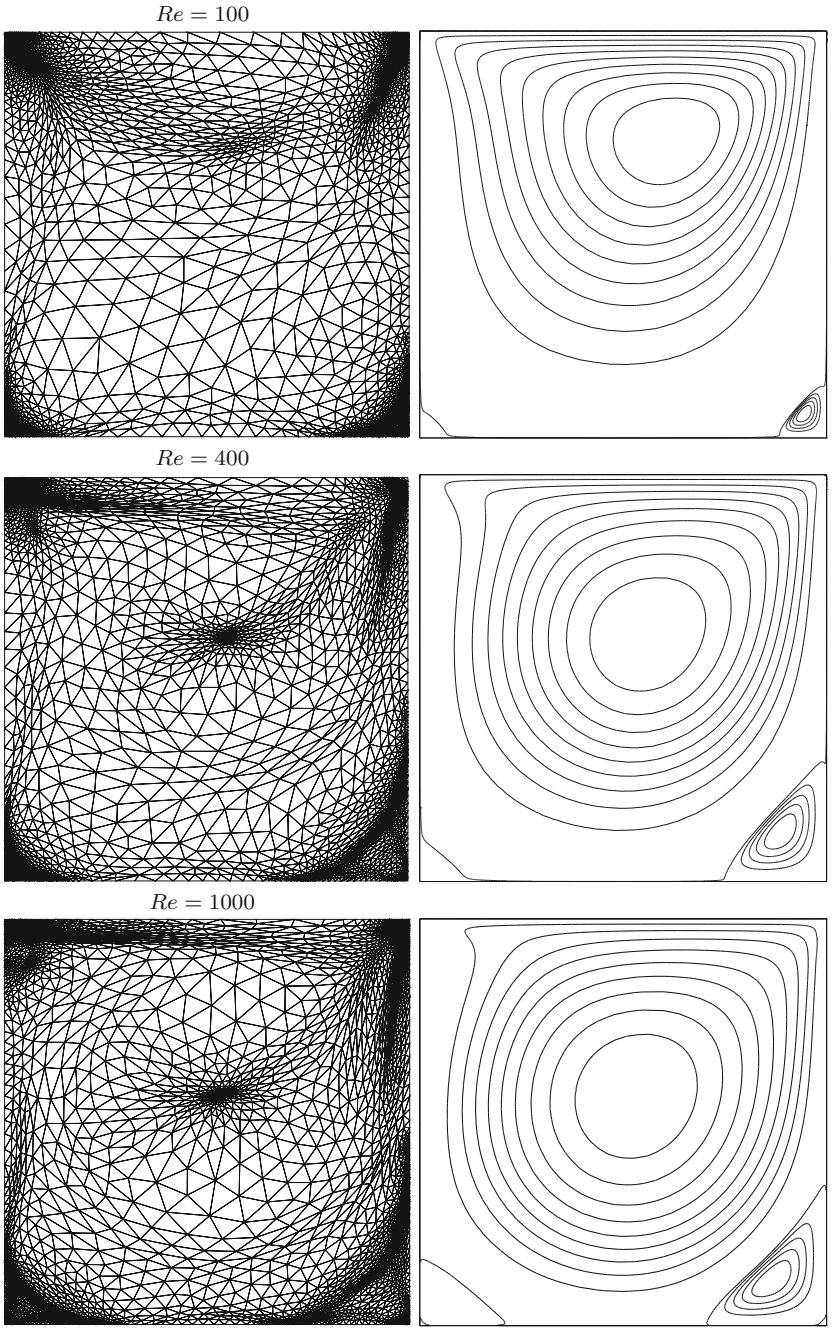

Fig. 1.20 The solution of the Navier–Stokes equations in the driven cavity for $Re = 100$, 400 and 1000 (from [284])

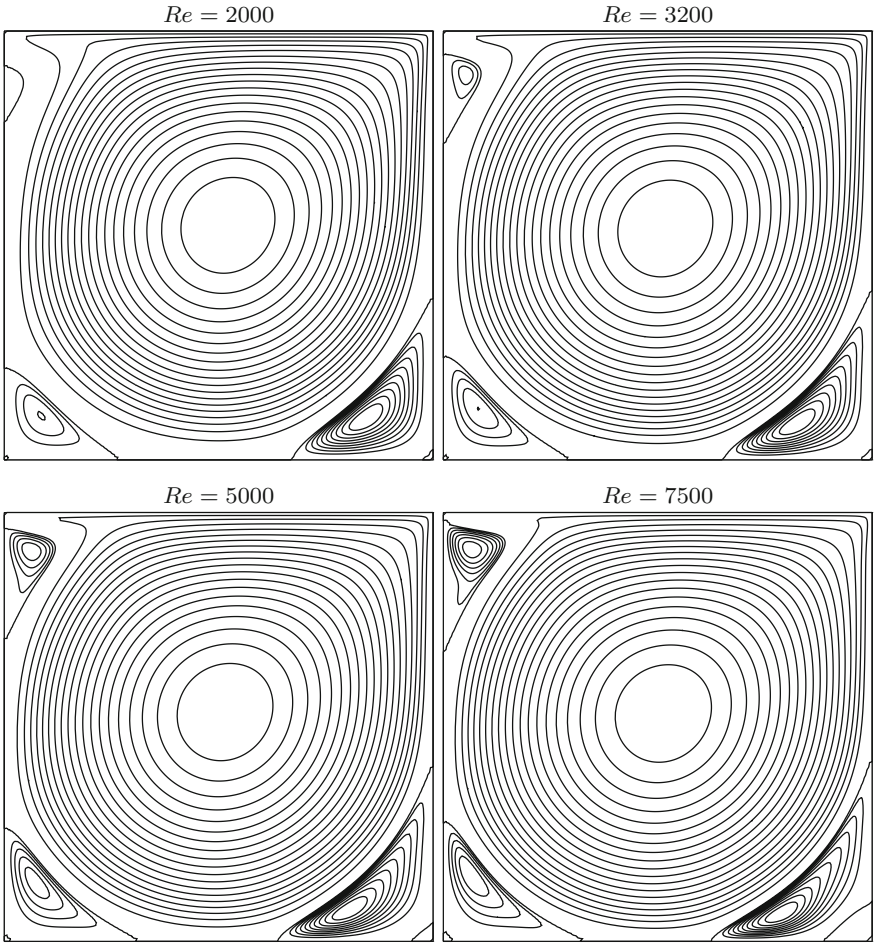

Fig. 1.21 The stationary solution of the Navier–Stokes equations in the driven cavity with the discontinuous Galerkin method (from [285])

in 2013 by Saramito [285], using the discontinuous Galerkin finite method together with a Newton algorithm. Figures 1.21 and 1.22 show solutions for the driven cavity at very high Reynolds number, up to $Re = 25000$. A third vortex develops at the top left corner for $Re = 3200$ while sub-vortices develops also inside the left and right vortices when $Re \geqslant 7500$. Solutions beyond the critical number are obtain by solving the stationary problem, and are not reachable with a time-dependent algorithm. The Newton algorithm will be presented in Chap. 2 for quasi-Newtonian fluids while the discontinuous Galerkin finite method will be developed in details in Chap. 4, in the context of viscoelastic fluids. The three-dimensional driven cavity has been investigated in [204] for $Re > 0$ by the method of characteristics (see also [203]).

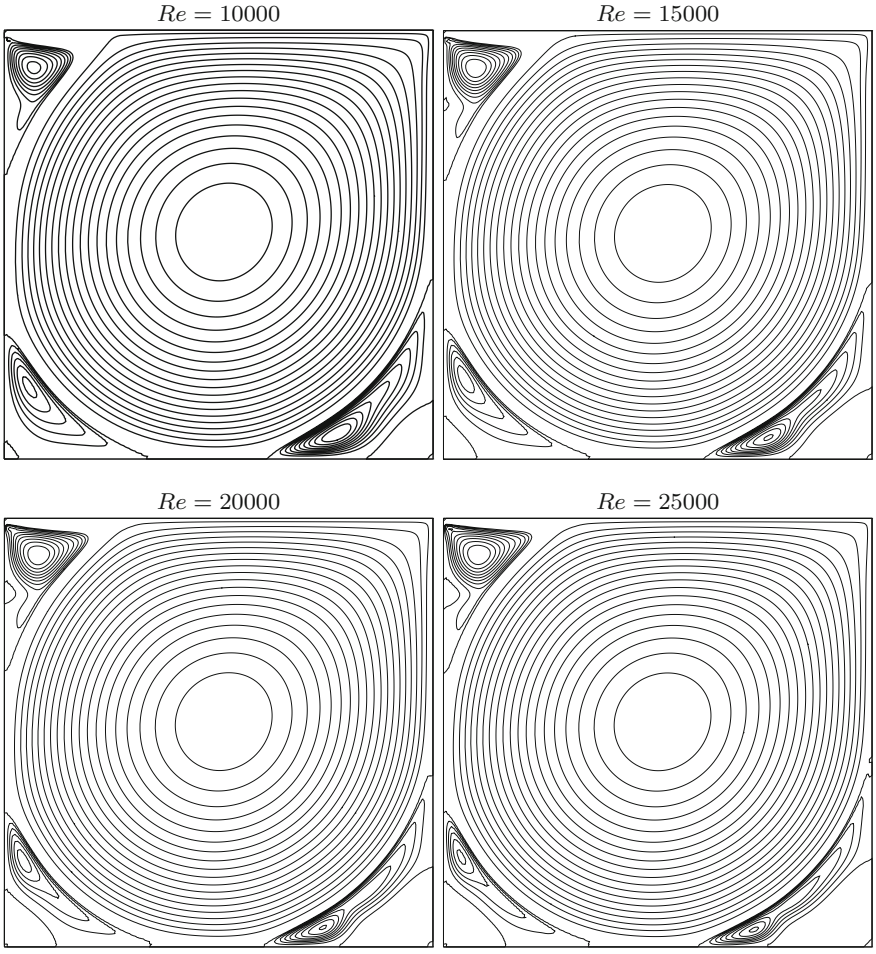

Fig. 1.22 The stationary solution of the Navier–Stokes equations in the driven cavity with the discontinuous Galerkin method (cont.) (from [285])

In conclusion, the exploration of the driven cavity at large Reynolds number is a fundamental challenge in computational fluid dynamics.

1.13 Iterative Resolution of the Stokes Problem

The generalized Stokes subproblem appears as a fundamental brick in all algorithms proposed all along the different chapters of this book for solving complex fluid flow problems. The direct solver is very efficient for two-dimensional problems, where the

fillin of the sparse matrix during the factorization is not too important. More precisely, Fig. 1.15 indicates the memory requirement which is proportional to the factorization time: $\mathcal{O}(n\ \log(n))$ in two dimension and $\mathcal{O}(n^2)$ in three dimension, where n denotes the mesh size. For three-dimensional meshes, this fillin becomes important and only meshes with small and medium sizes can be handled by computers when using direct methods. The main advantage of iterative methods is to avoid the factorization: the memory requirement reduces to the storage of the mesh and the sparse matrix, which is $\mathcal{O}(n)$.

Iterative solvers are able to handle the indetermination for the pressure. Recall that the pressure is defined up to an additive constant when using Dirichlet boundary conditions. Thus, only a simplified saddle point formulation is necessary and we can omit the Lagrange multiplier associated to the zero average for the pressure. Let L be the Lagrangian, defined for all $\boldsymbol{u}$ and p by

$$L(\boldsymbol{u},\ p) = \frac{1}{2}a(\boldsymbol{u},\ \boldsymbol{u}) + b(\boldsymbol{u},\ p) - \ell(\boldsymbol{u})$$

Note that the pressure appears as the Lagrange multiplier associated to the zero-divergence for the velocity.

Let us introduce the following *viscous dissipation energy* functional

$$J(\boldsymbol{u}) = \sup_{q \in L^2(\Omega)} L(\boldsymbol{u},\ q)$$

Note that this energy is finite if and only if $\boldsymbol{u}$ satisfies $\operatorname{div} \boldsymbol{u} = 0$. Otherwise, the maximization in q would be unbounded when q tends to infinity. Then, the problem reduces to the minimization of the viscous energy

$$\boldsymbol{u} = \arg\inf_{\boldsymbol{v} \in V(\boldsymbol{u}_\Gamma)} J(\boldsymbol{v})$$

Conversely, we define the *dual energy* functional

$$J_*(q) = -\inf_{\boldsymbol{v} \in V(\boldsymbol{u}_\Gamma)} L(\boldsymbol{v},\ q)$$

Note that J_* is convex, since L is concave in q. The problem can be expressed equivalently as a minimization problem in terms of the dual energy:

$$p = \arg\inf_{q \in L^2(\Omega)} J_*(q)$$

There are numerous efficient algorithms for the minimization of a convex function. The simplest one is certainly the fixed step descent method, also called the Uzawa algorithm. More improved algorithms exists; are the optimal step descent method, the conjugate gradient algorithm, the minimal residual one. Practical implementations of iterative Stokes solvers base either on the conjugate gradient or the minimal residual

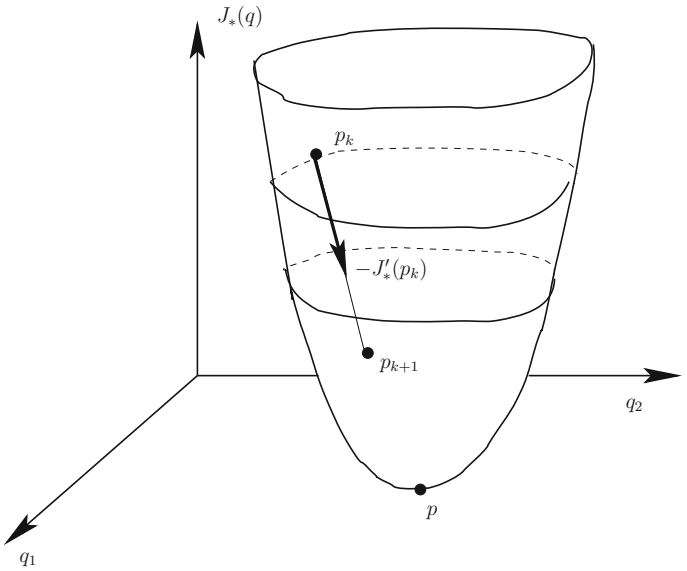

Fig. 1.23 The descent algorithm for a convex function

algorithm. See [12] for an exhaustive presentation of these algorithms and [284, 286] for a generic C++ implementation of them. For the purpose of simplicity, the Uzawa algorithm is presented here. Its abstract version for the minimization of the J_* functional writes (see also Fig. 1.23):

Algorithm 1.8 (*Uzawa algorithm – abstract version*)

- $k = 0$: let p_0 being given
- $k \geqslant 0$: let p_k being known, compute:

$$p_{k+1} = p_k - \beta \, J'_*(p_k)$$

where $\beta > 0$ is the fixed descent step.

In order to get a practical version of the Uzawa algorithm, the first step is to compute $J'_*(p_k)$. For this computation, we switch to the finite dimensional version of the Stokes problem, with the notations of Sect. 1.10. The linear system writes:

$$\begin{pmatrix} A & B^T \\ B & 0 \end{pmatrix} \begin{pmatrix} U \\ P \end{pmatrix} = \begin{pmatrix} F \\ G \end{pmatrix}$$

where A is a symmetric positive definite $n \times n$ matrix, B is a rectangular $n \times m$ matrix and $F \in \mathbb{R}^n$, $G \in \mathbb{R}^m$. Expanding the system leads to

$$\begin{aligned} AU + B^T P &= F \\ BU &= G \end{aligned}$$

Then, as A is non-singular, from the first equation, we get an explicit expression for U:

$$U = A^{-1}(F - B^T P)$$

Replacing in the second equation, we obtain

$$(BA^{-1}B^T)P = BA^{-1}F - G$$

Let $S = BA^{-1}B^T$ and $H = BA^{-1}F - G$. The S matrix is called the Schur complement of the mixed linear system. The problem reduces to

$$SP = H$$

As S involves A^{-1}, it is not recommended in practice to represent S by computing all its coefficients: while A and B are sparse, S is a full $m \times m$ matrix and it would requires m^2 memory entries. It is sufficient to be able to compute the effect of the multiplication between the matrix S and a vector. Solving the previous linear system is equivalent to solving the following quadratic minimization problem:

$$P = \underset{Q \in \mathbb{R}^m}{\arg\inf}\, J_*(Q)$$

with $J_*(Q) = \frac{1}{2} Q^T S Q - H^T Q$. The derivative of J_* is $J'_*(Q) = SQ - H$. Then, we are able to expand the computation of the Uzawa algorithm:

$$\begin{aligned} J'_*(P_k) &= SP_k - H \\ &= BA^{-1}B^T P_k - BA^{-1}F + G \\ &= BA^{-1}(B^T P_k - F) + G \\ &= -BU_k + G \end{aligned}$$

where $U_k = A^{-1}(F - B^T P_k)$.

Algorithm 1.9 (*Uzawa algorithm – practical version*)

- $k = 0$: let P_0 being given, find U_0 such that

$$AU_0 = F - B^T P_0$$

- $k \geqslant 0$: U_k and P_k known, compute:

$$\begin{aligned} R_k &:= G - B^T U_k \\ P_{k+1} &:= P_k - \beta R_k \end{aligned}$$

then find U_k such that

$$AU_{k+1} = F - B^T P_{k+1}$$

A classical stopping criterion is based on the norm of the residual R_k. Note that this algorithm involves only one resolution of a linear system per iteration, with the matrix A, when computing U_k in the last step. This inner resolution could also involve an iterative method, such as the conjugate gradient. There are many possible improvements, as replacing the Uzawa algorithm by the conjugate gradient one, and preconditioning, to accelerate the minimization of the residual. These strategies are implemented in the `Rheolef` library [284, 286] for the resolution of the three-dimensional Stokes problems.

1.14 Notes

Continuum mechanics – In this chapter, the Navier–Stokes equations were derived from two general principles: the conservations of mass and momentum. The derivation also used some regularity assumptions, such as the continuity of the stress tensor and the differentiability of the velocity vector. The development of continuum mechanics theories, including the Gauss and Cauchy theorems, based on weaker assumptions for the stress and the velocity is an active research area. For instance, in 2007, Chen et al. [50], using the measure theory, developed a rigorous extended continuum mechanics theory where stresses could develop discontinuities and shocks across surfaces. The mathematical description of the nature in general and of the fluid flows in particular is a ongoing human adventure that started during the 17th century with the pioneer work of Newton.

Non-symmetric stresses – In 1909, Eugène and François Cosserat, two brothers, proposed, on the basis of the Darboux theory of surfaces, a new description of continuum mechanics [62]. In particular, this theory predicts a possible non-symmetry of the total stress tensor. It extends the classical theory (see Theorem 1.6, p. 12) and the antisymmetric part of the stress tensor describes a couple stress field. Since the 1960s, this theory developed rapidly, stimulated by applications to some non-homogeneous materials, such as liquid crystals, suspensions, solid foams and materials with periodic micro-structure. For recent advances of such generalized continuum theories, see e.g. [24, 102] or the proceedings of the Euromech conference [201].

Textbooks – There are two classical textbooks on the Navier–Stokes equations. The first one, by Batchelor [13], written in 1967 and re-edited many times, presents the fluid mechanics point of view. The second textbook, by Temam [306], written in 1977 and re-edited also many times, groups mathematical results on these equations. While the Navier–Stokes equations have a long history, as presented at the end of Sect. 1.4, it remains today an active research area that takes two main branches. In 1934, Leray [184] published a major theoretical result. The first branch is interested in completing this result for the three-dimensional case. It is the subject of

one of the seven millennium prizes that were stated by the Clay mathematics institute in 2000. A correct solution to this problem would be awarded a one million US dollars prize from the institute. A recent presentation of mathematical aspect of the incompressible Navier–Stokes equation has been published in 2013 by Boyer and Fabrie [35]. The second branch aims is interested in improving the numerical algorithms and softwares for practical computations of approximations, when no explicit solutions are available.

Coupling – A common generalization of the Navier–Stokes equation is to suppose that the density ρ and the viscosity η depends upon another variable, e.g. the temperature for non-isothermal [187] fluids or the volume fraction for mixtures [129] or suspensions [130]. In that case, the Navier–Stokes equations are coupled with an additional equation for the evolution of this additional variable.

Algorithms and approximations – A classical textbook on the finite element method has been written in 1967 by Zienkiewicz and Taylor and re-edited in 2000: its third volume [320] is dedicated to fluid mechanics. While the present chapter propose both a direct and an iterative approach for solving the Stokes subproblems, there are many others iterative alternatives. In 1967, Chorin [51] suggested a pressure projection method that has been improved for over 40 years (see [132] for a review). In 1979, Girault and Raviart [118] grouped theoretical aspects of the finite element approximation of the Navier–Stokes equations in a major book. In this book, the authors suggested two algorithms for the resolution of the Stokes problem. These algorithms could be considered as obsolete today. The first algorithm bases on a regularization [118, p. 65] (also called penalization), that avoids the non-uniqueness of the pressure. A direct matrix resolution is then possible but the main drawbacks of this approach are that the discrete incompressibility constraint is not exactly satisfied and that the matrix is very ill conditioned. The second algorithm uses an augmented Lagrangian formulation initially proposed in 1983 by Fortin and Glowinski [107, p. 49]. It is an iterative algorithm and the incompressibility constraint is exactly satisfied at convergence but, at each step, the linear subproblem is also very ill conditioned. In 1982, Glowinski et al. [121, 124] proposed an operator splitting method combined with a second order in time θ-scheme for the time dependent Navier–Stokes equations. Note that operator splitting methods will be revisited in Chap. 4, in the context of viscoelastic fluids. The method of characteristics (Algorithm 1.2, p. 28) has been introduced in the 1980s. In 1982, Pironneau gave a first numerical analysis [241], improved in 1988 by Süli [299]. In 1987, Boukir et al. [33] suggested its application for high time order implicit schemes (Algorithm 1.3, p. 29) and the first computations with this scheme appeared later in 2004 [109]. In 1991, Brezzi and Fortin [38] systematically explored many possible finite element approximations of the Stokes and others mixed problems. The `Freefem++` [141] interpreter and the `Rheolef` [284, 286] library propose both recent and flexible software implementations of the finite element method and the method of characteristics, as presented in Sect. 1.7, together with applications to the Navier–Stokes equations. Many others free and non-free softwares are available today for computing some approximations

of the solutions of the Navier–Stokes equations and reviewing all of them is out of the scope of these notes.

Others approximations – There are alternatives to the finite element and finite difference methods for the approximation of fluid flow problems: for instance, the spectral method is also frequently used. In 1997, Bernardi and Maday [21] presented a mathematical review of this approach. The high order polynomial approximation of the spectral method combines with the flexibility of the finite element method into a new approach: the spectral/*hp* element method. In 1999, Karniadakis and Sherwin showed the efficiency of this approach in a nice re-edited book [165], which also demonstrates how the spectral/*hp* element method applies to the Navier–Stokes equations and proposes also a free C++ software called `Nektar++` [41]. The wavelet method is closely related to spectral methods: Perrier et al. [163] proposed in 2015 a promising divergence-free basis wavelet method.

Closely related to the method of characteristics is the vortex method, a meshless approach for hyperbolic problems as the Euler equations, and that could be extended also to include viscous terms. In 2000, Cottet and Koumoutsakos [63] presented some theoretical results related to the vortex methods, In 2005, Elman, Silvester and Wathen [87] explored several ways to improve the convergence of iterative algorithms for the Stokes problem using preconditioning techniques. In 2007, the pioneer's work of Kanschat [164] opened the door to robust approximations of the Navier–Stokes equation at high Reynolds numbers using discontinuous Galerkin methods. This variant of the finite element method will be presented in Chap. 4 for applications to viscoelasticity. In 2008, Hesthaven and Warburton [143] proposed a free software solution called `Nudge` for discontinuous Galerkin methods. The `Rheolef` library [285, 286] is another recent free software solution for solving flow problems with the discontinuous Galerkin method: solutions at very high Reynolds numbers were obtained (see Sect. 1.12) and the software is freely available.

Softwares – There are many available free softwares for the numerical resolution of the Navier–Stokes equations. It is out of the scope of the present notes to review all of them. The web page http://www.cfd-online.com/Wiki/Codes maintains a list of softwares that are in the public domain or available under some free software licenses. We already have presented some implementations with `Rheolef`, that is developed by the author. `Rheolef` is a free software that is available as a standard package under the Debian and Ubuntu GNU/Linux systems and could be installed from source code on others systems. It implements in C++ both the method of characteristic and the discontinuous Galerkin approaches. All the simulations of the forthcoming chapters, involving complex fluid models, are performed with `Rheolef`. `Freefem++` [141] is an interpreter that proposes a flexible software implementation of the finite element method and the method of characteristics, together with applications to the Navier–Stokes equations. `Nektar++` [41] implements in C++ the spectral/*hp* element method with successful computations for the Navier–Stokes equations. `Nudge` is an `octave` (or `matlab`) implementation of the discontinuous Galerkin method, with some applications to the Navier–Stokes equations.

Chapter 2
Quasi-Newtonian Fluids

Experimental observations show that the viscosity, as measured by viscosimeters, is constant for some fluids as water or honey, that are called Newtonian fluids (see Sect. 1.6, p. 21). Nevertheless, experiments show that the viscosity is no more constant for many others fluids, such as pastes or polymer solutions. These fluids are called non-Newtonian or complex fluids. Measurements showed that the viscosity varies upon the imposed rate of deformation. The simplest idea to describe complex fluids is to plot the viscosity measurements versus the imposed shear rate, and then, to fit the obtained curve with a simple template viscosity function, adjusting some few parameters. This is the main idea of quasi-Newtonian fluids models. Quasi-Newtonian fluids could be viewed as a first step inside the world of complex fluids: they could be considered as a simple approximation of more complex viscoplastic or viscoelastic fluids, that will be studied in Chaps. 3 and 4, respectively.

This chapter starts by reviewing some classical viscosity functions with few adjustable parameters. Then, the boundary value problem defining the non-Newtonian fluid is defined. The solution of both Poiseuille and Couette flows are then explicitly computed when using a simple viscosity function, the power law. When dealing with more general viscosity functions, geometries or flow condition, explicit computations are no more possible and we turn to the computation of an approximation of the solution. The problem is recast into the research of a saddle point of a Lagrangian and we obtain the variational formulation. Two algorithms are examined: the fixed point and the Newton methods. Algorithms are illustrated by some numerical computations for a Poiseuille flow in a pipe with a non-circular cross section.

2.1 Viscosity Function

Let us start with some few definitions.

Definition 2.1 (*tensor norm*)
For all $\boldsymbol{\tau} \in \mathbb{R}^{3\times 3}$, the following *tensor norm* is considered

$$|\boldsymbol{\tau}| = \left(\frac{\boldsymbol{\tau} : \boldsymbol{\tau}}{2}\right)^{\frac{1}{2}} = \left(\frac{1}{2}\sum_{i=1}^{3}\sum_{j=1}^{3}\tau_{i,j}^2\right)^{\frac{1}{2}}$$

P. Saramito, *Complex fluids*, Mathématiques et Applications 79,
DOI 10.1007/978-3-319-44362-1_2

Remark 2.1 (*choice of the tensor norm*)
An alternate definition of the tensor norm could be $|\boldsymbol{\tau}|_m = (\boldsymbol{\tau}:\boldsymbol{\tau})^{\frac{1}{2}}$. As $|\boldsymbol{\tau}|_m = \sqrt{2}|\boldsymbol{\tau}|$, these two norms are equivalent from a mathematical point of view and the only change is eventually the values of the material parameters involved in constitutive equations. Choosing $|.|$ instead of $|.|_m$ is motivated in this book by the following reason: for a simple shear flow, the diagonal components of $D(\boldsymbol{u})$ are zero while extra-diagonal components are counted twice in the $|.|_m$ norm, due to symmetry. The $1/2$ factor in the definition of the $|.|$ tensor norm deletes this twice counting effect. This simplification will be illustrated with the following Poiseuille and Couette examples, that are simple shear flows. Moreover, the choice of the $|.|$ tensor norm is conventional in rheology: values for material parameters of constitutive equations are estimated from experimental measurements on simple shear flows and using this choice for the tensor norm.

Definition 2.2 (*shear rate*)
The *shear rate*, denoted by $\dot{\gamma}$ is defined by $\dot{\gamma} = |2D(\boldsymbol{u})|$.

For simple shear flow, such as Poiseuille or Couette flows, $\dot{\gamma}$ coincide, up to the sign, with the time derivative of the shear deformation, often denoted as γ. For a general flow, $\dot{\gamma} = |2D(\boldsymbol{u})|$ is no more a time derivative of a quantity: this is just a conventional notation, used by extension. Recall (see Definition 1.9, p. 14) that the Cauchy stress tensor admits the decomposition $\boldsymbol{\sigma}_{\text{tot}} = \boldsymbol{\sigma} - p\boldsymbol{I}$ where $\boldsymbol{\sigma}$ is the stress deviator and p is the pressure.

Definition 2.3 (*quasi-Newtonian fluid*)
The fluid is said quasi-Newtonian when there exists a positive function $\eta : \mathbb{R}^+ \longrightarrow \mathbb{R}^+$ called the *viscosity function*, such that the stress deviator $\boldsymbol{\sigma}$ expresses as

$$\boldsymbol{\sigma} = 2\eta(|2D(\boldsymbol{u})|^2)\ \text{dev}\,(D(\boldsymbol{u})) \tag{2.1}$$

Note that the constitutive equation is non-linear: this is a major difference with Newtonian fluids. The viscosity function is supposed to be known by some experimental measurements. This function is expressed here for convenience in terms of the square of the shear rate, instead of the shear rate directly. Without any loss of generality, this choice will simplify later some computations. The simplest viscosity function is defined by the power law.

Definition 2.4 (*power law viscosity*) The power law expresses the viscosity as

$$\eta(\xi) = K\xi^{\frac{-1+n}{2}}, \quad \forall \xi \in \mathbb{R}^+ \tag{2.2}$$

where $n > 0$ and $K \geqslant 0$ are given real constants, called respectively the *power index* and the *consistency*.

Note that when $n = 1$ this function is constant and the fluid is Newtonian. In the context of polymer solutions, the power-law was proposed in 1929 by Ostwald [229]

and this author called it the Waele-Ostwald power law. Independently, in the context of steel metallurgy, also in 1929, Norton [225] proposed a one-dimensional version of the power law and in 1954, Hoff [144] generalized it to the three-dimensional case, using a tensor norm., and this law is referred as the Norton-Hoff one. In the context of glaciers and ice sheet models for climate change prediction the power law is referred as the Glen's law (see e.g. [70, p. 85]). This viscosity function is useful because of its simplicity, but only approximately describes the behavior of a real non-Newtonian fluid. For example, if n were less than one, the power law predicts that the effective viscosity would decrease with increasing shear rate indefinitely, requiring a fluid with infinite viscosity at rest and zero viscosity as the shear rate approaches infinity, but a real fluid has both a minimum and a maximum effective viscosity that depend on the physical chemistry at the molecular level. Therefore, the power law is only a good description of fluid behavior across the range of shear rates to which the coefficients were fitted. There are a number of other models that better describe the entire flow behavior of shear-dependent fluids, but they do so at the expense of simplicity, so the power law is still used to describe fluid behavior, permit mathematical predictions, and correlate experimental data.

Definition 2.5 (*Carreau's law viscosity*)
The Carreau's law expresses the viscosity as

$$\eta(\xi) = \eta_\infty + (\eta_0 - \eta_\infty)(1 + \lambda\xi)^{\frac{-1+n}{2}}, \quad \forall \xi \in \mathbb{R}^+ \tag{2.3}$$

where $n > 0$ and $\eta_0 \geqslant 0$, $\eta_\infty \geqslant 0$ and $\lambda \geqslant 0$ are given real constants, satisfying $\eta_0 \geqslant \eta_\infty$ when $n \leqslant 1$ and $\eta_0 \leqslant \eta_\infty$ when $n \geqslant 1$.

The Carreau's law is represented on Fig. 2.1. The Carreau's law was first proposed in 1968 by Carreau et al. [42]. A popular extension to the Carreau's law is the Yasuda [318] law, often called the Yasuda-Carreau's law and a closely related model is the Cross law [69]. Such models are of common use for blood flows (see e.g. [1]) with biological applications.

Note that when $n = 1$ then both the power law and the Carreau's law reduces to a Newtonian fluid model where the viscosity is constant. When $n < 1$, the viscosity is decreasing with the shear rate and the fluid is said *shear thinning* or *pseudo-plastic*. An example is solutions of large, polymeric molecules in a solvent with smaller molecules. It is generally supposed that the large molecular chains tumble at random and affect large volumes of fluid under low shear, but that they gradually align themselves in the direction of increasing shear and produce less resistance. A common household example of a strongly shear-thinning fluid is styling gel. If one were to hold a sample of hair gel in one hand and a sample of corn syrup or glycerin in the other, they would find that the hair gel is much harder to pour off the fingers (a low shear application), but that it produces much less resistance when rubbed between the fingers (a high shear application). When $n > 1$, the viscosity is increasing with the shear rate and the fluid is said *shear thickening* or *dilatant*. Such fluids are rarely encountered, but one common example is an uncooked paste of

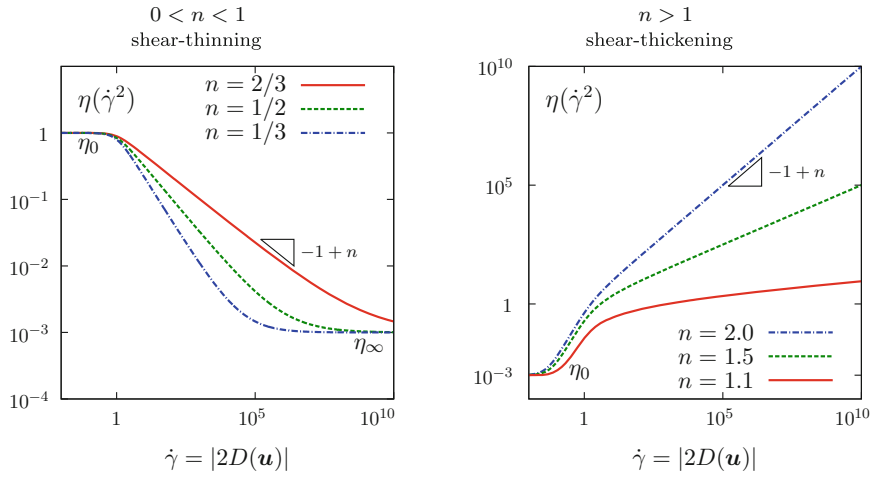

Fig. 2.1 Quasi-Newtonian flow: Carreau's law for the viscosity

cornstarch and water: under high shear rates the water is squeezed out from between the starch molecules, which are able to interact more strongly.

2.2 Problem Statement

As we consider here isothermal liquids, the density could be supposed as constant and the material as incompressible. The mass and momentum conservation equations (1.3) and (1.17) are completed with (1.22) for the Cauchy stress tensor and the constitutive equation (2.1) for quasi-Newtonian fluids. The set of equations is closed by appropriate initial and boundary conditions. The problem writes:

(P): find $\boldsymbol{u}$ and p, defined in $]0, T[\times\Omega$, such that

$$\rho\left(\frac{\partial \boldsymbol{u}}{\partial t} + \boldsymbol{u}.\nabla\boldsymbol{u}\right) - \mathbf{div}\left\{2\eta(|2D(\boldsymbol{u})|^2)\, D(\boldsymbol{u})\right\} + \nabla p = \rho\boldsymbol{g} \ \text{ in } \ ]0, T[\times\Omega \tag{2.4a}$$

$$-\operatorname{div}\boldsymbol{u} = 0 \ \text{ in } \ ]0, T[\times\Omega \tag{2.4b}$$

$$\boldsymbol{u}(0) = \boldsymbol{u}_0 \ \text{ in } \ \Omega \tag{2.4c}$$

$$\boldsymbol{u} = \boldsymbol{u}_\Gamma \text{ on }]0, T[\times\partial\Omega \tag{2.4d}$$

2.3 Example: Poiseuille Flow

We consider a quasi-Newtonian fluid with a power law viscosity function. Let us reuse the notations of Sect. 1.5, p. 18 for the Poiseuille flow of a Newtonian fluid. Assume that the flow is laminar: the pressure is given by $p(x, y, z) = -fz + p_0$ where $f > 0$ and $p_0 \in \mathbb{R}$ are given. We first consider the case of a flow between two parallel plates. The velocity is parallel to the plates $\boldsymbol{u}(x) = (0, 0, u_z(x))$. Its gradient is given by

$$\nabla \boldsymbol{u} = \begin{pmatrix} 0 & 0 & 0 \\ 0 & 0 & 0 \\ u_z' & 0 & 0 \end{pmatrix}$$

and the shear rate by $\dot{\gamma} = |2D(\boldsymbol{u})| = |u_z'|$. The stationary problem (2.4a)–(2.4d) reduces to

(P): find $u_z :]-L, L[\longrightarrow \mathbb{R}$ such that

$$\begin{cases} -\left(K|u_z'|^{n-1}u_z'\right)' = f \text{ in }]-L, L[\\ u_z(-L) = u_z(L) = 0 \end{cases}$$

This problem presents four physical parameters: n, K, L and f. In order to reduce the set of parameters, let us perform a dimensional analysis. As usual, the dimensionless quantities are denoted with tildes:

$$\tilde{x} = \frac{x}{L} \text{ and } \tilde{u}(\tilde{x}) = \frac{u_z(L\tilde{x})}{U}$$

where $U > 0$ will be chosen later. After this change of unknown, the problem becomes:

(P): find $\tilde{u} :]-1, 1[\longrightarrow \mathbb{R}$ such that

$$\begin{cases} -\dfrac{KU^n}{fL^{1+n}}\left(|\tilde{u}'|^{n-1}\tilde{u}'\right)' = 1 \text{ in }]-1, 1[\\ \tilde{u}(-1) = \tilde{u}(1) = 0 \end{cases}$$

Then, choose $U = (fL^{1+n}/K)^{1/n}$: the factor in the first equation disappears and there is only one physical parameter in this dimensionless problem, the power law index n. It means that, for a fixed n, the solution of the original problem is invariant up to a linear change of unknown. By using the symmetry of the geometry, the problem also reduces to the $]0, 1[$ interval. The dimensionless problem becomes:

(P): find $\tilde{u} :]0, 1[\longrightarrow \mathbb{R}$ such that

$$\begin{cases} -\left(|\tilde{u}'|^{n-1}\tilde{u}'\right)' = 1 \text{ in }]0, 1[\\ \tilde{u}'(0) = 0 \text{ and } \tilde{u}(1) = 0 \end{cases}$$

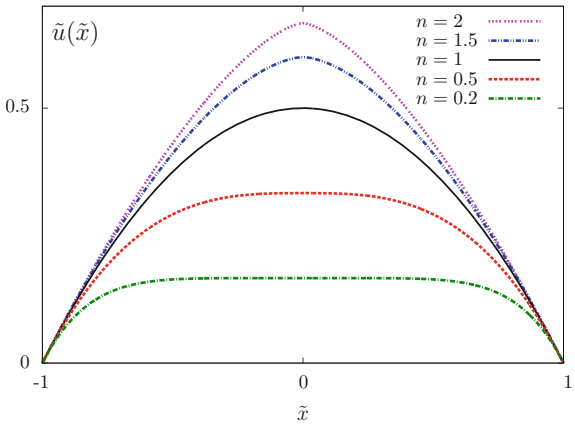

Fig. 2.2 Poiseuille flow with a power law viscosity

A first integration leads to: $-|\tilde{u}'|^{n-1}\tilde{u}' = \tilde{x} + c$ and $c = 0$ thanks to the symmetry condition $\tilde{u}'(0) = 0$. The previous relation leads to $\tilde{u}' < 0$ when $\tilde{x} \in]0, 1[$ and then $\tilde{u}' = -\tilde{x}^{1/n}$ when $\tilde{x} \in]0, 1[$. After a second integration and extending to $]-1, 1[$ by symmetry, we get $\tilde{u}(\tilde{x}) = \left(1 - |\tilde{x}|^{1+\frac{1}{n}}\right)/(1 + 1/n)$, for all $\tilde{x} \in]-1, 1[$. Finally, going back to dimensional quantities:

$$u_z(x) = \left(\frac{fL^{1+n}}{K}\right)^{\frac{1}{n}} \left(\frac{1 - \left(\frac{|x|}{L}\right)^{1+\frac{1}{n}}}{1 + \frac{1}{n}}\right), \quad \forall x \in]-L, L[.$$

Figure 2.2 plots the solution in dimensionless form for various values of the power law index n. When $n = 1$ we obtain the Newtonian solution already studied in Sect. 1.5, which is parabolic. Note that when $n < 1$, i.e. for shear thinning fluids, the solution is more flat: this is a very common experimental observation with many non-Newtonian fluids. Note also that when $n > 1$ the solution presents a peak at the center of the flow: the case $n > 1$ is less common. The case of a flow in a circular pipe requires similar computations: the solution is simply obtained by replacing f by $f/2$ and x by r in the previous expression.

2.4 Example: Couette Flow

We reuse the notations of Sect. 1.6, p. 21 for the Couette flow. For a laminar flow, the velocity writes $\boldsymbol{u} = (0, u_\theta(r), 0)$ in the cylindrical coordinate system (r, θ, z). By introducing the angular velocity $\omega(r)$ such that $u_\theta(r) = r\,\omega(r)$, the gradient of velocity writes

$$\nabla \boldsymbol{u} = \begin{pmatrix} 0 & 0 & 0 \\ r\omega' & 0 & 0 \\ 0 & 0 & 0 \end{pmatrix}$$

The shear rate is $\dot{\gamma} = r|w'|$. There are two main experimental situations: imposed torque and imposed angular velocity.

For an imposed torque, the stationary problem reduces to

(P): find $\sigma_{r\theta}$ and ω, defined in $]r_1, r_2[$, and p, defined in $]r_2[\times]0, z_0[$, such that

$$\rho\,\omega^2 r - \frac{\partial p}{\partial r} = 0 \quad \text{in }]r_1, r_2[\times]0, z_0[\tag{2.5a}$$

$$-\frac{1}{r^2}\left(r^2\left(K|r\omega'|^{-1+n} r\omega'\right)\right)' = 0 \quad \text{in }]r_1, r_2[\tag{2.5b}$$

$$-\frac{\partial p}{\partial z} = -\rho g \quad \text{in }]r_1, r_2[\times]0, z_0[\tag{2.5c}$$

$$K|r_1\omega'(r_1)|^{-1+n} r_1\omega'(r_1) = -f \text{ and } \omega(r_2) = \omega_2 \tag{2.5d}$$

Here, ω_2 is the angular velocity of the outer cylinder and f is a stress boundary data related to the imposed torque (see Sect. 1.6, p. 21). The problem presents eight physical parameters: $n, K, f, \omega_2, r_1, r_2, \rho, g$. In order to reduce the set of parameters, let us perform a dimensional analysis. As usual, the dimensionless quantities are denoted with tildes:

$$\tilde{r} = \frac{r}{r_2}, \quad \tilde{z} = \frac{z}{r_2}, \quad \tilde{\omega}(\tilde{r}) = \frac{\omega(r_2\tilde{r}) - \omega_2}{W}$$

where the characteristic angular velocity is $W = (f/K)^{\frac{1}{n}}$. After this change of unknowns, the reduced problem becomes:

(P): find $\tilde{\sigma}$ and $\tilde{\omega}$, defined in $]\beta, 1[$, and $\tilde{p}$, defined in $]\beta, 1[\times]0, \gamma[$, such that

$$Re\,\tilde{r}\tilde{\omega}^2 - \frac{\partial \tilde{p}}{\partial \tilde{r}} = 0 \quad \text{in }]\beta, 1[\times]0, \gamma[\tag{2.6a}$$

$$-\frac{1}{\tilde{r}^2}\left(\tilde{r}^{n+2}|\tilde{\omega}'|^{-1+n}\tilde{\omega}'\right)' = 0 \quad \text{in }]\beta, 1[\tag{2.6b}$$

$$-\frac{\partial \tilde{p}}{\partial \tilde{z}} = -\frac{Re}{Fr^2} \quad \text{in }]\beta, 1[\times]0, \gamma[\tag{2.6c}$$

$$\beta^n|\tilde{\omega}'(\beta)|^{-1+n}\tilde{\omega}'(\beta) = -1 \text{ and } \tilde{\omega}(1) = 0 \tag{2.6d}$$

Clearly, in (2.6a)–(2.6d), the computation of ω is decoupled to those of p, that could be performed later, using (2.6a) and (2.6c). The reduced problem (2.6b) and (2.6d) for computing the angular velocity involves two dimensionless numbers: the power index n and the geometry confinement $\beta = r_1/r_2 \in]0, 1[$. The two equations (2.6a) and (2.6c) for the pressure involve three additional dimensionless numbers: the Reynolds $Re = \rho W^2 r_2^2/\Sigma = \rho f r_2^2/\eta^2$, the Froude $Fr = (W r_2)/\sqrt{g r_2} = (f/\eta)\sqrt{r_2/g}$

and the cylinder vertical extension $\gamma = z_0/r_2$. Thus, let us focus on the computation of $\tilde{\omega}$. Integrating (2.6b) yields $\tilde{r}^{n+2}|\tilde{\omega}'|^{-1+n}\tilde{\omega}' = -c$ where c is an integration constant and the Neumann boundary condition (2.6d) at $\tilde{r} = \beta$ leads to $c = \beta^2$. Then $|\tilde{\omega}'|^{-1+n}\tilde{\omega}' = -\beta^2\tilde{r}^{-2-n}$ and thus $\tilde{\omega}' < 0$ in $[\beta, 1]$. Taking the absolute value of the previous relation leads to $|\tilde{\omega}'|^n = \beta^2\tilde{r}^{-2-n}$ or equivalently $|\tilde{\omega}'| = \beta^{2/n}\tilde{r}^{-(2+n)/n}$ and putting back the sign of $\tilde{\omega}'$ yields $\tilde{\omega}' = -\beta^{2/n}\tilde{r}^{-1-2/n}$. A second integration, together with the Dirichlet boundary condition (2.6d) at $\tilde{r} = 1$ leads to

$$\tilde{\omega}(\tilde{r}) = \frac{n\beta^{2/n}}{2}\left(\tilde{r}^{-2/n} - 1\right), \quad \forall \tilde{r} \in [\beta, 1]$$

Going back to dimensional quantities leads to the following expression of the velocity

$$u_\theta(r) = \omega_2 r + \frac{nf^{1/n}r}{2K^{1/n}}\left(\left(\frac{r_1}{r}\right)^{2/n} - \left(\frac{r_1}{r_2}\right)^{2/n}\right), \quad \forall r \in [r_1, r_2]$$

The solution is represented on Fig. 2.3. Note that when n decreases, the solution flattens at the vicinity of the outer cylinder. Conversely, when n becomes large, the solution becomes close to a linear function. The computation of the pressure is similar to those of the Newtonian case (see Sect. 1.6, p. 21). Finally, the case of an imposed angular velocity is similar to the case of an imposed torque and is left as an exercise to the reader.

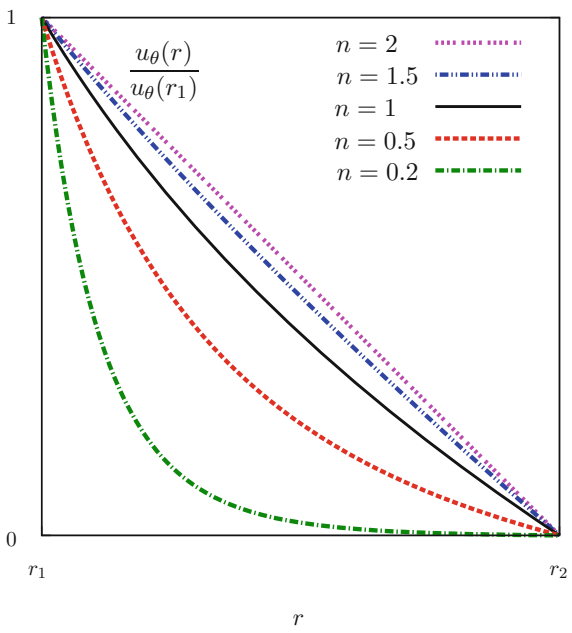

Fig. 2.3 Couette flow with a power law viscosity

For complex geometries or flow conditions, explicit solutions are no more possible and numerical approximation of the solutions is developed: this is the aim of the following sections.

2.5 Time Discretization

The methodology for the time discretization is then similar to those used for the Navier-Stokes equations, as presented in Sect. 1.7, p. 26. The method of characteristics is considered here for the discretization of the Lagrange derivative of the velocity by using a first order implicit scheme.

Algorithm 2.1 (*first order implicit scheme – quasi-Newtonian fluid*)

- $m = 0$: let $\boldsymbol{u}_0$, the initial condition, being given
- $m \geqslant 0$: let $\boldsymbol{u}_m$ being known, find $\boldsymbol{u}_{m+1}$ and p_{m+1} such that

$$\frac{\rho}{\Delta t}\boldsymbol{u}_{m+1} - \mathbf{div}\left\{2\eta\left(|2D\left(\boldsymbol{u}_{m+1}\right)|^2\right) D\left(\boldsymbol{u}_{m+1}\right)\right\} + \nabla p_{m+1} = \rho \boldsymbol{g} + \frac{\rho}{\Delta t}\boldsymbol{u}_m \circ X_m \text{ in } \Omega \tag{2.7a}$$

$$-\operatorname{div} \boldsymbol{u}_{m+1} = 0 \text{ in } \Omega \tag{2.7b}$$

$$\boldsymbol{u}_{m+1} = \boldsymbol{u}_\Gamma(t_{m+1}) \text{ on } \partial\Omega \tag{2.7c}$$

where X_m denotes the first order approximation of the characteristic line, defined by $X_m(\boldsymbol{x}) = \boldsymbol{x} - \Delta t\, \boldsymbol{u}_m(\boldsymbol{x})$ for all $\boldsymbol{x} \in \Omega$. Thus, at each step of this algorithm, there is a nonlinear subproblem to solve. Dropping the $m+1$ subscript for clarity, the subproblem writes:

(S): find $\boldsymbol{u}$ and p, defined in Ω, such that

$$\kappa\boldsymbol{u} - \mathbf{div}\left\{2\eta(|2D(\boldsymbol{u})|^2)\, D(\boldsymbol{u})\right\} + \nabla p = \boldsymbol{f} \text{ in } \Omega \tag{2.8a}$$

$$-\operatorname{div} \boldsymbol{u} = 0 \text{ in } \Omega \tag{2.8b}$$

$$\boldsymbol{u} = \boldsymbol{u}_\Gamma \text{ on } \partial\Omega \tag{2.8c}$$

where $\kappa \geqslant 0$, $\boldsymbol{f}$ and $\boldsymbol{u}_\Gamma$ are given. For simplicity and without loss of generality, we suppose in the rest of this chapter that $\kappa = 0$: the extension to $\kappa > 0$ do not present any difficulty. The resulting subproblem correspond to the stationary solution of the quasi-Newtonian fluid flow problem when inertia terms are neglected. Instead of a first order scheme, a higher order one could be used, e.g. Algorithm 1.3, p. 29: at each iteration, the subproblem would be similar.

2.6 Minimization Problem

We are looking to reformulate problem (2.8a)–(2.8c) as a minimization one. Let

$$J(\boldsymbol{u}) = \int_\Omega \mathscr{D}\left(|2D(\boldsymbol{u})|^2\right)\,\mathrm{d}x - \int_\Omega \boldsymbol{f}.\boldsymbol{u}\,\mathrm{d}x$$

where $\mathscr{D} : \mathbb{R}^+ \longrightarrow \mathbb{R}^+$ is a scalar differentiable function called the *energy of dissipation* function. We are looking for this function $\mathscr{D}$ such that the solution of the stationary problem (2.8a)–(2.8c) is also the solution of the following minimization problem

$$\boldsymbol{u} = \underset{\boldsymbol{v}\in K(\boldsymbol{u}_\Gamma)}{\arg\inf}\, J(\boldsymbol{v}) \tag{2.9}$$

where $K(\boldsymbol{u}_\Gamma)$ denotes the kernel of the divergence operator, as introduced in (1.46), p. 33, i.e. the set of divergence-free vector fields that satisfies also the Dirichlet boundary condition. As $\mathscr{D}$ is differentiable, the J functional is also differentiable. Let us compute its Gâteaux derivative. For any vector field $\boldsymbol{v}$, we have: by definition

$$J'(\boldsymbol{u}).(\boldsymbol{v}) = \lim_{\varepsilon\to 0} \frac{J(\boldsymbol{u}+\varepsilon\boldsymbol{v}) - J(\boldsymbol{u})}{\varepsilon}$$

Recall that the tensor norm is defined by $|\boldsymbol{\tau}|^2 = \boldsymbol{\tau}:\boldsymbol{\tau}/2$. Then $|2D(\boldsymbol{u})|^2 = 2D(\boldsymbol{u}):D(\boldsymbol{u})$ and

$$\frac{\mathrm{d}}{\mathrm{d}\boldsymbol{u}}\left(|2D(\boldsymbol{u})|^2\right).(\boldsymbol{v}) = 4D(\boldsymbol{u}):D(\boldsymbol{v})$$

By expanding:

$$\begin{aligned} J(\boldsymbol{u}+\varepsilon\boldsymbol{v}) &= \int_\Omega \mathscr{D}\left(2D(\boldsymbol{u}+\varepsilon\boldsymbol{v}):D(\boldsymbol{u}+\varepsilon\boldsymbol{v})\right)\,\mathrm{d}x - \int_\Omega \boldsymbol{f}.(\boldsymbol{u}+\varepsilon\boldsymbol{v})\,\mathrm{d}x \\ &= \int_\Omega \mathscr{D}\left(|2D(\boldsymbol{u})|^2\right)\,\mathrm{d}x - \int_\Omega \boldsymbol{f}.\boldsymbol{u}\,\mathrm{d}x \\ &\quad + \varepsilon\left(\int_\Omega 4\mathscr{D}'\left(|2D(\boldsymbol{u})|^2\right)\,(D(\boldsymbol{u}):D(\boldsymbol{v}))\,\mathrm{d}x - \int_\Omega \boldsymbol{f}.\boldsymbol{v}\,\mathrm{d}x\right) \\ &\quad + \mathcal{O}(\varepsilon^2) \end{aligned}$$

Then, the directional derivative is identified as the second term in the expansion:

$$J'(\boldsymbol{u}).(\boldsymbol{v}) = \int_\Omega 4\mathscr{D}'\left(|2D(\boldsymbol{u})|^2\right)\,(D(\boldsymbol{u}):D(\boldsymbol{v}))\,\mathrm{d}x - \int_\Omega \boldsymbol{f}.\boldsymbol{v}\,\mathrm{d}x \tag{2.10}$$

From (2.8a), multiplying by $\boldsymbol{v}$ such that div $\boldsymbol{v} = 0$ and $\boldsymbol{v} = 0$ on $\partial\Omega$ and integrating, we obtain the following variational formulation of the problem:

$$\int_\Omega 2\eta(|2D(\boldsymbol{u})|^2)\,(D(\boldsymbol{u}) : D(\boldsymbol{v}))\,\mathrm{d}x - \int_\Omega \boldsymbol{f}.\boldsymbol{v}\,\mathrm{d}x = 0 \tag{2.11}$$

As J is differentiable, its minimum is characterized by $J'(\boldsymbol{u}).(\boldsymbol{v}) = 0$ for all div $\boldsymbol{v} = 0$ and $\boldsymbol{v} = 0$ on $\partial\Omega$. Thus, by identification between (2.10) and (2.11), we get:

$$\begin{aligned} &2\mathscr{D}'(\xi) = \eta(\xi),\ \forall \xi \in \mathbb{R}^+ \\ \Longleftrightarrow\ &2\mathscr{D}(\xi) = \frac{1}{2}\int_0^\xi \eta\,(\xi)\ \mathrm{d}\xi,\ \forall \xi \in \mathbb{R}^+ \end{aligned}$$

Let us compute the energy function for the two previous examples of viscosity functions.

Property 2.1 (power law viscosity)

$$\begin{aligned} \eta(\xi) &= K\xi^{\frac{-1+n}{2}} \\ \mathscr{D}(\xi) &= \frac{1}{2}\int_0^\xi K\xi^{\frac{-1+n}{2}}\,\mathrm{d}\xi = \frac{K}{1+n}\xi^{\frac{1+n}{2}} \end{aligned}$$

Property 2.2 (Carreau's law viscosity)

$$\begin{aligned} \eta(\xi) &= \eta_\infty + (\eta_0 - \eta_\infty)(1+\lambda\xi)^{\frac{-1+n}{2}} \\ \mathscr{D}(\xi) &= \frac{1}{2}\int_0^\xi \left(\eta_\infty + (\eta_0 - \eta_\infty)(1+\lambda\xi)^{\frac{-1+n}{2}}\right)\mathrm{d}\xi \\ &= \frac{\eta_\infty \xi}{2} + \frac{\eta_0 - \eta_\infty}{\lambda(n+1)}\left((1+\lambda\xi)^{\frac{1+n}{2}} - 1\right) \end{aligned}$$

The energy function is represented on Fig. 2.4 versus the shear rate $\dot{\gamma}$.

Let us consider the power low viscosity: the energy functional J involved by the minimization problem writes:

$$J(\boldsymbol{u}) = \frac{K}{1+n}\int_\Omega |2D(\boldsymbol{u})|^{1+n}\,\mathrm{d}x - \int_\Omega \boldsymbol{f}.\boldsymbol{v}\,\mathrm{d}x \tag{2.12}$$

For this case, we are able to be more precise about the required regularity of the test functions. Our aim is to ensure that the integrals involved in J are convergent, i.e. $J(\boldsymbol{u}) < +\infty$. The regularity assumptions are introduced via some *functional spaces*. First, let us introduce some standard Lebesgue and Sobolev functional spaces (see also [36]).

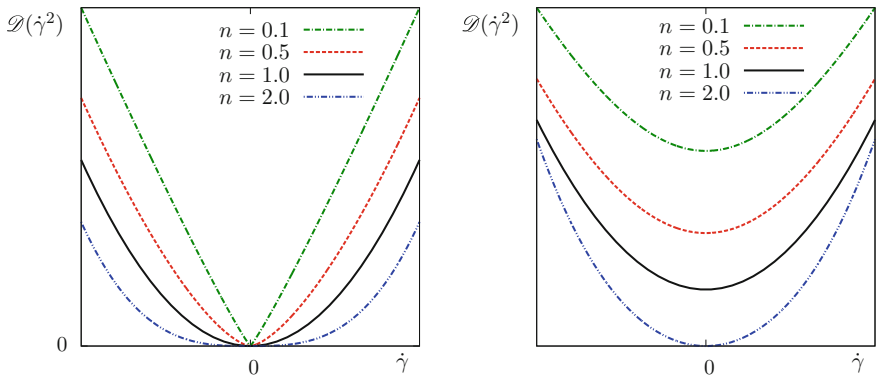

Fig. 2.4 Quasi-Newtonian fluid: energy function for the power law (*left*) and Carreau's law (*right*) viscosity functions

Definition 2.6 (*Lebesgue functional space*)

$$L^r(\Omega) = \left\{ \varphi : \Omega \to \mathbb{R}; \quad \int_\Omega |\varphi|^r \, \mathrm{d}x \; < \; +\infty \right\}, \quad \forall r \in [1, +\infty[$$

Note that this definition extends Definition 1.17, p. 32 to a general index r.

Definition 2.7 (*Sobolev functional space*)

$$W^{1,r}(\Omega) = \left\{ \varphi \in L^r(\Omega); \quad \nabla\varphi \in (L^r(\Omega))^3 \right\}, \quad \forall r \in [1, +\infty[$$
$$W_0^{1,r}(\Omega) = \left\{ \varphi \in W^{1,r}(\Omega); \quad \varphi = 0 \text{ on } \partial\Omega \right\}$$

Note that when $r = 2$ we have $W^{1,2}(\Omega) = H^1(\Omega)$, the Hilbert space introduced at Definition 1.18, p. 32. Note also that, in (2.12), the symmetric part of the gradient of velocity appears with a $r = 1 + n$ power index. Thus, the adequate functional space for the velocities is

$$V(\boldsymbol{u}_\Gamma) = \left\{ \boldsymbol{v} \in \left(W^{1,1+n}(\Omega)\right)^3; \quad \boldsymbol{v} = \boldsymbol{u}_\Gamma \text{ on } \partial\Omega \right\}$$

The associated kernel of the divergence operator writes:

$$K(\boldsymbol{u}_\Gamma) = \left\{ \boldsymbol{v} \in \left(W^{1,1+n}(\Omega)\right)^3; \quad \boldsymbol{v} = \boldsymbol{u}_\Gamma \text{ on } \partial\Omega \text{ and } \operatorname{div} \boldsymbol{v} = 0 \text{ in } \Omega \right\}$$

From the Sobolev trace theorem [36], a necessary and sufficient condition for the boundary condition $\boldsymbol{u}_\Gamma$ to satisfy $\boldsymbol{u}_\Gamma = \boldsymbol{u}_{|\partial\Omega}$ when $\boldsymbol{u} \in \left(W^{1,1+n}(\Omega)\right)^3$ is $\boldsymbol{u}_\Gamma \in \left(W^{1-\frac{n}{1+n},1+n}(\partial\Omega)\right)^3$. This is a regularity assumption on the boundary condition data of the problem. Note that the last term in (2.12), involves the integral

of $\boldsymbol{f}.\boldsymbol{v}$ for any $\boldsymbol{v} \in V(0) = \left(W_0^{1,1+n}(\Omega)\right)^3$. For this integral to be bounded, from a duality argument [36], this requires that the data $\boldsymbol{f} \in \left(W^{-1,1+n}(\Omega)\right)^3$. With this last assumption on the data of the problem, we are sure that all terms in the minimization have a sense.

Theorem 2.1 (existence and uniqueness of the stationary solution)
Assume that the viscosity function is given either by the power law or by the Carreau law. Then, the functional J is convex and problem (2.9) admits a unique solution. Moreover, this solution interprets as a weak solution of the stationary problem (2.8a)–(2.8c).

Proof The convexity of J follows from a Korn inequality [214] in the Sobolev space $W^{1,r}$ showed in 1971. In 1990 by Baranger and Najib [8] proved that the previous problem is well posed for the power law and the Carreau's one, and this result was improved in 2008 by Ervin et al. [95]. □

2.7 Saddle Point and Variational Formulations

In the previous section, we have shown that the minimization problem (2.9) is equivalent to find $\boldsymbol{u} \in K(\boldsymbol{u}_\Gamma)$ such that

$$\begin{aligned} & J'(\boldsymbol{u}).(\boldsymbol{v}) = 0, \ \forall \boldsymbol{v} \in K(0) \\ \Longleftrightarrow\ & a(\boldsymbol{u};\ \boldsymbol{u},\ \boldsymbol{v}) = \ell(\boldsymbol{v}),\ \forall \boldsymbol{v} \in K(0) \end{aligned}$$

where we have introduced the following forms

$$\begin{aligned} a(\bar{\boldsymbol{u}};\ \boldsymbol{u},\ \boldsymbol{v}) &= \int_\Omega 2\eta(|2D(\bar{\boldsymbol{u}})|^2)\, D(\boldsymbol{u}) : D(\boldsymbol{v})\, \mathrm{d}x, \quad \forall \bar{\boldsymbol{u}}, \boldsymbol{u}, \boldsymbol{v} \in \left(W^{1,1+n}(\Omega)\right)^3 \\ \ell(\boldsymbol{v}) &= \int_\Omega \boldsymbol{f}.\boldsymbol{v}\, \mathrm{d}x, \quad \forall \boldsymbol{v} \in \left(W^{1,1+n}(\Omega)\right)^3 \end{aligned}$$

Let us define the bilinear form

$$b(\boldsymbol{v}, q) = -\int_\Omega q \operatorname{div} \boldsymbol{v}\, \mathrm{d}x$$

and the Lagrangian

$$\begin{aligned} L(\boldsymbol{u}, p) &= J(\boldsymbol{u}) + b(\boldsymbol{u}, p) \\ &= \int_\Omega \mathscr{D}\left(|D(\boldsymbol{u})|^2\right)\, \mathrm{d}x - \int_\Omega \boldsymbol{f}.\boldsymbol{u}\, \mathrm{d}x - \int_\Omega p \operatorname{div} \boldsymbol{u}\, \mathrm{d}x \end{aligned}$$

The pressure appears in the Lagrangian as a Lagrange multiplier for the incompressibility constraint. The corresponding term requires the integration of $p \operatorname{div} \boldsymbol{u}$ for any $\boldsymbol{u} \in \left(W^{1,1+n}(\Omega)\right)^3$. By duality, a necessary and sufficient condition for this integral to be bounded (see [36]) is $p \in L^{1+\frac{1}{n}}(\Omega)$.

Following Sect. 1.8, in order to circumvent the indetermination of the pressure, defined up to an additive constant when using Dirichlet boundary conditions, let us introduce the space of zero-average pressures:

$$L_0^{1+\frac{1}{n}}(\Omega) = \left\{ q \in L^{1+\frac{1}{n}}(\Omega); \quad \int_\Omega q \, \mathrm{d}x = 0 \right\}$$

Finally, the minimization problem is equivalent to the following saddle point problem:

$$(\boldsymbol{u}, p) = \underset{\boldsymbol{v} \in V(\boldsymbol{u}_\Gamma)}{\arg\inf} \quad \sup_{q \in L_0^{1+n}(\Omega)} L(\boldsymbol{v}, q)$$

As the Lagrangian is differentiable, convex in $\boldsymbol{u}$ and linear in p, its unique saddle point is characterized by:

find $(\boldsymbol{u}, p) \in V(\boldsymbol{u}_\Gamma) \times L_0^{1+\frac{1}{n}}(\Omega)$ such that

$$\frac{\partial L}{\partial \boldsymbol{u}}(\boldsymbol{u}, p).(\boldsymbol{v}) = \frac{\partial L}{\partial p}(\boldsymbol{u}, p).(q) = 0, \quad \forall (\boldsymbol{v}, q) \in V(0) \times L_0^{1+\frac{1}{n}}(\Omega)$$

that writes equivalently:

(FV): find $(\boldsymbol{u}, p) \in V(\boldsymbol{u}_\Gamma) \times L_0^{1+\frac{1}{n}}(\Omega)$ such that

$$\begin{cases} a(\boldsymbol{u};\, \boldsymbol{u},\, \boldsymbol{v}) + b(\boldsymbol{v},\, p) = \ell(\boldsymbol{v}), \quad \forall \boldsymbol{v} \in V(0) \\ \quad b(\boldsymbol{u},\, q) \qquad\qquad\qquad\quad = 0, \quad \forall q \in L_0^{1+\frac{1}{n}}(\Omega) \end{cases}$$

This is the variational formulation of the problem. This problem is still non-linear: the form $a(.;\, .,\, .)$ is non-linear with respect to its first argument, due to the non-linearity of the viscosity function. The numerical treatment of this non-linearity requires some specific algorithms. Two of them are presented in the rest of this chapter: the fixed point algorithm and the Newton method.

2.8 Fixed Point Algorithm

Algorithm 2.2 (*fixed point*)

- $k = 0$: let $\boldsymbol{u}_0$ being given, e.g. the Newtonian solution
- $k \geqslant 0$: let $\boldsymbol{u}_{k-1}$ being known,

find $\boldsymbol{u}_k \in V(\boldsymbol{u}_\Gamma)$ and $p_k \in L_0^{1+\frac{1}{n}}(\Omega)$ such that

$$\begin{cases} a(\boldsymbol{u}_{k-1};\, \boldsymbol{u}_k,\, \boldsymbol{v}) + b(\boldsymbol{v},\, p_k) = (\boldsymbol{f},\, \boldsymbol{v}), & \forall \boldsymbol{v} \in V(0) \\ b(\boldsymbol{u}_k,\, q) = 0, & \forall q \in L_0^{1+\frac{1}{n}}(\Omega) \end{cases}$$

At the k-th step of this algorithm, there is a linear Stokes-like subproblem to solve. This subproblem is associated to a non-constant viscosity:

$$\eta_{k-1} = \eta\left(|2D(\boldsymbol{u}_{k-1})|^2\right)$$

where $\boldsymbol{u}_{k-1}$ is known from the previous step. Then, the form simply writes:

$$a(\boldsymbol{u}_{k-1};\, \boldsymbol{u},\, \boldsymbol{v}) = \int_\Omega 2\eta_{k-1}\, D(\boldsymbol{u}) : D(\boldsymbol{v})\, \mathrm{d}x, \quad \forall \boldsymbol{u}, \boldsymbol{v} \in \left(W^{1,1+n}(\Omega)\right)^3$$

This form is linear with respect to its second and third arguments. All algorithms developed in the Chap. 1, such as the direct and the iterative one, are easily adaptable to this problem. Thus, the sequence $(\boldsymbol{u}_k)_{k \geqslant 0}$ is practically computable. Is this sequence convergent, i.e.

$$\lim_{k \to +\infty} \boldsymbol{u}_k = \boldsymbol{u} \ ?$$

The answer to this question is difficult and requires some additional tools. Let G be the following operator:

$$\begin{aligned} G : V(\boldsymbol{u}_\Gamma) &\longrightarrow V(\boldsymbol{u}_\Gamma) \\ \bar{\boldsymbol{u}} &\longmapsto \hat{\boldsymbol{u}} = G(\bar{\boldsymbol{u}}) \end{aligned}$$

where $\hat{\boldsymbol{u}} \in V(\boldsymbol{u}_\Gamma)$ is defined, together with $\hat{p} \in L_0^{1+\frac{1}{n}}(\Omega)$, for any $\bar{\boldsymbol{u}} \in V(\boldsymbol{u}_\Gamma)$ as the unique solution of the following linear Stokes-likes system:

$$\begin{cases} a\left(\bar{\boldsymbol{u}};\, \hat{\boldsymbol{u}},\, \boldsymbol{v}\right) + b\left(\boldsymbol{v},\, \hat{p}\right) = (\boldsymbol{f},\, \boldsymbol{v}), & \forall \boldsymbol{v} \in V(0) \\ b\left(\hat{\boldsymbol{u}},\, q\right) = 0, & \forall q \in L_0^{1+\frac{1}{n}}(\Omega) \end{cases}$$

Note that the operator G, which associate to each $\bar{\boldsymbol{u}}$ the solution $\hat{\boldsymbol{u}}$ of the previous linear system, is not itself a linear operator. Indeed, when replacing $\bar{\boldsymbol{u}}$ by $\lambda\bar{\boldsymbol{u}}$ for any $\lambda \in \mathbb{R}$, we do not get $\lambda\hat{\boldsymbol{u}}$ as solution of the corresponding problem, since the form $a(.;\, .,\, .)$ is not linear with respect to its first argument. This is due to the non-linearity of the viscosity function. The non-linear problem is then reformulated in a concise way, as

$$(P) : \text{find } \boldsymbol{u} \in V(\boldsymbol{u}_\Gamma) \text{ such that } G(\boldsymbol{u}) = \boldsymbol{u}$$

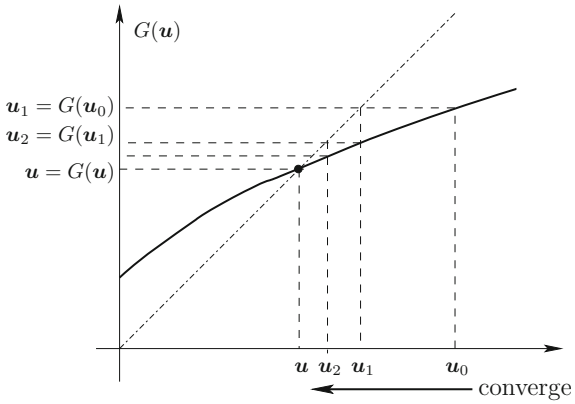

Fig. 2.5 Fixed point iteration: a convergent sequence

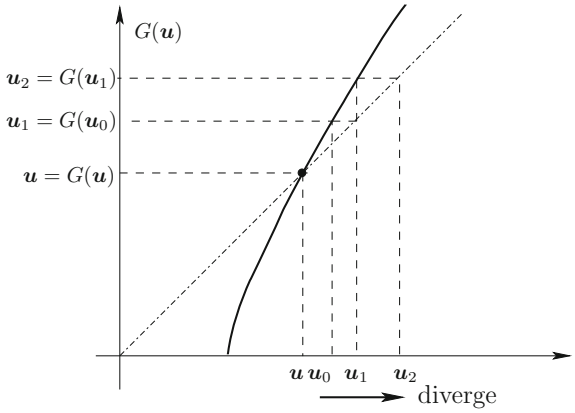

Fig. 2.6 Fixed point iteration: a divergent sequences

We says that the solution is a fixed point of G. Note also that $\boldsymbol{u}_k = G(\boldsymbol{u}_0)$ as G is the operator involved during one iteration. By recurrence, we have $\boldsymbol{u}_k = G^k(\boldsymbol{u}_0)$, i.e. the k-th iterate is obtained after k iterations of G.

Figures 2.5 and 2.6 present two typical sequences of the fixed point algorithm: one is convergent and the other is divergent. Let us try to elucidate the situation and find a necessary condition for the sequence to be convergent. Consider the following simple example:

$$\begin{aligned} G : \mathbb{R} &\longrightarrow \mathbb{R} \\ u &\longmapsto G(u) = \alpha u \end{aligned}$$

where $\alpha \in \mathbb{R}$. We have $u_k = G^k(u_0) = \alpha^k u_0$ and the sequence is convergent if and only if $|\alpha| < 1$. For the general case, the sequence is convergent when there exists a vicinity of $\boldsymbol{u}$ and containing $\boldsymbol{u}_0$ such that $|G'| < 1$ in this vicinity (see [319, p. 19]). In that case, we say that G is *contractive* in this vicinity. This result was due to Banach

in 1920. Nevertheless, in practice, and especially for our problem, it is difficult to prove the convergence of the sequence by this way. Numerical experimentations [284, Chap. 8] shows that the fixed point algorithm converges when the power index $n \in]0, 2[$ for a power law fluid. Thus, no all values of n are covered by this method. The following variant of the fixed point algorithms leads to improve the convergence rate of the algorithm and to build a convergent sequence for all power index.

Algorithm 2.3 (*Relaxed fixed point algorithm – abstract version*)

- $k = 0$: let $\boldsymbol{u}_0$ being given, e.g. the Newtonian solution
- $k \geqslant 0$: let $\boldsymbol{u}_{k-1}$ being known, compute

$$\boldsymbol{u}_k = \omega G\left(\boldsymbol{u}_{k-1}\right) + (1-\omega)\boldsymbol{u}_{k-1} \tag{2.13}$$

where $\omega > 0$ is a relaxation parameter.

This abstract algorithm involves the G operator: let us now unpack the G notation and get a practical version of the algorithm.

Algorithm 2.4 (*Relaxed fixed point algorithm – practical version*)
Let $\omega > 0$ be the relaxation parameter.

- $k = 0$: let $\boldsymbol{u}_0$ being given, e.g. the Newtonian solution
- $k \geqslant 0$: let $\boldsymbol{u}_{k-1}$ being known, let:

$$\eta_{k-1} = \eta\left(|2D\left(\boldsymbol{u}_{k-1}\right)|^2\right)$$
$$a\left(\boldsymbol{u}_{k-1};\, \boldsymbol{u},\, \boldsymbol{v}\right) = \int_{\Omega} 2\eta_{k-1}\, D(\boldsymbol{u}) : D(\boldsymbol{v})\, \mathrm{d}x$$

find $\boldsymbol{u}_* \in V\left(\boldsymbol{u}_\Gamma\right)$ and $p_k \in L_0^{1+\frac{1}{n}}(\Omega)$ such that

$$\begin{cases} a\left(\boldsymbol{u}_{k-1};\, \boldsymbol{u}_*,\, \boldsymbol{v}\right) + b\left(\boldsymbol{v},\, p_k\right) = \left(\boldsymbol{f},\, \boldsymbol{v}\right), & \forall \boldsymbol{v} \in V(0) \\ b\left(\boldsymbol{u}_*,\, q\right) = 0, & \forall q \in L_0^{1+\frac{1}{n}}(\Omega) \end{cases}$$

and set

$$\boldsymbol{u}_k = \omega \boldsymbol{u}_* + (1-\omega)\boldsymbol{u}_{k-1}$$

The last relation, that compute $\boldsymbol{u}_k$ as a linear combination of $\boldsymbol{u}_*$ and $\boldsymbol{u}_{k-1}$, interprets as an interpolation or extrapolation procedure, depending upon the value of ω. When, $0 < \omega < 1$, it is an *under-relaxation* method that slow down the changes from $\boldsymbol{u}_{k-1}$ to $\boldsymbol{u}_k$ by using and interpolation between $\boldsymbol{u}_k$ and $\boldsymbol{u}_*$. Conversely, when $\omega > 1$, it is an **over-relaxation** method, that increases the changes by using an extrapolation. Finally, when $\omega = 1$, we obtain the previous Algorithm 2.2 without relaxation. The relaxation could be used when $n > 2$ and then $0 < \omega < 1$ may be adjusted in order to obtain convergence. Also, when $n < 2$, adjusting $\omega > 1$ leads to improve the convergence rate, for an optimal efficiency. Numerical experimentations

[284, Chap. 8] shows that the optimal relaxation parameter ω_{opt} depends upon the power index n as $\omega_{\text{opt}} = \dfrac{2}{1+n}$. This value allows an optimal convergence rate of the relaxed fixed point algorithm for all values of the power index. Finally, observe that (2.13) writes equivalently

$$\frac{\boldsymbol{u}_k - \boldsymbol{u}_{k-1}}{\omega} + (I - G)(\boldsymbol{u}_{k-1}) = 0$$

Thus, the relaxation parameter interprets as a time step for an explicit first order scheme for the discretization of an evolutionary problem related to the $I - G$ operator. Increasing this time step as possible leads to reach faster the stationary solution, also solution of the fixed point problem. As the explicit scheme is only conditionally stable, there is a constraint upon the time step that should be taken sufficiently small.

2.9 Example: Poiseuille Flow in a Square Section

We consider the Poiseuille flow in pipe with a square cross section, as represented on Fig. 2.7 for a quasi-Newtonian fluid with a power law viscosity function. Assume that the flow is laminar: the pressure is given by $p(x, y, z) = -fz + p_0$ where $f > 0$ and $p_0 \in \mathbb{R}$ are given. The stationary velocity is parallel to the plates and depends only upon (x, y) in the section: $\boldsymbol{u}(x, y) = (0, 0, u_z(x, y))$. Its gradient is given by

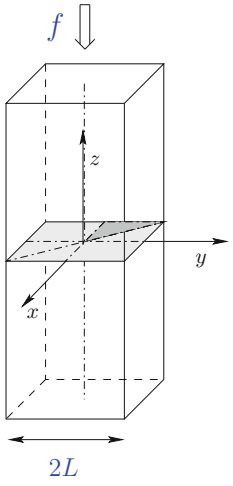

Fig. 2.7 Poiseuille flow in a square pipe section

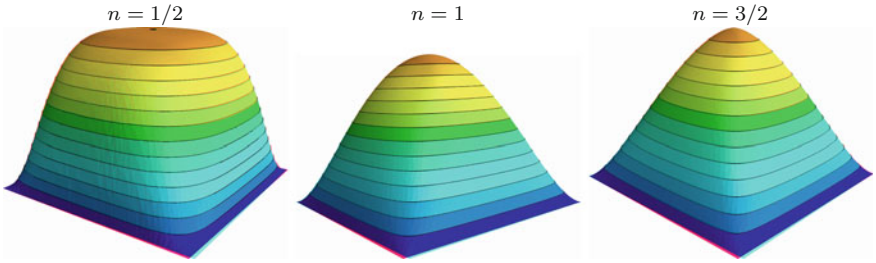

Fig. 2.8 Quasi-Newtonian fluids: Poiseuille flow in a square pipe section (from [284, Chap. 8])

$$\nabla \boldsymbol{u} = \begin{pmatrix} 0 & 0 & 0 \\ 0 & 0 & 0 \\ \dfrac{\partial u_z}{\partial x} & \dfrac{\partial u_z}{\partial y} & 0 \end{pmatrix}$$

and the shear rate by $\dot{\gamma} = |2D(\boldsymbol{u})| = |\nabla u_z|$. Note that the inertia term $(\boldsymbol{u}.\nabla)\boldsymbol{u}$ is zero. Indeed, the velocity is in the z direction while ∇ contains just two components $\partial/\partial x$ and $\partial/\partial y$ in the (O, x, y) plane. Then the operator $\boldsymbol{u}.\nabla$ is zero. The stationary problem (2.8a)–(2.8c) reduces to a two-dimensional one and the computational domain is the section of the pipe, denoted by Ω.

(P): find u_z defined in Ω such that

$$-\operatorname{div}\left(K|\nabla u_z|^{-1+n}\right)\nabla u_z\Big) = f \ \text{ in } \ \Omega \tag{2.14a}$$

$$u_z = 0 \ \text{ on } \ \partial\Omega \tag{2.14b}$$

This is problem is often referred as the p-Laplacian problem, with $p = 1 + n$. The dimensional analysis is similar to those of Sect. 2.3 and it remains only one relevant parameter in this problem, the power index n. Figure 2.8 presents the solution: it shares some similarities with the Poiseuille flow between two parallel plates (see Fig. 2.2, p. 68). Here the solution is no more explicit and it has been approximated by a finite element method and the non-linear problem has been solved by the relaxed fixed point Algorithm 2.4. The implementation uses the finite element library `Rheolef` and the C++ code is presented with details for this computation in [284, Chap 8].

2.10 Newton Algorithm

Figure 2.9 plots on the left the convergence to zero of the residual terms versus iterations in logarithmic scale. The fixed point algorithm converges linearly. The aim of this section is to study another method that presents superior convergence properties: Fig. 2.9 plots on the right the convergence of the Newton method. The curve is no more a strait line and the convergence is said super-linear. This very fast

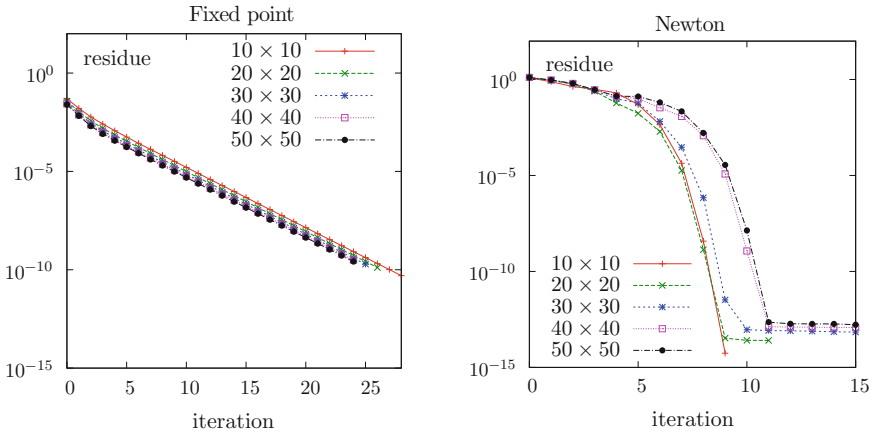

Fig. 2.9 Quasi-Newtonian fluids: convergence rate of the fixed point algorithm (*left*) and the Newton method (*right*), from [284, Chap. 8]

convergence of the residual terms to the machine precision is a definitive advantage of the Newton method, as compared with the fixed point algorithm. Note also that, for both algorithms, the number of iteration for reaching a prescribed precision is roughly mesh invariant.

Let:

$$F(\boldsymbol{u},p) = \begin{pmatrix} F_u(\boldsymbol{u},p) \\ F_p(\boldsymbol{u},p) \end{pmatrix} = \begin{pmatrix} -\mathbf{div}\left\{2\eta(|2D(\boldsymbol{u})|^2)\,D(\boldsymbol{u})\right\} + \nabla p - \rho\boldsymbol{g} \\ -\operatorname{div}\boldsymbol{u} \end{pmatrix} \tag{2.15}$$

With this notation, the problem is rewritten as

(P): find $\chi = (\boldsymbol{u}, p)$ such that $F(\chi) = 0$.

The principle of the Newton method is to build by recurrence a sequence $(\chi_k)_{k\geqslant 0}$. Figure 2.10 represents such a sequence, by plotting $F(\chi)$ versus χ. At step $k \geqslant 0$, assume that χ_k is known, and let us define χ_{k+1}. The tangent at the point $(\chi_k, F(\chi_k))$ is a line, i.e. the set of points (X, Y) such that

$$Y - F(\chi_k) = F'(\chi_k).(X - \chi_k)$$

where $F'(\chi).(\delta\chi)$ denotes the Gâteaux derivative at χ in a direction $\delta\chi$, defined by

$$F'(\chi).(\delta\chi) = \lim_{\varepsilon\to 0} \frac{F(\chi + \varepsilon\,\delta\chi) - F(\chi)}{\varepsilon}$$

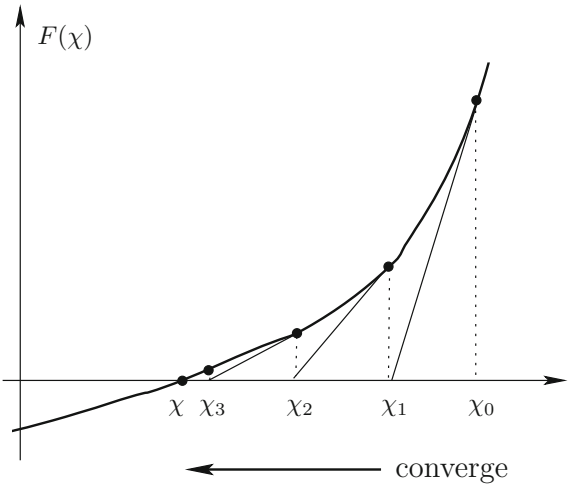

Fig. 2.10 Newton method: construction of a convergent sequence

The next iterate χ_{k+1} is defined such that the tangent line intersects the horizontal axis $Y = 0$ at $(X, Y) = (\chi_{k+1}, 0)$. Thus, χ_{k+1} is characterized by:

$$F'(\chi_k) \,.\, (\chi_{k+1} - \chi_k) = -F(\chi_k)$$

We are able to define an abstract version of the Newton method.

Algorithm 2.5 (*Newton algorithm – abstract version*)

- $k = 0$: let χ_0 being given
- $k \geqslant 0$: let χ_{k-1} being known, find $\delta\chi_k$ such that

$$F'(\chi_k).(\delta\chi_k) = -F(\chi_k)$$

and then

$$\chi_{k+1} = \chi_k + \delta\chi_k$$

While Fig. 2.10 presents a convergent sequence, Fig. 2.11 shows that the sequence is not always convergent: it seems to depend upon its starting point χ_0 and the properties of F. A necessary condition is that $F'(\chi)$ is non-singular for each element χ of the sequence: otherwise the sequence is not computable. This condition is not sufficient: in order to study the convergence properties, some second order derivative information is needed. The classical standard form to include this second order information is via a Lipschitz condition on F' (see e.g. [79, p. 11] or [3]). Nevertheless, in practice, it is difficult to prove the convergence of the sequence by this way and numerical experimentations show that the convergence of the method is very affected by the choice of the starting point χ_0. An efficient remedy is a variant called

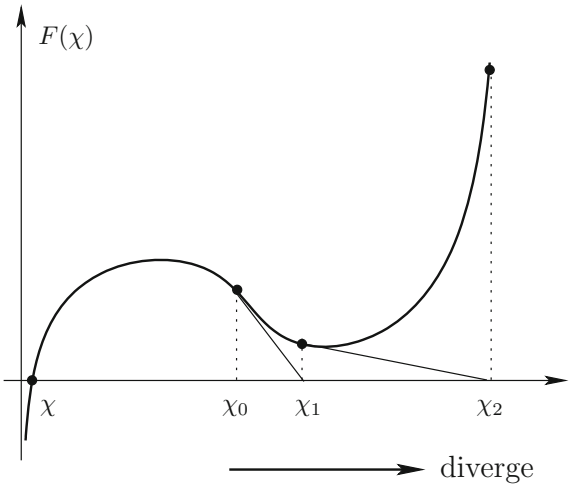

Fig. 2.11 Newton method: a divergent sequence

the *globalized Newton algorithm*, that guaranties that the sequence always converges from any starting point χ_0. This method simply modifies the last step of the algorithm as:

$$\chi_{k+1} = \chi_k + \lambda_k \delta\chi_k$$

where $\lambda_k \in]0, 1]$ is a damp coefficient. This coefficient is adjusted at each iteration and a practical and generic implementation can be found in the `Rheolef` library [284, Chap. 8]. Let us go back to our quasi-Newtonian fluid problem: the function F is defined by (2.15) and it remains to compute F', also called the Jacobian.

$$F'(\boldsymbol{u}, p).(\delta\boldsymbol{u}, \delta p) = \begin{pmatrix} \dfrac{\partial F_u}{\partial u}(\boldsymbol{u}, p).(\delta\boldsymbol{u}) + \dfrac{\partial F_u}{\partial p}(\boldsymbol{u}, p).(\delta p) \\ \dfrac{\partial F_p}{\partial u}(\boldsymbol{u}, p).(\delta\boldsymbol{u}) + \dfrac{\partial F_p}{\partial p}(\boldsymbol{u}, p).(\delta p) \end{pmatrix}$$

There are four directional derivatives to compute. Three of them are obtained without difficulty:

$$\begin{aligned} \frac{\partial F_p}{\partial p}(\boldsymbol{u}, p).(\delta p) &= 0 \\ \frac{\partial F_u}{\partial p}(\boldsymbol{u}, p).(\delta p) &= \nabla(\delta p) \\ \frac{\partial F_p}{\partial u}(\boldsymbol{u}, p).(\delta\boldsymbol{u}) &= -\operatorname{div}(\delta\boldsymbol{u}) \end{aligned}$$

The last one, $\dfrac{\partial F_u}{\partial u}(\boldsymbol{u}, p).(\delta \boldsymbol{u})$, requires more attention. We have

$$F_u(\boldsymbol{u}, p) = -\mathbf{div}\left\{2\eta(|2D(\boldsymbol{u})|^2)\, D(\boldsymbol{u})\right\}$$

Recall the definition of the tensor norm via the double dot product: $|\boldsymbol{\tau}|^2 = (\boldsymbol{\tau} : \boldsymbol{\tau})/2$. Then, we introduce an auxiliary function

$$f(\boldsymbol{u}) = |2D(\boldsymbol{u})|^2 = 2D(\boldsymbol{u}) : D(\boldsymbol{u})$$

Its directional derivative is

$$f'(\boldsymbol{u}).(\boldsymbol{v}) = 4D(\boldsymbol{u}) : D(\boldsymbol{v})$$

Let us introduce a second auxiliary function:

$$g(\boldsymbol{u}) = \eta\left(|2D(\boldsymbol{u})|^2\right) \;=\; (\eta \circ f)(\boldsymbol{u})$$

Its directional derivative is obtained by a derivation of the composition:

$$\begin{aligned} g'(\boldsymbol{u}).(\delta \boldsymbol{u}) &= (\eta' \circ f)(\boldsymbol{u})\; f'(\boldsymbol{u}).(\delta \boldsymbol{u}) \\ &= 4\eta'\left(|2D(\boldsymbol{u})|^2\right)\; (D(\boldsymbol{u}) : D(\delta \boldsymbol{u})) \end{aligned}$$

Finally, F_u expresses as:

$$F_u(\boldsymbol{u}, p) = -\mathbf{div}\left\{2g(\boldsymbol{u})\, D(\boldsymbol{u})\right\}$$

Its directional derivative is obtained by a derivation of the product:

$$\begin{aligned} \frac{\partial F_u}{\partial u}(\boldsymbol{u}, p).(\delta \boldsymbol{u}) &= -\mathbf{div}\left\{(2g'(\boldsymbol{u}).(\delta \boldsymbol{u}))\, D(\boldsymbol{u}) + 2g(\boldsymbol{u})\, D(\delta \boldsymbol{u})\right\} \\ &= -\mathbf{div}\left\{8\eta'(|2D(\boldsymbol{u})|^2)\, (D(\boldsymbol{u}) : D(\boldsymbol{v}))\, D(\boldsymbol{u})\right. \\ &\qquad \left. + 2\eta(|2D(\boldsymbol{u})|^2)\, D(\boldsymbol{v})\right\} \end{aligned}$$

Then, grouping, we obtain an expression of the Jacobian:

$$\begin{aligned} &F'(\boldsymbol{u}, p)(\delta \boldsymbol{u}, \delta p) \\ &= \begin{pmatrix} -\mathbf{div}\left\{2\eta(|2D(\boldsymbol{u})|^2)\, D(\delta \boldsymbol{u}) + 8\eta'(|2D(\boldsymbol{u})|^2)\, (D(\boldsymbol{u}) : D(\delta \boldsymbol{u}))\, D(\boldsymbol{u})\right\} + \nabla(\delta p) \\ -\operatorname{div}(\delta \boldsymbol{u}) \end{pmatrix} \end{aligned}$$

From the abstract version of the Newton algorithm, we obtain a concrete version for quasi-Newtonian fluids.

Algorithm 2.6 (*Newton algorithm – quasi-Newtonian fluids*)

- $k = 0$: let $(\boldsymbol{u}_0, p_0)$ being given, e.g. a Newtonian solution
- $k \geqslant 0$: let $(\bar{\boldsymbol{u}}, \bar{p}) = \left(\boldsymbol{u}^k, p_k\right)$ being the known current solution

1) compute the residue $(\boldsymbol{r}_u, r_p) = F(\bar{\boldsymbol{u}}, \bar{p})$
2) then, find the correction $(\delta\boldsymbol{u}, \delta p)$ such that

$$\begin{aligned} -\mathbf{div}\left\{2\eta(|2D(\bar{\boldsymbol{u}})|^2)\, D(\delta\boldsymbol{u}) + 8\eta'(|2D(\bar{\boldsymbol{u}})|^2)\, (D(\bar{\boldsymbol{u}}) : D(\delta\boldsymbol{u}))\; D(\bar{\boldsymbol{u}})\right\} & \\ +\nabla(\delta p) &= -\boldsymbol{r}_u \text{ in } \Omega \\ -\operatorname{div}(\delta\boldsymbol{u}) &= -r_p \text{ in } \Omega \\ \delta\boldsymbol{u} &= 0 \text{ on } \partial\Omega \end{aligned}$$

3) finally, apply the correction

$$\begin{aligned} \boldsymbol{u}_{k+1} &= \boldsymbol{u}_k + \delta\boldsymbol{u} \\ p_{k+1} &= p_k + \delta p \end{aligned}$$

This algorithm performs at each iteration three step. The first one is the computation of the residue, that could be used for a stopping criterion. The second step solves a linear system in order to compute the correction $(\delta\boldsymbol{u}, \delta p)$: this is the more computing time consuming step of the algorithm. The last step is simply an update, applying the correction.

The linear system concentrates now all our attention. In order to easily discretize this system, e.g. by a finite element method, we aim at obtaining a variational formulation. Let us introduce the following forms:

$$\begin{aligned} \tilde{a}(\bar{\boldsymbol{u}}; \delta\boldsymbol{u}, \delta\boldsymbol{v}) = & \int_\Omega 2\eta(|2D(\bar{\boldsymbol{u}})|^2)\, (D(\delta\boldsymbol{u}) : D(\delta\boldsymbol{v}))\, \mathrm{d}x \\ & + \int_\Omega 2\eta'(|2D(\bar{\boldsymbol{u}})|^2)\, (2D(\bar{\boldsymbol{u}}) : D(\delta\boldsymbol{u}))\, (2D(\bar{\boldsymbol{u}}) : D(\delta\boldsymbol{v}))\, \mathrm{d}x \\ b(\delta\boldsymbol{v}, \delta q) = & -\int_\Omega \delta q \operatorname{div}(\delta\boldsymbol{v})\, \mathrm{d}x \\ \ell_u(\delta\boldsymbol{v}) = & -\int_\Omega \boldsymbol{r}_u . \delta\boldsymbol{v}\, \mathrm{d}x \\ \ell_p(\delta q) = & -\int_\Omega r_p\, \delta q\, \mathrm{d}x \end{aligned}$$

The variational formulation of the linear problem involved by the Newton method writes:

(FV): find $\delta\boldsymbol{u} \in \left(H_0^1(\Omega)\right)^3$ and $\delta p \in L^2(\Omega)$ such that

$$\begin{cases} \tilde{a}(\bar{\boldsymbol{u}};\ \delta\boldsymbol{u},\ \delta\boldsymbol{v}) + b(\delta\boldsymbol{v},\ \delta p) = \ell_u(\delta\boldsymbol{v}), & \forall \delta\boldsymbol{v} \in \left(H_0^1(\Omega)\right)^3 \\ b(\delta\boldsymbol{u},\ \delta q) = \ell_p(\delta q), & \forall \delta q \in L^2(\Omega) \end{cases}$$

This problem appears as Stokes-like one. As the $a(.;.,.)$ involves some complex expressions, it is not clear whether is expression is well defined and if the problem is well posed. In order to give an answer to this question, we introduce some additional mathematical tools.

Definition 2.8 (*Lebesgue space*)

$$L^\infty(\Omega) = \left\{ \varphi : \Omega \to \mathbb{R};\ \sup_{\boldsymbol{x}\in\Omega} \text{ess}\ |\varphi(\boldsymbol{x})| < +\infty \right\}$$

This is the space of bounded functions in Ω, at least almost everywhere. Note that this definition extends the space $L^r(\Omega)$, introduced at Definition 2.6, p. 74, to the case $r = \infty$.

Definition 2.9 (*Sobolev space*)

$$W^{1,\infty}(\Omega) = \left\{ \varphi \in L^\infty(\Omega);\ \nabla\varphi \in \left(L^\infty(\Omega)\right)^3 \right\}$$

This is the space of functions with bounded gradients in Ω, at least almost everywhere. Also, this definition extends the space $W^{1,r}(\Omega)$, introduced at Definition 2.7, p. 74, to the case $r = \infty$. See [36] for complements about these spaces. Note that when $\bar{\boldsymbol{u}} \in \left(W^{1,\infty}(\Omega)\right)^3$, then $\tilde{a}(\bar{\boldsymbol{u}};\ \delta\boldsymbol{u},\ \delta\boldsymbol{v})$ is well defined, i.e. the integrals involved in the definition of $\tilde{a}$ are bounded for any $\delta\boldsymbol{u},\ \delta\boldsymbol{v} \in \left(H_0^1(\Omega)\right)^3$.

Theorem 2.2 (well-posedness of the subproblem)
Let $\bar{\boldsymbol{u}} \in \left(W^{1,\infty}(\Omega)\right)^3$. Suppose that $\tilde{a}(\bar{\boldsymbol{u}};.;.)$ is coercive in $\left(H_0^1(\Omega)\right)^3$ with respect to its second and third arguments. Then the sequence defined by the Newton method is well-defined.

Proof Each iteration of the Newton method involves a Stokes-like linear system, that falls intro the framework of mixed problems. A sufficient condition for this system to be well-posed [38] is that the $\tilde{a}$ form is coercive with respect to its second and third arguments. As this property is assumed by the theorem, the linear system are always well-posed and the sequence defined by the Newton method is then well-defined. □

It remains to study the coercivity of the $\tilde{a}$ form.

Lemma 2.1 (coercivity for shear-thickening fluids)
Let $\bar{\boldsymbol{u}} \in \left(W^{1,\infty}(\Omega)\right)^3$. Assume $\eta' > 0$ and either $\eta(0) > 0$ or $\inf \text{ess}_\Omega\ |D(\bar{\boldsymbol{u}})| > 0$. Then the $\tilde{a}(\bar{\boldsymbol{u}};.;.)$ form is coercive with respect to its second and third arguments.

Proof Recall the definition of the tensor norm via the double dot product: $|\boldsymbol{\tau}|^2 = (\boldsymbol{\tau}:\boldsymbol{\tau})/2$. Then, from the definition of $\tilde{a}$, we have:

$$\begin{aligned}\tilde{a}(\bar{\boldsymbol{u}};\delta\boldsymbol{u},\delta\boldsymbol{u}) = &\int_\Omega \eta(|2D(\bar{\boldsymbol{u}})|^2)\ \left(\frac{2D(\delta\boldsymbol{u}):2D(\delta\boldsymbol{u})}{2}\right)\mathrm{d}x\\ &+\int_\Omega 2\eta'(|2D(\bar{\boldsymbol{u}})|^2)\ \left(\frac{2D(\bar{\boldsymbol{u}}):2D(\delta\boldsymbol{u})}{2}\right)^2\mathrm{d}x\\ = &\int_\Omega \eta(|2D(\bar{\boldsymbol{u}})|^2)\ |D(\delta\boldsymbol{u})|^2\,\mathrm{d}x\\ &+\int_\Omega 2\eta'(|2D(\bar{\boldsymbol{u}})|^2)\ \left(\frac{2D(\bar{\boldsymbol{u}}):2D(\delta\boldsymbol{u})}{2}\right)^2\mathrm{d}x \qquad (2.16)\end{aligned}$$

As $\eta' > 0$ we get

$$\begin{aligned}\tilde{a}(\bar{\boldsymbol{u}};\delta\boldsymbol{u},\delta\boldsymbol{u}) &\geqslant \int_\Omega \eta(|2D(\bar{\boldsymbol{u}})|^2)\ |D(\delta\boldsymbol{u})|^2\,\mathrm{d}x\\ &\geqslant \inf_{\boldsymbol{x}\in\Omega}\operatorname{ess}\eta(|2D(\bar{\boldsymbol{u}})(\boldsymbol{x})|^2)\ \ \|2D(\delta\boldsymbol{u})\|^2_{L^2(\Omega)}\\ &\geqslant c_0^2\ \ \inf_{\boldsymbol{x}\in\Omega}\operatorname{ess}\eta(|2D(\bar{\boldsymbol{u}})(\boldsymbol{x})|^2)\ \ \|\delta\boldsymbol{u}\|^2_{H^1(\Omega)}\end{aligned}$$

where $c_0 > 0$ is the constant of the Lemma 1.2, p. 34. As η is a strictly increasing and non-negative function, we have

$$\tilde{a}(\bar{\boldsymbol{u}};\delta\boldsymbol{u},\delta\boldsymbol{u}) \geqslant c_0^2\ \eta(\xi_0)\ \ \|\delta\boldsymbol{u}\|^2_{H^1(\Omega)}$$

with $\xi_0 = \inf\operatorname{ess}_{\boldsymbol{x}\in\Omega}|2D(\bar{\boldsymbol{u}})(\boldsymbol{x})|^2$. By the assumption of the lemma, either $\xi_0 > 0$ and then $\eta(\xi_0) > 0$ or $\xi_0 = 0$ and $\eta(0) > 0$. In all cases, the form is coercive, with a coercivity constant $\alpha = c_0^2\eta(\xi_0) > 0$. □

Lemma 2.2 (coercivity for shear-thinning fluids)
Let $\bar{\boldsymbol{u}} \in \left(W^{1,\infty}(\Omega)\right)^3$.

Let

$$\nu(\xi) = \eta(\xi) + 2\eta'(\xi)\,\xi,\ \ \forall\xi\in\mathbb{R}^+$$

Assume $\eta' < 0$ *and either* $\nu > 0$ *or* $\nu \geqslant 0$ *and* $\nu' < 0$. *Then the* $\tilde{a}(\bar{\boldsymbol{u}};.;.)$ *is coercive with respect to its second and third arguments.*

Proof From Cauchy-Schwartz inequality:

$$\begin{aligned}\left(\frac{2D(\bar{\boldsymbol{u}}):2D(\delta\boldsymbol{u})}{2}\right)^2 &\leqslant \left(\frac{2D(\bar{\boldsymbol{u}}):2D(\bar{\boldsymbol{u}})}{2}\right)^2\left(\frac{2D(\delta\boldsymbol{u}):2D(\delta\boldsymbol{u})}{2}\right)^2\\ &= |2D(\bar{\boldsymbol{u}})|^2\ \ |2D(\delta\boldsymbol{u}))|^2\end{aligned}$$

Then, from (2.16) and using $\eta' < 0$, we get:

$$\begin{aligned}\tilde{a}(\bar{\boldsymbol{u}};\delta\boldsymbol{u},\delta\boldsymbol{u}) &\geqslant \int_\Omega \left\{\eta(|2D(\bar{\boldsymbol{u}})|^2) + 2\eta'(|2D(\bar{\boldsymbol{u}})|^2)\ |2D(\bar{\boldsymbol{u}})|^2\right\}\ |2D(\delta\boldsymbol{u})|^2\,\mathrm{d}x\\ &= \int_\Omega \nu(|2D(\bar{\boldsymbol{u}})|^2)\ |2D(\delta\boldsymbol{u})|^2\,\mathrm{d}x\\ &\geqslant \inf_{\boldsymbol{x}\in\Omega}\operatorname{ess}\nu(|2D(\bar{\boldsymbol{u}})(\boldsymbol{x})|^2)\ \ \|2D(\delta\boldsymbol{u})\|^2_{L^2(\Omega)}\\ &\geqslant c_0^2\ \inf_{\boldsymbol{x}\in\Omega}\operatorname{ess}\nu(|2D(\bar{\boldsymbol{u}})(\boldsymbol{x})|^2)\ \ \|\delta\boldsymbol{u}\|^2_{H^1(\Omega)}\end{aligned}$$

Let $\xi_0 = \inf \operatorname{ess}_{\boldsymbol{x}\in\Omega}|2D(\bar{\boldsymbol{u}})(\boldsymbol{x})|^2$ and $\xi_1 = \sup \operatorname{ess}_{\boldsymbol{x}\in\Omega}|2D(\bar{\boldsymbol{u}})(\boldsymbol{x})|^2$. Since $\bar{\boldsymbol{u}} \in \left(W^{1,\infty}(\Omega)\right)^3$, we have $\xi_1 = \|2D(\bar{\boldsymbol{u}})\|^2_{L^\infty(\Omega)} < +\infty$. When $\nu > 0$ then the coercivity is immediate. Otherwise, assume $\nu \geqslant 0$ and $\nu' < 0$. Then, as ν is a strictly decreasing function:

$$\inf_{\boldsymbol{x}\in\Omega}\operatorname{ess}\nu(|2D(\bar{\boldsymbol{u}})(\boldsymbol{x})|^2) \geqslant \nu(\xi_1)$$

As ν is strictly decreasing and positive, and ξ_1 is finite, then $\nu(\xi_1) > 0$ and the proof is complete. □

Note that Lemma 2.2 for shear-thickening fluids requires a strong assumption on $\bar{\boldsymbol{u}}$, namely $\inf \operatorname{ess}_\Omega |D(\bar{\boldsymbol{u}})| > 0$. It means that the rate of deformation tensor may be always nonzero, which is not physically relevant. For instance $D(\bar{\boldsymbol{u}})$ could vanishes on boundaries or symmetry axis. Conversely, Lemma 2.2 do not need such assumption and the sequence of the Newton method to be well-defined with more restrictive assumptions. Recall that the most physically relevant case is the shear-thinning case and this is a good news for practical applications. Let us study whether these assumptions lemma are satisfied by the two classical examples of viscosity functions, namely the power law and the Carreau's law.

Corollary 2.1 (power law)
For the power law (2.2)*, when* $n < 1$*, the sequence defined by the Newton method is well-defined.*

Proof From (2.2), we have

$$\begin{aligned}\eta'(\xi) &= \frac{(-1+n)K}{2}\xi^{\frac{-3+n}{2}} < 0, \quad \forall \xi > 0\\ \nu(\xi) &= nK\xi^{\frac{-1+n}{2}} \geqslant 0, \quad \forall \xi \geqslant 0\\ \nu'(\xi) &= \frac{n(-1+n)K}{2}\xi^{\frac{-3+n}{2}} < 0, \quad \forall \xi > 0\end{aligned}$$

Then, assumptions of Lemma 2.2 applies and the result follows from Theorem 2.2. □

Corollary 2.2 (Carreau's law)
For the Carreau's law (2.2)*, when* $n < 1$ *or* $n > 1$ *and* $\eta_0 > 0$*, the sequence defined by the Newton method is well-defined.*

Proof From (2.3), we have

$$\begin{aligned}
\eta'(\xi) &= \frac{(-1+n)\lambda}{2}(\eta_0 - \eta_\infty)(1+\lambda\xi)^{\frac{-3+n}{2}} \\
\nu(\xi) &= \eta_\infty + n\lambda(\eta_0 - \eta_\infty)(1+\lambda\xi)^{\frac{-1+n}{2}} \geqslant 0, \quad \forall \xi \in \mathbb{R}^+ \\
\nu'(\xi) &= \frac{n(-1+n)\lambda^2}{2}(\eta_0 - \eta_\infty)(1+\lambda\xi)^{\frac{-3+n}{2}}
\end{aligned}$$

When $n > 1$ and $\eta_0 > 0$, assumptions of Lemma 2.1 applies. Otherwise, when $n < 1$, assumptions of Lemma 2.2 applies. In both cases, the form is coercive and the result follows from Theorem 2.2. □

2.11 Notes

Starting from a software that solves the Navier-Stokes equation, quasi-Newtonian models can be easily implemented via the fixed point algorithm by updating the viscosity function at each iteration. The relaxed version of the fixed point algorithm enables some improvements of the convergence. Nevertheless, for serious application, the Newton method is more efficient. Since the viscosity is expected to vary in a very large range, particularly for the power law viscosity function that is unbounded, the linear Stokes subproblems of both the fixed point and the Newton algorithms are very ill conditioned. Thus, the direct Stokes solver is the method of predilection for medium sized problems. However, for some large scale problems, e.g. three-dimensional ones, iterative solvers could be preferred: they should be combined with an efficient preconditioner that takes into account the large variations of the viscosity. Such iterative solvers are proposed by many authors [128, 147, 219] for the nonlinear Stokes problem or the Jacobian of the Newton method. Section 2.9 showed that quasi-Newtonian power law fluids could also be viewed as a generalization of the well-known p-Laplacian problem. This link with the p-Laplacian problem is fruitful, as many numerical methods was tested on the p-Laplacian problem. In 1983, Fortin and Glowinski [107, p. 173] suggested to solve this problem by an augmented Lagrangian approach, but, as convergence properties of this method bases on the fixed point theorem, there is few hope to improve significantly the fixed point algorithm. Recent works focused on the Newton method. For instance, inexact Newton methods, where the Jacobian is approximately solved, are investigated in 2013 by Ern and Vohralík [91, 92] for the p-Laplacian problem.

Chapter 3
Viscoplastic Fluids

A toothpaste flows like a liquid through the squeezed tube and spreads over the toothbrush where it will remain at rest while the brush is brought up to the mouth. Then, it is largely deformed once again by agitation and friction against the teeth. Consider next an hair gel: it can flow easily like a simple viscous liquid if mixed with a spoon, but the bubbles formed within it will subsequently remain in the same place for years, as they would in a solid. Viscoplastic materials maintain their shape in the same way as solids under the effects of gravity, and yet are able to flow like liquids, i.e., deforming significantly when subject to a high enough stress. There is no phase transition, such as the transition between water and ice: once at rest the material presents the properties it had before flowing in the liquid regime. We are thus dealing with fluids in the sense that these materials can undergo any type of deformation without losing their intrinsic mechanical properties. According to the above description it is natural to distinguish two main states: a solid regime and a liquid regime. Thus the fundamental feature of these fluids is that they are able to flow (i.e., deform indefinitely) only if they are submitted to a stress above a critical value. Otherwise they deform in a finite way like solids.

These two examples of our daily experience point out the main feature of viscoplastic flows. The study of viscoplastic fluids is also motivated by many geophysical applications such as landslides, mud flows, snow avalanches and volcanic lava flows. The stability of building foundations in civil engineering and mechanical robustness of engine parts could also be formulated as viscoplastic flow problems. The flow characteristics of viscoplastic fluids are difficult to predict as they involve permanent or transient solid and liquid regions that are generally impossible to locate a priori. From mathematical point of view, these complex fluids are defined by a non-differentiable minimization problem and the corresponding constitutive equations are highly non-linear. For simple flows, as Poiseuille or Couette flows, explicit solution are exhibited. For more complex flows, the explicit computation of the solution is no more possible. In that case, classical numerical methods are no more possible for

P. Saramito, *Complex fluids*, Mathématiques et Applications 79,
DOI 10.1007/978-3-319-44362-1_3

such fluids: the numerical resolution requires some specific approaches. Two main classes of numerical algorithms are presented: the regularization approach and the augmented Lagrangian algorithm. This second approach uses some convex analysis tools that are developed in this chapter. The chapter closes with examples of numerical computations in a square pipe section, around an obstacle and in a driven cavity. This last example presents the combined effects of viscoplasticity and inertia.

3.1 Energy of Dissipation

For simplicity, we assume in this chapter that the density ρ is constant. This is a common assumption for isothermal liquids, in view of application of viscoplastic fluids. All the algorithms developed in this chapters extended to the case of compressible fluids. As in the previous chapter, the mass and momentum conservation equations (1.3) and (1.17) are completed with (1.22) for the Cauchy stress tensor. Thus, with these three unknowns, there are four unknowns, the velocity $\boldsymbol{u}$, the pressure p, the Cauchy stress tensor $\boldsymbol{\sigma}_{\text{tot}}$, and the stress deviator $\boldsymbol{\sigma}$. In order to close the system of equations, in the previous chapter, we provided a relation between the stress deviator $\boldsymbol{\sigma}$ and the rate of deformation $D(\boldsymbol{u})$. In this chapter, an additional highly non-linear relation will be provided in an indirect way. The main idea of viscoplastic fluid problem is to directly define the minimization problem with the help of an energy of dissipation function, while the relation between the stress deviator $\boldsymbol{\sigma}$ and the rate of deformation $D(\boldsymbol{u})$ will be deduced later. Recall the definition of the tensor norm via the double dot product: $|\boldsymbol{\delta}|^2 = (\boldsymbol{\delta}:\boldsymbol{\delta})/2$ for any $\boldsymbol{\delta} \in \mathbb{R}^{3\times 3}_s$.

Definition 3.1 (*Energy of dissipation*)

$$\mathscr{D}(\boldsymbol{\delta}) = \frac{K}{1+n}|2\boldsymbol{\delta}|^{1+n} + \sigma_0|2\boldsymbol{\delta}|, \quad \forall \boldsymbol{\delta} \in \mathbb{R}^{3\times 3}_s \tag{3.1}$$

where σ_0 is a positive constant called the *yield stress*. The parameters $n > 0$ is the power law index and $K > 0$ the consistency, as for quasi-Newtonian fluids defined by a power law viscosity.

Let us introduce the following functional, defined for all vector field $\boldsymbol{v}$ by

$$\begin{aligned} J(\boldsymbol{v}) &= \int_\Omega \mathscr{D}(D(\boldsymbol{v}))\,\mathrm{d}x - \int_\Omega \boldsymbol{f}.\boldsymbol{v}\,\mathrm{d}x \\ &= \frac{K}{1+n}\int_\Omega |2D(\boldsymbol{v})|^{1+n}\,\mathrm{d}x + \sigma_0 \int_\Omega |2D(\boldsymbol{v})|\,\mathrm{d}x - \int_\Omega \boldsymbol{f}.\boldsymbol{v}\,\mathrm{d}x \end{aligned} \tag{3.2}$$

Neglecting inertia terms, the stationary flow of a viscoplastic fluid is characterized as the solution of the following minimization problem:

$$\boldsymbol{u} = \underset{\boldsymbol{v}\in K(\boldsymbol{u}_\Gamma)}{\arg\inf}\ J(\boldsymbol{v})$$

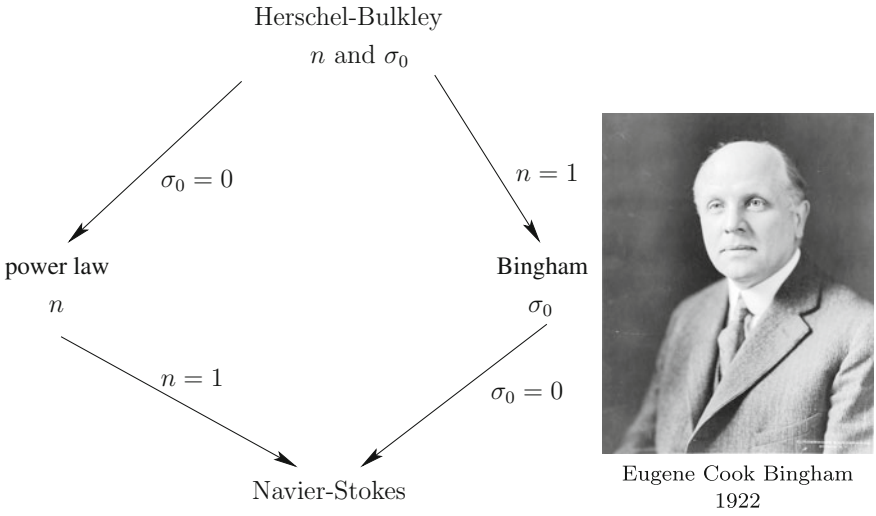

Fig. 3.1 (*Left*) viscoplastic fluids: a hierarchy of models; (*right*) E.C. Bingham (photo: Smithsonian museum, USA)

where $K(\boldsymbol{u}_\Gamma)$ denotes as usual the set of divergence-free vector fields that satisfies the boundary condition $\boldsymbol{u} = \boldsymbol{u}_\Gamma$ on $\partial\Omega$. The relation of the present fluid model with those of the previous chapters is represented on Fig. 3.1. When the power law index $n = 1$, the model is called the Bingham model and was introduced in 1922 by Bingham [26]. The present fluid model with $n > 0$ is called the Herschel–Bulkley model [142] and was introduced in 1926 by Herschel and Bulkley as an extension of the Bingham model. The development of viscoplastic model based on yield stress really started earlier: in 1900, when Schwedoff [291], while studying a gelatin suspension, proposed a more complex model, combining yield stress and elastic relaxation effects. Note that when $\sigma_0 = 0$, the present problem reduces to a quasi-Newtonian fluid flow problem with a power law viscosity function, as studied in the previous chapter: the J functional defined by (3.2) reduces to those defined in relation (2.12), p. 73. When both $\sigma_0 = 0$ and $n = 1$ the model describes a Newtonian fluid, represented by the Navier–Stokes equations.

3.2 Subdifferential

In the previous chapter, by differentiating J, we obtained the variational formulation, as $J'(\boldsymbol{u}).(\boldsymbol{v}) = 0$ for all test function $\boldsymbol{v}$. Here, there is a major difficulty, as J is not differentiable when $\sigma_0 \neq 0$. In order to understand the difficulty, let us consider the following function:

$$j(x) = \frac{K}{1+n}|x|^{1+n} + \sigma_0|x| - fx, \quad \forall x \in \mathbb{R}$$

The absolute value is not differentiable at $x = 0$ and so is the j function. As J is not differentiable we are not able to write a variational formulation by this way, and also, we are not able to write the set of equations for describing the fluid. The situation could appear as desperate, but there is a known remedy: to extend the definition of differentiation to any convex function. This is the notion of *subdifferential*, well-known in optimization and convex analysis.

The subdifferential is represented on Fig. 3.2. It is defined as the set of all the directions of strait lines passing in a point of the curve and that are globally below this curve.

Definition 3.2 (*Subdifferential*)
The subdifferential $\partial\mathscr{D}$ of a convex function $\mathscr{D}$ defined in $\mathbb{R}^{3\times3}_s$ is given by

$$\partial\mathscr{D}(\boldsymbol{\delta}_0) = \left\{\boldsymbol{\sigma} \in \mathbb{R}^{3\times3}_s;\ \mathscr{D}(\boldsymbol{\delta}_0) + \boldsymbol{\sigma} : (\boldsymbol{\delta} - \boldsymbol{\delta}_0) \leqslant \mathscr{D}(\boldsymbol{\delta}),\ \forall \boldsymbol{\delta} \in \mathbb{R}^{3\times3}_s\right\}$$

From Fig. 3.2, observe that the subdifferential can also be defined as the convex envelop of all directional – left and right – derivatives. This observation is the basis of the extension of generalized derivatives for non-convex functions, as proposed in 1990 by Clarkes [59]. As we do only consider convex energy functions in this chapter, the concept of subdifferential is sufficient for our purpose.

The major interest of subdifferential is the possibility to characterize the minimum of a convex function.

Theorem 3.1 (Characterization of the minimum)
For any convex function $\mathscr{D}$, $\boldsymbol{\delta}_0$ is a minimum of $\mathscr{D}$ if and only if $0 \in \partial\mathscr{D}(\boldsymbol{\delta}_0)$.

This result may be interpreted with the help of the graphical representation. Recall that all tangents at point $(\boldsymbol{\delta}_0, \mathscr{D}(\boldsymbol{\delta}_0))$ with direction $\boldsymbol{\sigma} \in \partial\mathscr{D}(\boldsymbol{\delta}_0)$ are below the convex

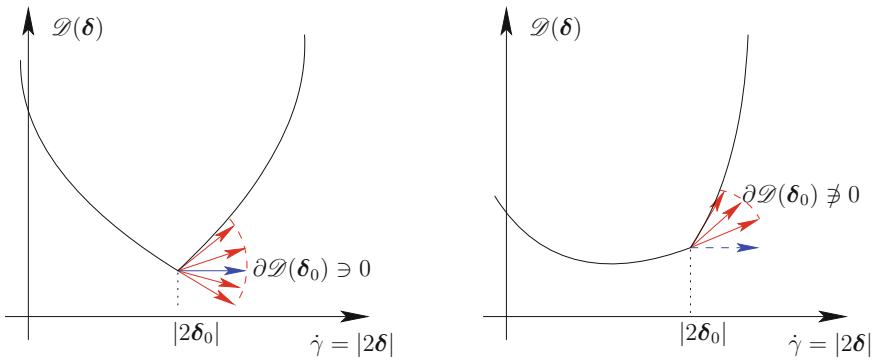

Fig. 3.2 Subdifferential of a convex function and its minimization

curve. If $0 \in \partial\mathscr{D}(\boldsymbol{\delta}_0)$, then the horizontal tangent is below the curve, and thus the point is a minimum.

As subdifferential is a major concept in this chapter, let us study some examples.

Example 3.1 (*Differentiable function*)

$$\begin{aligned} j(x) &\quad \text{is differentiable,} \quad \forall x \in \mathbb{R} \\ \partial j(x) &= \left\{ j'(x) \right\} \end{aligned}$$

Example 3.2 (*Almost differentiable function*)

$$j(x) \quad \text{is differentiable,} \quad \forall x \in \mathbb{R} \backslash \{x_0\}$$

$$\partial j(x) = \begin{cases} \left\{ j'(x) \right\} & \text{when } x \neq x_0 \\ \left[j'_-(x_0),\, j'_+(x_0) \right] & \text{when } x = x_0 \end{cases}$$

where $j'_-(x_0)$ and $j'_+(x_0)$ denotes the left and right derivatives at x_0, respectively.

Example 3.3 (*Subdifferential of the absolute value*)

$$j(x) = |x|, \quad \forall x \in \mathbb{R}$$

$$\partial j(x) = \begin{cases} \left\{ \dfrac{x}{|x|} \right\} & \text{when } x \neq 0 \\ [-1,\, 1] & \text{when } x = 0 \end{cases}$$

Example 3.4 (*Subdifferential of a combination with the absolute value*)

$$j(x) = \frac{|x|^{1+n}}{1+n} + |x|, \quad \forall x \in \mathbb{R}$$

$$\partial j(x) = \begin{cases} \left\{ x|x|^{-1+n} + \dfrac{x}{|x|} \right\} & \text{when } x \neq 0 \\ [-1,\, 1] & \text{when } x = 0 \end{cases}$$

After these preliminary examples, let us turn now to the more complex case of functions with a matrix argument.

Lemma 3.1 (Differentiable function with a matrix argument)
Let $f(\boldsymbol{\delta}) = |2\boldsymbol{\delta}|^2$, *for all* $\boldsymbol{\delta} \in \mathbb{R}^{3\times3}_s$. *Then* f *is differentiable and* $f'(\boldsymbol{\delta}) = 4\boldsymbol{\delta}$.

Proof Recall the definition of the tensor norm via the double dot product: $|\boldsymbol{\tau}|^2 = (\boldsymbol{\tau} : \boldsymbol{\tau})/2$ for any $\boldsymbol{\tau} \in \mathbb{R}^{3\times3}_s$. Then

$$
\begin{aligned}
f(\boldsymbol{\delta}) = |2\boldsymbol{\delta}|^2 \;&=\; \frac{2\boldsymbol{\delta}:2\boldsymbol{\delta}}{2} \;=\; 2\boldsymbol{\delta}:\boldsymbol{\delta} \\
\Longrightarrow\; f'(\boldsymbol{\delta}).(\boldsymbol{\xi}) &= 4\boldsymbol{\delta}:\boldsymbol{\xi}, \quad \forall \boldsymbol{\xi} \in \mathbb{R}^{3\times 3}_s \\
f'(\boldsymbol{\delta}) &= 4\boldsymbol{\delta}
\end{aligned}
$$

□

Lemma 3.2 (Matrix argument – continued)
Let $\mathscr{D}_1(\boldsymbol{\delta}) = \dfrac{K}{1+n}|2\boldsymbol{\delta}|^{1+n}$ *for all* $\boldsymbol{\delta} \in \mathbb{R}^{3\times 3}_s$. *Then* $\mathscr{D}_1$ *is differentiable and* $\mathscr{D}_1'(\boldsymbol{\delta}) = K\ |2\boldsymbol{\delta}|^{-1+n}\ 2\boldsymbol{\delta}$.

Proof Using the previous Lemma 3.1, we have:

$$
\begin{aligned}
\mathscr{D}_1(\boldsymbol{\delta}) = \frac{K}{1+n}|2\boldsymbol{\delta}|^{1+n} \;&=\; \frac{K}{1+n}\ f(\boldsymbol{\delta})^{\frac{1+n}{2}} \\
\mathscr{D}_1'(\boldsymbol{\delta}).(\boldsymbol{\xi}) = \frac{K}{2}\ f(\boldsymbol{\delta})^{\frac{-1+n}{2}}\ f'(\boldsymbol{\delta}).(\boldsymbol{\xi}) \;&=\; K\ |2\boldsymbol{\delta}|^{-1+n}\ 2\boldsymbol{\delta}:\boldsymbol{\xi} \\
\mathscr{D}_1'(\boldsymbol{\delta}) &= K\ |2\boldsymbol{\delta}|^{-1+n}\ 2\boldsymbol{\delta}
\end{aligned}
$$

□

Lemma 3.3 (Non-differentiable function with a matrix argument)
Let $\mathscr{D}_2$ *be the following non-differentiable function, defined for all* $\boldsymbol{\delta} \in \mathbb{R}^{3\times 3}_s$ *by*

$$\mathscr{D}_2(\boldsymbol{\delta}) = \sigma_0|2\boldsymbol{\delta}|$$

Then, its subdifferential is given by

$$
\partial\mathscr{D}_2(\boldsymbol{\delta}) = \begin{cases} \left\{\sigma_0\ \dfrac{2\boldsymbol{\delta}}{|2\boldsymbol{\delta}|}\right\} & \text{when } \boldsymbol{\delta} \neq 0 \\ \left\{\boldsymbol{\sigma} \in \mathbb{R}^{3\times 3}_s \ /\ |\boldsymbol{\sigma}| \leqslant \sigma_0\right\} & \text{when } \boldsymbol{\delta} = 0 \end{cases}
$$

Proof Using the notations of Lemma 3.1, we have: $\mathscr{D}_2(\boldsymbol{\delta}) = \sigma_0|2\boldsymbol{\delta}| \;=\; \sigma_0\ f(\boldsymbol{\delta})^{\frac{1}{2}}$. Let us consider first the simplest case when the matrix argument is not zero.

$$
\begin{aligned}
\mathscr{D}_2'(\boldsymbol{\delta}).(\boldsymbol{\xi}) = \sigma_0\ f(\boldsymbol{\delta})^{-\frac{1}{2}}\ f'(\boldsymbol{\delta}).(H) \;&=\; \sigma_0\ \frac{2\boldsymbol{\delta}:H}{|2\boldsymbol{\delta}|} \text{ when } \boldsymbol{\delta} \neq 0 \\
\mathscr{D}_2'(\boldsymbol{\delta}) = \sigma_0\ \frac{2\boldsymbol{\delta}}{|2\boldsymbol{\delta}|} &\text{ when } \boldsymbol{\delta} \neq 0
\end{aligned}
$$

When $\boldsymbol{\delta} = 0$, let us show that

$$\partial\mathscr{D}_2(0) = \left\{\boldsymbol{\sigma} \in \mathbb{R}^{3\times 3}_s \ /\ |\boldsymbol{\sigma}| \leqslant \sigma_0\right\}$$

The proof of this result is done in two steps. We fist assume that $|\boldsymbol{\sigma}| \leqslant \sigma_0$ and show that then $\boldsymbol{\sigma} \in \partial \mathscr{D}_2(0)$. Next, we show the reciprocal.

Step (1) Assume $|\boldsymbol{\sigma}| \leqslant \sigma_0$. By Definition 3.2 of the subdifferential:

$$\begin{aligned}\boldsymbol{\sigma} \in \partial \mathscr{D}_2(0) &\Longleftrightarrow \mathscr{D}_2(0) + \boldsymbol{\sigma} : (\boldsymbol{\delta} - 0) \leqslant \mathscr{D}_2(\boldsymbol{\delta}), \quad \forall \boldsymbol{\delta} \in \mathbb{R}^{3\times 3}_s \\ &\Longleftrightarrow \boldsymbol{\sigma} : \boldsymbol{\delta} \leqslant \sigma_0 |2\boldsymbol{\delta}| \text{ with } \mathscr{D}_2(\boldsymbol{\delta}) = \sigma_0 |2\boldsymbol{\delta}|\end{aligned}$$

From the Cauchy–Schwartz inequality:

$$\begin{aligned}\boldsymbol{\sigma} : \boldsymbol{\delta} &\leqslant (\boldsymbol{\sigma} : \boldsymbol{\sigma})^{\frac{1}{2}} (\boldsymbol{\delta} : \boldsymbol{\delta})^{\frac{1}{2}} \\ &= 2 \left(\frac{\boldsymbol{\sigma} : \boldsymbol{\sigma}}{2} \right)^{\frac{1}{2}} \left(\frac{\boldsymbol{\delta} : \boldsymbol{\delta}}{2} \right)^{\frac{1}{2}} \\ &= 2|\boldsymbol{\sigma}| \, |\boldsymbol{\delta}| \quad \text{with } |\boldsymbol{\sigma}| = \left(\frac{\boldsymbol{\sigma} : \boldsymbol{\sigma}}{2} \right)^{\frac{1}{2}} \\ &= |\boldsymbol{\sigma}| \, |2\boldsymbol{\delta}| \\ &\leqslant \sigma_0 \, |2\boldsymbol{\delta}| \quad \text{from assumption}\end{aligned}$$

Then $|\boldsymbol{\sigma}| \leqslant \sigma_0 \Longrightarrow \boldsymbol{\sigma} \in \partial \mathscr{D}_2(0)$
Step (2) Reciprocal. By contraposition:

$$\begin{aligned}\boldsymbol{\sigma} \in \partial \mathscr{D}_2(0) &\Longrightarrow |\boldsymbol{\sigma}| \leqslant \sigma_0 \\ \Longleftrightarrow \boldsymbol{\sigma} \notin \partial \mathscr{D}_2(0) &\Longleftarrow |\boldsymbol{\sigma}| > \sigma_0\end{aligned}$$

By Definition 3.2 of the subdifferential:

$$\begin{aligned}\boldsymbol{\sigma} \in \partial \mathscr{D}_2(0) &\Longleftrightarrow \mathscr{D}_2(0) + \boldsymbol{\sigma} : (\boldsymbol{\delta} - 0) \leqslant \mathscr{D}_2(\boldsymbol{\delta}), \ \forall \boldsymbol{\delta} \in \mathbb{R}^{3\times 3}_s \\ &\Longleftrightarrow \boldsymbol{\sigma} : \boldsymbol{\delta} \leqslant \sigma_0 |2\boldsymbol{\delta}|, \ \forall \boldsymbol{\delta} \in \mathbb{R}^{3\times 3}_s \\ \boldsymbol{\sigma} \notin \partial \mathscr{D}_2(0) &\Longleftrightarrow \exists \boldsymbol{\delta} \in \mathbb{R}^{3\times 3}_s \ / \ \boldsymbol{\sigma} : \boldsymbol{\delta} > \sigma_0 |2\boldsymbol{\delta}|\end{aligned}$$

Assume $|\boldsymbol{\sigma}| > \sigma_0 \geqslant 0$: then $\boldsymbol{\sigma} \neq 0$ and let $\boldsymbol{\delta} = \dfrac{\boldsymbol{\sigma}}{|\boldsymbol{\sigma}|}$

$$\begin{aligned}\boldsymbol{\sigma} : \boldsymbol{\delta} - \sigma_0 |2\boldsymbol{\delta}| &= \frac{(\boldsymbol{\sigma} : \boldsymbol{\sigma})}{|\boldsymbol{\sigma}|} - 2\sigma_0 \ = \ 2 \left(\frac{\boldsymbol{\sigma} : \boldsymbol{\sigma}}{2} \right) \frac{1}{|\boldsymbol{\sigma}|} - 2\sigma_0 \\ &= 2(|\boldsymbol{\sigma}| - \sigma_0) \ > \ 0\end{aligned}$$

Then $\boldsymbol{\sigma} \in \partial \mathscr{D}_2(0) \Longrightarrow |\boldsymbol{\sigma}| \leqslant \sigma_0$ and the proof is complete. □

Lemma 3.4 (Subdifferential of the energy of dissipation)
Let $\mathscr{D}$ be the energy of dissipation (3.1)*. Then, its subdifferential is given by*

$$\partial\mathscr{D}(\boldsymbol{\delta}) = \begin{cases} \left\{ \boldsymbol{\sigma} = 2K|2\boldsymbol{\delta}|^{-1+n}\,\boldsymbol{\delta} + \sigma_0 \dfrac{\boldsymbol{\delta}}{|\boldsymbol{\delta}|} \right\} & \textit{when } \boldsymbol{\delta} \neq 0 \\ \left\{ \boldsymbol{\sigma} \in \mathbb{R}^{3\times 3}_s \;/\; |\boldsymbol{\sigma}| \leqslant \sigma_0 \right\} & \textit{when } \boldsymbol{\delta} = 0 \end{cases} \tag{3.3}$$

Proof Observe that $\mathscr{D} = \mathscr{D}_1 + \mathscr{D}_2$ where $\mathscr{D}_1$ and $\mathscr{D}_2$ are defined in Lemmas 3.2 and 3.3 respectively. As both $\mathscr{D}_1$ and $\mathscr{D}_2$ are convex, its sum $\mathscr{D}$ is convex. Moreover

$$\boldsymbol{\sigma} \in \partial\mathscr{D}(\boldsymbol{\delta}) \Longleftrightarrow \exists\, \boldsymbol{\sigma}_1 \in \partial\mathscr{D}_1(\boldsymbol{\delta}),\ \boldsymbol{\sigma}_2 \in \partial\mathscr{D}_2(\boldsymbol{\delta}) \;/\; \boldsymbol{\sigma} = \boldsymbol{\sigma}_1 + \boldsymbol{\sigma}_2$$

The result follows from Lemmas 3.2 and 3.3. □

We are now able to define a viscoplastic fluid with a direct relation between the stress deviator $\boldsymbol{\sigma}$ and the rate of deformation $D(\boldsymbol{u})$.

Definition 3.3 (*Constitutive relation of a viscoplastic fluid*)
A viscoplastic fluid is defined by its Cauchy stress tensor $\boldsymbol{\sigma}_{\text{tot}} = \boldsymbol{\sigma} - p\,\boldsymbol{I}$ where the stress deviator $\boldsymbol{\sigma}$ satisfies the following constitutive relation:

$$\boldsymbol{\sigma} \in \partial\mathscr{D}(D(\boldsymbol{u})) \tag{3.4}$$

and where $\mathscr{D}$ is the energy of dissipation given in (3.1).

Note that, from Lemma 3.4, the constitutive relation (3.4) can be rewritten in a more explicit way:

$$\begin{cases} \boldsymbol{\sigma} = 2K|2D(\boldsymbol{u})|^{-1+n}\,D(\boldsymbol{u}) + \sigma_0 \dfrac{D(\boldsymbol{u})}{|D(\boldsymbol{u})|} & \text{when } D(\boldsymbol{u}) \neq 0 \\ |\boldsymbol{\sigma}| \leqslant \sigma_0 & \text{when } D(\boldsymbol{u}) = 0 \end{cases} \tag{3.5}$$

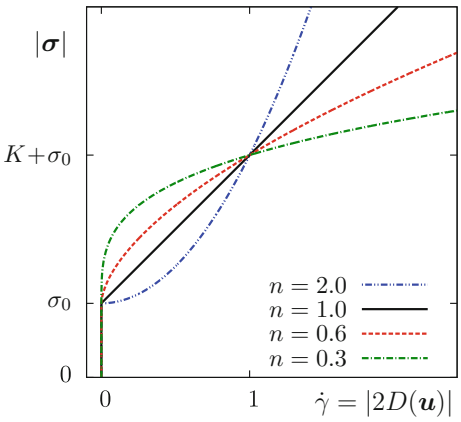

Fig. 3.3 Viscoplastic fluids: stress norm versus shear rate

Lemma 3.4 leads to a simple interpretation of the fluid behavior. Taking the norm of the previous relation leads to

$$\begin{array}{ll} |\boldsymbol{\sigma}| = K|2D(\boldsymbol{u})|^n + \sigma_0 & \text{when } D(\boldsymbol{u}) \neq 0 \\ |\boldsymbol{\sigma}| \leqslant \sigma_0 & \text{when } D(\boldsymbol{u}) = 0 \end{array}$$

This relation is represented on Fig. 3.3. Observe that when $D(\boldsymbol{u}) = 0$, then the stress is undetermined. We only known that it is below the yield stress value σ_0. These regions, where $D(\boldsymbol{u}) = 0$ will be characterized in the next section.

3.3 Problem Statement

Recall that, as we consider here liquids, the density could be supposed as constant and the material as incompressible. The mass and momentum conservation equations (1.3) and (1.17) are completed with (1.22) for the Cauchy stress tensor and the previous constitutive relation (3.5) for viscoplastic fluids. The system is closed by appropriate initial and boundary conditions. The time-dependent problem writes:

(P): find $\boldsymbol{\sigma}$, $\boldsymbol{u}$ and p, defined in $]0, T[\times\Omega$ such that

$$\begin{cases} \boldsymbol{\sigma} = 2K|2D(\boldsymbol{u})|^{-1+n} D(\boldsymbol{u}) + \sigma_0 \dfrac{D(\boldsymbol{u})}{|D(\boldsymbol{u})|}, & \text{when } D(\boldsymbol{u}) \neq 0 \\ |\boldsymbol{\sigma}| \leqslant \sigma_0 & \text{otherwise} \end{cases}$$

$$\begin{aligned} \rho\left(\frac{\partial \boldsymbol{u}}{\partial t} + \boldsymbol{u}.\nabla \boldsymbol{u}\right) - \mathbf{div}\,\boldsymbol{\sigma} + \nabla p &= \rho \boldsymbol{g} \quad \text{in }]0, T[\times\Omega \\ \operatorname{div} \boldsymbol{u} &= 0 \quad \text{in }]0, T[\times\Omega \\ \boldsymbol{u}(t=0) &= \boldsymbol{u}_0 \quad \text{in } \Omega \\ \boldsymbol{u} &= \boldsymbol{u}_\Gamma \quad \text{on }]0, T[\times\partial\Omega \end{aligned}$$

Note that the stress deviator appears now as an explicit unknown of the problem. This is a major difference with previous models, such as Newtonian and quasi-Newtonian fluids. The stress deviator can not be eliminated from the system, as it would cause a division by $|D(\boldsymbol{u})|$ that is expected to vanish in some large regions of the flow domain. The characterization of such regions is the aim of the next section.

3.4 Rigid Regions

The aim of this section is to characterize regions where $D(\boldsymbol{u}) = 0$.

Definition 3.4 (*Rigid region, rigid motion*)
At time t, a *rigid region* $\Omega_0(t) \subset \Omega$ is a subdomain of the flow domain with non-zero measure where the fluid is animated by a *rigid motion*, i.e. a combination of a solid

translation and a rotation:

$$\boldsymbol{u}(t,\boldsymbol{x}) = \boldsymbol{u}_0(t) + \boldsymbol{\omega}_0(t) \wedge \boldsymbol{x}, \quad \forall \boldsymbol{x} \in \Omega_0(t)$$

where $\boldsymbol{u}_0(t)$ and $\boldsymbol{\omega}_0(t) \in \mathbb{R}^3$ are respectively the translation and the angular rotation velocities, that are constants in all the subdomain $\Omega_0(t)$.

Theorem 3.2 (Rigid region and zero rate of deformation)
At time t, a subdomain $\Omega_0(t) \subset \Omega$ with non-zero measure is a rigid region if and only if $D(\boldsymbol{u}) = 0$ in $\Omega_0(t)$.

Proof Let us suppose first that $\Omega_0(t)$ is a rigid region and show that $D(\boldsymbol{u}) = 0$. By definition, the fluid is in rigid motion in $\Omega_0(t)$ when there exists $\boldsymbol{u}_0$ and $\boldsymbol{\omega}_0 \in \mathbb{R}^3$ such that $\boldsymbol{u}(t,\boldsymbol{x}) = \boldsymbol{u}_0 + \boldsymbol{\omega}_0 \wedge \boldsymbol{x}$ for all $\boldsymbol{x} \in \Omega_0(t)$. We decompose $\boldsymbol{x} = (x_i)_{1\leqslant i\leqslant 3}$ and $\boldsymbol{\omega}_0 = (\omega_i)_{1\leqslant i\leqslant 3}$ in a Cartesian coordinate system $(0, x_1, x_2, x_3)$. Expanding, we obtain

$$\boldsymbol{u}(t,\boldsymbol{x}) = \boldsymbol{u}_0 + \begin{pmatrix} \omega_2 x_3 - \omega_3 x_2 \\ \omega_3 x_1 - \omega_1 x_3 \\ \omega_1 x_2 - \omega_2 x_1 \end{pmatrix}$$

and then

$$\nabla \boldsymbol{u} = \begin{pmatrix} 0 & -\omega_3 & \omega_2 \\ \omega_3 & 0 & -\omega_1 \\ -\omega_2 & \omega_1 & 0 \end{pmatrix}$$

Observe that $\nabla \boldsymbol{u}$ is skew-symmetric and thus its symmetric part $D(\boldsymbol{u})$ is zero.

Conversely, we suppose that $D(\boldsymbol{u}) = 0$ and show that $\Omega_0(t)$ is a rigid region. The gradient of velocity $\nabla \boldsymbol{u}$ is the sum of its symmetric part $D(\boldsymbol{u})$, that is zero, and its skew-symmetric part, the vorticity tensor, which writes:

$$W(\boldsymbol{u}) = \frac{\nabla \boldsymbol{u} - \nabla \boldsymbol{u}^T}{2} = \begin{pmatrix} 0 & -\omega_{21} & \omega_{13} \\ \omega_{21} & 0 & -\omega_{32} \\ -\omega_{13} & \omega_{32} & 0 \end{pmatrix}$$

where

$$\omega_{i,j} = \frac{1}{2}\left(\frac{\partial u_i}{\partial x_j} - \frac{\partial u_j}{\partial x_i}\right), \quad 1 \leqslant i, j \leqslant 3 \text{ and } i \neq j$$

and $\boldsymbol{u} = (u_i)_{1\leqslant i\leqslant 3}$. Let us show that the $\omega_{i,j}$ are constant in $\Omega_0(t)$. For all $k = 1, 2, 3$ we have

$$\begin{aligned} \frac{\partial \omega_{i,j}}{\partial x_k} &= \frac{1}{2}\left(\frac{\partial^2 u_i}{\partial x_j \partial x_k} - \frac{\partial^2 u_j}{\partial x_i \partial x_k}\right) \\ &= \frac{1}{2}\left(\frac{\partial^2 u_i}{\partial x_j \partial x_k} + \frac{\partial^2 u_k}{\partial x_i \partial x_j} - \frac{\partial^2 u_j}{\partial x_i \partial x_k} - \frac{\partial^2 u_k}{\partial x_i \partial x_j}\right) \end{aligned}$$

$$= \frac{\partial}{\partial x_j}\left\{\frac{1}{2}\left(\frac{\partial u_i}{\partial x_k}+\frac{\partial u_k}{\partial x_i}\right)\right\}+\frac{\partial}{\partial x_i}\left\{\frac{1}{2}\left(\frac{\partial u_j}{\partial x_k}+\frac{\partial u_k}{\partial x_j}\right)\right\}$$
$$= 0$$

as $D(\boldsymbol{u}) = 0$. Finally, $\nabla \boldsymbol{u} = W(\boldsymbol{u})$ is constant and the result is obtained by integration. □

Remark 3.1 (*Arrested state and limit load analysis*)
Let us consider the case when $D(\boldsymbol{u}) = 0$ in all the domain Ω. It means that the material is in rigid motion, a combination of rotation and translation. In the special case of an homogeneous Dirichlet boundary condition, we obtain $\boldsymbol{u} = 0$ and then this case is called the *arrested state*. The stress deviator $\boldsymbol{\sigma}$ is then characterized as

$$-\mathbf{div}(\boldsymbol{\sigma}) = \boldsymbol{f} \text{ and } |\boldsymbol{\sigma}| \leqslant \sigma_0 \text{ in } \Omega \tag{3.6}$$

The problem of finding, for a given Ω and σ_0 the largest $|\boldsymbol{f}|$ such that this problem admits a solution is called a *limit load analysis*. This problem is difficult and important, as it has many application in mechanics, such as stability of building foundations in civil engineering, robustness of engine parts. On an example, the next section shows how to solve this problem.

3.5 Example: Poiseuille Flow

Let us reuse the notations of Sect. 1.5, p. 18 for the Poiseuille flow of a Newtonian fluid. Assume that the flow is laminar: the pressure is given by $p(x, y, z) = -fz + p_0$ where $f > 0$ and $p_0 \in \mathbb{R}$ are given. We first consider the flow between parallel plates. The velocity is parallel to the plates $\boldsymbol{u}(x) = (0, 0, u_z(x))$. Its gradient is given by

$$\nabla \boldsymbol{u} = \begin{pmatrix} 0 & 0 & 0 \\ 0 & 0 & 0 \\ u_z' & 0 & 0 \end{pmatrix}$$

and the shear rate by $\dot{\gamma} = |2D(\boldsymbol{u})| = |u_z'|$. As the stress deviator is proportional to the rate of deformation tensor $D(\boldsymbol{u})$, it is given by

$$\boldsymbol{\sigma} = \begin{pmatrix} 0 & 0 & \sigma_{xz} \\ 0 & 0 & 0 \\ \sigma_{xz} & 0 & 0 \end{pmatrix}$$

and its norm is $|\boldsymbol{\sigma}| = |\sigma_{xz}|$.

The problem reduces to

(P): find σ_{xz} and u_z defined in $]-L, L[$ such that

$$\begin{cases} \sigma_{xz} = \sigma_0 \dfrac{u_z'}{|u_z'|} + K|u_z'|^{-1+n} u_z' & \text{when } u_z' \neq 0 \\ |\sigma_{xz}| \leqslant \sigma_0 & \text{otherwise} \end{cases}$$

$$\begin{aligned} -\sigma_{xz}' &= f \text{ in }]-L, L[\\ u_z(-L) = u_z(L) &= 0 \end{aligned}$$

This problem presents five physical parameters: σ_0, n, K, L and f. In order to reduce the set of parameters, let us perform a dimensional analysis. As usual, the dimensionless quantities are denoted with tildes:

$$\tilde{x} = \frac{x}{L}, \quad \tilde{u}(\tilde{x}) = \frac{u_z(L\tilde{x})}{U}, \quad \tilde{\sigma}(\tilde{x}) = \frac{\sigma_{xz}(L\tilde{x})}{\Sigma}$$

where U and $\Sigma > 0$ will be chosen later. After this change of unknown, the problem becomes:

(P): find $\tilde{\sigma}$ and $\tilde{u}$ defined in $]-1, 1[$ such that

$$\begin{cases} \tilde{\sigma} = \dfrac{\sigma_0}{\Sigma} \dfrac{\tilde{u}'}{|\tilde{u}'|} + \dfrac{KU^n}{\Sigma L^n} |\tilde{u}'|^{-1+n} \tilde{u}' & \text{when } \tilde{u}' \neq 0 \\ |\tilde{\sigma}| \leqslant \dfrac{\sigma_0}{\Sigma} & \text{when } \tilde{u}' = 0 \\ -\tilde{\sigma}' = \dfrac{fL}{\Sigma} \text{ in }]-1, 1[\\ \tilde{u}(-1) = \tilde{u}(1) = 0 \end{cases}$$

Next, choose $\Sigma = fL$ and U such that $KU^n = \Sigma L^n$, i.e. $U = (fL^{1+n}/K)^{1/n}$. The factor in the first equation disappears and the right-hand-side in the third one is 1. There is only two physical dimensionless parameter in this problem: $Bi = \sigma_O/(fL)$, called the Bingham number, and the power law index n. It means that, for fixed Bi and n, the solution of the original problem is invariant up to a linear change of unknown. By using the symmetry of the geometry, the problem also reduces to the $]0, 1[$ interval. The dimensionless problem becomes:

(P): find $\tilde{\sigma}$ and $\tilde{u}$ defined in $]0, 1[$ such that

$$\tilde{\sigma} = Bi \frac{\tilde{u}'}{|\tilde{u}'|} + |\tilde{u}'|^{-1+n} \tilde{u}' \quad \text{when } \tilde{u}' \neq 0 \tag{3.7a}$$

$$|\tilde{\sigma}| \leqslant Bi \quad \text{when } \tilde{u}' = 0 \tag{3.7b}$$

$$-\tilde{\sigma}' = 1 \text{ in }]0, 1[\tag{3.7c}$$

$$\tilde{\sigma}(0) = 0 \text{ and } \tilde{u}(1) = 0 \tag{3.7d}$$

By integration, (3.7c) and (3.7d) leads to $\tilde{\sigma} = -\tilde{x}$. Consider a first case, when $|\tilde{\sigma}| \leqslant Bi$ or equivalently $\tilde{x} \leqslant Bi$. Then, from (3.7b), we obtain $\tilde{u}' = 0$. Thus $\tilde{u} = C$ where C is a constant.

Next, consider the second case, when $|\tilde{\sigma}| > Bi$ or equivalently $\tilde{x} > Bi$. Then, $\tilde{u}' \neq 0$ and, from (3.7a):

$$-\tilde{x} = \left(\frac{Bi}{|\tilde{u}'|} + |\tilde{u}'|^{-1+n}\right)\tilde{u}'$$

As $\tilde{x} > 0$, we get $\tilde{u}' < 0$ and then, taking the absolute value of the previous relation, we get $\tilde{x} = Bi + |\tilde{u}'|^n$ that writes equivalently $|\tilde{u}'| = (\tilde{x} - Bi)^{\frac{1}{n}}$. Then, restoring the sign of $\tilde{u}'$, we obtain

$$\tilde{u}' = -(\tilde{x} - Bi)^{\frac{1}{n}}$$

After a second integration, and jointing by continuity at $\tilde{x} = Bi$, we get:

$$\tilde{u}(\tilde{x}) = \begin{cases} -\dfrac{(\tilde{x} - Bi)^{1+\frac{1}{n}}}{1+\frac{1}{n}} + C & \text{when } \tilde{x} > Bi \\ C & \text{when } \tilde{x} \leqslant Bi \end{cases}$$

Finally, from (3.7d), the boundary condition $\tilde{u}'(1) = 0$ leads to the value of the constant C and

$$\tilde{u}(\tilde{x}) = \frac{\max(0, 1 - Bi)^{1+\frac{1}{n}} - \max(0,\ |\tilde{x}| - Bi)^{1+\frac{1}{n}}}{1 + \dfrac{1}{n}}, \quad \tilde{x} \in [-1, 1]$$

Note that when $Bi \geqslant 1$ we have $\tilde{u} = 0$: this is called the *arrested state*. In terms of dimensional variables, the condition $Bi \geqslant 1$ writes $f \leqslant \sigma_0/L$. It means that the pressure gradient force f is not sufficient to move the material in the pipe, and there is no flow. The quantity σ_0/L is called the limit load. It could be surprising, but remember how behaves a toothpaste and you will find this behavior more natural. Going back to dimensional quantities, the solution writes

$$u(x) = \frac{\max(0, L - \sigma_0/f)^{1+\frac{1}{n}} - \max(0,\ |x| - \sigma_0/f)^{1+\frac{1}{n}}}{\left(1 + \dfrac{1}{n}\right) K^{1/n}}, \quad x \in [-L, L]$$

The solution is represented on Fig. 3.4 for various values of the power law index n and $Bi = 1/2$. Observe the plug flow at the center of the flow: the material behaves as a rigid solid that translate with a constant velocity. Note that the plug region is a special case of a rigid regions, where the material is in translation, a spacial case of

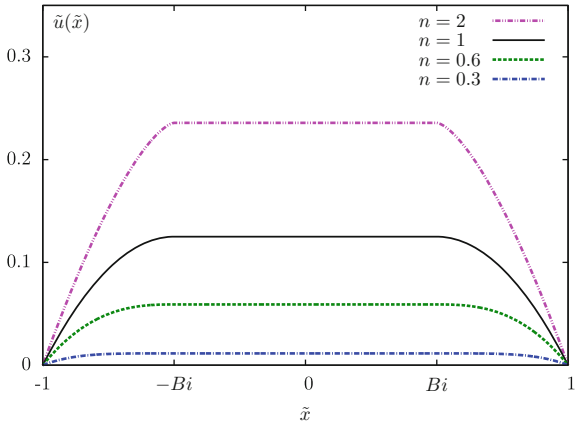

Fig. 3.4 Poiseuille flow with a viscoplastic fluid ($Bi = 1/2$)

rigid motion, Finally, the solution in a circular pipe is obtained by simply replacing f by $f/2$ and x by r in the previous expression.

3.6 Example: Couette Flow

We reuse the notations of Sect. 1.6, p. 21 for the Couette flow. For a laminar flow, the velocity writes $\boldsymbol{u} = (0, u_\theta(r), 0)$ in the cylindrical coordinate system (r, θ, z). By introducing the angular velocity $\omega(r)$ such that $u_\theta(r) = r\,\omega(r)$, the gradient of velocity writes

$$\nabla \boldsymbol{u} = \begin{pmatrix} 0 & 0 & 0 \\ r\omega' & 0 & 0 \\ 0 & 0 & 0 \end{pmatrix}$$

The shear rate is $\dot{\gamma} = r|w'|$ and the stress deviator $\boldsymbol{\sigma}$ has only one non-zero component $\sigma_{r\theta}$ while $|\boldsymbol{\sigma}| = |\sigma_{r\theta}|$. There are two main experimental situations: imposed torque and imposed angular velocity.

Imposed torque – The stationary problem reduces to

(P): find $\sigma_{r\theta}$ and ω, defined in $]r_1, r_2[$, and p, defined in $], r_2[\times]0, z_0[$, such that

$$\sigma_{r\theta} = \sigma_0 \frac{\omega'}{|\omega'|} + K|r\omega'|^{-1+n} r\omega' \text{ when } \omega' \neq 0 \tag{3.8a}$$

$$|\sigma_{r\theta}| \leqslant \sigma_0 \qquad \text{otherwise} \tag{3.8b}$$

$$\rho\,\omega^2 r - \frac{\partial p}{\partial r} = 0 \quad \text{in }]r_1, r_2[\times]0, z_0[\tag{3.8c}$$

$$-\frac{1}{r^2}\left(r^2\sigma_{r\theta}\right)' = 0 \quad \text{in }]r_1, r_2[\tag{3.8d}$$

$$-\frac{\partial p}{\partial z} = -\rho g \quad \text{in }]r_1, r_2[\times]0, z_0[\tag{3.8e}$$

$$\sigma_{r\theta}(r_1) = -f \text{ and } \omega(r_2) \;=\; \omega_2 \tag{3.8f}$$

Here, ω_2 is the angular velocity of the outer cylinder and f is a stress boundary data related to the imposed torque (see Sect. 1.6, p. 21). The problem presents nine physical parameters: $\sigma_0, n, K, f, \omega_2, r_1, r_2, \rho, g$. In order to reduce the set of parameters, let us perform a dimensional analysis. As usual, the dimensionless quantities are denoted with tildes:

$$\tilde{r} = \frac{r}{r_2}, \;\; \tilde{z} \;=\; \frac{z}{r_2}, \;\; \tilde{\omega}(\tilde{r}) \;=\; \frac{\omega(r_2\tilde{r}) - \omega_2}{W}, \;\; \tilde{\sigma}(\tilde{r}) \;=\; \frac{\sigma_{r\theta}(r_2\tilde{r})}{\Sigma}$$

where the characteristic stress is $\Sigma = f$ and the characteristic angular velocity W is such that $\Sigma = KW^n$ i.e. $W = (f/K)^{\frac{1}{n}}$. After this change of unknowns, the problem writes:

(P): find $\tilde{\sigma}$ and $\tilde{\omega}$, defined in $]\beta, 1[$, and $\tilde{p}$, defined in $]\beta, 1[\times]0, \gamma[$, such that

$$\tilde{\sigma} = Bi\frac{\tilde{\omega}'}{|\tilde{\omega}'|} + |\tilde{r}\tilde{\omega}'|^{-1+n}\tilde{r}\tilde{\omega}' \text{ when } \tilde{\omega}' \neq 0 \tag{3.9a}$$

$$|\tilde{\sigma}| \leqslant Bi \qquad \text{when } \tilde{\omega}' = 0 \tag{3.9b}$$

$$Re\,\tilde{r}\tilde{\omega}^2 - \frac{\partial \tilde{p}}{\partial \tilde{r}} = 0 \quad \text{in }]\beta, 1[\times]0, \gamma[\tag{3.9c}$$

$$-\frac{1}{\tilde{r}^2}\left(\tilde{r}^2\tilde{\sigma}\right)' = 0 \quad \text{in }]\beta, 1[\tag{3.9d}$$

$$-\frac{\partial \tilde{p}}{\partial \tilde{z}} = -\frac{Re}{Fr^2} \quad \text{in }]\beta, 1[\times]0, \gamma[\tag{3.9e}$$

$$\tilde{\sigma}(\beta) = -1 \text{ and } \tilde{\omega}(1) \;=\; 0 \tag{3.9f}$$

Clearly, in (3.9a)–(3.9f), the computation of $(\sigma_{r\theta}, \omega)$ is decoupled to those of p, that could be performed later, using (3.9c) and (3.9e). The reduced problem (3.9a), (3.9b), (3.9d) and (1.31d) for computing the stress and the angular velocity involves three dimensionless numbers: the Bingham number $Bi = \sigma_0/f$, the power index n and the geometry confinement $\beta = r_1/r_2 \in]0, 1[$. The two Eq. (1.31a) and (1.31c) for the pressure involve three additional dimensionless numbers: the Reynolds $Re = \rho W^2 r_2^2/\Sigma = \rho f r_2^2/\eta^2$, the Froude $Fr = (Wr_2)/\sqrt{gr_2} = (f/\eta)\sqrt{r_2/g}$ and the cylinder vertical extension $\gamma = z_0/r_2$. Thus, let us focus on the computation of $(\tilde{\sigma}_{r\theta}, \tilde{\omega})$. From (3.9d) we obtain $\tilde{\sigma}(\tilde{r}) = -c\tilde{r}^{-2}$ where $c \in \mathbb{R}$ is an integration constant that is given by the Neumann boundary condition (3.8f) as $c = \beta^2$. Then the stress $\tilde{\sigma}(\tilde{r}) = -\beta^2/\tilde{r}^2$ is completely solved, for all $\tilde{r} \in [\beta, 1]$. Consider a first case when $|\tilde{\sigma}| \leqslant Bi$ or equivalently $\tilde{r} \geqslant \tilde{r}_c$ where $\tilde{r}_c = \beta Bi^{-\frac{1}{2}}$ with the constraint that $\tilde{r}_c \in [\beta, 1]$. Then, from (3.9b), we have $\tilde{\omega}' = 0$ and, from the boundary condi-

tion (3.11) at $\tilde{r} = 1$, we get $\tilde{\omega} = 0$ in $[\tilde{r}_c, 1]$. Thus, there is a region $[\tilde{r}_c, 1]$ where the material is at the rest. Next, consider the second case when $|\tilde{\sigma}| > Bi$ or equivalently $\tilde{r} < \tilde{r}_c$. We have $\tilde{\omega}' \neq 0$ and from (3.9a):

$$-\frac{\beta^2}{\tilde{r}^2} = \left(\frac{Bi}{|\tilde{\omega}'|} + \tilde{r}^n |\tilde{\omega}'|^{-1+n}\right) \tilde{\omega}' \quad \text{in }]\beta, r_c[$$

Note that $\tilde{\omega}'(\tilde{r})$ has a negative sign for all $\tilde{r} \in]\beta, \tilde{r}_c[$. Taking the absolute value of the previous relation, we get $\beta^2 \tilde{r}^{-2} = Bi + \tilde{r}^n |\tilde{\omega}'|^n$ that writes equivalently $|\tilde{\omega}'| = \tilde{r}^{-1} \left(\beta^2 \tilde{r}^{-2} - Bi\right)^{\frac{1}{n}}$. Then, restoring the sign of $\tilde{\omega}'$, we obtain

$$\tilde{\omega}' = -\tilde{r}^{-1} \left(\beta^2 \tilde{r}^{-2} - Bi\right)^{\frac{1}{n}} \tag{3.10}$$

When integrating, there is no closed formula for $\tilde{\omega}$ for a general power index $n > 0$. Nevertheless, we are able to exhibit a closed formula for some special values of n, e.g. for rational values $n = 1, 1/2, 1/3, 2/3$, etc. For instance, for the Bingham model ($n = 1$), after integration and using the continuity $\tilde{\omega}(\tilde{r}_c) = 0$ at $\tilde{r} = \tilde{r}_c$:

$$\tilde{\omega}(\tilde{r}) = \frac{\beta^2}{2} \left(\tilde{r}^{-2} - \tilde{r}_c^{-2}\right) + Bi \log\left(\frac{\tilde{r}}{\tilde{r}_c}\right), \quad \forall \tilde{r} \in [\beta, \tilde{r}_c]$$

Merging these results, the solution of problem (3.9a)–(3.9f) writes

$$\begin{aligned}
\tilde{\sigma}(\tilde{r}) &= -\frac{c}{\tilde{r}^2} \\
\tilde{\omega}(\tilde{r}) &= \begin{cases} \dfrac{c}{2} \left(\tilde{r}^{-2} - \tilde{r}_c^{-2}\right) + Bi \log\left(\dfrac{\tilde{r}}{\tilde{r}_c}\right) & \text{when } \tilde{r} \in [\beta, \tilde{r}_c[\\ 0 & \text{when } \tilde{r} \in [\tilde{r}_c, 1] \end{cases} \\
\tilde{r}_c &= \max\left(\beta,\ \min\left(1,\ \beta Bi^{-\frac{1}{2}}\right)\right) \\
c &= \beta^2
\end{aligned}$$

There are three flow regimes:

- when $Bi \leqslant \beta^2$ i.e. $f > \sigma_0 \beta^{-2}$, then $\tilde{r}_c = \beta$ and there is no rigid region.
- when $\beta^2 < Bi < 1$ i.e. $\sigma_0 \beta^{-2} < f < \sigma_0$, then $\tilde{r}_c \in]\beta, 1[$ and there is both rigid and flowing regions.
- when $Bi \geqslant 1$ i.e. $f < \sigma_0$, then $\tilde{r}_c = 1$ and there is no flowing region: the fluid is at the rest, this is the arrested state.

The dimensional solution is then simply obtained by $\sigma_{r\theta}(r) = f \tilde{\sigma}(r/r_2)$, $\omega(r) = \omega_2 + (f/K)\, \tilde{\omega}(\tilde{r}/r_2)$ and $u_\theta(r) = r\, \omega(r)$. The pressure, due to inertial effects, is always obtained by integration of (3.8c) and (3.8e), as in the Newtonian case. The three flow regimes also interprets with dimensional data in terms of the torque F, as defined in (1.29), p. 23.

- When the torque is insufficient, $F \leqslant F_1$, there is no flow at all.
- When the torque is sufficiently high $F_1 < F < F_2$, the material is partially flowing, together with a dead region that decreases when the torque increases.
- When the torque is below a second critical value $F \geqslant F_2$, the material flows in all the gap between the two cylinders.

The critical torque values are given by $F_i = 2\pi\sigma_0 z_0 r_i^2$, $i = 1, 2$.

Imposed angular velocity – The previous problem was associated to a Neumann boundary conditions (3.8f) that corresponds to impose the inner cylinder torque. Another frequent and important case is to replace in (3.8f) the Neumann condition at $r = r_1$ by a Dirichlet one:

$$\omega(r_1) = \omega_1 \text{ and } \omega(r_2) \ = \ \omega_2$$

This corresponds to impose the cylinder inner angular velocity. The corresponding reduced problem presents seven physical parameters: $\sigma_0, n, K, \omega_1, \omega_2, r_1$ and r_2. The dimensionless quantities are:

$$\tilde{r} = \frac{r}{r_2}, \ \ \tilde{\omega}(\tilde{r}) \ = \ \frac{\omega(r_2\tilde{r}) - \omega_2}{\omega_1 - \omega_2}, \ \ \tilde{\sigma}(\tilde{r}) \ = \ \frac{\sigma_{r\theta}(r_2\tilde{r})}{\Sigma}$$

where $\Sigma = K(\omega_1 - \omega_2)^n$. The boundary condition of the dimensionless problem writes

$$\tilde{\omega}(\beta) = 1 \text{ and } \tilde{\omega}(1) \ = \ 0 \tag{3.11}$$

where $Bi = \sigma_0/(K(\omega_1 - \omega_2)^n)$. The dimensionless problem is defined by (3.9a)–(3.9d), (3.11) From the seven physical parameters of the dimensional problem, it remains in its dimensionless version only three dimensionless numbers: Bi, the Bingham number, n, the power law index, and β, the geometry confinement. From (3.9d) we obtain $\tilde{\sigma}(\tilde{r}) = -c\tilde{r}^{-2}$ where $c \in \mathbb{R}$ is an integration constant that should be determined. Consider a first case when $|\tilde{\sigma}| \leqslant Bi$ or equivalently $\tilde{r} \geqslant \tilde{r}_c$ with $\tilde{r}_c = \min\left(1, \sqrt{c/Bi}\right)$. Then, from (3.9b), we have $\tilde{\omega}' = 0$ and, from the boundary condition (3.11) at $\tilde{r} = 1$, we get $\tilde{\omega} = 0$ in $[\tilde{r}_c, 1]$. Next, consider the second case when $|\tilde{\sigma}| > Bi$ or equivalently $\tilde{r} < \tilde{r}_c$. We have $\tilde{\omega}' \neq 0$ and from (3.9a):

$$-\frac{c}{\tilde{r}^2} = \left(\frac{Bi}{|\tilde{\omega}'|} + \tilde{r}^n|\tilde{\omega}'|^{-1+n}\right)\tilde{\omega}' \ \text{ in }]\beta, r_c[$$

Note that $\tilde{\omega}'(\tilde{r})$ has a constant sign, opposite to those of c, for all $\tilde{r} \in]\beta, \tilde{r}_c[$. Then, $\tilde{\omega}$ is monotonically increasing or decreasing in this interval. From the boundary condition at $\tilde{r} = \beta$, we have $\tilde{\omega}(\beta) = 1$ and by continuity at $\tilde{r} = \tilde{r}_c$, we have $\tilde{\omega}(\tilde{r}) = 0$. Thus, $\tilde{\omega}$ is decreasing in this interval i.e. $\tilde{\omega}' < 0$ and $c > 0$. Taking the absolute value of the previous relation, we get $c\tilde{r}^{-2} = Bi + \tilde{r}^n|\tilde{\omega}'|^n$ that writes equivalently $|\tilde{\omega}'| = \tilde{r}^{-1}\left(c\tilde{r}^{-2} - Bi\right)^{\frac{1}{n}}$. Then, restoring the sign of $\tilde{\omega}'$, we obtain

$$\tilde{\omega}' = -\tilde{r}^{-1}\left(c\tilde{r}^{-2} - Bi\right)^{\frac{1}{n}} \tag{3.12}$$

As in the case of a Neumann boundary condition, consider the case of the Bingham model ($n = 1$). After integration and using the continuity $\tilde{\omega}(\tilde{r}_c) = 0$ at $\tilde{r} = \tilde{r}_c$:

$$\tilde{\omega}(\tilde{r}) = \frac{c}{2}\left(\tilde{r}^{-2} - \tilde{r}_c^{-2}\right) + Bi\log\left(\frac{\tilde{r}}{\tilde{r}_c}\right), \quad \forall \tilde{r} \in [\beta, \tilde{r}_c]$$

The boundary condition (3.11) at $\tilde{r} = \beta$ furnishes a relation for computing the integration constant c versus Bi and the confinement β:

$$\frac{c}{2}\left(\beta^{-2} - \tilde{r}_c^{-2}\right) + Bi\log\left(\frac{\beta}{\tilde{r}_c}\right) = 1 \quad \text{and} \quad \tilde{r}_c = \min\left(1, \sqrt{c/Bi}\right) \tag{3.13}$$

There is two cases, depending upon $\tilde{r}_c$. When $\tilde{r}_c = 1$ i.e. $c \geqslant Bi$, there is no rigid region. In that case, (3.13) yields $c = 2(1 - Bi\ \log(\beta))/(\beta^{-2} - 1)$ and the condition $c \geqslant Bi$ leads to $Bi \leqslant Bi_*(\beta)$ where

$$Bi_*(\beta) = \frac{2}{\beta^{-2} - 1 - 2\log\left(\beta^{-1}\right)}, \quad \beta \in]0, 1[$$

Otherwise, when $\tilde{r}_c < 1$ i.e. $Bi \geqslant Bi_*(\beta)$, there is a rigid region. In that case $c = Bi\,\tilde{r}_c^2$ and (3.13) becomes an equation for $\tilde{r}_c$ that writes, after rearrangements:

$$\left(\frac{\tilde{r}_c}{\beta}\right)^2 - 1 - 2\log\left(\frac{\tilde{r}_c}{\beta}\right) = \frac{2}{Bi}$$

A rapid inspection of the function $\varphi(\xi) = \xi^2 - 1 - 2\log(\xi)$ shows that φ is strictly increasing in $[1, +\infty[$ and $\varphi(1) = 0$. Thus, its inverse φ^{-1} is well-defined in $[0, +\infty[$ and could easily be computed. For instance, the Newton method allows to obtain its value in few iterations with the machine precision. Then, we have $\tilde{r}_c = \beta\,\varphi^{-1}(2Bi^{-1})$ and the integration constant is $c = Bi\,\tilde{r}_c^2$. Note that $\tilde{r}_c$ increases when Bi decreases.

Finally, grouping these results, the solution of problem (3.9a)–(3.9d) and (3.11) writes

$$\begin{aligned}
\tilde{\sigma}(\tilde{r}) &= -c\left(\frac{\tilde{r}_c}{\tilde{r}}\right)^2 \\
\tilde{\omega}(\tilde{r}) &= \begin{cases} \dfrac{c}{2}\left(\tilde{r}^{-2} - \tilde{r}_c^{-2}\right) + Bi\log\left(\dfrac{\tilde{r}}{\tilde{r}_c}\right) & \text{when } \tilde{r} \in [\beta, \tilde{r}_c[\\ 0 & \text{when } \tilde{r} \in [\tilde{r}_c, 1] \end{cases} \\
\tilde{r}_c &= \min\left(1,\ \beta\,\varphi^{-1}\left(2Bi^{-1}\right)\right) \\
\varphi(\xi) &= \xi^2 - 1 - 2\log(\xi), \quad \forall \xi \geqslant 0
\end{aligned}$$

$$c = \frac{2(1 + Bi\ \log(\tilde{r}_c/\beta))}{\beta^{-2} - \tilde{r}_c^{-2}}$$

Observe that the expression for $\tilde{\sigma}$ and $\tilde{\omega}$ are similar to those of the previous case of an imposed torque: only the expressions of $\tilde{r}_c$ and c are changed. Note that there are now only two flow regimes:

- $Bi \leqslant Bi_*(\beta)$: then $\tilde{r}_c = \beta$ and there is no rigid region.
- $Bi > Bi_*(\beta)$: then $\tilde{r}_c \in]\beta, 1[$ and there is both rigid and flowing regions.

Figure 3.5 plots the dimensionless solution of the Bingham model for a confinement $\beta = 1/2$ with $\tilde{r}_c = 3/4$ and 1, corresponding to $Bi \approx 4.555$ and $Bi = Bi_*(\beta) \approx 1.2394$ respectively. The *localization* of the flow in a region close to the inner cylinder is called *shear banding*. The dimensional solution is then simply obtained by $\sigma_{r\theta}(r) = K(\omega_1 - \omega_2)\tilde{\sigma}(r/r_2)$, $\omega(r) = \omega_2 + (\omega_1 - \omega_2)\tilde{\omega}(\tilde{r}/r_2)$ and $u_\theta(r) = r\,\omega(r)$. The pressure, due to inertial effects, is obtained by integration of (3.8c) and (3.8e), as in the Newtonian case. The two flow regimes also interprets in terms of the difference of angular velocities $\delta\omega = |\omega_1 - \omega_2|$:

- When $\delta\omega$ is insufficient, $\delta\omega < \delta\omega_*$, the material is partially flowing, together with a dead region that decreases when $\delta\omega$ increases.
- When $\delta\omega$ is below a critical value, $\delta\omega \geqslant \delta\omega_*$, the material flows in all the gap between the two cylinders.

The critical difference of angular velocities is given by

$$\delta\omega_* = \frac{\sigma_0}{2K}\left(\left(\frac{r_2}{r_1}\right)^2 - 1 - 2\log\left(\frac{r_2}{r_1}\right)\right)$$

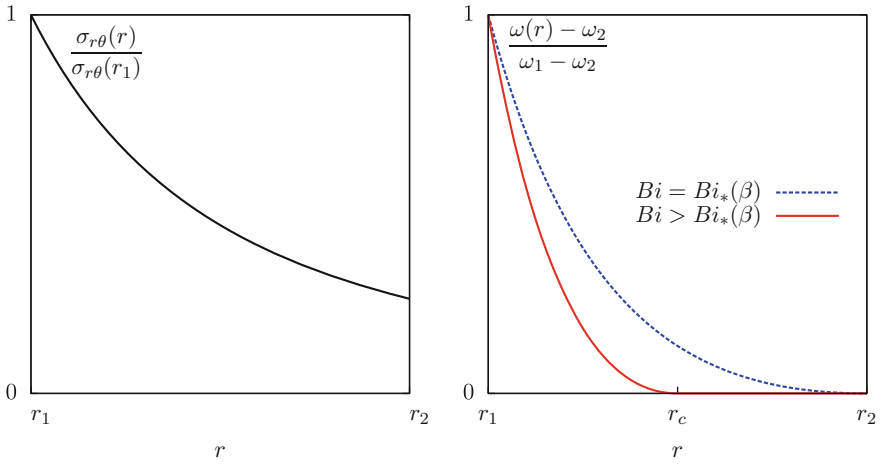

Fig. 3.5 Couette flow of a Bingham fluid ($\beta = 1/2$)

Finally, the case of the Couette flow of a Bingham fluid is completely solved with closed expressions for both an imposed torque and an imposed angular velocity. The case of an Herschel–Bulkley fluid with $n \neq 1$ is more complex. Equation (3.10) can be integrated in closed form when n is rational, e.g. $n = 1/2, n = 1/3, n = 2/3$, etc. The resulting expressions could be complex, but the general situation is similar to those of a Bingham fluid. For a general n value, Eq. (3.10) should be solved by a numerical method. This is the aim of the next sections.

3.7 Time Discretization

The methodology for the time discretization is similar to those used for the Navier–Stokes equations, as presented in Sect. 1.7, p. 26. The method of characteristics is considered here for the discretization of the Lagrange derivative of the velocity by using a first order implicit scheme.

Algorithm 3.1 (*First order implicit scheme – viscoplastic fluid*)

- $m = 0$: let $\boldsymbol{u}_0$, the initial condition, being given
- $m \geqslant 0$: let $\boldsymbol{u}_m$ being known, find $\boldsymbol{\sigma}_{m+1}$, $\boldsymbol{u}_{m+1}$ and p_{m+1} such that

$$\begin{cases} \boldsymbol{\sigma}_{m+1} = 2K\,|2D\,(\boldsymbol{u}_{m+1})|^{-1+n}\; D\,(\boldsymbol{u}_{m+1}) + \sigma_0 \dfrac{D\,(\boldsymbol{u}_{m+1})}{|D\,(\boldsymbol{u}_{m+1})\,|} \\ \qquad\qquad\qquad\qquad\qquad\qquad \text{when } D\,(\boldsymbol{u}_{m+1}) \neq 0 \\ |\boldsymbol{\sigma}_{m+1}| \leqslant \sigma_0 \qquad\qquad\qquad\qquad \text{otherwise} \end{cases}$$

$$\begin{aligned} \frac{\rho}{\Delta t}\boldsymbol{u}_{m+1} - \mathbf{div}\,\boldsymbol{\sigma} + \nabla p_{m+1} &= \rho \boldsymbol{g} + \frac{\rho}{\Delta t}\boldsymbol{u}_m \circ X_m \text{ in } \Omega \\ -\mathrm{div}\,\boldsymbol{u}_{m+1} &= 0 \text{ in } \Omega \\ \boldsymbol{u}_{m+1} &= \boldsymbol{u}_\Gamma(t_{m+1}) \text{ on } \partial\Omega \end{aligned}$$

where X_m denotes the first order approximation of the characteristic line, defined by $X_m(\boldsymbol{x}) = \boldsymbol{x} - \Delta t\, \boldsymbol{u}_m(\boldsymbol{x})$ for all $\boldsymbol{x} \in \Omega$. Thus, at each step of this algorithm, there is a nonlinear subproblem to solve. Dropping the $m+1$ subscript for clarity, the subproblem writes:

(P): find $\boldsymbol{\sigma}$, $\boldsymbol{u}$ and p, defined in Ω such that

$$\boldsymbol{\sigma} = 2K|2D(\boldsymbol{u})|^{-1+n}\, D(\boldsymbol{u}) + \sigma_0 \frac{D(\boldsymbol{u})}{|D(\boldsymbol{u})|} \quad \text{when } D(\boldsymbol{u}) \neq 0 \tag{3.14a}$$

$$|\boldsymbol{\sigma}| \leqslant \sigma_0 \quad \text{otherwise}$$

$$\kappa \boldsymbol{u} - \mathbf{div}\,\boldsymbol{\sigma} + \nabla p = \boldsymbol{f} \text{ in } \Omega \tag{3.14b}$$

$$\mathrm{div}\,\boldsymbol{u} = 0 \text{ in } \Omega \tag{3.14c}$$

$$\boldsymbol{u} = \boldsymbol{u}_\Gamma \text{ on } \partial\Omega \tag{3.14d}$$

where $\kappa \geqslant 0$, $\boldsymbol{f}$ and $\boldsymbol{u}_\Gamma$ are given. For simplicity and without loss of generality, we suppose in the rest of this chapter that $\kappa = 0$: the extension to $\kappa > 0$ do not present any difficulty. The resulting subproblem corresponds to the stationary solution of viscoplastic fluid flow problem when inertia terms are neglected.

3.8 Variational Formulation

For complex flows problems, the explicit computation of the solution is no more possible. In that case, we aim at computing an approximation by using numerical methods. The usual methodology for computing an approximation with the finite element method is to write first a variational formulation of the problem and next to replace the functional spaces by finite dimensional approximations. So, let us turn to the variational formulation of the problem.

Let us consider the decomposition $\mathscr{D} = \mathscr{D}_1 + \mathscr{D}_2$ of the energy of dissipation, as introduced in Lemma 3.4, where $\mathscr{D}_1$ and $\mathscr{D}_2$ was defined in Lemmas 3.2 and 3.3, respectively:

$$\mathscr{D}_1(\boldsymbol{\delta}) = \frac{K}{1+n}|2\boldsymbol{\delta}|^{1+n} \text{ and } \mathscr{D}_2(\boldsymbol{\delta}) = \sigma_0\,|2\boldsymbol{\delta}|, \quad \forall \boldsymbol{\delta} \in \mathbb{R}^{3\times 3}_s$$

Then, for all $\boldsymbol{\delta} \in \mathbb{R}^{3\times 3}_s$, we have

$$\begin{aligned}
&\boldsymbol{\sigma} \in \mathscr{D}(\boldsymbol{\delta}) \\
\Longleftrightarrow\ &\exists\, \boldsymbol{\sigma}_1 \in \partial\mathscr{D}_1(\boldsymbol{\delta}),\ \boldsymbol{\sigma}_2 \in \partial\mathscr{D}_2(\boldsymbol{\delta}) \,/\, \boldsymbol{\sigma} = \boldsymbol{\sigma}_1 + \boldsymbol{\sigma}_2 \\
\Longleftrightarrow\ &\exists\, \boldsymbol{\sigma}_2 \in \partial\mathscr{D}_2(\boldsymbol{\delta}) \,/\, \boldsymbol{\sigma} = 2K|2\boldsymbol{\delta}|^{-1+n}\boldsymbol{\delta} + \boldsymbol{\sigma}_2 \\
\Longleftrightarrow\ &\boldsymbol{\sigma} - 2K|2\boldsymbol{\delta}|^{-1+n}\boldsymbol{\delta} \in \partial\mathscr{D}_2(\boldsymbol{\delta}) \\
\Longleftrightarrow\ &\sigma_0|2\boldsymbol{\delta}| + (\boldsymbol{\sigma} - 2K|2\boldsymbol{\delta}|^{-1+n}\boldsymbol{\delta}) : \boldsymbol{\xi} \leqslant \sigma_0|2\boldsymbol{\xi}|, \quad \forall \boldsymbol{\xi} \in \mathbb{R}^{3\times 3}_s
\end{aligned}$$

Next, replace $\boldsymbol{\delta}$ by $D(\boldsymbol{u})$ and $\boldsymbol{\xi}$ by $D(\boldsymbol{v})$ and integrate over the flow domain Ω. This leads to a variational inequality.

$$a(\boldsymbol{u};\, \boldsymbol{u}, \boldsymbol{v}) + j(\boldsymbol{v}) - j(\boldsymbol{u}) \geqslant \int_\Omega \boldsymbol{\sigma} : D(\boldsymbol{v})\,\mathrm{d}x, \quad \forall \boldsymbol{v} \in K(0) \tag{3.15}$$

where the forms a and j are defined by

$$\begin{aligned}
a(\bar{\boldsymbol{u}};\, \boldsymbol{u}, \boldsymbol{v}) &= \int_\Omega 2K|2D(\bar{\boldsymbol{u}})|^{-1+n} D(\boldsymbol{u}) : D(\boldsymbol{v})\,\mathrm{d}x \\
j(\boldsymbol{u}) &= \int_\Omega \sigma_0|2D(\boldsymbol{u})|\,\mathrm{d}x
\end{aligned}$$

and $K(\boldsymbol{u}_\Gamma)$ denotes as usual the divergence-free vector field that satisfies the boundary condition:

$$K(\boldsymbol{u}_\Gamma) = \left\{ \boldsymbol{v} \in \left(W^{1,1+n}(\Omega)\right)^3 ;\ \operatorname{div} \boldsymbol{v} = 0 \text{ and } \boldsymbol{v} = \boldsymbol{u}_\Gamma \text{ on } \partial\Omega \right\}$$

Lets recall the conservation of momentum (3.14b)

$$-\mathbf{div}\,\boldsymbol{\sigma} + \nabla p = \boldsymbol{f} \text{ in } \Omega$$

Next, we multiply the previous relation by $\boldsymbol{v}$ satisfying $\boldsymbol{v} = 0$ on $\partial\Omega$, and we integrate over Ω. Applying the tensorial version of the divergence formula Corollary 1.3, p. 10, we obtain:

$$\int_\Omega \boldsymbol{\sigma} : D(\boldsymbol{v})\,\mathrm{d}x = \int_\Omega \boldsymbol{f}.\boldsymbol{v}\,\mathrm{d}x, \quad \forall \boldsymbol{v} \in K(0) \tag{3.16}$$

Summing (3.15) and (3.16) leads to the following variational formulation of the problem:

(FV): find $\boldsymbol{u} \in K(\boldsymbol{u}_\Gamma)$ such that

$$a(\boldsymbol{u};\ \boldsymbol{u}, \boldsymbol{v}) + j(\boldsymbol{v}) - j(\boldsymbol{u}) \geqslant \ell(\boldsymbol{v}), \quad \forall \boldsymbol{v} \in K(0)$$

where

$$\ell(\boldsymbol{v}) = \int_\Omega \boldsymbol{f}.\boldsymbol{v}\,\mathrm{d}x$$

Thus, there is no equations in the variational formulation: we finally obtain variational inequality. It is a major difference with the previous variational formulations in Chaps. 1 and 2. We can now reintroduce the pressure as a Lagrange multiplier and replace here the functional spaces by some finite dimensional counterparts. The result is a finite dimensional problem, composed of an huge system of non-linear inequalities. This problem is difficult to solve efficiently, even with the most recent algorithms. Nevertheless, these is at least two well-known ways to circumvent this difficulty: the regularization approach and the augmented Lagrangian algorithm. The following sections present these two methods before to show some examples of numerical computations.

3.9 Regularization Method

The main idea of the regularization method is to modify the problem is order go back to standard equations, where efficient algorithms are available. Let $\varepsilon \geqslant 0$ and set

$$\boldsymbol{\sigma}_\varepsilon = 2\left(K|2D(\boldsymbol{u})|^{-1+n} + \frac{\sigma_0}{\left(|2D(\boldsymbol{u})|^2 + \varepsilon^2\right)^{\frac{1}{2}}} \right) D(\boldsymbol{u})$$

where ε is the regularization parameter. When $\varepsilon = 0$, we go back to the previous constitutive equation when $D(\boldsymbol{u}) \neq 0$. When $\varepsilon > 0$, the previous relation is well-defined, even when $D(\boldsymbol{u}) = 0$. Next, let us define the following viscosity function (see Bercovier and Engelman [16]):

$$\eta_\varepsilon(\xi) = K\xi^{\frac{-1+n}{2}} + \frac{\sigma_0}{(\xi+\varepsilon^2)^{\frac{1}{2}}}, \ \forall \xi \in \mathbb{R}^+$$

Then, the previous relation writes:

$$\boldsymbol{\sigma}_\varepsilon = 2\eta_\varepsilon\left(|2D(\boldsymbol{u})|^2\right) D(\boldsymbol{u}) \tag{3.17}$$

When $\varepsilon > 0$, the fluid is a quasi-Newtonian one, as defined in Chap. 2. By this way, there is no more division by zero when $D(\boldsymbol{u}) = 0$ and we known efficient algorithm to solve such quasi-Newtonian fluid flow problems. Figure 3.6 plots the stress and the viscosity function versus the shear rate. From Sect. 2.6, we obtain the following expression of the energy function:

$$\mathscr{D}_\varepsilon(\xi) = \frac{1}{2}\int_0^\xi \eta_\varepsilon(s)\,\mathrm{d}s \ = \ \frac{K}{1+n}\xi^{\frac{1+n}{2}} + \frac{\sigma_0}{2}\left(\sqrt{\xi+\varepsilon^2} - \varepsilon\right)$$

This function is represented on Fig. 3.7 versus the shear rate: observe the convexity of the curve. Note also that the viscosity function is strictly decreasing (see also Fig. 3.6): the fluid is a shear-thinning one. Following Lemma 2.2, let us define

$$\begin{aligned}\nu_\varepsilon(\xi) &= \eta_\varepsilon(\xi) + 2\eta'_\varepsilon(\xi)\,\xi \\ &= nK\xi^{\frac{-1+n}{2}} + \sigma_0\varepsilon^2\left(\xi+\varepsilon^2\right)^{-3/2} \geqslant 0, \quad \forall \xi \in \mathbb{R}^+\end{aligned}$$

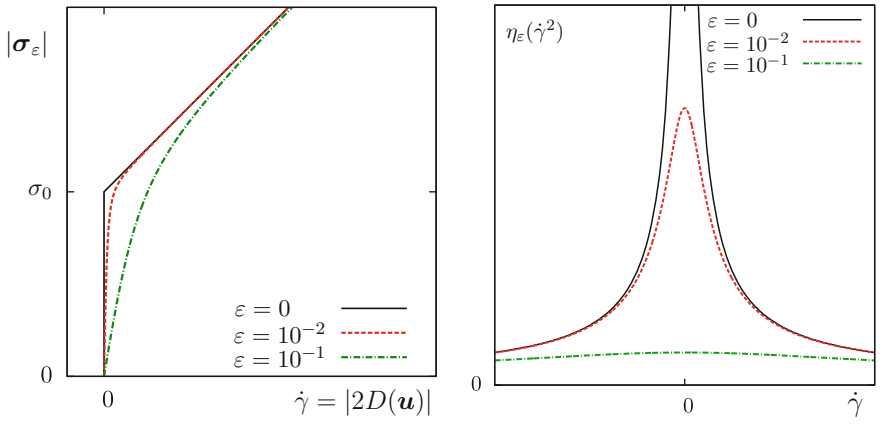

Fig. 3.6 Regularization for viscoplastic fluids: (*left*) the stress; (*right*) the viscosity

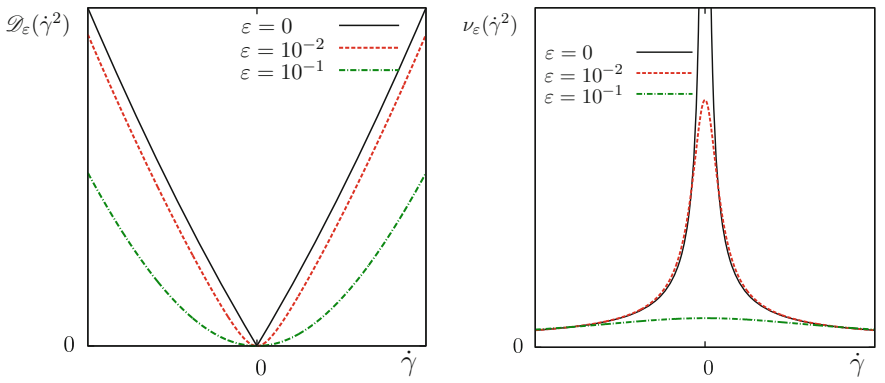

Fig. 3.7 Regularization for viscoplastic fluids: (*left*) energy; (*right*) coercivity criterion

Thus, hypothesis of Lemma 2.2 are satisfied and, from Theorem 2.2, the Newton method defines a well-defined sequence. A first weakness of this approach is the lack of general convergence results versus ε for the solution, denoted as $\boldsymbol{u}_\varepsilon$, of the regularized problem to the original solution $\boldsymbol{u}$ when $\varepsilon \longrightarrow 0$. In [123, p. 370] there is a convergence result for the Bingham model ($n = 1$) and the one-dimensional Poiseuille flow (Ω is a circular pipe section). This convergence result writes:

$$\|\boldsymbol{u} - \boldsymbol{u}_\varepsilon\|_{H^1(\Omega)} \leqslant c\,\varepsilon\sqrt{|\log\varepsilon|} \tag{3.18a}$$

$$\|\boldsymbol{u} - \boldsymbol{u}_\varepsilon\|_{L^\infty(\Omega)} \leqslant c\,\varepsilon \tag{3.18b}$$

where $c > 0$ is a constant independent of ε. There is no convergence results concerning the corresponding stress deviator $\boldsymbol{\sigma}_\varepsilon$ and, from numerical experiences, there is no evidence that this quantity converges to $\boldsymbol{\sigma}$. Recall that this quantity is crucial for the determination of rigid zones, characterized by $\{|\boldsymbol{\sigma}_\varepsilon| < \sigma_0\}$. Thus, we need a pointwise convergence (i.e. in L^∞ norm) of $\boldsymbol{\sigma}_\varepsilon$ to $\boldsymbol{\sigma}$ when ε tends to zero. From (3.17), observe that $\boldsymbol{\sigma}_\varepsilon$ involves a product of η_ε and $D(\boldsymbol{u}_\varepsilon)$. There is a trouble with rigid regions, where the fluid is in rigid motion, i.e. where $D(\boldsymbol{u}_\varepsilon)$ tends to zero with ε. Recall that the velocity and its gradient are convergent with ε. In that case, as the viscosity η_ε involves a division by $|D(\boldsymbol{u}_\varepsilon)|$, this viscosity tends to infinity, their product in the expression of $\boldsymbol{\sigma}_\varepsilon$ appears as indeterminate and there is no evidence that this product tends here to some finite value. Practical computations with the regularization methods are no able to observe any convergence of the stress deviator when ε tends to zero.

A second weakness of this approach is the disappearance of rigid regions, considered as $D(\boldsymbol{u}) = 0$. For instance, when solving the Poiseuille flow problem with this modified model, the velocity is no more constant at the center of the pipe. For the Couette flow, there is no more dead region and the position of the localization is difficult to determine. Finally, with this modified problem, there is no more *arrested state*: the flow do never stops when the load is lower than the critical value. The arrested

state and the limit load analysis could not be established clearly. The prediction of stability of building foundations in civil engineering or mechanical robustness of engine parts becomes thus problematic. Also when trying to predict natural hazards, such as landslides, mud flows, snow avalanches or volcanic lava flows, the disastrous event is always predicted, as the material can never be at the rest on a slope under the gravity forces. Nevertheless, this approach remains simple and also useful when computations do not aim at predicting accurately either the rigid regions or the arrested state. The next chapter presents a different approach that is able to address accurately both the rigid regions and the arrested state.

3.10 Augmented Lagrangian Algorithm

In Sect. 3.1 the problem was defined as a minimization one:

$$\boldsymbol{u} = \underset{\boldsymbol{v} \in K(\boldsymbol{u}_\Gamma)}{\arg\inf}\ J(\boldsymbol{v})$$

where

$$J(\boldsymbol{u}) = \frac{K}{1+n} \int_\Omega |2D(\boldsymbol{u})|^{1+n}\, \mathrm{d}x + \sigma_0 \int_\Omega |2D(\boldsymbol{u})|\, \mathrm{d}x - \int_\Omega \boldsymbol{f}.\boldsymbol{u}\, \mathrm{d}x$$

and where $K(\boldsymbol{u}_\Gamma)$ denotes as usual the set of divergence-free vector fields that satisfies the boundary condition $\boldsymbol{u} = \boldsymbol{u}_\Gamma$ on $\partial\Omega$. Let us reintroduce the pressure as a Lagrange multiplier associated to the divergence-free constraint. We also introduce a new independent variable $\boldsymbol{\delta}$ satisfying $\boldsymbol{\delta} = 2D(\boldsymbol{u})$. The relation $\boldsymbol{\delta} = 2D(\boldsymbol{u})$ is treated as a new constraint and is imposed with an additional Lagrange multiplier denoted as $\boldsymbol{\sigma}$. This notation is coherent, as $\boldsymbol{\sigma}$ will coincides with the stress deviator. The situation is as follows:

Constraint	Lagrange multiplier
$\operatorname{div} \boldsymbol{u} = 0$	p
$\boldsymbol{\delta} = D(\boldsymbol{u})$	$\boldsymbol{\sigma}$

Let us introduce the following Lagrangian:

$$\begin{aligned} L(\boldsymbol{u}, \boldsymbol{\delta};\ p, \boldsymbol{\sigma}) = {} & \frac{K}{1+n} \int_\Omega |\boldsymbol{\delta}|^{1+n}\, \mathrm{d}x + \sigma_0 \int_\Omega |\boldsymbol{\delta}|\, \mathrm{d}x - \int_\Omega \boldsymbol{f}.\boldsymbol{u}\, \mathrm{d}x \\ & - \int_\Omega p \operatorname{div} \boldsymbol{u}\, \mathrm{d}x + \frac{1}{2} \int_\Omega \boldsymbol{\sigma} : (2D(\boldsymbol{u}) - \boldsymbol{\delta})\, \mathrm{d}x \\ & + \frac{\alpha}{2} \int_\Omega |2D(\boldsymbol{u}) - \boldsymbol{\delta}|^2\, \mathrm{d}x \end{aligned} \tag{3.19}$$

Here, $\alpha \geqslant 0$ is an augmentation parameter and when $\alpha \neq 0$ the Lagrangian is called an *augmented Lagrangian*. The problem can be reformulated equivalently into a saddle point one:

$$(\boldsymbol{u}, \boldsymbol{\delta};\, p, \boldsymbol{\sigma}) \;=\; \underset{(\boldsymbol{v},\boldsymbol{\gamma})\in V(\boldsymbol{u}_\Gamma)\times L^2(\Omega)^{d\times d}_s}{\arg\inf} \;\; \underset{(q,\tau)\in L^2(\Omega)\times L^2(\Omega)^{d\times d}_s}{\sup} L(\boldsymbol{v}, \boldsymbol{\gamma}; q, \boldsymbol{\tau}) \tag{3.20}$$

where

$$V(\boldsymbol{u}_\Gamma) = \left\{ \boldsymbol{v} \in \left(H^1(\Omega)\right)^3 ;\; \boldsymbol{v} = \boldsymbol{u}_\Gamma \text{ on } \partial\Omega \right\}$$

Observe that the solution is independent upon the augmentation parameter: as the corresponding term involves the square of the constraint and this term vanishes for the solution. Observe also that the Lagrangian L is differentiable with respect to $\boldsymbol{u}$, p and $\boldsymbol{\sigma}$, but not with respect to $\boldsymbol{\delta}$. Recall that when L is differentiable, a saddle point is characterized as the solution of the following equations:

$$\frac{\partial L}{\partial \boldsymbol{v}} = \frac{\partial L}{\partial \boldsymbol{\delta}} = \frac{\partial L}{\partial p} = \frac{\partial L}{\partial \boldsymbol{\sigma}} = 0$$

Thus, here it is not possible since L is not differentiable vs $\boldsymbol{\delta}$. A similar difficulty was already pointed out in Sect. 3.2. But now, there is a way to circumvent this difficulty. Let us define the following *dual energy* functional:

$$J_*(\boldsymbol{\sigma}) = - \underset{(\boldsymbol{v},\boldsymbol{\gamma})\in V(\boldsymbol{u}_\Gamma)\times L^2(\Omega)^{3\times 3}_s}{\inf} \;\; \underset{q\in L^2(\Omega)}{\sup} L(\boldsymbol{v}, \boldsymbol{\gamma}; q, \boldsymbol{\sigma})$$

Note that J_* is differentiable, as L is differentiable with respect to $\boldsymbol{\sigma}$. Thus, a simple fixed step descent algorithm is possible.

Algorithm 3.2 (*Uzawa algorithm – abstract version*)

- $k = 0$: let $\boldsymbol{\sigma}_0$ being given
- $k \geqslant 0$: let $\boldsymbol{\sigma}_k$ being known, compute $\boldsymbol{\sigma}_{k+1} = \boldsymbol{\sigma}_k - \beta J'_*(\boldsymbol{\sigma}_k)$

Note that a similar dual descent approach was previously considered, at Sect. 1.13, p. 56, in the context of the Navier–Stokes equation, for defining an iterative solver of the Stokes problem. It remains to unpack the notation J_*, and specifically, to compute its derivative:

$$\begin{aligned} J'_*(\boldsymbol{\sigma}_k) &= -\frac{\partial L}{\partial \boldsymbol{\sigma}}(\boldsymbol{u}_k, \boldsymbol{\delta}_k;\; p_k, \boldsymbol{\sigma}_k) \\ &= \boldsymbol{\delta}_k - 2D(\boldsymbol{u}_k) \end{aligned}$$

where

$$(\boldsymbol{u}_k, \boldsymbol{\delta}_k;\, p_k) \;=\; \underset{(\boldsymbol{v},\boldsymbol{\gamma})\in V(\boldsymbol{u}_\Gamma)\times L^2(\Omega)^{3\times 3}_s}{\arg\inf} \quad \sup_{q\in L^2(\Omega)} L(\boldsymbol{v},\boldsymbol{\gamma};\, q, \boldsymbol{\sigma}_k)$$

The Uzawa algorithm writes now more explicitly.

Algorithm 3.3 (*Uzawa algorithm – semi-abstract version*)

- $k = 0$: let $\boldsymbol{\sigma}_0$ being given
- $k \geqslant 0$: let $\boldsymbol{\sigma}_k$ being known, compute

$$(\boldsymbol{u}_k, \boldsymbol{\delta}_k;\, p_k) = \underset{(\boldsymbol{v},\boldsymbol{\gamma})\in V(\boldsymbol{u}_\Gamma)\times L^2(\Omega)^{3\times 3}_s}{\arg\inf} \quad \sup_{q\in L^2(\Omega)} L(\boldsymbol{v},\boldsymbol{\gamma};\; q, \boldsymbol{\sigma}_k)$$

$$\boldsymbol{\sigma}_{k+1} = \boldsymbol{\sigma}_k + \beta(2D(\boldsymbol{u}_k) - \boldsymbol{\delta}_k)$$

Recall that L is differentiable with respect to $(\boldsymbol{u},\, p)$ but not with respect to $\boldsymbol{\delta}$. A good strategy is to decouple the minimization in these two directions. The computation is decomposed in two steps: we compute first $(\boldsymbol{u}_k,\, p_k)$ and then $\boldsymbol{\delta}_k$.

Algorithm 3.4 (*Uzawa algorithm – abstract decoupled version*)

- $k = 0$: let $\boldsymbol{\sigma}_0$ and $\boldsymbol{\delta}_{-1}$ being given
- $k \geqslant 0$: let $\boldsymbol{\sigma}_k$ and $\boldsymbol{\delta}_{k-1}$ being known, compute

$$(\boldsymbol{u}_k,\, p_k) = \underset{\boldsymbol{v}\in V(\boldsymbol{u}_\Gamma)}{\arg\inf} \quad \sup_{q\in L^2(\Omega)} L(\boldsymbol{v}, \boldsymbol{\delta}_{k-1};\; q, \boldsymbol{\sigma}_k) \tag{3.21a}$$

$$\boldsymbol{\delta}_k = \underset{\boldsymbol{\gamma}\in L^2(\Omega)^{3\times 3}_s}{\arg\inf} \; L(\boldsymbol{u}_k, \boldsymbol{\gamma};\; p_k, \boldsymbol{\sigma}_k) \tag{3.21b}$$

$$\boldsymbol{\sigma}_{k+1} = \boldsymbol{\sigma}_k + \beta(2D(\boldsymbol{u}_k) - \boldsymbol{\delta}_k) \tag{3.21c}$$

One iteration of the algorithm presents three steps. As L is differentiable with respect to $(\boldsymbol{u},\, p)$, the first step (3.21a) is quite standard. Moreover, a rapid inspection shows that L is quadratic in $\boldsymbol{u}$ and linear in p: the resulting problem is linear. As L is not differentiable with respect to $\boldsymbol{\delta}$, the second step (3.21b) is more complex. Finally, the third step (3.21c) is already explicit, and there is nothing to do.

Let us study the first step (3.21a):

$$(\boldsymbol{u}_k,\, p_k) = \underset{\boldsymbol{v}\in V(\boldsymbol{u}_\Gamma)}{\arg\inf} \quad \sup_{q\in L^2(\Omega)} L(\boldsymbol{v}, \boldsymbol{\delta}_{k-1};\; q, \boldsymbol{\sigma}_k)$$

$$\Longleftrightarrow \text{ find } (\boldsymbol{u}_k,\, p_k) \in V(\boldsymbol{u}_\Gamma) \times L^2(\Omega) \text{ such that}$$

$$\begin{cases} \dfrac{\partial L}{\partial \boldsymbol{u}}(\boldsymbol{u}_k, \boldsymbol{\delta}_{k-1};\; p_k, \boldsymbol{\sigma}_k).(\boldsymbol{v}) = 0, \quad \forall \boldsymbol{v} \in V(0) \\[2ex] \dfrac{\partial L}{\partial p}(\boldsymbol{u}_k, \boldsymbol{\delta}_{k-1};\; p_k, \boldsymbol{\sigma}_k).(q) = 0, \quad \forall q \in L^2(\Omega) \end{cases}$$

From the definition (3.19) of the augmented Lagrangian L, we obtain without difficulties the following Gâteaux derivatives:

$$\begin{aligned}\frac{\partial L}{\partial p}(\boldsymbol{u},\boldsymbol{\delta};\ p,\boldsymbol{\sigma}).(q) &= -\int_\Omega q\,\mathrm{div}\,\boldsymbol{u}\,\mathrm{d}x\\ \frac{\partial L}{\partial \boldsymbol{u}}(\boldsymbol{u},\boldsymbol{\delta};\ p,\boldsymbol{\sigma}).(\boldsymbol{v}) &= -\int_\Omega \boldsymbol{f}.\boldsymbol{v}\,\mathrm{d}x - \int_\Omega p\,\mathrm{div}\,\boldsymbol{v}\,\mathrm{d}x + \int_\Omega \boldsymbol{\sigma}:D(\boldsymbol{v})\,\mathrm{d}x\\ &\quad - \alpha\int_\Omega \boldsymbol{\delta}:D(\boldsymbol{v})\,\mathrm{d}x + 2\alpha\int_\Omega D(\boldsymbol{u}):D(\boldsymbol{v})\,\mathrm{d}x\end{aligned}$$

Then, the first step (3.21a) is equivalent to

(S_1): find $(\boldsymbol{u}_k,\ p_k)\in V(\boldsymbol{u}_\Gamma)\times L^2(\Omega)$ such that

$$\begin{aligned}&2\alpha\int_\Omega D(\boldsymbol{u}_k):D(\boldsymbol{v})\,\mathrm{d}x - \int_\Omega p_k\,\mathrm{div}\,\boldsymbol{v}\,\mathrm{d}x\\ &\qquad = \int_\Omega \boldsymbol{f}.\boldsymbol{v}\,\mathrm{d}x + \int_\Omega (\alpha\boldsymbol{\delta}_{k-1}-\boldsymbol{\sigma}_k):D(\boldsymbol{v})\,\mathrm{d}x,\quad \forall \boldsymbol{v}\in V(0)\\ &-\int_\Omega q\,\mathrm{div}\,\boldsymbol{u}_k\,\mathrm{d}x = 0,\quad \forall q\in L^2(\Omega)\end{aligned}$$

We recognize a Stokes-like problem. Let us introduce the following forms

$$a(\boldsymbol{u},\boldsymbol{v}) = 2\alpha\int_\Omega D(\boldsymbol{u}):D(\boldsymbol{v})\,\mathrm{d}x \ \text{ and } \ b(\boldsymbol{u},q) \ = \ -\int_\Omega q\,\mathrm{div}\,\boldsymbol{u}\,\mathrm{d}x$$

The decoupled Uzawa algorithm becomes:

Algorithm 3.5 (*Uzawa algorithm – semi-abstract decoupled version*)

- $k=0$: let $\boldsymbol{\sigma}_0$ and $\boldsymbol{\delta}_{-1}$ being given
- $k\geqslant 0$: let $\boldsymbol{\sigma}_k$ and $\boldsymbol{\delta}_{k-1}$ being known, compute

$$\ell_k(\boldsymbol{v}) = \int_\Omega \boldsymbol{f}.\boldsymbol{v}\,\mathrm{d}x + \int_\Omega (\alpha\boldsymbol{\delta}_{k-1}-\boldsymbol{\sigma}_k):D(\boldsymbol{v})\,\mathrm{d}x$$

find $(\boldsymbol{u}_k,\ p_k)\in V(\boldsymbol{u}_\Gamma)\times L^2(\Omega)$ such that

$$\begin{cases} a(\boldsymbol{u}_k,\boldsymbol{v}) + b(\boldsymbol{v},\ p_k) = \ell_k(\boldsymbol{v}),\ \forall \boldsymbol{v}\in V(0)\\ b(\boldsymbol{u}_k,q) \qquad\qquad\quad = 0, \qquad \forall q\in L^2(\Omega)\end{cases} \tag{3.22a}$$

$$\boldsymbol{\delta}_k = \underset{\boldsymbol{\gamma}\in L^2(\Omega)^{3\times 3}_s}{\arg\inf}\ L(\boldsymbol{u}_k,\boldsymbol{\gamma};\ p_k,\boldsymbol{\sigma}_k) \tag{3.22b}$$

$$\boldsymbol{\sigma}_{k+1} = \boldsymbol{\sigma}_k + \beta(2D(\boldsymbol{u}_k)-\boldsymbol{\delta}_k) \tag{3.22c}$$

It remains to work on the second step (3.22b) of this algorithm. Let us recall the definition (3.19) of the augmented Lagrangian:

$$L(\boldsymbol{u},\boldsymbol{\delta};\ p,\boldsymbol{\sigma}) = \frac{K}{1+n}\int_\Omega |\boldsymbol{\delta}|^{1+n}\,\mathrm{d}x + \sigma_0\int_\Omega |\boldsymbol{\delta}|\,\mathrm{d}x - \int_\Omega \boldsymbol{f}.\boldsymbol{u}\,\mathrm{d}x - \int_\Omega p\,\mathrm{div}\,\boldsymbol{u}\,\mathrm{d}x + \frac{1}{2}\int_\Omega \boldsymbol{\sigma}:(2D(\boldsymbol{u})-\boldsymbol{\delta})\,\mathrm{d}x + \frac{\alpha}{2}\int_\Omega |2D(\boldsymbol{u})-\boldsymbol{\delta}|^2\,\mathrm{d}x$$

Recall that L is not differentiable with respect to $\boldsymbol{\delta}$. Nevertheless, there is no space derivation, such as gradient of divergence, with respect to $\boldsymbol{\delta}$, and thus, the minimization can be performed pointwise for almost all $\boldsymbol{x}\in\Omega$:

$$\begin{aligned} \boldsymbol{\delta}_k &= \inf_{\boldsymbol{\delta}\in L^2(\Omega)_s^{3\times 3}} L(\boldsymbol{u}_k,\boldsymbol{\delta};\ p_k,\boldsymbol{\sigma}_k) \\ \Longleftrightarrow\quad \boldsymbol{\delta}_k(\boldsymbol{x}) &= \min_{\boldsymbol{\delta}\in\mathbb{R}_s^{3\times 3}} \Phi_{\boldsymbol{x}}(\boldsymbol{\delta}) \end{aligned}$$

where

$$\Phi_{\boldsymbol{x}}(\boldsymbol{\delta}) = \frac{\alpha}{2}|\boldsymbol{\delta}|^2 + \frac{K}{1+n}|\boldsymbol{\delta}|^{1+n} + \sigma_0|\boldsymbol{\delta}| - \frac{\boldsymbol{\chi}(\boldsymbol{x}):\boldsymbol{\delta}}{2},\quad \forall\boldsymbol{\delta}\in\mathbb{R}_s^{3\times 3} \tag{3.23a}$$

$$\boldsymbol{\chi}(\boldsymbol{x}) = \boldsymbol{\sigma}_k + 2\alpha D(\boldsymbol{u}_k) \tag{3.23b}$$

Note that the minimization problem involved in the second step of the algorithm has reduced from a minimization over $\left(L^2(\Omega)\right)_s^{3\times 3}$ to $\mathbb{R}_s^{3\times 3}$, which is a finite dimensional space. Observe also that $\Phi_{\boldsymbol{x}}$ is still not differentiable, but it is convex, and from Theorem 3.1, we have the following characterization of the minimum with the subdifferential:

$$\begin{aligned} \boldsymbol{\delta}_k(\boldsymbol{x}) &= \min_{\boldsymbol{\delta}\in\mathbb{R}_s^{3\times 3}} \Phi_{\boldsymbol{x}}(\boldsymbol{\delta}) \\ \Longleftrightarrow\quad &\text{find } \boldsymbol{\delta}_k(\boldsymbol{x})\in\mathbb{R}_s^{3\times 3} \text{ such that } 0\in\partial\Phi_{\boldsymbol{x}}(\boldsymbol{\delta}_k(\boldsymbol{x})) \end{aligned}$$

It remains to compute the subdifferential $\partial\Phi_{\boldsymbol{x}}$ with the help of optimization tools presented in Sect. 3.2, and since $\Phi_{\boldsymbol{x}}$ is the sum of a differentiable and a non-differentiable function, as in Lemma 3.4, we get:

$$\partial\Phi_{\boldsymbol{x}}(\boldsymbol{\delta}) = \begin{cases} \left\{\boldsymbol{\tau} = \dfrac{K}{2}|\boldsymbol{\delta}|^{-1+n}\boldsymbol{\delta} + \dfrac{\alpha}{2}\boldsymbol{\delta} + \dfrac{\sigma_0}{2}\dfrac{\boldsymbol{\delta}}{|\boldsymbol{\delta}|} - \dfrac{\boldsymbol{\chi}(\boldsymbol{x})}{2}\right\} & \text{when } \boldsymbol{\delta}\neq 0 \\ \left\{\boldsymbol{\tau} = \boldsymbol{\lambda} - \dfrac{\boldsymbol{\chi}(\boldsymbol{x})}{2};\ \boldsymbol{\lambda}\in\mathbb{R}_s^{d\times d} \text{ and } |\boldsymbol{\lambda}|\leqslant\dfrac{\sigma_0}{2}\right\} & \text{otherwise} \end{cases} \tag{3.24}$$

It remains to find $\boldsymbol{\delta}\in\mathbb{R}_s^{3\times 3}$ such that $0\in\partial\Phi_{\boldsymbol{x}}(\boldsymbol{\delta})$. This can be done in an elegant way with the help of some additional optimization tools.

Definition 3.5 (*Convex conjugate and Fenchel transformation*)
For any convex function Φ, the *convex conjugate* Φ^* is defined by the *Fenchel transformation*

$$\Phi^*(\boldsymbol{\tau}) = \boldsymbol{\tau} : \boldsymbol{\delta} - \Phi(\boldsymbol{\delta}), \quad \forall \boldsymbol{\tau} \in \partial\Phi(\boldsymbol{\delta}),\ \forall \dot{\boldsymbol{\varepsilon}} \in \mathbb{R}^{d\times d}_s$$

Property 3.1 (Subdifferential of the convex conjugate)
For any convex function Φ, we have for all $\boldsymbol{\tau}, \boldsymbol{\delta} \in \mathbb{R}^{d\times d}_s$

$$\boldsymbol{\tau} \in \partial\Phi(\boldsymbol{\delta}) \Longleftrightarrow \boldsymbol{\delta} \in \partial\Phi^*(\boldsymbol{\tau}) \iff \Phi(\boldsymbol{\delta}) + \Phi^*(\boldsymbol{\tau}) = \boldsymbol{\tau} : \boldsymbol{\delta}$$

Proof It is a classical result of convex analysis: see e.g. [263, p. 35]. □

Lemma 3.5 (Subdifferential of the convex conjugate of $\Phi_{\boldsymbol{x}}$)
The convex conjugate $\Phi^*_{\boldsymbol{x}}$ of the function $\Phi_{\boldsymbol{x}}$ defined by (3.23a) is differentiable and $\Phi^{*'}_{\boldsymbol{x}}(\boldsymbol{\tau}) = P(\boldsymbol{\tau} + \boldsymbol{\chi}(\boldsymbol{x}))$, for all $\boldsymbol{\tau} \in \mathbb{R}^{3\times 3}_s$, where P is the following projector, defined for all $\boldsymbol{\xi} \in \mathbb{R}^{3\times 3}_s$

$$P(\boldsymbol{\xi}) = \begin{cases} \psi^{-1}(|\boldsymbol{\xi}| - \sigma_0)\dfrac{\boldsymbol{\xi}}{|\boldsymbol{\xi}|} & \text{when } |\boldsymbol{\xi}| > \sigma_0 \\ \\ 0 & \text{otherwise} \end{cases} \tag{3.25}$$

and where ψ is the invertible function defined from $\mathbb{R}^+$ into $\mathbb{R}^+$ by

$$\psi(\xi) = K\xi^n + \alpha\xi, \quad \forall \xi \in \mathbb{R}^+ \tag{3.26}$$

Proof Since $\psi'(\xi) = nK\xi^{-1+n} + \alpha > 0$, $\forall \xi > 0$ then ψ is strictly increasing and invertible over $\mathbb{R}^+$. Thus, ψ^{-1} is well defined. Let us find $\boldsymbol{\delta} \in \mathbb{R}^{3\times 3}_s$ such that $\boldsymbol{\tau} \in \partial\Phi_{\boldsymbol{x}}(\boldsymbol{\delta})$. First, we are looking for $\boldsymbol{\delta} \neq 0$. In that case, from (3.24), $\Phi_{\boldsymbol{x}}$ is differentiable and

$$\begin{aligned} & \Phi'_{\boldsymbol{x}}(\boldsymbol{\delta}) = \boldsymbol{\tau} \\ \Longleftrightarrow\ & K|\boldsymbol{\delta}|^{-1+n}\boldsymbol{\delta} + \alpha\boldsymbol{\delta} + \sigma_0\frac{\boldsymbol{\delta}}{|\boldsymbol{\delta}|} = \boldsymbol{\tau} + \boldsymbol{\chi}(\boldsymbol{x}) \end{aligned} \tag{3.27}$$

For convenience, let $\boldsymbol{\xi} = \boldsymbol{\tau} + \boldsymbol{\chi}(\boldsymbol{x})$. By tacking the norm of the previous relation, we get

$$K|\boldsymbol{\delta}|^n + \alpha|\boldsymbol{\delta}| = |\boldsymbol{\xi}| - \sigma_0$$

As the left-hand-side is always strictly positive, a necessary condition for the solution $\boldsymbol{\delta}$ to be different from zero is $|\boldsymbol{\chi}(\boldsymbol{x})| - \sigma_0 > 0$. Then, the previous relation writes also

$$\begin{aligned} & \psi(|\boldsymbol{\delta}|) = |\boldsymbol{\xi}| - \sigma_0 \\ \iff & |\boldsymbol{\delta}| = \psi^{-1}(|\boldsymbol{\xi}| - \sigma_0) \end{aligned} \tag{3.28}$$

Note that (3.27) writes also equivalently:

$$\left(K|\boldsymbol{\delta}|^{-1+n} + \alpha + \frac{\sigma_0}{|\boldsymbol{\delta}|} \right) \boldsymbol{\delta} = \boldsymbol{\xi}$$

It means that the two matrix $\boldsymbol{\delta}$ and $\boldsymbol{\xi}$ shares the same direction, and, since for $\boldsymbol{\delta} \neq 0$, we can write

$$\frac{\boldsymbol{\delta}}{|\boldsymbol{\delta}|} = \frac{\boldsymbol{\xi}}{|\boldsymbol{\xi}|} \iff \boldsymbol{\delta} = \frac{|\boldsymbol{\delta}|}{|\boldsymbol{\xi}|}\,\boldsymbol{\xi} = \frac{\psi^{-1}(|\boldsymbol{\xi}| - \sigma_0)}{|\boldsymbol{\xi}|}\,\boldsymbol{\xi} \qquad \text{from (3.28)}$$

Finally, the case $\boldsymbol{\delta} = 0$ correspond to $|\boldsymbol{\xi}| \leqslant \sigma_0$ and the proof is complete. □

Note that for the Bingham model ($n = 1$) we have $\psi(\xi) = (K + \alpha)\xi$ and its inverse is explicit: $\psi^{-1}(\zeta) = (K + \alpha)^{-1}\zeta$. Otherwise, when $n \neq 1$, an efficient inversion of ψ based on the Newton method is possible: it converges up to the machine precision in few iterations. With the help of the previous Lemma 3.5, the second step (3.22b) of the decoupled Uzawa algorithm can be solved explicitly and it involves only a pointwise computation:

$$\begin{aligned} & \boldsymbol{\delta}_k(\boldsymbol{x}) = \underset{\boldsymbol{\delta} \in \mathbb{R}^{3\times 3}_s}{\arg\min}\, \Phi_{\boldsymbol{x}}(\boldsymbol{\delta}) \\ \iff & \text{find } \boldsymbol{\delta}_k(\boldsymbol{x}) \in \mathbb{R}^{3\times 3}_s \text{ such that } 0 \in \partial \Phi_{\boldsymbol{x}}(\boldsymbol{\delta}_k(\boldsymbol{x})) \\ \iff & \boldsymbol{\delta}_k(\boldsymbol{x}) = \Phi^{*'}_{\boldsymbol{x}}(0) = P\ (\boldsymbol{\sigma}_k(\boldsymbol{x}) + 2\alpha D(\boldsymbol{u}_k)(\boldsymbol{x})) \end{aligned}$$

where P has been defined in (3.25). We are now able to write the final version of the decoupled Uzawa algorithm.

Algorithm 3.6 (*Uzawa algorithm – final decoupled version*)

- $k = 0$: let $\boldsymbol{\sigma}_0$ and $\boldsymbol{\delta}_{-1}$ being given
- $k \geqslant 0$: let $\boldsymbol{\sigma}_k$ and $\boldsymbol{\delta}_{k-1}$ being known, compute

$$\ell_k(\boldsymbol{v}) = \int_\Omega \boldsymbol{f}.\boldsymbol{v}\,\mathrm{d}x + \int_\Omega (\alpha\boldsymbol{\delta}_{k-1} - \boldsymbol{\sigma}_k) : D(\boldsymbol{v})\,\mathrm{d}x$$

$$\text{find } (\boldsymbol{u}_k, p_k) \in V(\boldsymbol{u}_\Gamma) \times L^2(\Omega) \text{ such that}$$

$$\begin{cases} a(\boldsymbol{u}_k, \boldsymbol{v}) + b(\boldsymbol{v}, p_k) = \ell_k(\boldsymbol{v}), & \forall \boldsymbol{v} \in V(0) \\ b(\boldsymbol{u}_k, q) = 0, & \forall q \in L^2(\Omega) \end{cases} \tag{3.29a}$$

$$\boldsymbol{\delta}_k = P(\boldsymbol{\sigma}_k + 2\alpha D(\boldsymbol{u}_k)) \tag{3.29b}$$

$$\boldsymbol{\sigma}_{k+1} = \boldsymbol{\sigma}_k + \beta(2D(\boldsymbol{u}_k) - \boldsymbol{\delta}_k) \tag{3.29c}$$

The main computation time of this algorithm is spend by solving the Stokes-like problem, as others computations are pointwise and explicit. See Chap. 1 for efficient algorithms of the Stokes problem. A convenient choice for the descent step is $\beta = \alpha$, for which the algorithm is convergent, as shown in the following result.

Theorem 3.3 (Convergence of the augmented Lagrangian algorithm) *Assume that* $0 < \beta < \dfrac{1+\sqrt{5}}{2}\alpha$. *Then, for all augmentation parameter* $\alpha > 0$, *the sequence* $(\boldsymbol{\delta}_k, \boldsymbol{u}_k, \boldsymbol{\sigma}_k, p_k)_{k\geqslant 0}$ *defined by Algorithm 3.6 is convergent and its limit* $(\boldsymbol{\delta}, \boldsymbol{u}, \boldsymbol{\sigma}, p)$ *is the solution of the saddle point problem* (3.20). *Moreover, we have* $\boldsymbol{\delta} = 2D(\boldsymbol{u})$ *and* $(\boldsymbol{\sigma}, \boldsymbol{u}, p)$ *is a solution of* (3.14a)–(3.14d) *in a weak sens. It means that the Lagrange multiplier* $\boldsymbol{\sigma}$ *coincides with the stress deviator.*

Proof For the convergence of the sequence, see e.g. [122, p. 85]. From (3.29a)–(3.29b), and unpacking the notations $a(.,.)$, $b(.,.)$ and $\ell(.)$, at convergence of the algorithm, the limit satisfies

$$\int_\Omega 2\alpha D(\boldsymbol{u}) : D(\boldsymbol{v})\,\mathrm{d}x - \int_\Omega p\,\mathrm{div}(\boldsymbol{v})\,\mathrm{d}x = \int_\Omega \boldsymbol{f}.\boldsymbol{v}\,\mathrm{d}x + \int_\Omega (\alpha\boldsymbol{\delta} - \boldsymbol{\sigma}) : D(\boldsymbol{v})\,\mathrm{d}x, \quad \forall \boldsymbol{v} \in V(0) \tag{3.30a}$$

$$-\int_\Omega q\,\mathrm{div}(\boldsymbol{u})\,\mathrm{d}x = 0, \quad \forall q \in L^2(\Omega) \tag{3.30b}$$

$$\boldsymbol{\delta} - 2D(\boldsymbol{u}) = 0 \tag{3.30c}$$

$$\boldsymbol{\delta} = P(\boldsymbol{\sigma} + 2\alpha D(\boldsymbol{u})) \tag{3.30d}$$

Then, (3.30c) leads to $\boldsymbol{\delta} = 2D(\boldsymbol{u})$ and (3.30a) becomes, after performing an integration by part (see Property 1.6 p. 31)

$$\int_\Omega (-\mathbf{div}(\boldsymbol{\sigma}) + \nabla p - \boldsymbol{f}).\boldsymbol{v}\,\mathrm{d}x = 0, \quad \forall \boldsymbol{v} \in V(0)$$

It means $-\mathbf{div}(\boldsymbol{\sigma}) + \nabla p = \boldsymbol{f}$ in a weak sens, in $\left(H^{-1}(\Omega)\right)^3$ which is the topological dual of $V(0) = \left(H_0^1(\Omega)\right)^3$. Note that this relation corresponds to the conservation of momentum (3.14b). Conversely, (3.30b) means $\mathrm{div}(\boldsymbol{u}) = 0$ i.e. the incompressibility is satisfied in a weak sens, in $L^2(\Omega)$.

It remains to show that (3.30d) is equivalent to the constitutive equation. This is not obvious, as it contains some occurrences of α. Assume first that $|\boldsymbol{\sigma} + 2\alpha D(\boldsymbol{u})| > \sigma_0$. Then, from the definition (3.25) of P, we have

$$2D(\boldsymbol{u}) = \psi^{-1}(|\boldsymbol{\sigma} + 2\alpha D(\boldsymbol{u})| - \sigma_0)\frac{\boldsymbol{\sigma} + 2\alpha D(\boldsymbol{u})}{|\boldsymbol{\sigma} + 2\alpha D(\boldsymbol{u})|}$$

It implies that $D(\boldsymbol{u})$ and $\boldsymbol{\sigma}$ share the same direction. Taking the norm of the previous relation yields $|2D(\boldsymbol{u})| = \psi^{-1}(|\boldsymbol{\sigma} + 2\alpha D(\boldsymbol{u})| - \sigma_0)$ or equivalently, using

the definition (3.26) of ψ: $|\boldsymbol{\sigma} + 2\alpha D(\boldsymbol{u})| - \sigma_0 = \psi(|2D(\boldsymbol{u})|) = K|2D(\boldsymbol{u})|^n + \alpha|2D(\boldsymbol{u})|$. As $D(\boldsymbol{u})$ and $\boldsymbol{\sigma}$ share the same direction, this simplifies as $|\boldsymbol{\sigma}| = K|2D(\boldsymbol{u})|^n + \sigma_0$ which is independent of the augmentation parameter α. The condition $|\boldsymbol{\sigma} + 2\alpha D(\boldsymbol{u})| > \sigma_0$ is then equivalent to $K|2D(\boldsymbol{u})|^n + \alpha|2D(\boldsymbol{u})| > 0$ which is also equivalent to $D(\boldsymbol{u}) \neq 0$. As $D(\boldsymbol{u})$ and $\boldsymbol{\sigma}$ share the same direction and $D(\boldsymbol{u}) \neq 0$ we obtain

$$\boldsymbol{\sigma} = 2K|2D(\boldsymbol{u})|^{-1+n} D(\boldsymbol{u}) + \sigma_0 \frac{D(\boldsymbol{u})}{|D(\boldsymbol{u})|} \quad \text{when } D(\boldsymbol{u}) \neq 0$$

The second case $|\boldsymbol{\sigma} + 2\alpha D(\boldsymbol{u})| \leqslant \sigma_0$ yields, from the definition of P, $D(\boldsymbol{u}) = 0$ which means that this condition reduces to $|\boldsymbol{\sigma}| \leqslant \sigma_0$. Then, we have obtained exactly (3.14a) which completes the proof. □

3.11 Space Approximation

Let us study the approximate counterpart of the previous algorithm, as it reserves some subtleties and should be performed with care. In this section, for simplicity and without loss of generality for the study, we assume that the boundary data $\boldsymbol{u}_\Gamma = 0$. We deal with three finite dimensional spaces $T_h \subset \left(L^2(\Omega)\right)_s^{3\times 3}$, $V_h \subset \left(H_0^1(\Omega)\right)^3$ and $Q_h \subset L^2(\Omega)$. The space T_h is used for the symmetric tensors $\boldsymbol{\sigma}$ and $\boldsymbol{\delta}$ while V_h and Q_h are the velocity and pressure spaces. For the purpose of this study, let us introduce the operator R_h, defined as the L^2 projection from $\left(L^2(\Omega)\right)_s^{3\times 3}$ to T_h by

$$R_h(\boldsymbol{\gamma}) = \arg\inf_{\boldsymbol{\gamma}_h \in T_h} \int_\Omega |\boldsymbol{\gamma} - \boldsymbol{\gamma}_h|^2 \,\mathrm{d}x, \quad \forall \boldsymbol{\gamma} \in \left(L^2(\Omega)\right)_s^{3\times 3}$$

This is a differentiable minimization problem and its solution is characterized as the unique solution of the following variational formulation: find $R_h(\boldsymbol{\gamma}) \in T_h$ such that

$$\int_\Omega R_h(\boldsymbol{\gamma}) : \boldsymbol{\xi}_h \,\mathrm{d}x = \int_\Omega \boldsymbol{\gamma} : \boldsymbol{\xi}_h \,\mathrm{d}x, \quad \forall \boldsymbol{\gamma}_h \in T_h$$

Let us observe in the simplest case $\sigma_0 = 0$ and $n = 1$, i.e. for a Newtonian fluid, the result of the discrete version of the algorithm, after the replacement of functional spaces by their finite dimensional counterpart. At convergence, the solution is characterized by (3.30a)–(3.30d) and its approximation $(\boldsymbol{\sigma}_h, \boldsymbol{\delta}_h, \boldsymbol{u}_h, p_h) \in T_h^2 \times V_h \times Q_h$ by:

$$\begin{aligned} &\int_\Omega 2\alpha D(\boldsymbol{u}_h) : D(\boldsymbol{v}_h) \,\mathrm{d}x - \int_\Omega p_h \,\mathrm{div}(\boldsymbol{v}_h) \,\mathrm{d}x \\ &= \int_\Omega \boldsymbol{f}.\boldsymbol{v}_h \,\mathrm{d}x + \int_\Omega (\alpha\boldsymbol{\delta}_h - \boldsymbol{\sigma}_h) : D(\boldsymbol{v}_h) \,\mathrm{d}x, \quad \forall \boldsymbol{v}_h \in V_h \end{aligned} \tag{3.31a}$$

$$-\int_\Omega q_h \,\mathrm{div}(\boldsymbol{u}_h)\,\mathrm{d}x = 0, \quad \forall q_h \in L^2(\Omega) \tag{3.31b}$$

$$\boldsymbol{\delta}_h - 2R_h(D(\boldsymbol{u}_h)) = 0 \tag{3.31c}$$

$$\boldsymbol{\delta}_h = \frac{\boldsymbol{\sigma}_h + 2\alpha R_h(D(\boldsymbol{u}_h))}{K+\alpha} \tag{3.31d}$$

From (3.31c), we get $\boldsymbol{\delta}_h = 2R_h(D(\boldsymbol{u}_h))$ and then (3.31d) yields $\boldsymbol{\sigma}_h = 2KR_h(D(\boldsymbol{u}_h))$. Then, replacing in (3.31a) we obtain the following characterization of the pair $(\boldsymbol{u}_h, p_h) \in V_h \times Q_h$:

$$\begin{aligned}
\int_\Omega 2K R_h(D(\boldsymbol{u}_h)) : D(\boldsymbol{v}_h)\,\mathrm{d}x + 2\alpha \int_\Omega (I - R_h) D(\boldsymbol{u}_h) : D(\boldsymbol{v}_h)\,\mathrm{d}x \\
-\int_\Omega p_h \,\mathrm{div}(\boldsymbol{v}_h)\,\mathrm{d}x = \int_\Omega \boldsymbol{f}.\boldsymbol{v}_h\,\mathrm{d}x, \quad \forall \boldsymbol{v}_h \in V_h \\
-\int_\Omega q_h \,\mathrm{div}(\boldsymbol{u}_h)\,\mathrm{d}x = 0, \quad \forall q_h \in L^2(\Omega)
\end{aligned}$$

We recognize here a Stokes-like problem where the quadratic form depends, in general, upon the augmentation parameter α. Thus, its solution $(\boldsymbol{u}_h, p_h)$ depends also upon α. This is not a good news, as α could be chosen arbitrary large, for instance for improving the convergence properties of the augmented Lagrangian algorithm. Nevertheless, there is a special case for which the solution is independent upon α. Let us denote $D(V_h)$ the image by the $D(.)$ operator, i.e.the symmetric part of the vector gradient operator, of the finite dimensional vector field space V_h.

Property 3.2 (Choice of the stress approximation)
When $D(V_h) \subset T_h$, the solution of the approximate problem (3.31a)–(3.31d) *is independent upon α.*

Proof Observe that when $D(V_h) \subset T_h$, we have $R_h(D(\boldsymbol{v}_h)) = D(\boldsymbol{v}_h)$ for all $\boldsymbol{v}_h \in V_h$. Then $(\boldsymbol{u}_h, p_h) \in V_h \times Q_h$ is characterized as the solution of an usual discrete Stokes problem:

$$\begin{aligned}
\int_\Omega 2K D(\boldsymbol{u}_h) : D(\boldsymbol{v}_h)\,\mathrm{d}x - \int_\Omega p_h \,\mathrm{div}(\boldsymbol{v}_h)\,\mathrm{d}x = \int_\Omega \boldsymbol{f}.\boldsymbol{v}_h\,\mathrm{d}x, \quad \forall \boldsymbol{v}_h \in V_h \\
-\int_\Omega q_h \,\mathrm{div}(\boldsymbol{u}_h)\,\mathrm{d}x = 0, \quad \forall q_h \in L^2(\Omega)
\end{aligned}$$

while $\boldsymbol{\delta}_h = 2D(\boldsymbol{u}_h)$ and $\boldsymbol{\sigma}_h = 2KD(\boldsymbol{u}_h)$. □

Note that the when $\sigma_0 = 0$ and $n = 1$, the continuous problem (3.14a)–(3.14d) reduces to the so-called three-field Stokes problem.

(P): find $\boldsymbol{\sigma}$, $\boldsymbol{u}$ and p, defined in Ω, such that

$$\begin{array}{rrrl} \dfrac{1}{2K}\boldsymbol{\sigma} & - D(\boldsymbol{u}) & = & 0 \ \text{ in } \Omega \\ \mathbf{div}(\boldsymbol{\sigma}) & - \nabla p & = & -\boldsymbol{f} \text{ in } \Omega \\ & \operatorname{div} \boldsymbol{u} & = & 0 \ \text{ in } \Omega \\ & \boldsymbol{u} & = & 0 \text{ on } \partial\Omega \end{array}$$

Let us introduce the forms:

$$\begin{aligned} m(\boldsymbol{\sigma}, \boldsymbol{\tau}) &= \frac{1}{2K} \int_\Omega \boldsymbol{\sigma} : \boldsymbol{\tau} \, \mathrm{d}x, \quad \forall \boldsymbol{\sigma}, \boldsymbol{\tau} \in \left(L^2(\Omega)\right)_s^{3\times 3} \\ d(\boldsymbol{\sigma}, \boldsymbol{u}) &= -\int_\Omega \boldsymbol{\sigma} : D(\boldsymbol{u}) \, \mathrm{d}x, \quad \forall \boldsymbol{\sigma} \in \left(L^2(\Omega)\right)_s^{3\times 3}, \ \forall \boldsymbol{u} \in \left(H^1(\Omega)\right)^3 \\ b(\boldsymbol{u}, p) &= \int_\Omega p \operatorname{div} \boldsymbol{u} \, \mathrm{d}x, \quad \forall \boldsymbol{u} \in \left(H^1(\Omega)\right)^3, \ \forall p \in L^2(\Omega) \\ \ell(\boldsymbol{v}) &= -\int_\Omega \boldsymbol{f}.\boldsymbol{v} \, \mathrm{d}x, \quad \forall \boldsymbol{v} \in \left(H^1(\Omega)\right)^3 \end{aligned}$$

The variational formulation write:
(FV): find $\boldsymbol{\sigma} \in \left(L^2(\Omega)\right)_s^{3\times 3}$, $\boldsymbol{u} \in \left(H_0^1(\Omega)\right)^3$ and $p \in L^2(\Omega)$ such that

$$\begin{array}{rrrl} m(\boldsymbol{\sigma}, \boldsymbol{\tau}) + d(\boldsymbol{\tau}, \boldsymbol{u}) & & = & 0, \ \forall \boldsymbol{\tau} \in \left(L^2(\Omega)\right)_s^{3\times 3} \\ d(\boldsymbol{\sigma}, \boldsymbol{v}) & + b(\boldsymbol{v}, p) & = & \ell(\boldsymbol{v}), \ \forall \boldsymbol{u} \in \left(H_0^1(\Omega)\right)^3 \\ b(\boldsymbol{u}, q) & & = & 0, \ \forall p \in L^2(\Omega) \end{array}$$

This problem shares some structural similarities with the classical two-field Stokes system (see Sect. 1.8): this structure falls into the framework of mixed problems [38]. Here, there is two interlinked coupled pairs: a stress-velocity and a velocity-pressure one. When approximating this mixed problem with finite dimensional spaces $T_h \subset \left(L^2(\Omega)\right)_s^{3\times 3}$, $V_h \subset \left(H_0^1(\Omega)\right)^3$ and $Q_h \subset L^2(\Omega)$, we obtain two compatibility conditions (see Sect. 1.9), one for each coupling:

$$\exists \delta > 0 \ \text{ such that } \forall h > 0, \quad \inf_{\boldsymbol{v}_h \in K_h(0)} \sup_{\boldsymbol{\tau}_h \in T_h} \frac{d(\boldsymbol{\tau}_h, \boldsymbol{v}_h)}{\|\boldsymbol{\tau}_h\|_{L^2} \|\boldsymbol{v}_h\|_{H^1}} \geqslant \delta \tag{3.32a}$$

$$\exists \beta > 0 \ \text{ such that } \forall h > 0, \quad \inf_{q_h \in Q_h} \sup_{\boldsymbol{v}_h \in X_h} \frac{b(\boldsymbol{v}_h, q_h)}{\|\boldsymbol{v}_h\|_{H^1} \|q_h\|_{L^2}} \geqslant \beta \tag{3.32b}$$

there δ and β are two positive constants independent of the mesh size h and K_h denotes the kernel of the discrete b form:

$$K_h = \{\boldsymbol{v}_h \in \ / \ b(\boldsymbol{v}_h, q_h) = 0, \ \forall q_h \in Q_h\}$$

It means that the stress tensor can not be discretized arbitrarily: the stress discretization should be compatible with the velocity discretization. The situation is similar with the Stokes problem, where the velocity approximation should be compatible

with the pressure one. As we have both stresses, velocity and pressure, there is too interlinked compatibility conditions. The fist condition (3.32a) expresses a compatibility condition between T_h and V_h while the second (3.32b), between V_h and Q_h. Thus, these three finite dimensional spaces are linked and cannot be chosen arbitrarily. The simplest idea for building a successful combination of finite dimensional spaces, that satisfies simultaneously the two conditions, is to choose first a pair of spaces (V_h, Q_h) that satisfies the second condition (3.32b) and then choose $T_h = D(V_h)$, as suggested by the Property 3.2. It is a good idea, as shown in the following result.

Property 3.3 (Stress-velocity approximation compatibility)
When $D(V_h) \subset T_h$, the compatibility condition (3.32a) *is satisfied.*

Proof The compatibility condition (3.32a) expresses also: there exists a constant $\delta > 0$, such that, for all mesh size h, for all $\boldsymbol{v}_h \in V_h$, there exists $\boldsymbol{\tau}_h \in T_h$ such that

$$\int_\Omega \boldsymbol{\tau}_h : \ D(\boldsymbol{v}_h)\,\mathrm{d}x \ \geqslant \ \delta \|\boldsymbol{\tau}_h\|_{L^2} \|\boldsymbol{v}_h\|_{H^1}$$

Let any $\boldsymbol{v}_h \in V_h$ and choose $\boldsymbol{\tau}_h = 4D(\boldsymbol{v}_h) \in T_h$. Then, using Lemma 1.2, p. 34:

$$\begin{aligned}
\int_\Omega \boldsymbol{\tau}_h : D(\boldsymbol{v}_h)\,\mathrm{d}x &= \int_\Omega 4D(\boldsymbol{v}_h) : D(\boldsymbol{v}_h)\,\mathrm{d}x \\
&= \|2D(\boldsymbol{v}_h)\|_{L^2}^2 \\
&= \|2D(\boldsymbol{v}_h)\|_{L^2} \ \|\boldsymbol{\tau}_h\|_{L^2} \\
&\geqslant c_0 \|\boldsymbol{v}_h\|_{H^1} \ \|\boldsymbol{\tau}_h\|_{L^2}
\end{aligned}$$

Finally, the compatibility condition is satisfied with $\delta = c_0$, the constant of Lemma 1.2, which is independent of any mesh size. □

There is two classical discretization methods for the three-field Stokes problem that satisfy the compatibility conditions and ensure that the solution of the augmented Lagrangian is independent of the augmentation parameter. The first one is based one the Taylor–Hood $P_2 - P_1$ velocity-pressure finite element method. Then $T_h = D(V_h)$ is the space of piecewise discontinuous and affine polynomials (see Fig. 3.8). The second is based on the staggered grid finite difference method and is represented on Fig. 3.9. The velocity components are located at the middle of edges in two dimensions and at the center of faces in three dimensions. By this way, the finite difference approximation of the divergence of a velocity field is second order at the center of a cell, where the pressure is approximated. The diagonal stress components are located as the pressure, at the center of the cell, while extra-diagonal components are at the vertices of the cell in two dimensions and at the middle of the edges in three dimensions. Also, by this way, the finite difference approximation of the gradient of a velocity field is second order at the location of stress components.

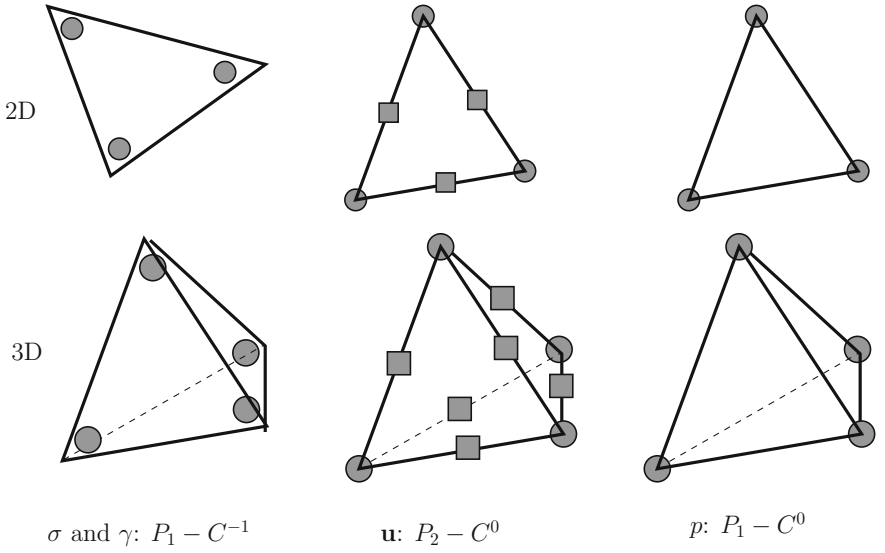

Fig. 3.8 Finite element for the three field Stokes problem [265]

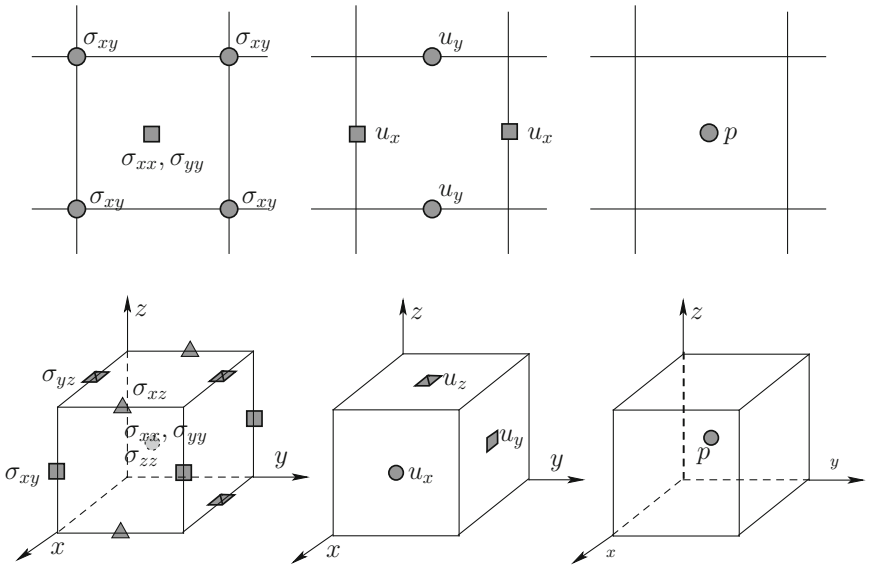

Fig. 3.9 Staggered grid scheme for the three field Stokes problem [277]

3.12 Example: Poiseuille Flow in a Square Section

We consider the Poiseuille flow in pipe with a square cross section, for a Bingham fluid described by a power law model. The flow conditions was presented in Sect. 2.9, p. 80. Assume that the flow is laminar: the pressure is given by $p(x, y, z) = -fz + p_0$ where $f > 0$ and $p_0 \in \mathbb{R}$ are given. The stationary velocity is parallel to the plates and depends only upon (x, y) in the section: $\boldsymbol{u}(x, y) = (0, 0, u_z(x, y))$. Its gradient is given by

$$\nabla \boldsymbol{u} = \begin{pmatrix} 0 & 0 & 0 \\ 0 & 0 & 0 \\ \dfrac{\partial u_z}{\partial x} & \dfrac{\partial u_z}{\partial y} & 0 \end{pmatrix}$$

and the shear rate by $\dot{\gamma} = |2D(\boldsymbol{u})| = |\nabla u_z|$. Note that the inertia term $(\boldsymbol{u}.\nabla)\boldsymbol{u}$ is zero. Indeed, the velocity is in the z direction while ∇ contains just two components $\partial/\partial x$ and $\partial/\partial y$ in the (O, x, y) plane. Then the operator $\boldsymbol{u}.\nabla$ is zero. The stationary problem reduces to a two-dimensional one and the computational domain is the section of the pipe, denoted by Ω. Let $\boldsymbol{\sigma}_z = (\sigma_{xz}, \sigma_{yz})$ denotes two-dimensional vector containing the shear components of the stress deviator. The problem writes:

(P): find $\boldsymbol{\sigma}_z$ and u_z, defined in Ω, such that

$$\begin{aligned} \boldsymbol{\sigma}_z = K|\nabla u_z|^{-1+n}\nabla u_z + \sigma_0 \frac{\nabla u_z}{|\nabla u_z|} \quad & \text{when } \nabla u_z \neq 0 \\ |\boldsymbol{\sigma}_z| \leqslant \sigma_0 \quad & \text{otherwise} \\ -\operatorname{div} \boldsymbol{\sigma}_z = f \text{ in } \Omega & \\ u_z = 0 \text{ on } \partial\Omega & \end{aligned}$$

The dimensional analysis is similar to those of Sect. 3.5. Let L, the half pipe with, be the characteristic length, $U = L^2 f/(2\eta)$ be the characteristic velocity and $\Sigma = \eta U/L = Lf/2$ be the characteristic stress. After a change to dimensionless variables, it remains only two relevant dimensionless parameters: the Bingham number $Bi = 2\sigma_0/(Lf)$ and the power index n. Note the two factor in the definition of the Bingham number: this factor is inserted for compatibility purpose with the values of the Bingham number used in [289], Fig. 3.10 represents the flow feature. As for the Poiseuille flow between parallel plates (see Sect. 3.5), the material presents a plug region in the center of the pipe, where the velocity is constant. Moreover, in the four outer corners, there are dead regions, where the material is at the rest.

Figure 3.11 presents the solution, as computed in 1997 by Taylor and Wilson [303] with the regularization method and $\varepsilon = 10^{-3}$. Note that, for $Bi = 0.8$, the rigid region are badly shaped, especially the dead regions that presents an *inverted* concavity, turned toward the *outside* of the pipe section. When $Bi = 1$, the dead regions are connected to the central plug, while sheared regions continue to exists at the vicinity to the wall. This situation is impossible. Using the regularized model due

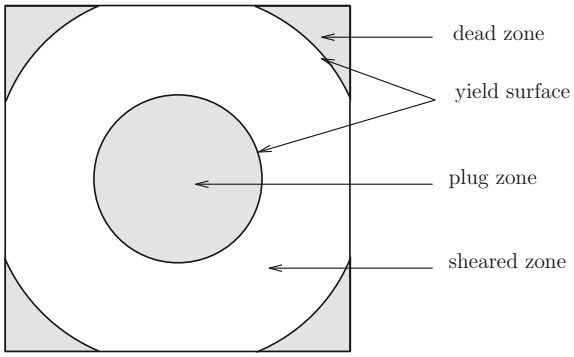

Fig. 3.10 Poiseuille flow of a viscoplastic fluid in a square pipe section: flow features and terminology

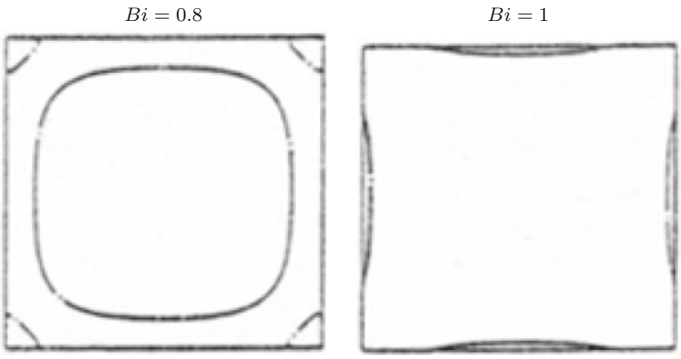

Fig. 3.11 Poiseuille flow of a Bingham fluid ($n = 1$) in a square pipe section: regularization method, by Taylor and Wilson [303]

to Papanastasiou [235], in 1999, Burgos and Alexandrou [40] obtained also similar connected plug and dead regions ([40], Fig. 8d, line 1, p. 494 and Fig. 9d, line 1, p. 495) and exhibited dead regions with inverted concavity ([40], Fig. 8d, line 2, p. 494). Theoretical studies showed that, for all $Bi > 0$:

(i) the existence and uniqueness of the plug region (showed in 1965 by Mosolov and Miasnikov [211]);
(ii) the existence of dead regions with concavity turned toward the inside osf the section (showed in 1966 by Mosolov and Miasnikov [212]).

Figure 3.12 presents some convergence problems with the regularization method when $\varepsilon \to 0$. The computations are performed with $\varepsilon = 10^{-13}$ in 1997 by Wang [312]. This author represented the $|2D(\boldsymbol{u})|$ iso-contours and pointed out the sensibility of the yield surfaces. While using a very small regularization parameter $\varepsilon = 10^{-13}$, there is no evidence of the convergence of the yield surfaces separating rigid and flowing regions.

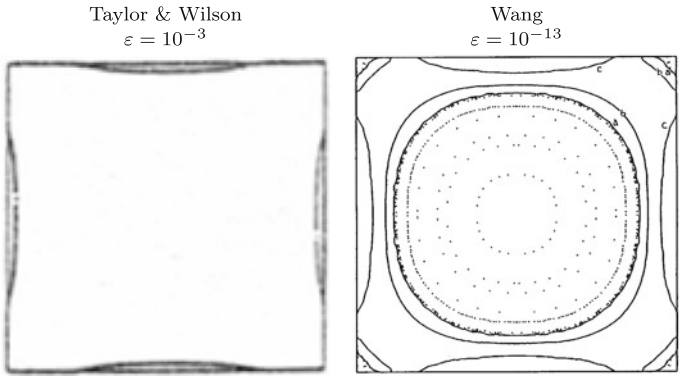

Fig. 3.12 Poiseuille flow of a viscoplastic fluid in a square pipe section: convergence problems with the regularization method [312]. On the *right*, $|2D(\boldsymbol{u})|$ iso-contours for (a) 10^{-2} (b) 10^{-3} (c) 8×10^{-7}

Figure 3.13 shows the solution for $Bi = 0.5, 0.9$ and 1.05, as computed in 2001 by Saramito and Roquet [289] with the augmented Lagrangian method and the decoupled Uzawa Algorithm 3.6. Exploiting three symmetries, the domain of computation is reduced to a triangular shaped region. The mixed problem is discretized by a continuous quadratic finite element method for the velocity u_z and a continuous affine one for the shear stress vector $\boldsymbol{\sigma}_z$. Computations was performed with the `Rheolef` library [284, 286]. An auto-adaptive mesh procedure was used, and the mesh is represented on the left of Fig. 3.13. The lines represents the iso-contours of the velocity component in the pipe axis direction. Dark lines indicate the velocity contours. Let us observe the flowing region $\{|\boldsymbol{\sigma}_z| \geqslant \sigma_0\}$, in gray, and the two rigid regions, in white $\{|\boldsymbol{\sigma}| < \sigma_0\}$. The first rigid region is a dead region, close to the outer corner. The second rigid region, at the center of the flow, is an inner plug, that translates with a constant velocity in the (Oz) direction. Observe the accurate detection of the yield surfaces separating the flowing and rigid regions. Let us now consider the dead region and its evolution with Bingham number. The dead region always presents a concavity turned towards the inside of the section, as pointed out by theoretical studies. Note that the plug region, associated with a rigid translation movement, and the dead region, associated with zero velocity, are always separated by the sheared region, where the velocity varies gradually. Our results are consistent with the properties showed by Mosolov and Miasnikov [211, 212]. In particular, plug and dead regions cannot be connected before the fluid comes to a full stop.

The inner plug is circle-like when small enough. As it grows, the inner plug gets flat due to its facing the wall. The shear region near the middle of the wall is thinner than the one along the diagonal, but it also decreases slowly, so that the shear region finally vanishes everywhere for the same critical Bingham number. The entire evolution of shear and rigid regions is described here. The fluid comes to a full stop for a Bingham number slightly greater than 1.05. For $Bi = 1.05$ (see Fig. 3.13), an almost totally yielded cross-section appears, with only a thin shear region. The

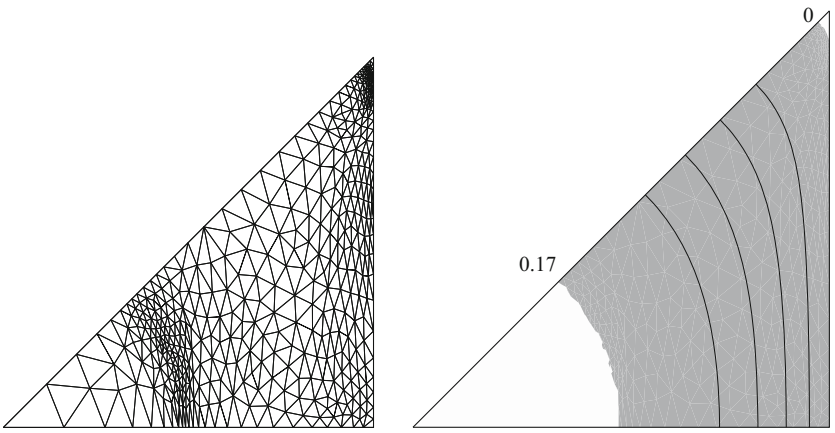

(a) $Bi = 0.5$

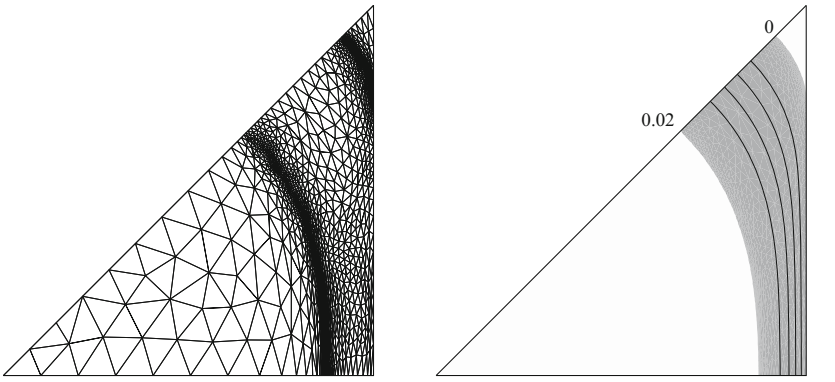

(b) $Bi = 0.9$

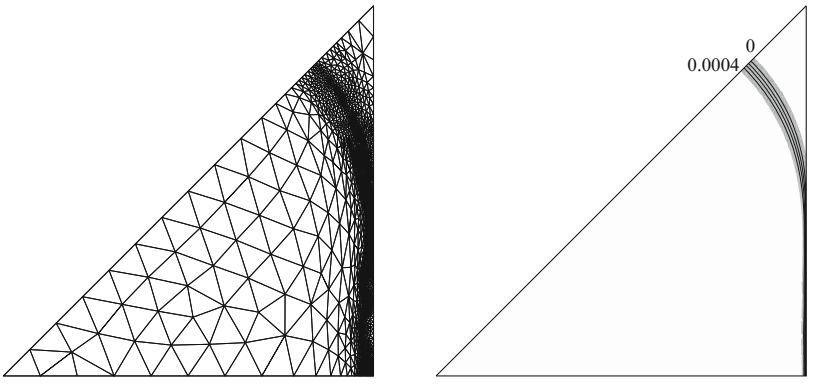

(c) $Bi = 1.05$

Fig. 3.13 Poiseuille flow in a square pipe section of a viscoplastic fluid: evolution versus Bi of velocity contours and flowing (in *gray*) and rigid (in *white*) regions

maximum velocity, i.e. velocity of the inner plug, is in this case roughly 10^3 times smaller than the corresponding one in the Newtonian case, which is associated with a wide area of the flow. The evolution shows that the fluid comes to a full stop for a finite critical Bingham number, namely $Bi_c \approx 1.05$. Recall that a similar result was obtained in Sect. 3.5 for the flow between parallel plates, with $Bi_c = 1$. For values of the Bingham number greater than Bi_c, the flow is totally stopped: this is the arrested state. By using variational methods, Mosolov and Miasnikov [211] exhibited for a square section the exact value: $Bi_c = 4/(2 + \sqrt{\pi}) \approx 1.0603178$.

3.13 Example: Flow Around an Obstacle

Figure 3.14 presents the flow of a moving cylinder between parallel plates in a viscoplastic fluid. The stationary problem is solved and the inertia term is neglected, as only slow flows are considered here. Figure 3.15 introduces some terminology associated to the flow features. The flow can be viewed as four kinds of distinct regions (see Fig. 3.15):

- A *flowing region* lies around the cylinder.
- A *surrounding dead region* contains the flowing region. Its boundary with the flowing region is called the *surrounding envelop*.
- Two rigid pike-shaped regions, called *pikes*, stick in front of and behind the cylinder, and are always included within the flowing region.
- Two oval rigid regions with pointed extremities, called *almonds*, lie inside the flowing region. Both are located between the wall and the cylinder, symmetrically with respect to the axis of the flow.

The stationary solution is supposed independent of z, in a Cartesian $(0, x, y, z)$ system, where Oz is the axis of the cylinder, and the problem reduces to a two-

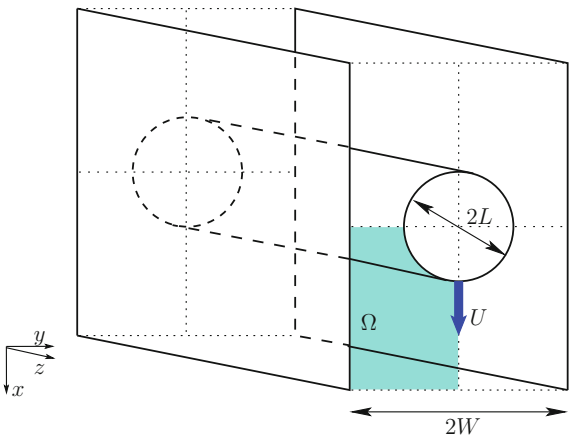

Fig. 3.14 Flow around a moving cylinder

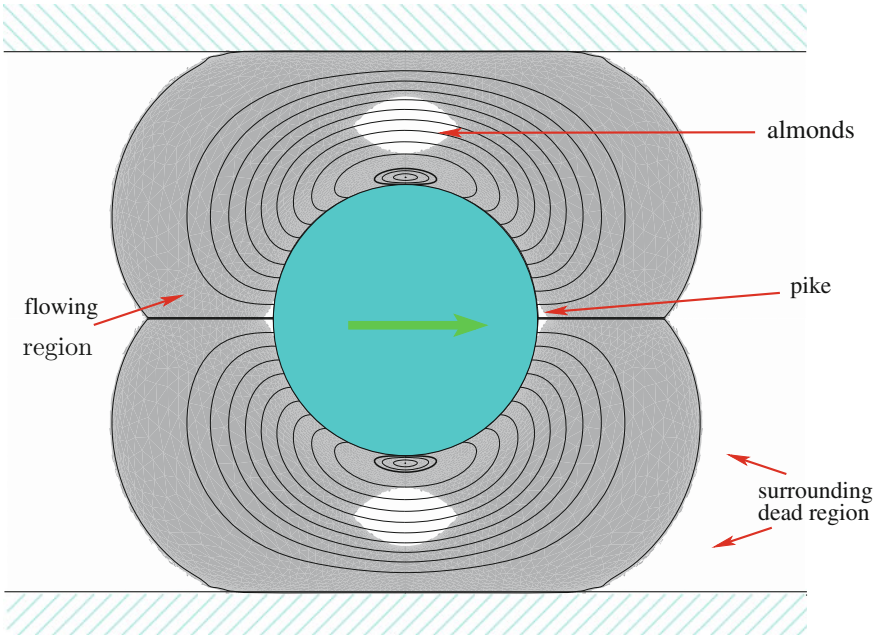

Fig. 3.15 Flow of a viscoplastic fluid around a moving cylinder: flow features and terminology

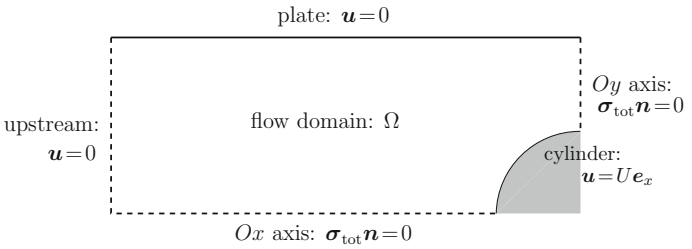

Fig. 3.16 Flow around a moving cylinder: boundary conditions

dimensional one. The domain of computation Ω is also reduced by exploiting the two axis of symmetry Ox and Oy. The problem is closed by non-slip Dirichlet conditions $\boldsymbol{u} = 0$ along the plate and $\boldsymbol{u} = U\boldsymbol{e}_x$ along the moving cylinder in the Ox direction (see Fig. 3.16). The upstream boundary is supposed to be sufficiently far from the cylinder for the fluid to be at the rest and the upstream boundary condition is $\boldsymbol{u} = 0$. The symmetries along the Ox and Oy axis express with a Neumann boundary condition $\boldsymbol{\sigma}_{\text{tot}}\boldsymbol{n} = 0$. A characteristic length is the cylinder radius L and a characteristic velocity is U, those of the cylinder. The dimensional analysis is similar to those of Sect. 3.5 and it remains only two relevant dimensionless parameters, the Bingham number $Bi = \sqrt{2}\sigma_0 L/(\eta U)$ and the power index n. Note the square root of two factor in the definition of Bi: this factor is inserted for compatibility purpose

with the values of the Bingham number used in [265], that was associated to a slightly different definition the tensor norm and, consequently, also to a different definition of the yield stress (see also Remark 2.1, p. 64). A third dimensionless number expresses the confinement of the geometry: $\beta = (W-L)/L$, where W is the half distance between the two parallel plates. In the present section, the power index is $n = 1$ i.e. we use the Bingham model and the confinement is $\beta = 1$. The problem is discretized by the finite element method showed on Fig. 3.8. The augmented Lagrangian method and the decoupled Uzawa Algorithm 3.6 are combined with an auto-adaptive mesh procedure, as presented in 2003 by Roquet and Saramito [265]. Computations was

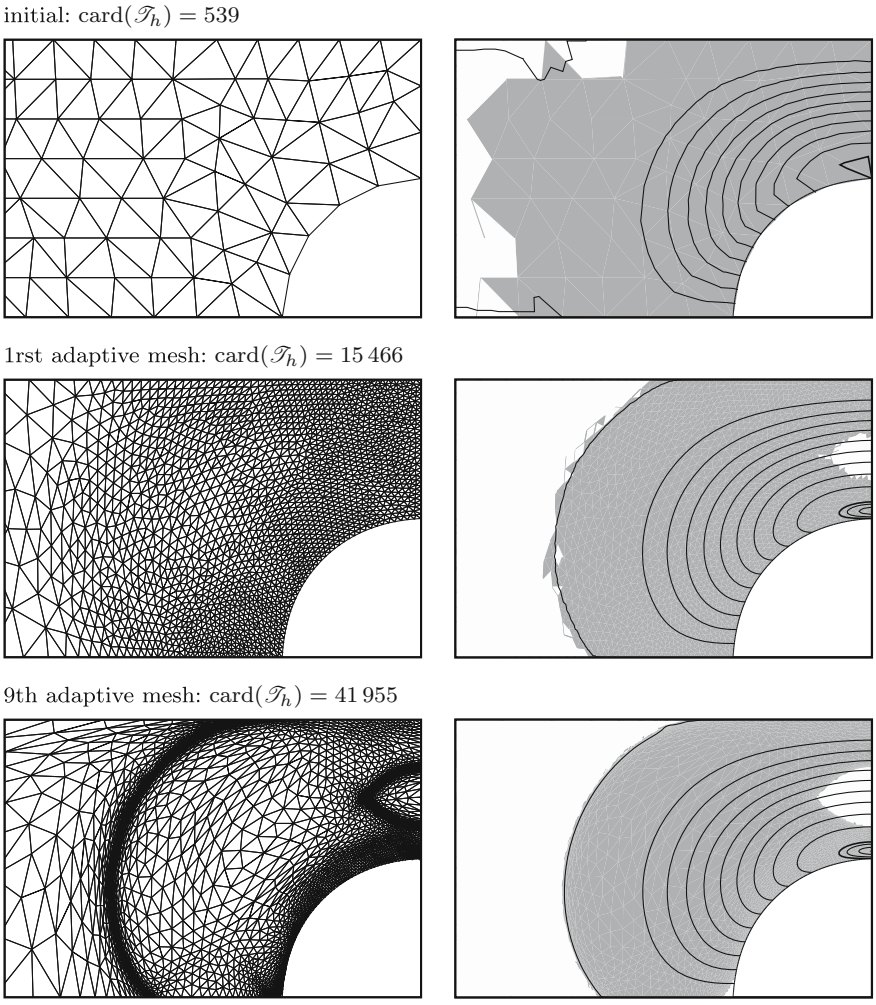

Fig. 3.17 Flow of a viscoplastic fluid around a moving cylinder: auto-adaptive mesh method when $Bi = 10$ and $n = 1$ [265]

performed with the `Rheolef` library [284, 286]. Figure 3.17 presents the successive iterates of the mesh adaptation procedure and the corresponding solutions. Flowing regions are in gray. Observe that this procedure is able to catch accurately the yield surfaces, separating flowing and solid rigid regions. Solution are also represented by the iso-contours of the stream function. Recall that the stream function has been introduced in Sect. 1.12, p. 49. For the moving cylinder problem, the stream function ψ is defined as the unique function that satisfies $-\Delta\psi = \partial_y u_x - \partial_x u_y$ in Ω with $\psi = Ux$ along the cylinder, $\psi = 0$ along the plate, the Ox axis and the upstream, and $\partial\psi/\partial\boldsymbol{n} = 0$ along the Oy axis. This is a Poisson problem with mixed Dirichlet-Neumann boundary conditions, that is completely standard. Ten positive and three negative equi-spaced iso-lines are represented on Fig. 3.17. As the flow is stationary, these lines correspond to the trajectories of the particles of material whose motion is due to the one of the cylinder and these lines are called streamlines. Each particle thrown in front of the cylinder comes back to its initial position after the cylinder has passed. Two kinds of streamlines can be identified. Some streamlines start horizontally from the cylinder, describe smooth curves which are surrounding the cylinder, and come back symmetrically in contact with it. In particular, the streamline $\psi = 0$ underlines the boundary of the envelop flowing region. Some others streamlines have

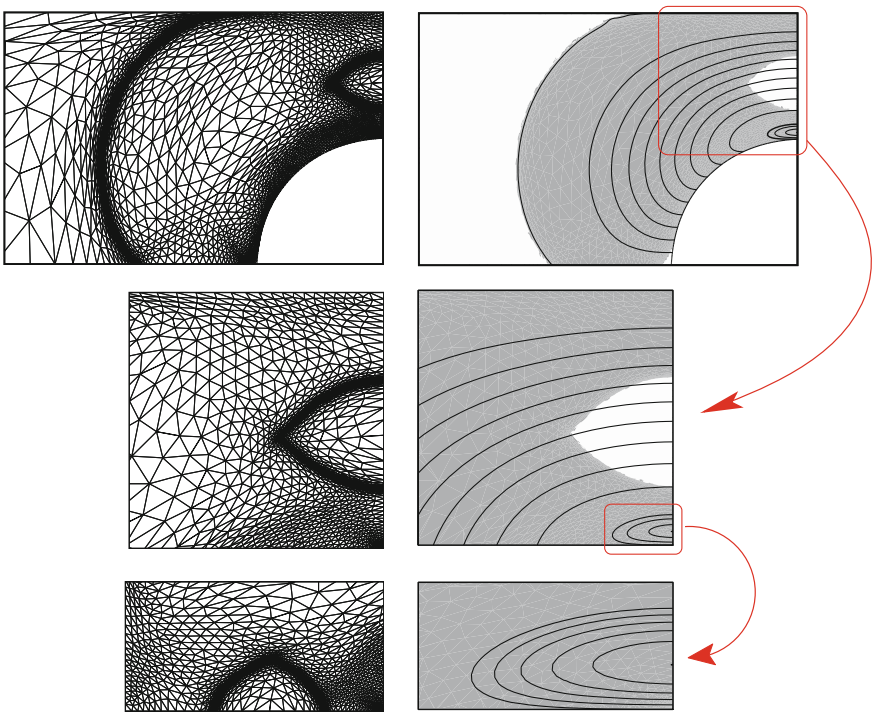

Fig. 3.18 Flow of a viscoplastic fluid around a moving cylinder: zoom on the adaptive mesh [265]

a closed loop pattern: there is a small vortex located just on the top of the cylinder. The boundary line of this vortex corresponds to the streamline $\psi = UL$. Finally, Fig. 3.18 presents a zoom of the last iteration of the adaptation procedure: observe the almond and the small vortex that sticks on the top of the cylinder. Finally, notice that, in [265], the effect of the confinement parameter β is also studied.

3.14 Example: Driven Cavity Flow

The cavity is a square of width L. The boundary velocity $\boldsymbol{u}_\Gamma$ is zero except on the top boundary $y = L$ where $\boldsymbol{u}_\Gamma = (1, 0)$ in a Cartesian coordinate system $(0, x, y)$. Here $U > 0$ denotes the constant top wall fluid velocity. The driven cavity flow of a Newtonian fluid was introduced in Sect. 1.12, p. 49. The dimensional analysis is performed as usual: it reduces the set of parameters to the Bingham number, defined by $Bi = \sigma_0/\Sigma$, the Reynolds number $Re = \rho U^2/\Sigma$, and the power law index n. Here, $\Sigma = K(U/L)^n$ denotes the characteristic stress used by the dimensionless procedure. The details of the computations can be found in Bernabeu et al. [18].

Figures 3.19 and 3.20 show the shape of the rigid zones and the streamlines when the Bingham number increases while $n = 1$ and when inertia effects are neglected ($Re = 0$). As expected, observe that when Bi increases the rigid zones develop. There are two main rigid zones. The first one sticks at the bottom of the cavity, growing from the two bottom left and right corners and merging. The material in this first rigid region is at the rest. The second one lies in the center of the cavity where

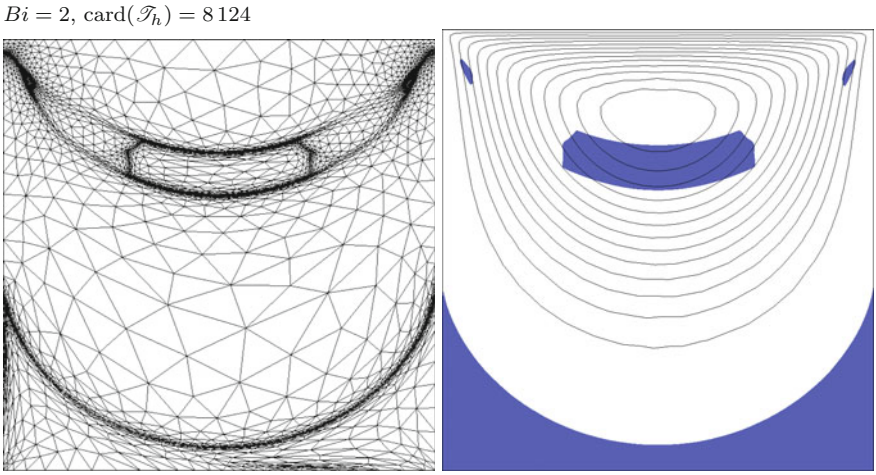

Fig. 3.19 Viscoplastic fluid in a driven cavity: influence of the Bingham number Bi when $n = 1$ and $Re = 0$

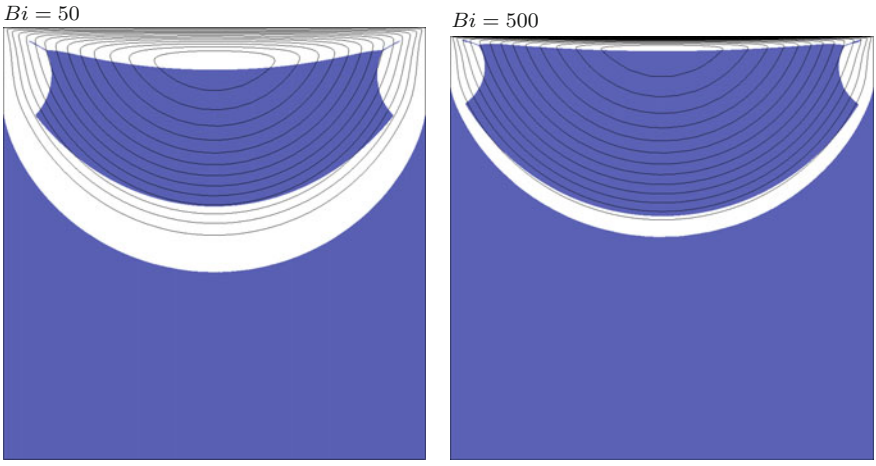

Fig. 3.20 Viscoplastic fluid in a driven cavity: influence of the Bingham number Bi when $n = 1$ and $Re = 0$ (cont.)

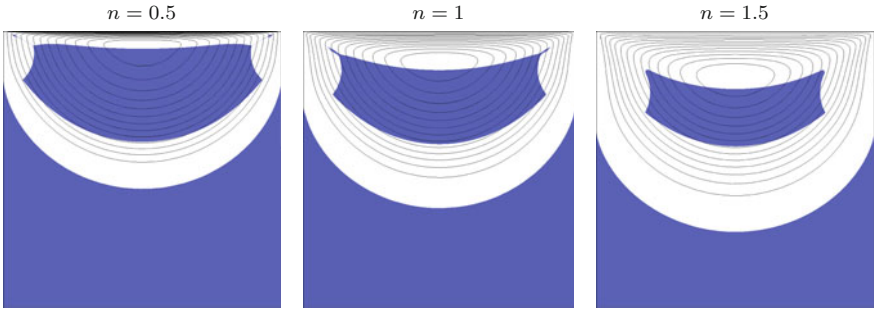

Fig. 3.21 Viscoplastic fluid in a driven cavity: influence of the power law index n when $Bi = 20$ and $Re = 0$

the material turns in a rigid motion. These two rigid regions develop with Bi and becomes asymptotically close for large Bi.

Figure 3.21 shows the flow evolution versus the power index n when $Bi = 20$ and when inertia effects are neglected ($Re = 0$). Observe that the rigid zones decrease when n increases.

Figure 3.22 presents inertia effects for the stationary solution of a viscoplastic fluid with $n = 1$ when $Re = 1000$ while Bi is varying. When Bi is small, the solution roughly looks like the Newtonian one at the same Reynolds number (see Fig. 1.20, p. 54). Observe several small rigid regions included inside the main recirculation and also inside the secondary vortices when $Bi = 0.1$. These small rigid regions are accurately computed, as shown on Fig. 3.23, thanks to a efficient anisotropic auto-adaptive mesh procedure provided by the `Rheolef` library [284, 286]. When $Bi = 1$, Fig. 3.22 shows that the two secondary vortices are completely at the rest

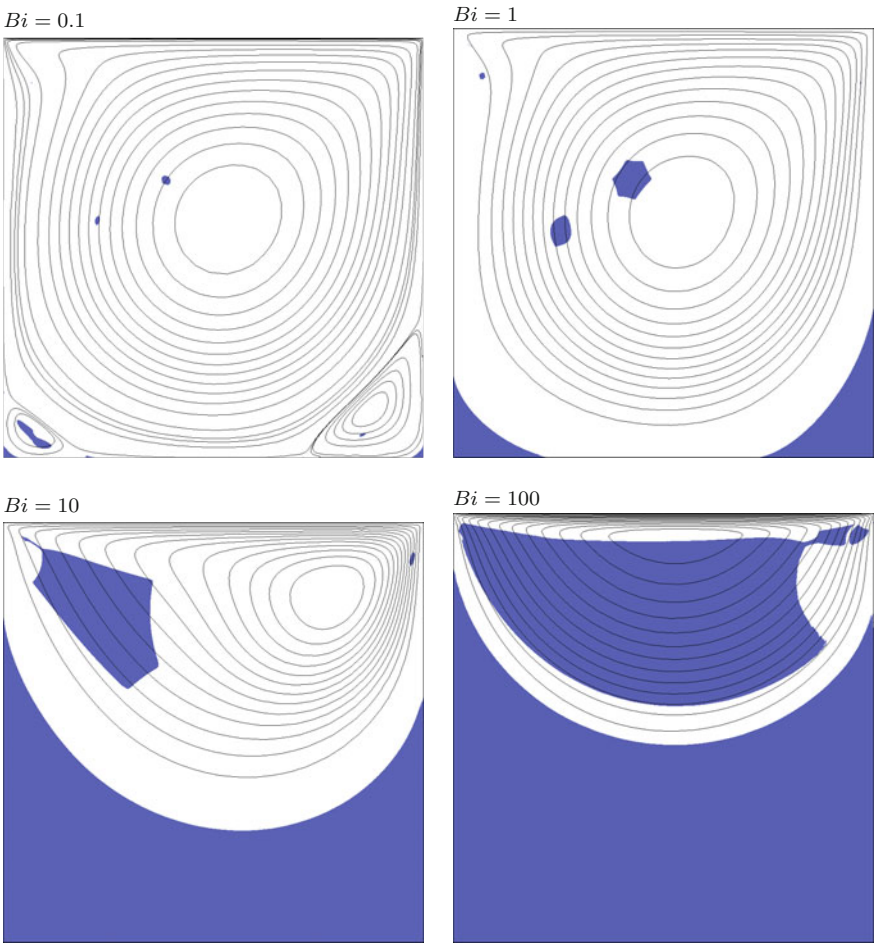

Fig. 3.22 Viscoplastic fluid in a driven cavity: influence of the Bingham number Bi when $n = 1$ and in presence of inertia effects $Re = 1000$

while the small rigid regions inside the main vortex develop. The zoom at the bottom of Fig. 3.23 shows some details of these rigid regions: one of them is an hexagon with concave sides and the other looks like the almond rigid region observed for the flow around an obstacle studied in the previous Sect. 3.13. When $Bi = 10$, the two rigid regions associated to secondary vortices merge at the bottom of the cavity. Also, the small rigid regions inside the main recirculation merge in a unique rotating rigid region. When $Bi = 100$, the two remaining rigid regions develop and occupy the most part of the flow domain. Observe that the flow remains unsymmetric, even when Bi is large: this asymmetry is due to inertia effects. Bernabeu [18] presents a comparison between these computations and two others one combining viscoplasticity and inertia

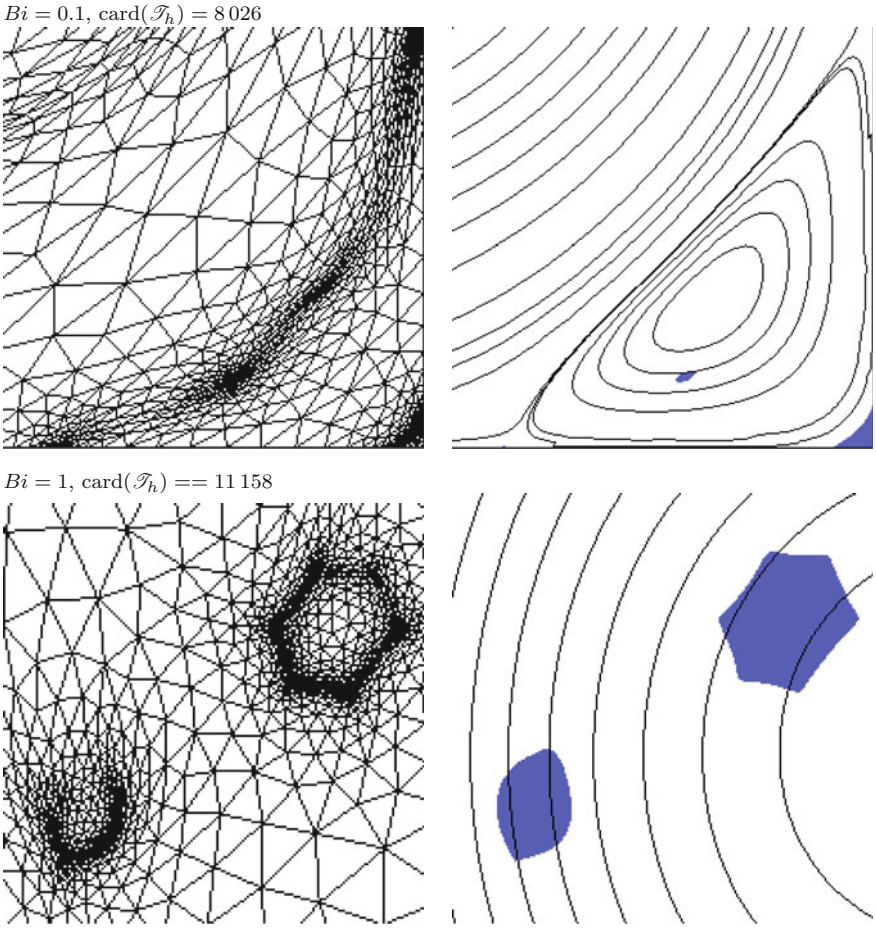

Fig. 3.23 Viscoplastic fluid in a driven cavity: zoom in the presence of inertia effects ($n = 1$, $Re = 1000$)

effects. The first one has been done in 2014 by Muravleva [216] by an augmented Lagrangian method and a staggered grid discretization. The second one is proposed by Syrakos et al. [301], by using a regularization method.

3.15 Notes

Models – The modeling of viscoplastic fluids started in 1900 when Schwedoff [291] studied gelatins with a one-dimensional time-dependent model involving a yield stress together with some elastic effects. The Schwedoff paper was the forerunner

to a multitude of papers on variable viscosity effects in a plethora of materials. Then, there was a tendency to label all anomalous behavior as manifestations of plasticity, with no clear idea as to what that meant. In 1922, Bingham published an important book [26] entitled *fluidity and plasticity* which contributed to clarify some ideas during this period. He presented a one-dimensional model with a yield stress, that appear as a particular case of the Schwedoff model when elastic effects are neglected. The modern story of viscoplastic fluids started later, in 1932, when Prager [244], using the von Mises [205] yielding criterion, proposed to extend the Bingham model to the three-dimensional case and Oldroyd, in 1947, in a collection of papers (see e.g. [226]) studied the Bingham three-dimensional model and its Herschel–Bulkley extension coupled with the Navier–Stokes equations for the motion of the fluid. In 1965, Mosolov and Miasnikov [211–213] showed explicit properties of the solution for a Poiseuille flow with non-circular cross section.

Algorithms – The first numerical computation appeared in 1972, when Fortin [104] presented his PhD and proposed a relaxed fixed point algorithm for the computation of a finite element approximation of the solution for a Poiseuille flow with a square cross section. In 1972, Duvaut and Lions [86] developed the theoretical framework of variational inequalities for many non-smooth problems, including Bingham flows, and in 1976, Glowinski, Lions and Tremolières, in a re-edited book [123], proposed the numerical analysis of their approximation. In 1980, Bercovier and Engelman [16] proposed a regularization approach with a viscosity function for this problem. Let us mention that the regularization approach is frequently used as a theoretical tool while investigating existence and regularity of solutions (see [123, p. 21] and more recently [197]).

During the 1970s, Rockafellar [264] developed the augmented Lagrangian algorithm for optimization problems and in 1980, Glowinski [120] and then Fortin and Glowinski [107] proposed to apply it to the solution of the linear Stokes problem and also to others non-linear problems such as Bingham fluid flows, and these authors developed an abstract framework. Algorithm 3.6 of the present book is an extension to the general Herschel–Bulkley model of the original Fortin and Glowinski algorithm ALG2 proposed for Bingham fluids. The presentation is here also different: it uses the nice and powerful tools of convex analysis, such as subdifferential and convex conjugate. In 1987, following Bercovier and Engelman, Papanastasiou [235] proposed another viscosity function for the regularization of Bingham flow problem. During the 1980s and the 1990s, numerical computations was dominated by the regularization method, perhaps due to its simplicity, while the augmented Lagrangian algorithm leaded not yet convincing results for viscoplastic flows. In 1989, Glowinski and le Tallec [122] revisited the augmented Lagrangian method, using new optimization and convex analysis tools, such as subdifferential, but no evidence of the efficiency of this approach to viscoplasticity was showed, while regularization approach becomes more popular in the 1990s with the work of mitsoulis et al. [206] and Wilson and Taylor [317]. Ionescu and Sofonea [152] studied theoretically the arrested state property of viscoplastic flows by using variational inequalities. The mixed approximation of the three-field Stokes problem with discontinuous stresses was introduced in 1989

by Fortin and Fortin [106] and re-analyzed in 1992 by Baranger and Sandri [9] in the context of viscoelastic fluids. Finally, in 2001, Saramito and Roquet [265, 289] showed for the first time the efficiency of the augmented Lagrangian algorithm when combined with auto-adaptive mesh methods for capturing accurately the yield surface.

In the 2000s, this approach became mature and a healthy competition developed between the regularization approach and the augmented Lagrangian one. Vola, Boscardin and Latché [311] obtained results for a driven cavity flow with the augmented Lagrangian algorithm while Mitsoulis et al. [207] presented computation for an expansion flow with regularization and Frigaard et al. [112, 215, 246] pointed out some drawbacks of the regularization approach. Finally, at the end of the 2000s decade, most supporters of the regularization method recognized the superiority of the augmented Lagrangian algorithm [81, 217] for obtaining accurate solutions. The free software `Rheolef` library, supporting both the augmented Lagrangian algorithm and an auto-adaptive mesh technique is now widely used for various flow applications (see e.g. [198, 246, 268–271]).

Newton algorithm – One of the most efficient algorithm to solve nonlinear problems is the Newton method, due to its super-linear convergence properties (see Sect. 2.10, p. 81). This approach has already been investigated for the regularized approach of the viscoplastic problem (see e.g. [25] and most recently [256–258] for the biviscous regularization) and it bases on the methodology introduced in Chap. 2. Applying the Newton method to the unregularized viscoplastic problem leads to a singular Jacobian matrix. This difficulty has been recently addressed by using the trusted region algorithm [309], that regularizes the Jacobian matrix but loses the superlinear convergence of the method. Recently, the present author [287] addressed directly the singularity of the Jacobian matrix in the Newton method and obtained a superlinear convergent algorithm for the unregularized viscoplastic fluid flow problem. This promising approach is a dramatic improvement, as compared with the augmented Lagrangian method.

Slip at the wall – The no-slip boundary condition at walls could be violated by viscoplastic fluids: for instance, a wet granular material or a dense suspension slide at the wall of a smooth tube and the reader could easily experiment it with a toothpaste tube. Viscoplastic fluid flow problems with yield slip at the wall was first investigated by using the augmented Lagrangian algorithm [266, 267] and recently investigated by using a regularized model [72].

Granular materials – Continuous models for granular materials such as Drucker-Prager [84] model and the so-called $\mu(I)$ rheology proposed in 2006 by Jop, Forterre and Pouliquen [158] appears as extensions of the Bingham and Herschel–Bulkley models, where the yield stress σ_0 is no more constant but pressure dependent. The Drucker-Prager models can be considered as a three-dimensional version of the Mohr-Coulomb yield surface model. In that case, the minimization problem is no more convex and minimization algorithms, such as the augmented Lagrangian one, are expected to reach some local extrema. In 2015, Ionescu et al. [151], using

an augmented Lagrangian algorithm, compared the Drucker-Prager and the $\mu(I)$ models with experiments on granular materials. Finally, a recent review of experimental observations performed with yield stress fluids has been written in 2014 by Coussot [65].

Coupling – Thermal effects was investigated by Vinay and Wachs [310] for oil applications and recently by Bernabeu et al. [18, 20] for volcanic lava flows. In that case, the yield stress σ_0 and the consistency K are no more constant but depend upon the temperature. Also, the change in time of the material properties of viscoplastic fluids, due for instance to damage and healing of some aggregates or micro-structure, has been investigated by Wachs [125]. In that case, the rheological parameters σ_0 and K depend upon a structural parameter, representing the damage or healing state of the material, and the model is completed by a coupled evolution equation for this parameter.

Shallow flows – The study of shallow approximations of viscoplastic fluids is motivated by many geophysical applications such as landslides, mud flows, snow avalanches and volcanic lava flows. An asymptotic analysis for these thin viscoplastic flow problems allows to reduce the three-dimensional problem into a two-dimensional surface one. Numerical approximations of thin viscoplastic problems are demonstrated for volcanic lava flow and simulations are compared with physical observations. See e.g. Bernabeu et al. [19, 20] and Bouchut et al. [32] for recent advances on this subject.

Chapter 4
Viscoelastic Fluids

The theory of viscoelastic fluids developed in the second half of the 20th century with the industrial production of molten and dilute polymers and the growth of engineering that generated many new products. Building constitutive equations for these fluids requires new tensorial tools from continuum mechanics, such as objective tensor derivatives, that are introduced in this chapter. The Poiseuille and Couette flow problems are then solved explicitly: this computation points out some mathematical specificities of viscoelastic fluid models, as the possible non-uniqueness of the stationary solution, together with some mechanical ones, such as normal stresses and the spectacular Weissenberg effect. For solving more general flows, two numerical approaches are developed: a θ-scheme algorithm, based on an operator splitting and a Newton method based on the log-conformation formulation. The discontinuous Galerkin finite element method is studied in details and then applied to the approximation of the constitutive equation. For the flow in an abrupt contraction and the flow in a driven cavity, examples of numerical computations are presented, illustrating the efficiency of these algorithm. Based on the log-conformation formulation, a global energy estimate is proved for this family of fluids.

4.1 Constitutive Equations

A viscoelastic fluid model is an attempt to represent, at a macroscopic scale, and by using the tools of continuum mechanics, a medium composed at a microscopic scale by a solution of long and flexible polymer molecules suspended in a solvent composed of small molecules, as shown on Fig. 4.1. By extension, viscoelastic models are able to represent some different materials that share similar mechanical properties at the macroscopic scale. The main difficulty consists in representing the behavior of a flexible polymer at the macroscopic scale. At the microscopic scale, the simplest representation is the dumbbell spring model, represented on Fig. 4.2. Let $\boldsymbol{q} = \overrightarrow{\boldsymbol{x}_1\boldsymbol{x}_2}$ be the vector from the two extremities $\boldsymbol{x}_1$ and $\boldsymbol{x}_2$ of the dumbbell. Then, at the microscopic scale, the elastic force is given by a Hookean elasticity relation:

P. Saramito, *Complex fluids*, Mathématiques et Applications 79,
DOI 10.1007/978-3-319-44362-1_4

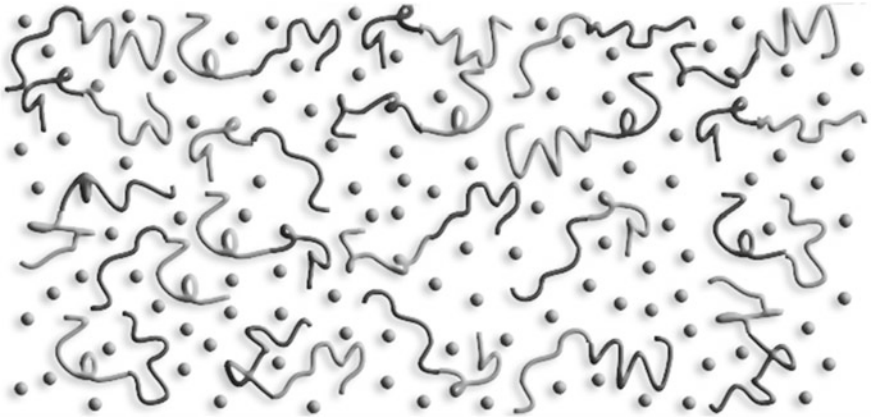

Fig. 4.1 Viscoelastic fluids: a suspension of polymer molecules

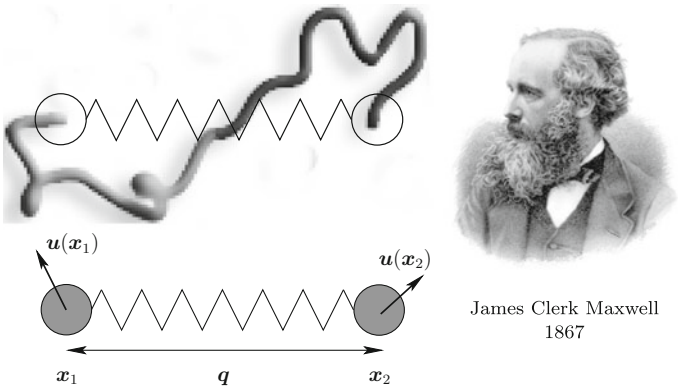

Fig. 4.2 (*left*) A polymeric chain and its representation as a dumbbell spring; (*right*) J.C. Maxwell, engraving by G.J. Stodart from a photograph by Fergus of Greenock

$$\boldsymbol{f} = \mu_0 \, \boldsymbol{q}$$

where μ_0 is the elastic modulus of the spring. At the macroscopic scale, this suspension is described in the continuum mechanics framework by an elastic stress tensor $\boldsymbol{\tau}$ that satisfies the following differential equation:

$$\frac{\dot{\boldsymbol{\tau}}}{\mu} + \frac{\boldsymbol{\tau}}{\eta_m} = 2D(\boldsymbol{u})$$

where μ is the elastic modulus of the material at the macroscopic scale and η_m is a viscosity coefficient that expresses the macroscopic effects of microscopic scale

friction between the long polymer molecules and the small solvent molecules. Here, $\dot{\boldsymbol{\tau}}$ denotes the Lagrangian derivative of the elastic stress tensor:

$$\dot{\boldsymbol{\tau}} = \frac{\partial \boldsymbol{\tau}}{\partial t} + (\boldsymbol{u}.\nabla)\boldsymbol{\tau} \tag{4.1}$$

Also, $D(\boldsymbol{u})$, denotes the rate of deformation tensor, i.e. the symmetric part of the gradient of velocity tensor. This combination of viscous and elastic effects is called *viscoelasticity*. Introducing the *relaxation time* $\lambda = \eta_m/\mu$, the previous equation writes equivalently:

$$\lambda \dot{\boldsymbol{\tau}} + \boldsymbol{\tau} = 2\eta_m D(\boldsymbol{u}) \tag{4.2a}$$

A differential model involving the elastic stress was first proposed in 1867 by Maxwell [202], who also contributed to the theory of electromagnetism. The complete and rigorous building from the microscopic scale description with Hookean dumbbells to the macroscopic description based on a linear differential equation involving the elastic stress can be found in [28, 174]. A common extension consists in taking into account the friction between the small solvent molecules at the microscopic scale. At the macroscopic scale, it can be expressed by introducing the viscosity η_s of the solvent. The Cauchy stress tensor is given by

$$\boldsymbol{\sigma}_{\text{tot}} = \boldsymbol{\tau} + 2\eta_s D(\boldsymbol{u}) - p.I \tag{4.2b}$$

Let us summarize the present situation: assuming that the density is constant, which is a reasonable assumption for a fluid, there are four unknowns $\boldsymbol{u}$, p, $\boldsymbol{\sigma}_{\text{tot}}$, $\boldsymbol{\tau}$ and four equations: the mass (1.3) and momentum (1.17) conservation equations and the constitutive equations (4.2a)–(4.2b). Oldroyd introduced in 1950 the important concept of the *objective derivative* of a tensor, that is the subject of the next section.

4.2 Objective Tensor Derivatives

Constitutive equations should be the same for an observer at rest and an observer that is animated by a rigid motion, i.e. a combination of rotation and translation. This principle applies to any moving frame, not only to Galilean frames, i.e. frame that moves with a constant translation. It is quite an obvious requirement in the sense that we do not expect stresses to develop in a body simply by running around it! In that case, the constitutive equation is said to be *objective*, or *frame invariant*, as it is invariant by a change of observer. Let the first observer be at the rest: it is represented by a coordinate system, e.g. $(0, x_1, x_2, x_3)$. A second observer develops in this coordinate system a motion that is a combination of rotation and translation, denoted respectively $\boldsymbol{R}(t)$ and $\boldsymbol{x}_0(t)$ at time t, as shown on Fig. 4.3. Let us denote by $\boldsymbol{x}$ the position of a material particle, as observed by the first observer, and $\hat{\boldsymbol{x}}$ the

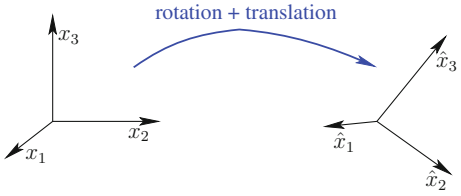

Fig. 4.3 Change of frame with a solid movement: rotation and translation

position of the same material particle as seen by the second observer. Then we have

$$\hat{\boldsymbol{x}} = \boldsymbol{R}(t)\,\boldsymbol{x} + \hat{\boldsymbol{x}}_0(t) + \boldsymbol{x} \tag{4.3}$$

The following theorem points out a major problem: the viscoelastic model (4.2a)–(4.2b) is non objective, and is thus invalid. But there is a solution, hence the reader can continue to read this chapter with no fear.

Theorem 4.1 (non-objectivity of the Lagrangian derivative)
The Lagrangian derivative of a vector, defined for all vector field $\boldsymbol{v}$ *by*

$$\dot{\boldsymbol{v}} = \frac{\partial \boldsymbol{v}}{\partial t} + (\boldsymbol{u}.\nabla)\boldsymbol{v}$$

is not objective. Also, the Lagrangian derivative of a tensor, as defined by (4.1)*, is not objective.*

Proof Let $\boldsymbol{v}$ be any vector field, as observed by the first observer. It transforms as $\hat{\boldsymbol{v}} = \boldsymbol{R}\boldsymbol{v}$. Taking its Lagrangian derivative leads to

$$\dot{\hat{\boldsymbol{v}}} = \boldsymbol{R}\,\dot{\boldsymbol{v}} + \dot{\boldsymbol{R}}\boldsymbol{v} \tag{4.4a}$$

As the last term in the previous relation do not vanish, the Lagrangian derivative of the vector is not objective. Let $\boldsymbol{\tau}$ be any tensor, e.g. the elastic stress tensor, as observed by the first observer. It transforms as $\hat{\boldsymbol{\tau}} = \boldsymbol{R}\boldsymbol{\tau}\boldsymbol{R}$. Taking its Lagrangian derivative leads to

$$\dot{\hat{\boldsymbol{\tau}}} = \boldsymbol{R}\,\dot{\boldsymbol{\tau}}\,\boldsymbol{R}^T + \dot{\boldsymbol{R}}\boldsymbol{\tau}\boldsymbol{R}^T + \boldsymbol{R}\boldsymbol{\tau}\dot{\boldsymbol{R}}^T \tag{4.4b}$$

As the two last terms in the previous relation do not vanish, the Lagrangian derivative of the tensor is not objective. □

Remark 4.1 (*Galilean frames and conservation of momentum*)
Note that the Lagrangian derivative of the velocity $\dot{\boldsymbol{u}}$ is also not frame invariant: rotations or non-constant translations change the acceleration. Thus, the conservation of linear momentum (1.17), p. 11, is also not frame invariant. Nevertheless, a rapid inspection shows that $\dot{\boldsymbol{u}}$ is invariant for a Galilean change of frame, i.e. for an observer that moves with a constant translation. With the present formalism, a Galilean change

of frame corresponds to $\boldsymbol{R}(t) = 0$ and $\boldsymbol{x}_0(t) = \boldsymbol{u}_0 t + \bar{\boldsymbol{x}}_0$ where $\boldsymbol{u}_0, \bar{\boldsymbol{x}}_0 \in \mathbb{R}^3$ are constant, i.e. independent of time. Thus, the conservation of linear momentum equation is invariant by any Galilean change of frame.

Theorem 4.2 (derivatives of the velocity)
The rate of deformation tensor is objective while the gradient of velocity and the vorticity are non-objective.

Proof The velocity of a material particle, observed at the position $\boldsymbol{x}$ by the first observer, is animated by a velocity $\boldsymbol{u} = \dot{\boldsymbol{x}}$. For the second observer, the same material particle is observed at position the $\boldsymbol{x}$ given by (4.3) and its velocity is

$$\begin{aligned} \hat{\boldsymbol{u}} &= \dot{\hat{\boldsymbol{x}}} \\ &= \dot{\boldsymbol{R}}\,\boldsymbol{x} + \boldsymbol{R}\,\dot{\boldsymbol{x}} + \dot{\hat{\boldsymbol{x}}}_0 \\ &= \dot{\boldsymbol{R}}\,\boldsymbol{x} + \boldsymbol{R}\,\boldsymbol{u} + \dot{\hat{\boldsymbol{x}}}_0 \end{aligned} \tag{4.5}$$

The gradient of velocity tensor $\nabla \boldsymbol{u} = \left(\dfrac{\partial u_i}{\partial x_j}\right)_{1 \leqslant i,j \leqslant 3}$ transforms in the frame of the second observer as

$$\hat{\nabla} \hat{\boldsymbol{u}} = \left(\frac{\partial \hat{u}_i}{\partial \hat{x}_j}\right)_{1 \leqslant i,j \leqslant 3} = \left(\sum_{k=1}^{3} \frac{\partial \hat{u}_i}{\partial x_k} \frac{\partial x_k}{\partial \hat{x}_j}\right)_{1 \leqslant i,j \leqslant 3} \tag{4.6}$$

Let us express the tensor $\left(\dfrac{\partial x_k}{\partial \hat{x}_j}\right)_{1 \leqslant i,j \leqslant 3}$ which is the inverse of $\left(\dfrac{\partial \hat{x}_i}{\partial x_j}\right)_{1 \leqslant i,j \leqslant 3}$. From (4.3), this last tensor is the rotation $\boldsymbol{R}$ of the second observer with respect to the first one. A classical property of a rotation tensor is

$$\boldsymbol{R}^{-1} = \boldsymbol{R}^T \tag{4.7}$$

It could be easily be checked. For instance, $\boldsymbol{R}$ can be expressed, for any $\boldsymbol{x}$, as

$$\boldsymbol{R}\boldsymbol{x} = \begin{pmatrix} 0 & -w_3 & w_2 \\ w_3 & 0 & -w_1 \\ -w_2 & w_1 & 0 \end{pmatrix} \begin{pmatrix} x_1 \\ x_2 \\ x_3 \end{pmatrix}$$

Thus $\boldsymbol{R}$ is antisymmetric and the inverse rotation $\boldsymbol{R}^{-1} = -\boldsymbol{R}^{-1} = \boldsymbol{R}^T$. Then $\left(\dfrac{\partial x_i}{\partial \hat{x}_j}\right)_{1 \leqslant i,j \leqslant 3} = \boldsymbol{R}^{-1} = \boldsymbol{R}^T$ and the expression (4.6) of the velocity gradient becomes successively

$$\begin{aligned}\hat{\nabla}\hat{\boldsymbol{u}} &= \nabla\hat{\boldsymbol{u}}\ \boldsymbol{R}^T \\ &= \nabla(\dot{\boldsymbol{R}}\boldsymbol{x} + \boldsymbol{R}\dot{\boldsymbol{x}} + \dot{\hat{\boldsymbol{x}}}_0)\ \boldsymbol{R}^T \\ &= (\dot{\boldsymbol{R}} + \boldsymbol{R}\nabla\dot{\boldsymbol{x}})\ \boldsymbol{R}^T \\ &= \boldsymbol{R}\ \nabla\boldsymbol{u}\ \boldsymbol{R}^T + \dot{\boldsymbol{R}}\ \boldsymbol{R}^T\end{aligned}$$

Thus, the gradient of velocity tensor is non-objective, as $\hat{\nabla}\hat{\boldsymbol{u}} \neq \boldsymbol{R}\ \nabla\boldsymbol{u}\ \boldsymbol{R}^T$. Next, let us turn to the rate of deformation tensor $D(\boldsymbol{u})$, that transforms as

$$\begin{aligned}\hat{D}(\hat{\boldsymbol{u}}) &= \frac{\hat{\nabla}\hat{\boldsymbol{u}} + \hat{\nabla}\hat{\boldsymbol{u}}^T}{2} \\ &= \boldsymbol{R}\ D(\boldsymbol{u})\ \boldsymbol{R}^T + \frac{1}{2}\left(\dot{\boldsymbol{R}}\boldsymbol{R}^T + \boldsymbol{R}\dot{\boldsymbol{R}}^T\right)\end{aligned}$$

From (4.7) we have $\boldsymbol{R}\ \boldsymbol{R}^T = \boldsymbol{I}$. Taking the Lagrangian derivative of this relation, we get

$$\dot{\boldsymbol{R}}\ \boldsymbol{R}^T + \boldsymbol{R}\dot{\boldsymbol{R}}^T = 0 \tag{4.8}$$

and then we obtain

$$\hat{D}(\hat{\boldsymbol{u}}) = \boldsymbol{R}\ D(\boldsymbol{u})\ \boldsymbol{R}^T$$

Thus, contrary to the gradient of velocity, the rate of deformation tensor is objective. Consider finally the vorticity tensor $2W(\boldsymbol{u})$ which transforms into

$$\begin{aligned}2\hat{W}(\hat{\boldsymbol{u}}) &= \hat{\nabla}\hat{\boldsymbol{u}} - \hat{\nabla}\hat{\boldsymbol{u}}^T \\ &= \quad \boldsymbol{R}\ \nabla\boldsymbol{u}\ \boldsymbol{R}^T \quad + \dot{\boldsymbol{R}}\boldsymbol{R}^T \\ &\quad -\boldsymbol{R}\ \nabla\boldsymbol{u}^T\ \boldsymbol{R}^T - \boldsymbol{R}\dot{\boldsymbol{R}}^T \\ &= \boldsymbol{R}\ 2W(\boldsymbol{u})\ \boldsymbol{R}^T + \dot{\boldsymbol{R}}\boldsymbol{R}^T - \boldsymbol{R}\dot{\boldsymbol{R}}^T\end{aligned}$$

From (4.8), we obtain

$$-\boldsymbol{R}\dot{\boldsymbol{R}}^T = \dot{\boldsymbol{R}}\boldsymbol{R}^T \tag{4.9}$$

and then

$$\hat{W}(\hat{\boldsymbol{u}}) = \boldsymbol{R}\ W(\boldsymbol{u})\ \boldsymbol{R}^T + \dot{\boldsymbol{R}}\boldsymbol{R}^T \tag{4.10}$$

Finally, the vorticity tensor is non-objective and the proof is complete. □

Corollary 4.1 (non-objectivity when using Lagrangian derivatives)
The viscoelastic model (4.2a)–(4.2b)*, that uses the Lagrangian derivative of a tensor, is non objective.*

Proof For the first observer, Eq. (4.2a) writes

$$\lambda\dot{\boldsymbol{\tau}} + \boldsymbol{\tau} - 2\eta_m D(\boldsymbol{u}) = 0$$

while, for the second one, the left-hand-side of the previous equation transforms as:

$$\lambda\dot{\hat{\boldsymbol{\tau}}} + \hat{\boldsymbol{\tau}} - 2\eta_m \hat{D}(\hat{\boldsymbol{u}}) = \boldsymbol{R}\ (\lambda\dot{\boldsymbol{\tau}} + \boldsymbol{\tau} - 2\eta_m D(\boldsymbol{u}))\ \boldsymbol{R}^T + \lambda(\dot{\boldsymbol{R}}\boldsymbol{\tau}\boldsymbol{R}^T + \boldsymbol{R}\boldsymbol{\tau}\dot{\boldsymbol{R}}^T)$$

While the first term is zero, the second one does not vanishes in general, and the equation is non objective. □

Note that a similar result could be obtained for any constitutive equation that uses the Lagrangian derivative of a vector.

Definition 4.1 (*Jaumann derivative*)
The Jaumann derivative of a vector field $\boldsymbol{v}$ is defined by

$$\begin{aligned}\frac{\mathscr{D}_0\boldsymbol{v}}{\mathscr{D}t} &= \dot{\boldsymbol{v}} - W(\boldsymbol{u})\boldsymbol{v} \\ &= \frac{\partial \boldsymbol{v}}{\partial t} + (\boldsymbol{u}.\nabla)\boldsymbol{v} - W(\boldsymbol{u})\boldsymbol{v}\end{aligned} \tag{4.11a}$$

The Jaumann derivative of a symmetric tensor $\boldsymbol{\tau}$ is defined by

$$\begin{aligned}\frac{\mathscr{D}_0\boldsymbol{\tau}}{\mathscr{D}t} &= \dot{\boldsymbol{\tau}} - W(\boldsymbol{u})\boldsymbol{\tau} + \boldsymbol{\tau}W(\boldsymbol{u}) \\ &= \frac{\partial \boldsymbol{\tau}}{\partial t} + (\boldsymbol{u}.\nabla)\boldsymbol{\tau} - W(\boldsymbol{u})\boldsymbol{\tau} + \boldsymbol{\tau}W(\boldsymbol{u})\end{aligned} \tag{4.11b}$$

Theorem 4.3 (objectivity of the Jaumann derivative)
The Jaumann derivatives of a vector field and of a symmetric tensor are objective.

Proof Consider the effect of the fluid rotation on a vector field $\boldsymbol{v}$: it is given by $W(\boldsymbol{u})\boldsymbol{v}$ and, from (4.10), it transforms as:

$$\begin{aligned}\hat{W}(\hat{\boldsymbol{u}})\ \hat{\boldsymbol{v}} &= (\boldsymbol{R}\ W(\boldsymbol{u})\ \boldsymbol{R}^T + \dot{\boldsymbol{R}}\ \boldsymbol{R}^T)\ (\boldsymbol{R}\ \boldsymbol{v}) \\ &= \boldsymbol{R}\ W(\boldsymbol{u})\ \boldsymbol{R}\ \boldsymbol{v} + \dot{\boldsymbol{R}}\ \boldsymbol{v}\end{aligned}$$

Note that the last term of the right-hand-side of the previous relation is the same as the last one in the right-hand-side of (4.4a), that expresses the Lagrangian derivative for the second observer. Since the Jaumann derivative (4.11b) is simply obtained by subtracting the fluid rotation effect from the Lagrangian derivative of a tensor, the proof is complete for a vector field.

Next, consider the effect of the fluid rotation on a stress tensor $\boldsymbol{\tau}$: it is the symmetric part of $2W(\boldsymbol{u})\boldsymbol{\tau}$, that writes:

$$W(\boldsymbol{u})\boldsymbol{\tau} + (W(\boldsymbol{u})\boldsymbol{\tau})^T = W(\boldsymbol{u})\boldsymbol{\tau} - \boldsymbol{\tau}W(\boldsymbol{u})$$

From (4.10), it transforms as:

$$\begin{aligned}
\hat{W}(\hat{\boldsymbol{u}})\,\hat{\boldsymbol{\tau}} - \hat{\boldsymbol{\tau}}\,\hat{W}(\hat{\boldsymbol{u}}) = \quad & (\boldsymbol{R}\,W(\boldsymbol{u})\,\boldsymbol{R}^T + \dot{\boldsymbol{R}}\,\boldsymbol{R}^T)\,(\boldsymbol{R}\,\boldsymbol{\tau}\,\boldsymbol{R}^T) \\
& -(\boldsymbol{R}\,\boldsymbol{\tau}\,\boldsymbol{R}^T)\,(\boldsymbol{R}\,W(\boldsymbol{u})\,\boldsymbol{R}^T + \dot{\boldsymbol{R}}\,\boldsymbol{R}^T) \\
= \; & \boldsymbol{R}\,(W(\boldsymbol{u})\,\boldsymbol{\tau} - \boldsymbol{\tau}\,W(\boldsymbol{u}))\,\boldsymbol{R}^T \\
& - \boldsymbol{R}\,\boldsymbol{\tau}\,\boldsymbol{R}^T\,\dot{\boldsymbol{R}}\,\boldsymbol{R}^T + \dot{\boldsymbol{R}}\,\boldsymbol{\tau}\,\boldsymbol{R}^T \\
= \; & \boldsymbol{R}\,(W(\boldsymbol{u})\,\boldsymbol{\tau} - \boldsymbol{\tau}\,W(\boldsymbol{u}))\,\boldsymbol{R}^T \\
& - \boldsymbol{R}\,\boldsymbol{\tau}\,\boldsymbol{R}^T\,(-\boldsymbol{R}\dot{\boldsymbol{R}}^T) + \dot{\boldsymbol{R}}\,\boldsymbol{\tau}\,\boldsymbol{R}^T \quad \text{from (4.9)} \\
= \; & \boldsymbol{R}\,(W(\boldsymbol{u})\,\boldsymbol{\tau} - \boldsymbol{\tau}\,W(\boldsymbol{u}))\,\boldsymbol{R}^T \\
& + \boldsymbol{R}\,\boldsymbol{\tau}\,\dot{\boldsymbol{R}}^T + \dot{\boldsymbol{R}}\,\boldsymbol{\tau}\,\boldsymbol{R}^T \quad \text{from (4.7)}
\end{aligned}$$

Note that the two last terms of the right-hand-side of the previous relation are the same as the two last one in the right-hand-side of (4.4b), that expresses the Lagrangian derivative for the second observer. Since the Jaumann derivative (4.11b) is simply obtained by subtracting the fluid rotation effect from the Lagrangian derivative of a tensor, the proof is complete. □

Figure 4.4 summarizes these properties for some quantities involved in the constitutive equation.

Definition 4.2 (*interpolated derivative*)
The interpolated derivative is defined for any vector field $\boldsymbol{v}$ and any symmetric tensor $\boldsymbol{\tau}$ by

$$\frac{\mathscr{D}_a\boldsymbol{v}}{\mathscr{D}t} = \frac{\partial\boldsymbol{v}}{\partial t} + (\boldsymbol{u}.\nabla)\boldsymbol{v} - W(\boldsymbol{u})\boldsymbol{v} - a\,D(\boldsymbol{u})\boldsymbol{v} \tag{4.12a}$$

$$\frac{\mathscr{D}_a\boldsymbol{\tau}}{\mathscr{D}t} = \frac{\partial\boldsymbol{\tau}}{\partial t} + (\boldsymbol{u}.\nabla)\boldsymbol{\tau} - W(\boldsymbol{u})\boldsymbol{\tau} + \boldsymbol{\tau}W(\boldsymbol{u}) - a\,(D(\boldsymbol{u})\boldsymbol{\tau} + \boldsymbol{\tau}D(\boldsymbol{u})) \tag{4.12b}$$

where $a \in \mathbb{R}$ is the interpolation parameter for this derivative.

The interpolated derivatives for tensors (4.12b) were proposed in 1972 by Gordon and Schowalters [126]. Note that when $a = 0$, the interpolated derivative coincides with the Jaumann derivative. When $a = 1$, this derivative is called the *upper convected* derivative or the *covariant* derivative. Note that this derivative is also called the Lie derivative in the context of the differential geometry (see e.g. [182, p. 385, Eq. (3.29)]). Conversely, when $a = -1$, it is called the *lower convected* derivative or the *contravariant* one. Thus, the a parameter interprets as an interpolation parameter between the upper and the lower convected derivatives. The last term of this derivative, with the a factor, represents the effect of the fluid deformation.

$$
\begin{array}{lll}
\text{position: } \boldsymbol{x} & \longmapsto & \hat{\boldsymbol{x}} = \boldsymbol{R}\,\boldsymbol{x} + \hat{\boldsymbol{x}}_0 + \boldsymbol{x} \\
\text{velocity: } \boldsymbol{u} = \dot{\boldsymbol{x}} & \longmapsto & \hat{\boldsymbol{u}} = \dot{\boldsymbol{R}}\,\boldsymbol{x} + \boldsymbol{R}\,\boldsymbol{u} + \dot{\hat{\boldsymbol{x}}}_0 \\
\nabla \boldsymbol{u} & \longmapsto & \hat{\nabla}\hat{\boldsymbol{u}} = \boldsymbol{R}\,\nabla \boldsymbol{u}\,\boldsymbol{R}^T + \dot{\boldsymbol{R}}\boldsymbol{R}^T \\
W(\boldsymbol{u}) & \longmapsto & \hat{W}(\hat{\boldsymbol{u}}) = \boldsymbol{R}\,W(\boldsymbol{u})\,\boldsymbol{R}^T + \dot{\boldsymbol{R}}\boldsymbol{R}^T \\
D(\boldsymbol{u}) & \longmapsto & \hat{D}(\hat{\boldsymbol{u}}) = \boldsymbol{R}\,D(\boldsymbol{u})\,\boldsymbol{R}^T \\
\text{vector: } \boldsymbol{v} & \longmapsto & \hat{\boldsymbol{v}} = \boldsymbol{R}\,\boldsymbol{v} \\
\dot{\boldsymbol{v}} & \longmapsto & \dot{\hat{\boldsymbol{v}}} = \boldsymbol{R}\,\dot{\boldsymbol{v}} + \dot{R}\boldsymbol{v} \\
W(\boldsymbol{u})\,\boldsymbol{v} & \longmapsto & \hat{W}(\hat{\boldsymbol{u}})\,\hat{\boldsymbol{v}} = \boldsymbol{R}W(\boldsymbol{u})\,\boldsymbol{v} + \dot{R}\boldsymbol{v} \\
\Longrightarrow \quad \dot{\boldsymbol{v}} - W(\boldsymbol{u})\,\boldsymbol{v} & \longmapsto & \dot{\hat{\boldsymbol{v}}} - \hat{W}(\hat{\boldsymbol{u}})\,\hat{\boldsymbol{v}} = \boldsymbol{R}\,(\dot{\boldsymbol{v}} - W(\boldsymbol{u})\,\boldsymbol{v}) \\
\text{tensor: } \boldsymbol{\tau} & \longmapsto & \hat{\boldsymbol{\tau}} = \boldsymbol{R}\,\boldsymbol{\tau}\,\boldsymbol{R}^T \\
\dot{\boldsymbol{\tau}} & \longmapsto & \dot{\hat{\boldsymbol{\tau}}} = \boldsymbol{R}\,\dot{\boldsymbol{\tau}}\,\boldsymbol{R}^T \\
 & & \quad + \ \dot{\boldsymbol{R}}\boldsymbol{\tau}\boldsymbol{R}^T + \boldsymbol{R}\boldsymbol{\tau}\dot{\boldsymbol{R}}^T \\
\Longrightarrow \quad \lambda\dot{\boldsymbol{\tau}} + \boldsymbol{\tau} - 2\eta_m D(\boldsymbol{u}) & \longmapsto & \lambda\dot{\hat{\boldsymbol{\tau}}} + \hat{\boldsymbol{\tau}} - 2\eta_m \hat{D}(\hat{\boldsymbol{u}}) \\
 & & \quad = \boldsymbol{R}\,(\lambda\dot{\boldsymbol{\tau}} + \boldsymbol{\tau} - 2\eta_m D(\boldsymbol{u}))\,\boldsymbol{R}^T \\
 & & \quad + \lambda(\dot{\boldsymbol{R}}\boldsymbol{\tau}\boldsymbol{R}^T + \boldsymbol{R}\boldsymbol{\tau}\dot{\boldsymbol{R}}^T) \\
W(\boldsymbol{u})\boldsymbol{\tau} - \boldsymbol{\tau}W(\boldsymbol{u}) & \longmapsto & \hat{W}(\hat{\boldsymbol{u}})\,\hat{\boldsymbol{\tau}} - \hat{\boldsymbol{\tau}}\,\hat{W}(\hat{\boldsymbol{u}}) \\
 & & \quad = \boldsymbol{R}\,(W(\boldsymbol{u})\,\boldsymbol{\tau} - \boldsymbol{\tau}\,W(\boldsymbol{u}))\,\boldsymbol{R}^T \\
 & & \quad + \ \dot{\boldsymbol{R}}\boldsymbol{\tau}\boldsymbol{R}^T + \boldsymbol{R}\boldsymbol{\tau}\dot{\boldsymbol{R}}^T \\
\Longrightarrow \quad \dot{\boldsymbol{\tau}} - W(\boldsymbol{u})\boldsymbol{\tau} + \boldsymbol{\tau}W(\boldsymbol{u}) & \longmapsto & \dot{\hat{\boldsymbol{\tau}}} - \hat{W}(\hat{\boldsymbol{u}})\,\hat{\boldsymbol{\tau}} + \hat{\boldsymbol{\tau}}\,\hat{W}(\hat{\boldsymbol{u}}) \\
 & & \quad = \boldsymbol{R}(\dot{\boldsymbol{\tau}} - W(\boldsymbol{u})\boldsymbol{\tau} + \boldsymbol{\tau}W(\boldsymbol{u}))\boldsymbol{R}^T
\end{array}
$$

Fig. 4.4 Change from observer for some quantities involved in the constitutive equation

Theorem 4.4 (objectivity of the interpolated derivatives)
The interpolated derivatives are objective.

Proof From Theorem 4.2, the rate of deformation tensor is objective. Thus, the additional terms with the interpolation parameter factor are also objective. □

The following result shows that the interpolated derivative of a deviatoric tensor is not in general deviatoric, at least when $a \neq 0$.

Lemma 4.1 (trace of the interpolated derivative)
For any symmetric tensor $\boldsymbol{\tau}$ *such that* $\operatorname{tr}(\boldsymbol{\tau}) = 0$ *we have*

$$\operatorname{tr}\left(\frac{\mathscr{D}_a\boldsymbol{\tau}}{\mathscr{D}t}\right) = -2a\ \operatorname{tr}\left(D(\boldsymbol{u})\boldsymbol{\tau}\right)$$

The interpolated derivative of a deviatoric tensor is not in general a deviatoric tensor, except when $a = 0$, i.e. for the Jaumann derivative.

Proof From Definition 4.2 of the interpolated derivative, we have

$$\operatorname{tr}\left(\frac{\mathscr{D}_a\boldsymbol{\tau}}{\mathscr{D}t}\right) = \left(\frac{\partial}{\partial t} + (\boldsymbol{u}.\nabla)\right)\operatorname{tr}(\boldsymbol{\tau}) + \operatorname{tr}\left(-W(\boldsymbol{u})\boldsymbol{\tau} + \boldsymbol{\tau}W(\boldsymbol{u})\right) \; - \; a \operatorname{tr}\left(D(\boldsymbol{u})\boldsymbol{\tau} + \boldsymbol{\tau}D(\boldsymbol{u})\right)$$

A rapid inspection of the two last terms of the right-hand-side shows that $\operatorname{tr}(-W(\boldsymbol{u})\boldsymbol{\tau} + \boldsymbol{\tau}W(\boldsymbol{u})) = 0$ and $\operatorname{tr}\left(D(\boldsymbol{u})\boldsymbol{\tau} + \boldsymbol{\tau}D(\boldsymbol{u})\right) = 2\operatorname{tr}\left(D(\boldsymbol{u})\boldsymbol{\tau}\right)$ which completes the first part of the proof. Note that, for any deviator tensor, its Jaumann derivative is also a deviator tensor. The remaining term $\operatorname{tr}\left(D(\boldsymbol{u})\boldsymbol{\tau}\right)$ is in general non-zero, even when both $D(\boldsymbol{u})$ and $\boldsymbol{\tau}$ are deviator tensors. □

Replacing the Lagrangian derivative by an interpolated one in (4.2a)–(4.2b) we obtain the following constitutive equation:

$$\boldsymbol{\sigma}_{\text{tot}} = \boldsymbol{\tau} + 2\eta_s D(\boldsymbol{u}) - p.I \tag{4.13a}$$

$$\lambda\frac{\mathscr{D}_a\boldsymbol{\tau}}{\mathscr{D}t} + \boldsymbol{\tau} = 2\eta_m D(\boldsymbol{u}) \tag{4.13b}$$

This is the Johnson–Segalman model, which was proposed in 1977 by Johnson and Segalman [157]. It is simply a generalization with interpolated derivatives of the two original models introduced by Oldroyd in 1950 [227]. The first Oldroyd model corresponds to the case $a = -1$, i.e. with the lower convected derivative, and is called the Oldroyd-A model, as it corresponds to equation labeled (A) in its 1950's celebrated paper. The second one corresponds to the case $a = 1$, i.e. with the upper convected derivative, and is called the Oldroyd-B model, as it corresponds to equation labeled (B) in the same paper. Its extension with the interpolated derivative, which is the Johnson–Segalman model, is often called a generalized Oldroyd model. Finally, when $\eta_s = 0$, i.e. when the solvent viscosity effect is neglected, the resulting constitutive equations are called the Maxwell viscoelastic model. It refers to Maxwell who published in 1867 the first paper [202] presenting a differential equation for the elastic stress.

Remark 4.2 (*pressure*)
Let us denotes $\bar{p}$ the pressure, defined in Definition 1.9, p. 14, as $\bar{p} = -(1/3)\operatorname{tr}(\boldsymbol{\sigma}_{\text{tot}})$. Taking the trace of (4.13a) yields $\bar{p} = p - (1/3)\operatorname{tr}(\boldsymbol{\tau})$. Recall that, from Lemma 4.1, the interpolated derivative of a deviatoric tensor is not deviatoric. From (4.13b), note that $\boldsymbol{\tau}$ is not in general a deviator. Then, the field p, which is the Lagrange multiplier associated to the incompressibility relation, does not coincide in general, with the pressure $\bar{p}$. These two quantities are equal when using the Jaumann derivative, i.e. when $a = 0$ and in that case $\boldsymbol{\tau}$ is a deviator.

Remark 4.3 (*Oldroyd's original formulation*)
The constitutive equations (4.13a)–(4.13b) could be expressed in term of $\boldsymbol{\sigma} = 2\eta_s D(\boldsymbol{u}) + \boldsymbol{\tau}$. We have:

$$\begin{aligned} \boldsymbol{\sigma}_{\text{tot}} &= \boldsymbol{\sigma} - p.I \\ \lambda \frac{\mathscr{D}_a \boldsymbol{\sigma}}{\mathscr{D}t} + \boldsymbol{\sigma} &= 2(\eta_s + \eta_m) D(\boldsymbol{u}) + 2\lambda\eta_s \frac{\mathscr{D}_a(D(\boldsymbol{u}))}{\mathscr{D}t} \end{aligned}$$

The original Oldroyd's expression of the constitutive equation was written with $\boldsymbol{\sigma}$ as in the previous equations, and using one viscosity $\eta = \eta_s + \eta_m$ and two times, a relaxation one λ and a retardation one $\lambda_s = \lambda\eta_s/\eta$. As is requires a second order derivative of the velocity field $\boldsymbol{u}$ in the right-hand-side, most formulations that focus on numerical approximations base on the formulation in terms of the elastic tensor $\boldsymbol{\tau}$. Note that, as pointed out in the previous remark, both tensors $\boldsymbol{\sigma}$ and $\boldsymbol{\tau}$ are not in general deviatoric, except when $a = 0$.

Let us summarize the situation: assuming that the density is constant, which is a reasonable assumption for isothermal liquids, there are four unknowns $\boldsymbol{u}$, p, $\boldsymbol{\sigma}_{\text{tot}}$, $\boldsymbol{\tau}$ and four equations: the mass (1.3) and the momentum (1.17) conservation equations and the constitutive equations (4.13a)–(4.13b).

4.3 Problem Statement

We are now able to close this system by initial and boundary conditions.

(P): find $\boldsymbol{\tau}$, $\boldsymbol{u}$ and p, defined in $]0, T[\times\Omega$ such that

$$\lambda\left(\frac{\partial\boldsymbol{\tau}}{\partial t} + (\boldsymbol{u}.\nabla)\boldsymbol{\tau} + \beta_a(\nabla\boldsymbol{u}, \boldsymbol{\tau})\right) + \boldsymbol{\tau} - 2\eta_m D(\boldsymbol{u}) = 0 \text{ in }]0, T[\times\Omega \tag{4.14a}$$

$$\rho\left(\frac{\partial\boldsymbol{u}}{\partial t} + (\boldsymbol{u}.\nabla)\boldsymbol{u}\right) - \mathbf{div}\,(\boldsymbol{\tau} + 2\eta_s D(\boldsymbol{u}) - p\,\boldsymbol{I}) = \rho\boldsymbol{g} \text{ in }]0, T[\times\Omega \tag{4.14b}$$

$$\operatorname{div}\boldsymbol{u} = 0 \text{ in }]0, T[\times\Omega \tag{4.14c}$$

$$\boldsymbol{\tau}(t=0) = \boldsymbol{\tau}_0 \text{ in } \Omega \tag{4.14d}$$

$$\boldsymbol{u}(t=0) = \boldsymbol{u}_0 \text{ in } \Omega \tag{4.14e}$$

$$\boldsymbol{\tau} = \boldsymbol{\tau}_\Gamma \text{ on }]0, T[\times\partial\Omega_- \tag{4.14f}$$

$$\boldsymbol{u} = \boldsymbol{u}_\Gamma \text{ on }]0, T[\times\partial\Omega \tag{4.14g}$$

where, for convenience, we have introduced the following notation

$$\beta_a(\nabla\boldsymbol{u}, \boldsymbol{\tau}) = \boldsymbol{\tau}\, W(\boldsymbol{u}) - W(\boldsymbol{u})\, \boldsymbol{\tau} - a\,(\boldsymbol{\tau}\, D(\boldsymbol{u}) + D(\boldsymbol{u})\, \boldsymbol{\tau}) \tag{4.15}$$

The material parameters are the relaxation time λ, the two viscosities η_m and η_s and the density ρ. There is some given data, as the initial conditions $\boldsymbol{\tau}_0$ and $\boldsymbol{u}_0$ and the

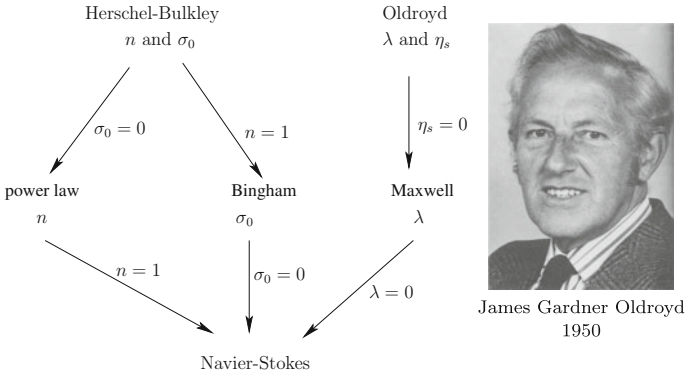

Fig. 4.5 Viscoelastic fluids: (*left*) the hierarchy of models and their relation with previous models presented in the book; (*right*) portrait of J.G. Oldroyd, from [237]

boundary conditions $\boldsymbol{\tau}_\Gamma$ and $\boldsymbol{u}_\Gamma$. Note that the boundary condition (4.14g) for the velocity imposes $\boldsymbol{u}$ on the whole boundary $\partial\Omega$, while the boundary condition (4.14f) imposes the elastic stress $\boldsymbol{\tau}$ only on the *upstream boundary*, defined by

$$\partial\Omega_-(t) = \{x \in \partial\Omega;\ \boldsymbol{u}_\Gamma(t,x).\boldsymbol{n}(x) < 0\}$$

This upstream boundary condition is associated to the transport operator $\boldsymbol{u}.\nabla$: as $\boldsymbol{\tau}$ is transported along the characteristic lines, i.e. the trajectories, a prescribed value of $\boldsymbol{\tau}$ should be given at the boundary point where the characteristic line enters in the flow domain. This boundary point belongs to the upstream boundary.

When $\lambda = 0$ the problem reduces to the Navier-Stokes equation with $\eta = \eta_m + \eta_s$ and when $\eta_m = 0$ it reduces to the Maxwell model. The relations between viscoelastic models and others models previously studied in the book are represented on Fig. 4.5. Note that the viscoplastic and viscoelastic model families develops two separated branches: a link between these branch will be created in the last chapter of the book, in the context of elastoviscoplastic models.

Several studies are concerned with the existence, uniqueness and regularity of a solution for this problem. In 1985, Renardy [253] proved the existence of a solution to the steady problem. In 1987, Guillopé and Saut [133] proved that there exists a unique strong solution local in time and that this solution is globally defined when the data and the retardation parameter α are small and the fluid is not too elastic (see also [188] for a different approach and Hakim [136] and Molinet and Talhouk [208], that removed the restriction on the smallness of the retardation parameter α). In 1998, Fernández-Cara, Guillopé and Ortega [99] extended this result to the large elasticity case and for an arbitrary large but finite final time T. In 2000, Lions and Masmoudi [191] obtained an improved result (T could be infinite) in the particular case of a Jaumann derivative ($a = 0$). In 2005, Kupferman, Mangoubi, and Titi [171] obtained a more explicit condition for the global in time existence of the solution

when $\Omega = \mathbb{R}^3$. In the next section, on the Poiseuille flow, we will exhibit by an explicit computation some situations of multiple stationary solutions and also a special case when there is no more stationary solutions. Finally, let us mention some recent works dealing with the Newtonian limit of viscoelastic models [209].

4.4 Example: Poiseuille Flow

Let us reuse the notations of Sect. 1.5, p. 18 for the Poiseuille flow of a Newtonian fluid. Assume that the flow is laminar: the pressure is given by $p(x, y, z) = -fz + p_0$ where $f > 0$ and $p_0 \in \mathbb{R}$ are given. We first consider the flow between parallel plates. The velocity is parallel to the plates $\boldsymbol{u}(x) = (0, 0, u_z(x))$. Its gradient is given by

$$\nabla \boldsymbol{u} = \begin{pmatrix} 0 & 0 & 0 \\ 0 & 0 & 0 \\ u_z' & 0 & 0 \end{pmatrix}$$

As major difference with both Newtonian, quasi-Newtonian and viscoplastic fluids, the stress is not in general proportional to the rate of deformation tensor $D(\boldsymbol{u})$, and could develop additional diagonal terms:

$$\boldsymbol{\tau} = \begin{pmatrix} \tau_{xx} & 0 & \tau_{xz} \\ 0 & 0 & 0 \\ \tau_{xz} & 0 & \tau_{zz} \end{pmatrix}$$

The two additional diagonal components are called *normal stress* components. Their apparition is the consequence of the introduction of the $\beta_a(\nabla \boldsymbol{u}, \boldsymbol{\tau})$ term of the tensor objective derivative, that mixts tensor components. Let us expand the $\beta_a(\nabla \boldsymbol{u}, \boldsymbol{\tau})$ term. From its definition (4.15) and after expansion:

$$\beta_a(\nabla \boldsymbol{u}, \boldsymbol{\tau}) = \begin{pmatrix} (1-a)u_z'\tau_{xz} & 0 & -\dfrac{1+a}{2}u_z'\tau_{xx} + \dfrac{1-a}{2}u_z'\tau_{zz} \\ 0 & 0 & 0 \\ -\dfrac{1+a}{2}u_z'\tau_{xx} + \dfrac{1-a}{2}u_z'\tau_{zz} & 0 & -(1+a)u_z'\tau_{xz} \end{pmatrix}$$

Note that both the inertia term $(\boldsymbol{u}.\nabla)\boldsymbol{u}$ and the elastic stress transport one $(\boldsymbol{u}.\nabla)\boldsymbol{\tau}$ are zero. Indeed, $\boldsymbol{u} = u_z\,\boldsymbol{e}_z$ while ∇ contains just one component $\partial/\partial x$ in the $\boldsymbol{e}_x$ direction and then the operator $\boldsymbol{u}.\nabla$ is zero. Thus, there is no associated upstream boundary condition for the elastic stress. Problem (4.14a)–(4.14g) becomes

(P): find τ_{xx}, τ_{zz}, τ_{xz} and u_z, defined in $]-L, L[$ such that

$$\begin{aligned} \lambda(1-a)u_z'\tau_{xz} + \tau_{xx} &= 0 \text{ in }]-L, L[\\ -\lambda(1+a)u_z'\tau_{xz} + \tau_{zz} &= 0 \text{ in }]-L, L[\end{aligned}$$

$$
\begin{aligned}
-\frac{\lambda(1+a)}{2}u_z'\tau_{xx} + \frac{\lambda(1-a)}{2}u_z'\tau_{zz} + \tau_{xz} - \eta_m u_z' &= 0 \text{ in }]-L, L[\\
-\tau_{xz}' - \eta_s u_z'' &= f \text{ in }]-L, L[\\
u_z(-L) = u_z(L) &= 0
\end{aligned}
$$

This problem presents six physical parameters: $\lambda \geqslant 0$, $a \in \mathbb{R}$, $\eta_m > 0$, $\eta_s \geqslant 0$, $f > 0$ and $L > 0$. In order to reduce the parameter set, let us perform a dimensional analysis. As usual, the dimensionless quantities are denoted with tildes:

$$
\tilde{x} = \frac{x}{L}, \quad \tilde{u}(\tilde{x}) = \frac{u_z(L\tilde{x})}{U} \text{ and } \tilde{\tau}_{ij}(\tilde{x}) = \frac{\tau_{ij}(\tilde{x})}{\Sigma}, \quad ij = xx, xz, zz
$$

where $\Sigma = (\eta_s + \eta_m)U/L$ and U will be chosen later. After this change of unknown, the problem becomes:

(P): find $\tilde{\tau}_{xx}$, $\tilde{\tau}_{zz}$, $\tilde{\tau}_{xz}$ and $\tilde{u}$, defined in $]-1, 1[$ such that

$$
\begin{aligned}
\frac{\lambda U}{L}(1-a)\tilde{u}'\tilde{\tau}_{xz} + \tilde{\tau}_{xx} &= 0 \text{ in }]-1, 1[\\
-\frac{\lambda U}{L}(1+a)\tilde{u}'\tilde{\tau}_{xz} + \tilde{\tau}_{zz} &= 0 \text{ in }]-1, 1[\\
\frac{\lambda U}{L}\left(-\frac{1+a}{2}\tilde{u}'\tilde{\tau}_{xx} + \frac{1-a}{2}\tilde{u}'\tilde{\tau}_{zz}\right) + \tilde{\tau}_{xz} - \frac{\eta_m}{\eta_s+\eta_m}\tilde{u}' &= 0 \text{ in }]-1, 1[\\
-\tilde{\tau}_{xz}' - \left(1 - \frac{\eta_m}{\eta_s+\eta_m}\right)\tilde{u}'' &= \frac{fL^2}{(\eta_s+\eta_m)U} \text{ in }]-1, 1[\\
\tilde{u}(-1) = \tilde{u}(1) &= 0
\end{aligned}
$$

Next, choose U such that $\dfrac{fL^2}{(\eta_s+\eta_m)U} = 1$ i.e. $U = fL^2/(\eta_s+\eta_m)$. Then, the right-hand-side in the fourth equation is 1. Let us introduce the two following dimensionless numbers:

$$
We = \frac{\lambda U}{L} \text{ and } \alpha = \frac{\eta_m}{\eta_s + \eta_m}
$$

The dimensionless number We is called the Weissenberg number while α is a viscosity ratio between the solvent and the polymer. The third parameter of the problem is the interpolation parameter a of the tensor derivative. Then, the dimensionless problem presents three parameters: We, α and a. Note that, when $\alpha = 1$, we obtain the Maxwell model. By using the symmetry of the geometry, the problem also reduces to the $]0, 1[$ interval. With these notations, the dimensionless problem becomes

(P): find $\tilde{\tau}_{xx}$, $\tilde{\tau}_{zz}$, $\tilde{\tau}_{xz}$ and $\tilde{u}$, defined in $]0, 1[$ such that

$$
We(1-a)\tilde{u}'\tilde{\tau}_{xz} + \tilde{\tau}_{xx} = 0 \text{ in }]0, 1[\tag{4.16a}
$$

$$
-We(1+a)\tilde{u}'\tilde{\tau}_{xz} + \tilde{\tau}_{zz} = 0 \text{ in }]0, 1[\tag{4.16b}
$$

$$
\frac{We}{2}\left(-(1+a)\tilde{u}'\tilde{\tau}_{xx} + (1-a)\tilde{u}'\tilde{\tau}_{zz}\right) + \tilde{\tau}_{xz} - \alpha\tilde{u}' = 0 \text{ in }]0, 1[\tag{4.16c}
$$

$$-\tilde{\tau}'_{xz} - (1-\alpha)\tilde{u}'' = 1 \text{ in }]0,1[\tag{4.16d}$$
$$\tilde{\tau}_{xz}(0) + (1-\alpha)\tilde{u}'(0) = 0 \tag{4.16e}$$
$$\tilde{u}(1) = 0 \tag{4.16f}$$

The symmetry condition (4.16e) along the plane $x = 0$ expresses the projection on the z axis of an homogeneous Neumann boundary $\boldsymbol{\sigma}_{\text{tot}}\boldsymbol{n} = 0$, where $\boldsymbol{n} = -\boldsymbol{e}_x$ is the outer unit normal of the symmetry plane. From (4.16a) and (4.16b) we get $\tilde{\tau}_{xx} = -We(1-a)\tilde{u}'\tilde{\tau}_{xz}$ and $\tilde{\tau}_{zz} = \quad We(1+a)\tilde{u}'\tilde{\tau}_{xz}$, respectively. Then (4.16c) yields $\left(1 + (1-a^2)We^2(\tilde{u}')^2\right)\tilde{\tau}_{xz} = \alpha\tilde{u}'$ that leads to

$$\tilde{\tau}_{xz} = \frac{\alpha\tilde{u}'}{1 + (1-a^2)\,We^2\,(\tilde{u}')^2} \tag{4.17}$$

A sufficient condition for the denominator to be non-vanishing is to restrict the tensor derivative interpolation parameter $a \in [-1, 1]$. For convenience, let us introduce the notation $k = \sqrt{1-a^2}\,We$. Integrating (4.16d) together with the symmetry condition (4.16e) leads to $\tilde{\tau}_{xz} + (1-\alpha)\tilde{u}' = -\tilde{x}$ and then (4.17) leads to

$$\begin{aligned} &\frac{\alpha\tilde{u}'}{\left(1 + k^2(\tilde{u}')^2\right)} + (1-\alpha)\tilde{u}' = -\tilde{x} \\ \iff &(1-\alpha)k^2(\tilde{u}')^3 + k^2\tilde{x}\,(\tilde{u}')^2 + \tilde{u}' + \tilde{x} = 0 \end{aligned} \tag{4.18}$$

This is a third order polynomial equation in $\tilde{u}'$. When $k = 0$, i.e. when $We = 0$ (Newtonian fluid) or $a = \pm 1$ (upper or lower tensor derivatives), it degenerates to a linear one, that solves easily. In that case, after a second integration and using the wall boundary condition (4.16f), we obtain

$$\begin{aligned} \tilde{u}(\tilde{x}) &= \frac{1-\tilde{x}^2}{2} \\ \tilde{\tau}_{xz}(\tilde{x}) &= -\alpha\tilde{x} \\ \tilde{\tau}_{xx}(\tilde{x}) &= -(1-a)We\alpha\tilde{x}^2 \\ \tilde{\tau}_{zz}(\tilde{x}) &= \quad (1+a)We\alpha\tilde{x}^2 \end{aligned}$$

Note that $\text{tr}(\boldsymbol{\tau}) = 2aWe\alpha\tilde{x}^2$ which is non-zero when $a = \pm 1$, as pointed out in Lemma 4.1, p. 151. The case of both the upper or the lower derivatives are then completely solved. Let us turn to the case of other interpolated derivatives, when $|a| < 1$ and $We \neq 0$. In that case $k > 0$ and, for convenience, let us perform a linear change of variable $\delta = -k\tilde{u}'$ and $\chi = k\tilde{x}$. With theses notations, (4.18) leads to the following characteristic equation:

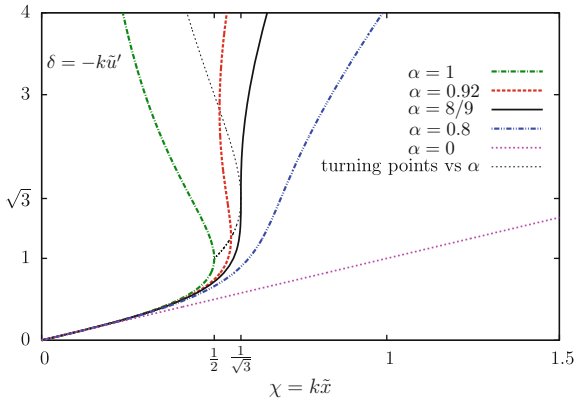

Fig. 4.6 Poiseuille flow of a viscoelastic fluid: characteristic curve

$$(1-\alpha)\delta^3 - \chi\,\delta^2 + \delta - \chi = 0$$
$$\iff \chi = \frac{\left(1+(1-\alpha)\delta^2\right)\delta}{1+\delta^2} \stackrel{def}{=} f(\delta)$$

The third order polynomial equation in δ degenerates to a second order one when $\alpha = 1$, i.e. for the Maxwell model: in that case it could be either zero or two solutions. Otherwise, when $\alpha < 1$, it could be either one or three solutions. Note that χ solves explicitly as an expression of δ called $f(\delta)$. This expression allows us to graphically represent the situation on Fig. 4.6. Observe that there is one *turning point* when $\alpha = 1$ and either zero on two turning points when $\alpha < 1$. The turning points $(\chi, \delta) = f(\delta), \delta)$ are given by the equation $f'(\delta) = 0$ that writes, after rearrangements:

$$(1-\alpha)\delta^4 + (2-3\alpha)\delta^2 + 1 = 0$$

When $\alpha < 1$, it is a bi-square equation and its discriminant is $\Delta = \alpha(9\alpha - 8)$. The situation could be summarized as

- $\alpha \leqslant 8/9$: there is no turning points
- $8/9 < \alpha < 1$: there is two turning points
- $\alpha = 1$: there is one turning point $(\chi, \delta) = (1/2, 1)$.

When $1 < \alpha < 8/9$, let $(\chi_i(\alpha), \delta_i(\alpha))$, $i = 1, 2$ denotes the two turning points, numbered such that $\chi_1(\alpha) < \chi_2(\alpha)$. More precisely:

$$\delta_1(\alpha) = \left(\frac{3\alpha - 2 + \sqrt{\alpha(9\alpha-8)}}{2(1-\alpha)}\right)^{1/2} \quad \text{and} \quad \chi_1(\alpha) = f(\delta_1(\alpha))$$
$$\delta_2(\alpha) = \left(\frac{3\alpha - 2 - \sqrt{\alpha(9\alpha-8)}}{2(1-\alpha)}\right)^{1/2} \quad \text{and} \quad \chi_2(\alpha) = f(\delta_2(\alpha))$$

The set of turning points $(\chi_i(\alpha),\ \delta_i(\alpha)), i = 1, 2$ when $\alpha \in [8/9, 1]$ is represented on Fig. 4.6 by a dotted thin line. Note that, when $\alpha = 8/9$, the two turning points merges at $(\chi, \delta) = (1/\sqrt{3}, \sqrt{3})$. When $\alpha = 1$, the first turning point is $(\chi, \delta) = (1/2, 1)$ and the second one diverges as $(\chi, \delta) = (0, +\infty)$. We are able to group these results.

Theorem 4.5 (Poiseuille flow of a generalized Oldroyd fluid model)

- *when* $a = \pm 1$ *or when* $\alpha \in [0, 8/9]$, *the problem admits a unique solution, for all* $We \geqslant 0$.
- *when* $|a| < 1$ *and* $\alpha \in]8/9, 1[$, *the problem admits a solution, for all* $We \geqslant 0$. *Moreover, this solution is unique when* $\sqrt{1 - a^2}\, We \leqslant \chi_1(\alpha)$.
- *when* $|a| < 1$ *and* $\alpha = 1$, *the problem admits a unique solution if and only if* $\sqrt{1 - a^2}\, We \leqslant 1/2$. *Otherwise, there is no solution.*

For practical computation, the solution of the third order characteristic equation could be obtained by e.g. the Cardano's explicit formula. This approach leads to an explicit formula for $\tilde{u}'$ versus $\tilde{x}$. Recall that the computation of the stress components is then explicit from $\tilde{u}'$. For obtaining $\tilde{u}$, no explicit primitive was found to $\tilde{u}'(\tilde{x})$ except when $\alpha = 1$ and a numeric integration should be used. A variant is to compute $\tilde{u}'$ versus $\tilde{x}$ by a Newton method: this approach was found to be more stable than the Cardano's formula for computing polynomial roots when using double precision floating point numbers, due to rounding effects. Figure 4.7 plots the solution when $\alpha = 8/9$. For $We = 1/2$, the solution when $a = 0$ is smooth and looks like the solution when $a = 0$. The corresponding stresses are also smooth. When We increases, more precisely when $\sqrt{1 - a^2}We > 1/\sqrt{3}$, the solution for $a = 0$ presents a singular point. At this flow regime, the flow rate increases dramatically and the difference of normal stresses $\tilde{\tau}_{zz} - \tilde{\tau}_{xx}$ also increases rapidly in a region adjacent to the wall. Figure 4.8 plots the solution when $\alpha = 0.95$. For small We, there is only one smooth solution. When $a = 0$ and We goes beyond a first critical value, others non-smooth solutions suddenly appear. When We increases beyond a second critical value, there is more smooth solutions. For the non-smooth solutions, the flow rate is high as compared with the smooth solution or with the solution at $a = 1$. Also, non-smooth solutions present discontinuities for the stress. Figure 4.9 shows the solution when $\alpha = 1$. For small We, there is only one smooth solution. For $We > 1/2$, there is no more solution when $a = 0$.

The solution in a circular pipe is obtained in a similar way: it suffice to replace f by $f/2$ and x by r in the dimensional expressions of the solutions.

The existence some multiple stationary solutions for the Poiseuille flow (Theorem 4.5) was first showed in [135, 276, p. 129]. It leads to questions about the stability of these solutions, especially for non-smooth ones. This question was investigated in 1990 by Guillopé and Saut [135]. The Maxwell model ($\alpha = 1$) appears to be very limited, as there is no solutions for sufficiently large We. Many numerical computations for complex flow geometries are based on intermediate values of α, such as $\alpha = 8/9$ or $\alpha = 1/2$.

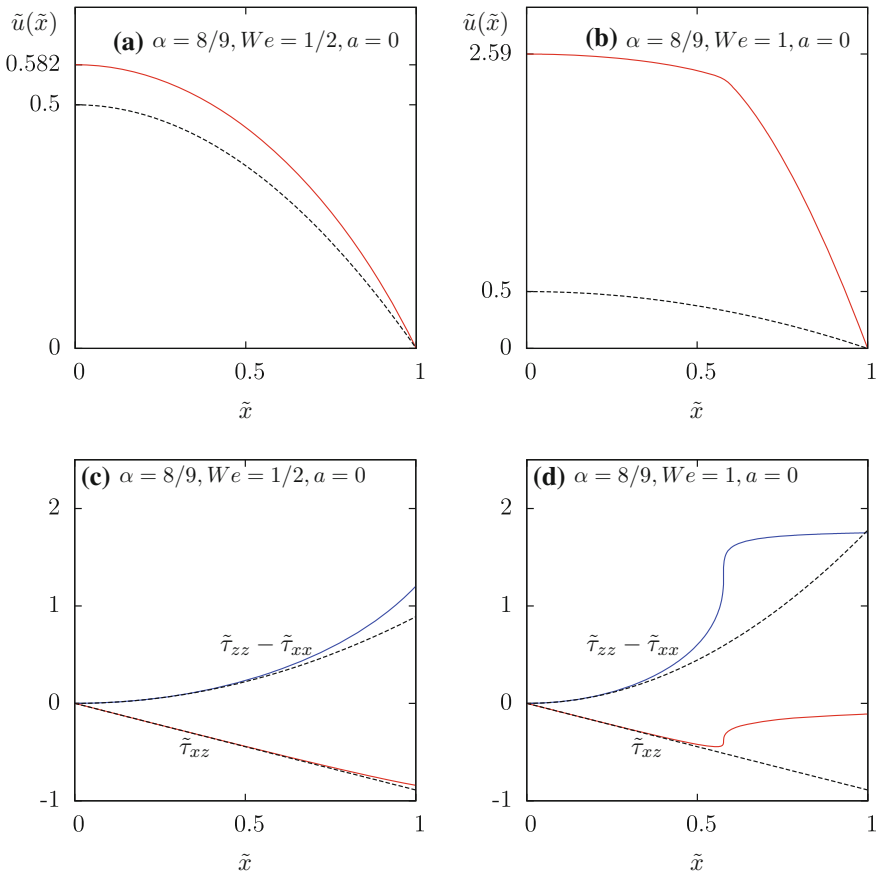

Fig. 4.7 Poiseuille flow of a viscoelastic fluid: the solution when $\alpha = 8/9$ and $a = 0$ (*solid lines*) and $a = 1$ (*dotted lines*)

4.5 Example: Couette Flow

We reuse the notations of Sect. 1.6, p. 21 for the Couette flow of a Newtonian fluid. For a laminar flow, the velocity writes $\boldsymbol{u} = (0, u_\theta(r), 0)$ in the cylindrical coordinate system (r, θ, z). By introducing the angular velocity $\omega(r)$ such that $u_\theta(r) = r\,\omega(r)$, the gradient of velocity writes

$$\nabla \boldsymbol{u} = \begin{pmatrix} 0 & 0 & 0 \\ r\omega' & 0 & 0 \\ 0 & 0 & 0 \end{pmatrix}$$

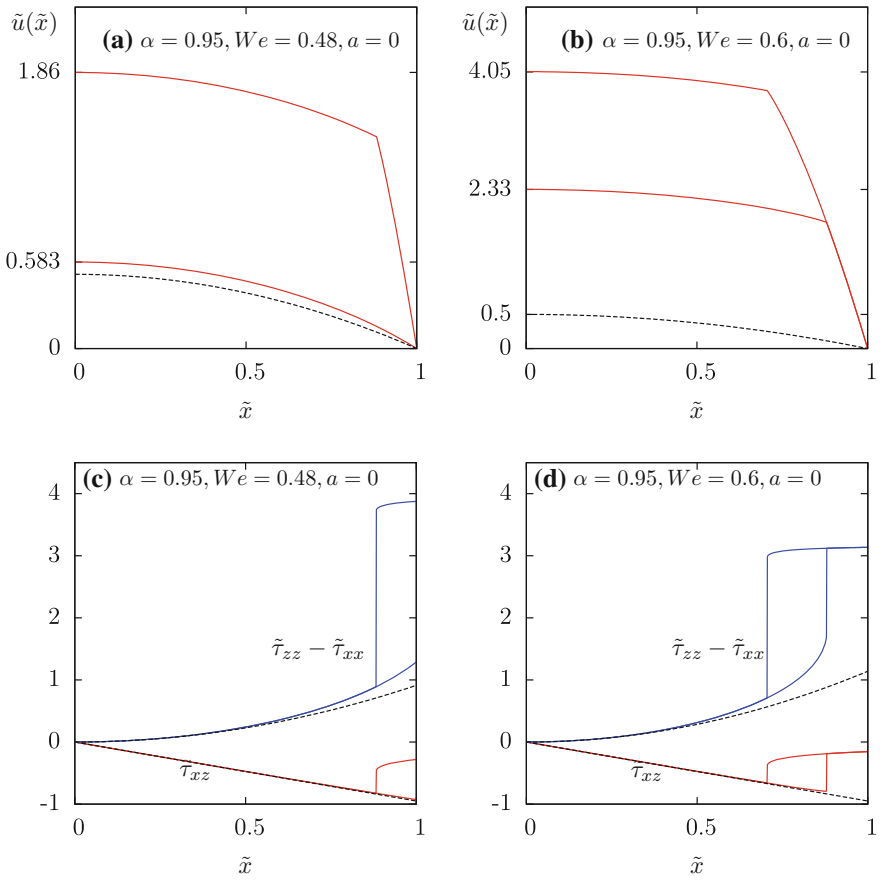

Fig. 4.8 Poiseuille flow of a viscoelastic fluid: the solutions when $\alpha = 0.95$ and $a = 0$ (*solid lines*) and the unique one when $a = 1$ (*dotted lines*)

As for the Poiseuille flow of a viscoelastic fluid, a major difference with Newtonian, quasi-Newtonian and viscoplastic fluid is that here, the stress is not in general proportional to the rate of deformation tensor $D(\boldsymbol{u})$. It could develop additional diagonal terms:

$$\boldsymbol{\tau} = \begin{pmatrix} \tau_{rr} & \tau_{r\theta} & 0 \\ \tau_{r\theta} & \tau_{\theta\theta} & 0 \\ 0 & 0 & 0 \end{pmatrix}$$

These two additional diagonal components are the *normal stress* components. Let us expand the interpolated derivative of this tensor for the stationary problem. As difference with the Cartesian coordinate system, the transport term $(\boldsymbol{u}.\nabla)\boldsymbol{\tau}$ is not zero in axisymmetric coordinate system (see e.g. [46, Appendix B]):

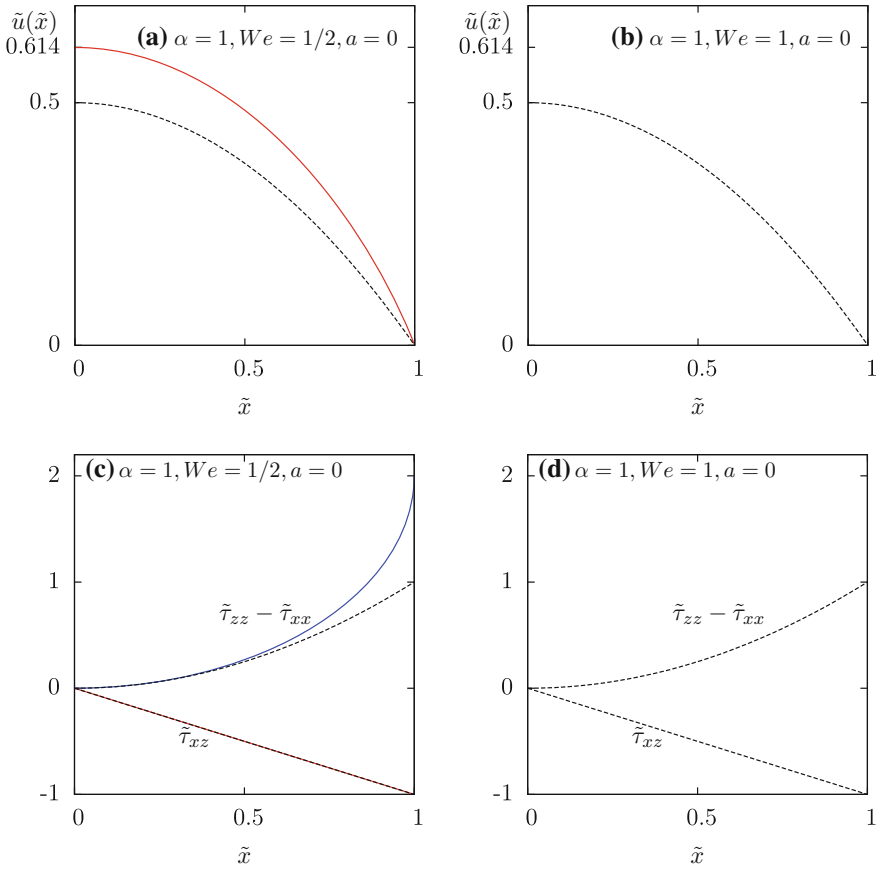

Fig. 4.9 Poiseuille flow of a viscoelastic fluid: the solution when $\alpha = 1$ and $a = 0$ (*solid lines*) and $a = 1$ (*dotted lines*)

$$(\boldsymbol{u}.\nabla)\boldsymbol{\tau} = \begin{pmatrix} -2\omega\tau_{r\theta} & \omega(\tau_{rr}-\tau_{\theta\theta}) & 0 \\ \omega(\tau_{rr}-\tau_{\theta\theta}) & 2\omega\tau_{r\theta} & 0 \\ 0 & 0 & 0 \end{pmatrix}$$

Let us expand the additional objective derivative term $\beta_a(\nabla\boldsymbol{u}, \boldsymbol{\tau})$. From its definition (4.15) and after expansion:

$$\begin{aligned} (\beta_a(\nabla\boldsymbol{u}, \boldsymbol{\tau}))_{rr} &= \left((1-a)r\omega' + 2\omega\right)\tau_{r\theta} \\ (\beta_a(\nabla\boldsymbol{u}, \boldsymbol{\tau}))_{r\theta} &= \frac{r\omega'}{2}\left((1-a)\tau_{\theta\theta} - (1+a)\tau_{rr}\right) - \omega(\tau_{rr}-\tau_{\theta\theta}) \\ (\beta_a(\nabla\boldsymbol{u}, \boldsymbol{\tau}))_{\theta\theta} &= -\left((1+a)r\omega' + 2\omega\right)\tau_{r\theta} \end{aligned}$$

Then

$$\frac{\mathscr{D}_a\boldsymbol{\tau}}{\mathscr{D}t} = \begin{pmatrix} (1-a)r\omega'\tau_{r\theta} & \frac{r\omega'}{2}\left((1-a)\tau_{\theta\theta} - (1+a)\tau_{rr}\right) & 0 \\ \frac{r\omega'}{2}\left((1-a)\tau_{\theta\theta} - (1+a)\tau_{rr}\right) & -(1+a)r\omega'\tau_{r\theta} & 0 \\ 0 & 0 & 0 \end{pmatrix}$$

There are two main experimental situations: imposed angular velocity and imposed torque.

Imposed torque – The stationary problem reduces to

(P): find τ_{rr}, $\tau_{r\theta}$, $\tau_{\theta\theta}$, ω, defined in $]r_1, r_2[$ and p, defined in $]r_1, r_2[\times]0, z_0[$, such that

$$\lambda(1-a)r\omega'\tau_{r\theta} + \tau_{rr} = 0 \tag{4.19a}$$

$$\frac{\lambda r\omega'}{2}\left((1-a)\tau_{\theta\theta} - (1+a)\tau_{rr}\right) + \tau_{r\theta} = \eta_m r\omega' \tag{4.19b}$$

$$-\lambda(1+a)r\omega'\tau_{r\theta} + \tau_{\theta\theta} = 0 \tag{4.19c}$$

$$\rho\,\omega^2 r + \tau'_{rr} + \frac{\tau_{rr} - \tau_{\theta\theta}}{r} - \frac{\partial p}{\partial r} = 0 \quad \text{in }]r_1, r_2[\times]0, z_0[\tag{4.19d}$$

$$-\frac{1}{r^2}\left(r^2\left(\eta_s r\omega' + \tau_{r\theta}\right)\right)' = 0 \quad \text{in }]r_1, r_2[\tag{4.19e}$$

$$-\frac{\partial p}{\partial z} = -\rho\boldsymbol{g} \quad \text{in }]r_1, r_2[\times]0, z_0[\tag{4.19f}$$

$$\eta_s r_1\omega'(r_1) + \tau_{r\theta}(r_1) = -f \text{ and } \omega(r_2) = \omega_2 \tag{4.19g}$$

where f is a boundary data associated to the torque $F = 2\pi z_0 r_1^2 f$ imposed on the inner cylinder (see Sect. 1.5, p. 18). The problem (4.19a)–(4.19g) presents ten physical parameters: λ, a, η_m, η_s, f, ω_2, r_1, r_2, ρ and $\boldsymbol{g}$. In order to reduce the set of parameters, let us perform a dimensional analysis. As usual, the dimensionless quantities are denoted with tildes:

$$\tilde{r} = \frac{r}{r_2},\ \tilde{z} = \frac{z}{r_2},\ \ \tilde{\omega}(\tilde{r}) = \frac{\omega(r_2\tilde{r}) - \omega_2}{W},\ \ \tilde{\boldsymbol{\tau}}(\tilde{r}) = \frac{\boldsymbol{\tau}(r_2\tilde{r})}{\Sigma},\ \ \tilde{p}(\tilde{r}, \tilde{z}) = \frac{p(r_2\tilde{r}, r_2\tilde{z})}{\Sigma}$$

where the characteristic stress is $\Sigma = f$ and the characteristic angular velocity W is such that $\Sigma = (\eta_m + \eta_s)W$ i.e. $W = f/(\eta_m + \eta_s)$. After this change of unknowns, the reduced problem becomes:

(P): find $\tilde{\tau}_{rr}$, $\tilde{\tau}_{r\theta}$, $\tilde{\tau}_{\theta\theta}$, $\tilde{\omega}$, defined in $]\beta, 1[$ and $\tilde{p}$, defined in $]\beta, 1[\times]0, \gamma[$ such that

$$We(1-a)\tilde{r}\tilde{\omega}'\tilde{\tau}_{r\theta} + \tilde{\tau}_{rr} = 0 \tag{4.20a}$$

$$\frac{We\,\tilde{r}\tilde{\omega}'}{2}\left((1-a)\tilde{\tau}_{\theta\theta} - (1+a)\tilde{\tau}_{rr}\right) + \tilde{\tau}_{r\theta} = \alpha\tilde{r}\tilde{\omega}' \tag{4.20b}$$

$$-We(1+a)\tilde{r}\tilde{\omega}'\tilde{\tau}_{r\theta} + \tilde{\tau}_{\theta\theta} = 0 \tag{4.20c}$$

$$Re\,\tilde{\omega}^2\tilde{r} + \tilde{\tau}'_{rr} + \frac{\tilde{\tau}_{rr} - \tilde{\tau}_{\theta\theta}}{r} - \frac{\partial\tilde{p}}{\partial\tilde{r}} = 0 \quad \text{in }]\beta, 1[\times]0, \gamma[\tag{4.20d}$$

$$-\frac{1}{\tilde{r}^2}\left(\tilde{r}^2\left((1-\alpha)\tilde{r}\tilde{\omega}' + \tilde{\tau}_{r\theta}\right)\right)' = 0 \quad \text{in }]\beta, 1[\tag{4.20e}$$

$$-\frac{\partial\tilde{p}}{\partial\tilde{z}} = -\frac{Re}{Fr^2} \quad \text{in }]\beta, 1[\times]0, \gamma[\tag{4.20f}$$

$$(1-\alpha)\beta\tilde{\omega}'(\beta) + \tilde{\tau}_{r\theta}(\beta) = -1 \text{ and } \tilde{\omega}(1) = 0 \tag{4.20g}$$

Clearly, the computation of $(\tilde{\tau}_{rr}, \tilde{\tau}_{r\theta}, \tilde{\tau}_{\theta\theta}, \tilde{\omega})$ is decoupled to those of $\tilde{p}$, that could be performed later, by integrating (4.20d) and (4.20f). The reduced problem for computing the elastic stress and the angular velocity involves only four dimensionless numbers: the Weissenberg number $We = \lambda f/(\eta_m + \eta_s)$, the tensor derivative interpolation parameter a, the viscosity ratio $\alpha = \eta_m/(\eta_s + \eta_m)$ and the geometry confinement $\beta = r_1/r_2 \in]0, 1[$. The two Eqs. (4.20d) and (4.20f) for $\tilde{p}$ involve three additional dimensionless numbers: the Reynolds $Re = \rho W^2 r_2^2/\Sigma = \rho f r_2^2/(\eta_m + \eta_s)^2$, the Froude $Fr = (Wr_2)/\sqrt{gr_2} = (f/(\eta_m + \eta_s))\sqrt{r_2/g}$ and the cylinder vertical extension $\gamma = z_0/r_2$. Combining (4.20a)–(4.20c), we obtain

$$\tilde{\tau}_{rr} = -We(1-a)\tilde{r}\tilde{\omega}'\tilde{\tau}_{r\theta} \tag{4.21}$$

$$\tilde{\tau}_{\theta\theta} = We(1+a)\tilde{r}\tilde{\omega}'\tilde{\tau}_{r\theta} \tag{4.22}$$

$$\tilde{\tau}_{r\theta} = \frac{\alpha\tilde{r}\tilde{\omega}'}{1 + We^2(1-a^2)(\tilde{r}\tilde{\omega}')^2} \tag{4.23}$$

Next, integrating (4.20e) yields

$$(1-\alpha)\tilde{r}\tilde{\omega}' + \tilde{\tau}_{r\theta} = -\frac{c}{\tilde{r}^2}$$

where $c \in \mathbb{R}$ is an integration constant. From (4.20g) we obtain $c = \beta^2$. Replacing $\tilde{\tau}_{r\theta}$ by its previous expression leads to

$$(1-\alpha)\tilde{r}\tilde{\omega}' + \frac{\alpha\tilde{r}\tilde{\omega}'}{1 + We^2(1-a^2)(\tilde{r}\tilde{\omega}')^2} = -\frac{\beta^2}{\tilde{r}^2}$$

Assume that the tensor derivative interpolation parameter $a \in [-1, 1]$ and let $k = We\sqrt{1-a^2}$. The previous relation writes equivalently

$$(1-\alpha)k^2\left(\tilde{r}\tilde{\omega}'\right)^3 + k^2\frac{\beta^2}{\tilde{r}^2}\left(\tilde{r}\tilde{\omega}'\right)^2 + \tilde{r}\tilde{\omega}' + \frac{\beta^2}{\tilde{r}^2} = 0$$

This is a third polynomial equation in $\tilde{r}\tilde{\omega}'$. When $k = 0$, i.e. when $We = 0$ or $a = \pm 1$ (upper or lower convected tensor derivatives), it degenerates to a linear equation that solves explicitly. In the case $a = \pm 1$, we obtain:

$$\tilde{\tau}_{rr}(\tilde{r}) = -\frac{(1-a)We\,\alpha\beta^4}{\tilde{r}^4}$$
$$\tilde{\tau}_{\theta\theta}(\tilde{r}) = \frac{(1+a)We\,\alpha\beta^4}{\tilde{r}^4}$$
$$\tilde{\tau}_{r\theta}(\tilde{r}) = -\frac{\alpha\beta^2}{\tilde{r}^2}$$
$$\tilde{\omega}(\tilde{r}) = \frac{\beta^2}{2}\left(\frac{1}{\tilde{r}^2} - 1\right)$$

The dimensional solution is then simply obtained by $\boldsymbol{\tau}(r) = f\tilde{\boldsymbol{\tau}}(r/r_2)$, $\omega(r) = \omega_2 + f\tilde{\omega}(r/r_2)/(\eta_m + \eta_s)$ and $u_\theta(r) = r\,\omega(r)$. Then, $\tilde{p}$ is obtained by integrating (4.19d)–(4.19f):

$$\begin{aligned}\tilde{p}(\tilde{r},\tilde{z}) &= \tilde{\tau}_{rr}(\tilde{r}) + \int_\beta^{\tilde{r}} \frac{\tilde{\tau}_{rr}(\tilde{r}) - \tilde{\tau}_{\theta\theta}(\tilde{r})}{\tilde{r}}\,\mathrm{d}\tilde{r} + Re\int_\beta^{\tilde{r}} \tilde{\omega}^2(\tilde{r})\tilde{r}\,\mathrm{d}\tilde{r} - \frac{Re\tilde{z}}{Fr^2} + \tilde{p}_0 \\ &= -\frac{We\,\alpha}{2}\left(1 - (2a-1)\left(\frac{\beta}{\tilde{r}}\right)^4\right) \\ &\quad + \frac{Re\beta^2}{8\tilde{r}^2}\left((\tilde{r}^2-\beta^2)\left(1+\beta^2\tilde{r}^2\right) - 4\beta^2\tilde{r}^2\log\left(\frac{\tilde{r}}{\beta}\right)\right) + \frac{Re\tilde{z}}{Fr^2} + \tilde{p}_0\end{aligned}$$

The first term represents the viscoelastic effects, with the We factor. The second term is the centripetal acceleration, with Re factor, the third one is the weight liquid effect and the last one, $\tilde{p}_0$, is an integration constant, as the pressure is defined up to a constant. In the vertical direction, this is the required pressure to keep the upper surface of the fluid horizontal. When the surface is not held horizontal but is free, this function will determine the shape of the free surface. Recall that, in the absence of viscoelastic effects ($We = 0$), the fluid is pushed in the direction of the outer cylinder (see Sect. 1.6, p. 21). When viscous effects are dominant, the Reynold number is small and in presence of viscoelasticity the first term is dominant. Let us consider the limit case $Re \approx 0$:

$$\frac{\partial\tilde{p}}{\partial\tilde{r}}(\tilde{r},\tilde{z}) = \frac{2(2a-1)We\,\alpha\beta^4}{3\tilde{r}^5} + \mathcal{O}(Re)$$

Observe that this quantity is negative while when $a = -1$ it is positive. Thus, when $a = 1$, the free surface may be expected to rise in a spectacular way near the inner cylinder: this climbing effect first observed experimentally in 1947 by Weissenberg [315, 316] is called the *positive Weissenberg effect*, represented on Fig. 4.10left. The plot on the right represents the pressure: observe that the fluid is pushed in the direction of the inner cylinder when viscoelastic effects are dominants, while it is pushed in the opposite direction when inertia effects are dominants. When

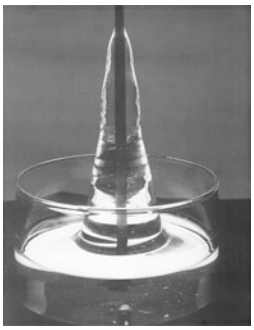

Karl Weissenberg
1947

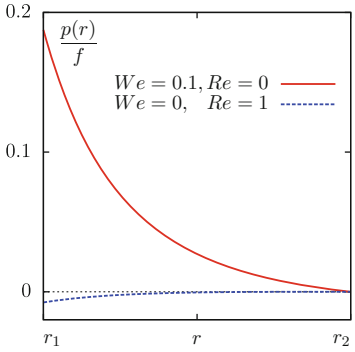

Fig. 4.10 (*left*) The Weissenberg effect, as observed with a polymer solution (from [30]); (*center*) photography of K. Weissenberg, from [302, p. 41]; (*right*) pressure, as computed with the Oldroyd model: $a = 1$, $\alpha = 1$, $\beta = 1/2$

$a = -1$, the free surface may be expected to sink down instead of rising up near the inner cylinder: this is the *negative Weissenberg effect*, also observed experimentally.

The case of both the upper or the lower derivatives are then completely solved. Let us turn to the case others interpolated derivatives, when $|a| < 1$ and $We \neq 0$. In that case $k > 0$ and, for convenience, let us perform a linear change of variable $\delta = -k\tilde{r}\tilde{\omega}'$ and $\chi = k\beta^2/\tilde{r}^2$. Then (4.23) becomes

$$(1-\alpha)\delta^3 - \chi\,\delta^2 + \delta - \chi = 0$$

This characteristic equation has already be studied in the previous section, for the Poiseuille flow. When $1 < \alpha < 8/9$, let $(\chi_i(\alpha), \delta_i(\alpha))$, $i = 1, 2$ denotes the two turning points, numbered such that $\chi_1(\alpha) < \chi_2(\alpha)$. The situation is summarized by the following result.

Theorem 4.6 (Couette flow of a generalized Oldroyd fluid model)

- *when $a = \pm 1$ or when $\alpha \in [0, 8/9]$, the problem admits a unique solution, for all $We \geqslant 0$.*
- *when $|a| < 1$ and $\alpha \in]8/9, 1[$, the problem admits a solution, for all $We \geqslant 0$. Moreover, this solution is unique when $\sqrt{1-a^2}\,We \leqslant \chi_1(\alpha)$ or $\sqrt{1-a^2}\,We\,\beta^2 \geqslant \chi_2(\alpha)$.*
- *when $|a| < 1$ and $\alpha = 1$, the problem admits a unique solution if and only if $\sqrt{1-a^2}\,We \leqslant 1/2$. Otherwise, there is no solution.*

The practical computation of the solution is also similar to those of the Poiseuille flow. Solving the third order polynomial equation leads to $\tilde{\omega}'(\tilde{r})$ and the components of the elastic stress $\tilde{\boldsymbol{\tau}}$ are then obtained by explicit expressions. Finally, a numerical integration yields $\tilde{\omega}(\tilde{r})$.

Imposed angular velocity – The solution is also explicit when $a = \pm 1$:

$$\tilde{\tau}_{rr}(\tilde{r}) = -\frac{4(1-a)We\,\alpha\beta^4}{(1-\beta^2)^2\tilde{r}^4}$$
$$\tilde{\tau}_{\theta\theta}(\tilde{r}) = \frac{4(1+a)We\,\alpha\beta^4}{(1-\beta^2)^2\tilde{r}^4}$$
$$\tilde{\tau}_{r\theta}(\tilde{r}) = -\frac{\alpha\beta^2}{(1-\beta^2)\tilde{r}^2}$$
$$\tilde{\omega}(\tilde{r}) = \frac{\beta^2}{1-\beta^2}\left(\frac{1}{\tilde{r}^2} - 1\right)$$

where $We = \lambda(\omega_1 - \omega_2)$. The dimensional solution is then simply obtained by $\boldsymbol{\tau}(r) = (\eta_m + \eta_s)(\omega_1 - \omega_2)\tilde{\boldsymbol{\tau}}(r/r_2)$, $\omega(r) = \omega_2 + (\omega_1 - \omega_2)\tilde{\omega}(r/r_2)$ and $u_\theta(r) = r\,\omega(r)$. Then, p is obtained by integrating (4.19d)–(4.19f), as in the case of a Neumann boundary condition. When $|a| < 1$, the resolution is more complex, since the integration constant c is no more known in the characteristic equation.

In 1993, Avgousti and Beris [7] showed that when the Weissenberg number becomes large, some instabilities appear and the flow of an Oldroyd fluid becomes three-dimensional. Note that these instabilities differ to the Taylor-Couette one [305], for a Newtonian fluid when the Reynolds number becomes large.

While the stationary Poiseuille and Couette flows could lead to explicit solutions, the case of more complex flow geometries and boundary conditions requires an approximation procedure. The following sections are devoted to numerical algorithms.

4.6 Time Discretization with the θ-Scheme Algorithm

This section is devoted to the development of an operator splitting algorithm for the numerical approximation of the solution to the time-dependent problem (4.14a)–(4.14g). The operator splitting algorithm is based on a second order semi-implicit scheme for the discretization versus time, the so-called θ-scheme. Problem (4.14a)–(4.14g) is first packaged in an abstract framework. The θ-scheme is then presented for this abstract framework. Finally, notations are expanded, in order to get a practical algorithm for our problem. Let

$$\mathcal{U} = \begin{pmatrix} \boldsymbol{\tau} \\ \boldsymbol{u} \\ p \end{pmatrix}, \quad \mathcal{U}_0 = \begin{pmatrix} \boldsymbol{\tau}_0 \\ \boldsymbol{u}_0 \\ 0 \end{pmatrix}, \quad \mathcal{F} = \begin{pmatrix} 0 \\ -\rho\boldsymbol{g} \\ 0 \end{pmatrix}, \quad M = \mathrm{diag}\left(\frac{\lambda}{2\eta_m}, -\rho, 0\right)$$

$$A(\mathcal{U}) = \begin{pmatrix} \dfrac{\lambda}{2\eta_m}(\boldsymbol{u}.\nabla\boldsymbol{\tau} + \beta_a(\nabla\boldsymbol{u},\boldsymbol{\tau})) + \dfrac{\boldsymbol{\tau}}{2\eta_m} & -D(\boldsymbol{u}) \\ \mathbf{div}\,(\boldsymbol{\tau}) & +\mathbf{div}\,(2\eta_s D(\boldsymbol{u})) - \nabla p \\ & \operatorname{div}\boldsymbol{u} \end{pmatrix}$$

Then, problem (4.14a)–(4.14g) writes:

(P): find $\mathcal{U}$ such that

$$M\frac{\partial \mathcal{U}}{\partial t} + A(\mathcal{U}) = \mathcal{F}$$
$$M\,\mathcal{U}(t=0) = M\,\mathcal{U}_0$$

The inertia term $(\boldsymbol{u}.\nabla)\boldsymbol{u}$ is neglected, as mostly slow flows are considered here. This is an usual assumption for such flow computation. For an easier readability, the boundary conditions for $\boldsymbol{\tau}$ and $\boldsymbol{u}$ are omitted in the abstract framework: they will be reintroduced when expanding the notations. The operator A is then split as

$$A = A_1 + A_2$$

where A_1 and A_2 are supposed to be *easier* to solve than A.

Algorithm 4.1 (θ*-scheme – abstract version*)
Let $\Delta t > 0$ be a time step and $\theta \in]0, 1/2[$.

- $m = 0$: let $\mathcal{U}_0$ being given.
- $m \geqslant 0$: let $\mathcal{U}_m$ being known, compute successively $\mathcal{U}_{m+\theta}$, $\mathcal{U}_{m+1-\theta}$ and $\mathcal{U}_{m+1}$ as

$$\begin{aligned} M\frac{\mathcal{U}_{m+\theta} - \mathcal{U}_m}{\theta\Delta t} &+ A_1(\mathcal{U}_{m+\theta}) + A_2(\mathcal{U}_m) &&= \mathcal{F}(t_{n+\theta}) \\ M\frac{\mathcal{U}_{m+1-\theta} - \mathcal{U}_{m+\theta}}{(1-2\theta)\Delta t} &+ A_1(\mathcal{U}_{m+\theta}) + A_2(\mathcal{U}_{m+1-\theta}) &&= \mathcal{F}(t_{n+1-\theta}) \\ M\frac{\mathcal{U}_{m+1} - \mathcal{U}_{m+1-\theta}}{\theta\Delta t} &+ A_1(\mathcal{U}_{m+1}) + A_2(\mathcal{U}_{m+1-\theta}) &&= \mathcal{F}(t_{n+1}) \end{aligned}$$

This algorithm involves three steps. During step 1, we search for $\mathcal{U}_{m+\theta}$ and solve a subproblem involving A_1. Then, during step 2, we search for $\mathcal{U}_{m+1-\theta}$ and solve a subproblem involving A_2. Finally, during step 3, we search for $\mathcal{U}_{m+1}$ and solve a subproblem, similar to those of step 1, involving A_1 (Fig. 4.11).

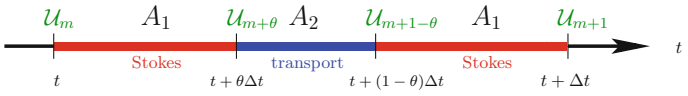

Fig. 4.11 The θ-scheme algorithm based on an operator splitting

For our problem, we choose to split operator A as

$$A_1(\mathcal{U}) = \begin{pmatrix} \dfrac{\boldsymbol{\tau}}{2\eta_m} & -D(\boldsymbol{u}) \\ \mathbf{div}\,(\boldsymbol{\tau}) + \mathbf{div}\,(2\eta_s D(\boldsymbol{u})) - \nabla p \\ \operatorname{div} \boldsymbol{u} \end{pmatrix}$$

$$A_2(\mathcal{U}) = \begin{pmatrix} \dfrac{\lambda}{2\eta_m}\,(\boldsymbol{u}.\nabla\boldsymbol{\tau} + \beta_a(\nabla\boldsymbol{u}, \boldsymbol{\tau})) \\ 0 \\ 0 \end{pmatrix}$$

Operator A_1 is a linear three-field Stokes operator (see Sect. 3.11, p. 123) while operator A_2 is a tensorial transport operator.

Let us unpack the notations for the step 1. Let $\boldsymbol{\tau}_m$ and $\boldsymbol{u}_m$ being known. The first subproblem writes:

(P_1): find $\boldsymbol{\tau}_{m+\theta}$, $\boldsymbol{u}_{m+\theta}$ and $p_{m+\theta}$ such that

$$\frac{\lambda}{2\eta_m}\left(\frac{\boldsymbol{\tau}_{m+\theta} - \boldsymbol{\tau}_m}{\theta\Delta t}\right) + \frac{\boldsymbol{\tau}_{m+\theta}}{2\eta_m} - D(\boldsymbol{u}_{m+\theta}) = -\frac{\lambda}{2\eta_m}(\boldsymbol{u}_m.\nabla\boldsymbol{\tau}_m + \beta_a(\nabla\boldsymbol{u}_m, \boldsymbol{\tau}_m)) \text{ in } \Omega \quad (4.24a)$$

$$-\rho\left(\frac{\boldsymbol{u}_{m+\theta} - \boldsymbol{u}_m}{\theta\Delta t}\right) + \mathbf{div}\,(\boldsymbol{\tau}_{m+\theta}) + \mathbf{div}\,(2\eta_s D(\boldsymbol{u}_{m+\theta})) - \nabla p_{m+\theta} = -\rho\boldsymbol{g} \text{ in } \Omega \quad (4.24b)$$

$$\operatorname{div} \boldsymbol{u}_{m+\theta} = 0 \text{ in } \Omega \quad (4.24c)$$

$$\boldsymbol{u}_{m+\theta} = \boldsymbol{u}_\Gamma(t_{m+\theta}) \text{ on } \partial\Omega \quad (4.24d)$$

Then, (4.24a) leads to an explicit expression of the elastic $\boldsymbol{\tau}_{m+\theta}$ tensor versus $\boldsymbol{u}_{m+\theta}$:

$$\boldsymbol{\tau}_{m+\theta} = \frac{1}{\lambda + \theta\Delta t}\left(\lambda\boldsymbol{\tau}_m + 2\eta_m\theta\Delta t\; D(\boldsymbol{u}_{m+\theta}) - \lambda\theta\Delta t\,\boldsymbol{\gamma}_m\right) \quad (4.25)$$

where $\boldsymbol{\gamma}_m = \boldsymbol{u}_m.\nabla\boldsymbol{\tau}_m + \beta_a(\nabla\boldsymbol{u}_m, \boldsymbol{\tau}_m)$ is a convenient notation, that depend only on known data at step 1. Substituting this expression of $\boldsymbol{\tau}_{m+\theta}$ in (4.24b) leads to reduce the subproblem at step 1 to the following velocity-pressure Stokes-like linear subproblem:

(S_1): find $\boldsymbol{u}_{m+\theta}$ and $p_{m+\theta}$ such that

$$\frac{\rho}{\theta\Delta t}\boldsymbol{u}_{m+\theta} - \mathbf{div}(2\eta_* D(\boldsymbol{u}_{m+\theta})) + \nabla p_{m+\theta} = \boldsymbol{f}_m \text{ in } \Omega \quad (4.26a)$$

$$-\operatorname{div} \boldsymbol{u}_{m+\theta} = 0 \text{ in } \Omega \quad (4.26b)$$

$$\boldsymbol{u}_{m+\theta} = \boldsymbol{u}_\Gamma(t_{m+\theta}) \text{ on } \partial\Omega \quad (4.26c)$$

with the notations

$$\eta_* = \eta_s + \left(\frac{\theta\Delta t}{\lambda + \theta\Delta t}\right)\eta_m \ > \ 0$$
$$\boldsymbol{f}_m = \rho\boldsymbol{g} + \frac{\rho}{\theta\Delta t}\boldsymbol{u}_m + \frac{1}{\lambda + \theta\Delta t}\mathbf{div}(\lambda\boldsymbol{\tau}_m - \lambda\theta\Delta t\,\boldsymbol{\gamma}_m)$$

Then, compute explicitly $\boldsymbol{\tau}_{m+\theta}$ from (4.25). The main computation time for step 1 is spend when solving the Stokes problem, as others computations are explicit. See Chap. 1 for efficient algorithms of the Stokes problem.

Let us turn to step 2 and unpack the notations. The second subproblem writes:

(P_2): find $\boldsymbol{\tau}_{m+1-\theta}$ and $\boldsymbol{u}_{m+1-\theta}$ such that

$$\frac{\lambda}{2\eta_m}\left(\frac{\boldsymbol{\tau}_{m+1-\theta} - \boldsymbol{\tau}_{m+\theta}}{(1-2\theta)\Delta t} + \boldsymbol{u}_{m+1-\theta}.\nabla\boldsymbol{\tau}_{m+1-\theta} + \beta_a(\nabla\boldsymbol{u}_{m+1-\theta}, \boldsymbol{\tau}_{m+1-\theta})\right)$$
$$= -\frac{\boldsymbol{\tau}_{m+\theta}}{2\eta_m} + D(\boldsymbol{u}_{m+\theta}) \qquad (4.27a)$$
$$-\rho\left(\frac{\boldsymbol{u}_{m+1-\theta} - \boldsymbol{u}_{m+\theta}}{(1-2\theta)\Delta t}\right) = -\rho\boldsymbol{g} - \mathbf{div}\left(\boldsymbol{\tau}_{m+\theta} + 2\eta_s D(\boldsymbol{u}_{m+\theta})\right) + \nabla p_{m+\theta} \qquad (4.27b)$$
$$\boldsymbol{\tau}_{m+1-\theta} = \boldsymbol{\tau}_\Gamma \text{ on } \partial\Omega_- \qquad (4.27c)$$

Note that (4.27b) looks like (4.24b) from step 1: there is only few changes between these equations, and combining them we get:

$$\frac{\boldsymbol{u}_{m+1-\theta} - \boldsymbol{u}_{m+\theta}}{(1-2\theta)\Delta t} = \frac{\boldsymbol{u}_{m+\theta} - \boldsymbol{u}_m}{\theta\Delta t}$$
$$\iff \boldsymbol{u}_{m+1-\theta} = \frac{1-\theta}{\theta}\boldsymbol{u}_{m+\theta} - \frac{1-2\theta}{\theta}\boldsymbol{u}_m \qquad (4.28)$$

As, both $\boldsymbol{u}_{m+\theta}$ and $\boldsymbol{u}_m$ are known at step 2, the computation of $\boldsymbol{u}_{m+1-\theta}$ is explicit. Finally, step 2 reduces to

(S_2): find $\boldsymbol{\tau}_{m+1-\theta}$ such that

$$\frac{\boldsymbol{\tau}_{m+1-\theta} - \boldsymbol{\tau}_{m+\theta}}{(1-2\theta)\Delta t} + \boldsymbol{u}_{m+1-\theta}.\nabla\boldsymbol{\tau}_{m+1-\theta} + \beta_a(\nabla\boldsymbol{u}_{m+1-\theta}, \boldsymbol{\tau}_{m+1-\theta}) = \boldsymbol{\chi}_{m+\theta} \qquad (4.29a)$$
$$\boldsymbol{\tau}_{m+1-\theta} = \boldsymbol{\tau}_\Gamma(t_{m+1-\theta}) \text{ on } \partial\Omega_- \qquad (4.29b)$$

where

$$\boldsymbol{\chi}_{m+\theta} = \frac{1}{\lambda}\left(2\eta_m D(\boldsymbol{u}_{m+\theta}) - \boldsymbol{\tau}_{m+\theta}\right)$$

This is a linear tensorial transport subproblem. This subproblem has not yet been studied: it will be done in a forthcoming section. Let us summarize the situation.

Algorithm 4.2 (*θ-scheme – viscoelastic fluid version*)

- $m = 0$: let $\boldsymbol{\tau}_0$ and $\boldsymbol{u}_0$ being given by initial conditions.
- $m \geqslant 0$: let $\boldsymbol{\tau}_m$ and $\boldsymbol{u}_m$ known,

(1) find $(\boldsymbol{u}_{m+\theta}, p_{m+\theta})$ as the solution of the Stokes problem (4.26a)–(4.26c) and then compute explicitly $\boldsymbol{\tau}_{m+\theta}$ from (4.25).
(2) compute explicitly $\boldsymbol{u}_{m+1-\theta}$ from (4.28) and then, find $\boldsymbol{\tau}_{m+1-\theta}$ as the solution of the tensorial transport problem (4.29a)–(4.29b).
(3) this step is similar to step 1, replacing indexes m and $m+\theta$ by $m+1-\theta$ and $m+1$, respectively.

This algorithm was proposed in 1990 by Saramito [276, 277]. It is a semi-implicit scheme that is conditionally stable: its stability was investigated in [278]. A good choice for the numerical parameter θ is $\theta = 1 - 1/\sqrt{2}$, as, in that case, the scheme is second order in time, and only first order for others choices of $\theta \in]0, 1/2[$. In 2008, Chrispell, Ervin and Jenkins investigates also the convergence of the discrete version of this algorithm [54, 55]. For practical viscoelastic computations that uses this scheme, see e.g. [54, 55, 277, 279, 288, 293, 300]. In the forthcoming Sect. 4.11, such a computation will be presented. Before to perform a computation, we need to study the space approximation and the resolution of the stress transport subproblem: this is the subject of the next sections.

4.7 Space Approximation

The generalized Oldroyd problem (4.14a)–(4.14g) involves three unknown $\boldsymbol{\tau}$, $\boldsymbol{u}$ and p. Also, step 1 in the previous algorithm involves a three-field Stokes problem. The variational formulation and the discretization of the three-field Stokes problem has been widely studied in Sect. 3.11, p. 123. An implementation of this algorithm by using the staggered grid finite difference method (see Fig. 3.8, p. 127) is presented in [277, 279]. An alternative is the finite-element approximation with the Taylor-Hood $P_2 - P_1$ element for the velocity-pressure pair and the P_1-discontinuous one for the stress, as represented on Fig. 3.8, p. 127. The P_1 discontinuous elements for the stress leads to the approximation by the discontinuous Galerkin method for the stress transport equation involved in step 2 of the present algorithm. This is the aim of the next section.

4.8 Tensorial Transport Subproblem

Dropping the subscript for simplicity, the tensorial transport problem (4.29a)–(4.29b) writes:

(P): find $\boldsymbol{\tau}$, defined in Ω, such that

$$\begin{cases} \boldsymbol{u}.\nabla\boldsymbol{\tau} + \beta_a(\nabla\boldsymbol{u}, \boldsymbol{\tau}) + \nu\boldsymbol{\tau} = \boldsymbol{\chi} \text{ in } \Omega \\ \qquad\qquad\qquad\qquad\quad \boldsymbol{\tau} = \boldsymbol{\tau}_\Gamma \text{ on } \partial\Omega_- \end{cases} \tag{4.30}$$

where $\nu = 1/((1-2\theta)\Delta t) > 0$, $\boldsymbol{u}$, $\boldsymbol{\chi}$ and $\boldsymbol{\tau}_\Gamma$ are given. This is a first order system of partial equations: as $\boldsymbol{\tau}$ is a 3×3 symmetric tensor, there are six equations and six unknowns. Its reduction to a two-dimensional geometries would reduce to three equations and three unknowns. This first order system of partial differential equations differs dramatically from the previous systems studied in this book, such as Stokes problems, that are second order systems of partial differential equations. For instance, the boundary conditions are imposed differently. For second order systems, they are imposed on the whole boundary $\partial\Omega$, e.g. Dirichlet or Neumann boundary conditions, while, for first order systems, they are imposed on the upstream boundary $\partial\Omega_-$. While it would seem unnatural to attempt a unified treatment, in 1968, Friedrichs [111], proposed such unification by introducing an abstract framework. This framework is fruitful, as it leads both to theoretical results about the existence of a solution and to variational formulations, that are required for the finite element discretization. Let us put our tensorial transport problem into the Friedrichs abstract framework. Suppose that $\boldsymbol{u} \in \left(C^1(\bar{\Omega})\right)^3$, $\boldsymbol{\chi} \in \left(L^2(\Omega)\right)_s^{3\times3}$ and $\boldsymbol{\tau}_\Gamma \in \left(L^2(\partial\Omega)\right)_s^{3\times3}$. We introduce the following notations:

$$A(\boldsymbol{\tau}) = (\boldsymbol{u}.\nabla)\boldsymbol{\tau} + \beta_a(\nabla\boldsymbol{u}, \boldsymbol{\tau}) + \nu\boldsymbol{\tau}, \ \forall\boldsymbol{\tau} \in \left(C^1(\bar{\Omega})\right)_s^{3\times3} \tag{4.31a}$$

$$B = \boldsymbol{u}.\boldsymbol{n} \tag{4.31b}$$

$$M = |\boldsymbol{u}.\boldsymbol{n}| \tag{4.31c}$$

With these notations, the tensorial transport problem (4.29a)–(4.29b) becomes:

(P): find $\boldsymbol{\tau} \in C^1(\bar{\Omega})_s^{3\times3}$ such that

$$\begin{cases} A\boldsymbol{\tau} = \boldsymbol{\chi} \text{ in } \Omega \\ (M-B)(\boldsymbol{\tau} - \boldsymbol{\tau}_\Gamma) = 0 \text{ on } \partial\Omega \end{cases} \tag{4.32}$$

Observe that $M - B$ is non-zero only on the upstream boundary condition and thus, this trick allows us to write a condition on the whole boundary. This is the strong formulation of the problem: it requires a strong assumption on the regularity of the solution $\boldsymbol{\tau}$: its continuous differentiability. This assumption will be relaxed later, in the context of a weak formulation, i.e. the variational formulation, which will accept less regular solutions, e.g. discontinuous ones. This is also consistent with the low regularity of the expected solution, which could be discontinuous, as observed for

the Poiseuille flow (see Sect. 4.4, p. 155). Let us study first the existence of a solution of the strong formulation. This study starts with two preliminary lemmas.

Lemma 4.2 (tensor derivative terms)
For all $\boldsymbol{\tau}, \boldsymbol{\gamma} \in \mathbb{R}^{3\times 3}$ *we have*

$$\beta_a(\nabla \boldsymbol{u}, \boldsymbol{\tau}) : \boldsymbol{\gamma} = -\boldsymbol{\tau} : \beta_{-a}(\nabla \boldsymbol{u}, \boldsymbol{\gamma})$$

Proof From the definition (4.15) of the bilinear form $\beta_a(.,.)$:

$$\begin{aligned} \beta_a(\nabla \boldsymbol{u}, \boldsymbol{\tau}) &= \quad \boldsymbol{\tau}\, W(\boldsymbol{u}) - W(\boldsymbol{u})\, \boldsymbol{\tau} - a\,(\boldsymbol{\tau}\, D(\boldsymbol{u}) + D(\boldsymbol{u})\, \boldsymbol{\tau}) \\ -\beta_{-a}(\nabla \boldsymbol{u}, \boldsymbol{\gamma}) &= -\boldsymbol{\gamma}\, W(\boldsymbol{u}) + W(\boldsymbol{u})\, \boldsymbol{\gamma} - a\,(\boldsymbol{\gamma}\, D(\boldsymbol{u}) + D(\boldsymbol{u})\, \boldsymbol{\gamma}) \end{aligned}$$

Since $W(\boldsymbol{u})$ is anti-symmetric:

$$\begin{aligned} (\boldsymbol{\tau} W(\boldsymbol{u}) - W(\boldsymbol{u})\boldsymbol{\tau}) : \boldsymbol{\gamma} &= \sum_{i,j,k=1}^{d} \tau_{ik} W_{kj}(\boldsymbol{u})\, \gamma_{ij} - \sum_{i,j,k=1}^{d} W_{ik}(\boldsymbol{u}) \tau_{kj}\, \gamma_{ij} \\ &= -\sum_{i,j,k=1}^{d} \tau_{ik}\, \gamma_{ij} W_{jk}(\boldsymbol{u}) + \sum_{i,j,k=1}^{d} \tau_{kj}\, W_{ki}(\boldsymbol{u}) \gamma_{ij} \\ &= \boldsymbol{\tau} : (-\boldsymbol{\gamma}\, W(\boldsymbol{u}) + W(\boldsymbol{u})\, \boldsymbol{\gamma}) \end{aligned}$$

Since $D(\boldsymbol{u})$ is symmetric:

$$(\boldsymbol{\tau}\, D(\boldsymbol{u}) + D(\boldsymbol{u})\, \boldsymbol{\tau}) : \boldsymbol{\gamma} = \boldsymbol{\tau} : (\boldsymbol{\gamma}\, D(\boldsymbol{u}) + D(\boldsymbol{u})\, \boldsymbol{\gamma})$$

Summing these two last equations leads to the result. □

Definition 4.3 (*formal adjoint*)
The formal adjoint of A is denoted A^* and is defined, for all $\boldsymbol{\tau} \in \left(C^1(\bar{\Omega})\right)_s^{3\times 3}$ by

$$A^*(\boldsymbol{\tau}) = -(\boldsymbol{u}.\nabla)\boldsymbol{\tau} - \beta_{-a}(\nabla \boldsymbol{u}, \boldsymbol{\tau}) + (\nu - \operatorname{div} \boldsymbol{u})\boldsymbol{\tau} \tag{4.33}$$

The formal adjoint interprets as the generalization of the transpose of a matrix: instead of a finite dimension space, it acts in an infinite dimensional functional space. The main motivation for defining the formal adjoint is the following integration by part property.

Lemma 4.3 (integration by part for A)
For all $\boldsymbol{\tau}, \boldsymbol{\gamma} \in C^1(\bar{\Omega})_s^{3\times 3}$, *the operator* A *and its formal adjoint* A^* *satisfy the following integration by part relation:*

$$\int_\Omega A(\boldsymbol{\tau}) : \boldsymbol{\gamma}\, \mathrm{d}x = \int_\Omega \boldsymbol{\tau} : A^*(\boldsymbol{\gamma})\, \mathrm{d}x + \int_{\partial\Omega} (\boldsymbol{\tau} : \boldsymbol{\gamma})\, \boldsymbol{u}.\boldsymbol{n}\, \mathrm{d}s$$

Proof An integration by part of the transport operator yields:

$$\int_\Omega (\boldsymbol{u}.\nabla\boldsymbol{\tau}):\boldsymbol{\gamma}\,\mathrm{d}x = -\int_\Omega \boldsymbol{\tau}:(\boldsymbol{u}.\nabla\boldsymbol{\gamma})\,\mathrm{d}x - \int_\Omega (\boldsymbol{\tau}:\boldsymbol{\gamma})\,\mathrm{div}\,\boldsymbol{u}\,\mathrm{d}x + \int_{\partial\Omega} (\boldsymbol{\tau}:\boldsymbol{\gamma})\,\boldsymbol{u}.\boldsymbol{n}\,\mathrm{d}s$$

Then, the result is obtained from the definition (4.31a) of A, the definition (4.33) of A^* and Lemma 4.2. □

Definition 4.4 (*symmetric part of an operator*)
The symmetric part of an operator A is defined by

$$A_s = \frac{A + A^*}{2}$$

Expanding the definition (4.31a) of A and the definition (4.33) of A^* leads to

$$\begin{aligned} A_s(\boldsymbol{\tau}) &= \left(\nu - \frac{1}{2}\mathrm{div}\,\boldsymbol{u}\right)\boldsymbol{\tau} + \frac{1}{2}\left(\beta_a(\nabla\boldsymbol{u},\boldsymbol{\tau}) - \beta_{-a}(\nabla\boldsymbol{u},\boldsymbol{\tau})\right) \\ &= \left(\nu - \frac{1}{2}\mathrm{div}\,\boldsymbol{u}\right)\boldsymbol{\tau} - a\left(\boldsymbol{\tau}\,D(\boldsymbol{u}) + D(\boldsymbol{u})\,\boldsymbol{\tau}\right) \end{aligned} \tag{4.34}$$

Definition 4.5 (*Friedrichs positive operator*)
An operator A is *Friedrichs positive* if and only if there exists a constant $a_0 > 0$ such that

$$\int_\Omega A_s(\boldsymbol{\tau}):\boldsymbol{\tau}\,\mathrm{d}x \geqslant a_0\|\boldsymbol{\tau}\|_{L^2(\Omega)},\ \forall\boldsymbol{\tau} \in \left(L^2(\Omega)\right)_s^{3\times 3}$$

The Friedrichs positivity could be interpreted as a variant of the coercivity for the symmetric part of the operator. The motivation of this definition of the positivity is the following result, proved in 1958 by Friedrichs [111]:

Theorem 4.7 (existence of a solution to the strong abstract formulation)
Suppose that the operator A is Friedrichs positive. Then the strong formulation (4.32) *of the problem admits a solution that is continuously differentiable.*

Corollary 4.2 (existence of a solution to the strong formulation)
Assume $\boldsymbol{u} \in \left(C^1(\bar{\Omega})\right)^3$. *Then, there exists* $\Delta t_c > 0$, *depending upon* $\theta \in]0, 1/2[$ *and* $\boldsymbol{u}$ *such that when* $\Delta t < \Delta t_c$, *the tensorial transport problem* (4.30) *admits a solution in* $\boldsymbol{\tau} \in \left(C^1(\bar{\Omega})\right)_s^{3\times 3}$.

Proof It remains to check that the assumption of Theorem 4.7, i.e. the positivity of A, is satisfied. From the expression (4.34) of the symmetric part of A, we have

$$\begin{aligned} \int_\Omega A_s(\boldsymbol{\tau}):\boldsymbol{\tau}\,\mathrm{d}x &\geqslant (2\nu - \|\mathrm{div}\,\boldsymbol{u}\|_{L^\infty})\,\|\boldsymbol{\tau}\|_{L^2}^2 - 2|a|\|D(\boldsymbol{u})\|_{L^\infty}\|\boldsymbol{\tau}\|_{L^2}^2 \\ &= (2\nu - \|\mathrm{div}\,\boldsymbol{u}\|_{L^\infty} - 2|a|\|D(\boldsymbol{u})\|_{L^\infty})\,\|\boldsymbol{\tau}\|_{L^2}^2 \end{aligned}$$

A sufficient condition for A_s to be Friedrichs positive is

$$2\nu - \|\mathrm{div}\,\boldsymbol{u}\|_{0,\infty,\Omega} - 2|a|\ \|D(\boldsymbol{u})\|_{0,\infty,\Omega} > 0$$

Recall that $\nu = 1/((1-2\theta)\Delta t)$. Then, this condition expresses in terms of Δt as

$$\Delta t \ < \ \Delta t_c = \frac{2}{(1-2\theta)\ (\|\mathrm{div}\,\boldsymbol{u}\|_{0,\infty,\Omega} + 2|a|\ \|2D(\boldsymbol{u})\|_{0,\infty,\Omega})} \tag{4.35}$$

□

Remark 4.4 (Jaumann derivative)
Note that when $\mathrm{div}\,\boldsymbol{u} = 0$ and $a = 0$ i.e. the Jaumann derivative, then from (4.35) we get $\Delta t_c = +\infty$. In that case, the strong formulation of the tensorial transport problem always admits a solution.

Note also that the previous result do not permit to prove the *uniqueness* of the solution: we only have its *existence*. Also, a variational formulation is required for the finite element approximation of the solution. These two points are the subject of the next section.

4.9 Variational Formulation

Friedrichs theory on first order systems do not use the concept of variational formulation. This development was performed later, in 2006, by Ern and Guermond in a series of papers [88, 89, 93] also regrouped in a book published in 2012 by di Pietro and Ern [240] in the context of discontinuous Galerkin methods. Let us consider the following functional space:

$$H = \left\{\boldsymbol{\tau} \in \left(L^2(\Omega)\right)_s^{3\times 3};\ \ A(\boldsymbol{\tau}) \in \left(L^2(\Omega)\right)_s^{3\times 3}\right\}$$

This space is equipped with a scalar product, defined for all $\boldsymbol{\tau}, \boldsymbol{\gamma} \in H$ by

$$(\boldsymbol{\tau}, \boldsymbol{\gamma})_H = \int_\Omega \boldsymbol{\tau} : \boldsymbol{\gamma}\, \mathrm{d}x + \int_\Omega A(\boldsymbol{\tau}) : A(\boldsymbol{\gamma})\, \mathrm{d}x$$

Equipped with this scalar product, the space H is an Hilbert space [90]. Next, we introduce the following forms

$$\begin{aligned} a(\boldsymbol{\tau}, \boldsymbol{\gamma}) &= \int_\Omega A(\boldsymbol{\tau}) : \boldsymbol{\gamma}\, \mathrm{d}x + \frac{1}{2}\int_{\partial\Omega} (M-B)\boldsymbol{\tau} : \boldsymbol{\gamma}\, \mathrm{d}x \\ \ell(\boldsymbol{\gamma}) &= \int_\Omega \boldsymbol{\chi} : \boldsymbol{\gamma}\, \mathrm{d}x + \frac{1}{2}\int_{\partial\Omega} (M-B)\boldsymbol{\tau}_\Gamma : \boldsymbol{\gamma}\, \mathrm{d}x \end{aligned}$$

Definition 4.6 (*weak solution*)
An element $\boldsymbol{\tau} \in H$ is a *weak* solution of problem (4.32) if and only if

$$a(\boldsymbol{\tau}, \boldsymbol{\gamma}) = \ell(\boldsymbol{\gamma}), \quad \forall \boldsymbol{\gamma} \in H \tag{4.36}$$

The variational formulation (4.36) requires less regularity (4.32) for the solution than the strong formulation: it assume $\boldsymbol{\tau} \in H$ instead of $\boldsymbol{\tau} \in \left(C^1(\bar{\Omega})\right)_s^{3\times 3}$. Note also that, while the boundary conditions was strongly imposed in (4.32), they are here only weakly imposed here, i.e. in a distributional sense that will be clarified later. The following lemma links the concept of Friedrichs positivity of the operator A to a concept of weak coercivity for the bilinear form $a(.,.)$.

Lemma 4.4 (positivity and coercivity)
Assume A is Friedrichs positive, with constant a_0. Then, the bilinear form $a(.,.)$ is coercive *in H for the semi-norm*

$$|\boldsymbol{\tau}|_M^2 = \int_\Omega \boldsymbol{\tau} : \boldsymbol{\tau} \, \mathrm{d}x + \int_{\partial\Omega} M(\boldsymbol{\tau}) : \boldsymbol{\tau} \, \mathrm{d}x$$

i.e. there exists a constant $\alpha_0 > 0$ such that

$$a(\boldsymbol{\tau}, \boldsymbol{\tau}) \geqslant \alpha_0 |\boldsymbol{\tau}|_M^2, \ \forall \boldsymbol{\tau} \in H$$

Proof Recall Lemma 4.3. The integration by parts extends to functions in H as:

$$\begin{aligned}
&\int_\Omega A(\boldsymbol{\tau}) : \boldsymbol{\gamma} \, \mathrm{d}x = \int_\Omega \boldsymbol{\tau} : A^*(\boldsymbol{\gamma}) \, \mathrm{d}x + \int_{\partial\Omega} (\boldsymbol{\tau} : \boldsymbol{\gamma}) \, \boldsymbol{u}.\boldsymbol{n} \, \mathrm{d}s, \quad \forall \boldsymbol{\tau}, \boldsymbol{\gamma} \in H \\
\Longrightarrow &\int_\Omega A(\boldsymbol{\tau}) : \boldsymbol{\tau} \, \mathrm{d}x = \int_\Omega \boldsymbol{\tau} : A^*(\boldsymbol{\tau}) \, \mathrm{d}x + \int_{\partial\Omega} (\boldsymbol{\tau} : \boldsymbol{\tau}) \, \boldsymbol{u}.\boldsymbol{n} \, \mathrm{d}s, \quad \forall \boldsymbol{\tau} \in H \\
\Longleftrightarrow &\int_\Omega \left(\frac{A - A^*}{2}\right)(\boldsymbol{\tau}) : \boldsymbol{\tau} \, \mathrm{d}x = \int_{\partial\Omega} B(\boldsymbol{\tau}) : \boldsymbol{\tau}) \, \mathrm{d}s
\end{aligned}$$

Then

$$\begin{aligned}
a(\boldsymbol{\tau}, \boldsymbol{\tau}) &= \int_\Omega A(\boldsymbol{\tau}) : \boldsymbol{\tau} \, \mathrm{d}x + \int_{\partial\Omega} \left(\frac{M - B}{2}\right) \boldsymbol{\tau} : \boldsymbol{\gamma} \, \mathrm{d}x \\
&= \int_\Omega \left(\frac{A + A^*}{2}\right)(\boldsymbol{\tau}) : \boldsymbol{\tau} \, \mathrm{d}x + \int_\Omega \left(\frac{A - A^*}{2}\right)(\boldsymbol{\tau}) : \boldsymbol{\tau} \, \mathrm{d}x \\
&\quad + \int_{\partial\Omega} \left(\frac{M - B}{2}\right) \boldsymbol{\tau} : \boldsymbol{\gamma} \, \mathrm{d}x \\
&= \int_\Omega A_s(\boldsymbol{\tau}) : \boldsymbol{\tau} \, \mathrm{d}x + \frac{1}{2} \int_\Omega B(\boldsymbol{\tau}) : \boldsymbol{\tau} \, \mathrm{d}x + \int_{\partial\Omega} \left(\frac{M - B}{2}\right) \boldsymbol{\tau} : \boldsymbol{\gamma} \, \mathrm{d}x \\
&= \int_\Omega A_s(\boldsymbol{\tau}) : \boldsymbol{\tau} \, \mathrm{d}x + \frac{1}{2} \int_\Omega M(\boldsymbol{\tau}) : \boldsymbol{\tau} \, \mathrm{d}x
\end{aligned}$$

$$\geqslant a_0 \int_\Omega \boldsymbol{\tau} : \boldsymbol{\tau} \, \mathrm{d}x + \frac{1}{2} \int_{\partial\Omega} M(\boldsymbol{\tau}) : \boldsymbol{\tau} \, \mathrm{d}x \quad \text{from positivity}$$
$$\geqslant \min(a_0, 1/2) \, |\boldsymbol{\tau}|_M^2$$

The result follows with $\alpha_0 = \min(a_0, 1/2)$. □

The first interest of the variational formulation is the following result, proved in 2012 by di Pietro and Ern [240, p. 308].

Theorem 4.8 (existence and uniqueness for the abstract problem)
Assume that A is Friedrichs positive. Then, there exists a unique weak solution $\boldsymbol{\tau}$ and it satisfies

$$A\boldsymbol{\tau} = \boldsymbol{\chi} \ \text{ in } \ \left(L^2(\Omega)\right)_s^{3\times 3}$$
$$(M - B)(\boldsymbol{\tau} - \boldsymbol{\tau}_\Gamma) = 0 \ \text{ in } H'$$

where H' denotes the topological dual of H.

Corollary 4.3 (existence and uniqueness for the tensorial transport problem)
Assume $\boldsymbol{u} \in \left(C^1(\bar{\Omega})\right)^3$. Then, there exists $\Delta t_c > 0$ expressed by (4.35), such that when $\Delta t < \Delta t_c$, the weak formulation of the tensorial transport problem admits a unique solution $\boldsymbol{\tau} \in H$.

Remark 4.5 (*Jaumann derivative*)
Note that when $\operatorname{div} \boldsymbol{u} = 0$ and $a = 0$ i.e. the Jaumann derivative, then from (4.35) we get $\Delta t_c = +\infty$. In that case, the weak formulation of the tensorial transport problem always admits a unique solution.

With these last results, the step 2 of the θ-scheme algorithm is well-posed. As steps 1 and 3 involve a Stokes subproblem that is also well-posed, then the whole iteration of the θ-scheme algorithm is well-defined, assuming that Δt is small enough. As the analysis of the continuous transport subproblem is now complete, let us now turn in the next section to the discretization of the transport subproblem.

4.10 Discontinuous Galerkin Method

This section presents the discretization of the tensorial transport problem by using the discontinuous Galerkin method. The main interest of this method is to extend to the finite element context the principle of the upstream uncentered finite difference method, also called *upwind method*. Why upwinding is required is not obvious: in order to understand this requirement, a small one-dimensional example is first presented. Then, the concept is extended to the general finite element context with the discontinuous Galerkin method. Let us consider the following one-dimensional problem.

(P): find $\tau :]0, 1[\longrightarrow \mathbb{R}$ such that

$$\begin{cases} \dfrac{\mathrm{d}\tau}{\mathrm{d}x} + \varepsilon\tau = 0 \ \text{ in }]0, 1[\\ \tau(0) = 1 \end{cases}$$

where $\varepsilon > 0$. The exact solution is known: $\tau(x) = \exp(-\varepsilon x)$. For the discretization of this one-dimensional problem, let us consider a uniform subdivision of the $[0, 1]$ interval in $N \geqslant 1$ elements. The element length is $h = 1/N$ and the i-th element is denoted by $K_i = [ih, (i+1)h], 0 \leqslant i \leqslant N-1$. The finite element space $T_h \subset L^2(\Omega)$ of continuous and piecewise linear functions is defined by

$$T_h = \left\{\gamma_h \in C^0(\bar{\Omega});\ \gamma_{h|K_i} \in P_1,\ 0 \leqslant i \leqslant N-1\right\}$$

Note that $\dim(T_h) = N + 1$. Let $(\varphi_i)_{0\leqslant i\leqslant N}$ be the Lagrange nodal basis defined by

$$\begin{cases} \varphi_i \in T_h, & 0 \leqslant i \leqslant N \\ \varphi_i(jh) = \delta_{i,j}, & 0 \leqslant i, j \leqslant N \end{cases}$$

The Lagrange nodal basis is represented on Fig. 4.12. Any $\tau_h \in T_h$ can be decomposed on this basis: there exists $(\tau_j)_{1\leqslant j\leqslant N} \in \mathbb{R}^{N+1}$, the coefficients of τ_h on this basis, such that

$$\tau_h(x) = \sum_{j=0}^{N} \tau_j\, \varphi_j(x), \quad \forall x \in \Omega$$

and we have $\tau_j = \tau_h(jh)$, for all j, $0 \leqslant j \leqslant N$, i.e. the coefficients of τ_h in the Lagrange basis are the values at the nodes of the subdivision. The approximate problem writes:

$(P)_h$: find $\tau_h \in T_h$ such that

$$\begin{cases} \tau_h(0) = 1 \\ \displaystyle\int_0^1 \left(\frac{\mathrm{d}\tau_h}{\mathrm{d}x} + \varepsilon\tau_h\right) \gamma_h \,\mathrm{d}x = 0, \quad \forall \gamma_h \in T_h \end{cases}$$

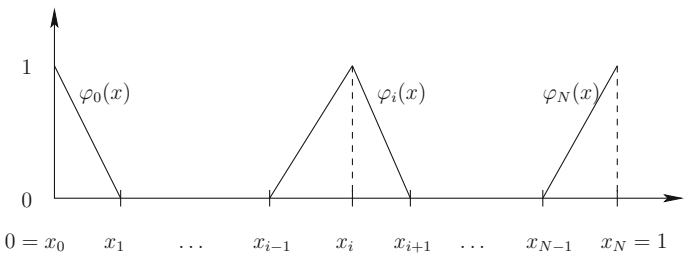

Fig. 4.12 The Lagrange nodal basis for the piecewise linear finite element method in one dimension

Using the decomposition of τ_h on the Lagrange basis and using as test function γ_h any φ_i, $1 \leqslant i \leqslant N$, we obtain the following finite dimensional linear system:

$(P)_h$: find $(\tau_i)_{0\leqslant i\leqslant N} \in \mathbb{R}^{N+1}$ such that

$$\left\{\begin{array}{r} \tau_0 = 1 \\ \displaystyle\sum_{j=0}^{N}\left(\int_0^1 (\varphi_j'(x)+\varepsilon\varphi_j(x))\varphi_i(x)\,\mathrm{d}x\right)\tau_j = 0,\ 1\leqslant i\leqslant N \end{array}\right.$$

$$\Longleftrightarrow \left\{\begin{array}{r} \tau_0 = 1 \\ \dfrac{\tau_{i+1}-\tau_{i-1}}{2h} + \dfrac{\varepsilon}{6}(\tau_{i+1}+4\tau_i+\tau_{i-1}) = 0,\ 1\leqslant i\leqslant N-1 \\ \dfrac{\tau_N-\tau_{N-1}}{h} + \dfrac{\varepsilon}{3}(2\tau_N+\tau_{N-1}) = 0 \end{array}\right.$$

This linear system involves a unsymmetric and tridiagonal matrix. Also, the finite element method appears as a *centered* second order finite difference scheme for the discretization of τ' as $\dfrac{\tau_{i+1}-\tau_{i-1}}{2h}$.

Figure 4.13 represents the solution for various mesh element sizes h. Observe that when h is not small enough, the solution presents some oscillations and takes negatives values while the exact solution is monotonically decreasing and always positive. This unsolicited behavior should be analyzed in depth. For convenience, let us introduce the notation $\mu = \varepsilon h/3$. The approximate problem becomes:

$(P)_h$: find $(\tau_i)_{0\leqslant i\leqslant N} \in \mathbb{R}^{N+1}$ such that

$$\left\{\begin{array}{r} \tau_0 = 1 \\ (\mu+1)\tau_{i+1} + 4\mu\,\tau_i + (\mu-1)\tau_{i-1} = 0,\ 1\leqslant i\leqslant N-1 \\ (2\mu+1)\tau_N + (\mu-1)\tau_{N-1} = 0 \end{array}\right.$$

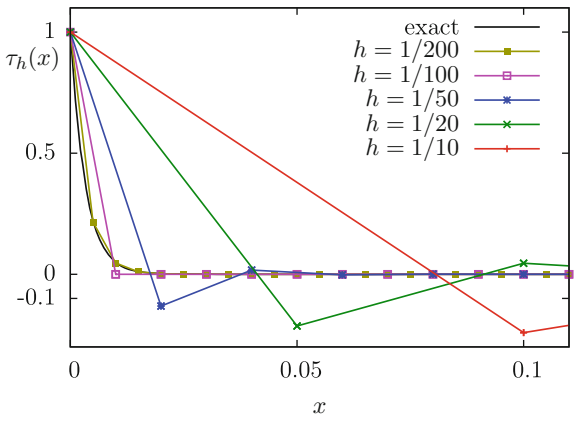

Fig. 4.13 The transport problem: approximation with the centered scheme of the one dimensional problem ($\varepsilon = 300$)

Let us search the solution using a double recurrence formula:

$$\tau_i = a{r_1}^i + b{r_2}^i, \quad 0 \leqslant i \leqslant N$$

The problem reduces to find $r_1, r_2, a, b \in \mathbb{R}^{N+1}$ such that

$$a + b = 0 \tag{4.37a}$$

$$\left((\mu+1){r_1}^2 + 4\mu r_1 + (\mu-1)\right) a r_1^{i-1} + \left((\mu+1){r_2}^2 + 4\mu r_2 + (\mu-1)\right) b r_2^{i-1} = 0, \ 1 \leqslant i \leqslant N-1 \tag{4.37b}$$

$$((2\mu+1)r_1 + (\mu-1))\, a r_1^{N-1} + ((2\mu+1)r_2 + (\mu-1))\, b r_2^{N-1} = 0 \tag{4.37c}$$

A necessary and sufficient condition is that r_1 and r_2 are the two roots of

$$(\mu+1)r^2 + 4\mu r + (\mu-1) = 0$$

Then, a,b are given by (4.37a)–(4.37c). Thus, we obtain an explicit expression for the approximate solution τ_h:

$$\tau_h(x) = \sum_{j=0}^{N} \tau_j \, \varphi_j(x), \quad \forall x \in \Omega$$

$$\tau_j = a r_1^j + b r_2^j, \quad 0 \leqslant j \leqslant N$$

where

$$r_1 = -2\mu + \sqrt{1 + 3\mu^2}$$

$$r_2 = -2\mu - \sqrt{1 + 3\mu^2}$$

Observe that $r_1 \in]0, 1[$ while $r_2 < 0$ and $\lim_{\mu \to +\infty} r_2 = -\infty$. Thus, the solution develops instabilities that could be important when $\mu = \epsilon h$ is not small enough. As h tends to zero, the solution will finish to converge and oscillations will decrease, but oscillations could appear for all fixed $h > 0$, depending on the value of ε. In conclusion, this discretization is not robust enough, and a better approach is known: the upwind method.

The upwind method is introduced with the following finite difference approximation of the one-dimensional transport problem:

$(P)_h$: find $\left(\tau_{i+\frac{1}{2}}\right)_{0 \leqslant i \leqslant N-1} \in \mathbb{R}^N$ such that

$$\begin{cases} \dfrac{\tau_{i+\frac{1}{2}} - \tau_{i-\frac{1}{2}}}{h} + \varepsilon \tau_{i+\frac{1}{2}} = 0, \quad 0 \leqslant i \leqslant N-1 \\ \tau_{-\frac{1}{2}} = 1 : \text{external trace} \end{cases}$$

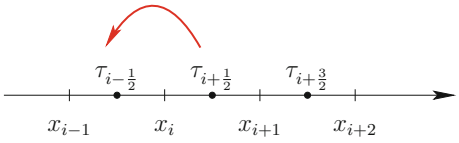

Fig. 4.14 The transport problem: upwind method

For convenience, the values of the function has been located at the center of the elements: the scheme is represented on Fig. 4.14. Observe the *left uncentered* first order finite difference scheme for the discretization of τ' as $\dfrac{\tau_{i+\frac{1}{2}} - \tau_{i-\frac{1}{2}}}{h}$. The boundary condition at $x = 0$ is weakly imposed via an external trace denoted as $\tau_{-\frac{1}{2}}$. The linear system is also triangular and unsymmetric. It writes also

$$\begin{cases} (1+\varepsilon h)\tau_{i+\frac{1}{2}} - \tau_{i-\frac{1}{2}} = 0, \quad 0 \leqslant i \leqslant N-1 \\ \tau_{-\frac{1}{2}} = 1 \end{cases}$$

The approximate solution admits an explicit expression:

$$\tau_{i+\frac{1}{2}} = \left(\frac{1}{1+\varepsilon h}\right)^{i+1}, \quad 0 \leqslant i \leqslant N-1$$

This approximate solution is always positive and monotonically decreasing: there is no more oscillations. Figure 4.15 plots this solution for various mesh sizes.

Let us turn now to an extension of the transport problem with a velocity. Consider one dimensional constant velocity u: we could either have $u < 0$ or $u > 0$. The extended problem writes:

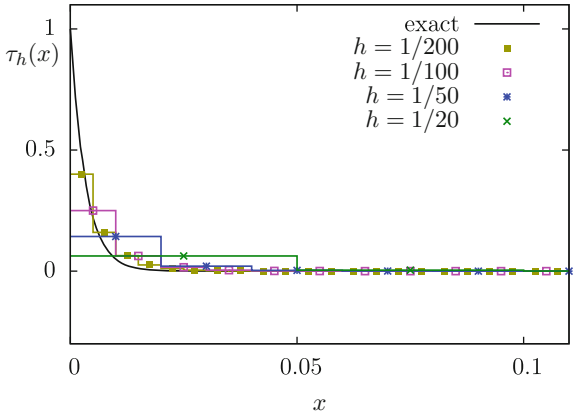

Fig. 4.15 The transport problem: approximation with the upwind method of the one dimensional problem ($\varepsilon = 300$)

(P): find τ defined in $]0,1[$ such that

$$\begin{cases} u\dfrac{\mathrm{d}\tau}{\mathrm{d}x} + \nu\tau = 0 \ \text{ in }]0,1[\\ \qquad \tau(0) = \tau_\Gamma \ \text{ when } u \geqslant 0 \\ \qquad \tau(1) = \tau_\Gamma \ \text{ when } u < 0 \end{cases}$$

where $\nu > 0$ is constant. Note that the upstream boundary moves from $x = 0$ when $u \geqslant 0$ to $x = 1$ when $u < 0$. The upwind discretization of this problem is given by:

$(P)_h$: find $\left(\tau_{i+\frac{1}{2}}\right)_{0\leqslant i\leqslant N-1} \in \mathbb{R}^N$ such that

$$\begin{cases} u\left(\dfrac{\tau_{i+\frac{1}{2}} - \tau_{i-\frac{1}{2}}}{h}\right) + \nu\tau_{i+\frac{1}{2}} = 0 \quad \text{when } u \geqslant 0 \\ \\ u\left(\dfrac{\tau_{i+\frac{3}{2}} - \tau_{i+\frac{1}{2}}}{h}\right) + \nu\tau_{i+\frac{1}{2}} = 0 \quad \text{when } u < 0 \\ \qquad\qquad\qquad\qquad\qquad\qquad 0 \leqslant i \leqslant N-1 \\ \qquad\qquad\qquad\qquad \tau_{-\frac{1}{2}} = \tau_\Gamma \quad \text{when } u \geqslant 0 \\ \\ \qquad\qquad\qquad\qquad \tau_{N+\frac{1}{2}} = \tau_\Gamma \quad \text{when } u < 0 \end{cases}$$

When $u \geqslant 0$, the scheme is *left uncentered*, i.e. the derivative τ' is discretized by $\dfrac{\tau_{i+\frac{1}{2}} - \tau_{i-\frac{1}{2}}}{h}$. Conversely, when $u < 0$, the scheme is *right uncentered*, i.e. the derivative τ' is discretized by $\dfrac{\tau_{i+\frac{3}{2}} - \tau_{i+\frac{1}{2}}}{h}$. Note that the boundary condition is weakly imposed via the external traces denoted as $\tau_{-\frac{1}{2}}$ and $\tau_{N+\frac{1}{2}}$. By using an absolute value, this discretization could be written equivalently in a more compact way:

(P): find $\left(\tau_{i+\frac{1}{2}}\right)_{0\leqslant i\leqslant N-1} \in \mathbb{R}^N$ such that

$$\begin{cases} \dfrac{|u|+u}{2}\left(\dfrac{\tau_{i+\frac{1}{2}} - \tau_{i-\frac{1}{2}}}{h}\right) \\ +\dfrac{|u|-u}{2}\left(\dfrac{\tau_{i+\frac{1}{2}} - \tau_{i+\frac{3}{2}}}{h}\right) + \nu\tau_{i+\frac{1}{2}} \qquad\qquad = 0, \quad 0 \leqslant i \leqslant N-1 \\ \dfrac{|u|+u}{2}\left(\tau_{-\frac{1}{2}} - \tau_\Gamma\right) + \dfrac{|u|-u}{2}\left(\tau_{N+\frac{1}{2}} - \tau_\Gamma\right) = 0 \end{cases}$$

This last expression extends from one-dimensional to multi-dimensional problems and also to high order polynomial approximations in the context of discontinuous Galerkin methods. This is not the only possible extension to the multi-dimensional case. Observe the following equivalent way to rewrite the previous discrete one-dimensional problem:

$$\left\{\begin{array}{l} \dfrac{|u|h}{2}\left(\dfrac{-\tau_{i+\frac{3}{2}}+2\tau_{i+\frac{1}{2}}-\tau_{i-\frac{1}{2}}}{h^2}\right) \\ \qquad +u\left(\dfrac{\tau_{i+\frac{3}{2}}-\tau_{i-\frac{1}{2}}}{2h}\right)+\nu\tau_{i+\frac{1}{2}} \qquad\qquad =0, \quad 0\leqslant i\leqslant N-1 \\ \dfrac{|u|+u}{2}\left(\tau_{-\frac{1}{2}}-\tau_\Gamma\right)+\dfrac{|u|-u}{2}\left(\tau_{N+\frac{1}{2}}-\tau_\Gamma\right)=0 \end{array}\right.$$

Note that the centered approximation $\dfrac{\tau_{i+\frac{3}{2}}-\tau_{i-\frac{1}{2}}}{2h}$ of the τ' derivative is back while there is a new term, that represents the discretization of a second order term τ'' multiplied by a factor $\dfrac{|u|h}{2}$. By an analogy with the heat equation, with both diffusion and convection terms, this factor appears as a *numerical diffusion* coefficient while the convection is played by the transport term. Thus, the discrete upwind method could also be obtained by a standard centered scheme, or a standard finite element approximation, of the following problem:

(Q): find τ defined in $]0,1[$ such that

$$\left\{\begin{array}{l} \dfrac{|u|h}{2}\tau''+u\dfrac{\mathrm{d}\tau}{\mathrm{d}x}+\nu\tau=0 \ \text{ in }]0,1[\\ \qquad\qquad\qquad\qquad \tau(0)=\tau_\Gamma \ \text{ when } u\geqslant 0 \\ \qquad\qquad\qquad\qquad \tau(1)=\tau_\Gamma \ \text{ when } u<0 \end{array}\right.$$

This approach, that adds to the initial problem an additional numerical diffusion terms that tends to zero with the mesh size h, extends naturally to multi-dimensional problems. The streamline upwind Petrov-Galerkin method [39] (SUPG) is certainly the most popular of the many possible extensions in this direction. Nevertheless, this approach presents also some drawbacks: it was found efficient for convection-dominated problems but, for pure transport problems and multi-dimensional problems, the solution still oscillates. In that case, the discontinuous Galerkin method was found to be superior. Moreover, in view of our applications based on discontinuous approximation of the stress tensor (see Sect. 4.7, p. 171), the discontinuous Galerkin method is a natural candidate. Let us consider the extension to the multi-dimensional case of the discontinuous Galerkin approach.

Let $\mathcal{T}_h$ be a finite element mesh of the tri-dimensional flow domain Ω. For any $k\geqslant 0$, we introduce the following piecewise k-order polynomial space:

$$T_h=\{\boldsymbol{\gamma}_h\in\left(L^2(\Omega)\right)_s^{3\times 3};\ \boldsymbol{\gamma}_{h|K}\in(P_k)_s^{3\times 3},\ \forall K\in\mathcal{T}_h\}$$

Note that functions of T_h are able to jump across inter-element boundaries. For instance, when $k=0$, the space T_h contains piecewise constant functions over the mesh.

Definition 4.7 (*external trace*)
Let $\boldsymbol{\tau}_h\in T_h$. For any element $K\in\mathcal{T}_h$, we denotes by $\boldsymbol{\tau}_{\text{ext}}$, and called the *external trace* of $\boldsymbol{\tau}_h\in T_h$ in K, the function defined on any face $\subset\partial K$ by the following rules:

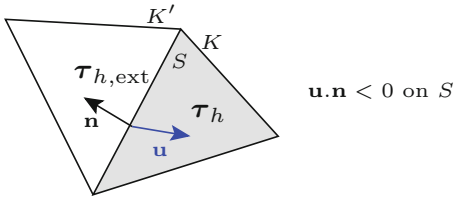

Fig. 4.16 Discontinuous Galerkin method: the external trace of a piecewise discontinuous function on an internal face of the mesh

- when $S \subset \partial\Omega$ is a boundary face, then $\boldsymbol{\tau}_{\text{ext}}$ is equal to $\boldsymbol{\tau}_{\Gamma,h}$, the Lagrange interpolation of the boundary condition $\boldsymbol{\tau}_\Gamma$.
- when S is an internal face, let $K' \in \mathcal{T}_h$ be the neighbor element, such that $S = \partial K \cap \partial K'$. Then, $\boldsymbol{\tau}_{\text{ext}}$ is the trace on S of the restriction $\boldsymbol{\tau}_h$ to K'.

Figure 4.16 represents the external trace of a piecewise polynomial function on an internal face. With this definition, the approximate tensorial transport problem writes:

$(P)_h$: find $\boldsymbol{\tau}_h \in T_h$ such that

$$\sum_{K\in\mathcal{T}_h}\left(\int_K (A(\boldsymbol{\tau}_h)-\boldsymbol{\chi}):\boldsymbol{\gamma}_h\,\mathrm{d}x + \sum_{S\subset\partial K}\int_S \left(\frac{|\boldsymbol{u}.\boldsymbol{n}|-\boldsymbol{u}.\boldsymbol{n}}{2}\right)(\boldsymbol{\tau}_h-\boldsymbol{\tau}_{h,ext}):\boldsymbol{\gamma}_h\,\mathrm{d}s\right)=0$$

for all $\boldsymbol{\gamma}_h \in T_h$. As the function $\boldsymbol{\tau}_h \in T_h$ is piecewise discontinuous, is derivative is not defined in all Ω. As the A operator, defined in (4.31a), involves derivatives, $A(\boldsymbol{\tau}_h)$ is also undefined on Ω. Nevertheless, the restriction to any element K of $\boldsymbol{\tau}_h$ is a polynomial function, which is differentiable. Then $A(\boldsymbol{\tau}_h)$ is defined inside any element K and the first term in the sum over $K \in \mathcal{T}$ is well defined. The second term in the sum corresponds to the upwind method and the weak imposition of the boundary condition. For any element K, $\boldsymbol{n}$ denotes the outer unit normal to K on ∂K. When $S \subset \partial K$ is a boundary face, i.e. $S \subset \partial\Omega$, then $\boldsymbol{n}$ coincides with the usual outer unit normal to Ω on $\partial\Omega$. When $\boldsymbol{u}.\boldsymbol{n} \geqslant 0$, this second term vanishes. Otherwise, when $\boldsymbol{u}.\boldsymbol{n} < 0$, it corresponds to the *upwind* method: the *wind*, i.e. the flow or the stream, goes inside the element, and the derivative are evaluated by taking into account the value of $\boldsymbol{\tau}_h$ in the neighbor element (see Fig. 4.16).

Note that, in this second term, any internal face S between to neighbor elements K_1 and K_2 will be counted two times: when the first sum over all elements K of the mesh reaches K_1, the side S is counted a first time, and next, when this sum reaches K_2, a second time. Note also that only one of the two counted terms is non-zero. For instance, if the flow goes from K_2 to K_1, then, the term over K_1 is non-zero while the term over K_2 is zero. This result is due to the change of sign of the outer normal when changing of neighbor element. Let us denote $\boldsymbol{n}_1$ (resp. $\boldsymbol{n}_2$) the outer unit normal on ∂K_1 (resp. ∂K_2) as represented on Fig. 4.17. Then $\boldsymbol{n}_1 = -\boldsymbol{n}_2$. For any internal face S of the mesh, we can choose arbitrarily its orientation and its corresponding normal vector, denoted as $\boldsymbol{n}$. In the case of the face S shared by the two elements K_1 and K_2, we arbitrarily choose the orientation of S such that $\boldsymbol{n} = \boldsymbol{n}_1 = -\boldsymbol{n}_2$. We denote by $\boldsymbol{\tau}_1$ (resp. $\boldsymbol{\tau}_2$) the restriction of $\boldsymbol{\tau}_h \in T_h$ to the element K_1 (resp. K_2) and

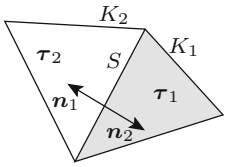

Fig. 4.17 Discontinuous Galerkin method: two neighbor elements and their opposite normals

do the same for the test function $\boldsymbol{\gamma}_h \in T_h$. The two terms involved by the internal face S can be rewritten as

$$\begin{aligned}
&\int_{S\cap\partial K_1} \left(\frac{|\boldsymbol{u}.\boldsymbol{n}_1|-\boldsymbol{u}.\boldsymbol{n}_1}{2}\right)(\boldsymbol{\tau}_1-\boldsymbol{\tau}_2)\,\boldsymbol{\gamma}_1\,\mathrm{d}s \\
&+\int_{S\cap\partial K_2} \left(\frac{|\boldsymbol{u}.\boldsymbol{n}_2|-\boldsymbol{u}.\boldsymbol{n}_2}{2}\right)(\boldsymbol{\tau}_2-\boldsymbol{\tau}_1)\,\boldsymbol{\gamma}_2\,\mathrm{d}s \\
&= \int_S \left(\frac{|\boldsymbol{u}.\boldsymbol{n}|}{2}(\boldsymbol{\tau}_1-\boldsymbol{\tau}_2):(\boldsymbol{\gamma}_1-\boldsymbol{\gamma}_2) - (\boldsymbol{u}.\boldsymbol{n})(\boldsymbol{\tau}_1-\boldsymbol{\tau}_2):\left(\frac{\boldsymbol{\gamma}_1+\boldsymbol{\gamma}_2}{2}\right)\right)\mathrm{d}s \\
&= \int_S [\![\boldsymbol{\tau}]\!]:\left(\frac{|\boldsymbol{u}.\boldsymbol{n}|}{2}[\![\boldsymbol{\gamma}]\!] - (\boldsymbol{u}.\boldsymbol{n})\{\boldsymbol{\gamma}\}\right)\mathrm{d}s
\end{aligned}$$

In the previous expression, some convenient notations has been introduced. These notations are standard in the context of the discontinuous Galerkin method. Here, $[\![\boldsymbol{\tau}]\!] = \boldsymbol{\tau}_1 - \boldsymbol{\tau}_2$ denotes the *jump* of $\boldsymbol{\tau}$ across the face and $\{\boldsymbol{\tau}\} = (\boldsymbol{\tau}_1+\boldsymbol{\tau}_2)/2$ denotes its *average*. Let us introduce the following forms, defined for all $\boldsymbol{\tau}, \boldsymbol{\gamma} \in T_h$ by

$$\begin{aligned}
a_h(\boldsymbol{\tau},\boldsymbol{\gamma}) = &\sum_{K\in\mathcal{T}_h}\int_K A(\boldsymbol{\tau}):\boldsymbol{\gamma}\,\mathrm{d}x + \frac{1}{2}\int_{\partial\Omega}(M-B)\boldsymbol{\tau}:\boldsymbol{\gamma}\,\mathrm{d}s \\
&+\sum_{S\in\mathscr{S}_h^{(i)}}\int_S [\![\boldsymbol{\tau}]\!]:\left(\frac{M}{2}[\![\boldsymbol{\gamma}]\!] + B\{\boldsymbol{\gamma}\}\right)\mathrm{d}s \\
\ell(\boldsymbol{\gamma}) = &\int_\Omega \boldsymbol{\chi}:\boldsymbol{\gamma}\,\mathrm{d}x + \frac{1}{2}\int_{\partial\Omega}(M-B)\boldsymbol{\tau}_\Gamma:\boldsymbol{\gamma}\,\mathrm{d}x
\end{aligned}$$

where $\mathscr{S}_h^{(i)}$ denotes the set of internal faces of the mesh $\mathcal{T}_h$. The sum over internal faces in the definition of $a_h(.,.)$ correspond to the upwind method. The boundary faces has been grouped in a boundary term and the boundary data $\boldsymbol{\tau}_\Gamma$ has been transfered to the right-hand-side, in the form $\ell(.)$, together with the data $\boldsymbol{\chi}$. With these definitions and notations, the approximate tensorial transport problem can be rewritten as:

$(P)_h$: find $\boldsymbol{\tau}_h \in T_h$ such that

$$a_h(\boldsymbol{\tau}_h,\boldsymbol{\gamma}_h) = \ell(\boldsymbol{\gamma}_h), \quad \forall \boldsymbol{\gamma}_h \in T_h \tag{4.38}$$

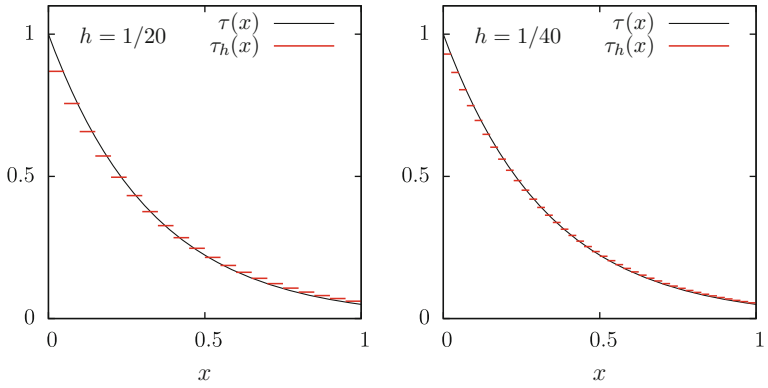

Fig. 4.18 The transport problem: approximation with the discontinuous Galerkin method of the one dimensional problem with $k = 0$ (from [285])

This is the classical formulation of the discontinuous Galerkin formulation. See [285, 286] for the practical implementation of this method in the `Rheolef` library. The solution of the previous one-dimensional transport is represented on Fig. 4.18 when using the discontinuous Galerkin method with $k = 0$, i.e. with piecewise constant approximations. Note the weak imposition of the boundary condition at $x = 0$: the value in the first element converges with mesh refinement to the imposed value at $x = 0$.

The theoretical error bound of this method for a scalar transport equation has been performed in 1986 by Johnson and Pitkäranta [156].

Theorem 4.9 (error bound for the discontinuous Galerkin method)
Let $\boldsymbol{\tau} \in H$ be the solution of the weak formulation (4.36) and $\boldsymbol{\tau}_h \in T_h$ be the solution of the discrete problem (4.38). Then, there exists a constant $C > 0$ such that

$$\|\boldsymbol{\tau} - \boldsymbol{\tau}_h\|_{L^2(\Omega)} \leqslant C h^{k+\frac{1}{2}}$$

Note that this error bound is not optimal, as the interpolation error in L^2 norm is $\mathcal{O}\left(h^{k+\frac{1}{2}}\right)$ when using k-th order polynomials. In 1988, Richter [260] showed that there possible, with some specially shaped mesh families, to obtain $\mathcal{O}(h^2)$ for P_1 discontinuous piecewise affine functions, and this result is then optimal. Peterson [236] showed that, when $k = 1$, the estimation $\mathcal{O}(h^{3/2})$ is sharp for a general family of quasi-uniform meshes. In 2010, the Richter's result has been extended by Cockburn et al. [61], Note also that the error estimate was extended in 1992 to the whole stationary viscoelastic flow problem by Baranger and Sandri [9]. The next section presents a practical flow computation of viscoelastic flow problem.

4.11 Example: Flow in an Abrupt Contraction

The flow in an abrupt contraction is represented in Fig. 4.19. We distinguish the planar abrupt contraction and the axisymmetric one. These geometries have practical applications in polymer processing and are also standard benchmarks for numerical computations. For an axisymmetric contraction, the Weissenberg number is defined as $We = 4\lambda U/L$ where U is the downstream average velocity, L the radius of the downstream pipe and λ is the relaxation time, obtained by a direct measurement. Note the 4 factor in the definition of the Weissenberg number: this factor is present for compatibility with the definition used in 1986 by Boger et al. [29]. An additional parameter is the contraction ratio $\beta = L_{\text{up}}/L$ where L_{up} denotes the ratio of the upstream pipe. In 1986, Boger et al. [29] published an experimentation of a polymer solution flowing in a abrupt contraction with a contraction ratio $\beta = 4$. These results are reproduced on Fig. 4.20. Observe the dramatic development of the recirculation zone as We increases. The numerical computations presented in on Fig. 4.21 was performed in 1994 by Saramito [279, 288] with a modified variant of the generalized Oldroyd model called the linear Phan-Thien and Tanner model [238]: in problem (4.14a)–(4.14g), the first Eq. (4.14a) is replaced by

$$\lambda\left(\frac{\partial\boldsymbol{\tau}}{\partial t}+(\boldsymbol{u}.\nabla)\boldsymbol{\tau}+\beta_a(\nabla\boldsymbol{u},\boldsymbol{\tau})\right)+\left(1+\frac{\xi\lambda}{\eta_m}\operatorname{tr}(\boldsymbol{\tau})\right)\boldsymbol{\tau}-2\eta_m D(\boldsymbol{u})=0$$

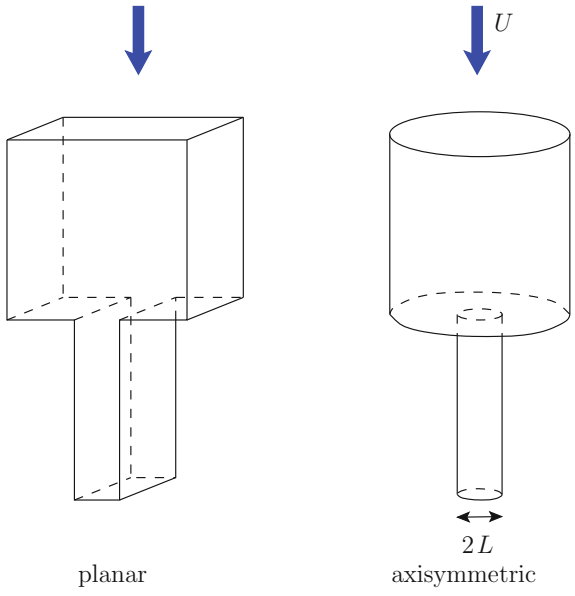

Fig. 4.19 Flow in an abrupt contraction: schematic view

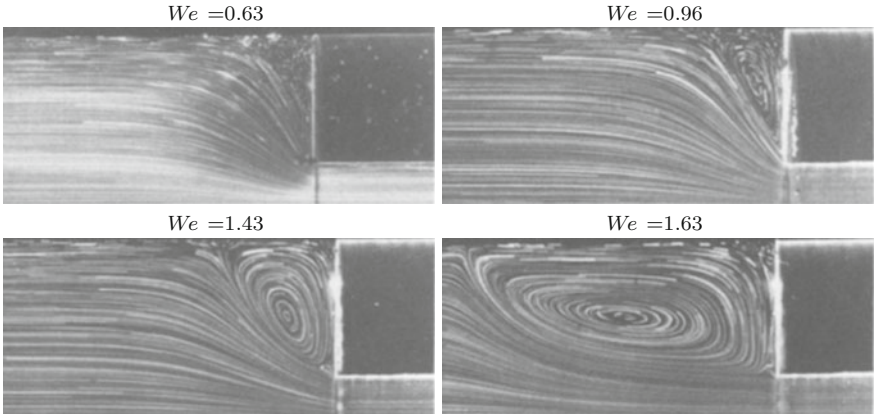

Fig. 4.20 Flow in an axisymmetric abrupt contraction: experimentation with a polymer solution (from [29])

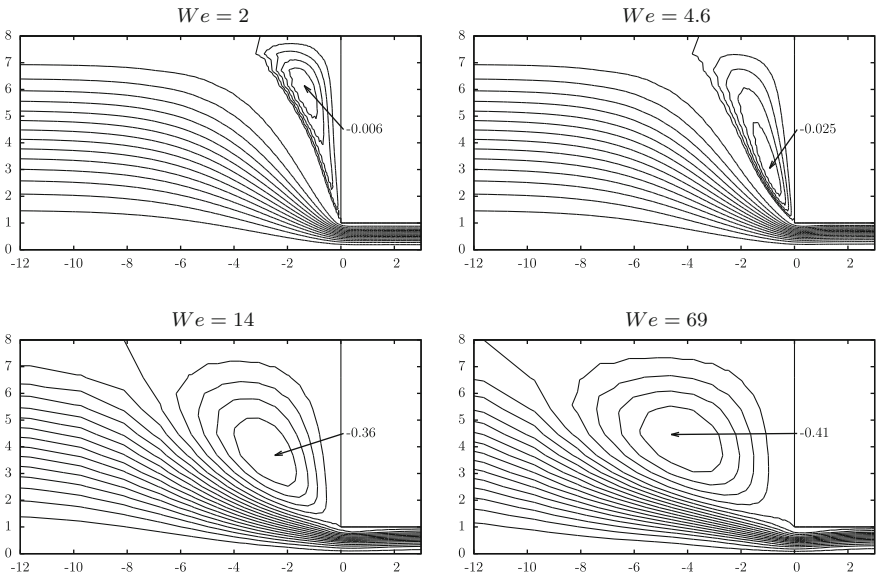

Fig. 4.21 Flow in an axisymmetric abrupt contraction: numerical solution with the Phan-Thien and Tanner viscoelastic flow model $\alpha = 0.875$, $a = 0.9$ and $\xi = 5 \times 10^{-4}$ (from [288])

Here, ξ is specific parameter of the Phan-Thien and Tanner model that acts on the trace of the elastic tensor, i.e. on elongational effects. When $\xi = 0$, this model reduces to the generalized Oldroyd one. Let (r, θ, z) be the cylindrical coordinate system. By symmetry, the solution is supposed to be independent of θ and the domain of computation reduces to a two-dimensional one: the solution depends only upon the r and z coordinates and the velocity writes $\boldsymbol{u} = (u_r, 0, u_z)$. Then, the rate of deformation tensor system writes in the cylindrical coordinate system:

$$2D(\boldsymbol{u}) = \begin{pmatrix} \dfrac{\partial u_r}{\partial r} & 0 & \dfrac{1}{2}\left(\dfrac{\partial u_r}{\partial z} + \dfrac{\partial u_z}{\partial r}\right) \\ 0 & \dfrac{u_r}{r} & 0 \\ \dfrac{1}{2}\left(\dfrac{\partial u_r}{\partial z} + \dfrac{\partial u_z}{\partial r}\right) & 0 & \dfrac{\partial u_z}{\partial z} \end{pmatrix}$$

Note u_r/r component: this component is non-zero in general and thus, the corresponding stress component $\tau_{\theta\theta}$ is also non-zero, even for a Newtonian fluid when the stress is proportional to $D(\boldsymbol{u})$. Thus, the general form of the symmetric elastic stress tensor is

$$\boldsymbol{\tau} = \begin{pmatrix} \tau_{rr} & 0 & \tau_{rz} \\ 0 & \tau_{\theta\theta} & 0 \\ \tau_{rz} & 0 & \tau_{zz} \end{pmatrix}$$

The system of equation is closed by boundary conditions. A non-slip boundary condition $\boldsymbol{u} = 0$ is imposed at the walls. The upstream boundary is supposed to be sufficiently far from the contraction for the solution to be fully developed: we impose both $\boldsymbol{\tau}$ and $\boldsymbol{u}$ as the solution of the Poiseuille flow in a circular pipe. This solution is similar to those of a flow between parallel plates, see Sect. 4.4 is approximated by a numerical computation when $a \neq \pm 1$. The pressure gradient of the Poiseuille flow is iteratively adjusted in order to reach the prescribed flow rate $q = \pi U L^2$ inside the contraction. Finally, at downstream and along the axis of symmetry, a Neumann boundary condition $\boldsymbol{\sigma}_{\text{tot}}\boldsymbol{n} = 0$ is imposed. The dimensional analysis is performed as usual: it reduces the set of parameters to five dimensionless parameters the Weissenberg number We, the viscosity ratio α, tensor derivative interpolation parameter a, the Phan-Thien and Tanner parameter ξ and the contraction ratio β. Here $\xi = 5 \times 10^{-4}$ and the tensor derivative interpolation parameter is $a = 0.9$ while the viscosity ratio is $\alpha = 0.875$ and the contraction ratio is $\beta = 8$. In the cylindrical coordinate system, the computation of the stream function requires a special definition (see Batchelor [13, p. 453]):

$$\boldsymbol{u} = (u_r, 0, u_z) = \left(\frac{1}{r}\frac{\partial \psi}{\partial z},\ 0,\ -\frac{1}{r}\frac{\partial \psi}{\partial r}\right)$$

Recall that

$$\mathbf{curl}\,\psi = \left(\frac{1}{r}\frac{\partial (r\psi)}{\partial r},\ 0,\ -\frac{\partial \psi}{\partial z}\right)$$

Thus, from this definition, in axisymmetric geometries $\boldsymbol{u} \neq \mathbf{curl}\,\psi$ and the definition of ψ differs from the Cartesian two- or three-dimensional cases (see Sect. 1.12, p. 49). Implementation details, C++ source code and practical computations of the Batchelor stream function can be found in the `Rheolef` library [284, Sect. 5.4]. Figure 4.21 represents the solution by its Stokes stream function. Observe that these simulations are able to predict the dramatic development of the recirculation zone as We increases. The numerical computations are qualitatively in agreement with

experiments. Nevertheless, the order of magnitude of the Weissenberg numbers do not correspond and there is no quantitative agreement. A possible explanation could be found by considering that the high complexity of polymer solutions are not fully expressed with simple microscopic scale dumbbell models (see Sect. 4.1, p. 143) and notes at the end of the chapter indicates. perspectives and futures works for the enrichment of the mathematical modeling of polymer solutions. The next section presents another direction of active research: the development of robust an efficient fully implicit algorithms for flow simulation.

4.12 Log-Conformation Tensor Formulation

This alternative formulation of viscoelastic fluid models is motivated by the following observations. In 1986, Keunings [167] pointed out that the maximum Weissenberg number We reached by all numerical computations of viscoelastic fluid flows was very low, depended upon the mesh size h and tended to zero with mesh refinement. Clearly, numerical methods was not able to compute a sequence of approximate solutions that converges with mesh refinement. This situation was referred as the *high Weissenberg number problem*. In 1987, Marchal and Crochet [199] presented the numerical simulation of an upper convected Oldroyd model up to $We = 60$ with a rough mesh and up to $We = 20$ with a finer mesh. It was the first time that computations was obtained to such high Weissenberg numbers. Nevertheless, the maximal Weissenberg number was still mesh dependent and decreasing with the mesh size h. In 1990, Saramito [276, 277], also using an upper convected Oldroyd model, pushed back the limit of the Weissenberg number to $We = 90$. In 2000, Keunings [168], in a review paper, point out that, while the limit Weissenberg number was pushed back and that important progresses where performed, the maximum Weissenberg We reached by all numerical computations of viscoelastic fluid flows was still mesh-dependent and decreasing with mesh refinement. In 2005, Fattal and Kupferman [98] introduced a new formulation of viscoelastic models with an upper convected tensor derivative based on the logarithm of the conformation tensor. These authors presented also numerical computations for the driven cavity flow benchmark, based on a time-dependent algorithm for reaching the stationary solution. While all previous computations for this difficult benchmark was limited to $We \leqslant 0.1$, they exhibited a stationary solution at $We = 3$. Moreover, they showed that the maximal Weissenberg number reached was no more mesh dependent: the high Weissenberg number problem was finally solved. In 2014, Saramito [283] proposed a variant of the logarithm of the conformation tensor formulation, extending it to the interpolated derivatives of tensors and using a fast Newton algorithm for reaching directly the stationary solutions, instead of a long time-dependent algorithm. Let us present now this formulation for the generalized Oldroyd model (4.13a)–(4.13b).

Definition 4.8 (*conformation tensor*)
The conformation tensor $\boldsymbol{c}$ is defined by

$$\boldsymbol{c} = \boldsymbol{\tau} + \frac{\eta_m}{a\lambda}\,\boldsymbol{I} \tag{4.39}$$

where $\boldsymbol{\tau}$ is the elastic stress tensor.

Remark 4.6 (*interpretation of the conformation tensor*)
The conformation tensor is related to the direction $\boldsymbol{q}$ of the polymers chains at the microscopic scale by:

$$\boldsymbol{c} = c_0 \int_{\boldsymbol{q}\in\mathbb{R}^3} \boldsymbol{q}\otimes\boldsymbol{q}\;\psi(t,\boldsymbol{x};\boldsymbol{q})\,\mathrm{d}q$$

where $c_0 > 0$ is a positive constant and $\psi(t,\boldsymbol{x};\boldsymbol{q})$ denotes the probability that the chain extends in the direction $\boldsymbol{q}$ at time $t \geqslant 0$ and at location $\boldsymbol{x} \in \Omega$ (see also Fig. 4.2, p. 144 and [28, 174] for more). The eigendirection associated to the largest eigenvalue of $\boldsymbol{c}$ represents the most probable direction of the chain.

Lemma 4.5 *The elastic stress and the conformation tensors satisfies:*

$$\lambda\frac{\mathscr{D}_a\boldsymbol{\tau}}{\mathscr{D}t} + \tau - 2\eta_m D(\boldsymbol{u}) = \lambda\frac{\mathscr{D}_a\boldsymbol{c}}{\mathscr{D}t} + \boldsymbol{c} - \frac{\eta_m}{a\lambda}\,\boldsymbol{I}$$

Proof From the definition (4.12b) of the interpolated tensor derivative:

$$\frac{\mathscr{D}_a\boldsymbol{I}}{\mathscr{D}t} = -2a\,D(\boldsymbol{u}) \tag{4.40}$$

Then, from (4.39), expanding the elastic tensor versus the conformation one, we get successively:

$$\begin{aligned}
\lambda\frac{\mathscr{D}_a\boldsymbol{\tau}}{\mathscr{D}t} + \tau - 2\eta_m D(\boldsymbol{u}) &= \lambda\frac{\mathscr{D}_a}{\mathscr{D}t}\left(\boldsymbol{c} - \frac{\eta_m}{a\lambda}\,\boldsymbol{I}\right) + \left(\boldsymbol{c} - \frac{\eta_m}{a\lambda}\,\boldsymbol{I}\right) - 2\eta_m D(\boldsymbol{u}) \\
&= \lambda\frac{\mathscr{D}_a\boldsymbol{c}}{\mathscr{D}t} - \frac{\eta_m}{a}\frac{\mathscr{D}_a\boldsymbol{I}}{\mathscr{D}t} - 2\eta_m D(\boldsymbol{u}) + \boldsymbol{c} - \frac{\eta_m}{a\lambda}\,\boldsymbol{I} \\
&= \lambda\frac{\mathscr{D}_a\boldsymbol{c}}{\mathscr{D}t} + \boldsymbol{c} - \frac{\eta_m}{a\lambda}\,\boldsymbol{I} \quad \text{from (4.40)}
\end{aligned}$$

which complete the proof. □

The formulation (4.14a)–(4.14g) of the problem in terms of the elastic tensor is then equivalent to the following one, in terms of the conformation tensor:

(C): find $\boldsymbol{c}$, $\boldsymbol{u}$ and p, defined in $]0, T[\times\Omega$, such that

$$\lambda\frac{\mathscr{D}_a\boldsymbol{c}}{\mathscr{D}t}+\boldsymbol{c}-\frac{\eta_m}{a\lambda}\boldsymbol{I}\ =\ 0 \tag{4.41a}$$

$$\rho\left(\frac{\partial\boldsymbol{u}}{\partial t}+(\boldsymbol{u}.\nabla)\boldsymbol{u}\right)-\mathbf{div}\,(\boldsymbol{c}+2\eta_s D(\boldsymbol{u}))-\nabla p\ =\ \rho\boldsymbol{g} \tag{4.41b}$$

$$\mathrm{div}\,\boldsymbol{u}\ =\ 0 \tag{4.41c}$$

$$\boldsymbol{c}(0)\ =\ \boldsymbol{c}_0\ \text{in}\ \Omega \tag{4.41d}$$

$$\boldsymbol{u}(0)\ =\ \boldsymbol{u}_0\ \text{in}\ \Omega \tag{4.41e}$$

$$\boldsymbol{c}\ =\ \boldsymbol{c}_\Gamma\ \text{on}\ ]0, T[\times\partial\Omega_- \tag{4.41f}$$

$$\boldsymbol{u}\ =\ \boldsymbol{u}_\Gamma\ \text{on}\ ]0, T[\times\partial\Omega \tag{4.41g}$$

Hulsen [150, p. 95] first showed that the tensor $\boldsymbol{c}$ is positive-definite, assuming that the initial condition $\boldsymbol{c}_0$ is positive-definite and that $\nabla\boldsymbol{u}$ is bounded. This result concerns the generalized Oldroyd model ($a\in[-1,1]$) and some of its extensions (Giesekus, etc.).

Theorem 4.10 (positivity of the conformation tensor)
Assume that the initial condition $\boldsymbol{c}_0$ is symmetric definite positive and that the velocity gradient is bounded $\boldsymbol{u}$ at any time. Then $\boldsymbol{c}(t)$ remains symmetric definite positive for any time $t>0$.

Remark 4.7 (*positivity and integral explicit expression*)
In 2011, Lee et al. [182, p. 385, Eq. (3.29)] showed that the conformation tensor $\boldsymbol{c}$ admits an explicit expression in integral form involving the unknown velocity field $\boldsymbol{u}$

$$\boldsymbol{c}(t,\boldsymbol{x})=\frac{\eta_m}{a\lambda}\int_{-\infty}^{t}\exp\left(-\frac{t-s}{\lambda}\right)\boldsymbol{F}(t,\boldsymbol{x};s)\boldsymbol{F}(t,\boldsymbol{x};s)^T\,\mathrm{d}s,\ \forall(t,\boldsymbol{x})\in]0,T[\times\Omega$$

where $\boldsymbol{F}(t,\boldsymbol{x};.)$ is a generalized Finger tensor, defined for all $(t_0,\boldsymbol{x}_0)\in]0,T[\times\Omega$ by the following Cauchy problem:

$$\begin{aligned}&\frac{D\boldsymbol{F}}{Ds}(t_0,\boldsymbol{x}_0;t)=\boldsymbol{g}_a(\boldsymbol{u})(t_0,\boldsymbol{x}_0)\ \boldsymbol{F}(t_0,\boldsymbol{x}_0;t),\ \forall t\in]0,T[\\&\boldsymbol{F}(t_0,\boldsymbol{x}_0;t_0)=\boldsymbol{I}\end{aligned}$$

where $\boldsymbol{g}_a(\boldsymbol{u})\ =\ W(\boldsymbol{u})+aD(\boldsymbol{u})$. Following Joseph [159, p. 15], remark that FF^T has real eigenvalues since FF^T is symmetric and that these eigenvalues are positive since F and F^T have the same eigenvalues. Thus the positivity of the conformation tensor $\boldsymbol{c}$ can also be deduced from its previous explicit expression.

The main idea of the logarithm of the conformation tensor starts from the Remark 4.4, p. 175 and Remark 4.5, p. 177. These remarks point out that the tensorial transport equation is not positive in the Friedrichs sense, except in the special case of the

Jaumann derivative: the bilinear form is Friedrichs positive only in the context of a time-dependent algorithm and with a time step sufficiently small. As an analogy, consider the scalar transport problem, Remark 4.5

$$\tau' + \varepsilon\tau = 0, \quad \varepsilon \geqslant 0 \text{ or } \varepsilon < 0$$

Then, the solution $\tau(t) = \tau_0 \exp(-\varepsilon t)$ grows exponentially when $\varepsilon < 0$. In the tensorial case, the equivalent of the source term with the ε factor is the last term of the interpolated tensor derivative (4.12b). This term, with a factor a, the interpolation parameter, represents effect of the deformation of the fluid. When $a = 0$, the tensorial transport problem is always positive in the Friedrichs sense and there is no exponential growth of the tensor. When $a \neq 0$, there is a possible exponential growth of the tensor, depending of the deformation of the fluid. And this exponential growth could be extremely violent in boundary layers, where deformations are important, and this situation causes the failure of the numerical methods. The main idea of the present formulation is that if there is a possible exponential growth of the conformation tensor, then, its logarithm growth linearly. Indeed, let $\chi = \log(\tau)$: then, the previous scalar differential equation becomes:

$$\chi' + \varepsilon = 0$$

Let us extend this idea to the tensorial case: we start by defining the logarithm and the exponential of a tensor.

Lemma 4.6 (eigen decomposition of a real symmetric matrix)
For any real symmetric matrix $\boldsymbol{\tau} \in \mathbb{R}^{3\times 3}_s$ *there exists* $\boldsymbol{\Lambda} = \text{diag}(\lambda_i)_{1\leqslant i\leqslant 3}$, $(\lambda_i)_{1\leqslant i\leqslant 3} \in \mathbb{R}^3$, *the real eigenvalues, and* $\boldsymbol{q} \in \mathbb{R}^{3\times 3}$, $\boldsymbol{q}^{-1} = \boldsymbol{q}^T$, *the unitary eigenvector matrix, such that* $\boldsymbol{\tau} = \boldsymbol{q}\boldsymbol{\Lambda}\boldsymbol{q}^T$.

Definition 4.9 (*exponential of a matrix*)
For any real symmetric matrix $\boldsymbol{\tau} \in \mathbb{R}^{3\times 3}_s$, the exponential of this matrix is defined by $\exp(\boldsymbol{\tau}) = \boldsymbol{q}\exp(\boldsymbol{\Lambda})\boldsymbol{q}^T$ with the notations of Lemma 4.6 and $\exp(\boldsymbol{\Lambda}) = \text{diag}(\exp(\lambda_i))_{1\leqslant i\leqslant 3}$.

Definition 4.10 (*logarithm of a matrix*)
For any real symmetric definite positive matrix $\boldsymbol{\tau} \in \mathbb{R}^{3\times 3}_s$, the logarithm of this matrix is defined by $\log(\boldsymbol{\tau}) = \boldsymbol{q}\log(\boldsymbol{\Lambda})\boldsymbol{q}^T$ with the notations of Lemma 4.6 and $\log(\boldsymbol{\Lambda}) = \text{diag}(\log(\lambda_i))_{1\leqslant i\leqslant 3}$.

In 2014, Saramito [283] modified the original change of unknown introduced by Fattal and Kupferman [98] and proposed the following definition of the logarithm of the conformation tensor.

Definition 4.11 (*logarithm of the conformation tensor*)
The logarithm of the conformation tensor, denoted as $\boldsymbol{\chi}$ is equivalently defined in terms of the conformation tensor or in terms of the elastic stress tensor as

$$\boldsymbol{\chi} = \frac{\eta_m}{a\lambda} \log\left(\frac{a\lambda}{\eta_m}\boldsymbol{c}\right) = \frac{\eta_m}{a\lambda} \log\left(\boldsymbol{I} + \frac{a\lambda}{\eta_m}\boldsymbol{\tau}\right) \tag{4.42}$$

$$\iff \boldsymbol{c} = \frac{\eta_m}{a\lambda} \exp\left(\frac{a\lambda}{\eta_m}\boldsymbol{\chi}\right) \text{ and } \boldsymbol{\tau} = \frac{\eta_m}{a\lambda}\left(\exp\left(\frac{a\lambda}{\eta_m}\boldsymbol{\chi}\right) - \boldsymbol{I}\right) \tag{4.43}$$

Our objective is now to perform a change of unknown from $\boldsymbol{c}$ to $\boldsymbol{\chi}$ in problem (4.41a)–(4.41g). The main difficulty is to expand the interpolated tensor derivative $\frac{\mathscr{D}_a \boldsymbol{c}}{\mathscr{D}t}$ in terms of $\boldsymbol{\chi}$. The change of unknown will be performed in three successive steps:

1. write the constitutive equation on the eigenbasis
2. performs the change of unknown on the eigenbasis
3. go back from the eigenbasis to the usual basis.

The computations share with Sect. 4.2 some technical aspects, since we also perform here a change of basis. Let us start with the first step and write the constitutive equation on the eigenbasis. Applying Lemma 4.6 to the conformation tensor, there exists $\tilde{\boldsymbol{c}} = \text{diag}(c_i)_{1\leqslant i\leqslant 3}$, $c_i > 0$ and $\boldsymbol{q} \in \mathbb{R}^{3\times 3}$, $\boldsymbol{q}^{-1} = \boldsymbol{q}^T$ such that $\boldsymbol{c} = \boldsymbol{q}\tilde{\boldsymbol{c}}\boldsymbol{q}^T$. Let us denote for simplicity the Lagrangian derivative with a dot. By differentiation, we get:

$$\dot{\boldsymbol{c}} = \boldsymbol{q}\dot{\tilde{\boldsymbol{c}}}\boldsymbol{q}^T + \dot{\boldsymbol{q}}\tilde{\boldsymbol{c}}\boldsymbol{q}^T + \boldsymbol{q}\tilde{\boldsymbol{c}}\dot{\boldsymbol{q}}^T \tag{4.44}$$

Let us introduce the notation $\boldsymbol{r} = \boldsymbol{q}\dot{\boldsymbol{q}}^T$. As $\boldsymbol{q}$ is the unitary eigenvector matrix, we have $\boldsymbol{q}^T = \boldsymbol{q}^{-1}$ or equivalently $\boldsymbol{q}\boldsymbol{q}^T = \boldsymbol{I}$. By differentiation, we get:

$$\dot{\boldsymbol{q}}\boldsymbol{q}^T + \boldsymbol{q}\dot{\boldsymbol{q}}^T = 0 \iff \boldsymbol{r}^T = -\boldsymbol{r}$$

Thus, $\boldsymbol{r}$ is skew-symmetric: it means that $\boldsymbol{r}$ is a rotation tensor. The previous relation writes also:

$$\begin{aligned} \dot{\boldsymbol{q}} &= -\boldsymbol{q}\dot{\boldsymbol{q}}^T\boldsymbol{q} \;=\; -\boldsymbol{r}\boldsymbol{q} \\ \dot{\boldsymbol{q}}^T &= -\boldsymbol{q}^T\boldsymbol{r}^T \end{aligned}$$

Using theses expressions of $\dot{\boldsymbol{q}}$ and $\dot{\boldsymbol{q}}^T$ in (4.44), we get the following expression of $\dot{\boldsymbol{c}}$:

$$\dot{\boldsymbol{c}} = \boldsymbol{q}\dot{\tilde{\boldsymbol{c}}}\boldsymbol{q}^T - \boldsymbol{r}\boldsymbol{q}\tilde{\boldsymbol{c}}\boldsymbol{q}^T - \boldsymbol{q}\tilde{\boldsymbol{c}}\boldsymbol{q}^T\boldsymbol{r}^T \tag{4.45}$$

In order to have a full expression of $\dot{\boldsymbol{c}}$ on the eigenbasis, it remains to decompose also $\boldsymbol{r}$ on the eigenbasis. Let $\tilde{\boldsymbol{r}} = \boldsymbol{q}^T\boldsymbol{r}\boldsymbol{q}$: it is skew-symmetric (non-diagonal). Then $\boldsymbol{r} = \boldsymbol{q}\tilde{\boldsymbol{r}}\boldsymbol{q}^T$ and $\boldsymbol{r}^T = \boldsymbol{q}\tilde{\boldsymbol{r}}^T\boldsymbol{q}^T$. Finally, we get an expression of $\dot{\boldsymbol{c}}$ on the eigenbasis:

$$\dot{\boldsymbol{c}} = \boldsymbol{q}\left(\dot{\tilde{\boldsymbol{c}}} - \tilde{\boldsymbol{r}}\tilde{\boldsymbol{c}} - \tilde{\boldsymbol{c}}\tilde{\boldsymbol{r}}^T\right)\boldsymbol{q}^T \tag{4.46}$$

In order to express the interpolated tensor derivative on the eigenbasis, it remains to treat the additional terms. Note that, from its definition (4.12b), the interpolated tensor derivative writes also:

$$\begin{aligned}\frac{\mathscr{D}_a \boldsymbol{c}}{\mathscr{D}t} &= \dot{\boldsymbol{c}} - W(\boldsymbol{u})\boldsymbol{c} + \boldsymbol{c}W(\boldsymbol{u}) - a\left(D(\boldsymbol{u})\boldsymbol{c} + \boldsymbol{c}D(\boldsymbol{u})\right)\\ &= \dot{\boldsymbol{c}} - \boldsymbol{g}_a(\boldsymbol{u})\,\boldsymbol{c} - \boldsymbol{c}\,\boldsymbol{g}_a(\boldsymbol{u})^T\end{aligned}$$

where $\boldsymbol{g}_a(\boldsymbol{u}) = W(\boldsymbol{u}) + a D(\boldsymbol{u})$. Next, let $\tilde{\boldsymbol{g}}_a = \boldsymbol{q}^T \boldsymbol{g}_a(\boldsymbol{u})\boldsymbol{q}$. This writes equivalently $\boldsymbol{g}_a(\boldsymbol{u}) = \boldsymbol{q}\tilde{\boldsymbol{g}}_a\boldsymbol{q}^T$. Then, the interpolated tensor derivative is completely expressed on the eigenbasis as:

$$\frac{\mathscr{D}_a \boldsymbol{c}}{\mathscr{D}t} = \boldsymbol{q}\left(\dot{\tilde{\boldsymbol{c}}} - \left(\tilde{\boldsymbol{r}} + \tilde{\boldsymbol{g}}_a\right)\tilde{\boldsymbol{c}} - \tilde{\boldsymbol{c}}\left(\tilde{\boldsymbol{r}} + \tilde{\boldsymbol{g}}_a\right)^T\right)\boldsymbol{q}^T \tag{4.47}$$

Let us now express the constitutive equation (4.41a) on the eigenbasis. Replacing (4.47) in (4.41a), we obtain:

$$\dot{\tilde{\boldsymbol{c}}} = \frac{\eta_m}{a\lambda^2}\boldsymbol{I} - \frac{1}{\lambda}\tilde{\boldsymbol{c}} + \left(\tilde{\boldsymbol{r}} + \tilde{\boldsymbol{g}}_a\right)\tilde{\boldsymbol{c}} + \tilde{\boldsymbol{c}}\left(\tilde{\boldsymbol{r}} + \tilde{\boldsymbol{g}}_a\right)^T \tag{4.48}$$

The first step of the change of unknown is fully achieved and we now start the second step. Before to perform the change of unknown on the eigenbasis, let us introduce the following notations:

$$\begin{aligned}\tilde{\boldsymbol{d}} &= \boldsymbol{q}^T D(\boldsymbol{u})\,\boldsymbol{q} = (\tilde{d}_{i,j})_{1\leqslant i,j\leqslant 3} \text{ which is symmetric}\\ \text{and } \tilde{\boldsymbol{w}} &= \boldsymbol{q}^T W(\boldsymbol{u})\boldsymbol{q} = (\tilde{w}_{i,j})_{1\leqslant i,j\leqslant 3} \text{ which is skew-symmetric}\end{aligned}$$

Then, we have

$$\begin{aligned}\operatorname{diag}(\tilde{\boldsymbol{g}}_a) &= \operatorname{diag}(\tilde{\boldsymbol{w}} + a\tilde{\boldsymbol{d}}) = a\operatorname{diag}(\tilde{\boldsymbol{d}})\\ \operatorname{diag}\left(\tilde{\boldsymbol{g}}_a\tilde{\boldsymbol{c}}\right) &= \operatorname{diag}\left(\tilde{\boldsymbol{c}}\tilde{\boldsymbol{g}}_a^T\right) = a\operatorname{diag}(\tilde{\boldsymbol{d}})\,\tilde{\boldsymbol{c}}\\ \operatorname{diag}\left(\tilde{\boldsymbol{r}}\tilde{\boldsymbol{c}}\right) &= \operatorname{diag}\left(\tilde{\boldsymbol{c}}\tilde{\boldsymbol{r}}^T\right) = 0\end{aligned}$$

Selecting the diagonal part of the tensorial equation (4.48), we obtain the following expression:

$$\dot{\tilde{\boldsymbol{c}}} = \frac{\eta_m}{a\lambda^2}\boldsymbol{I} - \left(\frac{\boldsymbol{I}}{\lambda} - 2a\operatorname{diag}(\tilde{\boldsymbol{d}})\right)\tilde{\boldsymbol{c}} \tag{4.49}$$

Let $\tilde{\boldsymbol{\chi}} = \operatorname{diag}(\chi_i)_{1\leqslant i\leqslant 3}$ be the eigenvalues of the logarithm of the conformation tensor $\boldsymbol{\chi}$. These eigenvalues are given by: $\chi_i = \dfrac{\eta_m}{a\lambda}\log\left(\dfrac{a\lambda}{\eta_m}c_i\right)$, $1 \leqslant i \leqslant 3$. By differentiation, we get:

$$\dot{\chi}_i = \frac{\eta_m}{a\lambda}\frac{\dot{c}_i}{c_i} \quad 1 \leqslant i \leqslant 3$$

$$\begin{aligned}
\Longleftrightarrow \dot{\tilde{\boldsymbol{\chi}}} &= \frac{\eta_m}{a\lambda}\,\dot{\tilde{\boldsymbol{c}}}\,\tilde{\boldsymbol{c}}^{-1} \\
&= \frac{\eta_m}{a\lambda}\left(\frac{\eta_m}{a\lambda^2}\boldsymbol{I} - \left(\frac{\boldsymbol{I}}{\lambda} - 2a\,\mathrm{diag}(\tilde{\boldsymbol{d}})\right)\tilde{\boldsymbol{c}}\right)\tilde{\boldsymbol{c}}^{-1} \quad \text{from (4.49)} \\
&= \frac{2\eta_m}{\lambda}\,\mathrm{diag}(\tilde{\boldsymbol{d}}) - \frac{1}{\lambda}\left\{\frac{\eta_m}{a\lambda}\left(\boldsymbol{I} - \frac{\eta_m}{a\lambda}\tilde{\boldsymbol{c}}^{-1}\right)\right\} \qquad (4.50)
\end{aligned}$$

The definition of the logarithm of the conformation tensor (4.43) expresses also on the eigenbasis as $\tilde{\boldsymbol{c}}^{-1} = \dfrac{a\lambda}{\eta_m}\exp\left(-\dfrac{a\lambda}{\eta_m}\tilde{\boldsymbol{\chi}}\right)$. Replacing this expression in (4.50) leads to the following expression of $\dot{\tilde{\boldsymbol{\chi}}}$:

$$\dot{\tilde{\boldsymbol{\chi}}} = \frac{2\eta_m}{\lambda}\,\mathrm{diag}(\tilde{\boldsymbol{d}}) - \frac{1}{\lambda}\left\{\frac{\eta_m}{a\lambda}\left(\boldsymbol{I} - \exp\left(-\frac{a\lambda}{\eta_m}\tilde{\boldsymbol{\chi}}\right)\right)\right\} \qquad (4.51)$$

The second step of the change of unknown is now fully achieved. Let us start the last one and go back from the eigenbasis to the usual one. Expression (4.46) of the Lagrange derivative $\dot{\boldsymbol{c}}$ is also valid for $\dot{\boldsymbol{\chi}}$: replacing (4.46) $\dot{\boldsymbol{c}}$ and $\boldsymbol{c}$ by $\dot{\boldsymbol{\chi}}$ and $\boldsymbol{\chi}$, respectively, we get:

$$\begin{aligned}
\dot{\boldsymbol{\chi}} &= \boldsymbol{q}\left(\dot{\tilde{\boldsymbol{\chi}}} - \tilde{\boldsymbol{r}}\tilde{\boldsymbol{\chi}} - \tilde{\boldsymbol{\chi}}\tilde{\boldsymbol{r}}^T\right)\boldsymbol{q}^T \\
&= -\frac{1}{\lambda}\left\{\frac{\eta_m}{a\lambda}\left(\boldsymbol{I} - \exp\left(-\frac{a\lambda}{\eta_m}\boldsymbol{\chi}\right)\right)\right\} - \boldsymbol{q}\left(\tilde{\boldsymbol{r}}\tilde{\boldsymbol{\chi}} + \tilde{\boldsymbol{\chi}}\tilde{\boldsymbol{r}}^T - \frac{2\eta_m}{\lambda}\,\mathrm{diag}(\tilde{\boldsymbol{d}})\right)\boldsymbol{q}^T
\end{aligned}$$

This relation writes equivalently

$$\dot{\boldsymbol{\chi}} + \phi_a(\boldsymbol{\chi}, \nabla\boldsymbol{u}) + \frac{1}{\lambda}\left\{\frac{\eta_m}{a\lambda}\left(\boldsymbol{I} - \exp\left(-\frac{a\lambda}{\eta_m}\boldsymbol{\chi}\right)\right)\right\} = 0 \qquad (4.52)$$

where we have introduced the notation:

$$\phi_a(\boldsymbol{\chi}, \nabla\boldsymbol{u}) = \boldsymbol{q}\left(\tilde{\boldsymbol{r}}\tilde{\boldsymbol{\chi}} + \tilde{\boldsymbol{\chi}}\tilde{\boldsymbol{r}}^T - \frac{2\eta_m}{\lambda}\,\mathrm{diag}(\tilde{\boldsymbol{d}})\right)\boldsymbol{q}^T \qquad (4.53)$$

The notation in (4.53) suggests that the right-hand-side is completely computable from the two tensors $\boldsymbol{\chi}$ and $\nabla\boldsymbol{u}$ only. Indeed, $\tilde{\chi}$ contains the eigenvalues of $\boldsymbol{\chi}$ while $\boldsymbol{q}$ is the tensor of its eigenvectors. Next, $\tilde{\boldsymbol{d}}$ depends upon $\boldsymbol{q}$ and $D(\boldsymbol{u})$. Thus, its remains to show that $\tilde{\boldsymbol{r}}$ is computable from the two tensors $\boldsymbol{\chi}$ and $\nabla\boldsymbol{u}$. Taking the off diagonal part of (4.48) leads to

$$0 = (\tilde{r}_{ij} + \tilde{\boldsymbol{g}}_{ij})c_j + c_i(\tilde{r}_{ji} + \tilde{\boldsymbol{g}}_{ji}), \quad i \neq j \ \text{ and } \ 1 \leqslant i, j \leqslant 3$$

Then, using the skew symmetry of $\tilde{\boldsymbol{r}}$ i.e. $\tilde{r}_{ji} = -\tilde{r}_{ij}$ we get

$$\tilde{r}_{ij} \;=\; \frac{\tilde{\boldsymbol{g}}_{ji}c_i + \tilde{\boldsymbol{g}}_{ij}c_j}{c_i - c_j} \quad \text{when } c_i \neq c_j$$

Note that, from the definition $\boldsymbol{g}_a(\boldsymbol{u}) \;=\; W(\boldsymbol{u}) + a\,D(\boldsymbol{u})$, we have on the eigenbasis $\tilde{\boldsymbol{g}}_{ij} = \quad \tilde{w}_{ij} + a\tilde{d}_{ij}$ and $\tilde{\boldsymbol{g}}_{ji} = -\tilde{w}_{ij} + a\tilde{d}_{ij}$. Then

$$\tilde{r}_{ij} \;=\; -\tilde{w}_{ij} + a\tilde{d}_{ij}\left(\frac{c_i + c_j}{c_i - c_j}\right) \quad \text{when } c_i \neq c_j \tag{4.54}$$

As the relation (4.43) between the conformation tensor and its logarithm writes equivalently in the eigenbasis $c_i = \dfrac{\eta_m}{a\lambda}\exp\left(\dfrac{a\lambda}{\eta_m}\chi_i\right)$, we obtain

$$\tilde{r}_{ij} = -\tilde{w}_{ij} + \frac{a\,\tilde{d}_{ij}}{\tanh\left(\dfrac{a\lambda}{\eta_m}\left(\dfrac{\chi_i - \chi_j}{2}\right)\right)} \quad \text{when } \chi_i \neq \chi_j \tag{4.55}$$

where $\tanh(\xi) = (\exp(2\xi) - 1)/(\exp(2\xi) + 1)$, for all $\xi \in \mathbb{R}$.

Let $\tilde{\phi}_a = \boldsymbol{q}^T\phi_a(\boldsymbol{\chi}, \nabla\boldsymbol{u})\boldsymbol{q}$. Then, from (4.53) we have

$$\begin{aligned}
\tilde{\phi}_a &= \tilde{\boldsymbol{r}}\tilde{\boldsymbol{\chi}} + \tilde{\boldsymbol{\chi}}\tilde{\boldsymbol{r}}^T - \frac{2\eta_m}{\lambda}\,\mathrm{diag}(\tilde{\boldsymbol{d}}) \;=\; (\tilde{\phi}_{ij})_{1\leqslant i,j\leqslant 3} \\
\tilde{\phi}_{ij} &= \tilde{r}_{ij}\chi_j + \chi_i\tilde{r}_{ji} \quad \text{when } i \neq j \\
&= -\left(\chi_i - \chi_j\right)\tilde{r}_{ij} \\
&= \left(\chi_i - \chi_j\right)\tilde{w}_{ij} - \left(\frac{\dfrac{a\lambda}{\eta_m}\left(\dfrac{\chi_i - \chi_j}{2}\right)}{\tanh\left(\dfrac{a\lambda}{\eta_m}\left(\dfrac{\chi_i - \chi_j}{2}\right)\right)}\right)\frac{2\eta_m\tilde{d}_{ij}}{\lambda} \quad \text{from (4.55)}
\end{aligned}$$

Note that $\lim\limits_{\xi\to 0}\dfrac{\xi}{\tanh(\xi)} = 1$ and then $\tilde{\phi}_{ij} \;=\; -\dfrac{2\eta_m}{\lambda}\tilde{d}_{i,j}$ when $\chi_i - \chi_j = 0$. Finally

$$\phi_a(\boldsymbol{\chi}, \nabla\boldsymbol{u}) = \boldsymbol{\chi}W(\boldsymbol{u}) - W(\boldsymbol{u})\boldsymbol{\chi} - \frac{2\eta_m}{\lambda}D(\boldsymbol{u}) + \frac{\eta_m}{\lambda}\kappa\left(\frac{a\lambda}{\eta_m}\boldsymbol{\chi},\, 2D(\boldsymbol{u})\right)$$

where we have introduced the new following form $\kappa(.,.)$, defined for all $\boldsymbol{\beta} \in \mathbb{R}^{3\times 3}_s$ and $\boldsymbol{\gamma} \in \mathbb{R}^{3\times 3}$ by

$$\kappa(\boldsymbol{\beta},\boldsymbol{\gamma}) = \boldsymbol{q}\tilde{\kappa}\boldsymbol{q}^T \tag{4.56a}$$

$$\tilde{\kappa}_{ij} = \hat{\kappa}\left(\frac{\beta_i-\beta_j}{2}\right)\tilde{\gamma}_{i,j},\ 1\leqslant i,j\leqslant d \tag{4.56b}$$

$$\mathrm{diag}(\beta_i)_{1\leqslant i\leqslant 3} = \boldsymbol{q}^T\boldsymbol{\beta}\boldsymbol{q} \tag{4.56c}$$

$$(\tilde{\gamma}_{ij})_{1\leqslant i,j\leqslant 3} = \boldsymbol{q}^T\boldsymbol{\gamma}\boldsymbol{q} \tag{4.56d}$$

$$\hat{\kappa}(\xi) = \begin{cases} 0 & \text{when } \xi = 0 \\ 1-\dfrac{\xi}{\tanh(\xi)} & \text{otherwise} \end{cases} \tag{4.56e}$$

Finally, both $\phi_a(.,.)$ and $\kappa(.,.)$ are fully defined versus their arguments. With these notations, relation (4.52) writes equivalently

$$\begin{aligned}&\lambda\{\dot{\boldsymbol{\chi}} - W(\boldsymbol{u})\boldsymbol{\chi} + \boldsymbol{\chi}W(\boldsymbol{u})\}\\ &+\eta_m\kappa\left(\frac{a\lambda}{\eta_m}\boldsymbol{\chi},\ 2D(\boldsymbol{u})\right) + \frac{\eta_m}{a\lambda}\left(\boldsymbol{I} - \exp\left(-\frac{a\lambda}{\eta_m}\boldsymbol{\chi}\right)\right) = 2\eta_m D(\boldsymbol{u})\end{aligned}$$

We recognize in the previous expression a Jaumann derivative of the $\boldsymbol{\chi}$ tensor. Thus, this relation writes also

$$\lambda\frac{\mathscr{D}_0\boldsymbol{\chi}}{\mathscr{D}t} + \eta_m\kappa\left(\frac{a\lambda}{\eta_m}\boldsymbol{\chi},\ 2D(\boldsymbol{u})\right) + \frac{\eta_m}{a\lambda}\left(\boldsymbol{I} - \exp\left(-\frac{a\lambda}{\eta_m}\boldsymbol{\chi}\right)\right) = 2\eta_m D(\boldsymbol{u})$$

The third step of the change of unknown is complete. We known, from the analysis of the tensorial transport problem, that the Jaumann derivative develops better properties of positivity than the general interpolated tensor derivative: see Remark 4.4, p. 175 and Remark 4.5, p. 177. Finally, let us introduce, for all $\mu\in\mathbb{R}$, and $\boldsymbol{\chi}\in\mathbb{R}^{3\times 3}_s$ the following function:

$$f(\mu,\boldsymbol{\chi}) = \begin{cases} 0 & \text{when } \mu = 0 \\ \dfrac{\exp(\mu\boldsymbol{\chi})-\boldsymbol{I}}{\mu} - \boldsymbol{\chi} & \text{otherwise} \end{cases} \tag{4.57}$$

Finally, the log-conformation formulation of the generalized Oldroyd model writes:

(LC): find $\boldsymbol{\chi}$, $\boldsymbol{u}$ and p, defined in $]0,T[\times\Omega$, such that

$$\lambda\frac{\mathscr{D}_0\boldsymbol{\chi}}{\mathscr{D}t} + \boldsymbol{\chi} - f\left(\frac{a\lambda}{\eta_m},-\boldsymbol{\chi}\right) + \eta_m\kappa\left(\frac{a\lambda}{\eta_m}\boldsymbol{\chi},\ 2D(\boldsymbol{u})\right) - 2\eta_m D(\boldsymbol{u}) = 0 \tag{4.58a}$$

$$\rho\left(\frac{\partial\boldsymbol{u}}{\partial t} + (\boldsymbol{u}.\nabla)\boldsymbol{u}\right) - \mathbf{div}\left(\boldsymbol{\chi} + f\left(\frac{a\lambda}{\eta_m},\boldsymbol{\chi}\right) + 2\eta_s D(\boldsymbol{u}) - p\,\boldsymbol{I}\right) = 0 \tag{4.58b}$$

$$\mathrm{div}\,\boldsymbol{u} = 0 \tag{4.58c}$$

$$\boldsymbol{\chi}(t=0) = \boldsymbol{\chi}_0 \tag{4.58d}$$

$$\boldsymbol{u}(t=0) = \boldsymbol{u}_0 \tag{4.58e}$$

$$\boldsymbol{\chi} = \boldsymbol{\chi}_\Gamma = 0 \text{ on }]0,T[\times\partial\Omega_- \quad (4.58f)$$

$$\boldsymbol{u} = \boldsymbol{u}_\Gamma \text{ on }]0,T[\times\partial\Omega \quad (4.58g)$$

Note that when $\lambda = 0$ then, since $f(0,.) = \kappa(0,.) = 0$, the system reduces to the Navier-Stokes equation, as expected. Also, when $a = 0$, this formulation coincides with those in terms of the elastic tensor (4.14a)–(4.14g) and in that case $\boldsymbol{\chi} = \boldsymbol{\tau}$. Otherwise, when $a \neq 0$, (4.58a) is now non-linear in $\boldsymbol{\chi}$ but it involves, even when $a \neq 0$, a Jaumann derivative.

4.13 Energy Estimate

The aim of this section is to show an exponential decrease of the global free energy of the system for the generalized Oldroyd model with interpolated derivatives. The main idea is to choose an homogeneous boundary condition $\boldsymbol{u}_\Gamma = 0$ and to observe how the solution goes to zero from any initial condition. Such result is essential for checking whether the model is well-posed. When dealing with viscoplastic fluids in the previous Chap. 3, the convexity of the energy of dissipation was a guaranty that the problem was well-posed (see Chap. 3) and the idea is to define a similar concept for viscoelastic fluids. Since 1987, several energy estimate for the generalized Oldroyd model based on the elastic stress tensor formulation was proposed by Guillopé and Saut [133–135]. Lee et al. [182, p. 388] showed an a priori energy estimate for the conformation tensor $\boldsymbol{c}$ in L^1 norm when $a = 1$ i.e. the Oldroyd-B model. Thee authors observe that, in the space of symmetric definite tensors, the trace is related to the L^1 norm as

$$\|\boldsymbol{c}\|_{L^1} = \int_\Omega \mathrm{tr}(\boldsymbol{c})\,\mathrm{d}x$$

Let $\mathbb{R}^{3\times3}_{s*+}$ denotes the space of symmetric definite positive 3×3 matrix. Conversely, let $\mathbb{R}^{3\times3}_{s*}$ (resp. $\mathbb{R}^{3\times3}_{s+}$) denotes the space of symmetric definite (resp. positive) 3×3 matrix.

Free energy involving the logarithm of the conformation tensor is a classical concept for representing a local *free energy* stored by the micro-scale mechanical system (see e.g [28, 230, 313]). The idea using such *free energy* expression for obtaining an energy estimate was first introduced in 2007 by Lelièvre [34, 148]. This idea bases on the following lemma.

Lemma 4.7 (positivity of a free energy like expression)

$$\boldsymbol{c} - \log \boldsymbol{c} - \boldsymbol{I} \in \mathbb{R}^{3\times3}_{s+},\ \forall \boldsymbol{c} \in \mathbb{R}^{3\times3}_{s*+} \quad (4.59)$$

Proof As $\boldsymbol{c}$ is symmetric and real, we can work in its eigenbasis where eigenvalue are real and strictly positive. Then the proof reduces to show that $x - \log x - 1 \geqslant 0$

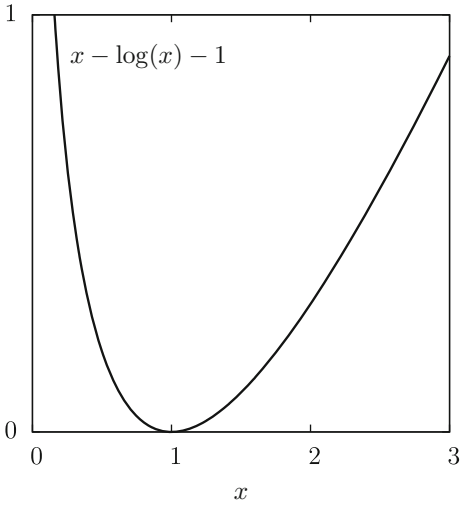

Fig. 4.22 Free energy like function for the logarithm of conformation tensor formulation of viscoelastic fluids

for all $x > 0$. This last result is obtained by a simple study of the corresponding function that is represented on Fig. 4.22. □

As a consequence, for all $\boldsymbol{c} \in \mathbb{R}^{3\times 3}_{s*+}$, we have $\boldsymbol{c} - \log\, \boldsymbol{c} - \boldsymbol{I} = 0$ if and only if $\boldsymbol{c} = \boldsymbol{I}$. Then, the following expression

$$\|\boldsymbol{\chi}\| = \int_{\Omega} \mathrm{tr}(\exp(\boldsymbol{\chi}) - \boldsymbol{\chi} - \boldsymbol{I})\, \mathrm{d}x$$

defines a norm on the space of symmetric tensors. For the present formulation, the free energy is defined by

$$\mathscr{F}(t) = \int_{\Omega} \left(\frac{1}{2a} \mathrm{tr}\,(\boldsymbol{\tau} - \boldsymbol{\chi}) + \frac{\rho}{2} |\boldsymbol{u}|^2 \right) \mathrm{d}x \tag{4.60}$$

where $\boldsymbol{\tau}$ is defined from $\boldsymbol{\chi}$ by (4.43). Note that this expression includes also the kinetic energy. The result showed in [34, 148] concerned the Oldroyd-B model ($a = 1$): it is extended in the present section to a general interpolated tensor derivative ($a \in [-1, 1]$). We start by some properties of the $\kappa(.,.)$ function and some technical lemmas before to show the main result.

Property 4.1 (Skew symmetry of κ)
The function κ defined by (4.56a)–(4.56e) satisfies the following properties:

1. *$\kappa(.,.)$ is nonlinear with respect to its first variable $\boldsymbol{\beta}$ and is linear with respect to its second variable $\boldsymbol{\gamma}$.*
2. *κ is traceless:*

$$\mathrm{tr}\, \kappa(\boldsymbol{\beta}, \boldsymbol{\gamma}) = 0, \ \forall \boldsymbol{\beta}, \boldsymbol{\gamma} \in \mathbb{R}^{3\times 3}_{s}$$

3. $\kappa(\boldsymbol{\beta}, \boldsymbol{\gamma}) = 0$ *when* $\boldsymbol{\beta}$ *and* $\boldsymbol{\gamma}$ *are aligned, i.e. when they share the same eigensystem. As a special case,* $\kappa(\boldsymbol{\beta}, \boldsymbol{\gamma}) = 0$ *when all eigenvalues of* $\boldsymbol{\beta}$ *are equal.*
4. κ *is skew-symmetric with respect to its first variable:*

$$\kappa(\boldsymbol{\beta}, \boldsymbol{\gamma}) : \boldsymbol{\beta} = 0, \ \forall \boldsymbol{\beta}, \boldsymbol{\gamma} \in \mathbb{R}_s^{3\times 3}$$

The skew symmetry extends to

$$\kappa(\boldsymbol{\beta}, \boldsymbol{\gamma}) : \boldsymbol{\sigma} = 0, \ \forall \boldsymbol{\beta}, \boldsymbol{\gamma}, \boldsymbol{\sigma} \in \mathbb{R}_s^{3\times 3} \text{ and } \boldsymbol{\beta} \text{ and } \boldsymbol{\sigma} \text{ share the same eigensystem} \tag{4.61}$$

5. κ *is continuously differentiable everywhere and*

$$\kappa(0, \boldsymbol{\gamma}) = 0 \ \text{ and } \ \frac{\partial \kappa}{\partial \boldsymbol{\beta}}(0, \boldsymbol{\gamma}) = 0, \ \forall \boldsymbol{\gamma} \in \mathbb{R}_s^{3\times 3}$$

Proof Note that, from (4.56a)–(4.56e), we have $\tilde{\kappa}_{k,k} = 0$ for all k, $1 \leqslant k \leqslant 3$ which leads to the traceless property. When $\boldsymbol{\beta}$ and $\boldsymbol{\gamma}$ are aligned then $\tilde{\boldsymbol{\gamma}}$ is diagonal and then $\tilde{\kappa}_{i,j} = 0$. The skew-symmetry result can be shown by the following development:

$$\begin{aligned}
\kappa(\boldsymbol{\beta}, \boldsymbol{\gamma}) : \boldsymbol{\beta} &= (\boldsymbol{q} \tilde{\kappa} \boldsymbol{q}^T) : (\boldsymbol{q}\, \tilde{\boldsymbol{\beta}}\, \boldsymbol{q}^T) \\
&= \sum_{i,j,k,l,m=1}^{3} \boldsymbol{q}_{i,j} \tilde{\kappa}_{j,k} \boldsymbol{q}_{l,k}\, \boldsymbol{q}_{i,m} \beta_m \boldsymbol{q}_{l,m} \\
&= \sum_{j,k,m=1}^{3} \delta_{j,m} \delta_{k,m} \tilde{\kappa}_{j,k} \beta_m \\
&\qquad \text{since } \sum_{i=1}^{3} \boldsymbol{q}_{i,j} \boldsymbol{q}_{i,m} = \delta_{j,m} \ \text{ and } \ \sum_{l=1}^{3} \boldsymbol{q}_{l,k} \boldsymbol{q}_{l,m} = \delta_{k,m} \\
&= \sum_{k=1}^{3} \tilde{\kappa}_{k,k} \boldsymbol{\beta}_k \\
&= 0 \ \text{ since } \tilde{\kappa}_{k,k} = 0
\end{aligned}$$

When $\boldsymbol{\beta} = 0$, then all eigenvalues of $\boldsymbol{\beta}$ are equal and then, from item 3, we have $\kappa(0, \boldsymbol{\gamma}) = 0$. The proof of the differentiability of κ is more technical and can be found in [283, Appendix A.2]. □

Lemma 4.8 (trace of a matrix product)

$$\operatorname{tr}(\boldsymbol{\sigma}\boldsymbol{\tau}) = \operatorname{tr}\left(\boldsymbol{\tau}^T \boldsymbol{\sigma}\right) = \boldsymbol{\sigma} : \boldsymbol{\tau}^T, \ \forall \boldsymbol{\sigma}, \boldsymbol{\tau} \in \mathbb{R}^{3\times 3} \tag{4.62}$$

Proof From a development

$$\mathrm{tr}(\boldsymbol{\sigma\tau}) = \sum_{i,j=0}^{d-1} \sigma_{i,j}\tau_{j,i} = \boldsymbol{\sigma} : \boldsymbol{\tau}^T$$

□

Lemma 4.9 (trace of a matrix logarithm)

$$\mathrm{tr}\ \log\ \boldsymbol{c} = \log\ \det \boldsymbol{c},\ \forall \boldsymbol{c} \in \mathbb{R}^{3\times 3}_{s*+} \tag{4.63}$$

Proof The trace and determinant are invariants: thus the trace (resp. the determinant) is the sum (resp. the product) of eigenvalues. The result is then simply a consequence that the a sum of logs is the log of the products. □

Lemma 4.10 (derivative of the trace)

$$\frac{\mathrm{d}}{\mathrm{d}t}(\mathrm{tr}\,\boldsymbol{c}) = \mathrm{tr}\left(\boldsymbol{c}\,\frac{\mathrm{d}}{\mathrm{d}t}(\log\ \boldsymbol{c})\right) = \left(\frac{\mathrm{d}}{\mathrm{d}t}(\log\ \boldsymbol{c})\right) : \boldsymbol{c},\ \forall \boldsymbol{c} \in C^1\left(]0, T[, \mathbb{R}^{3\times 3}_{s*+}\right) \tag{4.64}$$

Proof The matrix exponential is a C^∞ diffeomorphism from $\mathbb{R}^{3\times 3}_s$ to $\mathbb{R}^{3\times 3}_{s*+}$ by virtue of the local inversion theorem (see [272, ex. 65, p. 200]) whose inverse mapping coincide with the matrix logarithm. Then, there exists $\boldsymbol{b} \in C^1\left(]0, T[, \mathbb{R}^{3\times 3}_s\right)$ such that $\boldsymbol{c} = \exp(\boldsymbol{b})$ i.e. $\boldsymbol{b} = \log(\boldsymbol{c})$. Then

$$\frac{\mathrm{d}}{\mathrm{d}t}(\mathrm{tr}\,\boldsymbol{c}) = \mathrm{tr}\left(\frac{\mathrm{d}\boldsymbol{c}}{\mathrm{d}t}\right) = \mathrm{tr}\left(\frac{\mathrm{d}}{\mathrm{d}t}(\exp\ \boldsymbol{b})\right) = \mathrm{tr}\left((\exp\ \boldsymbol{b})\frac{\mathrm{d}\boldsymbol{b}}{\mathrm{d}t}\right) = \mathrm{tr}\left(\boldsymbol{c}\,\frac{\mathrm{d}}{\mathrm{d}t}(\log\ \boldsymbol{c})\right)$$

The last equality follows as $\dfrac{\mathrm{d}}{\mathrm{d}t}(\log\ \boldsymbol{c})$ is symmetric. □

Lemma 4.11 (derivative of the determinant – Jacobi formula)

$$\frac{\mathrm{d}}{\mathrm{d}t}(\det \boldsymbol{c}) = \mathrm{tr}\left(\det(\boldsymbol{c})\ \boldsymbol{c}^{-1}\ \frac{\mathrm{d}\boldsymbol{c}}{\mathrm{d}t}\right),\ \forall \boldsymbol{c} \in C^1\left(]0, T[, \mathbb{R}^{3\times 3}_{s*}\right) \tag{4.65}$$

Proof See [195, Sect. 8.3, p. 169]. □

Lemma 4.12 (derivative of the trace of the logarithm)

$$\frac{\mathrm{d}}{\mathrm{d}t}\mathrm{tr}(\log(\boldsymbol{c})) = \mathrm{tr}\left(\boldsymbol{c}^{-1}\frac{\mathrm{d}\boldsymbol{c}}{\mathrm{d}t}\right) = \left(\frac{\mathrm{d}\boldsymbol{c}}{\mathrm{d}t}\right) : \boldsymbol{c}^{-1},\ \forall \boldsymbol{c} \in C^1\left(]0, T[, \mathbb{R}^{3\times 3}_{s*+}\right) \tag{4.66}$$

Proof

$$\begin{aligned}\frac{\mathrm{d}}{\mathrm{d}t}\mathrm{tr}(\log(\boldsymbol{c})) &= \frac{\mathrm{d}}{\mathrm{d}t}\log\det\boldsymbol{c}, \quad \text{from (4.63)}\\ &= (\det\boldsymbol{c})^{-1}\frac{\mathrm{d}}{\mathrm{d}t}(\det\boldsymbol{c})\\ &= (\det\boldsymbol{c})^{-1}\mathrm{tr}\left(\det(\boldsymbol{c})\boldsymbol{c}^{-1}\frac{\mathrm{d}\boldsymbol{c}}{\mathrm{d}t}\right), \quad \text{from (4.65)}\\ &= \mathrm{tr}\left(\boldsymbol{c}^{-1}\frac{\mathrm{d}\boldsymbol{c}}{\mathrm{d}t}\right)\end{aligned}$$

The last equality of the lemma is obtained from (4.62). □

Theorem 4.11 (exponential decrease of the free energy)
Let $(\boldsymbol{\chi}, \boldsymbol{u}, p)$ *be a smooth solution of* (4.58a)–(4.58g) *with homogeneous Dirichlet condition* $\boldsymbol{u}_\Gamma = 0$ *and a symmetric definite positive initial value* $\boldsymbol{c}_0$. *Then the free energy defined by* (4.60) *decreases exponentially.*

Proof Note that, when the initial value $\boldsymbol{c}_0$ is symmetric definite positive, from Theorem 4.10, $\boldsymbol{c} - \log\boldsymbol{c} - \boldsymbol{I}$ is well defined and from Lemma 4.7, it is positive. Multiplying (4.58b) by $\boldsymbol{u}$ and integrating leads to

$$\frac{\rho}{2}\frac{\mathrm{d}}{\mathrm{d}t}\int_\Omega |\boldsymbol{u}|^2\,\mathrm{d}x + 2\eta_s\int_\Omega |D(\boldsymbol{u})|^2\,\mathrm{d}x + \int_\Omega \left(\boldsymbol{\chi} + f\left(\frac{a\lambda}{\eta_m}, \boldsymbol{\chi}\right)\right) : D(\boldsymbol{u})\,\mathrm{d}x = 0$$

From the definition (4.57) of f and (4.58c):

$$\left(\boldsymbol{\chi} + f\left(\frac{a\lambda}{\eta_m}, \boldsymbol{\chi}\right)\right) : D(\boldsymbol{u}) = \frac{\eta_m}{a\lambda}\exp\left(\frac{a\lambda}{\eta_m}\boldsymbol{\chi}\right) : D(\boldsymbol{u})$$

and then

$$\frac{\rho}{2}\frac{\mathrm{d}}{\mathrm{d}t}\int_\Omega |\boldsymbol{u}|^2\,\mathrm{d}x + 2\eta_s\int_\Omega |D(\boldsymbol{u})|^2\,\mathrm{d}x + \frac{\eta_m}{a\lambda}\int_\Omega \exp\left(\frac{a\lambda}{\eta_m}\boldsymbol{\chi}\right) : D(\boldsymbol{u})\,\mathrm{d}x = 0 \quad (4.67)$$

Taking the trace of (4.58a) and integrating yields

$$\lambda\frac{\mathrm{d}}{\mathrm{d}t}\int_\Omega \mathrm{tr}(\boldsymbol{\chi})\,\mathrm{d}x + \int_\Omega \mathrm{tr}\left(\boldsymbol{\chi} - f\left(\frac{a\lambda}{\eta_m}, -\boldsymbol{\chi}\right)\right)\mathrm{d}x = 0$$

where we have used the antisymmetry of $\kappa(.,.)$ and (4.58c). From the definition (4.57) of f:

$$\lambda\frac{\mathrm{d}}{\mathrm{d}t}\int_\Omega \mathrm{tr}(\boldsymbol{\chi})\,\mathrm{d}x + \int_\Omega \frac{\eta_m}{a\lambda}\mathrm{tr}\left(\boldsymbol{I} - \exp\left(-\frac{a\lambda}{\eta_m}\boldsymbol{\chi}\right)\right)\mathrm{d}x = 0 \quad (4.68)$$

Contracting (4.58a) with $\exp\left(\frac{a\lambda}{\eta_m}\chi\right)$ and integrating yields

$$\begin{aligned}
&\lambda\int_\Omega \frac{D\boldsymbol{\chi}}{Dt}:\exp\left(\frac{a\lambda}{\eta_m}\boldsymbol{\chi}\right)\,\mathrm{d}x+\lambda\int_\Omega(\boldsymbol{\chi}W(\boldsymbol{u})-W(\boldsymbol{u})\boldsymbol{\chi}):\exp\left(\frac{a\lambda}{\eta_m}\boldsymbol{\chi}\right)\,\mathrm{d}x\\
&+\int_\Omega\left(\boldsymbol{\chi}-\boldsymbol{g}\left(\frac{a\lambda}{\eta_m},-\boldsymbol{\chi}\right)\right):\exp\left(\frac{a\lambda}{\eta_m}\boldsymbol{\chi}\right)\,\mathrm{d}x\\
&+\eta_m\int_\Omega\kappa\left(\frac{a\lambda}{\eta_m}\boldsymbol{\chi},\ D(\boldsymbol{u})\right):\exp\left(\frac{a\lambda}{\eta_m}\boldsymbol{\chi}\right)\,\mathrm{d}x\\
&-2\eta_m\int_\Omega D(\boldsymbol{u}):\exp\left(\frac{a\lambda}{\eta_m}\boldsymbol{\chi}\right)\,\mathrm{d}x=0
\end{aligned}\tag{4.69}$$

From the antisymmetry of $W(\boldsymbol{u})$ and the symmetry of $\boldsymbol{\chi}$ and $\exp\left(\frac{a\lambda}{\eta_m}\boldsymbol{\chi}\right)$ we have:

$$(\boldsymbol{\chi}W(\boldsymbol{u})-W(\boldsymbol{u})\boldsymbol{\chi}):\exp\left(\frac{a\lambda}{\eta_m}\boldsymbol{\chi}\right)=0$$

From property (4.61), as $\boldsymbol{\chi}$ and $\exp\left(\frac{a\lambda}{\eta_m}\boldsymbol{\chi}\right)$ share the same eigensystem:

$$\kappa\left(\frac{a\lambda}{\eta_m}\boldsymbol{\chi},\ D(\boldsymbol{u})\right):\exp\left(\frac{a\lambda}{\eta_m}\boldsymbol{\chi}\right)=0$$

From the definition (4.57) of f:

$$\begin{aligned}
\left(\boldsymbol{\chi}-\boldsymbol{g}\left(\frac{a\lambda}{\eta_m},-\boldsymbol{\chi}\right)\right):\exp\left(\frac{a\lambda}{\eta_m}\boldsymbol{\chi}\right)&=\frac{\eta_m}{a\lambda}\left(\boldsymbol{I}-\exp\left(-\frac{a\lambda}{\eta_m}\boldsymbol{\chi}\right)\right):\exp\left(\frac{a\lambda}{\eta_m}\boldsymbol{\chi}\right)\\
&=\frac{\eta_m}{a\lambda}\mathrm{tr}\left(\exp\left(\frac{a\lambda}{\eta_m}\boldsymbol{\chi}\right)-\boldsymbol{I}\right)
\end{aligned}$$

Applying Lemma 4.10 with $\exp\left(\frac{a\lambda}{\eta_m}\boldsymbol{\chi}\right)$

$$\frac{D\boldsymbol{\chi}}{Dt}:\exp\left(\frac{a\lambda}{\eta_m}\boldsymbol{\chi}\right)=\frac{D}{Dt}\mathrm{tr}\left(\frac{\eta_m}{a\lambda}\exp\left(\frac{a\lambda}{\eta_m}\boldsymbol{\chi}\right)\right)$$

Then (4.69) becomes

$$\begin{aligned}
&\lambda\frac{\mathrm{d}}{\mathrm{d}t}\int_\Omega\mathrm{tr}\left(\frac{\eta_m}{a\lambda}\exp\left(\frac{a\lambda}{\eta_m}\boldsymbol{\chi}\right)\right)\,\mathrm{d}x+\int_\Omega\frac{\eta_m}{a\lambda}\mathrm{tr}\left(\exp\left(\frac{a\lambda}{\eta_m}\boldsymbol{\chi}\right)-\boldsymbol{I}\right)\,\mathrm{d}x\\
&-2\eta_m\int_\Omega D(\boldsymbol{u}):\exp\left(\frac{a\lambda}{\eta_m}\boldsymbol{\chi}\right)\,\mathrm{d}x=0
\end{aligned}\tag{4.70}$$

Combining (4.67) – $(1/(2a\lambda))\times$ (4.68) + $(1/(2a\lambda))\times$ (4.70)

$$\frac{\mathrm{d}}{\mathrm{d}t}\int_\Omega \left(\frac{1}{2a}\mathrm{tr}\left(\frac{\eta_m}{a\lambda}\exp\left(\frac{a\lambda}{\eta_m}\boldsymbol{\chi}\right)-\frac{\eta_m}{a\lambda}\boldsymbol{I}-\boldsymbol{\chi}\right)+\frac{\rho}{2}|\boldsymbol{u}|^2\right)\mathrm{d}x$$
$$+\frac{1}{2a\lambda}\int_\Omega \mathrm{tr}\left(\frac{\eta_m}{a\lambda}\exp\left(\frac{a\lambda}{\eta_m}\boldsymbol{\chi}\right)-\frac{2\eta_m}{a\lambda}\boldsymbol{I}+\frac{\eta_m}{a\lambda}\exp\left(-\frac{a\lambda}{\eta_m}\boldsymbol{\chi}\right)\right)\mathrm{d}x$$
$$+2\,\eta_s\int_\Omega |D(\boldsymbol{u})|^2\,\mathrm{d}x=0$$

Let $\boldsymbol{b}=\frac{\eta_m}{a\lambda}\exp\left(\frac{a\lambda}{\eta_m}\boldsymbol{c}\right)$. Applying Lemma 4.7 to $\boldsymbol{b}^{-1}$ leads to $\mathrm{tr}\left(\boldsymbol{b}^{-1}+\log\,\boldsymbol{b}-\boldsymbol{I}\right)\geqslant 0$ and then

$$\begin{aligned}\mathrm{tr}\left(\boldsymbol{b}-2\,\boldsymbol{I}+\boldsymbol{b}^{-1}\right)&=\mathrm{tr}\,(\boldsymbol{b}-\log\,\boldsymbol{b}-\boldsymbol{I})+\mathrm{tr}\left(\boldsymbol{b}^{-1}+\log\,\boldsymbol{b}-\boldsymbol{I}\right)\\&\geqslant \mathrm{tr}\,(\boldsymbol{b}-\log\,\boldsymbol{b}-\boldsymbol{I})\end{aligned}$$

The previous relation becomes

$$\frac{\mathrm{d}}{\mathrm{d}t}\int_\Omega \left(\frac{1}{2a}\mathrm{tr}\left(\frac{\eta_m}{a\lambda}\exp\left(\frac{a\lambda}{\eta_m}\boldsymbol{\chi}\right)-\frac{\eta_m}{a\lambda}\boldsymbol{I}-\boldsymbol{\chi}\right)+\frac{\rho}{2}|\boldsymbol{u}|^2\right)\mathrm{d}x$$
$$+\int_\Omega \left(\frac{1}{2a\lambda}\mathrm{tr}\left(\frac{\eta_m}{a\lambda}\exp\left(\frac{a\lambda}{\eta_m}\boldsymbol{\chi}\right)-\frac{\eta_m}{a\lambda}\boldsymbol{I}-\boldsymbol{\chi}\right)+2\eta_s|D(\boldsymbol{u})|^2\right)\mathrm{d}x\leqslant 0$$

From Lemma 1.2, p. 34, there exists a constant $c_0>0$ depending only upon Ω such that $c_0\|\boldsymbol{u}\|_{0,2,\Omega}\leqslant\|D(\boldsymbol{u})\|_{0,2,\Omega}$. Then, using the definition (4.43) of $\boldsymbol{\tau}$ we get:

$$\frac{\mathrm{d}}{\mathrm{d}t}\int_\Omega \left(\frac{1}{2a}\mathrm{tr}\,(\boldsymbol{\tau}-\boldsymbol{\chi})+\frac{\rho}{2}|\boldsymbol{u}|^2\right)\mathrm{d}x+\int_\Omega\left(\frac{1}{2a\lambda}\mathrm{tr}\,(\boldsymbol{\tau}-\boldsymbol{\chi})+2\eta_s c_0^2|\boldsymbol{u}|^2\right)\mathrm{d}x\leqslant 0$$

Finally

$$\mathscr{F}'(t)+c_1\mathscr{F}(t)\leqslant 0,\quad \forall t\in\,]0,T[$$

where $c_1=\min\left(\frac{1}{\lambda},\,\frac{4c_0^2\eta_s}{\rho}\right)$. Then, by integration, we obtain $\mathscr{F}(t)\leqslant e^{-c_1 t}\mathscr{F}(0)$ which completes the proof. □

4.14 Example: Driven Cavity Flow

The cavity is a square of width L. The boundary velocity $\boldsymbol{u}_\Gamma$ is zero except on the top boundary $y=L$ where $\boldsymbol{u}_\Gamma(x,L)=(16Ux^2(L-x)^2/L^2,\,0)$ in a Cartesian coordinate system $(0,x,y)$. Here $U>0$ denotes the maximal fluid velocity, that

is reached at the center of the top boundary, while it vanishes at its extremities, i.e. the top left and right corners. Note that this boundary condition differs from those of Sect. 1.12, p. 49, where a constant horizontal velocity was used. The inertia term $(\boldsymbol{u}.\nabla)\boldsymbol{u}$ is neglected, as mostly slow flows are considered here. This is an usual assumption for such flow computation. The dimensional analysis is performed as usual: it reduces the set of parameters to the Weissenberg number, defined by $We = \lambda U/L$, the viscosity ratio $\alpha = \eta_m/(\eta_s + \eta_m)$ and the interpolation parameter of the tensor derivative a. Computations in this section are performed with $\alpha = 1/2$ and $a = 1$ i.e. an upper-convected derivative associated to the Oldroyd-B model. The problem is discretized by the Scott–Vogelius P_2-continuous/P_1-discontinuous finite element pair [292] for the velocity-pressure and the P_1-discontinuous element for the stress. The Scott–Vogelius element pair satisfies exactly the incompressibility relation at the discrete level, which is an improvement as compared with the usual Taylor Hood $P_2 - P_1$ continuous element. In [283], a damped Newton algorithm is proposed for the direct computation of stationary solutions. The implementation of the damped strategy bases on the `Rheolef` library [284, 286, Chap. 8]. For a presentation of the Newton method, see Sect. 2.10, p. 81. Figure 4.23a plots the L^2 norm of the residual term of the stationary problem versus the iteration number of the damped Newton method. The loop is initialized from the Newtonian solution, associated to $We = 0$ and the solution is then computed directly for a specific We. Recall that, without the log-conformation formulation, and before 2005, all numerical computations was limited to $We \leqslant 0.1$ for this benchmark problem. Here, observe the super-linear convergence in log scale, up to $We = 0.5$: the solution is reached with less than ten resolution of linear system, with a residual term close to the machine precision. Observe also that the number of iteration for reaching a prescribed precision is

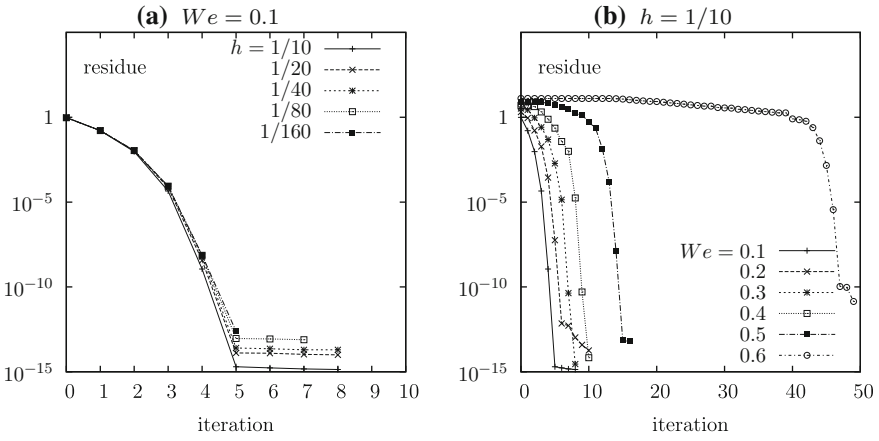

Fig. 4.23 Convergence of the damped Newton algorithm, starting from the solution at $We = 0$ for the viscoelastic Oldroyd-B model on the driven cavity with $\alpha = 1/2$: **a** versus We for a uniform mesh with $h = 1/10$; **b** versus mesh refinement h for $We = 0.1$

roughly mesh invariant. For the last test case, $We = 0.6$ the damped strategy of the Newton method still allows the convergence of the algorithm at the price of a larger number of iteration and the loss of the super-linear convergence. In that case, an Euler-Newton continuation algorithm, which restarts from a previous computed solution at a smaller We, is more efficient. A Weissenberg number increment of 0.1 is used. With this algorithm, each step uses about five resolutions of the Jacobian linear system and the solution at $We = 1$ can be reached from the solution at $We = 0$ with about fifty resolutions of linear systems. Observe also that, for both algorithms, the number of iteration for reaching a prescribed precision is roughly mesh invariant. The current implementation is combined with an auto-adaptive mesh procedure and uses the `Rheolef` library [284–286].

Figure 4.24 shows the adapted meshes and stream function iso-contours for $We = 1, 2$ and 3. The stream function for the driven cavity has already been introduced in Sect. 1.12, p. 49. Ten negative and fifteen positive equi-spaced iso-contours are represented on each plot. Observe that viscoelastic effects break the symmetry observed for the velocity field of cavity flows of viscous Newtonian fluids when inertia terms are neglected. At low Weissenberg number, the flow remains two-dimensional but the center of the primary recirculating vortex in the cavity shifts progressively upstream (left). These results are in qualitative agreement with experimental results [234]. Note also that inertia in viscous Newtonian fluids (i.e. $We = 0$ and $Re > 0$) has opposite effects (see e.g. [285, part 2]): the center of the primary recirculating vortex in the cavity shifts downstream (right).

Figures 4.25 and 4.26 show zooms on the left and right secondary vortices. While the main vortex moves from left to right when We increases, the left vortex grows and the right one decreases in activity. Note that this is also in opposition with inertial effects for viscous Newtonian fluids, as shown in Sect. 1.12, p. 49.

4.15 Notes

Textbooks – In 1987 Bird et al. [27, 28] written a two volume book that is still today the standard reference for the mathematical modeling of viscoelastic fluids. Others classical textbooks on viscoelastic models was written in 1974 by Astarita and Marrucci [5], in 1988 by Larson [174] and in 1997 by Huilgol and Phan-Thien [149]. Experimental observations and details about measurements can be found in Barnes et al. [11] or in Boger and Walters [30], illustrated with impressive photographies. The history of the mathematical analysis of viscoelastic flow problems is presented at the end of Sect. 4.3 while Sect. 4.12 proposes a short review of the development of numerical methods. Textbooks on the mathematical analysis of viscoelastic models was published in 1990 by Joseph [159], then in 2000 by Renardy [254], followed in 2002 by Fernández-Cara, Guillén and Ortega [100]. Textbooks specifically dedicated to numerical methods for viscoelastic fluids was published in 1984 by Crochet et al. [68] and, in 2002, by Owens and Philips [233]. Both these books pointed out

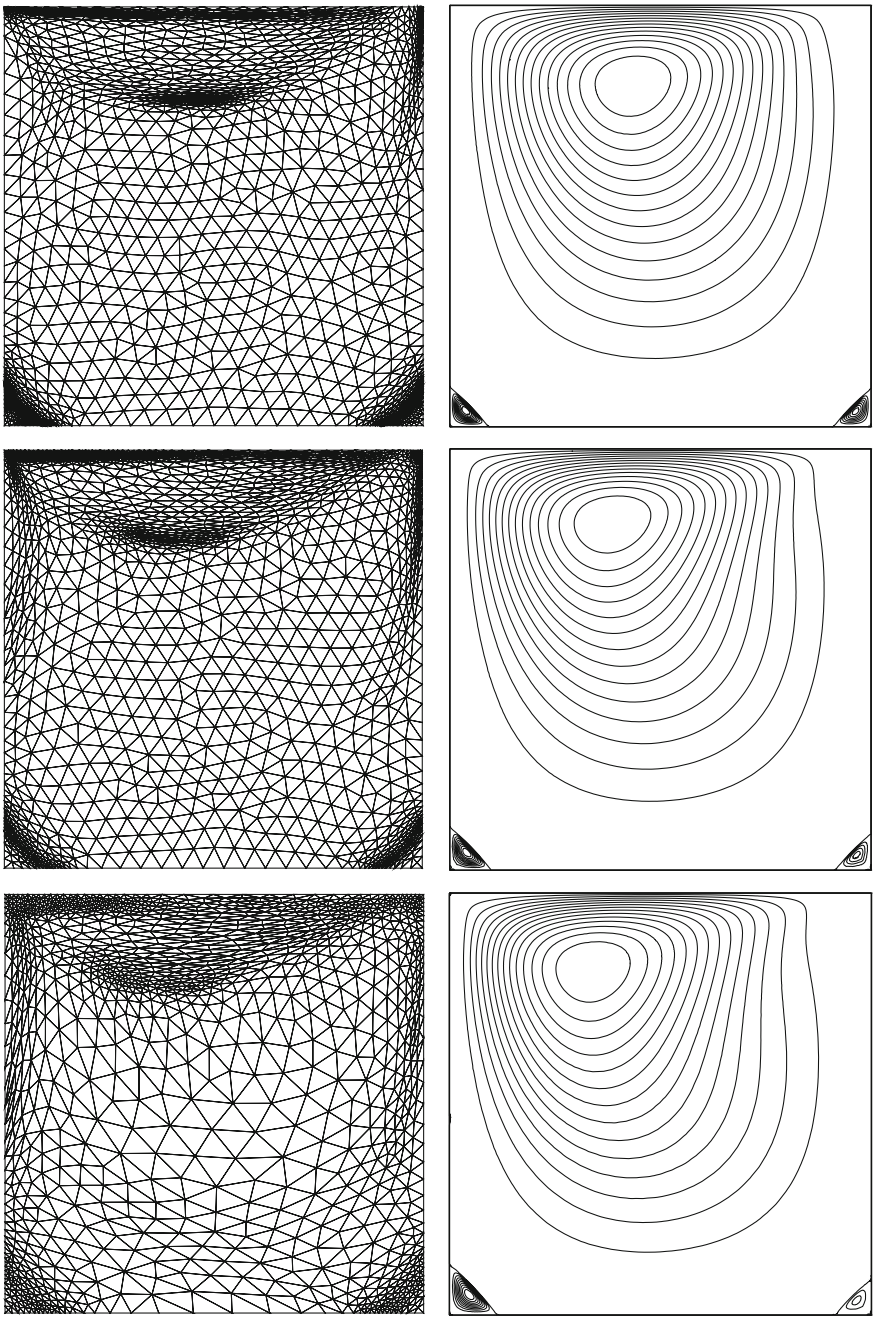

Fig. 4.24 Viscoelastic Oldroyd-B model on the driven cavity with $\alpha = 1/2$. Adapted mesh and stream function iso-contours. From *top* to *bottom*: $We = 1$, 2 and 3

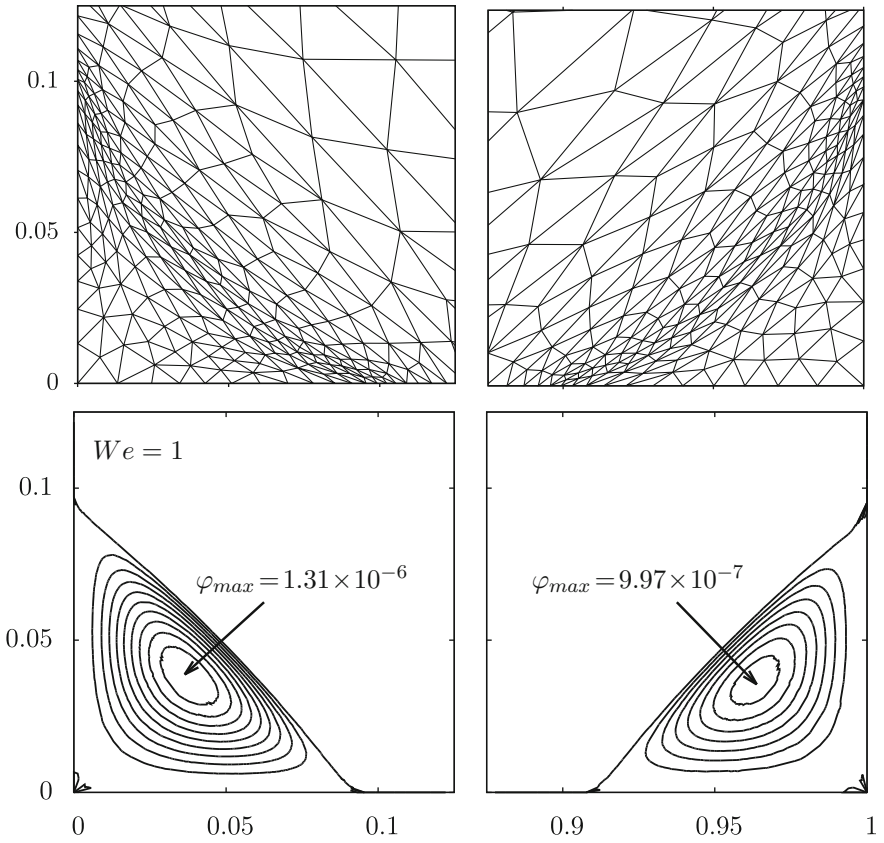

Fig. 4.25 Viscoelastic Oldroyd-B model on the driven cavity with $\alpha = 1/2$. Zoom around vortex for $We = 1$

the high Weissenberg number problem that limited numerical computations. Recall that this problem was solved later, in 2005, as shown in Sect. 4.12.

Algorithms – Earlier computations performed in 1987 by Marchal and Crochet [108, 199] on the stationary problem used a Newton method and a direct solver for the Jacobian. Next, in 1990, Fortin and Fortin [103] experimented an iterative solver for the Jacobian and Saramito [276, 277] proposed the θ-scheme, that allowed to decouple the computation of stresses and velocities (see Sect. 4.6). Decoupled methods had the advantage to be less memory consuming on computers. In 1995, Guénette and Fortin [131] proposed a closely related decoupled idea, the discrete elastic-viscous stress splitting algorithm (DEVSS). Coupled methods made a come back in 2010 with Damanik et al. [71] and Saramito [283] for the log-conformation reformulation of the constitutive equation (see Sect. 4.12).

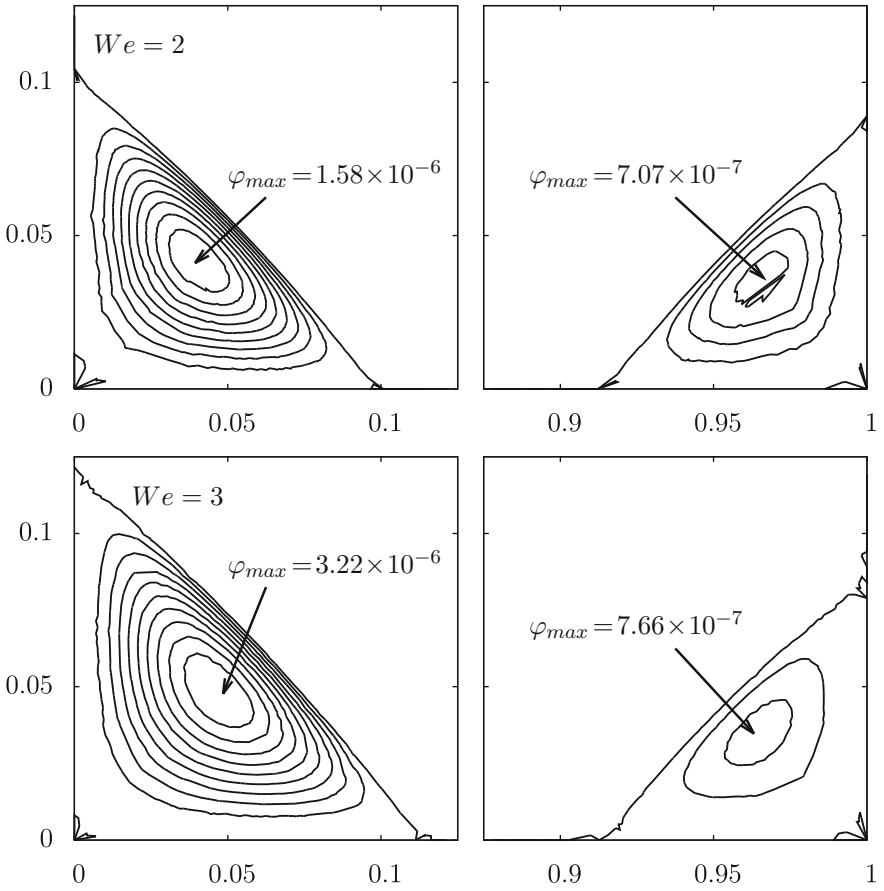

Fig. 4.26 Viscoelastic Oldroyd-B model on the driven cavity with $\alpha = 1/2$. Zoom around vortex for $We = 2$ and 3

Approximations – The compatibility condition between stress and velocity approximations was first pointed out in 1987 by Marchal and Crochet [199] who introduced for quadrangular elements a 4×4 bilinear subdivision of stresses together with biquadratic velocities. This compatibility condition was studied in Sect. 3.11, p. 123, in the context of viscoplastic fluids. Discontinuous stress approximation was introduced in 1989 by Fortin and Fortin [106]. In 1992, Baranger and Sandri [9, 10] reanalyzed the mixed three-field Stokes approximation (see Sect. 4.7) and shown that compatibility condition does not need to be imposed if a solvent viscous contribution is present ($\eta_s > 0$) which allows a much larger class of discretization for stresses. High order polynomial approximations, up to degree 18, was recently addressed in 2013 by Claus and Phillips [60], using the Dubiner modal expansion basis developed by Karniadakis and Sherwin [165], the so-called spectral/*hp* approximation.

Upwinding – The discontinuous Galerkin method is an efficient approach for the discretization of the constitutive equation. This method has been introduced in 1973 by Reed and Hill [252] in the context of steady neutron transport, while its numerical analysis was performed in 1974 by Lesaint and Raviart [185, 186]. Its application to viscoelastic fluids was first experimented in 1989 by Fortin and Fortin [106]. Note that this method has been efficiently extended to equations with diffusion and an application to the Navier-Stokes equation is illustrated in Sect. 1.12. The method of characteristics is an alternative for the discretization of the constitutive equation: it has been proposed in 1987 by Fortin and Esselaoui [15, 105] for viscoelastic fluid. Another alternative is the streamline upwind Petrov Galerkin (SUPG) method: it was first considered in 1987 by Marchal and Crochet [199] and in 2008, Chrispell et al. [54] combined it with the θ-scheme algorithm. Note that this approach requires continuous approximation for stresses.

Models – The present chapter focuses on the generalized Oldroyd model, for which the differential constitutive equation is linear with respect to the elastic stress. The availability of the Oldroyd model to predict non-zero normal stresses and the experimentally observed Weissenberg effect was pointed out in 1958 by Oldroyd [228]. The climbing free surface was computed with the Oldroyd model using a finite element simulation in 1992 by Debbaut and Hocq [76]. Numerical results based on this model are qualitatively in agreement with observation, as shown on Sect. 4.11, but differs quantitatively when compared with experimental measurements. With the long term aim to obtain models able to predict the flow of real viscoelastic fluids, various theories proposed more sophisticated viscoelastic fluid models and the numerical methods presented along this chapter extends to many quasi-linear variants of the Oldroyd model. For instance, Sect. 4.11 presented numerical computations performed with one of them, the Phan-Thien and Tanner model.

Order fluid models – Order fluid models was introduced in 1955 by Rivlin and Ericksen [262] and a recent mathematical review has been proposed in 2011 by Girault and Hecht [117]. Order fluid models could be considered as an intermediate complexity step between quasi-Newtonian models and viscoelastic models and are few used for practical computations in the complex fluid community. See also [233, p. 30] for a discussion on the limitations of order fluid models.

Integral models – Remark 4.7, p. 192, exhibited an explicit expression for the conformation tensor $\boldsymbol{c}$ versus the velocity field $\boldsymbol{u}$ for the generalized Oldroyd model. This expression was proposed inn 2011 by Lee et al. [182, p. 383] and extended also to various models such as the Phan-Thien and Tanner one. This explicit expression involves a single-integral over time and along trajectories. Viscoelastic models of integral type are the generalization of such integral expressions that cannot be equivalently transformed back into partial differential equations (see e.g. [27, Chap. 8] for such models). Then, coupling with the mass and momentum conservations leads to an integro-differential problem. For practical computations with integral models, either a Lagrangian or a streamline integration formulation must be adopted (see [233, p. 163] for a review on this subject). Following Joseph et al. [159, 160], in 1994,

Kwon and Leonov [172, 173] analyzed the stability of the solutions of integral models for small disturbance of data, the so-called Hadamard and dissipative stabilities. This aspect is essential for numerical computations: the solution should not be too sensitive to rounding and approximations. These authors concluded that "*there is no viscoelastic single-integral constitutive equations of factorable type proposed in the literature which can satisfy all the Hadamard and dissipative stability criteria*". In 2013, Chupin [57, 58] presented a global existence result for a modified integral model that include an additional solvent viscosity $\eta_s > 0$. This solvent viscosity is similar to those added in the Maxwell model to obtain the Oldroyd one.

Micro-macro models – Section 4.1 introduces the Oldroyd model as a microscopic scale composed of a dumbbell dilute solution. The equivalence between the Oldroyd model and this microscopic scale description of Hookean dumbbells has been proved, based on the Fokker–Planck equation. in 1987 by Bird et al. [28] and in 1988 by Larson [174]. Another popular variant of the dumbbell model is the finitely extensible non-linear elastic (FENE) model [314] (see also [28]), i.e. a finitely extensible spring at the microscopic scale. It simply expresses that polymer molecules are not infinitely extensible. From this microscopic scale description, and due to its non-linearity, there is no equivalent macroscopic scale model. Nevertheless, an useful approximation to the FENE dumbbell leads to a closed-form differential equation for the elastic stress, the FENE-P model, that looks like the Oldroyd and the Phan-Thien Tanner models, and all the numerical methods presented in this chapter extend also the FENE-P model. The development of micro-macro models is an active area and recent reviews on this subject has been written in 2004 by Keunings [169], in 2011 by Lozinski et al. [193] and in 2012 by Le Bris and Lelièvre [180]. The first research direction aims at obtaining exact or, in most cases, approximate closed form equations at the macroscopic scale and then perform computations. The second research direction aims at overcome the approximation required by the closed form: it perform computations based on the micro scale constitutive equation, coupled with usual mass and momentum conservation equations at macroscopic scale. This approach is referred as a micro-macro computation. Two main numerical approaches has been developed for that purpose, the stochastic simulations and the computations based on the Fokker–Planck equation. In 2014, Griebel and Rüttgers [127] compared the solutions of both the FENE model and its closed form approximation, the FENE-P model, for the flow in an abrupt contraction. These authors used the stochastic simulation method. They showed that these two models significantly differ at steady state and concluded that the FENE-P model does not deliver a good approximation to the FENE model. Computations based on the Fokker–Planck equation developed also rapidly. In 2012, Maitrejean et al. [196] applied it to the flow in a driven cavity.

Turbulence, fiber suspension, liquid crystals – In 1957, Rivlin [261] remarked the analogy between viscoelastic fluids and turbulence closure. It has been extensively employed by the turbulence modeling community, leading to the so-called tensorial $R_{ij} - \varepsilon$ model (see e.g. [177, 297] and [80, Chap. 6]) that extends the scalar $k - \varepsilon$ turbulence model. The study of fiber suspensions started in 1922 when Jeffery [155] studied the motion and orientation of ellipsoidal particles immersed in a viscous

fluid and proposed a model where the orientation information is stored in a tensor that satisfies a differential equation. In 1988, Lipscomb et al. [192], using numerical computations, explored models that incorporates the particle orientation into the stress equation. Recent computations based either on closed form models (see e.g. Latz et al. [176]) or on micro-macro methods (see e.g. Pruliere et al. [245]). Liquid crystal models involves also orientation: in 2007, Sonnet and Ramage [295] computed the flow in a driven cavity of a liquid crystal by using a differential model involving an orientation tensor that satisfies a quasi-linear differential equation with objective tensor derivative. Thus, the method studied in this chapter could be applied to a wide variety of contexts, using some quasi-linear extensions of the Oldroyd model. Finally, the Oldroyd model appears as a template for various modeling such as polymer solutions, turbulence, fiber suspensions and liquid crystals. The following chapter presents elastoviscoplastic fluid models, that could be viewed as a quasi-linear extensions of the Oldroyd model.

Instabilities – Viscoelastic instabilities was introduced in this chapter at Sects. 4.4 and 4.5 for Poiseuille and Couette flows, respectively. The stability issue for viscoelastic flows is an important and challenging problem. For instance, in polymer processing, one wants to explain, predict or avoid possible instabilities. The review papers of Larson [175] and Saut [290] are good starting points for respectively experimental and mathematical approaches (see also [255, p. 250]). Experimental explanations are not yet well understood: its causes are multiple and include e.g. slip at the wall. Conversely, mathematical explanations are also multiple and include change of type of the governing equations, i.e. Hadamard instabilities [159, 160]. In 2012, Saut [290, p. 371] pointed out that, in contrast with the Newtonian case, none of the theoretical results necessary to justify rigorously stability issues have been fully established for the equations governing viscoelastic flows. In any case, viscoelastic instabilities differ from the instabilities which occur in Newtonian flows at high Reynolds numbers (see Sect. 1.6, p. 21). Instabilities that happen at moderate Reynolds numbers, and even at zero Reynolds number, are basically due to the elastic effects.

Chapter 5
Elastoviscoplastic Fluids

The study of elastoviscoplastic models is motivated by a wide range of applications, such as the development of biological tissues, the behavior of cell cytoskeleton and of blood flows in medium arteries. Also, elastoviscoplastic models apply to liquid foams, some polymer solutions or melts in industrial processing, hot metal forming, soil mechanics for geophysical applications such as meteoritic impact or tectonic dynamic of earth. Many of the materials we encounter in our daily life are neither perfectly elastic solids nor simple Newtonian fluids: an attempt to describe these materials as being either fluid or solid often fail. Such materials are sometimes grouped into the term of soft condensed matter which encompasses a broad range of soft materials from colloidal assemblies and gels to emulsions and non-Brownian suspensions. See [31] for a recent review on soft materials. Recent elastoviscoplastic fluid models are able to describe such complex behavior efficiently. Elastoviscoplastic fluid models are more complicated than viscoplastic or viscoelastic one. The elaboration of constitutive equations for such materials requires some precaution: equations should be objective and satisfy the second principle of thermodynamics.

This chapter starts with an introduction to thermodynamics and then develops a robust framework for the development of rheological models: the generalized standard materials. While, in general, checking that a constitutive equation satisfies the second principle is a difficult task, for all constitutive equations developed in this specific framework, the second principle is automatically satisfied. Moreover, this framework opens large possibilities for the development of new constitutive equations. Several examples of such standard materials are studied. All models introduced in the previous chapters of this book fall into this theoretical framework. The elastoviscoplastic model, that combines viscoplastic and viscoelastic effects in the same model, is then elaborated with details. The Poiseuille and Couette flows are then presented for elastoviscoplastic fluids. Finally, the flow around an obstacle is investigated and numerical computations are compared with experimental measurements. This chapter closes with historical notes and new trends and applications of elastoviscoplastic fluids.

P. Saramito, *Complex fluids*, Mathématiques et Applications 79,
DOI 10.1007/978-3-319-44362-1_5

5.1 Conservation of Energy

The first principle of the thermodynamics is the conservation of energy:

Postulate 5.1 *(conservation of energy – non-local form)*
For every material system, at each time, the time derivative of the energy is the sum of the power of the external forces applied to, and of the rate of heat received by the system.

As for the conservation of mass and momentum in Chap. 1, our first aim is to express this postulate by using mathematical notations. At any time $t \geqslant 0$, for any material system $\mathcal{V}(t) \subset \Omega$ transported by the velocity $\boldsymbol{u}$, the energy is the sum of the kinetic energy and the internal energy. The density of the kinetic energy is $\rho|\boldsymbol{u}|^2/2$. We assume that there exists a measure denoted by e and called the *mass density of specific internal energy* of the system, such that ρe is the volume density of internal energy. Then, the energy of any material system $\mathcal{V}(t) \subset \Omega$ is expressed by

$$\int_{\mathcal{V}(t)} \rho \left(\frac{|\boldsymbol{u}|^2}{2} + e \right) \mathrm{d}x$$

The external forces applied are of two kinds: the volume forces, applied inside $\mathcal{V}(t)$, and the surface forces, applied on $\partial\mathcal{V}(t)$. Following the notations introduced in Sect. 1.2, p. 4, the density of internal forces is denoted by ρg and those of surface forces by $\boldsymbol{s}(., \boldsymbol{n})$ where $\boldsymbol{n}$ denotes, as usual, the outer unit normal on $\partial\mathcal{V}(t)$. Then, the power of external forces applied is

$$\int_{\mathcal{V}(t)} \rho\, g.\boldsymbol{u}\, \mathrm{d}x + \int_{\partial\mathcal{V}(t)} \boldsymbol{s}(t, \boldsymbol{x}, \boldsymbol{n}).\boldsymbol{u}\, \mathrm{d}s$$

Recall that, thanks to the Cauchy theorem 1.3, p. 6, the density of surface forces writes $\boldsymbol{s}(., \boldsymbol{n}) = \boldsymbol{\sigma}_{\mathrm{tot}}\boldsymbol{n}$ where $\boldsymbol{\sigma}_{\mathrm{tot}}$ denotes the Cauchy stress tensor.

Conversely, the rate of heat received by the system is of two kinds: volume heat and surface heat. The rate of heat received in the small and arbitrary volume $\mathcal{V}(t) \subset \Omega$ is performed by distance actions, e.g. radiative effects, and its density is denoted by r. Those received on its boundary $\partial\mathcal{V}(t)$ is performed by contact and friction actions, i.e. conduction inside the material, as $\mathcal{V}(t) \subset \Omega$ is inside the flow domain, and its density is denotes by $\chi(., \boldsymbol{n})$. Then, the rate of heat of the material system $\mathcal{V}(t)$ is

$$\int_{\mathcal{V}(t)} r\, \mathrm{d}x + \int_{\partial\mathcal{V}(t)} \chi(t, \boldsymbol{x}, \boldsymbol{n})\, \mathrm{d}s$$

Then, the mathematical expression of the conservation of energy in any material system $\mathcal{V}(t) \subset \Omega$ writes

$$\frac{\mathrm{d}}{\mathrm{d}t}\left(\int_{\mathcal{V}(t)}\rho\left(\frac{|\boldsymbol{u}|^2}{2}+e\right)\mathrm{d}x\right)$$
$$=\int_{\mathcal{V}(t)}\rho\, g.\boldsymbol{u}\,\mathrm{d}x+\int_{\partial\mathcal{V}(t)}(\boldsymbol{\sigma}_{\mathrm{tot}}\boldsymbol{n}).\boldsymbol{u}\,\mathrm{d}s+\int_{\mathcal{V}(t)}r\,\mathrm{d}x+\int_{\partial\mathcal{V}(t)}\chi(t,\boldsymbol{x},\boldsymbol{n})\,\mathrm{d}s \quad (5.1)$$

In order to obtain the conservation of energy in local form, the next step is to obtain an integral over $\mathcal{V}(t)$. There are three terms that are not directly written as an integral over $\mathcal{V}(t)$. The first one is the left-hand-side, which could be treated by using the Reynolds formula. The second is the second term of the right-hand-side, which will requires some rearrangements followed by the Stokes formula. The third one is the last term of the right-hand-side, which will requires a special treatment. Let us start by the following corollary of the Reynolds theorem that will be used several times in this chapter.

Corollary 5.1 (weighted Reynolds formula)
For all sufficiently regular φ defined in Ω and all material system $\mathcal{V}(t)\subset\Omega$ transported by the velocity field $\boldsymbol{u}$, we have

$$\frac{\mathrm{d}}{\mathrm{d}t}\left(\int_{\mathcal{V}(t)}\rho\,\varphi\,\mathrm{d}x\right)=\int_{\mathcal{V}(t)}\rho\left(\frac{\partial\varphi}{\partial t}+\boldsymbol{u}.\nabla\varphi\right)\mathrm{d}x \quad (5.2)$$

Proof From the Reynolds theorem 1.1, p. 3, we get successively:

$$\frac{\mathrm{d}}{\mathrm{d}t}\left(\int_{\mathcal{V}(t)}\rho\,\varphi\,\mathrm{d}x\right)=\int_{\mathcal{V}(t)}\left(\frac{\partial(\rho\varphi)}{\partial t}+\mathrm{div}(\rho\varphi\boldsymbol{u})\right)\mathrm{d}x$$
$$=\int_{\mathcal{V}(t)}\left(\frac{\partial\rho}{\partial t}+\mathrm{div}(\rho\boldsymbol{u})\right)\varphi\,\mathrm{d}x+\int_{\mathcal{V}(t)}\rho\left(\frac{\partial\varphi}{\partial t}+\boldsymbol{u}.\nabla\varphi\right)\mathrm{d}x$$

Then, using the conservation of mass Eq. (1.3), p. 4, the first term of the right-hand-side is zero, which completes the proof. □

Applying the previous theorem with $\varphi=|\boldsymbol{u}|^2/2+e$ leads to

$$\frac{\mathrm{d}}{\mathrm{d}t}\left(\int_{\mathcal{V}(t)}\rho\left(\frac{|\boldsymbol{u}|^2}{2}+e\right)\mathrm{d}x\right)=\int_{\mathcal{V}(t)}\rho\,(\dot{\boldsymbol{u}}.\boldsymbol{u}+\dot{e})\,\mathrm{d}x \quad (5.3)$$

where the dot denotes as usual the Lagrangian derivative $\dot{\varphi}=\dfrac{\partial\varphi}{\partial t}+\boldsymbol{u}.\nabla\varphi$ for any sufficiently regular function φ. Next, let us decompose $\boldsymbol{\sigma}_{\mathrm{tot}}=(\sigma_{i,j})_{1\leqslant i,j\leqslant 3}$ in a Cartesian coordinate system $(0,x_1,x_2,x_3)$. Recall that the Cauchy stress tensor is symmetric, thanks to Theorem 1.6, p. 12. Thus, $(\boldsymbol{\sigma}_{\mathrm{tot}}\boldsymbol{n}).\boldsymbol{u}=(\boldsymbol{\sigma}_{\mathrm{tot}}\boldsymbol{u}).\boldsymbol{n}$. Then, applying the Stokes corollary 1.2, p. 10, with $\boldsymbol{v}=\boldsymbol{\sigma}_{\mathrm{tot}}\boldsymbol{u}$, we get successively

$$\int_{\partial\mathcal{V}(t)}(\boldsymbol{\sigma}_{\mathrm{tot}}\boldsymbol{u}).\boldsymbol{n}\,\mathrm{d}s=\int_{\mathcal{V}(t)}\mathrm{div}(\boldsymbol{\sigma}_{\mathrm{tot}}\boldsymbol{u})\,\mathrm{d}x$$

$$= \int_{\mathcal{V}(t)} \left(\sum_{i,j=1}^{3} \frac{\partial}{\partial x_i} \left(\sigma_{i,j}\, u_j \right) \right) \mathrm{d}x$$
$$= \int_{\mathcal{V}(t)} \left(\sum_{i,j=1}^{3} \frac{\partial \sigma_{i,j}}{\partial x_i} u_j + \sigma_{i,j} \frac{\partial u_j}{\partial x_i} \right) \mathrm{d}x$$

As $\boldsymbol{\sigma}_{\text{tot}}$ is symmetric, we have $\sigma_{i,j} = \sigma_{j,i}$, $1 \leqslant i, j \leqslant 3$ and then

$$\sum_{i,j=1}^{3} \frac{\partial \sigma_{i,j}}{\partial x_i} u_j = \sum_{i,j=1}^{3} \frac{\partial \sigma_{j,i}}{\partial x_i} u_j = \mathbf{div}(\boldsymbol{\sigma}_{\text{tot}}).\boldsymbol{u}$$
$$\sum_{i,j=1}^{3} \sigma_{i,j} \frac{\partial u_j}{\partial x_i} = \sum_{i,j=1}^{3} \frac{\sigma_{i,j} + \sigma_{j,i}}{2} \frac{\partial u_j}{\partial x_i}$$
$$= \frac{1}{2} \sum_{i,j=1}^{3} \sigma_{i,j} \frac{\partial u_j}{\partial x_i} + \frac{1}{2} \sum_{i,j=1}^{3} \sigma_{j,i} \frac{\partial u_j}{\partial x_i}$$
$$= \frac{1}{2} \boldsymbol{\sigma}_{\text{tot}} : \nabla \boldsymbol{u}^T + \frac{1}{2} \boldsymbol{\sigma}_{\text{tot}} : \nabla \boldsymbol{u}$$
$$= \boldsymbol{\sigma}_{\text{tot}} : D(\boldsymbol{u})$$

Thus

$$\int_{\partial \mathcal{V}(t)} (\boldsymbol{\sigma}_{\text{tot}} \boldsymbol{u}).\boldsymbol{n}\, \mathrm{d}s = \int_{\mathcal{V}(t)} \left(\mathbf{div}(\boldsymbol{\sigma}_{\text{tot}}).\boldsymbol{u} + \boldsymbol{\sigma}_{\text{tot}} : D(\boldsymbol{u}) \right) \mathrm{d}x \tag{5.4}$$

Using (5.3) and (5.4), the conservation of energy (5.1) becomes, after rearrangements:

$$\int_{\mathcal{V}(t)} \left(\rho \dot{\boldsymbol{u}} - \mathbf{div}(\boldsymbol{\sigma}_{\text{tot}}) - \rho g \right) .\boldsymbol{u}\, \mathrm{d}x + \int_{\mathcal{V}(t)} \left(\rho \dot{e} - \boldsymbol{\sigma}_{\text{tot}} : D(\boldsymbol{u}) - r \right) \mathrm{d}x$$
$$= \int_{\partial \mathcal{V}(t)} \chi(t, \boldsymbol{x}, \boldsymbol{n})\, \mathrm{d}s$$

Using the conservation of momentum (1.17), p. 11, the first term of the left-hand-side is zero and the conservation of energy reduces to

$$\int_{\mathcal{V}(t)} \left(\rho \dot{e} - \boldsymbol{\sigma}_{\text{tot}} : D(\boldsymbol{u}) - r \right) \mathrm{d}x = \int_{\partial \mathcal{V}(t)} \chi(t, \boldsymbol{x}, \boldsymbol{n})\, \mathrm{d}s \tag{5.5}$$

Theorem 5.1 (existence of the heat flux vector field)
Let φ be a bounded function defined in Ω and χ be a continuous function called the normal rate of heat, defined in $\Omega \times S$ where $S = \{\boldsymbol{\nu} \in \mathbb{R}^3 \,;\ |\boldsymbol{\nu}| = 1\}$ denotes the unit sphere. Assume that

$$\int_{\partial\mathcal{V}} \chi(\boldsymbol{x}, \boldsymbol{n})\, \mathrm{d}s = \int_{\mathcal{V}} \varphi(\boldsymbol{x})\, \mathrm{d}x, \quad \forall \mathcal{V} \subset \Omega$$

where $\boldsymbol{n}$ *denotes the unit outward normal on* $\partial\mathcal{V}$*. Then,* χ *could be extended with respect to its second argument from* S *to* $\mathbb{R}^3$ *as a linear operator, i.e. there exists a vector* $\boldsymbol{q}$*, called the* heat flux*, such that*

$$\chi(\boldsymbol{x}, \boldsymbol{\nu}) = -\boldsymbol{q}(\boldsymbol{x}).\boldsymbol{\nu} \tag{5.6}$$

for all $\boldsymbol{x} \in \Omega$ *and* $\boldsymbol{\nu} \in \mathbb{R}^3$.

Proof Note that this theorem is similar to the Cauchy theorem 1.3, p. 6. The proof is then obtained by choosing, in the Cauchy theorem, vectors $\boldsymbol{s}$ and $\boldsymbol{f}$ whose all components are equal to χ and φ, respectively. □

Note the presence of the minus sign in (5.6): its presence is conventional in the definition of the heat flux. Applying the previous theorem with $\varphi = \rho\dot{e} - \boldsymbol{\sigma}_{\text{tot}} : D(\boldsymbol{u}) - r$, relation (5.5) becomes

$$\int_{\mathcal{V}(t)} (\rho\dot{e} - \boldsymbol{\sigma}_{\text{tot}} : D(\boldsymbol{u}) - r)\, \mathrm{d}x = -\int_{\partial\mathcal{V}(t)} \boldsymbol{q}.\boldsymbol{n}\, \mathrm{d}s$$

Then, applying the Stokes corollary 1.2, p. 10, to the right-hand-side with $\boldsymbol{v} = \boldsymbol{q}$ yields

$$\int_{\mathcal{V}(t)} (\rho\dot{e} - \boldsymbol{\sigma}_{\text{tot}} : D(\boldsymbol{u}) + \operatorname{div} \boldsymbol{q} - r)\, \mathrm{d}x = 0$$

This relation is true at any time $t > 0$ and for any material system $\mathcal{V}(t) \subset \Omega$. Thus, from Lemma 1.1, the relation is true locally at point in Ω and we finally obtain the following local form of the conservation of energy.

Theorem 5.2 (conservation of energy – local form)

$$\rho\left(\frac{\partial e}{\partial t} + \boldsymbol{u}.\nabla e\right) + \operatorname{div} \boldsymbol{q} = \boldsymbol{\sigma}_{\text{tot}} : D(\boldsymbol{u}) + r \quad \textit{in }]0, +\infty[\times \Omega \tag{5.7}$$

5.2 Second Principle of Thermodynamics

Postulate 5.2 *(second principle of thermodynamics – non-local form)*
For every material system, at each time, the time derivative of the entropy is greater than or equal to the rate of external heat supply to the system.

As for the conservation of energy during the previous section, our first aim is to express this postulate by using mathematical notations. We assume that there exists

a measure denoted by s and called the *mass density of specific entropy* of the system, such that ρs is the volume density of entropy. Then, at any time $t \geqslant 0$, for any material system $\mathcal{V}(t) \subset \Omega$, the entropy of this system is expressed by

$$\int_{\mathcal{V}(t)} \rho\, s \, \mathrm{d}x$$

The rate of external supply to the system is of two kinds, the volume rate and the surface one:

$$\int_{\mathcal{V}(t)} \frac{r}{\theta} \, \mathrm{d}x + \int_{\partial\mathcal{V}(t)} \frac{\chi(t, \boldsymbol{x}, \boldsymbol{n})}{\theta} \, \mathrm{d}x$$

Here, r denotes the volume rate of heat density, $\chi(t, \boldsymbol{x}, \boldsymbol{n})$ the surface one and θ is the absolute temperature: it is a strictly positive scalar field. The idea of the division by the temperature interprets as: a rate of heat supply at high temperature has a higher quality than a heat supply at a lower temperature. Recall that, thanks to Theorem 5.1, there exists a flux $\boldsymbol{q}$ such that $\chi(t, \boldsymbol{x}, \boldsymbol{n}) = \boldsymbol{q}.\boldsymbol{n}$. Then, the second principle of thermodynamics writes:

$$\frac{\mathrm{d}}{\mathrm{d}t}\left(\int_{\mathcal{V}(t)} \rho\, s \, \mathrm{d}x\right) \geqslant \int_{\mathcal{V}(t)} \frac{r}{\theta} \, \mathrm{d}x - \int_{\partial\mathcal{V}(t)} \frac{\boldsymbol{q}.\boldsymbol{n}}{\theta} \, \mathrm{d}x$$

Applying the weighted Reynolds corollary 5.1 to the left-hand-side with $\varphi = s$ and the Stokes corollary 1.2, p. 10, to the second term of the right-hand-side with $\boldsymbol{v} = \boldsymbol{q}/\theta$ leads to

$$\int_{\mathcal{V}(t)} \left(\rho \dot{s} + \operatorname{div}\left(\frac{\boldsymbol{q}}{\theta}\right) - \frac{r}{\theta}\right) \mathrm{d}x \geqslant 0$$

This relation is true at any time $t > 0$ and for any material system $\mathcal{V}(t) \subset \Omega$. It is possible to adapt Lemma 1.1, p. 3, to an inequality instead of an equality: the proof of this variant do not pose any difficulty and is left as an exercise to the reader. Thus, the relation is true locally at point in Ω and we finally obtain the following local form of the conservation of energy.

Theorem 5.3 (second principle of thermodynamics – local form)

$$\rho \dot{s} + \operatorname{div}\left(\frac{\boldsymbol{q}}{\theta}\right) - \frac{r}{\theta} \geqslant 0 \quad \textit{in }]0, T[\times \Omega \tag{5.8}$$

Note that, in difference to the first principle, the second principle is an inequality.

Definition 5.1 (*Helmholtz free energy*)
The *free energy*, also called *Helmholtz energy*, is defined by

$$\mathscr{E} = e - s\theta \tag{5.9}$$

Theorem 5.4 (Clausius–Duhem inequality)
The second principle writes equivalently in terms of the free energy:

$$-\rho\left(\dot{\mathscr{E}}+s\dot{\theta}\right)+\boldsymbol{\sigma}_{\text{tot}}:D(\boldsymbol{u})-\nabla\theta.\boldsymbol{q}\geqslant 0\quad in\ ]0,T[\times\Omega \tag{5.10}$$

Proof By differentiation of (5.9) we get

$$\begin{aligned}&\dot{\mathscr{E}}=\dot{e}-\dot{s}\theta-s\dot{\theta}\\ \Longleftrightarrow\ &\rho\theta\dot{s}=\rho\dot{e}-\rho\left(\dot{\mathscr{E}}+s\dot{\theta}\right)\end{aligned}$$

Multiplying (5.8) by θ and expanding leads to

$$\rho\theta\dot{s}+\theta\,\text{div}\left(\frac{\boldsymbol{q}}{\theta}\right)-r\geqslant 0$$

Then, replacing $\rho\theta\dot{s}$ by its previous expression in terms of the free energy leads to

$$\rho\dot{e}-\rho\left(\dot{\mathscr{E}}+s\dot{\theta}\right)+\text{div}(\boldsymbol{q})-\boldsymbol{q}.\nabla\theta-r\geqslant 0$$

Finally, replacing $\rho\dot{e}$ by its expression from (5.7) directly yields the result. Conversely, replacing $\mathscr{E}$ by $e+s\theta$ in the Clausius–Duhem inequality leads to the second principle by the same way. □

In 1822, Fourier [110] proposed the following equation between the heat flux and the temperature.

Definition 5.2 (*Fourier equation*)
The heat flux expresses as

$$\boldsymbol{q}=-\boldsymbol{k}(\theta)\nabla\theta \tag{5.11}$$

where $\boldsymbol{k}(\theta)$ is a symmetric positive tensor called the *diffusion*.

Note that, in its simplest version, $\boldsymbol{k}(\theta)=k\,\boldsymbol{I}$, where the diffusion k is a positive constant. An anisotropic material could be represented with a tensor.

Lemma 5.1 (direction of the heat flux)
Suppose that the heat flux is given by the Fourier equation (5.11)*. Then, the heat flux and the gradient of temperature make an obtuse angle, i.e.*

$$-\frac{\boldsymbol{q}.\nabla\theta}{\theta}\ \geqslant\ 0 \tag{5.12}$$

Proof From (5.11) we have

$$-\frac{\boldsymbol{q}.\nabla\theta}{\theta}=(\boldsymbol{k}(\theta)\nabla\theta).\nabla\theta\ \geqslant\ 0$$

since $\boldsymbol{k}(\theta)$ is a symmetric positive tensor. □

This properties expresses with mathematical notations that the heat flux goes from warm regions to cold ones.

Remark 5.1 (*heat equation*)
When there is no phase transition, the energy e is a smooth function of the temperature and $\dot{e} = c_p\dot{\theta}$, where c_p is the specific heat capacity. Then, using (5.11), the conservation of energy (5.7) becomes,

$$\rho c_p\dot{\theta} - \operatorname{div}(\boldsymbol{k}(\theta)\nabla\theta) = \boldsymbol{\sigma}_{\text{tot}} : D(\boldsymbol{u}) + r \quad \text{in }]0, T[\times\Omega$$

This is the usual heat equation.

Remark 5.2 (*Thers heat flux constitutive equations*)
Note that the Fourier equation is not the only possible way to link the heat flux $\boldsymbol{q}$ and the temperature θ. Various modifications have been proposed over the years. The best known is the Maxwell-Cattane one (see e.g. [56]) that introduces a time delay in the Fourier equation.

5.3 Framework for Constitutive Equations

The elaboration of constitutive equations for complex materials requires some precaution. These equations should be objective, i.e. invariant by change of observers, as pointed out in Sect. 4.2. They also should satisfy the second principle of thermodynamics. In general, checking that a constitutive equation satisfies the second principle is a difficult task. In this section, we present a robust framework for the development of rheological models called the *generalized standard materials*. This framework was initially developed in the 1970s decade by Germain [115] and Halphen and Nguyen [137], for solid materials under the small deformation assumption. Recall that, under the small deformation assumption, the Lagrange derivative and the partial derivative with respect to time can be identified, i.e. if $\boldsymbol{\varepsilon}$ denotes the linearized deformation tensor, then the rate of deformation tensor $D(\boldsymbol{u})$ is identified with $\dot{\boldsymbol{\varepsilon}}$, the partial derivative with respect to time of the linearized deformation tensor. For all constitutive equations developed in this framework, the second principle is automatically satisfied, at least for small deformations, and the development of new constitutive equations becomes easier. Its extension to fluids and large deformations is discussed later in this chapter, together with examples.

5.3.1 Generalized Standard Materials

Definition 5.3 (*standard generalized material*)
A *standard generalized material* is completely defined by two functionals: $\mathscr{E}(\theta, \chi)$, the free energy and $\mathscr{D}(\dot{\chi})$, the energy of dissipation, where $\chi = (\chi_1, \chi_2, \ldots, \chi_m)$,

is the vector of thermodynamical states, of size $m \geqslant 1$ and $\dot{\chi}$ is its Lagrangian derivative. By convention, $\chi_1 = \varepsilon$ is the linearized deformation tensor. When $m \geqslant 2$, $(\chi_i)_{2 \leqslant i \leqslant m}$ represents $m-1$ thermodynamical *internal variables*. Then, the constitutive equations of the material are given by

$$\begin{aligned} \boldsymbol{\sigma}_{\text{tot}} = &\quad \rho \frac{\partial \mathscr{E}}{\partial \varepsilon}(\theta, \chi) + \frac{\partial \mathscr{D}}{\partial \dot{\varepsilon}}(\dot{\chi}) \\ 0 = &\quad \rho \frac{\partial \mathscr{E}}{\partial \chi_i}(\theta, \chi) + \frac{\partial \mathscr{D}}{\partial \dot{\chi}_i}(\dot{\chi}), \quad 2 \leqslant i \leqslant m \\ s = &\quad -\frac{\partial \mathscr{E}}{\partial \theta}(\theta, \chi) \end{aligned}$$

This definition extends to the case where the energy of dissipation $\mathscr{D}$ is not differentiable, e.g. for materials with plasticity. In that case, the constitutive equations of a standard generalized material involve the subdifferential of $\mathscr{D}$ (see Definition 3.2, p. 94) and write

$$\boldsymbol{\sigma}_{\text{tot}} - \rho \frac{\partial \mathscr{E}}{\partial \varepsilon}(\theta, \chi) \in \frac{\partial \mathscr{D}}{\partial \dot{\varepsilon}}(\dot{\chi}) \tag{5.13a}$$

$$-\rho \frac{\partial \mathscr{E}}{\partial \chi_i}(\theta, \chi) \in \frac{\partial \mathscr{D}}{\partial \dot{\chi}_i}(\dot{\chi}), \quad 2 \leqslant i \leqslant m \tag{5.13b}$$

$$s + \frac{\partial \mathscr{E}}{\partial \theta}(\theta, \chi) = 0 \tag{5.13c}$$

A major difficulty for many constitutive equations is to check that the second principle of thermodynamics is satisfied. A definitive advantage for generalized standard materials is the possibility to have a sufficient condition on the dissipation of energy for the second principle to be satisfied, and that this condition is easy to check. The following result presents this property.

Theorem 5.5 (convexity and second principle)
Assume that the energy of dissipation $\mathscr{D}$ is convex, $\mathscr{D} \geqslant 0$ and $\mathscr{D}(0) = 0$ and that the heat flux is given by the Fourier equation (5.11)*. Then the second principle of thermodynamics is satisfied.*

Proof Let $Z = (Z_1, \ldots, Z_m) \in \partial \mathscr{D}(\dot{\chi})$ be any element of the subdifferential of the energy of dissipation. As $\mathscr{D}$ is convex, from the Definition 3.2, p. 94, of the subdifferential, we have, for all $\dot{Y}$:

$$\mathscr{D}(\dot{\chi}) + Z.(\dot{Y} - \dot{\chi}) \leqslant \mathscr{D}(\dot{Y})$$

Choosing $\dot{Y} = 0$, we get $\mathscr{D}(\dot{\chi}) + Z.(0 - \dot{\chi}) \leqslant \mathscr{D}(0)$. Since, from theorem's hypothesis, $\mathscr{D}(0) = 0$, this writes also $Z.\dot{\chi} \geqslant \mathscr{D}(\dot{\chi})$ and since $\mathscr{D} \geqslant 0$, it becomes $Z.\dot{\chi} \geqslant 0$. The constitutive equations (5.13a)–(5.13b) of a generalized standard material write equivalently

$$Z_0 = \left(\boldsymbol{\sigma}_{\text{tot}} - \rho \frac{\partial \mathscr{E}}{\partial \boldsymbol{\varepsilon}}(\theta, \chi), \quad \left(-\rho \frac{\partial \mathscr{E}}{\partial \chi_i}(\theta, \chi) \right)_{2 \leqslant i \leqslant m} \right) \in \partial \mathscr{D}(\dot{\chi})$$

For this particular element Z_0 of the subdifferential of the energy of dissipation, the property $Z_0.\dot{\chi} \geqslant 0$ is also satisfied. Let us denote $\dot{\chi} = \left(\dot{\boldsymbol{\varepsilon}}, \quad (\dot{\chi}_i)_{2 \leqslant i \leqslant m}\right)$. Then

$$Z_0.\dot{\chi} \;\geqslant\; 0 \Longleftrightarrow \left(\boldsymbol{\sigma}_{\text{tot}} - \rho \frac{\partial \mathscr{E}}{\partial \boldsymbol{\varepsilon}}(\theta, \chi) \right).\dot{\boldsymbol{\varepsilon}} - \sum_{i=2}^{m} \rho \frac{\partial \mathscr{E}}{\partial \chi_i}(\theta, \chi).\dot{\chi}_i \;\geqslant\; 0 \qquad (5.14)$$

The derivative of the free energy $\mathscr{E}$ develops as:

$$\begin{aligned} \dot{\mathscr{E}}(\theta, \chi).(\dot{\theta}, \dot{\chi}) &= \frac{\partial \mathscr{E}}{\partial \theta}(\theta, \chi).\dot{\theta} + \frac{\partial \mathscr{E}}{\partial \boldsymbol{\varepsilon}}(\theta, \chi).\dot{\boldsymbol{\varepsilon}} + \sum_{i=2}^{m} \frac{\partial \mathscr{E}}{\partial \chi_i}(\theta, \chi).\dot{\chi}_i \\ &= -s\,\dot{\theta} + \frac{\partial \mathscr{E}}{\partial \boldsymbol{\varepsilon}}(\theta, \chi).\dot{\boldsymbol{\varepsilon}} + \sum_{i=2}^{m} \frac{\partial \mathscr{E}}{\partial \chi_i}(\theta, \chi).\dot{\chi}_i \quad \text{from (5.13c)} \end{aligned}$$

Then, combining with inequality (5.14) leads to

$$-\rho \left(\dot{\mathscr{E}}(\theta, \chi).(\dot{\theta}, \dot{\chi}) + s\,\dot{\theta} \right) + \boldsymbol{\sigma}_{\text{tot}} : \dot{\boldsymbol{\varepsilon}} \geqslant 0$$

Then, under the small deformation assumption, identifying the partial derivative with respect to time $\dot{\boldsymbol{\varepsilon}}$ of the linearized deformation tensor with the rate of deformation $D(\boldsymbol{u})$ yields

$$-\rho \left(\dot{\mathscr{E}} + s\dot{\theta} \right) + \boldsymbol{\sigma}_{\text{tot}} : D(\boldsymbol{u}) - \nabla\theta.\boldsymbol{q} \geqslant 0$$

Finally, as the heat flux is given by the Fourier equation (5.11), from (5.12), it satisfies $-\nabla\theta.\boldsymbol{q} \geqslant 0$ and the previous inequality reduces to the Clausius–Duhem inequality (5.10) which is, from Theorem 5.4, equivalent to the second principle.

□

5.3.2 *Example: Elastic Material*

Figure 5.1 represents an Hookean elastic material both as a rheological diagram and as a generalized standard material. Here μ is the elasticity parameter of the material and μ_c a compressibility parameter. The rheological diagram contains a spring, associated to the elasticity. The spring stores the potential energy, and its element goes to the free energy, while there is no dissipation of energy. With this choice of $\mathscr{E}$ and $\mathscr{D}$, the constitutive equations (5.13a)–(5.13b) reduce, as $\mathscr{E}$ is differentiable and $\mathscr{D}$ is zero, to $\boldsymbol{\sigma}_{\text{tot}} = \rho \mathscr{E}'(\boldsymbol{\varepsilon})$. From the definition of the tensor norm, we have $|\boldsymbol{\varepsilon}|^2 = (\boldsymbol{\varepsilon} : \boldsymbol{\varepsilon})/2$ and

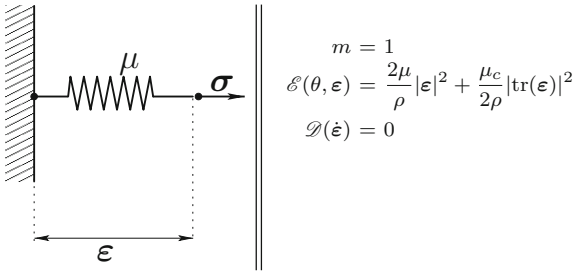

Fig. 5.1 Generalized standard materials: an elastic material

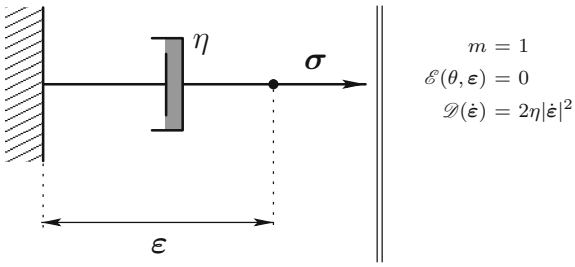

Fig. 5.2 Generalized standard materials: the Newtonian fluid model

then $\rho\mathscr{E}(\varepsilon) = \mu\,(\varepsilon:\varepsilon) + \dfrac{\mu_c}{2}\,|\mathrm{tr}(\varepsilon)|^2$. A short computation shows that the derivative of $|\mathrm{tr}(\varepsilon)|^2$ with respect to ε is $2\,\mathrm{tr}(\varepsilon)\,\boldsymbol{I}$. Thus, we obtain $\boldsymbol{\sigma}_{\mathrm{tot}} = 2\mu\varepsilon + \mu_c \mathrm{tr}(\varepsilon)\,\boldsymbol{I}$ which is the expected result.

5.3.3 *Example: Newtonian Fluid*

Figure 5.2 represents the Newtonian fluid model both as a rheological diagram and as a generalized standard material. Recall that the Newtonian fluid was already introduced in Sect. 1.3, p. 13. The rheological diagram contains a dash-pot, associated to the viscous effect. This element leads to a dissipation effect that goes to the dissipation energy, while the free energy is zero. With these choices for $\mathscr{E}$ and $\mathscr{D}$, the constitutive equations (5.13a)–(5.13b) reduce, as $\mathscr{D}$ is differentiable and $\mathscr{E}$ is zero, to $\boldsymbol{\sigma}_{\mathrm{tot}} = \mathscr{D}'(\dot{\varepsilon})$. From the definition of the tensor norm $|\dot{\varepsilon}|^2 = (\dot{\varepsilon}:\dot{\varepsilon})/2$ we have $\mathscr{D}(\dot{\varepsilon}) = \eta\,\dot{\varepsilon}:\dot{\varepsilon}$ and we obtain $\boldsymbol{\sigma}_{\mathrm{tot}} = 2\eta\dot{\varepsilon}$. When the density ρ is constant, the mass conservation leads to the incompressibility constraint $\mathrm{div}\,\boldsymbol{u} = 0$. Since $\dot{\varepsilon} = D(\boldsymbol{u})$ and $\mathrm{tr}(D(\boldsymbol{u})) = \mathrm{div}\,\boldsymbol{u}$, this constraint expresses also as $\mathrm{tr}(\dot{\varepsilon}) = 0$. The following definition and lemma will help us to deal with incompressible fluids.

Definition 5.4 (*deviatoric indicator*)
The *deviatoric indicator* is defined for all $\boldsymbol{\delta} \in \mathbb{R}^{3\times 3}_s$ by

$$\mathbb{I}_{\mathrm{dev}}(\boldsymbol{\delta}) = \begin{cases} 0 & \text{when } \mathrm{tr}(\boldsymbol{\delta}) = 0 \\ +\infty & \text{otherwise} \end{cases} \tag{5.15}$$

Lemma 5.2 (incompressible material)
Let ϕ_0 be a convex function defined in $\mathbb{R}^{3\times 3}_s$ such that $\phi_0(\boldsymbol{\delta}) < +\infty$ for all $\boldsymbol{\delta} \in \mathbb{R}^{3\times 3}_s$. Let $\phi = \phi_0 + \mathbb{I}_{\text{dev}}$. Then, for all $\boldsymbol{\tau} \in \mathbb{R}^{3\times 3}_s$, the following problems are equivalent:

$$\begin{aligned} & \textit{find } \boldsymbol{\delta} \in \partial\phi^*(\boldsymbol{\tau}) \\ \Longleftrightarrow\ & \textit{find } \boldsymbol{\delta} \in \mathbb{R}^{3\times 3}_s \textit{ and } p \in \mathbb{R} \textit{ such that} \\ & \begin{cases} \partial\phi_0(\boldsymbol{\delta}) - p\,\boldsymbol{I} \ni \boldsymbol{\tau} \\ \operatorname{tr}(\boldsymbol{\delta}) = 0 \end{cases} \end{aligned}$$

Proof Let $\boldsymbol{\tau} \in \mathbb{R}^{3\times 3}_s$ and let us search for $\boldsymbol{\delta} \in \partial\phi^*(\boldsymbol{\tau})$. When $\operatorname{tr}(\boldsymbol{\delta}) \neq 0$, then $\partial\phi(\boldsymbol{\delta}) = \emptyset$. Using Property 3.1, p. 120, that characterizes the subdifferential, we have $\boldsymbol{\tau} \in \partial\phi(\boldsymbol{\delta}) \Longleftrightarrow \boldsymbol{\delta} \in \partial\phi^*(\boldsymbol{\tau})$ and then, the problem $\boldsymbol{\delta} \in \partial\phi^*(\boldsymbol{\tau})$ has no solution. Consider next the case $\operatorname{tr}(\boldsymbol{\delta}) = 0$. By Definition 3.2, p. 94, of the subdifferential

$$\begin{aligned} \partial\phi(\boldsymbol{\delta}) &= \left\{\boldsymbol{\tau} \in \mathbb{R}^{3\times 3}_s\ ;\ \phi_0(\boldsymbol{\delta}) + \boldsymbol{\tau} : (\boldsymbol{\xi} - \boldsymbol{\delta}) \leqslant \phi_0(\boldsymbol{\xi}),\ \ \forall \boldsymbol{\xi} \in \mathbb{R}^{3\times 3}_s \text{ and } \operatorname{tr}(\boldsymbol{\xi}) = 0\right\} \\ &= \left\{\boldsymbol{\tau} \in \mathbb{R}^{3\times 3}_s\ ;\ j_{\boldsymbol{\tau}}(\boldsymbol{\delta}) \leqslant j_{\boldsymbol{\tau}}(\boldsymbol{\xi}),\ \ \forall \boldsymbol{\xi} \in \mathbb{R}^{3\times 3}_s \text{ and } \operatorname{tr}(\boldsymbol{\xi}) = 0\right\} \end{aligned}$$

where $j_{\boldsymbol{\tau}}$ is defined for all $\boldsymbol{\xi} \in \mathbb{R}^{3\times 3}_s$ and $\operatorname{tr}(\boldsymbol{\xi}) = 0$ by $j_{\boldsymbol{\tau}}(\boldsymbol{\xi}) = \phi_0(\boldsymbol{\xi}) - \boldsymbol{\tau} : \boldsymbol{\xi}$. As $\boldsymbol{\tau} \in \partial\phi(\boldsymbol{\delta}) \Longleftrightarrow \boldsymbol{\delta} \in \partial\phi^*(\boldsymbol{\tau})$, then $\boldsymbol{\delta}$ is characterized as the minimum of $j_{\boldsymbol{\tau}}$ over the set of traceless symmetric 3×3 matrices, that we note $\mathbb{R}^{3\times 3}_{s,dev}$ for convenience:

$$\boldsymbol{\delta} = \underset{\boldsymbol{\xi} \in \mathbb{R}^{3\times 3}_{s,dev}}{\arg\min}\ j_{\boldsymbol{\tau}}(\boldsymbol{\xi})$$

This is a constrained minimization problem. Let us introduce the corresponding Lagrangian $L_{\boldsymbol{\tau}}(\boldsymbol{\xi}, q) = j_{\boldsymbol{\tau}}(\boldsymbol{\xi}) + q \operatorname{tr}(\boldsymbol{\xi})$. The minimization problem is equivalent to the following saddle point problem

$$(\boldsymbol{\delta},\, p) = \underset{\boldsymbol{\xi} \in \mathbb{R}^{3\times 3}_{s,dev}}{\arg\min} \max_{q \in \mathbb{R}} L_{\boldsymbol{\tau}}(\boldsymbol{\xi}, q)$$

The saddle point $(\boldsymbol{\delta},\, p) \in \mathbb{R}^{3\times 3}_s \times \mathbb{R}$ is characterized as

$$\frac{\partial L_{\boldsymbol{\tau}}}{\partial \boldsymbol{\xi}}(\boldsymbol{\delta},\, p) \ni 0 \ \text{ and } \ \frac{\partial L_{\boldsymbol{\tau}}}{\partial q}(\boldsymbol{\delta},\, p) = 0$$

which writes equivalently, after expanding the subdifferentials:

$$\begin{aligned} & \text{find } \boldsymbol{\delta} \in \mathbb{R}^{3\times 3}_s \text{ and } p \in \mathbb{R} \text{ such that} \\ & \begin{cases} \partial\phi_0(\boldsymbol{\delta}) - p\,\boldsymbol{I} \ni \boldsymbol{\tau} \\ \operatorname{tr}(\boldsymbol{\delta}) = 0 \end{cases} \end{aligned}$$

which completes the proof. □

For an incompressible fluid the energy of dissipation is defined by $\mathscr{D}(\dot{\varepsilon}) = 2\eta|\dot{\varepsilon}|^2 + \mathbb{I}_{\text{dev}}(\dot{\varepsilon})$. Then, the constitutive equations (5.13a)–(5.13b) reduce, as $\mathscr{E}$ is zero, to $\boldsymbol{\sigma}_{\text{tot}} \in \partial\mathscr{D}(\dot{\varepsilon})$. From Lemma 5.2, the constitutive equation reduces to $\boldsymbol{\sigma}_{\text{tot}} = -p\,\boldsymbol{I} + 2\eta\dot{\varepsilon}$ when the incompressibility constraint $\text{tr}(\dot{\varepsilon}) = 0$ is satisfied, which is the expected result. It means that this constraint is imposed via a Lagrange multiplier p, that coincides with the pressure. Recall that this constitutive equation was previously presented in Sect. 1.3, p. 13.

5.3.4 Example: Herschel–Bulkley Model

Figure 5.3 represents the Herschel–Bulkley [142] model both as a rheological diagram and as a generalized standard material. Recall that the Herschel–Bulkley model was already introduced by its energy of dissipation in (3.1), p. 92, up to the deviatoric indicator $\mathbb{I}_{\text{dev}}$ additional term. Thus, this is an equivalent definition of the Herschel–Bulkley model. The rheological diagram contains a dry-friction element, associated to plasticity and a dash-pot, associated to the non-linear viscous effect, i.e. the consistency and the power law index. All these elements lead to dissipation effects that go to the dissipation energy, while the free energy is zero. With this choice of $\mathscr{E}$ and $\mathscr{D}$, the constitutive equations (5.13a)–(5.13b) write also $\boldsymbol{\sigma}_{\text{tot}} \in \partial\mathscr{D}(\dot{\varepsilon})$. Let φ_0 the convex function defined, for all $\dot{\varepsilon} \in \mathbb{R}^{3\times3}$ by $\varphi_0(\dot{\varepsilon}) = \dfrac{K}{1+n}|2\dot{\varepsilon}|^{1+n} + \sigma_0|2\dot{\varepsilon}|$. Then $\mathscr{D} = \varphi_0 + \mathbb{I}_{\text{dev}}$ and, from Lemma 5.2, when $\text{tr}(\dot{\varepsilon}) = 0$, the constitutive equation reduces to $\boldsymbol{\sigma}_{\text{tot}} + p\,\boldsymbol{I} \in \partial\varphi_0(\dot{\varepsilon})$ where p is the pressure. Using Property 3.1, p. 120, that characterizes the subdifferential, this writes equivalently as $\dot{\varepsilon} \in \partial\varphi_0^*(\boldsymbol{\sigma}_{\text{tot}} + p\,\boldsymbol{I})$ where φ_0^* denotes the convex conjugate, that was introduced at Definition 3.5, p. 120. The following property leads to a new formulation of this model that will be reused later in this chapter.

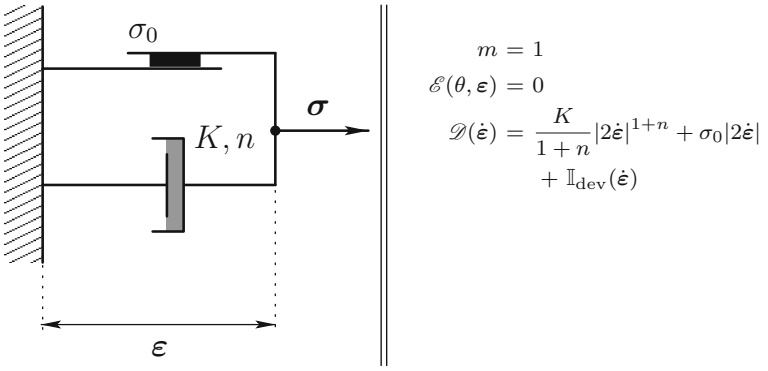

Fig. 5.3 Generalized standard materials: the Herschel–Bulkley model

Lemma 5.3 (convex conjugate of the Herschel–Bulkley dissipation)
Let $\varphi = \varphi_0 + \mathbb{I}_{\mathrm{dev}}$ where φ_0 is the convex function defined, for all $\dot{\boldsymbol{\varepsilon}} \in \mathbb{R}^{3\times 3}$ by $\varphi_0(\dot{\boldsymbol{\varepsilon}}) = \frac{K}{1+n}|2\dot{\boldsymbol{\varepsilon}}|^{1+n} + \sigma_0|2\dot{\boldsymbol{\varepsilon}}|$. The convex conjugate φ^*, as introduced in Definition 3.5 p. 120, is differentiable and it derivative is given, for all $\boldsymbol{\tau} \in \mathbb{R}^{3\times 3}_s$ by

$$\varphi^{*\prime}(\boldsymbol{\tau}) = \begin{cases} \dfrac{1}{2}\left(\dfrac{|\mathrm{dev}(\boldsymbol{\tau})| - \sigma_0}{K}\right)^{\frac{1}{n}} \dfrac{\mathrm{dev}(\boldsymbol{\tau})}{|\mathrm{dev}(\boldsymbol{\tau})|} & \text{when } |\mathrm{dev}(\boldsymbol{\tau})| > \sigma_0 \\ 0 & \text{otherwise} \end{cases}$$
$$= \frac{1}{2}\max\left(0,\ \frac{|\mathrm{dev}(\boldsymbol{\tau})| - \sigma_0}{K\ |\mathrm{dev}(\boldsymbol{\tau})|^n}\right)^{\frac{1}{n}} \mathrm{dev}(\boldsymbol{\tau})$$

Proof The subdifferential of φ_0 was already computed in Lemma 3.4, p. 97. For any $\dot{\boldsymbol{\varepsilon}} \in \mathbb{R}^{3\times 3}_s$ we have

$$\partial\varphi_0(\dot{\boldsymbol{\varepsilon}}) = \begin{cases} \left\{\boldsymbol{\tau} = 2K|2\dot{\boldsymbol{\varepsilon}}|^{-1+n}\dot{\boldsymbol{\varepsilon}} + \sigma_0\dfrac{\dot{\boldsymbol{\varepsilon}}}{|\dot{\boldsymbol{\varepsilon}}|}\right\} & \text{when } \dot{\boldsymbol{\varepsilon}} \neq 0 \\ \{\boldsymbol{\tau} \in \mathbb{R}^{d\times d}_s;\ |\boldsymbol{\tau}| \leqslant \sigma_0\} & \text{otherwise} \end{cases}$$

For any $\dot{\boldsymbol{\varepsilon}} \in \mathbb{R}^{3\times 3}_s$ such that $\dot{\boldsymbol{\varepsilon}} \neq 0$ we have $\boldsymbol{\tau} \in \partial\varphi_0(\dot{\boldsymbol{\varepsilon}})$ if and only if

$$\boldsymbol{\tau} = \left(2^n K|\dot{\boldsymbol{\varepsilon}}|^{-1+n} + \sigma_0\frac{1}{|\dot{\boldsymbol{\varepsilon}}|}\right)\dot{\boldsymbol{\varepsilon}}$$

Then, for any $\dot{\boldsymbol{\varepsilon}} \in \mathbb{R}^{3\times 3}_s$ such that $\mathrm{tr}(\dot{\boldsymbol{\varepsilon}}) = 0$ and $\dot{\boldsymbol{\varepsilon}} \neq 0$ we have, from Lemma 5.2, that $\boldsymbol{\tau} \in \partial\varphi(\dot{\boldsymbol{\varepsilon}})$ if and only if $\boldsymbol{\tau} + p\,\boldsymbol{I} \in \partial\varphi_0(\dot{\boldsymbol{\varepsilon}})$ where p is the Lagrange multiplier associated to the deviatoric constraint. From the previous relation, we have

$$\boldsymbol{\tau} + p\,\boldsymbol{I} = \left(2^n K|\dot{\boldsymbol{\varepsilon}}|^{-1+n} + \sigma_0\frac{1}{|\dot{\boldsymbol{\varepsilon}}|}\right)\dot{\boldsymbol{\varepsilon}}$$

Then, taking the deviatoric part of the previous relation yields

$$\mathrm{dev}(\boldsymbol{\tau}) = \left(2^n K|\dot{\boldsymbol{\varepsilon}}|^{-1+n} + \sigma_0\frac{1}{|\dot{\boldsymbol{\varepsilon}}|}\right)\dot{\boldsymbol{\varepsilon}} \tag{5.16}$$

since $\dot{\boldsymbol{\varepsilon}}$ is traceless. Next, taking the tensor norm of the previous relation yields $|\mathrm{dev}(\boldsymbol{\tau})| = K|2\dot{\boldsymbol{\varepsilon}}|^n + \sigma_0$. This writes equivalently as an expression of $|\dot{\boldsymbol{\varepsilon}}|$ versus $|\mathrm{dev}(\boldsymbol{\tau})|$ i.e. $|\dot{\boldsymbol{\varepsilon}}| = \frac{1}{2}\left(\frac{|\mathrm{dev}(\boldsymbol{\tau})| - \sigma_0}{K}\right)^{\frac{1}{n}}$. Relation (5.16) also expresses that the two tensors $\dot{\boldsymbol{\varepsilon}}$ and $\mathrm{dev}(\boldsymbol{\tau})$ share the same direction. These tensors are also non-

zero and thus $\dfrac{\dot{\varepsilon}}{|\dot{\varepsilon}|} = \dfrac{\mathrm{dev}(\boldsymbol{\tau})}{|\mathrm{dev}(\boldsymbol{\tau})|}$. Finally, using the previous expression of $|\dot{\varepsilon}|$ versus $|\mathrm{dev}(\boldsymbol{\tau})|$, we get:

$$\dot{\varepsilon} = |\dot{\varepsilon}| \frac{\mathrm{dev}(\boldsymbol{\tau})}{|\mathrm{dev}(\boldsymbol{\tau})|} = \frac{1}{2}\left(\frac{|\mathrm{dev}(\boldsymbol{\tau})| - \sigma_0}{K}\right)^{\frac{1}{n}} \frac{\mathrm{dev}(\boldsymbol{\tau})}{|\mathrm{dev}(\boldsymbol{\tau})|}$$

The case $\dot{\varepsilon} = 0$ corresponds to $|\mathrm{dev}(\boldsymbol{\tau})| \leqslant \sigma_0$, and the proof is complete. □

Using $\dot{\varepsilon} = D(\boldsymbol{u})$, this result leads to a new formulation of the Herschel–Bulkley fluid problem:

(P): find $\boldsymbol{\sigma}$, $\boldsymbol{u}$ et p, defined in $]0, T[\times\Omega$ such that

$$\begin{aligned}
\max\left(0, \frac{|\boldsymbol{\sigma}| - \sigma_0}{K|\boldsymbol{\sigma}|^n}\right)^{\frac{1}{n}} \boldsymbol{\sigma} - 2D(\boldsymbol{u}) &= 0 \text{ in }]0, T[\times\Omega \\
\rho\left(\frac{\partial \boldsymbol{u}}{\partial t} + \boldsymbol{u}.\nabla\boldsymbol{u}\right) - \mathbf{div}\,\boldsymbol{\sigma} + \nabla p &= \rho g \text{ in }]0, T[\times\Omega \\
\mathrm{div}\,\boldsymbol{u} &= 0 \text{ in }]0, T[\times\Omega \\
\boldsymbol{u}(t=0) &= \boldsymbol{u}_0 \text{ in } \Omega \\
\boldsymbol{u} &= \boldsymbol{u}_\Gamma \text{ on }]0, T[\times\partial\Omega
\end{aligned}$$

Note that here $\boldsymbol{\sigma}$ is, by construction, proportional to the rate of deformation tensor. It is a deviatoric tensor and thus $\mathrm{dev}(\boldsymbol{\sigma})$ has been replaced by $\boldsymbol{\sigma}$ in the previous equations.

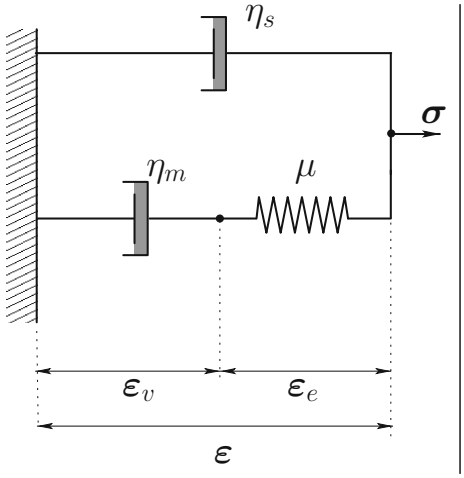

$$\begin{aligned}
m &= 2 \\
\mathscr{E}(\theta, \boldsymbol{\varepsilon}, \boldsymbol{\varepsilon}_e) &= \frac{2\mu}{\rho}|\boldsymbol{\varepsilon}_e|^2 \\
\mathscr{D}(\dot{\boldsymbol{\varepsilon}}, \dot{\boldsymbol{\varepsilon}}_e) &= 2\eta_s|\dot{\boldsymbol{\varepsilon}}|^2 + 2\eta_m|\dot{\boldsymbol{\varepsilon}} - \dot{\boldsymbol{\varepsilon}}_e|^2 \\
&\quad + \mathbb{I}_{\mathrm{dev}}(\dot{\boldsymbol{\varepsilon}})
\end{aligned}$$

Fig. 5.4 Generalized standard materials: the Oldroyd [227] model

5.3.5 Example: Oldroyd Model

Figure 5.4 represents the Oldroyd [227] model both as a rheological diagram and as a generalized standard material. Recall that the Oldroyd model was already introduced in Sect. 4.3, p. 153 as a set of partial differential equations, so the presentation is here different. Let us check that these presentations are equivalent. The rheological diagram contains a spring, associated to the elasticity, and two dash-pots, associated to the viscous effects. The spring stores the potential energy, and its element goes to the free energy, while the two viscous effects go to the energy of dissipation. The diagram involves two deformations, a viscous and an elastic one, and the total deformation is $\varepsilon = \varepsilon_v + \varepsilon_e$. As these three deformations are not independent, we select two of them, say $(\varepsilon, \varepsilon_e)$ as independent variables, where ε_e represents a thermodynamical internal variable. With this choice of $\mathscr{E}$ and $\mathscr{D}$, the constitutive equations (5.13a)–(5.13b) write

$$\begin{cases} \boldsymbol{\sigma}_{\text{tot}} = \rho \dfrac{\partial \mathscr{E}}{\partial \boldsymbol{\varepsilon}}(\boldsymbol{\varepsilon}, \boldsymbol{\varepsilon}_e) + \dfrac{\partial \mathscr{D}}{\partial \dot{\boldsymbol{\varepsilon}}}(\dot{\boldsymbol{\varepsilon}}, \dot{\boldsymbol{\varepsilon}}_e) \\ 0 = \rho \dfrac{\partial \mathscr{E}}{\partial \boldsymbol{\varepsilon}_e}(\boldsymbol{\varepsilon}, \boldsymbol{\varepsilon}_e) + \dfrac{\partial \mathscr{D}}{\partial \dot{\boldsymbol{\varepsilon}}_e}(\dot{\boldsymbol{\varepsilon}}, \dot{\boldsymbol{\varepsilon}}_e) \end{cases}$$

Then, from Lemma 5.2 when $\operatorname{tr}(\dot{\boldsymbol{\varepsilon}}) = 0$ and introducing the pressure p, these relations are equivalent to

$$\begin{aligned} &\begin{cases} \boldsymbol{\sigma}_{\text{tot}} + p\,\boldsymbol{I} = 2\eta_s \dot{\boldsymbol{\varepsilon}} + 2\eta_m(\dot{\boldsymbol{\varepsilon}} - \dot{\boldsymbol{\varepsilon}}_e) \\ 0 = 2\mu \boldsymbol{\varepsilon}_e - 2\eta_m(\dot{\boldsymbol{\varepsilon}} - \dot{\boldsymbol{\varepsilon}}_e) \end{cases} \\ \Longleftrightarrow\ &\begin{cases} \boldsymbol{\sigma}_{\text{tot}} = -p\,\boldsymbol{I} + 2\eta_s \dot{\boldsymbol{\varepsilon}} + \boldsymbol{\tau} \\ \lambda \dot{\boldsymbol{\tau}} + \boldsymbol{\tau} = 2\eta_m \dot{\boldsymbol{\varepsilon}} \end{cases} \end{aligned}$$

where we have defined the elastic stress $\boldsymbol{\tau} = 2\mu\boldsymbol{\varepsilon}_e$ and the relaxation time $\lambda = \eta_m/\mu$. The Lagrangian derivative of the elastic stress tensor $\dot{\boldsymbol{\tau}}$ is not objective, as shown in Sect. 4.2, p. 145. It should be replaced by an objective one, e.g. the interpolated one $\dfrac{\mathscr{D}_a \boldsymbol{\tau}}{\mathscr{D}t}$. Note that these derivatives coincide under the *small deformation* assumption, which consists here to neglect the additional terms of the objective derivative. When the density ρ is constant, the mass conservation leads to the incompressibility constraint $\operatorname{div} \boldsymbol{u}$. This constraint is imposed via a Lagrange multiplier, that coincides with the pressure. We then replace $\boldsymbol{\sigma}_{\text{tot}}$ by $\boldsymbol{\sigma}_{\text{tot}} + p\,\boldsymbol{I}$. Finally, recall that $\dot{\boldsymbol{\varepsilon}} = D(\boldsymbol{u})$. Then, we obtain

$$\begin{aligned} \boldsymbol{\sigma} &= -p\,\boldsymbol{I} + 2\eta_s D(\boldsymbol{u}) + \boldsymbol{\tau} \\ \lambda \frac{\mathscr{D}_a \boldsymbol{\tau}}{\mathscr{D}t} + \boldsymbol{\tau} &= \eta_m \dot{\boldsymbol{\varepsilon}} \end{aligned}$$

These relations coincide with (4.13a)–(4.13b) that was introduced in Chap. 4. The system of equations is closed by adding the mass and momentum conservation and boundary and initial conditions.

5.4 Problem Statement

The previous examples showed how to define some already known models by using the thermodynamical framework. Let us now use this framework to define a new model, that was not yet studied in this book. Figure 5.5 represents the elastoviscoplastic model proposed in 2007 by Saramito [280, 281], both as a rheological diagram and as a generalized standard material. The rheological diagram contains a spring, associated to the elasticity, two dash-pots, associated to the viscous effects and a dry-friction element, associated to plasticity. The spring stores the potential energy, and its element goes to the free energy, while the two viscous effects and the dry-friction goes to the energy of dissipation. The diagram involves two deformations, a viscous and an elastic one, and the total deformation is $\boldsymbol{\varepsilon} = \boldsymbol{\varepsilon}_v + \boldsymbol{\varepsilon}_e$. As these three deformations are not independent, we select two of them, says $(\boldsymbol{\varepsilon}, \boldsymbol{\varepsilon}_e)$ as independent variables, where $\boldsymbol{\varepsilon}_e$ represents a thermodynamical internal variable. Note that, as both $\boldsymbol{\varepsilon}$ and $\boldsymbol{\varepsilon}_p$ are deviatoric tensors, then $\boldsymbol{\varepsilon}_e$ is also a deviator. As this model was not yet introduced in this book, let us derive it as a set of partial differential equations. With this choice of $\mathscr{E}$ and $\mathscr{D}$, the constitutive equations (5.13a)–(5.13b) write

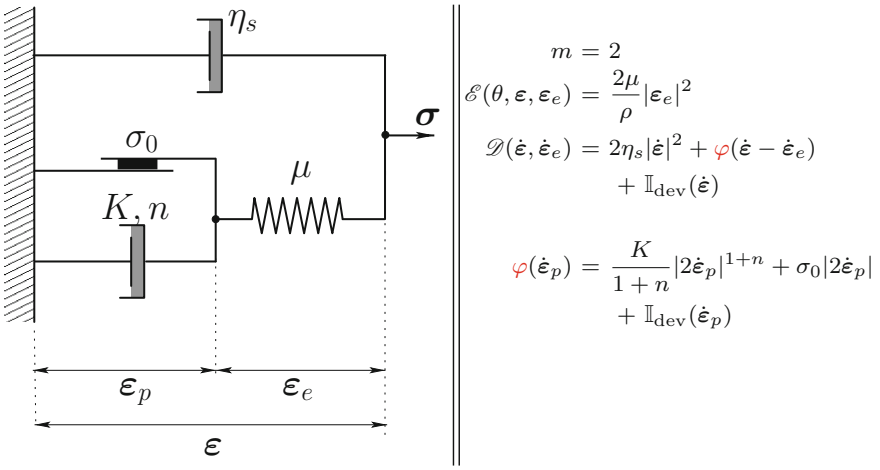

Fig. 5.5 Generalized standard materials: The elastoviscoplastic model [280, 281]

$$\begin{cases} \boldsymbol{\sigma}_{\text{tot}} \in \rho \dfrac{\partial \mathscr{E}}{\partial \boldsymbol{\varepsilon}}(\boldsymbol{\varepsilon}, \boldsymbol{\varepsilon}_e) + \dfrac{\partial \mathscr{D}}{\partial \dot{\boldsymbol{\varepsilon}}}(\dot{\boldsymbol{\varepsilon}}, \dot{\boldsymbol{\varepsilon}}_e) \\ 0 \in \rho \dfrac{\partial \mathscr{E}}{\partial \boldsymbol{\varepsilon}_e}(\boldsymbol{\varepsilon}, \boldsymbol{\varepsilon}_e) + \dfrac{\partial \mathscr{D}}{\partial \dot{\boldsymbol{\varepsilon}}_e}(\dot{\boldsymbol{\varepsilon}}, \dot{\boldsymbol{\varepsilon}}_e) \end{cases}$$

From Lemma 5.2, we introduce the pressure p associated to $\operatorname{tr}(\dot{\boldsymbol{\varepsilon}}) = 0$. The previous relations write equivalently

$$\begin{cases} \boldsymbol{\sigma}_{\text{tot}} + p\, \boldsymbol{I} \in 2\eta_s \dot{\boldsymbol{\varepsilon}} + \partial\varphi(\dot{\boldsymbol{\varepsilon}} - \dot{\boldsymbol{\varepsilon}}_e) \\ 0 \in 2\mu \boldsymbol{\varepsilon}_e - \partial\varphi(\dot{\boldsymbol{\varepsilon}} - \dot{\boldsymbol{\varepsilon}}_e) \end{cases}$$

Let us introduce the elastic stress $\boldsymbol{\tau} = 2\mu\boldsymbol{\varepsilon}_e$. Note that, since $\boldsymbol{\varepsilon}_e$ is a deviator, then $\boldsymbol{\tau}$ is also a deviator. These relations becomes

$$\begin{cases} \boldsymbol{\sigma}_{\text{tot}} = -p\, \boldsymbol{I} + 2\eta_s \dot{\boldsymbol{\varepsilon}} + \boldsymbol{\tau} \\ \boldsymbol{\tau} \in \partial\varphi\left(\dot{\boldsymbol{\varepsilon}} - \dfrac{\dot{\boldsymbol{\tau}}}{2\mu}\right) \end{cases}$$

Using Property 3.1, p. 120, that characterizes the subdifferential of the convex conjugate, we have equivalently

$$\begin{cases} \boldsymbol{\sigma}_{\text{tot}} = -p\, \boldsymbol{I} + 2\eta_s \dot{\boldsymbol{\varepsilon}} + \boldsymbol{\tau} \\ \dot{\boldsymbol{\varepsilon}} - \dfrac{\dot{\boldsymbol{\tau}}}{2\mu} \in \partial\varphi^*(\boldsymbol{\tau}) \end{cases}$$

Note that the functional φ coincides with the energy of dissipation of the Herschel–Bulkley model: its convex conjugate is differentiable and its derivative has already been computed in Lemma 5.3. A necessary condition is that the tensor $\dot{\boldsymbol{\varepsilon}} - \dfrac{\dot{\boldsymbol{\tau}}}{2\mu}$ is deviatoric. As $\dot{\boldsymbol{\varepsilon}}$ is deviatoric, the tensor derivative $\dot{\boldsymbol{\tau}}$ should also be a deviatoric. We have

$$\begin{cases} \boldsymbol{\sigma}_{\text{tot}} = -p\, \boldsymbol{I} + 2\eta_s \dot{\boldsymbol{\varepsilon}} + \boldsymbol{\tau} \\ \dot{\boldsymbol{\varepsilon}} - \dfrac{\dot{\boldsymbol{\tau}}}{2\mu} = \varphi^{*\prime}(\boldsymbol{\tau}) = \dfrac{1}{2} \max\left(0,\ \dfrac{|\operatorname{dev}(\boldsymbol{\tau})| - \sigma_0}{K\ |\operatorname{dev}(\boldsymbol{\tau})|^n}\right)^{\frac{1}{n}} \operatorname{dev}(\boldsymbol{\tau}) \\ \operatorname{tr}(\dot{\boldsymbol{\tau}}) = 0 \end{cases}$$

$$\iff \begin{cases} \boldsymbol{\sigma}_{\text{tot}} = -p\, \boldsymbol{I} + 2\eta_s \dot{\boldsymbol{\varepsilon}} + \boldsymbol{\tau} \\ \dfrac{\dot{\boldsymbol{\tau}}}{\mu} + \max\left(0,\ \dfrac{|\operatorname{dev}(\boldsymbol{\tau})| - \sigma_0}{K\ |\operatorname{dev}(\boldsymbol{\tau})|^n}\right)^{\frac{1}{n}} \operatorname{dev}(\boldsymbol{\tau}) = 2\dot{\boldsymbol{\varepsilon}} \\ \operatorname{tr}(\dot{\boldsymbol{\tau}}) = 0 \end{cases} \tag{5.17}$$

The derivative $\dot{\boldsymbol{\tau}}$ of the elastic tensor is not objective, as shown in Sect. 4.2, p. 145. It should be replaced by an objective one and also this objective derivative should be deviatoric. Recall that, from Lemma 4.1, p. 151, the interpolated derivative of a

deviatoric tensor is not in general deviatoric, at least when $a \neq 0$, which poses a problem for the replacement of the Lagrangian derivative $\dot{\boldsymbol{\tau}}$ by an objective one. A first approach to get around this difficulty was proposed in [280, 281]. The idea is to relax the deviatoric constraint on the elastic stress tensor $\boldsymbol{\tau}$ while using the interpolated tensor derivative. Then, replacing $\dot{\boldsymbol{\varepsilon}}$ by $D(\boldsymbol{u})$, the constitutive equations (5.17) become

$$\left\{\begin{array}{l} \boldsymbol{\sigma}_{\text{tot}} \;=\; -p\,\boldsymbol{I} + 2\eta_s D(\boldsymbol{u}) + \boldsymbol{\tau} \\ \dfrac{1}{\mu}\dfrac{\mathscr{D}_a\boldsymbol{\tau}}{\mathscr{D}t} + \max\left(0,\; \dfrac{|\text{dev}(\boldsymbol{\tau})| - \sigma_0}{K\;|\text{dev}(\boldsymbol{\tau})|^n}\right)^{\frac{1}{n}} \boldsymbol{\tau} \;=\; 2D(\boldsymbol{u}) \end{array}\right. \tag{5.18}$$

Following Remark 4.2, p. 152, the pressure is defined as $\bar{p} = -(1/3)\text{tr}(\boldsymbol{\sigma}_{\text{tot}}) = p - (1/3)\text{tr}(\boldsymbol{\tau})$. It does not in general coincide with p, which is the Lagrange multiplier associated to the incompressibility relation. These two quantities coincide only when using the Jaumann derivative.

A second approach to get around this difficulty is proposed here. The idea is to maintain the deviatoric constraint on the elastic stress tensor $\boldsymbol{\tau}$ while using the following deviatoric variant of the interpolated tensor derivative.

Definition 5.5 (*deviatoric interpolated tensor derivative*)
The *deviatoric interpolated derivative* is defined, for any symmetric tensor $\boldsymbol{\tau}$ by

$$\begin{aligned} \left(\frac{\mathscr{D}_a\boldsymbol{\tau}}{\mathscr{D}t}\right)_{\text{d}} &= \frac{\mathscr{D}_a\boldsymbol{\tau}}{\mathscr{D}t} \;+\; \frac{2a}{3}\text{tr}\left(D(\boldsymbol{u})\boldsymbol{\tau}\right)\,\boldsymbol{I} \\ &= \frac{\partial\boldsymbol{\tau}}{\partial t} + (\boldsymbol{u}.\nabla)\boldsymbol{\tau} - W(\boldsymbol{u})\boldsymbol{\tau} + \boldsymbol{\tau}W(\boldsymbol{u}) \\ &\qquad - a\left(D(\boldsymbol{u})\boldsymbol{\tau} + \boldsymbol{\tau}D(\boldsymbol{u}) - \frac{2}{3}\text{tr}\left(D(\boldsymbol{u})\boldsymbol{\tau}\right)\,\boldsymbol{I}\right) \end{aligned} \tag{5.19}$$

where $a \in \mathbb{R}$ is the parameter of the derivative.

Note that, when $a = 0$, the deviatoric interpolated tensor derivative coincides with the Jaumann derivative.

Property 5.1 (deviatoric interpolated tensor derivative)
The deviatoric interpolated derivative is objective and, when acting on any symmetric deviatoric tensor, it is a symmetric deviatoric tensor.

Proof From Theorem 4.4, p. 151, the interpolated derivative $\dfrac{\mathscr{D}_a\boldsymbol{\tau}}{\mathscr{D}t}$ is objective. Note that, from Lemma 4.1, $\left(\dfrac{\mathscr{D}_a\boldsymbol{\tau}}{\mathscr{D}t}\right)_{\text{d}}$ is simply the deviatoric part of the interpolated derivative when its argument $\boldsymbol{\tau}$ is a deviatoric tensor. As the deviatoric part and the trace are linear and frame invariant operators, the deviatoric interpolated derivative is also objective. □

With this second workaround, the elastic stress tensor $\boldsymbol{\tau}$ is a deviator, the derivative $\dot{\boldsymbol{\tau}}$ is replaced by the deviatoric interpolated derivative $\left(\frac{\mathscr{D}_a \boldsymbol{\tau}}{\mathscr{D}t}\right)_{\mathrm{d}}$ and $\dot{\boldsymbol{\varepsilon}}$ by $D(\boldsymbol{u})$. The elastoviscoplastic model (5.17) becomes

$$\begin{cases} \boldsymbol{\sigma} \;=\; -p\,\boldsymbol{I} + 2\eta_s D(\boldsymbol{u}) + \boldsymbol{\tau} \\ \dfrac{1}{\mu}\left(\dfrac{\mathscr{D}_a \boldsymbol{\tau}}{\mathscr{D}t}\right)_{\mathrm{d}} + \max\left(0,\ \dfrac{|\boldsymbol{\tau}| - \sigma_0}{K\,|\boldsymbol{\tau}|^n}\right)^{\frac{1}{n}} \boldsymbol{\tau} \;=\; 2D(\boldsymbol{u}) \end{cases}$$

Note that, in that case, the pressure coincides with p, the Lagrange multiplier associated with the incompressibility relation. The system of equations is closed by adding the mass and momentum conservations and boundary and initial conditions. The elastoviscoplastic fluid problem writes:

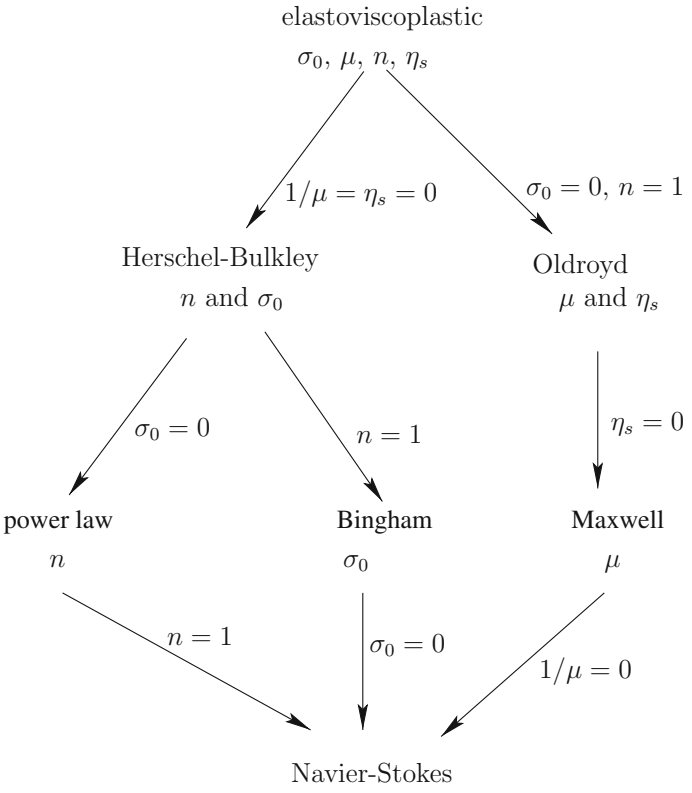

Fig. 5.6 Elastoviscoplastic fluids: a hierarchy of models

(P): find $\boldsymbol{\tau}$, $\boldsymbol{u}$ and p, defined in $]0, T[\times\Omega$ such that

$$\frac{1}{\mu}\left(\frac{\mathscr{D}_a\boldsymbol{\tau}}{\mathscr{D}t}\right)_{\mathrm{d}} + \max\left(0, \frac{|\boldsymbol{\tau}| - \sigma_0}{K\ |\boldsymbol{\tau}|^n}\right)^{\frac{1}{n}} \boldsymbol{\tau} - 2D(\boldsymbol{u}) = 0 \tag{5.20a}$$

$$\rho\left(\frac{\partial \boldsymbol{u}}{\partial t} + \boldsymbol{u}.\nabla\boldsymbol{u}\right) - \mathbf{div}(\boldsymbol{\tau} + 2\eta_s D(\boldsymbol{u}) - p\,\boldsymbol{I}) = \rho g \tag{5.20b}$$

$$\operatorname{div}\boldsymbol{u} = 0 \tag{5.20c}$$

$$\boldsymbol{\tau}(t=0) = \boldsymbol{\tau}_0 \text{ in } \Omega \tag{5.20d}$$

$$\boldsymbol{u}(t=0) = \boldsymbol{u}_0 \text{ in } \Omega \tag{5.20e}$$

$$\boldsymbol{\tau} = \boldsymbol{\tau}_\Gamma \text{ on }]0, T[\times\partial\Omega_- \tag{5.20f}$$

$$\boldsymbol{u} = \boldsymbol{u}_\Gamma \text{ on }]0, T[\times\partial\Omega \tag{5.20g}$$

When the elastic effect vanishes $1/\mu = 0$ and $\eta_s = 0$ we obtain the Herschel–Bulkley model, as formulated in Sect. 5.3.4. Conversely, when the plastic effects vanish, i.e. $\sigma_0 = 0$ and when $n = 1$ the elastoviscoplastic model reduces to a generalized Oldroyd model, associated to the deviatoric interpolated derivative. When both elastic and plastic effects vanishes, i.e. $1/\mu = 0$ and $\sigma_0 = 0$, and $n = 1$, we obtain a Newtonian fluid with a viscosity $\eta_s + \eta_m$. The hierarchy of models is represented on Fig. 5.6. Finally, this elastoviscoplastic model combines and covers the different models studied all along this books. Note that this model was introduced in 2007 by Saramito [280, 281] in a slightly different variant: instead of a deviatoric interpolated derivative, an usual interpolated derivative was considered. These two variants coincide when $a = 0$, i.e. when using the Jaumann derivative in (5.20a). Let us study on some practical flow examples the features of this model.

5.5 Example: Poiseuille Flow

Let us reuse the notations of Sect. 1.5, p. 18 for the Poiseuille flow of a Newtonian fluid. Assume that the flow is laminar: the pressure is given by $p(x, y, z) = -fz + p_0$ where $f > 0$ and $p_0 \in \mathbb{R}$ are given. We first consider the flow between parallel plates. The velocity is parallel to the plates $\boldsymbol{u}(x) = (0, 0, u_z(x))$. Its gradient is given by

$$\nabla\boldsymbol{u} = \begin{pmatrix} 0 & 0 & 0 \\ 0 & 0 & 0 \\ u_z' & 0 & 0 \end{pmatrix}$$

As for viscoelastic fluids and as a major difference with both Newtonian, quasi-Newtonian and viscoplastic fluids, the stress is not in general proportional to the rate of deformation tensor $D(\boldsymbol{u})$, and could develop additional diagonal terms. When using deviatoric interpolated tensor derivatives, the elastic stress tensor $\boldsymbol{\tau}$ is deviatoric. It writes:

$$\boldsymbol{\tau} = \begin{pmatrix} \tau_{xx} & 0 & \tau_{xz} \\ 0 & 0 & 0 \\ \tau_{xz} & 0 & -\tau_{xx} \end{pmatrix}$$

The diagonal component τ_{xx} is called the *normal stress* component. Its apparition is due to the introduction of the $\beta_a(\nabla \boldsymbol{u}, \boldsymbol{\tau})$ term of the tensor objective derivative, that mixes tensor components. Let us expand the $\beta_a(\nabla \boldsymbol{u}, \boldsymbol{\tau})$ term. From its Definition 4.15 and after expansion

$$\text{dev}\,(\beta_a(\nabla \mathbf{u}, \tau)) = \begin{pmatrix} u_z' \tau_{xz} & 0 & -u_z' \tau_{xx} \\ 0 & 0 & 0 \\ -u_z' \tau_{xx} & 0 & -u_z' \tau_{xz} \end{pmatrix}$$

Note that this tensor is independent from the interpolation parameter a of the tensor derivative. Note also that both the inertia term $(\boldsymbol{u}.\nabla)\boldsymbol{u}$ and the elastic stress transport one $(\boldsymbol{u}.\nabla)\boldsymbol{\tau}$ are zero. Indeed, $\boldsymbol{u} = u_z\, \boldsymbol{e}_z$ while ∇ contains just one component $\partial/\partial x$ in the $\boldsymbol{e}_x$ direction and then the operator $\boldsymbol{u}.\nabla$ is zero. Thus, there is no associated upstream boundary condition for the elastic stress. Problem (5.20a)–(5.20g) becomes

(P): find τ_{xx}, τ_{xz} and u_z, defined in $]-L, L[$ such that

$$\begin{aligned} \frac{u_z' \tau_{xz}}{\mu} + \kappa \tau_{xx} &= 0 \ \text{ in } \ ]-L, L[\\ -\frac{u_z' \tau_{xx}}{\mu} + \kappa \tau_{xz} &= u_z' \ \text{ in } \ ]-L, L[\\ -\tau_{xz}' - \eta_s u_z'' &= f \ \text{ in } \ ]-L, L[\\ u_z(-L) = u_z(L) &= 0 \end{aligned}$$

where $\kappa = \max\left(0, \dfrac{|\boldsymbol{\tau}| - \sigma_0}{K|\tau|^n}\right)^{\frac{1}{n}}$ and $|\boldsymbol{\tau}|^2 = \tau_{xx}^2 + \tau_{xz}^2$. This problem presents six physical parameters: μ, σ_0, K, n, f and L. Note that the interpolation parameter a of the tensor derivative does not appear, as we use the deviatoric tensor derivative. In order to reduce the parameter set, let us perform a dimensional analysis. As usual, the dimensionless quantities are denoted with tildes:

$$\tilde{x} = \frac{x}{L}, \quad \tilde{u}(\tilde{x}) = \frac{u_z(L\tilde{x})}{U} \ \text{ and } \ \tilde{\boldsymbol{\tau}}(\tilde{x}) = \frac{\boldsymbol{\tau}(\tilde{x})}{\Sigma}$$

where Σ and U will be chosen later. After this change of unknown, the problem becomes:

$(\tilde{P})$: find $\tilde{\tau}_{xx}$, $\tilde{\tau}_{xz}$ and $\tilde{u}$, defined in $]-1, 1[$ such that

$$\frac{\Sigma}{\mu} \tilde{u}' \tilde{\tau}_{xz} + \frac{L}{U} \left(\frac{\Sigma}{K}\right)^{\frac{1}{n}} \tilde{\kappa} \tilde{\tau}_{xx} = 0 \ \text{ in } \ ]-1, 1[$$

$$
\begin{aligned}
-\frac{\Sigma}{\mu}\tilde{u}'\tilde{\tau}_{xx} + \frac{L}{U}\left(\frac{\Sigma}{K}\right)^{\frac{1}{n}}\tilde{\kappa}\tilde{\tau}_{xz} &= \tilde{u}' \ \text{ in } \ ]-1,1[\\
-\tilde{\tau}'_{xz} - \frac{K_s U}{\Sigma L}\tilde{u}'' &= \frac{fL}{\Sigma} \ \text{ in } \ ]-1,1[\\
\tilde{u}(-1) = \tilde{u}(1) &= 0
\end{aligned}
$$

with $\tilde{\kappa} = \max\left(0, \dfrac{|\tilde{\tau}| - Bi}{|\tilde{\tau}|^n}\right)^{\frac{1}{n}}$ and $Bi = \sigma_0/\Sigma$. Let us choose $\Sigma = fL$ and U such that $K(U/L)^n + \eta_s(U/L) = fL$. Let $We = fL/\mu$ and $\alpha = K(U/L)^n/\Sigma = 1 - \eta_s U/(\Sigma L)$. Exploiting the symmetry of the solution, the previous problem becomes:

(P): find $\tilde{\tau}_{xx}$, $\tilde{\tau}_{xz}$ and $\tilde{u}$, defined in $]0,1[$ such that

$$
\begin{aligned}
We\,\tilde{u}'\tilde{\tau}_{xz} + \alpha^{-\frac{1}{n}}\tilde{\kappa}\tilde{\tau}_{xx} &= 0 \ \text{ in } \ ]0,1[\\
-We\,\tilde{u}'\tilde{\tau}_{xx} + \alpha^{-\frac{1}{n}}\tilde{\kappa}\tilde{\tau}_{xz} &= \tilde{u}' \ \text{ in } \ ]0,1[\\
\tilde{\tau}'_{xz} + (1-\alpha)\tilde{u}'' &= -1 \ \text{ in } \ ]0,1[\\
\tilde{\tau}_{xz}(0) + (1-\alpha)\tilde{u}'(0) = 0 \ \text{ and } \ \tilde{u}(1) &= 0
\end{aligned}
$$

This problem involves only four parameters: $We \geqslant 0$, the Weissenberg number, $Bi \geqslant 0$, the Bingham number, $\alpha \in]0,1]$. the viscosity ratio and n, the power law index. We are looking to compute an explicit solution and, for simplicity, we consider the case $n = 1$ and $\alpha = 1$. The previous problem simplifies as:

(P): find $\tilde{\tau}_{xx}$, $\tilde{\tau}_{xz}$ and $\tilde{u}$, defined in $]0,1[$ such that

$$
\begin{aligned}
We\,\tilde{u}'\tilde{\tau}_{xz} + \tilde{\kappa}\tilde{\tau}_{xx} &= 0 \ \text{ in } \ ]0,1[\\
-We\,\tilde{u}'\tilde{\tau}_{xx} + \tilde{\kappa}\tilde{\tau}_{xz} &= \tilde{u}' \ \text{ in } \ ]0,1[\\
-\tilde{\tau}'_{xz} &= 1 \ \text{ in } \ ]0,1[\\
\tilde{\tau}_{xz}(0) = 0 \ \text{ and } \ \tilde{u}(1) &= 0
\end{aligned}
$$

with $\tilde{\kappa} = \max(0, 1 - Bi/|\tilde{\boldsymbol{\tau}}|)$. By integration, we get $\tilde{\tau}_{xz}(x) = -\tilde{x}$ which is completely solved and the problem reduces to:

(P): find $\tilde{\tau}_{xx}$ and $\tilde{u}$, defined in $]0,1[$ such that

$$
\begin{aligned}
-We\,\tilde{x}\tilde{u}' + \tilde{\kappa}\tilde{\tau}_{xx} &= 0 \ \text{ in } \ ]0,1[&& \text{(5.21a)} \\
-We\,\tilde{u}'\tilde{\tau}_{xx} - \tilde{x}\tilde{\kappa} &= \tilde{u}' \ \text{ in } \ ]0,1[&& \text{(5.21b)} \\
\tilde{u}(1) &= 0 && \text{(5.21c)}
\end{aligned}
$$

with $\tilde{\kappa} = \max\left(0, 1 - Bi/\sqrt{\tilde{x}^2 + \tilde{\tau}_{xx}^2}\right)$. Let us first consider the case when $\tilde{\tau}_{xx}$ and $\tilde{x}$ are such that $\tilde{x}^2 + \tilde{\tau}_{xx}^2 \leqslant Bi^2$. Then $\tilde{\kappa} = 0$ and from (5.21a) we have $-We\,\tilde{x}\tilde{u}' = 0$. In that case, if also $We > 0$ and $\tilde{x} \neq 0$, then, necessarily, we have $\tilde{u}' = 0$. It means that we are in a rigid region and $\tilde{\tau}_{xx}(\tilde{x})$ is undetermined, provided that $|\tilde{\tau}_{xx}(\tilde{x})| \leqslant \sqrt{Bi^2 - \tilde{x}^2}$. The value of the normal stress component $\tilde{\tau}_{xx}(\tilde{x})$ in the rigid region

could be considered as arbitrary. In a time-dependent flow problem, it is provided by the initial condition and it is called the *residual stress*. Here, let us suppose this value is constant, given and equal to $\tilde{\tau}_0 \in \mathbb{R}$. Then, the rigid region terminates at $\tilde{x}_c = \sqrt{Bi^2 - \tilde{\tau}_0^2}$. In particular, when $\tilde{\tau}_0 = 0$, e.g. when the material is initially not pre-stressed, we obtain $\tilde{x}_c = Bi$ as for the Poiseuille flow of a Bingham fluid (see Sect. 3.5, p. 101). Thus, the localization $\tilde{x}_c = Bi$ of the rigid region depends upon the given residual stress $\tilde{\tau}_0$. While it is well determined in a time-dependent problem, it remains undetermined in a stationary one.

Next, let us consider the case when $\tilde{x}^2 + \tilde{\tau}_{xx}^2 > Bi^2$. In that case $\tilde{\kappa} \neq 0$. Multiplying (5.21a) by $\tilde{\tau}_{xx}$, multiplying (5.21b) by $\tilde{\tau}_{xz} = -\tilde{x}$ and summing, we get:

$$|\tilde{\boldsymbol{\tau}}|^2 - Bi\,|\tilde{\boldsymbol{\tau}}| + \tilde{x}\tilde{u}' = 0$$

where $|\tilde{\boldsymbol{\tau}}|^2 = \tilde{x}^2 + \tilde{\tau}_{xx}^2$. This is a second order polynomial equation in $|\tilde{\boldsymbol{\tau}}|$. As $\tilde{x}\tilde{u}' \leqslant 0$, the discriminant $\Delta = Bi^2 - 4\tilde{x}\tilde{u}' \geqslant Bi^2 \geqslant 0$ and there are two roots. The only positive root is $|\tilde{\boldsymbol{\tau}}| = \left(Bi + \sqrt{\Delta}\right)/2$. Then $\tilde{\kappa} = 1 - Bi/|\tilde{\boldsymbol{\tau}}| = \left(\sqrt{\Delta} - Bi\right) / \left(\sqrt{\Delta} + Bi\right)$ depends only upon $\tilde{u}'$ and $\tilde{x}$. From (5.21a) we obtain $\tilde{\tau}_{xx}$ as an expression of $\tilde{u}'$ and $\tilde{x}$ only:

$$\tilde{\tau}_{xx} = \frac{We\,\tilde{x}\tilde{u}'}{\kappa}$$

Replacing in (5.21b) we obtain an equation for $\tilde{u}'$ only:

$$\frac{We^2\,\tilde{x}(\tilde{u}')^2}{\kappa} + \tilde{x}\kappa + \tilde{u}' = 0$$

After multiplying by $\tilde{x}$ and rearranging:

$$\tilde{x}^2 = \frac{\left(-\tilde{x}\tilde{u}'\right)\tilde{\kappa} - We^2\left(-\tilde{x}\tilde{u}'\right)^2}{\tilde{\kappa}^2} \tag{5.22}$$

Let us introduce the dimensionless number $\varepsilon_y = We\,Bi$. From the definition of We and Bi we have $\varepsilon_y = \sigma_0/\mu$ that depend only upon the material parameters of the fluid and no more upon the flow conditions. The number ε_y interprets as a characteristic deformation supported by the material when the stress reaches the yield stress value σ_0. Let $X = 4x/Bi$ and $Y = -4xu'/Bi^2$. After rearrangements, we get from (5.22) an explicit expression of X^2 versus Y as:

$$X^2 = f(Y) = \frac{Y^2\left\{4 - \varepsilon_y^2\left(\sqrt{1+Y}+1\right)^2\right\}}{\left(\sqrt{1+Y}-1\right)^2} \tag{5.23}$$

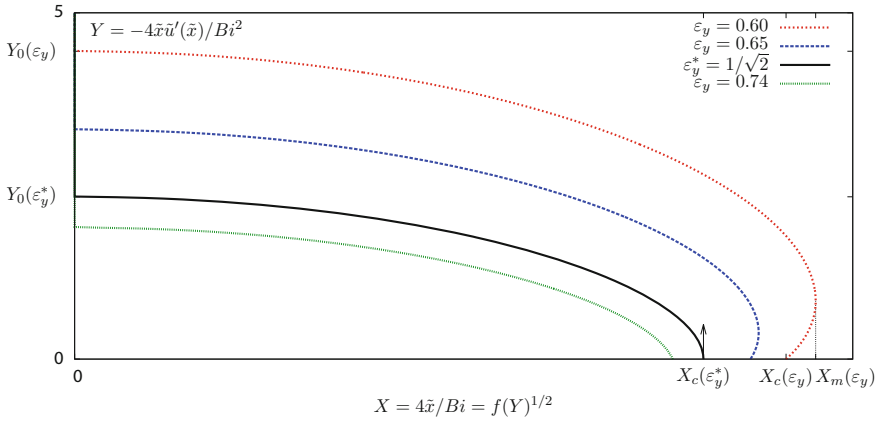

Fig. 5.7 Poiseuille flow of an elastoviscoplastic fluid: turning point $Y = -4\tilde{x}\tilde{u}'(x)/Bi^2$ versus $X = 4\tilde{x}/Bi$ for various values of $\varepsilon_y = We\,Bi$

Figure 5.7 plots X versus Y for various ε_y: clearly, f is not always invertible and presents some turning points for sufficiently large ε_y. It remains to study f with details in order to know when f is invertible or not. Let us compute $f(0)$. Observe that $\sqrt{1+Y} = 1 + Y/2 - Y^2/8 + Y^3/16 + \mathcal{O}(Y^4)$. We are able to extend f by continuity at $Y = 0$ and by expansion we find $f(0) = 16(1-\varepsilon_y^2)$. A necessary condition for the solution to exists is $f(0) \geqslant 0$ i.e. $\varepsilon_y \leqslant 1$. At the boundary between the flowing and the rigid region we have $\tilde{u}' = 0$ i.e. $Y = 0$ and the corresponding abscissa is $X_c = f(Y=0)^{1/2}$ i.e. $\tilde{x}_c = Bi\ f(0)^{1/2}/4 = Bi(1-\varepsilon_y^2)^{1/2}$. It means that $\tilde{u}'(\tilde{x}_c) = 0$. Note that, in the limit case $\tilde{x}_c = 1$, we have $\tilde{u}'(\tilde{x}) = 0$ in all $[0, 1]$. Then, from the boundary condition (5.21c) at $\tilde{x} = 1$, we get $\tilde{u} = 0$ in all $[0, 1]$. This is the arrested state, the material is at rest. Conversely, the flowing condition is $\tilde{x}_c < 1$. Using $\varepsilon_y = We\,Bi$, it writes equivalently $We > \varepsilon_y(1-\varepsilon_y^2)^{1/2}$ and the situation is represented on Fig. 5.8.

Next, let us study the branch $f(Y)$ for $Y \geqslant 0$. From (5.23), the denominator is always positive while the numerator is able to change sign for sufficiently large Y. As f may be positive for the solution $X = f(Y)^{1/2}$ to exist, a necessary condition is $2/\varepsilon_y - 1 \geqslant \sqrt{1+Y}$. As $\varepsilon_y < 1$, the left-hand-side is positive and, taking the square of the previous inequality, we get $Y \leqslant Y_0 = 4(1-\varepsilon_y)/\varepsilon_y^2$. Thus $f(Y_0) = 0$ with $Y_0 > 0$ as $\varepsilon_y < 1$. Since $f(0) > 0$ and f is continuous in $[0, Y_0]$, this implies that f is decreasing on at least one part of $[0, Y_0]$. Moreover, as f is continuous over $[0, Y_0]$, it reaches its maximum on this interval. This maximum could be reached either inside $]0, Y_0[$ or at Y_0, depending upon the value of ε_y, as shown on Fig. 5.7. When this maximum is reached inside $]0, Y_0[$, it is associated to a turning point, denoted as (X_m, Y_m) where $X_m = f(Y_m)^{1/2}$. The turning points are given by the equation $f'(Y) = 0$ with

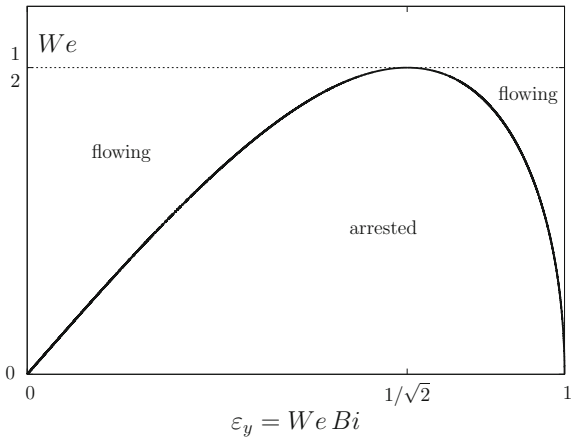

Fig. 5.8 Poiseuille flow of an elastoviscoplastic fluid: condition for the arrested state

$$f'(Y) = \frac{2Y\left\{-\varepsilon_y^2 Y^2 + 2Y + 4 - 4\sqrt{1+Y}\right\}}{\sqrt{1+Y}\left(\sqrt{1+Y}-1\right)^3} \tag{5.24}$$

When Y is large, higher order terms dominate the numerator and $f'(Y) < 0$. Let us compute $f'(0)$ by extending f' at $Y = 0$ by continuity. After expansion at $Y = 0$, we get $f'(0) = 8(1 - 2\varepsilon_y^2)$. Then $f'(0) > 0$ if and only if $\varepsilon_y \leqslant \varepsilon_y^* = 1/\sqrt{2}$. In that case, as $f'(Y)$ changes of sign when Y increases and there always exists a turning point $Y_m > 0$. This turning point Y_m is a zero of the numerator in (5.24) i.e. $-\varepsilon_y^2 Y^2 + 2Y + 4 = 4\sqrt{1+Y}$. Taking the square of the two sides and rearranging, as $Y_m \neq 0$, the previous equation for Y_m is equivalent to:

$$\varepsilon_y^4 Y^2 - 4\varepsilon_y^2 Y + 4 - 8\varepsilon_y^2 = 0$$

This is a second order polynomial equation with two positive roots and its lowest root corresponds to the turning point:

$$Y_m = \frac{2\left(1-\sqrt{2}\varepsilon_y\right)}{\varepsilon_y^2}, \quad X_m = f(Y_m)^{1/2} = \frac{2}{\varepsilon_y}$$

The maximal value $X_m = 4\tilde{x}_m/Bi = 2/\varepsilon_y$ corresponds to a necessary condition for the solution to exists: $\tilde{x}_m \geqslant 1$. Using $\varepsilon_y = We\,Bi$, it writes equivalently $We \leqslant 1/2$. For a practical computation of the solution, we first compute $\tilde{u}'(\tilde{x})$ at fixed $\tilde{x}$ by solving $X^2 = f(Y)$ with a Newton method, as f' is available. Then, $\tilde{u}(\tilde{x})$ is obtained by a numerical integration. The solution is represented on Fig. 5.9 for various We.

Depending upon the residual stress $\tilde{\tau}_0 \in [-Bi\,\varepsilon_Y, Bi\,\varepsilon_Y]$, the localization of the rigid region $\tilde{x}_c \in [\tilde{x}_c^-, \tilde{x}_c^+]$ where $\tilde{x}_c^- = Bi\left(1-\varepsilon_y^2\right)^{1/2}$ and $\tilde{x}_c^+ = Bi$. The regular solution is represented on Fig. 5.9. It corresponds to $\tilde{x}_c = \tilde{x}_c^- = Bi\left(1-\varepsilon_y^2\right)^{1/2}$

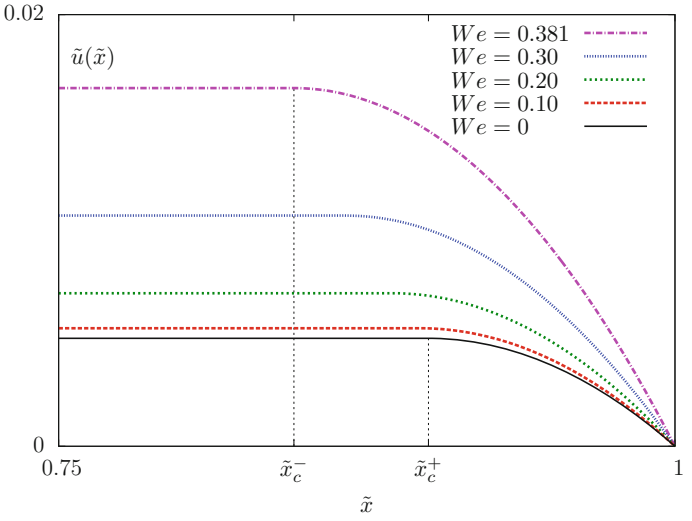

Fig. 5.9 Poiseuille flow of an elastoviscoplastic fluid: ($\alpha = 1$, $Bi = 0.9$): The C^1 solution for various values of We

and $\tilde{\tau}_0 = \pm Bi\, \varepsilon_y$. In that case $|\tilde{\boldsymbol{\tau}}(\tilde{x}_c^-)| = \left(\tilde{\tau}_0^2 + (\tilde{x}_c^-)^2\right)^{1/2} = Bi$. Another possible choice is $\tilde{\tau}_0 = 0$. In that case $\tilde{x}_c = \tilde{x}_c^+ = Bi$ and $|\tilde{\boldsymbol{\tau}}(\tilde{x}_c^+)| = \tilde{x}_c^+ = Bi$. We also have $\tilde{u}'(\tilde{x}) = 0$ for all $\tilde{x} \in [0, Bi[$ and the right limit of $\tilde{u}'(\tilde{x})$ at $\tilde{x} = \tilde{x}_c^+ = Bi$ is non-vanishing: $\tilde{u}'$ presents a discontinuity at $\tilde{x} = Bi$. Finally, when $\tilde{\tau}_0$ covers the interval $[0, Bi\, \varepsilon_y]$, then the localization of the rigid zone $\tilde{x}_c$ covers $[\tilde{x}_c^-, \tilde{x}_c^+]$. The width of this interval of possible localization is $\tilde{x}_c^+ - \tilde{x}_c^- = Bi\left(1 - \left(1 - \varepsilon_y^2\right)^{1/2}\right)$: it growths with both Bi and ε_y. Thus, there is a continuum of solutions and only one solution is C^1, all the others are only C^0. The solutions are represented on Fig. 5.10. For comparison, the solution with a Bingham fluid ($We = 0$) at the same Bingham number is also represented with dotted lines.

We are able to group these results.

Theorem 5.6 (Poiseuille flow of an elastoviscoplastic fluid)
Assume $n = 1$ and $\alpha = 1$. Then, the problem admits a stationary solution if and only if $We \leqslant 1/2$. Moreover, when $We \leqslant \varepsilon_y(1 - \varepsilon_y^2)^{1/2}$, the unique solution is zero and otherwise, there is a continuum of solutions and one of them is smooth.

The non-existence of the stationary solution when $We > 1/2$ could be disappointing: recall that this situation is inherited from the Maxwell viscoelastic model (see Sect. 4.4, p. 155). For viscoelastic fluids, a classical remedy is to add a solvent viscosity $\eta_s > 0$: for the dimensionless problem, this corresponds to $\alpha \in]0, 1[$. This remedy extends to the present elastoviscoplastic model and the case $n = 1$ and $\alpha \in]0, 1[$ could also be investigated in a similar way, with explicit computations. After some computations, it is possible to check that the present model always admits

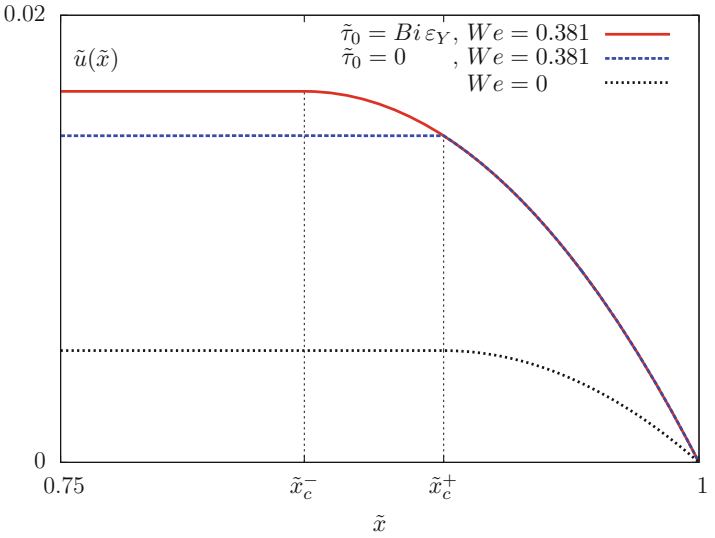

Fig. 5.10 Poiseuille flow of an elastoviscoplastic fluid: ($\alpha = 1$, $Bi = 0.9$, $We = 0.381$): existence of C^0 solutions and the C^1 one; also for comparison, the solution with the Bingham fluid ($We = 0$)

a solution when $\alpha \in]0, 1[$. Moreover, when choosing α small enough, the turning point can be avoided, as in the viscoelastic case.

In conclusion, the stationary flow of an elastoviscoplastic fluid is not unique, even for small dimensionless numbers: it depends upon the residual stress. Note that, in that case, the time dependent problem admits a unique solution, as stresses are provided by initial conditions. This feature dramatically differs from both viscoplastic and viscoelastic fluids. This major feature of elastoviscoplastic fluids is investigated in the following section together with some comparisons with experimental measurements.

5.6 Example: Couette Flow

Figure 5.11 presents the Couette flow of a liquid foam. The Couette flow has been already introduced in Sect. 1.6, p. 21 for a Newtonian fluid. Here, a two-dimensional Couette flow of a foam, confined between two parallel plates of glass, is considered. The inner cylinder moves at angular velocity ω_1 while the outer cylinder is at the rest ($\omega_2 = 0$). Experiments with foams or emulsions, especially in two dimensions, enable an easy visualization of the micro-structure: bubbles or droplets act as tracers for the velocity, the elastic deformation and plasticity. At a larger scale, such materials enable also visualization of global flow heterogeneities. Many studies focus on the velocity profile that can localize near the moving walls: measurements exhibit the coexistence between a flowing region and a region moving as a whole, similar to what

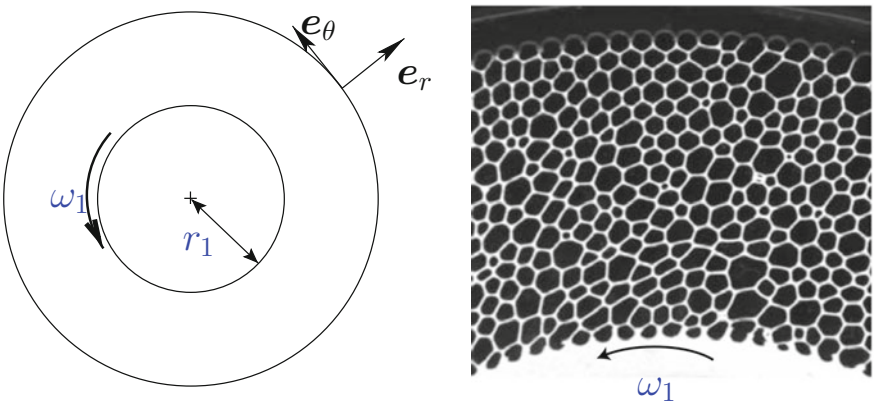

Fig. 5.11 Couette flow of an elastoviscoplastic fluid: (*left*) geometry; (*right*) a liquid foam between two parallel plates (from Debrégeas et al. [162])

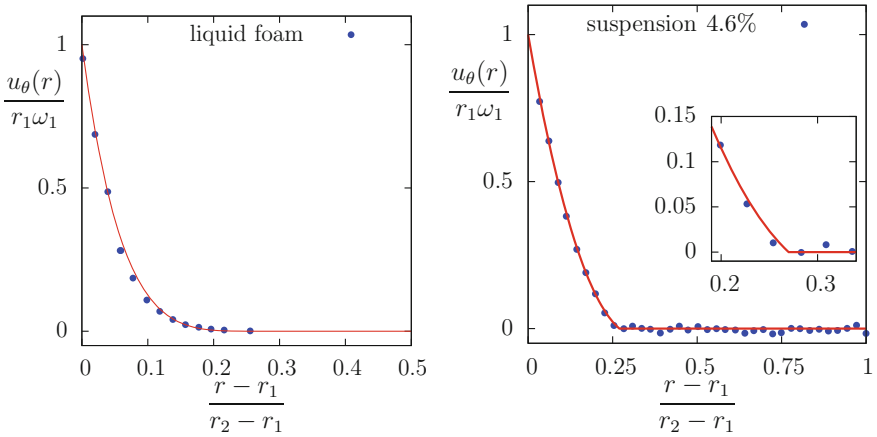

Fig. 5.12 Couette flow of an elastoviscoplastic fluid: (*left*) smooth and (*right*) abrupt velocity profiles. Experimental measurements from Debrégeas et al. [77] and Coussot et al. [67]

has been observed for two- or three-dimensional shear flows of emulsions, colloids or wet granular materials. This observation is also called *shear banding*.

The first study, performed in 2001 by Debrégeas et al. [77] with a liquid foam, reveals a smooth transition between the flowing and non-flowing regions, as shown on Fig. 5.12. The next year, Coussot et al. [67], using both an emulsion and a suspension, exhibited an abrupt transition between the two regions. Next, in 2003, Salmon et al. [273, 274], using worm-like micelles, and in 2004, Lauridsen et al. [178] using a liquid foam, found an abrupt profile. The abrupt profile was also confirmed for a liquid foam in 2006 by Gilbreth et al. [116] and in 2008, by Dennin [78]. In 2008, the debate intensifies when Kätgert et al. [166] observed a smooth profile with a liquid

Fig. 5.13 Couette flow of an elastoviscoplastic fluid: 10 years of debates

year	profile	authors	material
2001	smooth	Debrégeas *et al.*	liquid foam
2002	abrupt	Coussot *et al.*	suspensions, emulsions
2003	abrupt	Salmon *et al.*	worm-like micelles
2004	abrupt	Lauridsen *et al.*	liquid foam
2006	abrupt	Gilbreth *et al.*	liquid foam
2008	abrupt	Dennin	liquid foam
2008	smooth	Kätgert *et al.*	liquid foam
2010	smooth	Coussot *et al.*	suspensions, emulsions
2010	smooth	Ovarlez *et al.*	liquid foam
2010	smooth	Kätgert *et al.*	liquid foam

foam and in 2010, Coussot, Ovarlez et al. [66, 232], using liquid foam, an emulsion and a suspension, observed also a smooth profile. These differences between experimental observations are summarized on Fig. 5.13: they were not clearly understood until, in 2012, Cheddadi et al. [49] proposed an interpretation of the experimental observations, based on a theoretical and numerical investigation using the elastoviscoplastic model presented in this chapter. These results are presented in this section.

The elastoviscoplastic model (5.20a)–(5.20g) is considered here. The solvent viscosity effect is neglected i.e. $\eta_s = 0$. Also, instead of a deviatoric interpolated derivative, in (5.20a), an upper-convected derivative is considered, as in (5.18). This modification corresponds to the model version proposed by Saramito [280, 281]. For the present computation, the upper-convective derivative is considered, i.e. derivative material parameter $a = 1$. For a laminar flow, the velocity writes $\boldsymbol{u} = (0, u_\theta)$ in the two-dimensional polar coordinate system (r, θ). Moreover u_θ depends only upon the time t and r. Its gradient is given by

$$\nabla \boldsymbol{u} = \begin{pmatrix} 0 & 0 \\ \dfrac{\partial u_\theta}{\partial r} - \dfrac{u_\theta}{r} & 0 \end{pmatrix}$$

As for the Poiseuille flow of a viscoelastic fluids (see Sect. 4.4, p. 155), the stress is not in general proportional to the rate of deformation tensor $D(\boldsymbol{u})$, and could develop additional diagonal terms:

$$\boldsymbol{\tau} = \begin{pmatrix} \tau_{rr} & \tau_{r\theta} \\ \tau_{\theta r} & \tau_{\theta\theta} \end{pmatrix}$$

The two additional diagonal components are called *normal stress* components. After expansion of the equations on the axis, the problem writes:

(P): find $\tau_{rr}, \tau_{r\theta}, \tau_{\theta\theta}$ and u_θ defined in $]0, T[\times]r_1, r_2[$ such that

$$\frac{1}{\mu}\frac{\partial \tau_{rr}}{\partial t} + \max\left(0, \frac{|\mathrm{dev}(\boldsymbol{\tau})| - \sigma_0}{K\,|\mathrm{dev}(\boldsymbol{\tau})|^n}\right)^{\frac{1}{n}} \tau_{rr} = 0$$

$$
\begin{aligned}
\frac{1}{\mu}\left(\frac{\partial \tau_{r\theta}}{\partial t} - \dot{\varepsilon}_{r\theta}\tau_{rr}\right) + \max\left(0, \frac{|\mathrm{dev}(\boldsymbol{\tau})| - \sigma_0}{K\,|\mathrm{dev}(\boldsymbol{\tau})|^n}\right)^{\frac{1}{n}} \tau_{r\theta} &= \dot{\varepsilon}_{r\theta} \\
\frac{1}{\mu}\left(\frac{\partial \tau_{\theta\theta}}{\partial t} - 2\dot{\varepsilon}_{r\theta}\tau_{r\theta}\right) + \max\left(0, \frac{|\mathrm{dev}(\boldsymbol{\tau})| - \sigma_0}{K\,|\mathrm{dev}(\boldsymbol{\tau})|^n}\right)^{\frac{1}{n}} \tau_{\theta\theta} &= 0 \\
\rho\frac{\partial u_\theta}{\partial t} - \frac{1}{r^2}\frac{\partial}{\partial r}\left(r^2\tau_{r\theta}\right) &= 0 \\
u_\theta(r_1) = r_1\omega_1 \text{ and } u_\theta(r_2) &= 0 \\
\tau_{rr}(t=0),\ \tau_{r\theta}(t=0),\ \tau_{\theta\theta}(t=0) &\quad \text{are given}
\end{aligned}
$$

with the notation $\dot{\varepsilon}_{r\theta} = \dfrac{\partial u_\theta}{\partial r} - \dfrac{u_\theta}{r}$ and $|\mathrm{dev}(\boldsymbol{\tau})|^2 = \tau_{r\theta}^2 + (\tau_{rr} - \tau_{\theta\theta})^2/4$. A characteristic length is $L = r_2 - r_1$, the distance between the two cylinders, and a characteristic velocity is $U = \omega_1 r_1$, the velocity of the inner cylinder. Then, a characteristic time is U/L, a characteristic stress is $K(U/L)^n = K(\omega_1 r_1/(r_2 - r_1))^n$ and the problem can be rewritten in dimensionless form. There are three dimensionless numbers: the Weissenberg number $We = 2^{\frac{n-1}{2}} K U^n/(\mu L^n)$, the Bingham one $Bi = 2^{1-\frac{n}{2}}\sigma_0 L^n/(K U^n)$ and the power law index n. Note the power of two factors in the definition of Bi and We: these factors are inserted for compatibility purpose with the values of the Bingham and Weissenberg numbers used in [49], that were associated to a slightly different definition the tensor norm and, consequently, also to a different definition of the yield stress and the consistency (see also Remark 2.1, p. 64). With these definitions, a characteristic deformation of the material when the stress reaches the yield value is given by $\varepsilon_y = \sigma_0/\mu = \sqrt{2}We\,Bi$. This quantity was introduced in the previous paragraph when studying the Poiseuille flow. A supplementary dimensionless number characterize the confinement of the Couette geometry: $\beta = r_1/r_2$. When the two radii are close, this number is close to one. Conversely, when the curvature is extreme, e.g. when the inner radius becomes small, this number tends to zero. In the study presented by Cheddadi et al. [49], this number was fixed to $\beta = 71/122 \approx 0.582$, as in the experimental setup of both Debrégeas et al. [77]. and Coussot et al. [67]. The influence of the following initial condition for the stress is investigated:

$$
\boldsymbol{\tau}(t=0) = \begin{pmatrix} 0 & 0 \\ 0 & \tau_{\theta\theta}^* \end{pmatrix}
$$

where $\tau_{\theta\theta}^* \in \mathbb{R}$ is a given constant. Two extremal cases and an intermediate one are studied:

$\tau_{\theta\theta}^*$	interpretation
$+2\sigma_0$	pre-stress
0	no pre-stress
$-2\sigma_0$	pre-stress

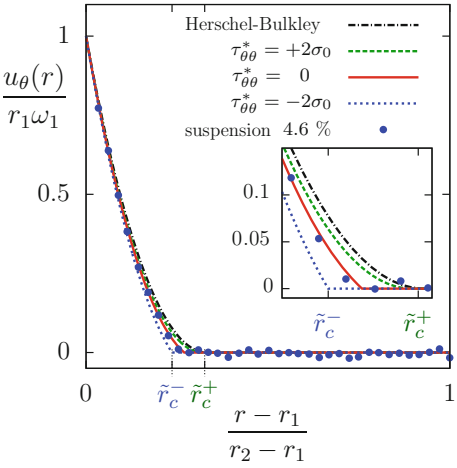

Fig. 5.14 Couette flow of an elastoviscoplastic fluid: computation of an abrupt profile with $We = 0.026$, $Bi = 27$, $n = 1$, $a = 1$ by Cheddadi et al. [49] and measurements by Coussot et al. [67]

The numerical computations are shown on Fig. 5.14 together with experimental measurements by Coussot et al. [67]. Observe the good concordance between the computation and the experimental measurement when $\tau^*_{\theta\theta} = 0$ i.e. when the material is not pre-stressed: it was the case of the present experimental setup in Coussot et al. [67]. In that case, the profile is abrupt, both for the experimental observation and the numerical simulation. Conversely, the pre-stress cases $\tau^*_{\theta\theta} = \pm 2\sigma_0$ lead to different profiles, either abrupt or smooth: they do not correspond to any observation by Coussot et al. [67]. Also, it is coherent with the experimental setup, as the materials was not pre-stressed for this experiment. Finally, the velocity profile obtained with the Herschel–Bulkley model is represented: it is smooth and does not correspond to the experimental measurement. The dimensionless numbers We and Bi were evaluated from the physical parameters σ_0, K, n and μ that were obtained by experimental measurements.

Figure 5.15 shows another computation together with experimental measurements by Debrégeas et al. [77]. Observe the good concordance between the computation and the experimental measurement when $\tau^*_{\theta\theta} = 2\sigma_0$ i.e. when the material is pre-stressed: it was the case of the present experimental setup. In the experiment, a steady state was reached after a transient regime. The rotation direction was then inverted, and after a second transient another steady state was reached: this was when measurements are recorded. In that case, the profile was smooth, both for the experimental observation and the numerical simulation.

There is a complex interplay between elasticity, viscosity and plasticity, which together, accounts for experimental observations. Even in such a simple geometry, the effects of orientations are important, so that a tensorial elastoviscoplastic description is necessary to capture many aspects of the physics. There is a memory effect of the preparation of the material through the initial stress condition and a persistence of residual normal stresses. Observe that, from the system of equations, if we add a

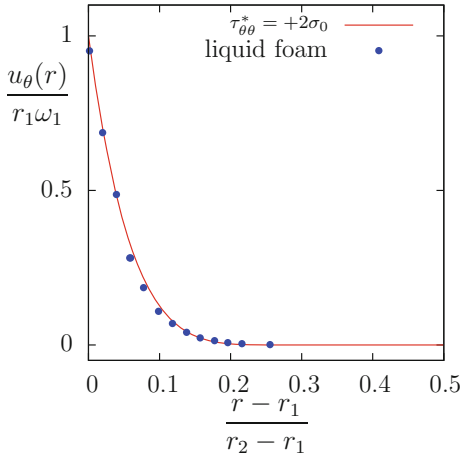

Fig. 5.15 Couette flow of an elastoviscoplastic fluid: computation of a smooth profile with $We = 0.035$, $Bi = 10$, $n = 1/3$, $a = 1$ by Cheddadi et al. [49] and measurements by Debrégeas et al. [77]

constant value to $\boldsymbol{\tau}$ such that $|\boldsymbol{\tau}_d|$ remains under the yield stress value σ_0, then the stationary solution is unchanged. Such stresses that persists in the material are called *residual stress*. The steady solution is non-unique: one is smooth and some others are non-smooth. These features can be predicted neither by the viscoplastic models nor by the viscoelastic one.

Finally, it appears that the steady Couette flow of such complex fluid, which has stimulated so many debates, is not unique. Note that a similar observation was already pointed out in the previous section for the Poiseuille flow. Thus, all observations, either smooth of abrupt, could be interpreted as simply depending on the way the fluid was prepared before the experiment.

5.7 Example: Flow Around an Obstacle

Figure 5.16 shows the two-dimensional flow of a liquid foam between to parallel glasses around a circular obstacle. In 2013, Cheddadi et al. [47, 49] performed the corresponding numerical computations and some comparisons with experimental measurements. The comparisons found an excellent agreement with the spatial distribution of all important features. They found accurate predictions of the experimental fields of velocity, elastic deformation, and plastic deformation rate in terms of magnitude, direction, and anisotropy. These results demonstrated that the behavior of soft glassy materials cannot be reduced to an intermediate between that of a solid and that of a liquid: the viscous, the elastic and the plastic contributions to the flow, as well as their couplings, must be treated simultaneously.

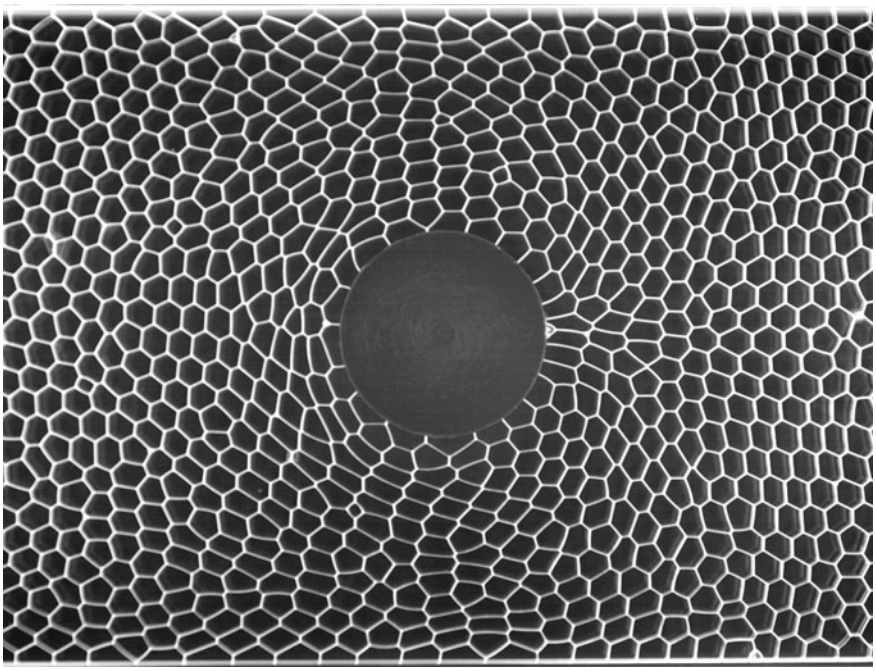

Fig. 5.16 Liquid foam flowing around an obstacle (from Raufaste [251])

Observe on Fig. 5.16 that there is a symmetry with respect to the horizontal Ox axis while the upstream-downstream one is broken: close to the obstacle, the bubbles downstream (left) are stretched while there are compressed upstream (right). The computational domain is reduced to the half top of the flow domain. The boundary conditions are similar to those of Sect. 3.3, p. 99, and represented on Fig. 3.16, except that both the upstream and the downstream parts are here included in the computational domain Ω. The elastoviscoplastic model (5.20a)–(5.20g) is considered here with a power law index $n = 1$. Also, instead of a deviatoric interpolated derivative, in (5.20a), an upper-convected derivative is considered, as in (5.18). This modification corresponds to the model version proposed by Saramito [280, 281].

Let $\lambda = \eta_m/\mu$ be the relaxation time. A characteristic length is the radius L of the obstacle and a characteristic velocity is the upstream velocity U of the fluid. There are four dimensionless numbers: the Weissenberg number $We = \lambda U/L$, the Bingham number $Bi = \sqrt{2}\sigma_0 L/((\eta_s + \eta_m)U)$, the solvent ratio $\alpha = \eta_m/(\eta_s + \eta_m)$ and the parameter of the interpolated derivative a. Note the square root of two factor in the definition of Bi: this factor is inserted for compatibility with the value of the Bingham number used in [47], that was associated to a slightly different definition of the tensor norm and, consequently, also to a different definition of the yield stress (see also Remark 2.1, p. 64). A fifth dimensionless number is the Reynold $Re = \rho U L/(\eta_s + \eta_m)$ that is estimated of about 5×10^{-3} and the inertia term is simply neglected in (5.20b).

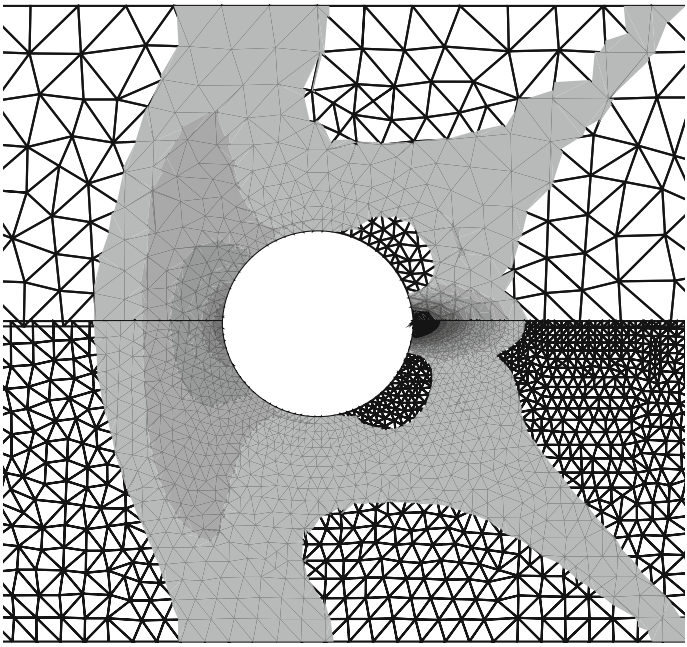

Fig. 5.17 Elastoviscoplastic fluid around an obstacle with $We = 0.075$, $Bi = 8$, $\alpha = 0.9$ and $a = 1$: flowing regions $\{\boldsymbol{x} \in \Omega;\ |\boldsymbol{\tau}_d(\boldsymbol{x}| \geqslant Bi\}$. Mesh sensitivity: (*top*) with a coarse mesh; (*bottom*) with a fine mesh, reflected (from [47])

Unlike for most liquid flows, but in agreement with foam flow experiments [82], bubbles slide along the obstacle and the borders with a negligible friction. Thus, a slip boundary condition is used along the obstacle and the lateral wall. Slip boundary conditions allow to impose a uniform velocity in the x direction on the upstream boundary. A zero stress is used as upstream boundary condition. The problem is solved by an operator splitting method, the θ-scheme algorithm, similar to those presented in Sect. 4.6, p. 167. Then, viscoplasticity and viscoelasticity are split and solved separately.

Figure 5.17 shows the contours of the flowing regions: the finer mesh predicts the same flowing area as the coarser one, which validates the convergence by the mesh insensitivity of our computations. Recall that regions where $|\text{dev}(\boldsymbol{\tau})| < Bi$ behave as elastic solid. The convergence is confirmed on Fig. 5.18 by cuts of velocity and stress components along the horizontal axis. The mesh sensitivity is imperceptible for the velocity plot while it is slightly visible upstream for the stresses. In particular, computations with both meshes predict the same *overshoot* of the velocity after the obstacle, which is one of the salient features of this setup. Such an overshoot, also referred to as *negative wake* in the literature, has already been evidenced, both experimentally and numerically with viscoelastic materials at high velocity (see [48] for a short review) and elastoviscoplastic materials such as carbopol, with spherical

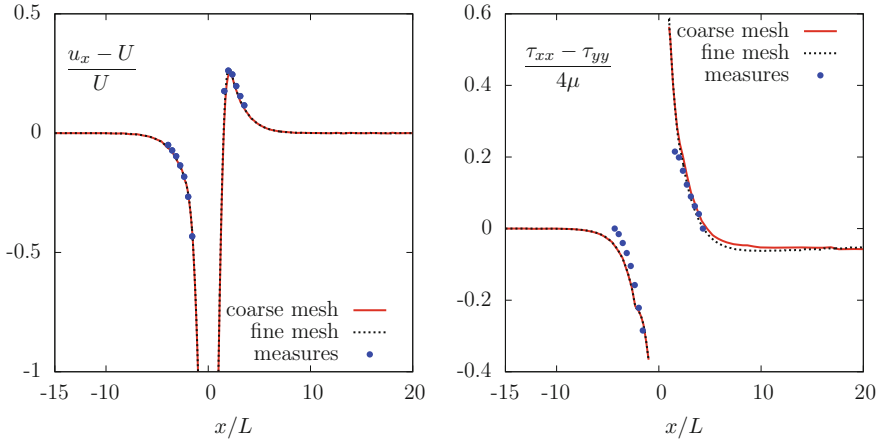

Fig. 5.18 Elastoviscoplastic fluid around an obstacle with $We = 0.075$, $Bi = 8$, $\alpha = 0.9$ and $a = 1$: (*left*) velocity and (*right*) normal stress difference along the horizontal axis (from [47])

objects settling [248] or flow perpendicular to a disc [161]. Experimental measurements are obtained as averages over bubbles. These experiments exhibit a strong fore-aft asymmetry with negative wake even in the case of slow flows, which cannot be predicted neither by viscoelastic or viscoplastic models. As carbopol is a shear thinning yield stress fluid with elastic properties, it seems that the present approach with the elastoviscoplastic model could be successfully applied to interpret these experiments.

Finally, Fig. 5.19 presents a comparison on the whole domain of the solution (half top) with experimental measurements (half bottom, reflected). Observe the excellent concordance of the stream function, represented with thin lines. The streamlines are represented in the referential of the moving obstacle, as if the fluid was at rest and the obstacle was moving. See Sect. 3.13, p. 132 for the computation of the stream function around a moving obstacle. Let us compare these streamlines with those of a viscoplastic fluid, on Fig. 3.17. Observe here that the upstream/downstream symmetry is lost, due to elastic effects, while a viscoplastic fluid flow maintains this symmetry (see Sect. 3.13, p. 132). The velocity field is represented with arrows. For a two-dimensional geometry, the deviatoric part of the elastic deformation tensor $\varepsilon_e = \tau/(2\mu)$ has two real eigenvalues that have opposite signs. The positive eigenvalue is represented as a circle with radius proportional to this eigenvalue and the corresponding eigenvector is represented as a line across the circle. The black arrow at bottom left represents the scale of the entrance velocity U. Conversely, the bottom left bar represents the characteristic stress used for scaling the elastic eigenvalues.

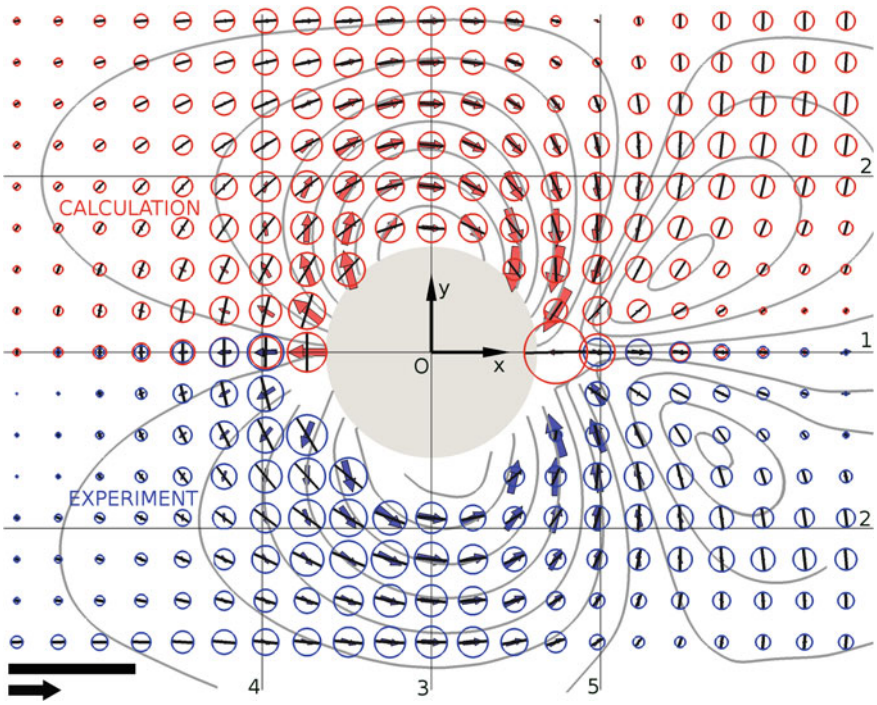

Fig. 5.19 Elastoviscoplastic fluid around an obstacle with $We = 0.08$, $Bi = 5$, $\alpha = 10/11 \approx 0.91$ and $a = 0$. Comparison with measures on a liquid foam (from [48])

5.8 Notes

History – The development of a viscoplastic model based on yield stress started in 1900 when Schwedoff [291], studying a gelatin suspension, presented a one-dimensional plastic version of the Maxwell viscoelastic model [202]:

$$\begin{cases} \dot{\varepsilon} = 0, & \text{when } \tau \leqslant \sigma_0, \\ \lambda \dfrac{\mathrm{d}\tau}{\mathrm{d}t} + (\tau - \sigma_0) = \eta_m \dot{\varepsilon}, & \text{when } \tau > \sigma_0, \end{cases} \tag{5.25}$$

where τ is the stress, $\dot{\varepsilon}$ the rate of deformation, $\eta_m > 0$ the viscosity, $\sigma_0 \geqslant 0$ the yield stress and $\lambda \geqslant 0$ a relaxation time. In steady shear flow this reduces to $\tau = \sigma_0 + \eta_m \dot{\varepsilon}$ when $\tau > \sigma_0$. In 1922, Bingham [26] proposed the one-dimensional stress-deformation rate equation for a viscous fluid with a yield stress:

$$\max\left(0, \frac{|\tau| - \sigma_0}{|\tau|}\right) \tau = \eta_m \dot{\varepsilon} \iff \begin{cases} |\tau| \leqslant \sigma_0 & \text{when } |\dot{\varepsilon}| = 0, \\ \tau = \eta_m \dot{\varepsilon} + \sigma_0 \dfrac{\dot{\varepsilon}}{|\dot{\varepsilon}|} & \text{otherwise.} \end{cases} \tag{5.26}$$

Note that this model is equivalent – up to the sign of $\dot{\varepsilon}$, assumed positive – to the steady case of the model proposed by Schwedoff. Numerous attempts have been made to modify this simple equation to account for more complex behavior of such materials. In 1926, Herschel and Bulkley [142] proposed to model the observed shear stress dependence of the viscosity on the shear rate $\dot{\varepsilon}$ after yielding by explicitly defining the viscosity η_m as a power-law function of $|\dot{\varepsilon}|$. In 1932, Prager [244], using the von Mises [205] yielding criterion, proposed to extend the Bingham model to the three-dimensional case and Oldroyd, in 1947, in a collection of papers (see e.g. [226]) studied the Bingham three-dimensional model and its Herschel–Bulkley extension coupled with the Navier-Stokes equations for the motion of the fluid. Oldroyd also proposed a three-dimensional constitutive equation which combines the yielding criterion together with a linear Hookean elastic behavior before yielding and a viscous behavior after yielding. In the one-dimensional case, the model can be written as:

$$\begin{cases} \tau = \mu\varepsilon & \text{when } \tau \leqslant \sigma_0, \\ \left(\dfrac{|\tau| - \sigma_0}{|\tau|}\right) \tau = \eta_m \dot{\varepsilon} & \text{when } \tau > \sigma_0. \end{cases} \tag{5.27}$$

When compared to (5.25), this model is qualitatively different: the material is no longer rigid before yielding. Here, the yield stress σ_0 is related to the yield deformation $\varepsilon_0 = \sigma_0/\mu$. Since the first equation in (5.27) describes stresses in term of deformation ε and the second equation in (5.27) in term of deformation rate $\dot{\varepsilon}$, the stress-deformation curve predicted by this model must exhibit a discontinuity at the yield deformation $\dot{\varepsilon} = \dot{\varepsilon}_0$ at which the stress jumps from $\tau = \sigma_0$ to $\tau = \sigma_0 + \eta\dot{\varepsilon}$. This is an approximation of the true behavior of materials: the real deformation at the transition is expected to be smooth, at least continuous. In 1950, Oldroyd [227] developed a theory for the invariant forms of constitutive equations and proposed a three-dimensional viscoelastic model, that can be expressed in its one-dimensional version as:

$$\lambda \frac{\mathrm{d}\tau}{\mathrm{d}t} + \tau = \eta_m \dot{\varepsilon} \tag{5.28}$$

where the total stress $\sigma = \eta_s \dot{\varepsilon} + \tau$. In this approach the stress τ is the elastic part of the total stress, from which the elastic deformation can be obtained. The constant $\eta_s > 0$ is a second viscosity, called the solvent viscosity in the context of polymer solutions.

A one-dimensional version of the elastoviscoplastic model proposed by Saramito [280, 281] and presented in this chapter, Eq. (5.20a), appears as combination of the two previous Bingham (5.26) and Oldroyd (5.28) models:

$$\lambda \frac{\mathrm{d}\tau}{\mathrm{d}t} + \max\left(0, \frac{|\tau| - \sigma_0}{|\tau|}\right) \tau = \eta_m \dot{\varepsilon}. \tag{5.29}$$

where the total stress is $\sigma = \eta_s \dot{\varepsilon} + \tau$. When $\lambda = \eta =_s 0$ we obtain the Bingham (5.26) model while when $\sigma_0 = 0$ our model reduces to the Oldroyd (5.28) one. Observe

that (5.29) differs both from (5.25) and (5.27). Schwedoff proposed a rigid behavior $\dot{\varepsilon} = 0$ when $|\tau| \leqslant \sigma_0$ and Oldroyd (5.27) proposed a brutal change of model when reaching the yield value. The elastoviscoplastic model proposed by Saramito [280, 281] presented a continuous change from a solid to a fluid behavior of the material.

A number of other closely related models have appeared in the literature. In 1991, Beris et al. [83], in order to recover a continuous approximation of the solution of the elastic-viscoplastic model (5.27) proposed by Oldroyd, introduced an ad-hoc recovery procedure. Before yielding, the material behaves as an elastic solid while after yielding it behaves as a power-law viscous non-Newtonian fluid. Despite the lack of a thermodynamical analysis of their model, these authors have been able to propose, based on their computational results, a useful Cox-Merz rule extension that was found to be in good agreement with experimental data on a suspension of silicon particles in polyethylene. In 2003, Puzrin and Houlsby [250, p. 254] inserted friction and a spring into the viscoelastic Kelvin-Voigt model and the resulting model is represented in Fig. 5.20a. Before yielding, the friction is rigid and the material behaves as an elastic solid, thanks to the spring μ. After yielding, the deformation is governed by the so-called *standard* model: a Kelvin-Voigt element plus a spring in series (see e.g. [200, p. 42]). The predicted elongation under a constant traction is presented on Fig. 5.20b. The elongation jumps immediately at $t = 0$ from $\varepsilon = 0$ to $\varepsilon = \overline{\sigma}/\mu$, since the spring element has no time scale. Next, when $t > 0$, if $\overline{\sigma} \leqslant \sigma_0$, then the elongation remains constant, since the spring is fully extended. Otherwise, if $\overline{\sigma} > \sigma_0$, the elongation grows and tends to a bounded value: the material behaves as a solid. By this way Puzrin and Houlsby were able to capture some relevant aspects of the behavior of saturated clays. These authors have proposed in a collection of papers [146, 249] many variants of their model. Nevertheless, it is not applicable to material such as human blood or liquid foams that deform under a low stress and flow under a sufficient stress. In 1990 Isayev and Fan [154] proposed a viscoelastic plastic constitutive equation for flow of particles filled polymers. The main idea of these authors is to insert a friction and a spring into the viscoelastic Oldroyd model and the resulted model is represented on Fig. 5.20c. Before yielding, the friction is rigid and the material behaves as a simple elastic solid, thanks to the spring μ. After yielding, the deformation is described by the Oldroyd viscoelastic model. These authors have added in parallel other Maxwell elements in order to replace the Oldroyd viscoelastic element by a multi-mode Leonov viscoelastic model. The predicted elongation under a constant traction is presented on Fig. 5.20d. As for the Puzrin-Houlsby model, the elongation jumps immediately at $t = 0$ from $\varepsilon = 0$ to $\varepsilon = \overline{\sigma}/\mu$. Next, when $t > 0$, if $\overline{\sigma} \leqslant \sigma_0$, then the elongation remains constant. Otherwise, if $\overline{\sigma} > \sigma_0$, the elongation grows and is not bounded: in that case, the material behaves as a fluid. The friction element was able to describe the stress generated in the disperse phase of the filled polymer melts and this contribution has represented an important conceptual advance in this domain. Since the effect of added solid particles in a polymer melt is usually to reduce the viscoelasticity, the need of this kind of formulation arises primarily in the case of highly viscoelastic polymers such as rubbers. Nevertheless, the model presented in Fig. 5.20e, f is a definite improvement: the instantaneous jump at $t = 0$ followed by a constant elongation under traction of both the Puzrin-Houlsby and the

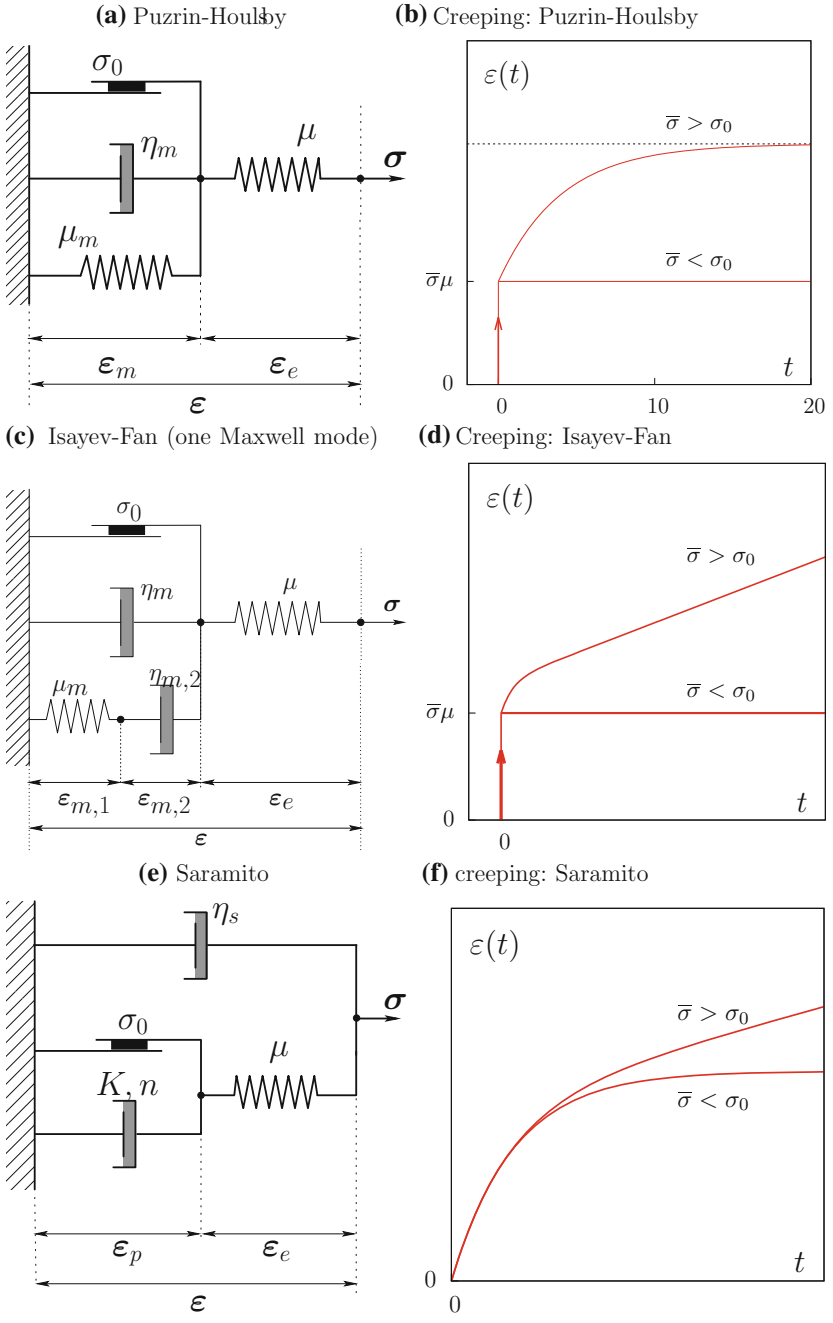

Fig. 5.20 Comparison of some rheological models: (*left*) diagram; (*right*) creeping curves

year	contribution	before yielding	after yielding	3D	TH
1900	Schwedoff [290]	rigid solid	viscoelastic fluid		
1922	Bingham [26]	rigid solid	Newtonian fluid	*X*	*X*
1926	Herschel-Bulkley [142]	rigid solid	power-law fluid	*X*	*X*
1947	Oldroyd [227]	elastic fluid	Newtonian fluid	**X**	*X*
1990	Isayev-Fan [154]	elastic solid	viscoelastic fluid	**X**	**X**
1991	Beris *et al.* [83]	elastic solid	power-law fluid	**X**	
2003	Puzrin-Houlsby [249, p. 254]	elastic solid	viscoelastic solid	**X**	**X**
2007	Saramito [279, 280]	viscoelastic solid	viscoelastic fluid	**X**	**X**
2008	Bénito *et al.* [14]	viscoelastic solid	viscoelastic fluid	**X**	**X**

Fig. 5.21 Summary of the referenced contributions on elastoviscoplastic models

one-mode simplified Isayev-Fan models is replaced by a smoother behavior. Finally, let us mention the tensorial model proposed by Bénito et al. [14] that combines viscoelastic and viscoplastic properties.

Figure 5.21 presents an historical summary of such models and signals their associated main features before and after yielding. The `3D` column is marked when the model has been written in a general sense, e.g. with objective derivatives. The `TH` column is also marked when the model satisfies the second law of thermodynamics. The italic mark *X* in the `3D` or the `TH` columns means that the corresponding property has been derived later. For instance, the Bingham and the Herschel–Bulkley models were first proposed in a one-dimensional context, next extended to 3D and finally found to satisfy the second law of thermodynamics.

Thermodynamics – During the 1970s decade Germain [115] and Halphen and Nguyen [137] developed a thermodynamic framework for generalized standard materials. It furnished a robust theoretical tools for managing efficiently constitutive equations. See e.g. Le Tallec [181, p. 26], Maugin [200] or Nguyen [224] for concise and more recent presentations of this framework.

Extensions – The class of elastoviscoplastic models opens the door to many applications. In order to study crater dynamics during meteoritic impacts, drop impact of carbopol are studied in [194], both experimentally and using numerical computations, based on the elastoviscoplastic model introduced in this chapter. The modeling of biological tissue [308] in large deformation, such as embryo-genesis and morpho-genesis involves recently elastoviscoplastic models. In 2015, Dansereau et al. [74] (see also [73]) proposed a viscoelastic model taking into account damage and applied it for the prediction of the global arctic sea ice behavior and this model is being integrated in the NEMO-LIM3 global ocean-sea ice model. In that case, the model is coupled with a structural parameter, representing the damage and healing of the ice sheet material. This coupling with a structural parameter is closely related to thixotropic fluids, as the material properties are changing in time. In 2011, for oil applications, Wachs investigated viscoplastic coupling with either thermal or thixotropic effects [125]. Souza Mendes proposed [296] a regularized viscoplastic model combining both elastic and thixotropic effects, and recently, this model has been numerically investigated in [189].

References

1. F. Abraham, M. Behr, M. Heinkenschloss, Shape optimization in unsteady blood flow: a numerical study of non-Newtonian effects. Comput. Meth. Biomech. Biomed. Engrg. **8**(3), 201–212 (2005)
2. J. d' Alembert. *Essai d'une nouvelle théorie de la résistance des fluides* (David l'aîné, Paris, 1752). http://gallica.bnf.fr/ark:/12148/bpt6k206036b.r=.langFR
3. I.K. Argyros, *Convergence and Applications of Newton-Type Iterations* (Springer, Heidelberg, 2008)
4. C. Ashcraft, J.W.H. Liu, Robust ordering of sparse matrices using multisection. SIAM J. Matrix Anal. Appl. **19**(3), 816–832 (1998)
5. G. Astarita, G. Marrucci, *Principles of non-Newtonian Fluid Mechanics* (Mc Graw-Hill, New-York, 1974)
6. F. Auteri, N. Parolini, L. Quartapelle, Numerical investigation on the stability of singular driven cavity flow. J. Comput. Phys. **183**(1), 1–25 (2002)
7. M. Avgousti, A.N. Beris, Non-axisymmetric modes in viscoelastic Taylor–Couette flow. J. Non-Newton. Fluid Mech. **50**(2), 225–251 (1993)
8. J. Baranger, K. Najib, Analyse numérique des écoulements quasi-Newtoniens dont la viscosité obéit à la loi puissance ou la loi de Carreau. Numer. Math. **58**(1), 35–49 (1990)
9. J. Baranger, D. Sandri, Finite element approximation of viscoelastic fluid flow: existence of approximate solutions and error bounds Part I. discontinuous constraints. Numer. Math. **63**, 13–27 (1992)
10. J. Baranger, D. Sandri, A formulation of Stokes's problem and the linear elasticity equations suggested by the Oldroyd model for viscoelastic flow. M2AN **26**(2), 331–345 (1992)
11. H.A. Barnes, J.F. Hutton, K. Walters, *An Introduction to Rheology* (Elsevier, Amsterdam, 1989)
12. R. Barrett, M. Berry, T.F. Chan, J. Demmel, J.M. Donato, J. Dongarra, V. Eijkhout, R. Pozow, C. Romine, H. van der Vorst, *Templates for the Solution of Linear Systems*, 2nd edn. (SIAM, Philadelphia, 1994). http://www.netlib.org/templates
13. G.K. Batchelor, *An Introduction to Fluid Dynamics*, 6th edn. (Cambridge University Press, UK, 1967)
14. S. Bénito, C.-H. Brunneau, T. Colin, C. Gay, F. Molino, An elasto-visco-plastic model for immortal foams or emulsions. Eur. Phys. J. E **25**, 225–251 (2008)
15. M. Bensaada, D. Esselaoui, P. Saramito, Error estimate for the characteristic method involving Oldroyd derivative in a tensorial transport problem. Electr. J. Differ. Equ. **11**, 53–59 (2004). (Conference)
16. M. Bercovier, M. Engelman, A finite-element method for incompressible non-Newtonian flows. J. Comput. Phys. **36**, 313–326 (1980)

P. Saramito, *Complex fluids*, Mathématiques et Applications 79,
DOI 10.1007/978-3-319-44362-1

17. A. Bermudez, M.R. Nogueiras, C. Vasquez, Numerical analysis of convection-diffusion-reaction problem with higher order characteristics/finite elements. Part II: fully discretized and quadrature formulas. SIAM J. Numer. Anal. **44**(5), 1854–1876 (2006)
18. N. Bernabeu, Modélisation multi-physique des écoulements viscoplastiques – application aux coulées de lave volcaniques. Ph.D. thesis, Université de Grenoble (2015)
19. N. Bernabeu, P. Saramito, C. Smutek, Numerical modeling of shallow non-newtonian flows: Part II. viscoplastic fluids and general tridimensional topographies. Int. J. Numer. Anal. Model. **11**(1), 213–228 (2014)
20. N. Bernabeu, P. Saramito, C. Smutek, *Modelling Lava Flow Advance Using a Shallow-depth Approximation for Three-dimensional Cooling of Viscoplastic Flows, Chap. 27* (The Geological Society, London, 2016)
21. C. Bernardi, Y. Maday, Spectral methods, in *Handbook of Numerical Analysis*, vol. 5. Techniques of scientific computing (part 2), Chap. 2, ed by P.G. Ciarlet, J.-L. Lions (Elsevier, Amsterdam, 1997), pp. 209–277
22. D. Bernouilli, *Hydrodynamica* (J.H. Decker, Basiliensis, 1738). http://docnum.u-strasbg.fr/u?/coll12,57982
23. D. Bernouilli, *Hydrodynamics, Chap. 1* (Dover, Mineola, 1968), pp. 1–350
24. J. Besson, G. Cailletaud, J.-L. Chaboche, S. Forest, M. Blétry, *Non-linear Mechanics of Materials* (Springer, Heidelberg, 2010)
25. C.R. Beverly, R.I. Tanner, Numerical analysis of three-dimensional bingham plastic flow. J. Non-Newton. Fluid Mech. **42**(1), 85–115 (1992)
26. E.C. Bingham, *Fluidity and Plasticity* (Mc Graw-Hill, New York, 1922). http://www.archive.org/download/fluidityandplast007721mbp/fluidityandplast007721mbp.pdf
27. R. Bird, R.C. Armstrong, O. Hassager, *Dynamics of Polymeric Liquids*, vol. 1, 2nd edn., Fluid Mechanics (Wiley, New York, 1987)
28. R. Bird, R.C. Armstrong, O. Hassager, *Dynamics of Polymeric Liquids*, vol. 2, Kinetic Theory (Wiley, New York, 1987)
29. D.V. Boger, D.U. Hur, R.J. Binnington, Further observations of elastic effects in tubular entry flows. J. Non-Newton. Fluid Mech. **20**, 31–49 (1986)
30. D.V. Boger, K. Walters, *Rheological Phenomena in Focus* (Elsevier, Amsterdam, 1993)
31. D. Bonn, J. Paredes, M.M. Denn, L. Berthier, T. Divoux, S. Manneville, Yield stress materials in soft condensed matter. Submitted (2015). http://arxiv.org/abs/1502.05281
32. F. Bouchut, I. Ionescu, A. Mangeney, A shallow model including static-flowing transition for viscoplastic Drucker-Prager materials. Submitted (2015). https://hal.archives-ouvertes.fr/hal-01081213
33. K. Boukir, Y. Maday, B. Metivet, E. Razafindrakoto, A high-order characteristic/finite element method for the incompressible Navier–Stokes equations. Int. J. Numer. Meth. Fluids **25**, 1421–1454 (1997)
34. S. Boyaval, T. Lelièvre, C. Mangoubi, Free-energy-dissipative schemes for the Oldroyd-B model. ESAIM Math. Model. Numer. Anal. **43**(03), 523–561 (2009)
35. F. Boyer, P. Fabrie, *Mathematical Tools for the Study of the Incompressible Navier–Stokes Equations and Related Models*, 2nd edn. (Springer, Heidelberg, 2013)
36. H. Brezis, *Functional Analysis, Sobolev Spaces and Partial Differential Equations* (Springer, Heidelberg, 2011)
37. F. Brezzi, On the existence, uniqueness and approximation of saddle-point problems arising from Lagrangian multipliers. RAIRO Anal. Numer. **8**(2), 129–151 (1974)
38. F. Brezzi, M. Fortin, *Mixed and Hybrid Finite Element Methods* (Springer, Hiedelberg, 1991)
39. A.N. Brooks, T.J.R. Hughes, Streamline upwind/Petrov–Galerkin formulations for convection dominated flows with particular emphasis on the incompressible Navier–Stokes equations. Comput. Meth. Appl. Mech. Eng. **32**(1–3), 199–259 (1982)
40. G.R. Burgos, A.N. Alexandrou, Flow development of Herschel–Bulkley fluids in a sudden three-dimensional square expansion. J. Rheol. **43**, 485–498 (1999)

41. C.D. Cantwell, D. Moxey, A. Comerford, A. Bolis, G. Rocco, G. Mengaldo, D. de Grazia, S. Yakovlev, J.-E. Lombard, D. Ekelschot, B. Jordi, H. Xu, Y. Mohamied, C. Eskilsson, B. Nelson, P. Vos, C. Biotto, R.M. Kirby, S.J. Sherwin, Nektar++: an open-source spectral/hp element framework. Comput. Phys. Commun. **192**, 205–219 (2015)
42. P.J. Carreau, I.F. MacDonald, R.B. Bird, A nonlinear viscoelastic model for polymer solutions and melts (II). Chem. Eng. Sci. **23**(8), 901–911 (1968)
43. A. Cauchy, Recherches sur l'équilibre et le mouvement intérieur des corps solides ou fluides, élastiques ou non-élastiques. Bull. Soc. Philomath., 9–19 (1823); Oeuvres complètes **2**(2), 300–304 (1882). http://gallica.bnf.fr/ark:/12148/bpt6k901948.r=Cauchy%2C+Augustin-Louis+completes.langFR
44. A. Cauchy, De la pression ou tension dans un corps solide. Exercices de mathématiques **2**, 42–56 (1827); Oeuvres complètes **2**(7), 55–78 (1882). http://gallica.bnf.fr/ark:/12148/bpt6k901990.r=Cauchy%2C+Augustin-Louis+completes.langFR
45. CGAL: computational geometry algorithm library (2015). http://doc.cgal.org
46. I. Cheddadi, Contribution à la modélisation numérique des écoulements de mousse. Ph.D. thesis, Université de Grenoble (2010). http://tel.archives-ouvertes.fr/tel-00497436
47. I. Cheddadi, P. Saramito, A new operator splitting algorithm for elastoviscoplastic flow problems. J. Non-Newton. Fluid Mech. **202**, 13–21 (2013)
48. I. Cheddadi, P. Saramito, B. Dollet, C. Raufaste, F. Graner, Understanding and predicting viscous, elastic, plastic flows. Eur. Phys. J. E. Soft Matter **34**(1), 11001 (2011)
49. I. Cheddadi, P. Saramito, F. Graner, Steady Couette flows of elastoviscoplastic fluids are non-unique. J. Rheol. **56**(1), 213–239 (2012)
50. G.-Q. Chen, W.P. Ziemer, M. Torres, Gauss–Green theorem for weakly differentiable vector fields, sets of finite perimeter, and balance laws. Comm. Pure Appl. Math. **62**(2), 242–304 (2009)
51. A.J. Chorin, The numerical solution of the Navier–Stokes equations for an incompressible fluid. Bull. Am. Math. Soc. **73**(6), 928–931 (1967)
52. A.J. Chorin, J.E. Marsden, *A Mathematical Introduction to Fluid Mechanics*, 3rd edn. (Springer, Heidelberg, 2000)
53. P. Chossat, G. Iooss, *The Couette–Taylor problem* (Springer, Heidelberg, 1994)
54. J.C. Chrispell, V.J. Ervin, E.W. Jenkins, A fractional step θ-method for viscoelastic fluid flow using a SUPG approximation. Int. J. Comput. Sci. **2**(3), 336–351 (2008)
55. J.C. Chrispell, V.J. Ervin, E.W. Jenkins, A fractional step θ-method approximation of time-dependent viscoelastic fluid flow. J. Comput. Appl. Math. **232**(2), 159–175 (2009)
56. C.I. Christov, On frame indifferent formulation of the Maxwell–Cattaneo model of finite-speed heat conduction. Mech. Res. Commun. **36**(4), 481–486 (2009)
57. L. Chupin, Existence results for the flow of viscoelastic fluids with an integral constitutive law. J. Math. Fluid Mech. **15**(4), 1–24 (2013)
58. L. Chupin, Global existence results for some viscoelastic models with an integral constitutive law. SIAM J. Math. Anal. **46**(3), 1859–1873 (2014)
59. F.H. Clarke, *Optimization and Nonsmooth Analysis* (SIAM, Philadelphia, 1990)
60. S. Claus, T.N. Phillips, Viscoelastic flow around a confined cylinder using spectral/hp element methods. J. Non-Newton. Fluid Mech. **200**, 131–146 (2013)
61. B. Cockburn, B. Dong, J. Guzmán, J. Qian, Optimal convergence of the original DG method on special meshes for variable transport velocity. SIAM J. Numer. Anal. **48**(1), 133–146 (2010)
62. E. Cosserat, F. Cosserat, *Théorie des corps déformables* (Hermann, Paris, 1909)
63. G.-H. Cottet, P.D. Koumoutsakos, *Vortex Methods: Theory and Practice* (Cambridge University Press, UK, 2000)
64. M. Couette, Études sur le frottement des liquides. Ph.D. thesis, Faculté des Sciences de Paris, Paris (1890)
65. P. Coussot, Yield stress fluid flows: a review of experimental data. J. Non-Newton. Fluid Mech. **211**, 31–49 (2014)

66. P. Coussot, G. Ovarlez, Physical origin of shear-banding in jammed systems. Eur. Phys. J. E **33**(3), 183–188 (2010)
67. P. Coussot, J.S. Raynaud, F. Bertrand, P. Moucheront, J.P. Guilbaud, H.T. Huynh, S. Jarny, D. Lesueur, Coexistence of liquid and solid phases in flowing soft-glassy materials. Phys. Rev. Lett. **88**(21), 218301 (2002)
68. M.J. Crochet, A.R. Davis, K. Walters, *Numerical Simulation of Non-Newtonian Flow* (Elsevier, Amsterdam, 1984)
69. M.M. Cross, Rheology of non-Newtonian fluids: a new flow equation for pseudoplastic systems. J. Colloid Sci. **20**(5), 417–437 (1965)
70. K.M. Cuffey, W.S.B. Paterson, *The Physics of Glaciers* (Academic Press, Amsterdam, 2010)
71. H. Damanik, J. Hron, A. Ouazzi, S. Turek, A monolithic FEM approach for the log-conformation reformulation (LCR) of viscoelastic flow problems. J. Non-Newton. Fluid Mech. **165**(19), 1105–1113 (2010)
72. Y. Damianou, M. Philippou, G. Kaoullas, G.C. Georgiou, Cessation of viscoplastic poiseuille flow with wall slip. J. Non-Newton. Fluid Mech. **203**, 24–37 (2014)
73. V. Dansereau, J. Weiss, P. Saramito, P. Lattes, A Maxwell-elasto-brittle rheology for sea ice modelling. The Cryosphere Discussions, 2016:1–0 (2016). http://www.the-cryosphere-discuss.net/tc-2015-200
74. V. Dansereau, J. Weiss, P. Saramito, P. Lattes, E. Coche, A Maxwell-elasto-brittle rheology for sea ice modeling. Mercat. Ocean Newslett. **51**, 35–40 (2015)
75. O. Darrigol, *Worlds of Flow: A History of Hydrodynamics from the Bernoulli to Prandt* (Oxford University Press, Oxford, 2005)
76. B. Debbaut, B. Hocq, On the numerical simulation of axisymmetric swirling flows of differential viscoelastic liquids: the rod climbing effect and the Quelleffekt. J. Non-Newton. Fluid Mech. **43**(1), 103–126 (1992)
77. G. Debrégeas, H. Tabuteau, J.-M. di Meglio, Deformation and flow of a two-dimensional foam under continuous shear. Phys. Rev. Lett. **87**, 178305 (2001)
78. M. Dennin, Discontinuous jamming transitions in soft materials: coexistence of flowing and jammed states. J. Phys. Condens. Matter **20**(2), 283103 (2008)
79. P. Deuflhard, *Newton Methods for Nonlinear Problems: Affine Invariance and Adaptive Algorithms* (Springer, Heidelberg, 2004)
80. M.O. Deville, T.B. Gatski, *Mathematical Modeling for Complex Fluids and Flows* (Springer, Heidelberg, 2012)
81. Y. Dimakopoulos, M. Pavlidis, J. Tsamopoulos, Steady bubble rise in Herschel–Bulkley fluids and comparison of predictions via the augmented Lagrangian method with those via the Papanastasiou model. J. Non-Newton. Fluid Mech. **200**, 34–51 (2013)
82. B. Dollet, F. Graner, Two-dimensional flow of foam around a circular obstacle: local measurements of elasticity, plasticity and flow. J. Fluid Mech. **585**, 181–211 (2007)
83. D. Doraiswamy, A.N. Mujumdar, I. Tsao, A.N. Beris, S.C. Danforth, A.B. Metzner, The Cox–Merz rule extended: a rheological model for concentrated suspensions and other materials with a yield stress. J. Rheol. **35**(4), 647–685 (1991)
84. D.C. Drucker, W. Prager, Soil mechanics and plastic analysis for limit design. Q. Appl. Math. **10**(2), 157–165 (1952)
85. G. Duvaut, *Mécanique des milieux continus* (Masson, Paris, 1990)
86. G. Duvaut, J.L. Lions, *Les inéquations en mécanique et physique* (Dunod, Paris, 1972)
87. H.C. Elman, D.J. Silvester, A.J. Wathen, *Finite Elements and Fast Iterative Solvers with Applications in Incompressible Fluid Dynamics* (Oxford University Press, UK, 2005)
88. A. Ern, J.L. Guermond, Discontinuous Galerkin methods for Friedrichs' systems. II. Second-order elliptic PDEs. SIAM J. Numer. Anal. **44**(6), 2363–2388 (2006)
89. A. Ern, J.-L. Guermond, Discontinuous Galerkin methods for Friedrichs' systems. Part III. multifield theories with partial coercivity. SIAM J. Numer. Anal. **46**(2), 776–804 (2008)
90. A. Ern, J.-L. Guermond, G. Caplain, An intrinsic criterion for the bijectivity of Hilbert operators related to Friedrich' systems. Commun. Partial Diff. Equ. **32**(2), 317–341 (2007)

91. A. Ern, M. Vohralík, Adaptive inexact Newton methods: a posteriori error control and speed-up of calculations. SIAM News **46**(1) (2013)
92. A. Ern, M. Vohralík, Adaptive inexact Newton methods with a posteriori stopping criteria for nonlinear diffusion PDEs. SIAM J. Sci. Comput. **35**(4), A1761–A1791 (2013)
93. A. Ern, J.L. Guermond, Discontinuous Galerkin methods for Friedrichs' symmetric systems. I. General theory. SIAM J. Numer. Anal. **44**(2), 753–778 (2006)
94. E. Erturk, T.C. Corke, C. Gökçol, Numerical solutions of 2-D steady incompressible driven cavity flow at high Reynolds numbers. Int. J. Numer. Meth. Fluids **48**, 747–774 (2005)
95. V.J. Ervin, J.S. Howell, I. Stanculescu, A dual-mixed approximation method for a three-field model of a nonlinear generalized Stokes problem. Comput. Methods Appl. Mech. Eng. **197**, 2886–2900 (2008)
96. L. Euler, Principes généraux du mouvement des fluides. Mém. Acad. Sci. Berl. **11**, 217–273 (1757). https://math.dartmouth.edu/~euler/docs/originals/E225.pdf
97. L. Euler, Principles of the motion of fluids. Phys. D **237**(14), 1840–1854 (2008). English translation by W. Pauls of the Latin original paper from 1756
98. R. Fattal, R. Kupferman, Time-dependent simulation of viscoelastic flows at high Weissenberg number using the log-conformation representation. J. Non-Newton. Fluid Mech. **126**(1), 23–37 (2005)
99. E. Fernández-Cara, F. Guillén, R.R. Ortega, Some theoretical results concerning non-Newtonian fluids of the Oldroyd kind. Ann. Scuola Norm. Sup. Pisa Cl. Sci. **26**(1), 1–29 (1998)
100. E. Fernández-Cara, F. Guillén, R.R. Ortega, Mathematical modeling and analysis of viscoelastic fluids of the Oldroyd kind, in *Handbook of Numerical Analysis. Volume 8. Solutions of Equations in* $\mathbb{R}^n$ *(Part 4). Techniques of Scientific Computing (Part 4). Numerical Methods for Fluids (Part 2)*, ed. by P.G. Ciarlet, J.-L. Lions (Elsevier, Amsterdam, 2002), pp. 543–661
101. R.A. Finkel, J.L. Bentley, Quad trees a data structure for retrieval on composite keys. Acta Informatica **4**(1), 1–9 (1974)
102. S. Forest, *Milieux continus généralisés et matériaux hétérogènes* (École des mines, Paris, 2006)
103. A. Fortin, M. Fortin, A preconditioned generalized minimal residual algorithm for the numerical solution of viscoelastic fluid flows. J. Non-Newton. Fluid Mech. **36**, 277–288 (1990)
104. M. Fortin, Calcul numérique des écoulements des fluides de Bingham et des fluides newtoniens incompressibles par la méthode des éléments finis. Ph.D. thesis, Université Paris VI (1972)
105. M. Fortin, D. Esselaoui, A finite element procedure for viscoelastic flows. Int. J. Numer. Methods Fluids **7**(10), 1035–1052 (1987)
106. M. Fortin, A. Fortin, A new approach for the FEM simulation of viscoelastic flows. J. Non-Newton. Fluid Mech. **32**(3), 295–310 (1989)
107. M. Fortin, R. Glowinski, *Augmented Lagrangian Methods* (Elsevier, Amsterdam, 1983)
108. M. Fortin, R. Pierre, On the convergence of the mixed method of Crochet and Marchal for viscoelastic flows. Comp. Meth. Appl. Mech. Eng. **73**(3), 341–350 (1989)
109. G. Fourestey, S. Piperno, A second-order time-accurate ALE Lagrange–Galerkin method applied to wind engineering and control of bridge profiles. Comput. Methods Appl. Mech. Eng. **193**, 4117–4137 (2004)
110. J. Fourier, Théorie analytique de la chaleur. Firmin Didot père et fils (1822). http://gallica.bnf.fr/ark:/12148/bpt6k1045508v.r=fourier+chaleur.langFR
111. K.O. Friedrichs, Symmetric positive linear differential equations. Comm. Pure Appl. Math. **11**, 333–418 (1958)
112. I.A. Frigaard, C. Nouar, On the usage of viscosity regularisation methods for visco-plastic fluid flow computation. J. Non-Newton. Fluid Mech. **127**(1), 1–26 (2005)
113. T. Gelhard, G. Lube, M.A. Olshanskii, J.H. Starcke, Stabilized finite element schemes with LBB-stable elements for incompressible flows. J. Comput. Appl. Math. **177**, 243–267 (2005)
114. A. George, Nested dissection of a regular finite element mesh. SIAM J. Numer. Anal. **10**, 345–363 (1973)
115. P. Germain, *Cours de mécanique des milieux continus* (Masson, Paris, 1973)

116. C. Gilbreth, S. Sullivan, M. Dennin, Flow transition in two-dimensional foams. Phys. Rev. E **74**, 031401 (2006)
117. V. Girault, F. Hecht, Numerical methods for grade-two fluid models: finite-element discretizations and algorithms, in *Handbook of Numerical Analysis, Chap. 1*, vol. 16, Numerical Methods for Non-Newtonian Fluids, ed. by P.G. Ciarlet, J.-L. Lions (Elsevier, Amsterdam, 2011), pp. 1–209
118. V. Girault, P.A. Raviart, *Finite Element Approximation of the Navier–Stokes Equations* (Springer, Heidelberg, 1979)
119. V. Girault, P.A. Raviart, *Finite Element Methods for the Navier–Stokes Equations: Theory and Algorithms* (Springer, Heidelberg, 1986)
120. R. Glowinski, *Lecture on Numerical Methods for Nonlinear Variational Problems* (Springer, Heidelberg, 1980)
121. R. Glowinski, Finite element methods for incompressible viscous flow, in *Handbook of Numerical Analysis, Chap. 1*, vol. 9, Numerical Methods for Fluids (Part 3) (Elsevier, Amsterdam, 2003), pp. 3–1176
122. R. Glowinski, P. Le Tallec, *Augmented Lagrangian and Operator Splitting Methods in Nonlinear Mechanics* (SIAM, Philadelphia, 1989)
123. R. Glowinski, J.L. Lions, R. Trémolières, *Numerical Analysis of Variational Inequalities* (Elsevier, Amsterdam, 1981)
124. R. Glowinski, B. Mantel, J. Périaux, *Numerical Solution of the Time Dependent Navier–Stokes Equations for Incompressible Viscous Fluids by Finite Element and Alternating Direction Methods* (Academic Press, London, 1982), pp. 309–336
125. R. Glowinski, A. Wachs, On the numerical simulation of viscoplastic fluid flow, in *Handbook of Numerical Analysis, Chap. 6*, vol. 16, Numerical Methods for Non-Newtonian Fluids, ed. by P.G. Ciarlet, J.-L. Lions (Elsevier, Amsterdam, 2011), pp. 483–717
126. R.J. Gordon, W.R. Schowalter, Anisotropic fluid theory: a different approach to the dumbbell theory of dilute polymer solutions. J. Rheol. **16**, 79–97 (1972)
127. M. Griebel, A. Rüttgers, Multiscale simulations of three-dimensional viscoelastic flows in a square-square contraction. J. Non-Newton. Fluid Mech. **205**, 41–63 (2014)
128. P.P. Grinevich, M.A. Olshanskii, An iterative method for the Stokes type problem with variable viscosity. SIAM J. Sci. Comput. **31**(5), 3959–3978 (2009)
129. S. Gross, A. Reusken, *Numerical Methods for Two-Phase Incompressible Flows* (Springer, Heidelberg, 2011)
130. E. Guazzelli, J.F. Morris, *A Physical Introduction to Suspension Dynamics* (Cambridge University Press, UK, 2011)
131. R. Guénette, M. Fortin, A new mixed finite element method for computing viscoelastic flows. J. Non-Newton. Fluid Mech. **60**(1), 27–52 (1995)
132. J.L. Guermond, P. Minev, J. Shen, An overview of projection methods for incompressible flows. Comput. Methods Appl. Mech. Eng. **195**, 6011–6045 (2006)
133. C. Guillopé, J.C. Saut, Résultats d'existence pour les fluides viscoélastiques à loi de comportement de type différentiel. C. R. Acad. Sci. Paris, Sér. 1 **305**(11), 489–492 (1987)
134. C. Guillopé, J.C. Saut, Existence results for the flow of viscoelastic fluid a differential constitutive law. Nonlinear Anal. **15**(9), 849–869 (1989)
135. C. Guillopé, J.C. Saut, Global existence and one-dimensional nonlinear stability of shearing motions of viscoelastic Oldroyd type. M2AN **24**(3), 369–401 (1990)
136. A. Hakim, Mathematical analysis of viscoelastic fluids of White–Metzner type. J. Math. Anal. Appl. **185**(3), 675–705 (1994)
137. B. Halphen, Q.S. NGuyen, Sur les matériaux standards généralisés. J. Méca **14**, 39–63 (1975)
138. F.H. Harlow, J.E. Welch, Numerical calculation of time-dependent viscous incompressible flow of fluid with free surface. Phys. Fluids **8**(12), 2182–2189 (1965)
139. F. Hecht, Construction d'une base de fonctions P_1 non conforme à divergence nulle dans $\mathbb{R}^3$. RAIRO Anal. Numer. **15**(2), 119–150 (1981)
140. F. Hecht, BAMG: bidimensional anisotropic mesh generator (2006). http://www.ann.jussieu.fr/~hecht/ftp/bamg

141. F. Hecht, Freefem++ user's manual, version 3.29 (2014)
142. W.H. Herschel, T. Bulkley, Measurement of consistency as applied to rubber-benzene solutions. Proc. Am. Soc. Test. Mater. **26**(2), 621–633 (1926)
143. J.S. Hesthaven, T. Warburton, *Nodal Discontinuous Galerkin Methods: Algorithms, Analysis and Applications* (Springer, Heidelberg, 2008)
144. N.J. Hoff, Approximate analysis of structures in the presence of moderately large creep deformations. Q. Appl. Math. **12**(1), 49 (1954)
145. A.J. Hoffman, M.S. Martin, D.J. Rose, Complexity bounds for regular finite difference and finite element grids. SIAM J. Numer. Anal. **10**(2), 364–369 (1973)
146. G.T. Houlsby, A.M. Puzrin, Rate-dependent plasticity models derived from potential functions. J. Rheol. **41**, 113–126 (2002)
147. J. Hron, A. Ouazzi, S. Turek, *A Computational Comparison of Two FEM Solvers for Nonlinear Incompressible Flow* (Springer, Heidelberg, 2003), pp. 87–109
148. D. Hu, T. Lelièvre, New entropy estimates for the Oldroyd-B model and related models. Commun. Math. Sci. **5**(4), 909–916 (2007)
149. R.R. Huilgol, N. Phan-Thien, *Fluid Mechanics of Viscoelasticity: General Principles, Constitutive Modelling and Numerical Techniques* (Elsevier, Amsterdam, 1997)
150. M.A. Hulsen, A sufficient condition for a positive definite configuration tensor in differential models. J. Non-Newton. Fluid Mech. **38**(1), 93–100 (1990)
151. I. Ionescu, A. Mangeney, F. Bouchut, O. Roche, Viscoplastic modelling of granular column collapse with pressure and rate dependent viscosity. J. Non-Newton. Fluid Mech. **219**, 1–18 (2015)
152. I. Ionescu, M. Sofonea, *Functional and Numerical Methods in Viscoplasticity* (Oxford University Press, UK, 1993)
153. F. Irgens, *Continuum Mechanics* (Springer, Heidelberg, 2008)
154. A.I. Isayev, X. Fan, Viscoelastic plastic constitutive equation for flow of particle filled polymers. J. Rheol. **34**, 35–54 (1990)
155. G.B. Jeffery, The motion of ellipsoidal particles immersed in a viscous fluid. Proc. R. Soc. Lond. A **102**(715), 161–179 (1922)
156. C. Johnson, J. Pitkäranta, An analysis of the discontinuous Galerkin method for a scalar hyperbolic equation. Math. Comp. **46**(173), 1–26 (1986)
157. M.W. Johnson, D. Segalman, A model for viscoelastic fluid behavior which allows non-affine deformation. J. Non-Newton. Fluid Mech. **2**, 255–270 (1977)
158. P. Jop, Y. Forterre, O. Pouliquen, A constitutive law for dense granular flows. Nature **441**, 727–730 (2006)
159. D.D. Joseph, *Fluid Dynamics of Viscoelastic Liquids* (Springer, Heidelberg, 1990)
160. D.D. Joseph, M. Renardy, J.-C. Saut, Hyperbolicity and change of type in the flow of viscoelastic fluids. Arch. Rational Mech. Anal. **87**(3), 213–251 (1985)
161. L. Jossic, F. Ahonguio, A. Magnin, Flow of a yield stress fluid perpendicular to a disc. J. Non-Newton. Fluid Mech. **191**, 14–24 (2013)
162. A. Kabla, J. Scheibert, G. Debrégeas, Quasistatic rheology of foams II. Continuous shear flow. J. Fluid Mech. **587**, 45–72 (2007)
163. S. Kadri-Harouna, V. Perrier, Divergence-free wavelet projection method for incompressible viscous flow. SIAM Multiscale Model. Simul. **13**(1), 399–422 (2015). Hal-00798417
164. G. Kanschat, *Discontinuous Galerkin Methods for Viscous Incompressible Flow* (Springer, Heidelberg, 2007)
165. G.E. Karniadakis, S.J. Sherwin, *Spectral/hp Element Methods for Computational Fluid Dynamics*, 2nd edn. (Oxford University Press, UK, 2005)
166. G. Katgert, M.E. Möbius, M. van Hecke, ate dependence and role of disorder in linearly sheared two-dimensional foams. Phys. Rev. Lett. **101**, 058301 (2008)
167. R. Keunings, On the high Weissenberg number problem. J. Non-Newton. Fluid Mech. **20**, 209–226 (1986)
168. R. Keunings, A survey of computational rheology, in *Proceedings of the XIIIth International Congress on Rheology*, vol. 1, pp. 7–14 (2000)

169. R. Keunings, Micro-macro methods for the multiscale simulation of viscoelastic flow using molecular models of kinetic theory (The british society of Rheology, 2004), pp. 67–98
170. D.E. Knuth, *The Art of Computer Programming*, vol. 3, Sorting and Searching (Addison Wesley, Reading, 1973)
171. R. Kupferman, C. Mangoubi, E.S. Titi, A Beale–Kato–Majda breakdown criterion for an Oldroyd-B fluid in the creeping flow regime. Submitted (2014). http://arxiv.org/abs/0709.1455
172. Y. Kwon, A.I. Leonov, On instabilities of single-integral constitutive equations for viscoelastic liquids. Rheol. Acta **33**(5), 398–404 (1994)
173. Y. Kwon, A.I. Leonov, Stability constraints in the formulation of viscoelastic constitutive equations. J. Non-Newton. Fluid Mech. **58**(1), 25–46 (1995)
174. R.G. Larson, *Constitutive Equations for Polymer Melts and Solutions* (Butterworths, Boston, 1988)
175. R.G. Larson, Instabilities in viscoelastic flows. Rheol. Acta **31**(3), 213–263 (1992)
176. A. Latz, U. Strautins, D. Niedziela, Comparative numerical study of two concentrated fiber suspension models. J. Non-Newton. Fluid Mech. **165**(13), 764–781 (2010)
177. B.E. Launder, G. Reece, W. Rodi, Progress in the development of a Reynolds-stress turbulence closure. J. Fluid Mech. **68**(03), 537–566 (1975)
178. J. Lauridsen, G. Chanan, M. Dennin, Velocity profiles in slowly sheared bubble rafts. Phys. Rev. Lett. **93**(1), 018303 (2004)
179. P.D. Lax, A.N. Milgram, *Parabolic Equations: Contributions to the Theory of Partial Differential Equations*, vol. 33, Annals of Mathematics Studies (Princeton University Press, Princeton, 1954)
180. C. Le Bris, T. Lelièvre, Micro-macro models for viscoelastic fluids: modelling, mathematics and numerics. Sci. China Math. **55**(2), 353–384 (2012)
181. P. Le Tallec, *Numerical Analysis of Viscoelastic Problems* (Masson, Paris, 1990)
182. Y.-L. Lee, J. Xu, C.-S. Zhang, Stable finite element discretizations for viscoelastic flow models, in *Handbook of numerical analysis, Chap. 4*, vol. 16, Numerical Methods for Non-Newtonian Fluids, ed. by P.G. Ciarlet, J.-L. Lions (Elsevier, Amsterdam, 2011), pp. 371–432
183. S. Lefschetz, *Differential Equations, Geometric Theory*, 2nd edn. (Wiley, New York, 1962)
184. J. Leray, Sur le mouvement d'un liquide visqueux emplissant l'espace. Acta Math. **63**, 193–248 (1934)
185. P. Lesaint, Finite element methods for the transport equation. M2AN **8**(1), 67–94 (1974)
186. P. Lesaint, P.A. Raviart, *On a Finite Element Method for Solving the Neutron Transport Equation, Chap. 4* (Academic Press, New York, 1974), pp. 89–124
187. R.W. Lewis, P. Nithiarasu, K.N. Seetharamu, *Fundamentals of the Finite Element Method for Heat and Fluid Flow* (Wiley, New York, 2004)
188. F.-H. Lin, C. Liu, P. Zhang, On hydrodynamics of viscoelastic fluids. Comm. Pure Appl. Math. **58**(11), 1437–1471 (2005)
189. F.B. Link, S.L. Frey, R.L. Thompson, M.F. Naccache, P.R. de Souza Mendes, Plane flow of thixotropic elasto-viscoplastic materials through a 1:4 sudden expansion. J. Non-Newton. Fluid Mech. **220**, 162–174 (2015)
190. J.-L. Lions, *Quelques méthodes de résolution des problèmes aux limites non linéaires* (Gauthier-Villars, Paris, 1969)
191. P.L. Lions, N. Masmoudi, Global solutions for some Oldroyd models of non-Newtonian flows. Chin. Ann. Math. Ser. B **21**(2), 131–146 (2000)
192. G.G. Lipscomb, M.M. Denn, D.U. Hur, D.V. Boger, The flow of fiber suspensions in complex geometries. J. Non-Newton. Fluid Mech. **26**(3), 297–325 (1988)
193. A. Lozinski, R.G. Owens, T.N. Phillips, The Langevin and Fokker–Planck equations in polymer rheology, in *Handbook of Numerical Analysis, Chap. 2*, vol. 16, Numerical Methods for Non-Newtonian Fluids, ed. by P.G. Ciarlet, J.-L. Lions (Elsevier, Amsterdam, 2011), pp. 211–303
194. L.-H. Luu, Y. Forterre, Drop impact of yield-stress fluids. J. Fluid Mech. **632**, 301–327 (2009)

195. J.R. Magnus, H. Neudecker, *Matrix differential calculus with applications in statistics and econometrics*, 3rd edn. (Wiley, New York, 2007)
196. G. Maîtrejean, A. Ammar, F. Chinesta, M. Grmela, Deterministic solution of the kinetic theory model of colloidal suspensions of structureless particles. Rheol. Acta **51**(6), 527–543 (2012)
197. J. Málek, M. Ružička, V.V. Shelukhin, Herschel–Bulkley fluids: existence and regularity of steady flows. Math. Models Meth. Appl. Sci. **15**(12), 1845–1861 (2005)
198. A. Maleki, S. Hormozi, A. Roustaei, I.A. Frigaard, Macro-size drop encapsulation. J. Fluid Mech. **769**, 482–521 (2015)
199. J.M. Marchal, M.J. Crochet, A new mixed finite element for calculating viscoelastic flow. J. Non-Newton. Fluid Mech. **26**, 77–144 (1987)
200. G.A. Maugin, *The Thermomechanics of Plasticity and Fracture* (Cambridge University Press, UK, 1992)
201. G.A. Maugin, A.V. Metrikine, *Mechanics of Generalized Continua: One Hundred Years After the Cosserats* (Springer, Heidelberg, 2010)
202. J.C. Maxwell, On the dynamical theory of gases. Phil. Trans. R. Soc. Lond. **157**, 49–88 (1867)
203. S. Melchior, V. Legat, P. Van Dooren, A.J. Wathen, Analysis of preconditioned iterative solvers for incompressible flow problems. Int. J. Numer. Methods Fluids **68**(3), 269–286 (2012)
204. P.D. Minev, C.R. Ethier, A characteristic/finite element algorithm for the 3-D Navier–Stokes equations using unstructured grids. Comput. Methods Appl. Mech. Eng. **178**(1–2), 39–50 (1998)
205. R. von Mises, Mechanik der festen Körper im plastich-deformablen Zustand. Nachrichten Ges. Wiss. Göttingen, 582–592 (1913)
206. E. Mitsoulis, S.S. Abdali, N.C. Markatos, Flow simulation of Herschel–Bulkley fluids through extrusion dies. Can. J. Chem. Eng. **71**, 147–160 (1993)
207. E. Mitsoulis, R.R. Huilgol, Entry flows of Bingham plastics in expansions. J. Non-Newton. Fluid Mech. **122**, 45–54 (2004)
208. L. Molinet, R. Talhouk, On the global and periodic regular flows of viscoelastic fluids with a differential constitutive law. Nonlinear Diff. Equ. Appl. **11**(3), 349–359 (2004)
209. L. Molinet, R. Talhouk, Newtonian limit for weakly viscoelastic fluid flows of Oldroyd type. SIAM J. Math. Anal. **39**(5), 1577–1594 (2008)
210. K.W. Morton, A. Priestley, E. Süli, Stability of the Lagrange–Galerkin method with non-exact integration. M2AN **22**(4), 625–653 (1988)
211. P.P. Mosolov, V.P. Miasnikov, Variational methods in the theory of the fluidity of a viscous-plastic medium. J. Appl. Math. Mech. **29**(3), 545–577 (1965)
212. P.P. Mosolov, V.P. Miasnikov, On stagnant flow regions of a viscous-plastic medium in pipes. J. Appl. Math. Mech. **30**(4), 841–853 (1966)
213. P.P. Mosolov, V.P. Miasnikov, On qualitative singularities of the flow of a viscoplastic medium in pipes. J. Appl. Math. Mech. **31**(3), 609–613 (1967)
214. P.P. Mosolov, V.P. Mjasnikov, A proof of Korn inequality. Sov. Math. **12**, 1618–1622 (1971)
215. M.A. Moyers-Gonzalez, I.A. Frigaard, Numerical solution of duct flows of multiple visco-plastic fluids. J. Non-Newton. Fluid Mech. **127**, 227–241 (2004)
216. L. Muravleva, Uzawa-like methods for numerical modeling of unsteady viscoplastic Bingham medium flows. Appl. Numer. Math. **93**, 140–149 (2015)
217. L. Muravleva, E. Muravleva, G.C. Georgiou, E. Mitsoulis, Numerical simulations of cessation flows of a Bingham plastic with the augmented Lagrangian method. J. Non-Newton. Fluid Mech. **165**, 544–550 (2010)
218. C. Navier, Mémoire sur les lois du mouvement des fluides. Mémoires de l'académie royale des sciences de l'institut de France **6**, 381–449 (1823)
219. A. Nejat, A. Jalali, M. Sharbatdar, A Newton-Krylov finite volume algorithm for the power-law non-Newtonian fluid flow using pseudo-compressibility technique. J. Non-Newton. Fluid Mech. **166**, 1158–1172 (2011)
220. I. Newton, *Philosophiae Naturalis Principia Mathematica*, 3rd edn. (A. Guil. and J. Innys, London, 1726). http://www.e-rara.ch/doi/10.3931/e-rara-1235

221. I. Newton, *Principes mathématiques de la philosophie naturelle, tome 1* (J. Gabay, Paris, 1759). Traduction par É. du Châtelet. http://gallica.bnf.fr/ark:/12148/bpt6k29037w
222. I. Newton, *Principes mathématiques de la philosophie naturelle, tome 2* (J. Gabay, Paris, 1759). Traduction par É. du Châtelet. http://gallica.bnf.fr/ark:/12148/bpt6k290387
223. I. Newton, *The mathematical principles of natural philosophy (1687)* (D. Adee, New York, 1846). Translated by A. Motte
224. Q.-S. Nguyen, *Stability and Nonlinear Solid Mechanics* (Wiley, New York, 2000)
225. F.H. Norton, *The Creep of Steel at High Temperatures* (McGraw-Hill, New York, 1929)
226. J.G. Oldroyd, A rational formulation of the equations of plastic flow for a Bingham fluid. Proc. Camb. Philos. Soc. **43**, 100–105 (1947)
227. J.G. Oldroyd, On the formulation of rheological equations of states. Proc. R. Soc. Lond. A **200**, 523–541 (1950)
228. J.G. Oldroyd, Non-Newtonian effects in steady motion of some idealized elastico-viscous liquids. Proc. R. Soc. Lond. A Math. Phys. Sci. **245**(1241), 278–297 (1958)
229. W. Ostwald, Ueber die rechnerische darstellung des strukturgebietes der viskosität. Kolloid-Zeitschrift **47**(2), 176–187 (1929)
230. H.C. Öttinger, *Beyond Equilibrium Thermodynamics* (Wiley, New York, 2005)
231. M.L. Ould Salihi, Couplage de méthodes numériques en simulation directe d'écoulements incompressibles. Ph.D. thesis, Université J. Fourier, Grenoble (1998)
232. G. Ovarlez, K. Krishan, S. Cohen-Addad, Investigation of shear banding in three-dimensional foams. Europhys. Lett. **91**, 68005 (2010)
233. R. Owens, T. Phillips, *Computational Rheology* (Imperial College Press, London, 2002)
234. P. Pakdel, S.H. Spiegelberg, G.H. McKinley, Cavity flows of elastic liquids: two-dimensional flows. Phys. Fluids **9**(11), 3123 (1997)
235. T.C. Papanastasiou, Flow of materials with yield. J. Rheol. **31**, 385–404 (1987)
236. T.E. Peterson, A note on the convergence of the discontinuous Galerkin method for a scalar hyperbolic equation. SIAM J. Numer. Anal. **28**(1), 133–140 (1991)
237. C. Petrie, H. Giesekus, James Gardner Oldroyd (1921–1982). Rheol. Acta **22**(1), 1–3 (1983)
238. N. Phan-Thien, R.I. Tanner, A new constitutive equation derived from network theory. J. Non-Newton. Fluid Mech. **2**(4), 353–365 (1977)
239. J.M. Piau, M. Bremond, J.M. Couette, M. Piau, Maurice Couette, one of the founders of rheology. Rheol. Acta **33**(5), 357–368 (1994)
240. D.A. di Pietro, A. Ern, *Mathematical Aspects of Discontinuous Galerkin Methods* (Springer, Heidelberg, 2012)
241. O. Pironneau, On the transport-diffusion algorithm and its applications to the Navier–Stokes equations. Numer. Math. **38**(3), 309–332 (1982)
242. H. Poincarré, *La science et l'hypothèse* (1902). www.ebooksgratuits.com/ebooks.php
243. J.-L.-M. Poiseuille, Recherches expérimentales sur le mouvement des liquides dans les tubes de très-petits diamètres. Imprimerie royale (1844). http://books.google.fr/books?id=uBN1Q-IRzTMC&printsec=frontcover&hl=fr#v=onepage&q&f=false
244. W. Prager, K. Hohenemser, Über die Ansätze der Mechanik isotroper Kontinua. Z. Angew. Math. Mech. **12**, 216–226 (1932)
245. E. Pruliere, A. Ammar, N. El Kissi, F. Chinesta, Recirculating flows involving short fiber suspensions: numerical difficulties and efficient advanced micro-macro solvers. Arch. Comput. Methods Eng. **16**(1), 1–30 (2009)
246. A. Putz, I.A. Frigaard, Creeping flow around particle in a Bingham fluid. J. Non-Newton. Fluid Mech. **165**(5–6), 263–280 (2010)
247. A. Putz, I.A. Frigaard, D.M. Martinez, On the lubrication paradox and the use of regularisation methods for lubrication flows. J. Non-Newton. Fluid Mech. **163**, 62–77 (2009)
248. A.M.V. Putz, T.I. Burghelea, A. Frigaard, D.M. Martinez, Settling of an isolated spherical particle in a yield stress shear thinning fluid. Phys. Fluids **20**, 033102 (2008)
249. A.M. Puzrin, A.M. Asce, G.T. Houlsby, Rate-dependent hyperplasticity with internal functions. J. Eng. Mech. **129**(3), 252–263 (2003)

250. A.M. Puzrin, G.T. Houlsby, A thermomechanical framework for rate-independent dissipative materials with internal functions. Int. J. Plast. **17**, 1147–1165 (2001)
251. C. Raufaste, Rhéologie et imagerie des écoulements 2D de mousse: approche expérimentale, numérique et théorique. Ph.D. thesis, Université J. Fourier, Grenoble (2007)
252. W.H. Reed, T.R. Hill, Triangular mesh methods for the neutron transport equation. Technical report LA-UR-73-0479, Los Alamos Scientific Laboratory, USA (1973). http://lib-www.lanl.gov/cgi-bin/getfile?00354107.pdf
253. M. Renardy, Existence of slow steady flows of viscoelastic fluids with differential constitutive equations. Z. Angew. Math. u. Mech. **65**(9), 449–451 (1985)
254. M. Renardy, *Mathematical Analysis of Viscoelastic Flows* (SIAM, Philadelphia, 2000)
255. M. Renardy, *Mathematical Analysis of Viscoelastic Fluids, Chap. 5* (Elsevier, Amsterdam, 2008), pp. 229–265
256. J.C. de los Reyes, S.A. González Andrade, Numerical simulation of two-dimensional Bingham fluid flow by semismooth Newton methods. J. Comput. Appl. Math. **235**, 11–32 (2010)
257. J.C. de los Reyes, S.A. González Andrade, A combined BDF-semismooth Newton approach for time-dependent Bingham flow. Numer. Methods Part. Diff. Equ. **28**(3), 834–860 (2012)
258. J.C. de los Reyes, S.A. González Andrade, Numerical simulation of thermally convective viscoplastic fluids by semismooth second order type methods. J. Non-Newton. Fluid Mech. **193**, 43–48 (2013)
259. O. Reynolds, An experimental investigation of the circumstances which determine whether the motion of water shall be direct or sinuous, and of the law of resistance in parallel channels. Proc. R. Soc. Lond. **35**, 84–99 (1883). https://archive.org/details/philtrans09957627
260. G.R. Richter, An optimal-order error estimate for the discontinuous galerkin method. Math. Comput. **50**(181), 75–88 (1988)
261. R.S. Rivlin, The relation between the flow of non-Newtonian fluids and turbulent Newtonian fluids. Q. Appl. Maths. **15**, 212–215 (1957)
262. R.S. Rivlin, J.L. Ericksen, Stress-deformation relations for isotropic materials. J. Rat. Mech. Anal. **4**, 323–425 (1955)
263. R.T. Rockafellar, *Conjugate Duality and Optimization* (SIAM, Philadelphia, 1974)
264. R.T. Rockafellar, Augmented Lagrangians and applications of the proximal point algorithm in convex programming. Math. Oper. Res. **1**(2), 97–116 (1976)
265. N. Roquet, P. Saramito, An adaptive finite element method for Bingham fluid flows around a cylinder. Comput. Appl. Methods Mech. Eng. **192**(31–32), 3317–3341 (2003)
266. N. Roquet, P. Saramito, Stick-slip transition capturing by using an adaptive finite element method. M2AN **38**(2), 249–260 (2004)
267. N. Roquet, P. Saramito, An adaptive finite element method for viscoplastic flows in a square pipe with stick-slip at the wall. J. Non-Newton. Fluid Mech. **155**, 101–115 (2008)
268. A. Roustaei, Yield stress fluid flows in uneven geometries: applications to the oil and gas industry. Ph.D. thesis, University of British Columbia, Vancouver, Canada (2016)
269. A. Roustaei, I.A. Frigaard, The occurrence of fouling layers in the flow of a yield stress fluid along a wavy-walled channel. J. Non Newton. Fluid Mech. **198**, 109–124 (2013)
270. A. Roustaei, I.A. Frigaard, Residual drilling mud during conditioning of uneven boreholes in primary cementing. Part 2: steady laminar inertial flows. J. Non-Newton. Fluid Mech. **226**, 1–15 (2015)
271. A. Roustaei, A. Gosselin, I.A. Frigaard, Residual drilling mud during conditioning of uneven boreholes in primary cementing. Part 1: rheology and geometry effects. J. Non-Newton. Fluid Mech. **220**, 87–98 (2015)
272. F. Rouvière, *Petit guide de calcul différentiel à l'usage de la licence et de l'agrégation*, 2nd edn. (Casini, Paris, 2003)
273. J.-B. Salmon, S. Manneville, A. Colin, Shear banding in a lyotropic lamellar phase. i. time-averaged velocity profiles. Phys. Rev. E **68**, 051503 (2003)
274. J.-B. Salmon, S. Manneville, A. Colin, Shear banding in a lyotropic lamellar phase. ii. temporal fluctuations. Phys. Rev. E **68**, 051504 (2003)

275. H. Samet, *The Design and Analysis of Spatial Data Structure* (Addison Wesley, Reading, 1990)
276. P. Saramito, Simulation numérique d'écoulements de fluides viscoélastiques par éléments finis incompressibles et une méthode de directions alternées; applications. Ph.D. thesis, Institut National Polytechnique de Grenoble (1990)
277. P. Saramito, Numerical simulation of viscoelastic fluid flows using incompressible finite element method and a θ-method. M2AN **28**(1), 1–35 (1994)
278. P. Saramito, Operator splitting for viscoelastic fluid with a differential constitutive law. C. R. Acad. Sci. Paris Ser. II **319**(3), 267–270 (1994)
279. P. Saramito, Efficient simulation of nonlinear viscoelastic fluid flows. J. Non-Newton. Fluid Mech. **60**, 199–223 (1995)
280. P. Saramito, A new constitutive equation for elastoviscoplastic fluid flows. J. Non-Newton. Fluid Mech. **145**(1), 1–14 (2007)
281. P. Saramito, A new elastoviscoplastic model based on the Herschel–Bulkley viscoplasticity. J. Non-Newton. Fluid Mech. **158**(1–3), 154–161 (2009)
282. P. Saramito, *Language C++ et calcul scientifique* (College Publications, London, 2013)
283. P. Saramito, On a modified non-singular log-conformation formulation for Johnson–Segalman viscoelastic fluids. J. Non-Newton. Fluids Mech. **211**, 16–30 (2014)
284. P. Saramito, *Efficient C++ Finite Element Computing with Rheolef* (CNRS and LJK, Grenoble, 2015). http://cel.archives-ouvertes.fr/cel-00573970
285. P. Saramito, *Efficient C++ Finite Element Computing with Rheolef: Volume 2: Discontinuous Galerkin Methods*, vol. 2 (CNRS and LJK, Grenoble, 2015). http://cel.archives-ouvertes.fr/cel-00863021
286. P. Saramito, *Rheolef: An Efficient C++ Finite Element Environment* (Rheolef editorial board, 2015). http://www-ljk.imag.fr/membres/Pierre.Saramito/rheolef
287. P. Saramito, A damped newton algorithm for computing viscoplastic fluid flows. J. Non-Newton. Fluid Mech. (2016, in press, to appear). https://hal.archives-ouvertes.fr/hal-01228347/document
288. P. Saramito, J.-M. Piau, Flow characteristics of viscoelastic fluids in an abrupt contraction by using numerical modeling. J. Non-Newton. Fluid Mech. **52**, 263–288 (1994)
289. P. Saramito, N. Roquet, An adaptive finite element method for viscoplastic fluid flows in pipes. Comput. Methods Appl. Mech. Eng. **190**(40–41), 5391–5412 (2001)
290. J.-C. Saut, *Lectures on the Mathematical Theory of Viscoelastic Fluids* (Higher Education Press, Beijing; International Press, Boston, 2012), pp. 325–393
291. T. Schwedoff, La rigidité des liquides, in *Congrès Int. Physique, Paris*, vol. 1, pp. 478–486 (1900)
292. L.R. Scott, M. Vogelius, Norm estimates for a maximal right inverse of the divergence operator in spaces of piecewise polynomials. M2AN **19**(1), 111–143 (1985)
293. N.D. Scurtu, Stability analysis and numerical simulation of non-Newtonian fluids of Oldroyd kind. Ph.D. thesis, U. Nürnberg, Deutschland (2005)
294. J. Shen, Hopf bifurcation of the unsteady regularized driven cavity flow. J. Comp. Phys. **95**, 228–245 (1991)
295. A.M. Sonnet, A. Ramage, Computational fluid dynamics for nematic liquid crystals, in *21st International Liquid Crystral Conference, Keystone, Colorado, USA* (2007)
296. P.R. de Souza Mendes, Thixotropic elasto-viscoplastic model for structured fluids. Soft Matter **7**(6), 2471–2483 (2011)
297. C.G. Speziale, B.A. Younis, S.A. Berger, Analysis and modelling of turbulent flow in an axially rotating pipe. J. Fluid Mech. **407**, 1–26 (2000)
298. G. Stokes, On the theories of internal frictions of fluids in motion and of the equilibrium and motion of elastic solids. Trans. Camb. Phil. Soc. **8**, 287–319 (1845)
299. E. Süli, Convergence and nonlinear stability of the Lagrange–Galerkin method for the Navier–Stokes equations. Numer. Math. **53**(4), 459–483 (1988)
300. R. Sureshkumara, M.D. Smith, R.C. Armstrong, R.A. Brown, Linear stability and dynamics of viscoelastic flows using time-dependent numerical simulations. J. Non-Newton. Fluid Mech. **82**, 57–104 (1999)

301. A. Syrakos, G.C. Georgiou, A.N. Alexandrou, Performance of the finite volume method in solving regularised Bingham flows: inertia effects in the lid-driven cavity flow. J. Non-Newton. Fluid Mech. **208**, 88–107 (2014)
302. R.I. Tanner, K. Walters, *Rheology: An Historical Perspective* (Elsevier, Amsterdam, 1998)
303. A.J. Taylor, S.D.R. Wilson, Conduit flow of an incompressible, yield-stress fluid. J. Rheol. **41**(1), 93–101 (1997)
304. C. Taylor, P. Hood, A numerical solution of the Navier–Stokes equations using the finite element technique. Comput. Fluids **1**(1), 73–100 (1973)
305. G.I. Taylor, Stability of a viscous liquid contained between two rotating cylinders. Phil. Trans. R. Soc. Lond. A **223**, 289–343 (1923)
306. R. Temam, *Navier–Stokes Equations and Nonlinear Functional Analysis*, 2nd edn. (SIAM, Philadelphia, 1995)
307. R. Temam, A. Miranville, *Mathematical Modeling in Continuum Mechanics*, 2nd edn. (Cambridge University Press, UK, 2005)
308. S. Tlili, C. Gay, F. Graner, P. Marcq, F. Molino, P. Saramito, Colloquium: mechanical formalism for tissue dynamics. Eur. Phys. J. E **38**, 33–63 (2015)
309. T. Treskatis, M.A. Moyers-Gonzalez, C.J. Price, A trust-region SQP method for the numerical approximation of viscoplastic fluid flow. Submitted (2015). http://arxiv.org/pdf/1504.08057.pdf
310. G. Vinay, A. Wachs, J.-F. Agassant, Numerical simulation of non-isothermal viscoplastic waxy crude oil flows. J. Non-Newton. Fluid Mech. **128**(2), 144–162 (2005)
311. D. Vola, L. Boscardin, J.C. Latché, Laminar unsteady flows of Bingham fluids: a numerical strategy and some benchmark results. J. Comput. Phys. **187**, 441–456 (2003)
312. Y. Wang, Comment on "Conduit flow of an incompressible, yield-stress fluid". J. Rheol. **41**, 93–101 (1997); J. Rheol. **41**(6), 1387–1389 (1997)
313. P. Wapperom, M.A. Hulsen, Thermodynamics of viscoelastic fluids: the temperature equation. J. Rheol. **42**, 999 (1998)
314. H.R. Warner, Kinetic theory and rheology of dilute suspensions of finitely extendible dumbbells. Ind. Eng. Chem. Fundam. **11**(3), 379–387 (1972)
315. K. Weissenberg, A continuum theory of rheological phenomena. Nature **159**(4035), 310–311 (1947)
316. K. Weissenberg, Rheology of hydrocarbon gels. Proc. R. Soc. Lond. Ser. A **200**(1061), 183–188 (1950)
317. S.D.R. Wilson, A.J. Taylor, The channel entry problem for a yield stress fluid. J. Non-Newton. Fluid Mech. **65**, 165–176 (1996)
318. K.Y. Yasuda, R.C. Armstrong, R.E. Cohen, Shear flow properties of concentrated solutions of linear and star branched polystyrenes. Rheol. Acta **20**(2), 163–178 (1981)
319. E. Zeidler, *Applied Functional Analysis*, vol. 1, Application to Mathematical Physics (Springer, Heidelberg, 1995)
320. O.C. Zienkiewicz, R.L. Taylor, *The finite element method*, vol. 3, 5th edn., Fluid Dynamics (Butterworth-Heinemann, Newton, 2000)

Index

P. Saramito, *Complex fluids*, Mathématiques et Applications 79,
DOI 10.1007/978-3-319-44362-1